Article:
Wu, C., Huang, Q., Xu, Z. et al. (92 more authors) (2024) A comprehensive review of carbon capture science and technologies. Carbon Capture Science & Technology, 11. 100178. ISSN 2772-6568

https://doi.org/10.1016/j.ccst.2023.100178

Carbon Capture Science & Technology 11 (2024) 100178

Contents lists available at ScienceDirect

Carbon Capture Science & Technology

journal homepage: www.elsevier.com/locate/ccst

Review

A comprehensive review of carbon capture science and technologies

Chunfei Wu[a,*], Qi Huang[a], Zhicheng Xu[b], Ayesha Tariq Sipra[b], Ningbo Gao[b,†], Luciana Porto de Souza Vandenberghe[c,†], Sabrina Vieira[c], Carlos Ricardo Soccol[c], Ruikai Zhao[d], Shuai Deng[d,†], Sandra K.S. Boetcher[e,†], Shijian Lu[f,*], Huancong Shi[g], Dongya Zhao[h,†], Yupeng Xing[h], Yongdong Chen[i,†], Jiamei Zhu[j], Dongdong Feng[k,†], Yu Zhang[k], Lihua Deng[k], Guoping Hu[l,†], Paul A. Webley[m], Daxin Liang[n,†], Zhichen Ba[n], Agata Mlonka-Mędrala[o], Aneta Magdziarz[o,†], Norbert Miskolczi[p,†], Szabina Tomasek[p], Su Shiung Lam[q,†], Shin Ying Foong[q], Hui Suan Ng[r], Long Jiang[s,†], Xinlong Yan[t], Yongzhuo Liu[u], Ying Ji[s], Hongman Sun[v,†], Yu Zhang[v], Haiping Yang[w,†], Xiong Zhang[w], Mingzhe Sun[x], Daniel C.W. Tsang[x,†], Jin Shang[y], Christoph Muller[z,*], Margarita Rekhtina[z], Maximilian Krödel[z], Alexander H. Bork[z], Felix Donat[z], Lina Liu[aa,†], Xin Jin[h,†], Wen Liu[bb,†], Syed Saqline[bb], Xianyue Wu[bb], Yongqing Xu[cc], Asim Laeeq Khan[dd,†], Zakawat Ali[dd], Haiqing Lin[ee,†], Leiqing Hu[ee], Jun Huang[ff,†], Rasmeet Singh[ff], Kaifang Wang[gg,hh], Xuezhong He[gg,hh,†], Zhongde Dai[ii,†], Shouliang Yi[jj,*], Alar Konist[kk,†], Mais Hanna Suleiman Baqain[kk], Yijun Zhao[k], Shaozeng Sun[k], Guoxing Chen[ll,†], Xin Tu[mm], Anke Weidenkaff[ll,nn], Sibudjing Kawi[oo,†], Kang Hui Lim[oo], Chunfeng Song[pp,†], Qing Yang[qq,†], Zhenyu Zhao[rr], Xin Gao[rr,†], Xia Jiang[ss,†], Haiyan Ji[ss], Toluleke E. Akinola[tt], Adekola Lawal[uu], Olajide S. Otitoju[tt], Meihong Wang[tt,*], Guojun Zhang[vv], Lin Ma[vv,†], Baraka C. Sempuga[ww], Xinying Liu[ww,†], Eni Oko[xx,†], Michael Daramola[yy], Zewei Yu[zz], Siming Chen[f], Guojun Kang[f], Qingfang Li[aaa], Li Gao[aab], Ling Liu[f], Hui Zhou[cc,*]

[a] School of Chemistry and Chemical Engineering, Queen's University Belfast, Belfast, BT7 1NN, UK
[b] School of Energy and Power Engineering, Xi'an Jiaotong University, Xi'an, Shaanxi, 710049, China
[c] Department of Bioprocess Engineering and Biotechnology, Federal University of Paraná, Brazil
[d] State Key Laboratory of Engines, Tianjin University, Tianjin 300350, China
[e] Embry-Riddle Aeronautical University, Daytona Beach, Florida 32114 USA
[f] China University of Mining and Technology, China
[g] Huzhou Research Institute of Zhejiang University, China
[h] College of Chemistry & Chemical Engineering, China University of Petroleum (East China), Qingdao 266580, China
[i] College of Chemistry and Chemical Engineering, Southwest Petroleum University, Chengdu 610500, China
[j] School of Chemical Engineering and Technology, China University of Mining & Technology, Xuzhou, Jiangsu 221116, China
[k] School of Energy Science and Engineering, Harbin Institute of Technology, 150001, China
[l] Key Laboratory of Rare Earths, Ganjiang Innovation Academy, Chinese Academy of Sciences, Ganzhou, Jiangxi, 341000, China
[m] Department of Chemical Engineering, Monash University, Victoria 3800, Australia
[n] Key Laboratory of Bio-based Material Science and Technology (Ministry of Education), Northeast Forestry University, Harbin 150040, China
[o] AGH University of Krakow, Al. A. Mickiewicza 30, 30-059 Krakow, Poland

* Corresponding authors.
E-mail addresses: c.wu@qub.ac.uk (C. Wu), lushijian@cumt.edu.cn (S. Lu), muelchri@ethz.ch (C. Muller), slyi@chbe.gatech.edu (S. Yi), meihong.wang@sheffield.ac.uk (M. Wang), zhouhui.10@tsinghua.org.cn (H. Zhou).

† **Section leaders**: 2.1&2.2 - Professor Ningbo Gao; 2.3 - Professor Luciana Porto de Souza Vandenberghe; 2.4 - Professor Shuai Deng; 2.4 & 5.3 - Professor Sandra Boetcher; 3.1.1.5 – Professor Dongya zhao; 3.1.2 - Professor Yongdong Chen; 3.1.3 - Dr Dongdong Feng; 3.2.1 - Dr Guoping Hu; 3.2.2-Dr Daxin Liang; 3.2.3.1 - Dr Aneta Magdziarz; 3.2.3.2 - Dr Norbert Miskolczi; 3.2.3.3 - Professor Su Shiung Lam; 3.2.4 - Dr Long Jiang; 3.2.5.1 - Dr Hongman Sun; 3.2.5.2 - Professor Haiping Yang; 3.2.5.3 - Professor Dan Tsang; 3.4.1, 3.4.2 & 3.5.1 - Professor Christoph Muller; 3.4.3 - Dr Lina Liu; 3.5.2 – Dr Xin Jin; 3.5.3, 5.1.2 & 5.3 - Dr Wen Liu; 4.1 & 4.2.1 - Dr Asim Khan 4.2 - Professor Haiqing Lin; 4.3, 3.2.2, 3.2.5.1 - Professor Jun Huang; 4.4 - Dr Xuezhong He; 4.5 - Dr Zhongde Dai; 5.1.1Professor Alar Konist; 5.1.4 - Dr Guoxing Chen; 5.2 - Dr Sibudjing Kawi; 5.3 Professor Chunfeng Song; 5.3.8 - Professor Qing Yang; 5.4 – Professor Xin Gao; 5.5 – Professor Xia Jiang; 6.1&6.2 - Professor Meihong Wang; 6.3 & 6.4 - Professor Lin Ma 6.5 -Professor Xinying Liu; 6.6 - Dr Eni Oko; 7.1 – Professor Shijian Lu; 7.2 – Dr Siming Chen; 7.3 – Dr Ling Liu

https://doi.org/10.1016/j.ccst.2023.100178
Received 6 September 2023; Received in revised form 3 December 2023; Accepted 8 December 2023

[p] MOL Department of Hydrocarbon and Coal Processing, University of Pannonia, H-8200, Veszprém, Egyetem u. 10, Hungary
[q] Institute of Tropical Aquaculture and Fisheries (AKUATROP), Universiti Malaysia Terengganu, 21030 Kuala Nerus, Terengganu, Malaysia
[r] Centre for Research and Graduate Studies, University of Cyberjaya, Persiaran Bestari, 63000 Cyberjaya, Selangor, Malaysia
[s] Institute of Refrigeration and Cryogenics, Zhejiang University, Hangzhou, 310027, China
[t] School of Chem. Eng. Technol., China University of Mining and Technology, Xuzhou 221116, China
[u] College of Chemical Engineering, Qingdao University of Science & Technology, Qingdao, 266042, China
[v] State Key Laboratory of Heavy Oil Processing, College of Chemistry and Chemical Engineering, China University of Petroleum, Qingdao 266580, China
[w] State Key Laboratory of Coal Combustion, School of Energy and Power Engineering, Huazhong University of Science and Technology, Wuhan, 430074, China
[x] Department of Civil and Environmental Engineering, The Hong Kong University of Science and Technology, Clear Water Bay, Hong Kong
[y] School of Energy and Environment, City University of Hong Kong, Tat Chee Avenue, Kowloon, Hong Kong, China
[z] Institute of Energy and Process Engineering, ETH Zürich, Leonhardstrasse 21, Zürich 8092, Switzerland
[aa] College of Environmental Science and Engineering, Ministry of Education Key Laboratory of Pollution Processes and Environmental Criteria, Nankai University, Tianjin 300350, China
[bb] School of Chemistry, Chemical Engineering and Biotechnology, Nanyang Technological University, 62 Nanyang Drive, Singapore 637459, Singapore
[cc] Department of Energy and Power Engineering, Tsinghua University, Beijing, 100084, China
[dd] Chemical Engineering Department, COMSATS University Islamabad, Lahore, Pakistan
[ee] Department of Chemical and Biological Engineering, University at Buffalo, The State University of New York, Buffalo, NY 14260, USA
[ff] School of Chemical and Biomolecular Engineering, University of Sydney, Sydney, Australia
[gg] Department of Chemical Engineering, Guangdong Technion - Israel Institute of Technology, 241 Daxue Road, Shantou, Guangdong, 515063, China
[hh] The Wolfson Department of Chemical Engineering, Technion - Israel Institute of Technology, Haifa 3200003, Israel
[ii] College of Carbon Neutrality Future Technology, Sichuan University, Chengdu 610065, China
[jj] Department of Energy, National Energy Technology Laboratory, Pittsburgh, PA 15236, USA
[kk] Department of Energy Technology, Tallinn University of Technology, 19086, Tallinn, Estonia
[ll] Fraunhofer Research Institution for Materials Recycling and Resource Strategies IWKS, Brentanostraße 2a, 63755 Alzenau, Germany
[mm] Department of Electrical Engineering and Electronics, University of Liverpool, Liverpool L69 3GJ, UK
[nn] Department of Materials and Earth Sciences, Technical University Darmstadt, Alarich-Weiss-Str. 2, 64287 Darmstadt, Germany
[oo] Department of Chemical and Biomolecular Engineering, National University of Singapore, P.O. Box 117585, Singapore
[pp] School of Environmental Science and Engineering, Tianjin University, Tianjin, China
[qq] School of Energy and Power Engineering, Huazhong University of Science and Technology, Wuhan, China
[rr] School of Chemical Engineering and Technology, Tianjin University, Tianjin 300072, China
[ss] College of Carbon Neutrality Future Technology, Sichuan University, Chengdu, 610065, China
[tt] Department of Chemical and Biological Engineering, University of Sheffield, Sheffield S1 3JD, UK
[uu] Petrofac, Woking GU21 5BH, UK
[vv] Department of Mechanical Engineering, University of Sheffield, Sheffield S1 3JD, UK
[ww] Institute for Catalysis and Energy Solutions, University of South Africa, c/o Christiaan de Wet & Pioneer Avenue, Florida, 1709, Johannesburg, South Africa
[xx] School of Engineering, Newcastle University, Newcastle upon Tyne NE1 7RU, UK
[yy] Department of Chemical Engineering, Faculty of Engineering, Built Environment and Information Technology, University of Pretoria, Pretoria, South Africa
[zz] International CCS Knowledge Centre, 198–10 Research Drive Regina, SK S4S 7J7, Canada
[aaa] Sinopec Engineering Incorporation, Dongying, Shandong, 257088, China
[aab] China Energy Jin Jie Power Station, Yulin, Shanxi, 719319, China

1. Introduction

CO_2 is one of the major anthropogenic greenhouse gases in the atmosphere contributing to global warming (Blamey et al., 2010; Mikkelsen et al., 2010). In the last half-century, the concentration of CO_2 has exhibited a dramatic growth from about 310 to over 415 ppm owing to the large-scale utilization of fossil fuels and various chemical refinery processes (Hu et al., 2016; Lackner, 2003; Yu et al., 2008). Thus, worldwide efforts have been devoted to developing new technologies for reducing CO_2 emissions and most of the United Nations members have approved Paris Climate Agreements for greenhouse gas reduction (He et al., 2016; Jacobson, 2009; Obergassel et al., 2016; Wang et al., 2011). The 21st conference on global warming (COP21) reached a landmark agreement (the Paris Agreement) to limit the increase of the global average temperature to 2.0 °C in 2100 (Rhodes, 2016). CO_2 emissions from energy- and industry-related sources must decrease dramatically after 2030 and reach net-zero levels between 2050 and 2060 (Rogelj et al., 2016) to enable this target to be reached.

Carbon capture removing CO_2 before releasing it into the atmosphere plays an important role in a zero and/or negative CO_2 emission. It has three categories: pre-combustion, post-combustion, and oxyfuel combustion. For oxyfuel combustion, pure oxygen is used in combustion to produce flue gas with high purity of CO_2. In the pre-combustion CO_2 capture process, fuels are partially oxidized by steam or oxygen to produce synthetic gas, followed by water gas shift reaction to form hydrogen-enriched gas. The third category of CO_2 capture is post-combustion, which refers to capturing CO_2 after the combustion of hydrocarbon fuels. Among these CO_2 capture technologies, post-combustion with amine solvents is the state-of-the-art mature technology (Rochelle, 2009). In addition, directly capturing CO_2 from the air could meet global climate goals. However, a new study reported that the process needs as much as a quarter of global energy supplies in 2100 (Realmonte et al., 2019).

The direct use of carbonaceous fuels such as fossil fuels and biomass is unavoidable in the future. Therefore, a large amount of CO_2 is still expected to be emitted into the atmosphere. Therefore, post-combustion CO_2 capture, oxyfuel combustion and direct air capture (DAC) represent key technologies to reduce CO_2 emissions and mitigate climate change. Review papers are available regarding the development of carbon capture technologies (Al-Hamed and Dincer, 2021; Buckingham et al., 2022; Mikulčić et al., 2019). However, a more comprehensive review of carbon capture will be beneficial to the research community. Therefore, this paper provides a thorough description and analysis of carbon capture technologies, including solid and liquid-based sorbents for capturing CO_2 from different sources (e.g. flue gas, biogas, syngas and air). Various liquid solvents, including amines, ion liquid and ammonia, were studied. In addition, solid adsorbents were analysed based on their working temperatures, such as low-temperature adsorbents (carbon, biochar, zeolite, amine-loaded solid, covalent organic frameworks (COFs) and aerogels), medium-temperature adsorbents (MgO and K_2CO_3) and high-temperature adsorbents (CaO). In Section 4 of this review paper, membrane-based CO_2 separation is critically analysed, followed by the investigation of oxyfuel combustion, chemical looping, cryogenic CO_2 capture, and bioenergy-related CO_2 capture. Process modelling using Aspen, CFD and machine learning for CO_2 capture is also included and critically analysed in this review paper. Furthermore, techno-economic analysis and evaluation of typical large-scale CO_2 capture plants were carried out.

2. CO_2 capture from various CO_2 sources

2.1. Flue gas as the CO_2 source

2.1.1. Current status of flue gas

Currently, as the world's second-largest energy source, coal contributes to more than 40 % of the total global emissions (Rahman et al., 2017; Younas et al., 2020). Around 60 % and 39 % of the total carbon emissions from the electricity industry were derived from coal-fired and natural gas-fired power plants, respectively (Administration, 2020). Therefore, carbon capture from flue gas as the CO_2 source is the key to achieving net-zero global CO_2 emissions. In addition, capturing and utilising CO_2 in flue gas will reduce the pressure of greenhouse gas emissions and generate substantial economic benefits (Khalifa et al., 2022; Maina et al., 2021).

Carbon capture from flue gas refers to the process of separating and collecting CO_2 from industrial production and energy use, such as power plants, cement manufacturing and stainless-steel factory, etc. (Cheng et al., 2022; Wang and Song, 2020a). CO_2 emissions from fossil fuel-fired flue gas in the power industry are characterised by large flue gas volume, low CO_2 partial pressure (0.03-0.2 bar), high total emissions and relatively low CO_2 concentration (3–20 %) (Buvik et al., 2021; Figueroa et al., 2008). Usually, the flue gas from other manufacturing industries contains a higher CO_2 concentration than that from the power plant. As for the components of flue gas from power plants, except for N_2 in air, CO_2, O_2 and H_2S are approximately 20 %, 5 % and < 1 %, respectively, produced by complete fuel combustion, together with large amounts of water vapour generation (Cheah et al., 2015; Maina et al., 2021; Wang and Song, 2020a). The properties of a few typical flue gases from different sources are summarised in Table 2.1.

2.1.2. Challenges to CO_2 capture from flue gas

Until now, the use of fossil fuels is still increasing for electricity generation in future (Zou et al., 2017). Thereby, as an "end-of-pipe" process, post-combustion carbon capture is the most widely used and mature carbon capture technology due to its good viability and feasibility for existing power plants, without the requirement for large-scale renovation and upgrading (Cheng et al., 2022; Han et al., 2020; Zhao et al., 2018). The main post-combustion CO_2 capture technologies include absorption separation (physical and chemical absorption) (Fang et al., 2020; Wang et al., 2015), adsorption separation (physical and chemical adsorption) (Wilcox et al., 2014; Zhao et al., 2018) and membrane separation (Feron et al., 2020; Han et al., 2020). According to the statistics, there are more than 60 % of post-combustion technologies employing absorption-based methods. Among those, the chemical absorption method, represented by the MEA absorption, is considered the most promising for industrial applications because of its applicability to large air volumes and simplicity of operation, which mainly consists of two important processes, including chemical absorption of CO_2 in the absorption tower and thermal regeneration of the absorber in the desorption tower (Akeeb et al., 2022).

However, carbon capture from flue gas sources is still confronted with major challenges, restraining its further development and commercialisation (D'Alessandro et al., 2010; Notz et al., 2011). First, after fossil fuel combustion, there is a high volumetric flow rate together with a large amount of CO_2 in flue gas derived from most conventional thermal power plants, which is in the temperature range of 50-150 °C because of a series of gas cleaning procedures after fuel combustion. Then, the discharge flue gas is mainly in atmospheric pressure, but the partial pressure of CO_2 is at a relatively low level due to insufficient volumetric concentration of CO_2 in flue gas, as discussed above. Last, the surplus O_2 used during the combustion process results in the presence of SO_x and NO_x, and the humidity due to the existing steam poses additional difficulties for the currently preferred CO_2 capture process, such as amine-based absorption technology.

Solid amine-based adsorbents are promising candidates for carbon capture from flue gas, especially at low CO_2 partial pressure (10–15 %) (Wang and Song, 2020a). However, the low oxidative stability of amines could significantly influence the performance of flue gas carbon capture using amine-based adsorbents, because the presence of O_2 (3-4 %) can result in the rapid oxidative degradation of amines (Sreedhar et al., 2017). Min et al. investigated amine-based solids for CO_2 capture by enhancing the oxidation resistance of polyethyleneimine (PEI)/silica adsorbent, as shown in Fig. 2.1, with two strategies adopted. First, 1, 2-epoxybutane was used to functionalise PEI to produce tethered 2-hydroxybutyl groups. Besides, metals that could assist amine oxidation were poisoned through using chelator. After improvement, only a surprisingly low decay of CO_2 capture capacity (8.5 %) was observed under aging by flue gas with oxygen at 110 °C after 30 d, 50 times higher stability compared with conventional PEI/silica (Min et al., 2018). This work may provide the further commercialisation prospect of these adsorbents when used for carbon capture from flue gas containing oxygen, which may cause the oxidation of adsorbents (Bali et al., 2013; Heydari-Gorji and Sayari, 2012).

It is known that traditional amine-containing adsorbents are vulnerable to acidic conditions in flue gas caused by SO_x and NO_x, which could lead to irreversible poisoning effects and, eventually, fast deactivation of sorbents. Thus, the basic sites in amine-based adsorbents can be significantly influenced by acidic compounds (Maina et al., 2021; Zhao et al., 2018). Hence, designing and developing SO_x- and NO_x-resistant amine-

Table 2.1
Typical CO_2 concentration and impurities of flue gas from various sources.

Flue gas source	CO_2 conc. (vol%)	Pressure (atm)	CO_2 partial pressure (atm)	Impurities	Ref.
Aluminum production	1-2	1	0.01-0.02	SO_x and NO_x present, fluoride	Husebye et al., 2012
Gas turbine exhaust	3-4	1	0.03-0.04	low SO_x and NO_x levels, O_2: 12 %-15 %	Samanta et al., 2011
Fired boiler of oil refinery and petrochemical plant	~8	1	0.08	SO_x and NO_x present	Wang and Song, 2020a
Natural gas fired boilers	7-10	1	0.07-0.10	SO_x and NO_x present	Wang and Song, 2020a
Oil-fired boilers	11-13	1	0.11-0.13	high SO_x and NO_x levels, O_2: 2 %-5 %	Wang and Song, 2020a
Coal-fired boilers	12-14	1	0.12-0.14	high SO_x and NO_x levels, O_2: 2 %-5 %	Samanta et al., 2011
IGCC syngas turbine	12-14	1	0.12-0.14	low SO_x and NO_x levels	Wang and Song, 2020a; Song et al., 2019b
Hydrogen production	15-20	22-27	3-5	high NO_x levels	Husebye et al., 2012
Steel production (Blast furnace)	20-27	1-3	0.2-0.6	SO_x and NO_x present	Husebye et al., 2012
Cement process	14-33	1	0.14-0.33	SO_2 and NO_x, trace elements, particulates	Husebye et al., 2012

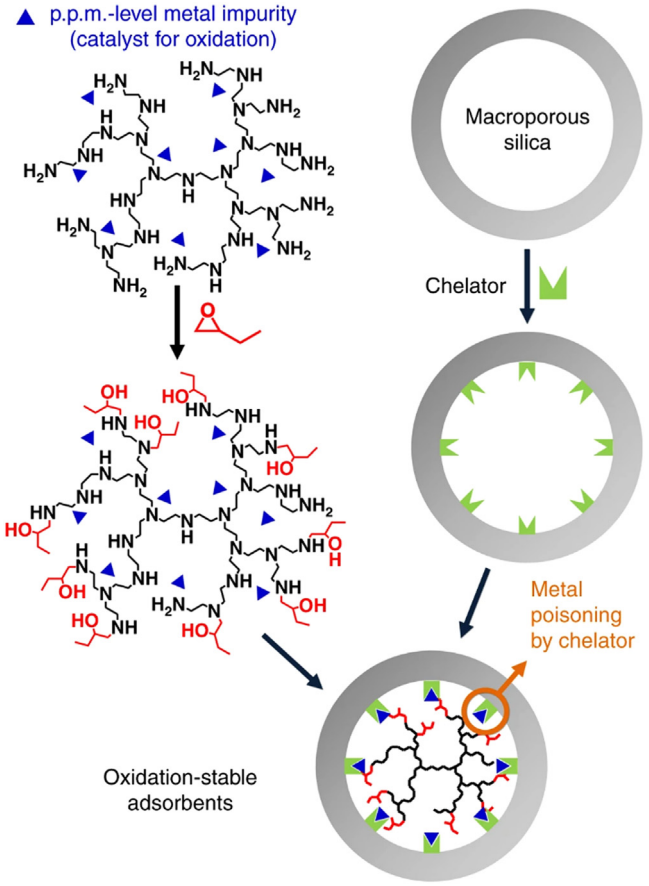

Fig. 2.1. Synthesis of oxidation-stable PEI functionalised CO_2 adsorbent (Min et al., 2018). (For interpretation of the references to color in this figure legend, the reader is referred to the web version of this article.)

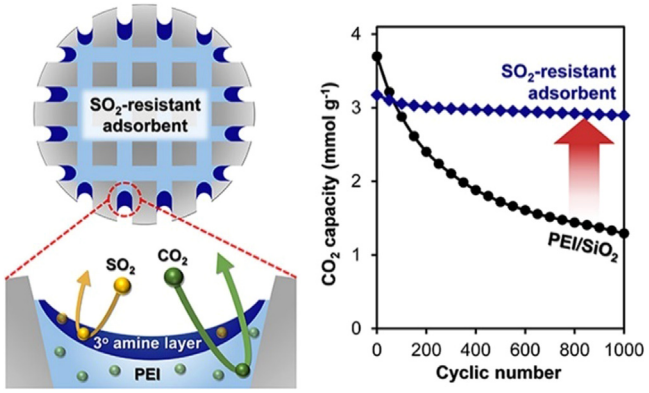

Fig. 2.2. Synthesis of SO_2-resistant CO_2 adsorbent. Tertiary-amine-rich layer plays a role of protection for CO_2 capture by beneath PEI layer (Kim et al., 2019). (For interpretation of the references to color in this figure legend, the reader is referred to the web version of this article.)

based adsorbents are of great importance for carbon capture from flue gas in terms of solid adsorption technologies. Kim and co-workers (Kim et al., 2019) employed a facile fabrication route to impregnate porous silica with PEI to form a surface layer composed of tertiary amines, which exhibited improved SO_2 resistance during flue gas CO_2 capture. As shown in Fig. 2.2, the tertiary amine layer can capture SO_2 to enhance CO_2 adsorption by the beneath layer. The results showed that, compared with conventional PEI/silica for 65.1 % carbon uptake ability, this novel sorbent achieved a significant reduction of capacity loss (only 8.52 %) after 1000 cycles for simulated flue gas carbon capture with 50 ppm SO_2 (Kim et al., 2019). In addition to the improvement of adsorbents for carbon capture from flue gas with existing impurities of SO_x and NO_x as CO_2 resources, another method is to establish desulfurisation and denitrification units for enhancing sorbents regenerability during real-world power plant applications.

In most cases of practical power plants, the flue gas after post-combustion could be in humid conditions between 40 °C to 80 °C. The presence of moisture in wet flue gas may be detrimental to carbon capture, because the resulting steam not only results in competitive adsorption to CO_2, but could decompose the adsorbents due to their low hydrothermal stability (Ray et al., 2021). However, modifying the existing power plant for pretreatment of water removal in flue gas may significantly aggregate the economic burden of the overall process. Therefore, novel sorbent materials should be designed and fabricated with high hydrothermal stability and high CO_2 uptake selectivity.

Soubeyrand-Lenoir et al. (2012) studied three different MOFs (HKUST-1, UiO-66 (Zr) and MIL-100 (Fe)) for CO_2 uptake with varying relative humidity (RH). As shown in Fig. 2.3a, 5 times higher carbon capture ability (105 mg/g) was achieved by MIL-100 (Fe) with escalating RH from 3 % to 40 %, compared with the other two MOFs. As depicted in Fig. 2.3b, the filled water on MIL-100 (Fe) formed microporous pockets to enhance CO_2 capture (A, B and C). However, the water in microporous MOFs could antagonise the carbon uptake by blocking CO_2 molecules (D and E) (Soubeyrand-Lenoir et al., 2012). In addition to the route of water-enhanced CO_2 uptake from flue gas reported in the above research, there are other key strategies for improving the carbon capture from wet flue gas, including hydrophobic modifications, the introduction of functional groups and amine modifications.

Therefore, it is essential to optimise the post-combustion CO_2 capture processes to deal with flue gas impurities, for example, O_2, moisture, SO_x and NO_x, in terms of cost reduction, sorbents performance and regeneration, together with power plant units of drying, desulfurisation and denitrification. First, it is recommended to develop advanced materials with favourable stability, high capture capacity and low cost for promotion of the CO_2 capture from flue gas. Second, system and process optimisation is also crucial to make the new approach from bench-scale experiments to practical application. Besides, most of the research work in current literature used simulated gas or pure CO_2 as the carbon sources. In the future, the real-world flue gas with impurities should be applied for carbon capture investigations, in order to obtain more viable and feasible processes for carbon capture from flue gas to facilitate CO_2 reduction, collection and utilisation.

2.2. Syngas as the CO_2 source

2.2.1. Characteristics of syngas

Syngas is comprised of methane (CH_4), hydrogen (H_2), carbon monoxide (CO), water vapours (H_2O), carbon dioxide (CO_2), condensable compounds, and hydrocarbons (HCs). It is the major product of the gasification of carbonaceous materials, like natural gas, heavy oil and coal. Syngas is a favourable alternative fuel because it burns cleanly and has low greenhouse gas emissions. Its composition largely depends on the choice of feedstock and the production process. The main source of carbon dioxide emissions is coal. Syngas obtained from coal is non-renewable; however, producing syngas from coal gasification by Integrated Gasification Combined Cycle (IGCC) power plants will help reduce CO_2 emissions compared to burning coal directly (Casleton et al., 2008).

As described in the previous section, there are three key approaches for capturing CO_2 from fossil fuel-based power plants: post-combustion, oxy-fuel combustion and pre-combustion. In an IGCC power plant with pre-combustion carbon capture, syngas generated from the gasification of coal are processed in a water-gas shift (WGS) unit where after desulfurisation most of CO is converted to CO_2 and steam. This allows for

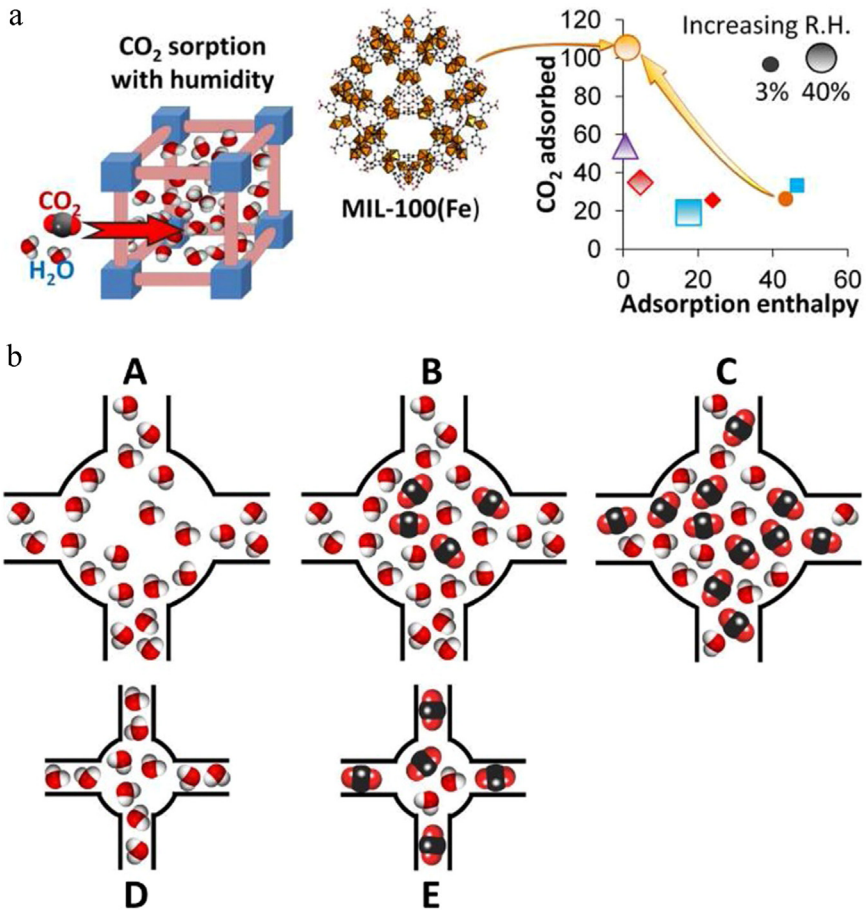

Fig. 2.3. Three MOF samples studied under various R.H. levels (a); Schematic representation of possible mechanisms of CO_2 adsorption in the presence of humidity (b) (Soubeyrand-Lenoir et al., 2012). (For interpretation of the references to color in this figure legend, the reader is referred to the web version of this article.)

Table 2.2
Advantages of syngas over flue gas in terms of CO_2 capture (Wang and Song, 2020b).

Factors	Pre-combustion (Syngas)	Post-combustion (Flue gas)
CO_2 Partial pressure	High	Low
CO_2 concentration	High (~40 %)	Low (~3-15 %)
Plant modifications	Minimal; requires the addition of only absorber and regenerator	Needs larger and more expensive equipment due to less CO_2 concentration in the exhaust stream

the separation of CO_2 before the combustion of the fuel (H_2) (Subraveti et al., 2019b). The CO_2 in the syngas can be separated by various methods like adsorption, absorption, membranes etc. According to Table 2.2, CO_2 concentration in the syngas is much higher compared to flue gas, pre-combustion CO_2 capture is a potentially cheaper method than post-combustion CO_2 capture. This is because, for an equal quantity of CO_2 captured, a relatively smaller volume of gas needs to be processed, resulting in lower capital costs due to smaller equipment size. Therefore, syngas is a better and more economical source for CO_2 capture as compared to flue gas in IGCC power plants (Trapp et al., 2015). However, further research needs to be carried out in order to integrate pre-combustion CO_2 capture technologies into IGCC power plants successfully.

2.2.2. *Challenges of CO_2 capture from syngas*

Since gasification is required to produce syngas in the pre-combustion process, various factors in the gasification process can pose challenges to CO_2 capture from syngas. The gasification can be classified into oxygen-blown and air-blown processes. The oxygen-blown gasifier contains no nitrogen, having an evidently different composition from the air-blown gasifier syngas, which have a large nitrogen content (Cao et al., 2021). Therefore, both processes can have different configurations for the CO_2 capture process. The type of fuel (coal, oil, natural gas or biomass) can also affect the composition of syngas, which in turn affects the CO_2 capture system. Coal is an abundant fossil fuel used for electricity production. Besides, it's up-gradation and developments in better efficiency at present power plants, researchers are concentrating on the growth of innovative technologies, for example, supercritical and ultra-supercritical coal fired power plants and IGCCs. Amongst these technologies, IGCCs exhibit the most promising efficiency and environmental performance, along with the facility to incorporate various kinds of feedstock (James et al., 2019). These power plants are also good for low carbon applications, as syngas has a higher concentration of CO_2 which favours the separation process. At present, absorption is considered to be the most reliable method for CO_2 separation from syngas. The absorption process can utilise chemical solvents like aqueous solutions of amines or hot potassium carbonate and physical solvents (Rectisol, Selexol, Purisol) (Notz et al., 2011). As IGCC power plants yield high partial pressure of CO_2 in the syngas with higher plant operating pressure, physical solvents are deemed more appropriate than chemical ones for CO_2 absorption (Jansen et al., 2015). Therefore, vast research has been performed on pre-combustion CO_2 capture processes using various physical solvents (Park et al., 2015; Siefert et al., 2016; Smith et al., 2022). The cost of carbon capture IGCC facility depends on thermal recovery and pumping, heating and cooling of the liquid and gas stream. Compared to other commercial physical solvent processes, the Selexol process has lower strength, which would result in reduced lower heating value, thereby increasing the overall plant efficiency (Cormos, 2011; Dave et al., 2016). Alternative methods for CO_2 capture are gaining research attention, such as the utilisation of H_2 or CO_2-selective

membranes. The type of membrane selection also depends on the gasification process, which subsequently affects the cost of the pre-combustion capture process (Scholes et al., 2012). Furthermore, the syngas flow rate, hydrogen production, output power, hydrocarbon flow rate, and apparent thermal efficiency also affect the CO_2 capture system. Therefore, all these factors must be considered while selecting appropriate CO_2 capture systems.

From the above discussion, it can be concluded that pre-combustion carbon capture is considered to be the most effective method as compared to other carbon capture methods. This is because of high CO_2 partial pressure. Separating carbon dioxide from syngas is considerably easier than in the post-combustion carbon capture system. Moreover, pre-combustion holds better environmental, economic and social impact as compared to other carbon capture technologies (Olabi et al., 2022). Recently, two commercial pre-combustion carbon capture facilities have been working in the United States, where around 90 % of CO_2 is captured by using physical solvent absorption processes (Olabi et al., 2022). Two more power plants are operating in Spain and Netherlands, but only a part of syngas is being treated for carbon capture (Rubin et al., 2012). Therefore, there is a need to study the commercialisation prospects of the pre-combustion carbon capture process extensively.

2.3. Biogas as the CO_2 source

2.3.1. Biogas production and the upgrade necessity

Anaerobic digestion is a process that involves organic matter digestion to form biogas through hydrolysis, acidogenesis, acetogenesis, and methanogenesis (Fu et al., 2021). The produced biogas is considered to be one of the most important renewable energy sources, whose technology has been used worldwide for organic waste treatment and bioenergy production. In fact, the world is impacted by limited energy alternatives and significant environmental problems, which have stimulated the search for new bioenergy and environmental solutions. That is why the biogas industry has faced accelerated development and increase in the last decades. The annual biogas production in Europe and China is expected to reach 300 billion m^3 by 2020 (Fu et al., 2021), representing around 1.43 exajoules (Sönnichsen, 2022).

Traditionally, most of the raw biogas is used to produce electricity and heat directly (Khan et al., 2021). In general, biogas is a mixture of gases consisting of 50–75 % methane (CH_4), 25–50 % carbon dioxide (CO_2), 0–10 % nitrogen (N_2), 0–3 % hydrogen sulfide (H_2S), 0–1 % hydrogen (H_2) and a minimal concentration of other gases (Aghel et al., 2022). With this composition, it does not meet natural gas specifications, so the content of CH_4 in biogas should be upgraded, and, in this case, it can be called biomethane or natural gas, enlarging its commercial value and range of applications, such as vehicle fuel (Yanuka-Golub et al., 2019). Natural gas contains 98–75 % of CH_4, promoting higher burning energy, with higher burning velocity and flammability. Also, when used as vehicle fuel, CO_2 gas occupies more space in the cylinder tanks, which leads to the necessity of additional energy during biogas compression, thus, increasing costs. So, CO_2 content must be reduced through biogas upgrade solutions for the elimination of impurities using different techniques (Aghel et al., 2022a).

2.3.2. Developed technologies for CO_2 capture from biogas

The main applied technologies worldwide for biogas upgrade are: absorption (water scrubbing, chemical absorption, physical absorption), swing adsorption (temperature, electrical, pressure), and membrane-based gas permeation are employed worldwide for biogas up-gradation (Shah et al., 2021) (Fig. 2.4). High-pressure water scrubbing is the most simple and reliable biogas absorption technology. This technology promotes large-volume biogas processing. However, it presents higher electricity consumption (0.30–33.0 kWh/Nm^3) (Aghel et al., 2022a). So, the development and optimisation of biogas upgrade must pass through less energy consumption and the generation of methane-rich gas high-energy biogas. In situ technologies for methane enrichment have been explored, which include cryogenic separation, and hybrid membrane-cryogenic technologies to limit energy costs and improve CO_2 capture efficiency (Shah et al., 2021). Apparently, hybrid technologies seem to be more economic, but they must still be tested on a large scale (Scholz et al., 2013). Table 2.3 presents the characteristics, parameters, and advantages of the most employed biogas purification techniques, which will be described as follows (Fu et al., 2021; Shah et al., 2021).

Water purification is the most common and well-developed method for removing CO_2 from biogas, and is based on the principle of physical absorption of gas in water, because of the property of gas solubility. Temperature is a factor that directly influences the process, because the solubility of gases increases with the decrease in temperature. Pressurised biogas is injected through the bottom of the absorption column, and water is channelled inward through the top of a column. The absorption of CO_2 in the water washing process is usually performed at 8–10 bar, although pressures are also used in the range of 10–20 bar. Biogas flows up in the column, and water flows from the top to the bottom of the column. Biomethane with more than 90 % CH_4 is obtained from the top of the purifier, while water containing CO_2 and absorbed H_2S is channelled from the bottom of the column to a flash vessel. Pressure reduction (2.5-3.5 bar) is applied, which results in the release of a gaseous mixture rich in CO_2 (80–90 %) (Kapoor et al., 2019). The main advantages of this technology are simplicity of design, low overall cost, and low loss of methane during the process (less than 2 %). The accumulation of elemental sulphur, corrosion, and unpleasant odour, results of simultaneous absorption of H_2S in water, are problems that occur in this process.

Aqueous organic or inorganic compounds are used to bind the CO_2 or H_2S molecules contained in biogas. The commonly used chemical solvents are amines and aqueous solutions of alkaline salts (sodium hydroxide, potassium, ammonium, and calcium) (Abdeen et al., 2016). The solubility of CO_2 in sodium hydroxide is higher than amines. For example, to absorb 1 ton of CO_2, 1.39 tons of monoethanolamine will be required, and 0.9 tons of sodium hydroxide are needed (Angelidaki et al., 2018). Aqueous alkaline salts are more economical and readily available compared to amines; however, the regeneration of alkaline solutions is expensive due to the high energy requirement. However, if carbonation products from the inorganic absorption process are used in other applications, such as chemical manufacturing, the process may be advantageous. The chemical purification system consists of a packaged bed column integrated into a desorption unit equipped with a reboiler. In chemical purification, biogas is injected into the packaged bed absorber operating at 1–2 bar from the bottom, and the chemical solvent is supplied from the top counter. The CO_2-rich solution obtained from the bottom of the absorber is pumped into a stripping column through a heat exchanger. Solvent regeneration is performed in the stripping column at a pressure of 1.5 bar and heating it to 120–160 °C (Ullah Khan et al., 2017). Foaming, the cost of chemicals, solvent loss due to evapouration and contaminant accumulation, amine degradation, solvent losses, composition problems, corrosion, and operational problems make this system complex compared to other techniques (Kapoor et al., 2019).

Organic solvents, such as methanol mixtures and polyethylene glycol dimethyl ethers, can be used for the physical absorption of CO_2 from biogas. The use of organic solvents has advantages: reduction of recycling rates of absorbents, investment, and operating costs. In addition, another advantage of organic solvent is the low vapour pressure of polyethylene glycol dimethyl ethers, which leads to a low solvent loss during the washing process. During the process, the raw biogas is compressed to 7-8 bar, and the column is cooled to 20 °C before injection into the absorption. The organic solvent is also cooled before being injected from the top. After washing, the organic solvent is regenerated by heating and depressurisation at 80 °C and 1 bar, respectively, in a desorption column. The first step of the process is the compression and cooling of the crude biogas (7-8 bar, 20 °C), followed by its injection into the bottom of the absorption column. The regeneration of the organic solvent is done in the desorption column by heating it to 80 °C while

Table 2.3
Biogas purification technologies and their characteristics (Modified from (Fu et al., 2021; Shah et al., 2021)).

Technology	Operation	Pressure (bar)	Electrical Consumption (kWh/Nm^3)	Methane losses (%)	Methane purity (%)	Investment (€/Nm^3 biogas)	Maintenance per year (€/year)	Advantages	Disadvantages
Water scrubbing	Absorption	6 – 10	0.30 – 33.0	< 1 %	>97 %	**0.13 – 15**	**15,000**	Easy to handle and simple in operation; The large volume of processed gas; Useful in cold regions where CO_2 solubility increases; High methane purity with less methane loss.	High investment High pressure and energy needed A huge amount of water needed High risk of biological contamination
Chemical scrubbing	Absorption	1 – 1.5	< 0.15	< 0.1 %	**>99 %**	**0.28**	59,000	High efficiency; High CH_4 purity up to 99 %; Easy operation; Low CH_4 loss (<0.1 %); Simultaneous removal of CO_2 and H_2S.	High investment in amine solvents; Toxic solvents are needed; Solutions are needed for reasonable disposal.
Solvents scrubbing	Absorption	4-7	< 0.25 – 0.33	2 – 4 %	>96 %	0.25	39,000	Fewer liquid inputs, smaller dimensions of the upgrading unit; High CH_4 purity up to 98 %; Simultaneous removal of CO_2 and H_2S; Simple process and easy operation; Low CH_4 loss.	Use of toxic organic solvents; Difficult regeneration of organic solvents (presence of CO_2); High temperatures are required for H_2S separation.
Membrane separation	Permeation	20-36	< 0.18 – 0.35	< 5 %	90 – 99 %	0.22	25,000	Dry process; High selectivity to impurities; Removes water vapour; Less mechanical deterioration; No usage of chemicals.	High cost of membranes; Multiple steps are required for high purity; Low membrane selectivity; Pretreatment is needed
Cryogenic separation	Compression and condensation	40	< 0.18 – 0.66	< 0.1 %	>99 %	0.40-0.44	-	Methane purity is high No use of chemicals and water Possible reuse of CO_2	High investment and operation costs; High energy is needed; Under development.
Pressure swing adsorption	Adsorption/ desorption	4 -8	0.25	< 3 %	>96 %	0.26	56,000	Dry process No solvent to dispose No water requirement No microbial impurity Adsorbent usable for up to 3 years	Higher CH_4 loss; Prepurification equipment is needed to remove H_2S from biogas; Pre-drying is needed for water remove from biogas; Contamination by impurities in the biogas.
Biological methods	Photosynthetic reaction	Atmospheric	-	-	>99 %	-	-	High methane recovery up to ~97 % Transformation of CO_2 into other products Production of active biomass Low requirements in terms of land and water	High investment cost and energy; Low photosynthetic CO_2 uptake; Natural sources are required; High risk of biological contamination.
	Chemoautotrophic reaction	Atmospheric	-	-	>99 %	-	-	High selectivity, process efficiency, and CH_4 purity Conversion of CO_2 into CH_4; Reduction of CO_2 emission; Moderate temperatures and atmospheric pressure; Can be integrated with the AD process; Environmentally friendly.	A high amount of reductant is needed; This technology is still under development.

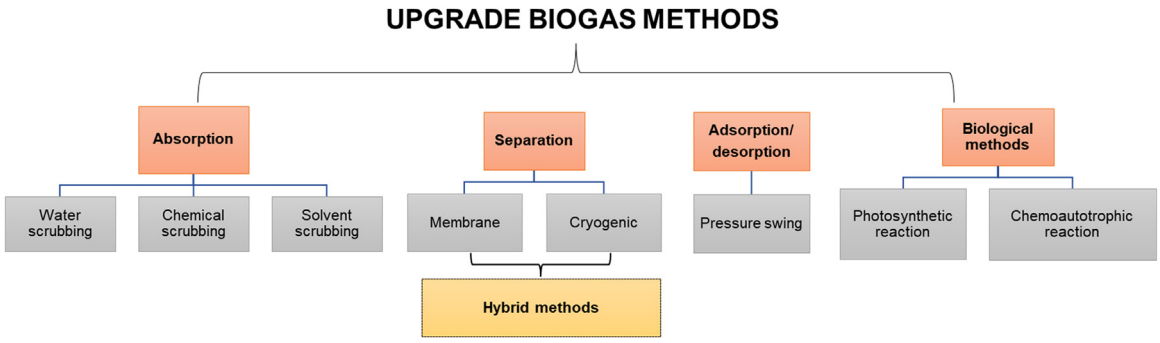

Fig. 2.4. Methods for CO_2 capture from biogas. (For interpretation of the references to color in this figure legend, the reader is referred to the web version of this article.)

the pressure is decreased to 1 bar. The final methane content in the biogas updated using this technology can reach 96–98.5 % and less than 2 % of CH_4 losses, which can be achieved in an optimised plant on a full scale.

Adsorption involves the selective adhesion or bonding of one or more components to the surface of a microporous solid. The adsorption is classified according to the adsorbent regeneration method. The procedure can occur: a) in a cyclic operation by closing the inlet valve or by using a vacuum (vacuum swing adsorption -VSA), by reducing the pressure to atmospheric level (pressure swing adsorption - PSA), or by varying temperature (30–120 °C) that is carried out at the same pressure level (temperature swing adsorption - TSA) (Nie et al., 2013). Pressure swing adsorption - PSA presents interesting advantages to remove CO_2 from biogas because it employs compact equipment, has low energy requirements, and requires low investment. It is safe, simple, and stable compared to other methods. Another point is that it is suitable for small-scale plants (Aghel et al., 2020). It uses structural adsorbents in the form of granules, pellets, and laminates to separate CO_2 from biogas, which is based on size-selective adsorption strategies (Kadam and Panwar, 2017). Porous carbon is widely used in gas phase separation, and it can be produced by the thermal decomposition of natural and synthetic polymers. However, natural polymers are advantageous due to their high availability and lower costs. Activated carbon is commonly used as an adsorbent due to its high surface area, developed microporosity, thermal stability, ease of reduction, and low production costs (Aghel et al., 2022a).

Vacuum pressure oscillation adsorption (VPSA) technology for CO_2 removal from biogas has low capital investment and low energy consumption and greater applicability in areas with water deficiency (Shen et al., 2018). In adsorption, atoms, molecules or ions adhere to the surface of materials creating an adsorbent layer on the adsorbent surface. Gas adsorption can be based on temperature and pressure, as high pressures and low temperatures promote adsorption efficiency (Zhou et al., 2017). VPSA methods drew more attention to the removal of CO_2 from biogas due to its low capital investment and low energy consumption, which can be applied in areas with water deficiency (Shen et al., 2018).

Cryogenic processes are based on temperature differences for the liquefaction of biogas compounds (Ma et al., 2018). The separation depends on different sublimation points where CH_4 (−161.5 °C) has a lower sublimation point than CO_2 (−78.5 °C). Another strategy is the gradual temperature reduction, which allows the selective separation of CH_4 from other components (Aghel et al., 2022a). In this case, biogas is cooled and compressed until CO_2 is liquefied. With the lower sublimation point of CH_4, the two gases can be separated through distillation (Budzianowski et al., 2017). In cryogenic separation, the difference in the boiling point of the various gas components is explored to separate the components, and obtain high content of CH_4 and CO_2 recovery, generating biomethane of high purity and with minimal methane losses (<1 %). In addition, liquid CO_2 can be generated (usually up to 98 % purity), and this high-purity liquid CO_2 can be produced at a high-pressure level, which makes it interesting, especially about storage, saving dense compression of energy to store CO_2 as gas (Hashemi et al., 2019). However, some obstacles are encountered by separating CO_2 under the required very low-temperature conditions, hindering its development and applicability: the dense consumption of energy via refrigeration cycles used for separation and the formation of dry ice due to cryogenic separation of CO_2, which generates serious operating problems such as clogging of pipes or other equipment (Yousef et al., 2018b). Although the separation by this method is interesting because it results in very high-purity gas, this method has high electricity consumption and requires a cryogenic production technology of up to −125 °C temperature at pressures of 20–50 bar (Mehrpooya et al., 2020). In a study on cryogenic technologies for biogas update and CO_2 separation, three main systems were identified. In the first system, the biogas is first cooled, and the water is removed, then it is cooled, compressed, and gets CO_2 liquid. In the distillation system, a distillation column is used to remove and liquefy CO_2. In the desublimation process, CO_2 is removed during its phase change from steam to solid inside a heat exchanger (Tan et al., 2017).

Biological biogas update involves the application of microorganisms for the conversion of CO_2 and H_2 into methane. The two metabolic pathways involved in the updating of biological biogas are that with hydrogenotrophic methanogens involved in the direct conversion of CO_2 into CH_4, and another with homoacetogenic bacteria that first convert CO_2 into acetate, and then for conversion into methane by acetoclastic methane (Kapoor et al., 2019).

In biological upgrading methods, microorganisms are employed as catalysts to convert CO_2 and H_2 into CH_4. Different advantages of biological processes can be pointed out over chemical processes, such as the use of moderate temperatures and atmospheric pressure, compared to chemical processes. In addition, higher resistance to gas contaminations, including H_2S, organic acids, and NH_4 is observed (Aghel et al., 2022a). The most important advantage of biological processes is that CO_2 is captured and recycled to be used in the production of new bioproducts. Biological upgrading methods can involve methanogens binding CO_2 into CH_4, dicarboxylic-acid-producing bacteria binding CO_2 into dicarboxylic acids such as biosuccinic acid, or algae binding CO_2 into algal biomass (Fu et al., 2021).

In the last years, microalgae, bacteria, or archaea have been used in upgrading biogas processes (Zhu et al., 2020). According to processes' configurations, these technologies are classified into *in situ* biogas upgrading, *ex situ* biogas upgrading, and hybrid biogas upgrading. In situ configuration, H_2 is injected directly into the biogas reactor to capture the endogenously produced CO_2. In the *ex-situ* strategy, H_2 and biogas are injected into a separate reactor. Hybrid upgrading is a combination of in situ and *ex situ* strategies, where the initial *in situ* process occurs in a favourable pH for biological processes, while the last upgrading step is

carried out in an ex-situ process. An advantage of *in situ* biogas upgrading is the integration of biomethanation and biogas upgrading in the same bioreactor in an economically and feasible way (Fu et al., 2021).

2.4. Direct air capture (DAC)

2.4.1. Technological family of DAC

Large-scale direct air capture (DAC) has been considered since the late 1990s as an additional way to mitigate the growing atmospheric CO_2 concentrations. Lackner et al. (1999), Zeman and Lackner (2004) presented an optimistic look regarding DAC. Although ambient CO_2 concentrations are very low, DAC may not totally be unfeasible and detailed a carbon-capture approach utilising Ca $(OH)_2$. A number of DAC approaches have been proposed using adsorption and absorption technologies, although the topic is still developing (Goeppert et al., 2012; Jones, 2011). DAC is a technique for permanently capturing and storing CO_2 in geological storage sites by separating it from ambient air using chemical, physical, or mechanical methods. Since the CO_2 in the atmosphere is quite diluted (~415 ppm), substantial energy is required while utilising specialised materials. Therefore, the process design and ensuing techno-economic and environmental performances will have a significant impact on their future deployment and participation in climate change mitigation (Qiu et al., 2022).

Pressure swing adsorption (PSA) is utilised in many industrial processes to separate specified gas species from a mixture of gases (usually air). An adsorbent bed (e.g., activated carbon, zeolites, etc.) is used to trap target gas species while the mixture is pressurised. When the pressure is released, the trapped gas species are released. Membranes, such as zeolites, have the potential to become useful for DAC (Gao et al., 2022a; Hong, 2022). Another promising technology is utilising nitrogen-enriched biochar as a CO_2 adsorbent (Sanz-Pérez et al., 2016).

Another technology for carbon capture is temperature swing adsorption (TSA), which alternates the temperature of the sorbent to adsorb and desorb CO_2. TSA is attractive because it is generally less costly than PSA (Zhao et al., 2017c). Veselovskaya et al. (2013) presented an extensive study of utilising K_2CO_2 in g-AL_2O_3 as a composite inorganic sorbent for a TSA cycle for direct air capture.

Removing CO_2 from the atmosphere using alkaline solutions has been investigated since the 1940s (A and Dodge, 1946; Tepe and Dodge, 1943). In various wet-scrubbing techniques, CO_2 is absorbed into a NaOH solution, which leaves behind an aqueous solution of NaOH and Na_2CO_3. Packed scrubbing towers (Baciocchi et al., 2006; Zeman, 2007) and large convective towers (Lackner et al., 1999) are the most frequently used designs for putting NaOH in contact with CO_2. Other investigators (Stolaroff et al., 2008) have generated a fine spray of the absorbing solution to the air through an open tower. It has since been proposed that DAC using CO_2 absorption exclusively by an aqueous solution of NaOH is unfeasible economically (Socolow et al., 2011).

Another alternative to chemisorption- and physisorption-based approaches is to take advantage of the temperature advantage that naturally cold climates, such as the arctic and Antarctica, can provide to desublimate CO_2 directly from the air. Since the outside air temperature is very cold, the idea is not as much energy is needed to cool the air to desublimate CO_2. DAC via cryogenic heat exchangers is still very nascent. Serious consideration to such devices started in the early 2010s with lab-scale benchtop demonstrations (Agee et al., 2013; Agee and Orton, 2016). Follow-on work by several other studies quantified the theoretical energy associated with DAC cryogenic carbon capture plants placed in arctic climates (Boetcher et al., 2020; Perskin et al., 2022; von Hippel, 2018).

2.4.2. DAC performance from real world

2.4.2.1. Performance map of DAC: adsorption as a case study. The chronological results of the amount and proportion of publications on direct air capture (DAC) since 2004 are presented in Fig. 2.5. The keywords of (TS= (direct air capture or DAC) AND TS= (CO_2 or carbon dioxide)) NOT (DT== ("PATENT")) is applied for the literature research. Until July 2022, a total of 1673 articles were collected, with a significant increase in the past four years. Furthermore, the keywords of (TS= (direct air capture or DAC) AND TS= (CO_2 or carbon dioxide) AND TS= (sorbent or *sorbent)) NOT (DT== ("PATENT")) were applied to final obtain 306 articles among these published articles on DAC sorbents, accounting for 18.2 % of the total number of articles. Such results are applied to establish a data pool of DAC performance to explore specific development trends.

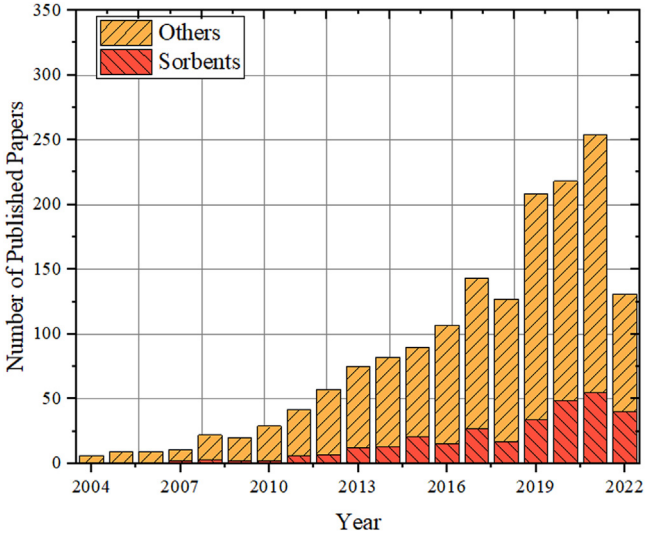

Fig. 2.5. The database pool of DAC performance from 2004 to 2022 (Data collected in July 2022 based on search results of papers from Web of Science). (For interpretation of the references to color in this figure legend, the reader is referred to the web version of this article.)

However, after a detailed screening of summarised data, it could be found that the real-world performance of DAC has not yet demonstrable a clear development trend among various technologies. Due to the relatively active status of research and demonstration, adsorption DAC is taken as the example of the technological family to demonstrate the real-world performance analysis of DAC (Baus and Nehr, 2022; Belmabkhout et al., 2010; Chaikittisilp et al., 2011; Chan et al., 2013; Custelcean et al., 2021; Elfving and Sainio, 2021; Fujikawa et al., 2021; Hemmatifar et al., 2022; Keith et al., 2018; Keller et al., 2018; Mazzotti et al., 2013; Mukherjee et al., 2019; Ruuskanen et al., 2021; Sadiq et al., 2020; Sinha et al., 2017; Sinha and Realff, 2019; Wang et al., 2014; Wang et al., 2020; Wurzbacher et al., 2016; Xu et al., 2020; Zhu et al., 2021). Two main performance indicators of adsorption capacity and energy consumption are employed in Fig. 2.6 with three physical scales: adsorbent-scale, contactor-scale, and system-scale. Due to a lack of standard methods of test and data-report on DAC with different TRLs (Technology Readiness Levels), it is challenging to conduct a fair performance comparison without a classification on various physical scales.

In addition to direct screening of Fig. 2.6, several points are summarised as follows based on the current data pool:

(1) The adsorbents with large sorption capacities, fast reaction kinetics, strong selectivity, as well as low energy consumption, are so-called 'intrinsic' pursuit of researches not only on adsorbent scale, but also on contactor and system scale.
(2) The adsorption heat of adsorbent is expected to on a reasonable level of 45-92 kJ/mol CO_2 for potential scale-application of DAC. Thus, amine-modified porous materials have become a primary option due to their excellent comprehensive properties.
(3) Moisture cannot be ignored in the DAC performance analysis, especially some active candidates of adsorbent, such as amine-modified porous materials. Though the presence of water could

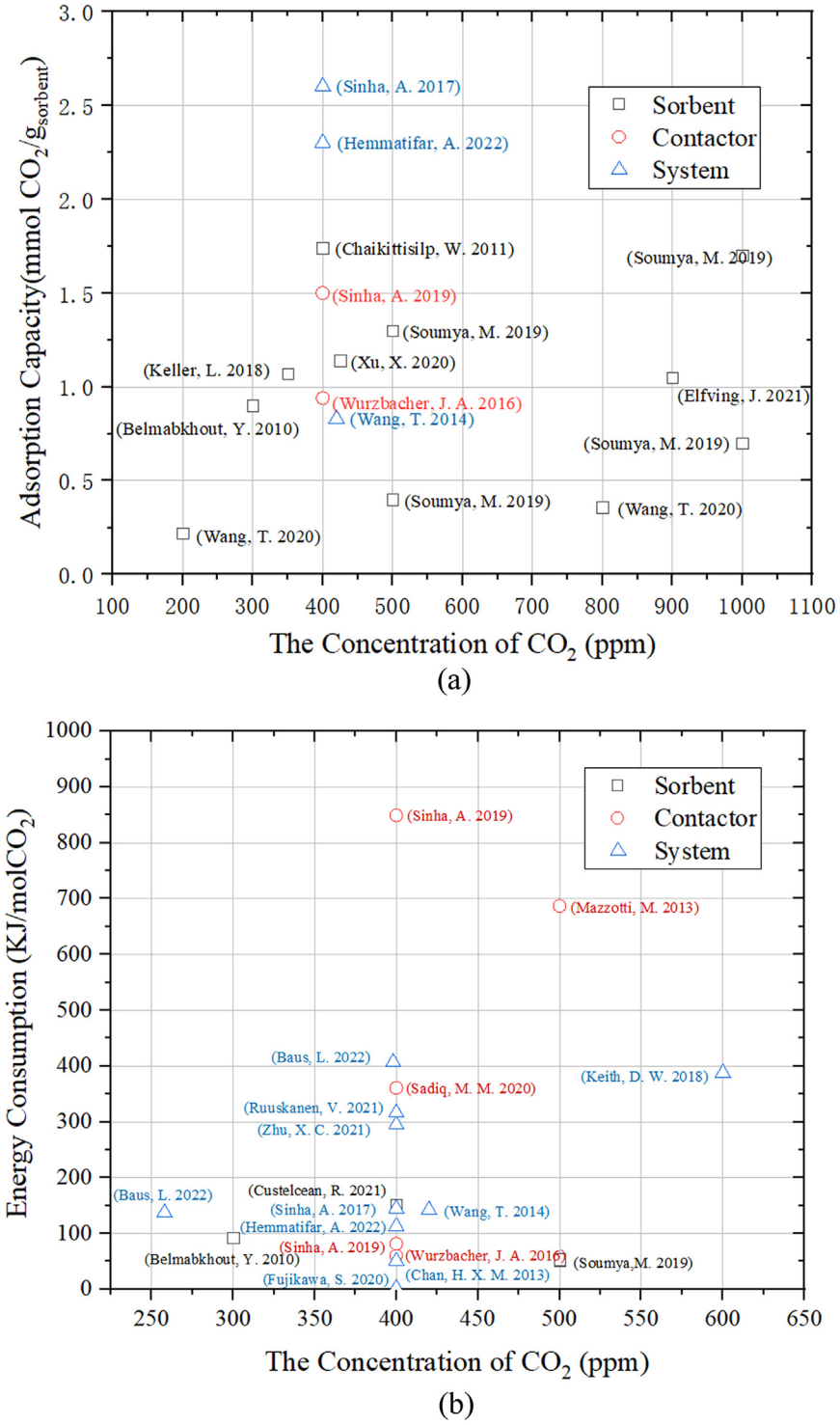

Fig. 2.6. Performance map of adsorption DAC (a) Adsorption Capacity (b) Energy Consumption. (For interpretation of the references to color in this figure legend, the reader is referred to the web version of this article.)

increase the capture performance on some specific moisture level, the adsorption of water would increase the heat of adsorption during the desorption process (Jung and Lee, 2020). Drechsler proposed that a well-designed desorption step of DAC could significantly reduce the co-desorption effect of moisture, and the heat of water vapour can be recovered to further compensate for the desorption heat loss (Drechsler and Agar, 2020).

(4) Currently, the condition window for DAC research is commonly in a range of 400–420 ppm and 20–25 °C. Considering scenarios of carbon sources are still emerging for potential exploration in industrial, building, etc. sectors, some relatively concentrated range, e.g. 5 % vol, of distributed carbon source, could lead DAC application to a wonderland, with improved capture performance and lower energy-consumption (Zhao et al., 2019b), though it may increase the complexity of the capture system to a certain extent.

(5) Integrating DAC technology with other technologies could result in an intensive process with a reasonable energy-consumption and improved energy-efficiency of the entire system (Wang et al., 2014).

2.4.2.2. Re-thinking the methodology of performance evaluation of DAC. The efficient operation with reasonable energy consumption is a key prerequisite to the practical application of DAC. Hence, a clear and complete performance evaluation method, especially on energy-consumption or energy-efficient aspects, is critical to scale-up. Chen et al. (2021) employed the benchmarking analysis method to compare the energy-consumption results of temperature swing adsorption (TSA) carbon capture systems with various psychical boundaries. It was found that the selection of benchmarking boundary has an important influence on the performance evaluation results, as shown in Table 2.4.

In Table 2.4, e_1–e_7 are elements of energy consumption during the heating process, depending on which scale is applied in performance evaluation, which commonly includes the sensible heat of adsorbent, the sensible heat of adsorbed gas, the heat of desorption, the sensible heat of adsorption chamber, the heat dissipation of adsorption chamber, the sensible heat of pipelines and auxiliary equipment, and the heat dissipation of pipelines and auxiliary equipment. The e_8 and e_9 are the energy consumption of the blower and the vacuum pump, respectively. By analysing the elements of the energy consumption of DAC technology in Table 2.4, it can be found that there are a few consensuses on which evaluation framework should be applied for the performance analysis of DAC, as a standard framework. Such a knowledge gap would lead to a direct performance comparison among various studies difficult. A simplified guideline would be helpful: according to the specific research aim, the energy consumption of DAC, taking adsorption-kind technology as an example, could be divided into three physical scales: the adsorbent, the adsorption chamber, and the adsorption system. Such rough classification, at least, could be considered as a small step in the scholar community to re-think whether the current confused methodology of performance evaluation is beneficial to the development of DAC.

2.4.2.3. Discussion on DAC performance in real world. In addition to capturing rate and purity, energy consumption is taken into consideration in the performance evaluation framework with the emerging attention on initial investment and operation management of DAC. Although it is a widely-applied indicator for the performance evaluation of DAC, the specific amount of energy consumption during operation is deeply affected by operating conditions such as the composition of the air source and the temperature of the heat source (e.g. heat regeneration). Hence, it is challenging to compare the performance of various DAC systems directly without specific descriptions of design or operation conditions. In addition, this indicator should clearly reflect the energy-saving potential of various DAC technology, as well as the maturity degree of technology, in a direct way.

The efficiency of the second law of thermodynamics (ESLT), which has been successfully applied in the performance evaluation of heat pump, organic rankie cycle, etc., can also be applied in the performance evaluation of DAC to solve the above-mentioned problems (Landelle et al., 2017). Generally, the ESLT is applied to evaluate the irreversibility of the energy system with a viewpoint of thermodynamics, which could be considered as an indicator to demonstrate the ratio of performance of actual DAC to that of real DAC. In reference Zhao et al. (2017a), it is expressed as follows:

$$\eta_{2nd} = \frac{W_{min}}{W_{ac}} = \frac{W_{min}}{W_{min} + LW}, \tag{2.1}$$

where W_{ac} is the equivalent work input of the actual system; W_{min} is the minimum separation work, that is, the work required for the reversible separation of the ideal mixture under constant temperature and pressure; $LW = T_0 \Delta S$ and indicates the irreversibility of the actual system.

Based on the common calculation method, the ESLT of DAC cases from the pool of existing publications is obtained. Due to the lack of real performance data of DAC, more cases of carbon capture are included. The final-chosen cases include absorption, sorption, membrane separation, cryogenics, and integrated technologies (Berstad et al., 2022; Bounaceur et al., 2006; Cau et al., 2014; Clausse et al., 2011;

Table 2.4
The boundary with various elements of energy-consumption: TSA DAC system as a case study.

Reference	Organisation	Heat consumption (MJ/kg)	Electricity consumption (MJ/kg)	e_1	e_2	e_3	e_4	e_5	e_6	e_7	e_8	e_9
Deutz et al. (Deutz and Bardow, 2021)	RWTH Aachen University; ETH Zurich	11.9	2.52	√	√	√	√	√			√	√
Young et al. (Young et al., 2021)	Heriot-Watt University	9.93	0.8	√	√	√	√	√			√	√
Zhu et al. (Zhu et al., 2021)	Shanghai Jiao Tong University	16.23	1.3	√	√	√	√	√			√	√
Sinha et al. (Sinha et al., 2017, 2020)	Georgia Institute of Technology	0.77	2.5	√		√	√				√	√
Wurzbacher et al. (Wurzbacher et al., 2012)	ETH Zurich; Climeworks Ltd.	11.2	0.28	√	√	√						√

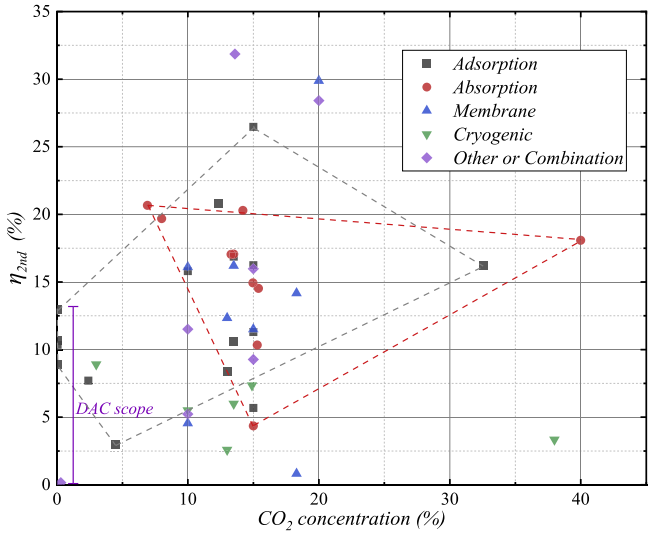

Fig. 2.7. The efficiency of the second law of thermodynamic of different technologies (Zhao et al., 2017a). (For interpretation of the references to color in this figure legend, the reader is referred to the web version of this article.)

Cormos, 2015; Giordano et al., 2017; Grande and Rodrigues, 2008; Hussain and Hägg, 2010; Jiang et al., 2020; Kim and Lee, 2016; Knapik et al., 2018; Krekel et al., 2018; Landelle et al., 2017; Li et al., 2020, 2022; Li et al., 2016; Lin et al., 2021; Lindqvist et al., 2014; Liu et al., 2020; Matthews and Lipiński, 2012; Mletzko et al., 2016; Oexmann et al., 2008; Oreggioni et al., 2015; Pirngruber et al., 2013; Rezaei et al., 2022; Ruan et al., 2014; Sanpasertparnich et al., 2010; Seo et al., 2022; Shen et al., 2012, 2017; Song et al., 2017; Tajima et al., 2004; Tian et al., 2021; Tuinier et al., 2011a, 2011b; Veneman et al., 2015; Versteeg and Rubin, 2011; Wang and Gan, 2014; Wurzbacher et al., 2012; Xie et al., 2014; Zhang et al., 2016; Zhao et al., 2017a), as well as some DAC cases.

As can be seen in Fig. 2.7, the ESLT of adsorption-based carbon capture and DAC ranges from 3–26 %, while the absorption-based technologies range from 4–21 %. The area enclosed by the grey and red dotted lines represents the ELST ranges of the state-of-art of adsorption and absorption technologies, respectively. It is worth noting that the purple area shows ELST of DAC-related technologies is in a range of 0.15–13 %. The fact of ESLT of DAC is relatively lower compared to that of high-concentration CO_2 capture. It is implied that the current knowledge system has weaker support for DAC than that of carbon capture; more efforts should be input into the DAC field to explore its potential for system optimisation.

2.4.3. DAC cost from the real world

2.4.3.1. Cost controversy of DAC. The cost of DAC is uncertain and hotly disputed. Due to the limited research that has been done, the available data are not unified and sometimes even inconsistent. The reason is that the research methods are different, and the method of data report is not systematic and comprehensive. The results of different research projects are inconsistent, and the results of the same project are constantly updated to overturn the existing knowledge. Currently, the cost of DAC typically includes the investment cost, operating cost, material loss, and system maintenance cost of the DAC equipment. Other studies also consider the cost of CO_2 transportation, storage, and utilisation. Early studies on CO_2 capture from the atmosphere primarily focused on producing synthetic fuels (Steinberg and Dang, 1977). Subsequently, the concept of DAC was proposed in the field of carbon capture and storage (CCS) (Lackner et al., 1999). Fig. 2.8 shows the context of the DAC cost battle in recent years.

Some researchers believe that the cost of DAC will be so high that investment in DAC is a mistake because it undermines the incentives for a major clean-modification of the original energy structure. In 2003,

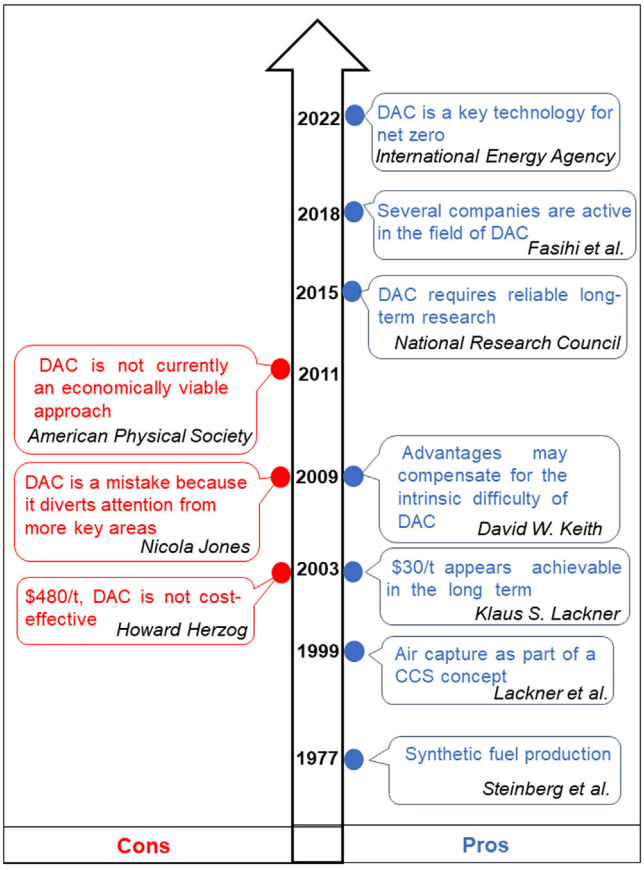

Fig. 2.8. Controversy of DAC development. (For interpretation of the references to color in this figure legend, the reader is referred to the web version of this article.)

Howard Herzog of the Massachusetts Institute of Technology calculated that the cost of DAC technology was as high as $480–540/t (H, 2003). In 2009, Jones N. of Columbia University argued that the study on DAC may be a complete mistake because it diverted attention and resources from other important fields (Jones, 2009). In 2011, the American Physical Society released a report on *Direct Air Capture of* CO_2 *with Chemicals,* and stated that DAC was not an economically feasible solution to mitigate climate change (Socolow et al., 2011). The report used a simplified method to calculate the CO_2 avoidance cost of DAC using a sodium hydroxide solution that was $600/t. In comparison, the CO_2 avoidance cost of post combustion carbon capture from flue gas using the same solution was only $80/t. Hence, the cost of DAC is approximately eight times that of the post combustion carbon capture. In addition, the report also states that DAC cost is likely to decline as technology advances and new concepts are introduced. However, industry experience suggests that considering the necessary compromises in material selection, process conditions, component efficiency, and component lifetime, the cost of all systems will increase after the pilot operation. Therefore, the report concluded that the adoption of DAC technology should be postponed.

In stark contrast, supporters argue that DAC is relatively inexpensive and plays a key role in managing carbon dioxide emissions. In 2003, Klaus S. Lackner of Columbia University showed that the cost of CO_2 emission reduction would be reduced in the long run (Lackner, 2003). In 2009, David W. Keith reported that although the DAC cost would be higher than the cost of power plants with post combustion carbon capture under the same economic conditions. However, DAC enables the partial decoupling of carbon capture from the energy infrastructure, easing the constraints that arise when new energy technologies must be integrated into the existing infrastructures and making it easier to build

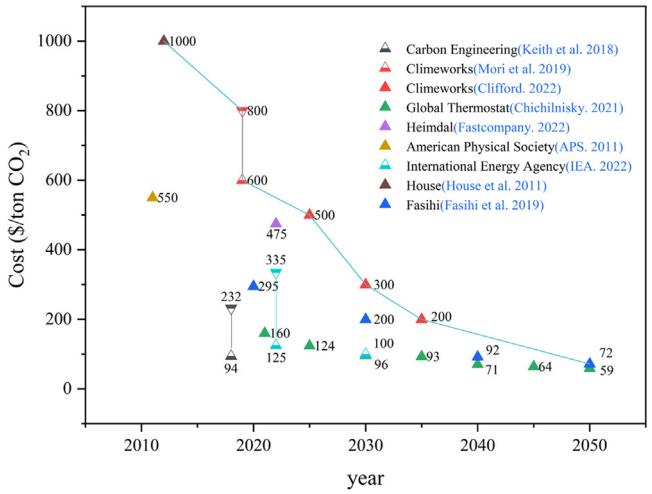

Fig. 2.9. The cost summary of DAC. (For interpretation of the references to color in this figure legend, the reader is referred to the web version of this article.)

a capture plant near the best sequestration sites (Keith, 2009). These advantages can compensate for the inherent difficulties of DAC.

After the report of 2014 International Panel on Climate Change (IPCC) (Pachauri and Meyer, 2014), the international academic community generally changed their views on DAC. In 2015, the National Research Council of the United States released a report stating that long-term research support for DAC is required (Board and Council, 2015). Subsequently, Keith et al. designed a plant for DAC using a potassium hydroxide (KOH) sorbent and calcium-alkali coupling cycle. A detailed calculation showed that the cost of CO_2 was \$94–232/t (Keith et al., 2018). DAC has gradually become a major research focus in the United States, Europe, China, and Japan. For example, the Negative Carbon Plan launched by the U.S. Department of Energy in November 2021 enlisted DAC technology as a key development goal. This strategy aims to reduce the DAC cost to less than \$100/t.

2.4.3.2. How high is the DAC cost in the real-world right now?. As shown in Fig. 2.9, many scholars have conducted an economic evaluation of DAC (Baylin-Stern et al., 2022; Chichilnisky, 2021; Clifford, 2022; Fasihi et al., 2019; House et al., 2011; Keith et al., 2018; Mori et al., 2019; Peters, 2022; Socolow et al., 2011). In Mori et al. (2019) conducted a cost assessment of the pilot DAC plant of Climeworks in Iceland. Since the technology and commercial scale was still in the development stage, the cost was approximately \$600–800/t. In 2022, according to Fast company, a start-up company called Heimdal launched the first ocean-assisted carbon removal plant in Hawaii that is currently capable of capturing CO_2 at the cost of \$475/t (Peters, 2022). Some researchers believe that the DAC cost will show a clear downward trend in the long term. In a techno-economic assessment of DAC plants by Fasihi et al. (2019) in 2019, it was reported that the cost of DAC systems would be significantly reduced with large-scale applications in the 2040s and 2050s. By using a low-temperature sorption DAC system that utilises a hybrid photovoltaic power cell system in Morocco as an example, the CO_2 capture costs in 2020, 2030, 2040, and 2050 were estimated to be \$295, \$200, \$92, and \$72/t, respectively. Jan Wurzbacher, co-founder and co-CEO of Climeworks, told CNBC in an interview that the company is focusing on cost reduction in addition to increasing capacity (Clifford, 2022). It is expected that the cost in 2025, 2030, and 2035, can be reduced to \$500, \$300, and \$200/t, respectively. In December 2021, NOAH Zurich report, Graciela Chichilnisky described the DAC technology of Global Thermostat that captures carbon dioxide from the air using waste heat at 85 °C and a proprietary solvent. According to the use of the captured carbon (e.g., beverage filling, carbon dioxide concrete, synthetic fuels, and sequestration), Global Thermostat has divided the 2020 to 2050 period into nine phases and assessed the cost of each phase. It is estimated that the cost will be as low as \$54/t by 2050 (Chichilnisky, 2021). According to the IEA's report on DAC in Baylin-Stern et al. (2022), assuming different capture technologies, energy prices, and financial assumptions, the cost of DAC capture under a large-scale application of 1 Mt CO_2/year is estimated to be in the range of \$125–335/t. In addition, the IEA also predicts that by 2030, the cost of DAC is likely to be less than \$100/t with the large-scale application of the technology.

2.4.3.3. High or relatively high cost?. Currently, the high cost has become the primary factor that limits the commercialisation of DAC technology. However, a good question that needs to be addressed is whether the DAC cost is high or relatively high compared to the environmental cost. The hidden cost can be quantified to a certain extent using external tools such as a carbon tax. As shown in Fig. 2.10, as the amount of captured carbon increases, the cost of DAC increases as well. According to IEA, the cost of DAC under large-scale application conditions (1 Mt CO_2/year) is between \$125–335/t. Low heat and electricity prices could reduce the projected cost to just above the industry target of \$100/t (Baylin-Stern et al., 2022). If the captured carbon could be monetised using some form of carbon pricing scheme, the levelized cost of DAC would be well below \$100/t. Furthermore, a carbon price above \$160/t could make DAC-based capture profitable.

Due to the high flexibility of DAC technology in terms of plant site selection, the best power generation and heating technology could be used in areas with high renewable energy potentials. By 2030, the cost of DAC could be reduced to less than \$100/t. In addition to strong policy and financial support, technological research and development may also cause industrial upgrades. Therefore, cost reduction could be achieved through technological research and development, learning-by-doing, and large-scale implementation (Fasihi et al., 2019).

Other factors, such as social acceptability, policies, and regulations, can also play a critical role in the cost of DAC (Chauvy and Dubois, 2022). For instance, DAC systems would be difficult to be adopted without a policy-driven carbon tax price. It is worth mentioning that most of the key levers in existing studies are also necessary to facilitate the implementation of other low-carbon technologies, such as photovoltaics and wind power (Chauvy and Dubois, 2022). Therefore, a cost assessment of DAC should not merely focus on a step-by-step reduction of the cost of the DAC technology itself, but a moderately accurate quantitative method should be developed for the environmental cost related to global warming.

2.4.4. Perspectives on DAC

In order to meet specific climate targets, such as those outlined in the Paris agreement, it is imperative that all CO_2 removal technologies be explored (Allen, 2019; Shayegh et al., 2021). Capturing CO_2 at the source, such as at power plants, may not be enough. Other avenues, such as DAC, although more costly than capturing at the source, will be required. Although several groups are conducting research on various DAC approaches such as adsorption, absorption, and cryogenic capture, considerable research will need to go into scaling up these technologies so that they can be feasibly implemented in real-world systems. The risks of implementing such systems are enormous, including environmental, ethical, and technical risks (Lenzi, 2018). Furthermore, massive spending, estimated to reach a third of government general expenditures in developed countries, will be required (Bednar et al., 2019).

The five pillars of DAC, as shown in Fig. 2.11, are (1) capture technology, (b) energy demand, (c) cost, (d) environmental impact, and (e) political support (Ozkan et al., 2022). Currently, DAC technologies need to be improved to reduce costs. Costs of less than \$100/tonne of CO_2 are needed to make DAC viable economically. The costs include capital equipment, maintenance, and operation due to the very low concentrations of CO_2 found in the atmosphere.

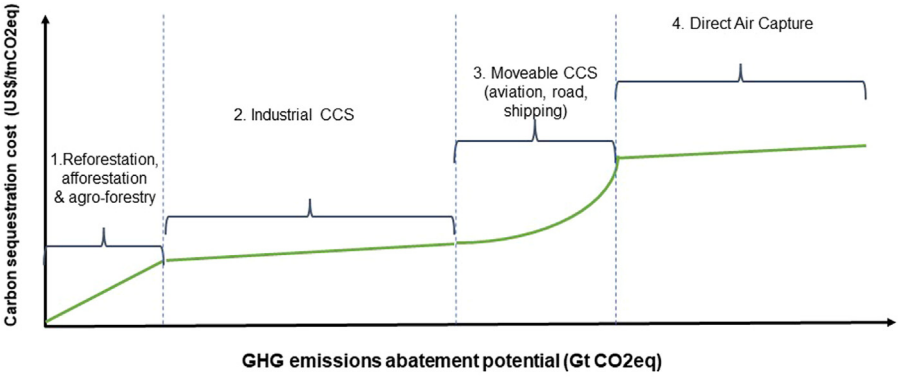

Fig. 2.10. Carbon abatement cost curve (Research, 2019). (For interpretation of the references to color in this figure legend, the reader is referred to the web version of this article.)

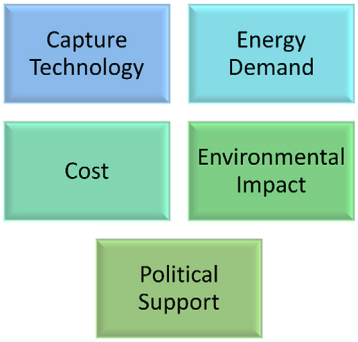

Fig. 2.11. The five of DAC as outlined by Ozkan et al. (2022). (For interpretation of the references to color in this figure legend, the reader is referred to the web version of this article.)

According to a recent report (Budinis., 2022), there are currently 18 DAC plants in Europe, Canada, and the United States that are in operation that captures nearly 0.01 $MtCO_2$/year. As stated by the "net-zero emissions by 2050 scenario," (IEA, 2021) DAC should be scaled-up to capture at least 60 Mt/CO_2 by 2030. The first 1 Mt/CO_2 DAC plant is expected to be fully operating in the United States by 2025, with even more DAC facilities planned.

3. CO_2 capture with sorbents

3.1. Liquid-based sorbents amine solutions

3.1.1. Amine solution

Chemical absorption using amine solvent is a relatively mature post-combustion CO_2 capture method at present, which has realized industrial application from large fixed emission sources such as coal/gas power plant flue gas (Wang et al., 2021; Zhang and Liu, 2013) It is an important technical route to achieve large-scale CO_2 reduction at this stage, and it is also the only low-concentration CO_2 capture technology in the world that can achieve large-scale commercial applications (Weidong et al., 2009). Taking monoethanolamine (MEA) as an example, CO_2 can react with it to form corresponding water-soluble salt and release CO_2 when heating it at 100~140 °C, thus realizing the capture and enrichment of CO_2. The CO_2-rich MEA solvent enters the digestion unit after being heated by the heat exchanger and releases CO_2. However, the shortcomings of the chemical absorption method using amine solvents are also very obvious (Xuepeng, 2014) Due to the large flue gas flow and low CO_2 partial pressure, the investment cost and operation energy consumption of the chemical absorption method are high. Secondly, amine solvents such as MEA have poor stability and are easy to degrade in contact with oxygen in the air. (Lin Haizhou et al. (2019)) In addition, it is necessary to control the concentration of sulphur oxide and nitrogen oxide in the combustion tail gas of the separation unit below 10 ppm to prevent the amine liquid from reacting with the above impurities and deteriorating rapidly. In addition, this kind of solution is highly corrosive and requires relatively expensive pipeline and equipment investment in the early stage.

The average energy consumption of amine chemical absorption carbon capture technology in China is about 2.4~3.2 GJ/t CO_2, reaching the same level in the world, but it is still in the industrial demonstration stage due to lack of large-scale industrial or commercial application. China has designed large-scale and major CCUS demonstration projects, such as the Huaneng Shanghai Shidongkou Carbon Capture Demonstration Project (100000 tons/year) put into operation in 2009, the Shengli Oil Field Flue Gas Carbon Capture Project (40000 tons/year) put into operation in 2010, the CCUS Test Platform Project of China Resources Power Haifeng Company (20000 tons/year) put into operation in 2019, and the National Energy Group Jinjie Carbon Capture Demonstration Project (150000 tons/year) put into operation in 2021, The relatively mature chemical absorption technology of mixed amine solution is adopted.

Internationally, the amine liquid chemical absorption method has a high maturity and is widely used in the existing coal-fired power plants and other flue gas CO_2 capture, and has completed the industrial demonstration and large-scale commercial operation stage internationally. In 2014, Canada put into operation the SaskPower boundary dam project with a capacity of 1 million tons/year, the United States put into operation the world's largest PetraNova project with a capacity of 1.4 million tons/year in 2017, and Japan put into operation the Mikawa biomass combustion power plant with a capacity of 150000 tons/year carbon capture project in 2020, all of which use amine chemical absorption capture technology. The average energy consumption of amine regeneration is 2.6~3.0 GJ/tCO_2.

3.1.1.1. Mixed amine solution. The mixed amine technology combines the advantages of different organic amines. (Han Shuyi et al. (2014)) It reduces the energy consumption of regeneration by optimizing the proportion of amine liquid in different proportions and is widely used in the post-combustion chemical absorption method at this stage. A mini review studied several commercial amine blend solvents licensed by companies such as BASF, DOW, Fluor Daniel Co. MHI Shell Co, etc., with high "energy efficiency". Aghel et al. (2022b) Most primary amines exhibit enthalpy of CO_2 solubility that represents CO_2 absorption heat about 80–90 kJ/mol CO_2, and secondary amines contain lower enthalpy of 70–75 kJ/mol, and tertiary amines contain the reduced enthalpy within the range of 40–55 kJ/mol. (Flores-Segura and Torres, 1997) The lower enthalpy of amine reflects lower heat duties but with higher absorption rates. The amine blends can reach very low heat duty and moderate absorption rates with optimized combination ratios.

Based on literature review, Table 3.1 plotted 5 famous branches of solvent improvement / blended amine solution, along with the most re-

Table 3.1
Major solvent improvement methods in amine blend in CO_2 absorption.

System	Use of reagent	Time
MEA based blended amine	MEA + R3N	Since 2005
PZ based blended amine	PZ + K_2CO_3, PZ + R3N	Since 2005
AMP based blended amine	AMP + DETA, AMP + EAE, AMP + DETA + PZ	Since 2016
The selection rules developed based on structure -performance correlation	MDEA, DEEA, 1DMA-2P, 3DMA-1P	Since 2016
The "absorption-desorption parameter" studies of single and blended amines	BEA, AMP, BEA + AMP	Since 2017
The "coordinative effect" of MEA + RR'NH of single amine	MEA (activator) + DEA (domiant)	Since 2018

cent 6th one: tri-blends containing coordinative effects. The 1st branch was famous and common, which is blending MEA with various tertiary amines MEA + R_3N (5 + 0~2 mol/L) since 2005. (Decardi-Nelson et al., 2017; Gao et al., 2017; Liao et al., 2017; Liu H et al., 2017; Raphael Idem et al., 2006; Roongrat et al., 2005; Sema et al., 2012; Shi et al., 2014b; Srisang et al., 2018; Zhang et al., 2019) Several typical examples were MEA + MDEA, MEA + DEAB, MEA + DEEA and etc. (Decardi-Nelson et al., 2017; Gao et al., 2017; Liao et al., 2017; Liu H et al., 2017; Raphael et al., 2006; Roongrat et al., 2005; Sema et al., 2012; Srisang et al., 2018; Vega et al., 2020; Zhang et al., 2019) It integrated the advantages of MEA (quick CO_2 absorption reaction rates) with tertiary amines (lower energy cost and larger cyclic capacity) and offset the disadvantage of MEA (higher energy cost of desorption and smaller cyclic capacity) with tertiary amine (slower absorption rates). For example, Zhang et al. used MEA (5M), MEA MDEA (5:1 molar ratio, total content 6M) and MEA-1DMA2P (5:1 molar ratio, total content 6M) as blended amine solution. The results show that as an additive in MEA, 1DMA2P has better potential than MDEA to generate bicarbonate ions under the condition of poor CO_2 load and reduce the regeneration energy. (Zhang et al., 2016) The 2nd branch was mixing piperazine (PZ) with various types of tertiary amines PZ + R_3N or K_2CO_3, etc. (Brúder et al., 2011; Cullinane and Rochelle, 2004; Gao et al., 2018; Li et al., 2014; Zhao et al., 2017) The concept integrates the advantage of PZ (faster absorption rate) with tertiary amine (lower energy cost and larger cyclic capacity) and offsets the disadvantage of PZ (easy to precipitate and poison to human life) and tertiary amine (lower absorption rates).

The 3rd branch was blending AMP based amine with either bi-amine blends or tri- amine blends, which fully exerted the advantage of AMP (higher desorption performance with moderate absorption performance). The carbamate of AMP was unstable, which was easy to hydrolyze under heat. Ciftja et al. (2014) After 2016, a large number of studies involved tri-solvents of MEA + AMP + PZ, (Nwaoha et al., 2017, 2016b) MDEA + DETA + AMP (Nwaoha et al., 2016a) and bi-solvents: AMP + PZ, (Brúder et al., 2011) and AMP + DETA, (Wai et al., 2018). Zhang et al. studied the regeneration behaviour of 6M MEA-AMP-PZ (monoethanolamine, 2-amino-2-methyl-1-propanol and piperazine) tri-solvent mixtures loaded with CO_2 with different AMP/PZ molar ratios and blank mixtures at 96 °C. For non-catalytic operation, the results show that compared with 5M MEA, all three solvent mixed amines greatly increase the CO_2 desorption rate, and cycle capacity and reduce the relative heat load. ^{13}C NMR analysis showed that 3M MEA-2.5M AMP-0.5M PZ blend with the highest AMP/PZ ratio produced the largest amount of bicarbonate and less carbamate, which led to the best desorption performance (Zhang et al., 2018c).

The 4th branch started to investigate the chemical property of amines by their molecular structure (hindrance), kinetics (k_2) and basicity (pKa), and correlate the performance with its CO_2 absorption and desorption performance such as absorption rates, equilibrium CO_2 solubility (α_{eq}), heat duty (H), etc. (Singto et al., 2016). Several studies developed various selection rules of tertiary amines (R_3N), (Xiao et al., 2016) which is named as "fast screen method" in 2016. (Xiao et al., 2016) Other studies (Singto et al., 2016), (Luo et al., 2016; Muchan et al., 2017) also reported the selection rules of different amines based on "structure-activity correlations" based on equilibrium solubility, pKa analysis, and absorption rates after 2016–2017.

The 5th branch developed a set of comprehensive "absorption-desorption" parameters of various single amines, such as primary, secondary and tertiary amines in order to compare various single amines at a consistent level. Later on, these sets of parameters were extended to a blended amine solution (Shi et al., 2018). The absorption and desorption parameters integrated the initial absorption rates, equilibrium CO_2 solubility, initial desorption rates, heat duty and cyclic capacity, etc. into two equations. That study discovered that BEA and AMP possessed optimised absorption parameters and desorption parameters (Narku-Tetteh et al., 2017). AMP had a very high desorption parameter with a relatively adequate absorption parameter, while BEA had a very high absorption parameter with relatively good desorption parameter (Narku-Tetteh et al., 2017). Based on intensive analysis, the 2 + 2 mol/L BEA + AMP blended amine solvents were prepared, and tested with heterogeneous catalysts in both absorber and desorber in a batch process and bench scale pilot plant study (Afari et al., 2018; Narku-Tetteh et al., 2018; Natewong et al., 2019; Prasongthum et al., 2019). After studies of these 5 branches, the methodologies of liquid amine solutions were upgraded to highly accurate quantitative analysis. The preparation method was developed from "combination of the advantage of two amine blends" since 2005, (Roongrat et al., 2005) to "structure-activity correlation" since 2016 (Singto et al., 2016) and "absorption-desorption parameter analyses" since 2017 (Narku-Tetteh et al., 2017). The research focus was always at "heat duty oriented analysis" (energy efficient and low cost) by analysing the individual energy contribution: such as absorption enthalpy, sensible heat, and heat of vapourization (Narku-Tetteh et al., 2018; Nwaoha et al., 2017).

The 6th branch was developed in 2018. It is the application of "coordinative effect" onto "bi-solvents" or "tri-solvents", together with absorption-desorption parameters analysis (Narku-Tetteh et al., 2017) of the 5th branch to analyse the performance of amine solution comprehensively. Firstly, Liu et al.[31] and Shi et al. (2020), (2018) discovered "coordinative effect" of MEA + RR'NH, which could facilitate CO_2 absorption (Shi et al., 2022) and desorption (Shi et al., 2020, 2018) simultaneously. This performance was contradictive to the general rule that MEA enhance CO_2 absorption performance and weakens desorption performance. (Nwaoha et al., 2017). The coordinative effect was already verified to exist within MEA + DEA (RR'NH) bi-solvent at the ratio of 0~0.5/2 (Shi et al., 2020) and MEA + BEA (RR'NH) + AMP tri-solvent at 0.1~0.5 + 2 + 2 mol/L[34]. Experimental results confirmed that their absorption and desorption performance was better than that of BEA + AMP 2 + 2 mol/L simultaneously (Hsa et al. 2021). Recently, other similar tri-solvents with the coordinative effect of MEA + EAE + AMP (Shi et al., 2022; Zhang et al., 2022) MEA + BEA + DEEA (Shi et al., 2022) were also studied by Shi et al. and exhibited higher absorption desorption performance.

3.1.1.2. Non-aqueous amine solution. It has been well understood that energy consumption was the main factor affecting the efficiency of power plants when employing the CO_2 capture process (Chakma, 1995; Oexmann and Kather, 2010; Tan et al., 2011). Water evapouration in conventional aqueous amine solutions is the major reason for the high energy consumption (Guo et al., 2014; Leites, 1998; Li et al., 2012). Using organic solvents instead of water provides significant advantages. For example, it can reduce decomposition at high temperature and

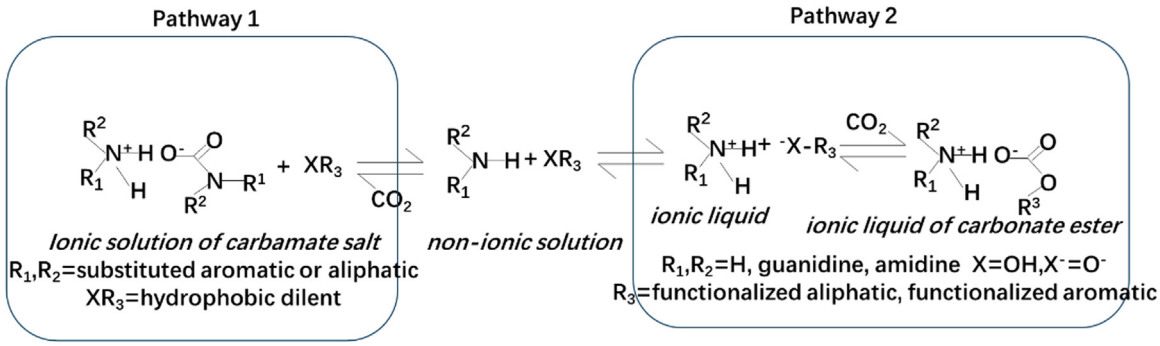

Fig. 3.1. Reaction pathways for RTI's NASs. (For interpretation of the references to color in this figure legend, the reader is referred to the web version of this article.)

energy cost in the regeneration step due to their low heat of vapourization and high boiling temperature (Barzagli et al., 2013; Yu et al., 2013). Recently, non-aqueous amine solutions have been extensively investigated. Lail et al. (2014) developed improved RILs called "non aqueous solvents" (NASs). These solvents are composed of hydrophobic, steric, carbamate forming amine (with low water solubility) and an unspecified amount of low vapour pressure organic diluents to produce NASs with minimum foaming, viscosity reduction and water accumulation. Two families of promising NASs have been discovered and the general reaction pathways with CO_2 are depicted in Fig. 3.1.

Barpaga et al. (2022) found that dilute water solvents have unique thermodynamic and physical properties that can be used to improve efficiency Water-poor solvents have shown water resistance. The reboiler load is lower and the mass transfer rate is higher than expected, but the increase of intrinsic viscosity must be balanced. David et al. Heldebrant et al. (2017) also studied the comprehensive examination of GAP/TEG solvent system at a molecular level to slow down hydrolysis and reduce viscosity. This discovery makes it possible to design one-component silicone-free diamine derivatives, which can reduce viscosity by adding selective chemical groups at specific positions, direct placement and directional hydrogen bonding. Compared with the original GAP/TEG formulation, the viscosity is reduced by 98 %. Chen et al. (2015) studied that compared with the use of triethylene glycol (TEG) or diethylene glycol (DEG) cosolvent, the CO_2 capture formula produced by ethyl monoethanolamine (EMEA) solution in tertiary ethanolamine cosolvent (such as diethylethanolamine (DEAA) or MDEA) has higher equilibrium solubility and high cycle capture capacity. DEEA participates in chemical absorption by extracting protons from EMEA carbamate intermediates. Moreover, using tertiary amine DEEA in non-aqueous solvent has better performance than using alcohol and glyco (Chen, S. et al., 2016).

Sada et al. studied the kinetics of CO_2 absorption with mono- and diethanolamine in non-aqueous solvents, such as methanol, ethanol and 2-propanol (Sada et al., 1985). Versteeg et al. developed a CO_2 absorption system of MDEA in ethanol and concluded that in non-aqueous solutions, no reaction, even no alkycarbonate formation, occurred between CO_2 and tertiary alkanolamines (Versteeg and van Swaaij, 1988). Sami et al. observed the pseudo-first-order rate constant value for the reaction of aniline/cyclohexamine/hexamine with carbon dioxide in ethanol and the results favoured the zwitterion intermediate mechanism (Ali et al., 2000). Park et al. measured the chemical absorption rate of CO_2 with DEA, DIPA, TEA and MDEA in non-aqueous solvents, such as methanol, ethanol, n-propanol, n-butanol (NBA), ethylene glycol, propylene glycol, and propylene carbonate (Hwang et al., 2010; Park et al., 2006, 2005, 2006). Tan et al. explored the CO_2 capture process with a mixture composed of MEA and triethylene glycol (TEG) (Tan et al., 2011). Li et al. studied the mixed non-aqueous solutions of MEA, DEA, and diglycolamine (DGA) with polyethylene glycol (PEG) as non-aqueous solvent for CO_2 capture (Li et al., 2012). Zheng et al. examined the CO_2 solubility in the non-aqueous solutions of AMP−diethylene glycol (DEG) and AMP−triethylene glycol (TEG) (Zheng et al., 2012). Guo et al. investigated a mixture of 2- (2-aminoethylamine)ethanol with benzylalcohol (BP) as absorbent for CO_2 capture. Guo et al. (2014) Barpaga team (Cantu et al., 2020) developed and studied the aqueous diamine solvent N1- (2-ethoxyethyl)-N_2, N_2-diisopropylethane-1,2-diamine (2-EEDIPEDA).

The CO_2 capture performance of the solvent was evaluated from the aspects of adsorption characterization such as vapour-liquid equilibrium adsorption kinetics and viscosity, and it was found that its performance was ahead of that of aqueous dilute amine solvent and its economic cost was as low as 46.8 USD/ton. The results of Fu et al. (2020) showed that the viscosity of the three EHA non-aqueous solutions was smaller (<3 mPa·s) at the temperature range of 303.2 K ~ 323.2 K, which was conducive to the mass transfer and initial absorption rate of CO_2 absorption. These three non-aqueous adsorbents had good application potential in the process of CO_2 capture.

Zheng et al. (2016) studied the process mechanism of lean water CO_2 combined with organic liquid (CO_2BOL) solvent platform and polar swing assisted regeneration (PSAR). From thermodynamics, dynamics and bench scale data, combined with Aspen Plus, the full-size process performance under three CO_2BOL/PSAR conditions were predicted, the material performance was discussed, and the viscosity was determined as the key characteristic that most seriously limited the viability of the water-poor solvent platform.

The Water-poor solvents retain the chemical selectivity of water amine and utilise the lower specific heat of organic matter relative to water to reduce the load of the reboiler, that is, the energy required for the regeneration of solvent. In terms of time and cost, the dilute water solvent can be used as a drop-in solvent substitute that can use the first and second generation of water amine infrastructure. In addition to the characteristics of high boiling point, low specific heat and low evapouration enthalpy of organic solvent, the use of organic solvent instead of water to build an anhydrous absorbent system is expected to reduce the energy consumption of regeneration, and also reduce solvent loss and equipment corrosion. The future experimental work will focus on testing the new iteration of a similar amino-based dilute water solvent with different hydrophilicity to understand the impact on carbon dioxide capture while developing new configuration and process design to further improve the efficiency and cost of the solvent, and testing the use of lean water solvent for carbon dioxide capture after combustion with large-scale platform, testing its efficiency and calculating its cost.

3.1.1.3. Phase-change amine solution. Recently, biphasic solvents, forming two immiscible phases (CO_2-rich and CO_2-lean phases) during the CO_2 capture process, have attracted increasing interest because the process only transports the CO_2-rich phase into the desorption tower, which greatly reduces the volume of solution to be desorbed and regenerated and reduces the energy consumption for water evapouration and

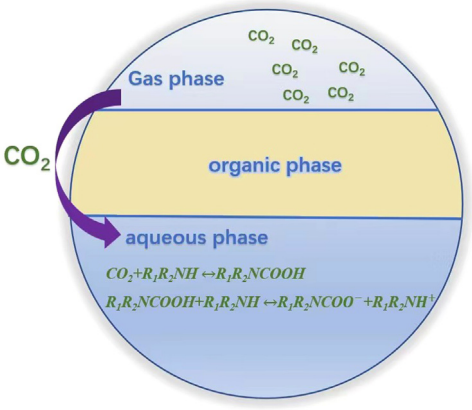

Fig. 3.2. Phase separation schematic diagram of biphasic solvents. (For interpretation of the references to color in this figure legend, the reader is referred to the web version of this article.)

sensible heat, thus reducing the energy consumption for regeneration reduced (Raynal et al., 2011; Zhou et al., 2019). A biphasic solvent typically consists of active amines and a phase-separation agent. As shown in Fig. 3.2, the active amine is a primary or secondary amine with a fast reaction rate, and the phase separation agent is a tertiary amine that cannot react directly with CO_2, so it plays a role as a catalyst in the absorption process (Ye et al., 2015).

The primary or secondary amine (R_1R_2NH) can absorb CO_2 and form a carbamate acid (Reaction 3.1), which can then be deprotonated by a base (Reaction 3.2) such as tertiary amine. The formation of the carbamate greatly increases the solvent polarity and changes the density. Phase separation occurs if the carbamate is immiscible with a phase-separation agent. Phase separation can occur, a phenomenon known as the salting-out effect.

$$CO_2 + R_1R_2NH \Leftrightarrow R_1R_2NCOOH \tag{3.1}$$

$$R_1R_2NCOOH + R_1R_2NH \Leftrightarrow R_1R_2NCOO^- + R_1R_2NH_2^+ \tag{3.2}$$

Tertiary amines such as *N*,*N*-diethylethanolamine (DEEA), *N*, *N*-dimethylcyclohexylamine (DMCA), and pentamethyldiethylenetriamine (PMDTA) are used as phase-separation agent because of their low polarity, which allows the salting out of the carbamate to form aqueous and organic phase (Liu et al., 2019a; Liu et al., 2019b; Pinto et al., 2014a, 2014b; Ye et al., 2015; Zhang et al., 2018). Pinto et al. proposed an aqueous biphasic solvent comprising 5 M DEEA mixed with 2 M *N*-methyl-1,3-diaminopropane (MAPA), compared with 5 M MEA, the DEEA-MAPA biphasic solvent requires lower heat to absorb, and can regenerate at high pressure or low temperature, which has a high cyclic absorption capacity (2 mol kg^{-1}) and a low regeneration energy consumption (2.2–2.4 GJ t^{-1} CO_2) (Pinto et al., 2014b). Zhang et al. studied the phase change behaviour of five different tertiary amines (DEEA, DMCA, PMDETA, 3- (diethylamino)-1,2-propanediol (DEAPD), and bis (2-dimethylaminoethyl)ether (BDMAEE)) on triethylenetetramine (TETA), total amine concentration is 4M, the molar ratio of DMCA and TETA is 3:1. and found that TETA-BDMAEE and TETA-PMDETA were inferior to MEA in absorption capacity, TETA-DEAPD had the strongest absorption capacity, but due to the low hydrophobicity of DEAPD no phase separation occurred during absorption, TETA-DEEA formed a homogeneous phase at high CO_2 loading, and only TETA-DMCA showed high stability in absorption capacity and phase change behaviour, the rate of CO_2 absorption into this biphasic solvent was comparable to that of the 5 M MEA solution, while the regeneration energy reduced by approximately 40 % compared with that achieved with MEA (Zhang et al., 2018). Zhou et al. explored a novel biphasic solvent comprising PMDTA and diethylenetriamine (DETA) with a CO_2-absorption loading of 0.613 mol CO_2•mol^{-1} amine, in which 99.7 % of the absorbed CO_2 was distributed in the lower phase, accounting for 57 % of the total volume. The regeneration energy was reduced to 2.40 GJ t^{-1} CO_2. (Lv et al., 2019; Zhou et al., 2017).

Organic physical solvents such as diethylene glycol dimethyl ether (DGM), diethylene glycol diethyl ether, 1-propanol, *N*-heptanol, and sulfone are often used as physical solvents and phase splitters (Luo et al., 2016; Wang et al., 2019; Xu et al., 2019). For example, Wang et al. (2021) used 1-propanol as a phase splitter mixed with an aqueous MEA solvent and triggered the liquid–liquid phase-change. Compared with pure MEA solution, the cycle capacity was increased from 1.01 mol/kg to 2.51 mol/kg after the addition of 1-propanol, and the biphasic solvent was able to reduce the energy consumption to 2.87 GJ t^{-1} CO_2 (Wang et al., 2019). Liu et al. developed 2-amino-2-methyl-l-propanol (AMP)/MEA blend-based biphasic solvents using diethylene glycol dimethyl ether and sulfolane as phase splitters, and shows that AMP/MEA blends with physical solvents have higher CO_2 absorption rate, with the most excellent being 69 % higher CO_2-absorption capacity and 36 % lower regeneration energy than those achieved using 30 wt% MEA (Liu et al., 2019a). Hu et al. developed a biphasic solvent consisting of 2- (methylamino) ethanol (MAE), 3- (dimethylamino)propan-1-ol (3DMA1P), DGM and water with a CO_2 loading of 1.59 mol/kg, which is 74.2 % higher compared to 30 wt% MEA, and demonstrated by simulation that the concentration of DGM has an effect on the absorption rate of CO_2 (Hu et al., 2022).

Non-aqueous solutions generally use organic reagents as solvents such as alcohols, polyethers, and alcohol (Tao et al., 2018; Zhuang and Clements, 2018). However, precipitation often occurs when alcohols or polyethers are used as phase splitters, forming a solid–liquid biphasic solvent (Chen et al., 2020). The liquid-solid biphasic solvents have significant advantages such as good absorption performance and low regeneration energy consumption, but the formation of solid products makes it difficult to transport to the resolution tower for desorption and regeneration. In addition, it can cause operational problems such as equipment fouling and plugging. Therefore, liquid–liquid biphasic solvents are more attractive. Zhou et al. proposed a novel non-aqueous liquid–liquid biphasic solvent composed of 2- ((2-aminoethyl)-amino)ethanol (AEEA) as an active amine, dimethyl sulfoxide (DMSO) as a diluent, and *N*, *N*, *N′*, *N″*, *N″*-pentamethyldiethylenetriamine (PMDETA) as a phase splitter with a high CO_2-absorption loading (1.75 mol mol^{-1}); 96.8 % of the absorbed CO_2 was in the lower phase. The regeneration energy consumption could be reduced to 1.66 GJ $t^{-1}CO_2$. Moreover, the biphasic solvent in the CO_2 saturated state did not exhibit corrosion behaviour on carbon steel CO_2 absorption products with high polarity are more willing to dissolve in the polar DMSO solvent rather than in the less polar PMDETA, resulting in phase-change behaviour (Li et al., 2021; Zhou et al., 2020). Hence, phase-change behaviour can be obtained by modifying the solvent polarity. Note that the polarity of the phase-splitting agent should be lower than those of the active amine and diluent.

3.1.1.4. Amine solution regeneration using catalysts. The addition of solid acid catalysts to CO_2-rich amine solution is considered as one of the potential methods to reduce the energy consumption for CO_2 regeneration, as it can help decompose the carbamate by providing protons to increase the desorption rate and reduce the desorption temperature (Sun et al., 2021; Zhang et al., 2019b). The principle of catalytic desorption with solid acid catalyst is shown in Fig. 3.3.

Domestic and international research based on solid acid catalysts has focused on metal oxides, zeolites, mesoporous silica, sulfated metal oxides, and composite catalysts (Alivand et al., 2020; Zhang et al., 2019b). Metal oxides have a wide range of industrial applications as solid acid catalysts because of the acidic sites provided by surface defects (Lewis acidity, Brønsted acidity). The addition of γ-Al_2O_3 as a catalyst to the rich solution was first proposed by Idem et al., and experimental data showed a 27 % decrease in energy consumption for the regeneration

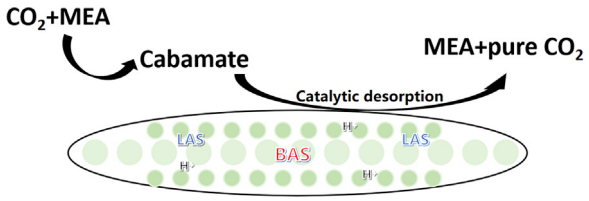

Fig. 3.3. Principle of catalytic desorption with a solid acid catalyst (Xing et al., 2021). (For interpretation of the references to color in this figure legend, the reader is referred to the web version of this article.)

of 5 M MEA aqueous solution (Shi et al., 2014a; 2014b). The catalytic properties of metal oxides (TiO_2, SiO_2) were investigated by Wang et al. and compared with γ-Al_2O_3. The result showed that TiO_2 was the most effective and that the addition of TiO_2 to MEA increased the desorption rate by more than 10 % and reduced the desorption time by more than 40 % compared to MEA with no catalysts (Wang, T. et al., 2016). Bhatti et al. systematically investigated the desorption kinetics of MEA aqueous solutions with metal oxide catalyse and found that V_2O_5, MoO_3, Ag_2O, and Nb_2O_5 exhibited better catalytic performance due to the presence of both Lewis and Brewster acids on the surface (Bhatti et al., 2018a, 2017, 2018b). Ji et al. (2022) found that adding ZrO $(OH)_2$ and FeOOH to CO_2-rich amine solution can reduce the desorption heat load by 45 % and 47 %, respectively. Jiang et al. prepared metal hydroxyl oxide AlOOH and applied it to CO_2 desorption, and found that the addition of AlOOH increased the desorption rate by 560 % and the amount of desorption by 251 % (Jiang et al., 2022).

Previous studies have shown that the addition of synthetic zeolites (HZSM-5, HY, HB, SAPO-34) to the CO_2-rich amine solutions can also improve CO_2 desorption performance. Xu et al. found that HZSM-5 could effectively promote CO_2 regeneration and reduce regeneration energy consumption by 23.9 % (Xu et al., 2020). Bhatti et al. prepared a range of HZSM-5 with different properties and investigated its catalytic performance in CO_2-rich amine solutions and found that optimally adjusted HZSM-5 could reduce the relative heat load by 62.7 % (Bhatti et al., 2020). Zhang et al. found that HB with a larger mesoporous specific surface area and more Brønsted acid centers could improve CO_2 desorption performance by 1360.8 % and reduce regeneration energy consumption by 66.1 % (Zhang et al., 2019a). Through their study, Srisang et al. found that the catalytic performance of HY in CO_2-rich amine solutions was significantly inferior to HZSM-5 (Srisang et al., 2017). A commercial SAPO-34 had a similar surface area, average pore width and Bronsted to Lewis acid ratio to HZSM-5, but SAPO-34 showed a lower catalytic efficiency in CO_2-rich amine solutions than HZSM-5 due to the lower number of total acid sites on SAPO-34 compared to HZSM-5 (Zhang et al., 2018c). Natural zeolites are considered an ideal alternative to CO_2 desorption catalysts due to their unique advantages such as low price and high availability. However, only H-mordenite zeolite was reported to be applied as a catalyst for CO_2 desorption, showing similar catalytic performance to HZSM-5 (Zhang et al., 2019a). Mesoporous silica such as MCM-41 and SBA-15 has also been used to catalyse CO_2 desorption due to their regular mesoporous structure and small amounts of Brønsted acid. However, their catalytic performance was inferior under the same conditions compared to that of HZSM-5 (Gao et al., 2020; Liu H et al., 2017; Zhang et al., 2017).

Sulphated metal oxides exhibit more acidic sites due to the presence of sulphur atoms in their structure (Almeida et al., 2008; HINO and ARATA, 1979; López et al., 2000). As reported in previous years, the catalytic effects of sulfated zirconia (SO_4^{2-}/ZrO_2), sulfated TiO_2 (SO_4^{2-}/TiO_2), and sulfated Fe_2O_3 (SO_4^{2-}/Fe_2O_3) was inferior to HZSM-5 and MCM-41 because of the lower number of Lewis and Brønsted acid sites and mesoporosity (Ali Saleh Bairq et al., 2019; Xing, Lei et al., 2021). Idem et al. investigated the preparation of solid super acid catalyst Ce $(SO_4)_2/ZrO_2$ and its catalytic effect on CO_2 desorption and found that Ce $(SO_4)_2/ZrO_2$ has a large number of Brønsted acid sites even well beyond HZSM-5 (Natewong et al., 2019; Prasongthum et al., 2019). Hybrid composite catalysts are usually composed of two materials with different properties, which combine the unique advantages of different materials to further reduce energy consumption for CO_2 regeneration.

For instance, composite amine catalyst γ-Al_2O_3/ HZSM-5 is more effective in catalysing desorption than γ-Al_2O_3 or HZSM-5 alone (Liang et al., 2016b; Zhang et al., 2018b). The catalysts were prepared by loading SO_4^{2-}/ZrO_2 onto mesoporous structures (e.g., γ-Al_2O_3, SiO_2, SBA-15, and MCM-41) and used to catalyse CO_2 desorption with a higher catalytic effect than HZSM-5 (Ali Saleh Bairq et al., 2019; Gao et al., 2020; Zhang et al., 2018a, 2019b). Gao et al. synthesized composite catalyst SO_4^{2-}/ZrO_2/SBA-15 and used it to reduce heat duty for the regeneration of CO_2-loaded MEA solution. The results of the study showed that SO_4^{2-}/ZrO_2/SBA-15 increased the desorption factor by 100–200 % and reduced energy consumption for regeneration by 20–26.50 % (Gao et al., 2020). A series of composite catalysts (CMK-3-SiO_2, CMK-3-MCM-41 and CMK-3-SBA-15) were prepared, and their catalytic performance was compared and analysed by Bairq et al. It was found that CMK-3-SiO_2 gave the best catalytic performance, being able to reduce the energy requirement by 37.41 % and increase the desorption rate by 195 % (Bairq et al., 2020).

3.1.1.5. Life cycle assessment of amine solutions based carbon capture.

3.1.1.5.1. Introduction. LCA is an important environmental management tool. The term “life cycle” refers to the whole process of an object from raw materials, through production and use, to abandonment (that is, from cradle to grave). The International Organization for Standardization (ISO) defines LCA as the assessment of environmental factors and potential impacts in the life cycle and mentions that LCA is generally carried out through four stages (target and scope definition, inventory analysis, impact assessment, and interpretation) to quantify the main potential environmental impacts associated with related products or services. Literature (Wang et al., 2022) introduces the four stages of LCA in detail:

1. Definition of objectives and scope: “clear objectives,” “determine the boundary,” "time span of evaluation," and "specify the functional units of quantitative description."
2. Inventory analysis: collect relevant data and prepare a list of inputs and outputs related to the environment and resources of the evaluated objects. When the data is missing or unclear, it needs to be analysed at the interpretation stage.
3. Impact assessment: The results of the inventory analysis are classified according to the type of impact, and the assessment method is selected and quantified for the resulting environmental impact.
4. Interpretation: analyse the results of the impact assessment phase, improve the data through sensitivity and uncertainty analysis, and draw conclusions.

In this paper, the life cycle impact of a part of the CCS system (the amine solution carbon capture system) is studied. The important problems involved in the LCA of an amine solution carbon capture system are analysed, and the limitations and shortcomings of the system are pointed out.

3.1.1.5.2. Life cycle assessment of amine solution carbon capture systems.

Goals and Scope

At present, the life cycle evaluation of carbon capture systems in amine solutions is very limited. Tim Grant et al. studied the life cycle evaluation of coal-fired power plants using MEA and potassium carbonate solution as absorbents (Grant et al., 2014). Ben Young et al. evaluated the life cycle of CCS in oil refineries, amine production plants, and coal-fired power plants in the United States (Young et al., 2019). There is extensive research on the life cycle evaluation of carbon capture systems, but there is a lack of research on amine-based carbon capture systems. The carbon capture system is a part of the CCS system, and the research on it can learn to a certain extent from the research experience

of the CCS system life cycle. When the object of LCA is transferred from the CCS system to the ammonium solution carbon capture system, the focus of LCA should turn to the impact of the ammonium solution carbon capture system on the environment without considering the impact of the sequestration part on the environment.

In LCA, the definition of the functional unit should be based on its ability to serve as a reference for the impact of the evaluated system on the environment to facilitate the comparison between different studied systems. In general, functional units need to be defined in terms of research objectives, and the defined functional units need to be consistent with the goals of the overall system. Most research has focused on the environmental burden of CCS systems using different absorbents. Since most studies are based on coal-fired power plants, the LCA of CCS systems usually uses a functional unit based on power generation without capturing a certain amount of CO_2 as a functional unit. For example, Letitia Petrescu et al. (2017) selected 1 MWH of net generation as a functional unit in the LCA of a supercritical pulverised coal power plant with post-combustion carbon capture and storage (Petrescu et al., 2017). Francois Saunier et al. (2019) selected "separation of 1 tonne of CO_2 from smoke streams from a 550 MW coal-fired power plant in the Midwest of the United States in 2017" as a functional unit in a study on bio-catalysing and facilitating a comparison of the LCA of a K2 carbonate process with amine-based carbon capture technologies (Saunier et al., 2019). The purpose of defining functional units in this way is to compare the environmental impacts of different CO_2 separation methods. In future studies, more consideration should be given to defining CO_2-based functional units to make better comparisons between different studies.

The whole amine solution carbon capture system is a relatively complete process in the CCS system, which connects all devices in series by absorbing and desorbing carbon dioxide. By determining system boundaries, relevant processes can be included in the LCA of the target system, performing a full life cycle evaluation or a partial life cycle evaluation on the target system. In general, the boundaries of the target system should encompass the entire process from cradle to grave. For example, the boundaries of the life cycle evaluation of CCS systems for sub-critical coal-fired power plants include the entire chain of CCS systems, i.e., the entire process from generation to CO_2 storage (Giordano et al., 2018). Generally, the boundary of the target system should be selected according to different research purposes. When defining the system boundary, we can purposefully simplify the system boundary according to the research focus, which helps us better study the relatively complex system. However, the boundary of the target system should be simplified in line with the actual situation rather than arbitrarily. In particular, processes with less than 1 % environmental impact are considered negligible. Kristina Zakuciova et al. defined the system boundary as the operation part of the power plant and the activated carbon production, emission treatment, carbon dioxide capture process, and waste generation in the life cycle evaluation of coal-fired power plants and carbon capture systems based on activated carbon (Zakuciová et al., 2020). However, the definition of the system boundary does not need to consider the operation part of the power plant or the production of activated carbon. Instead, it needs to focus on the production and deterioration processes of the amine solution. Since this paper only takes the carbon capture system as the object, carbon dioxide compression, transport, and oil displacement are excluded from the system boundary. When comparing amine solution carbon capture systems applied to different combustion power generation plants, it should be fully considered that the different coal-fired power plants may have an impact on the life cycle evaluation of amine solution carbon capture systems.

Inventory analysis

The rationality, timeliness, and accuracy of the required data can affect the final evaluation results to a large extent. When the available data cannot support the research, a variety of assumptions need to be added to the target system, which may affect the accuracy of the evaluation to some extent, and the relevant database cannot provide comprehensive life cycle inventory (LCI) data. Real data, rather than average or average data, should be used as far as possible for LCA, as many aspects, such as average data in geographical space, time span, and technical level, may lead to large errors in LCA. The improvement of the accuracy and timeliness of the data involved in the studied system can provide more experience for the construction of various carbon capture systems. Usually, researchers are faced with the problem of limited available data, so they will use relevant average data for research, which will reduce the accuracy of the results. It is particularly important to reduce the difficulty and improve the accuracy of data collection. In addition, with the continuous innovation of target system technology, researchers need more and more types of data, so they should pay more attention to data collection.

Most of the information used in this study is taken from published works, studies by international and national agencies (such as the IEA, IPCC, and Global CCS Institute), and a number of commercial databases (like Ecoinvent, Environmental Footprint, and Impact World +). In the areas of agriculture, building, chemical manufacture, power generation, fishing, metals, refineries, textiles, tourism, transportation, waste treatment and recycling, water supply, etc., the Ecoinvent database includes 140 nations. Due to the openness, depth, and dependability of its data, it is frequently utilised by businesses and has more than 18,000 data for roughly 3,200 items. The geographic variability of the data can be reduced in the IMPACT World Plus database, which provides country- or region-specific characterisation parameters.

Impact assessment

Two accepted approaches to life cycle impact assessment are problem-oriented midpoint impacts and damage-oriented end effects. The former was chosen in most LCA studies of amine-based carbon capture systems. Selecting appropriate impact categories is the first and most significant step for the first method. The selection of impact categories usually depends on the purpose of the study, the time span considered in the study, and the geographical location of the object of study (Wang et al., 2022). The role of carbon capture systems is to reduce greenhouse gas emissions by separating CO_2 from fixed emission sources, which include cement, steel production, hydrogen production from fossil fuels, waste incineration, power generation, and other industries. However, the construction and operation of the infrastructure for carbon capture systems, as well as the production, regeneration, and degradation of amine solutions, will cause certain negative environmental impacts. Therefore, we should not only select the “global warming potential” (GWP) as the impact category but also select other impact categories for comprehensive analysis and assessment in the LCA studies of amine-based carbon capture systems. Table 3.2 lists the impact categories selected in the LCA study of the amine-based carbon capture system.

Interpretation

There is a certain gap between the results of the LCA and the actual situation, so we need to analyse the cause of this gap. In the process of LCA, the evaluation is not accurate due to the data (such as the gap in the application of existing databases and some data caused by the integration of heterogeneous data sets). Furthermore, the emission trends of small-scale-related emissions have expanded to large-scale applications with factors that cause large errors and other factors that make the results of the life cycle subject to a certain degree of uncertainty. Therefore, we need to analyse the life cycle results and uncertainty to optimise the results of the parameters. Therefore, we should solve these uncertain issues in future research (Gibon et al., 2015).

Sensitivity and uncertainty analysis

The application of the CCS system can reduce the GWP indicator of the coal power generation system, but it will also affect some other environmental indicators to a certain extent. In the literature (Petrescu and Cormos, 2017), the condition of the IGCC power plant without CCS is compared with the IGCC power plant with calcium circulation for the carbon dioxide capture before burning. The results showed that the GWP of the CCS coal-fired power plant was 917.25 kg CO_2-EQ/MWH,

Table 3.2
Selected impact categories for LCA studies on carbon capture in amine solutions.

Study	GWP	AP	EP	PCOP	ADP	HTP	ETP	ODP	PMFP
Kathrin Volkart (2013)				√		√			√
Longlong Tang (2014)	√	√	√	√	√	√	√		
Tim Grant (2014)	√	√	√	√	√	√	√		
Utrecht University (2014)		√	√	√		√		√	√
Xiangping Zhang (2014)	√	√	√	√		√	√	√	√
M.A. Morales Mora (2016)	√								
Stefanie Troy (2016)	√	√	√	√	√	√	√		√
Tang Daqing (2016)	√	√	√	√	√	√	√	√	√
Letitia Petrescu (2017)	√	√	√	√	√	√	√	√	
Lorena Giordano (2018)	√	√	√	√	√	√	√	√	
Ben Young (2019)	√	√		√	√				√
Yi-Ming Wei (2019)	√	√	√	√	√	√	√	√	
Albert Ratner (2020)	√	√	√			√		√	
Alireza Aslani (2022)	√	√	√		√	√	√	√	√
Andrea Mio (2022)		√	√	√	√	√	√	√	

GWP = Global Warming Potential.; AP = Acidification Potential; EP = Eutrophication Potential; PCOP = Photochemical Oxidation Potential; ADP = Abiotic Depletion Potential; HTP = Human Toxicity Potential; ETP = Ecotoxicity Potential;
ODP = Ozone Depletion Potential; PMFO = Particulate Matter Formation

and the GWP was 373.09 kg CO_2-EQ/MWH under CCS. The use of CCS reduced GWP by more than 50 %. However, other environmental indicators have increased. The AP index of the power plant system that has not been used in CCS technology was 0.49 kg SO_2-EQ/MWH. After using the CCS technology, the AP index increased to 1.47 kg SO_2-EQ/MWH. The literature (Petrescu et al., 2017) compared the SC pulverised coal power plant without CCS with the SC pulverised coal power plant using amine-based (MDEA) combustion CCS. The GWP value of an SC pulverised coal power plant without CCS is 970.37 kg CO_2 equiv./MWh, and the total GWP value of an SC pulverised coal power plant using amine (MDEA) combustion was 495.93 kg CO_2 equiv./MWh. However, after the application of amine-based combustion, the AP environmental index has reached 4.57 kg SO_2 eq/MWh, while the AP index of pulverised coal power plants without CCS is 0.49 kg SO_2 eq/MWh, with an increase of about 9 times. Not only that, EP, ADP, and other relevant environmental indicators have also increased to varying degrees. According to the analysis, the MDEA production process and the upstream and downstream processes of CCS have made great contributions to these growth indicators. Therefore, the reduction of CO_2 emission in the power generation system can not only focus on the emissions of the power plant itself but also combine the whole process to analyse the environmental benefits of the system comprehensively. In addition, the cost of establishing the emission reduction system should also be considered.

The fate of some other harmful substances other than carbon dioxide is also an important uncertainty. The amine solution absorbent may absorb other harmful substances besides carbon dioxide during the actual absorption process, which may make the whole system have better environmental performance. If the power plant system can effectively treat these substances, some environmental assessment indicators will be greatly reduced, and the environmental impact of the entire system will be smaller (Pehnt and Henkel, 2009). In addition, the energy efficiency of the system itself has an important impact on LCA. The literature (Young et al., 2019) indicated that in ammonia production systems and petroleum production systems, when the energy efficiency of the system was improved, almost the entire life cycle impact was reduced by 20–30 %, and the photochemical smoke formation potential (PSFP) in ammonia production systems reduced by 60 %. The PSFP effect of CO_2 reduction per unit equivalent ammonia production system was greatest, while the increase in PSFP was minimal when energy efficiency was sensitive. Therefore, when a more energy-efficient carbon capture system is used, the environmental impact of the entire system can be significantly improved.

3.1.1.5.3. Environmental impact of amine solution carbon capture systems. After the application of a carbon capture system to a coal-fired power plant, its direct CO_2 emissions decrease, but other negative environmental impacts increase. It was pointed out (Young et al., 2019) that the operation of carbon capture systems and the degradation of amine solutions caused negative impacts on the environment, such as abiotic depletion, acidification, and eutrophication. In another literature (Volkart et al., 2013), LCA was performed on a coal-fired power plant with a carbon capture system. The results showed that the plant was superior to the plant without a carbon capture system in terms of the impact categories of GWP and AP but had greater negative impacts on other impact categories (such as HTP, PMFP, ETP, ADP, etc.).

To justify whether the carbon capture system reduces the environmental burden, it is necessary to understand whether the environmental benefits generated by the system are higher than the environmental damage it brings. As a result, the method of a damage-oriented end impact assessment must be introduced for further analysis. For example, the end-point impact assessment method was applied for human health, and ecological environment damage was used to conduct an LCA for biomass co-fired power plants combined with CO_2 capture systems (Schakel et al., 2014). The results showed that the overall environmental performance of the power plant was improved, even though the CO_2 capture system itself produced various negative environmental impacts.

In the carbon capture system, the production and degradation of chemical absorbents are one of the main factors that cause negative environmental impacts, and different absorbents have different impacts on the environment. In the literature Barbera et al. (2022) and Grant et al. (2014), carbon capture systems with different absorbents (monoethanolamine (MEA) and potassium carbonate) were compared. The results showed that in the natural gas power plant with a carbon capture system, the GWP of MEA was lower than that of potassium carbonate, but its ETP and HTP were higher than those of potassium carbonate. In the lignite power plant with a carbon capture system, the potassium carbonate process showed less environmental impact than MEA on the basic environmental indicators such as GWP, ETP, HTP, and ADP. It can be seen that the selection of absorbents depends on CO_2 emission sources, and selecting different absorbents for different CO_2 emission sources can improve the overall environmental performance. In addition, LCA was carried out on two carbon capture systems with MEA and strong hydroxide as absorbents (Zahedi et al., 2022). The results showed that except for eutrophication and nonbiological resource consumption, MEA had less impact on the environment than strong hydroxide in other impact categories. In addition to chemical absorbent separation, CO_2 capture systems can also use membrane separation methods to separate CO_2. Compared with MEA, membrane separation not only consumes less energy but also has a lower negative environmental impact (Giordano et al., 2018; Zhang et al., 2014) .

The energy consumption of the CO_2 capture system can be reduced by using clean energy to supply energy to the MEA regeneration system. It was found that the temperature range of the solar collector had a good match with the regeneration temperature of MEA; thus solar energy can be used to supply heat for the MEA regeneration system. Junyao Wang et al. (2017) analysed the solar-assisted coal-fired power plant with a CO_2 capture system by using the LCA method. The results showed that when the CO_2 capture rate was 90 %, in terms of GHG reduction performance, the implementation of CCS reduced the life cycle GHG emissions by 67.1 % and 73.7 % for coal-fired power plants with an amine-based CO_2 capture system and solar-assisted repowering of coal-fired power plants, respectively. This was because solar energy reduced greenhouse gases for carbon capture power plants more than the greenhouse gases emitted by the construction and operation of solar heat collection systems. Therefore, the application of solar heat collection systems is conducive to reducing the negative environmental impact of coal-fired power plants with CO_2 capture systems.

According to the LCA findings, carbon capture systems based on amine solutions can increase environmental performance while lowering greenhouse gas emissions and CO_2 levels. Additionally, it can be shown from a comparison of amine solution and other chemical absorbents that there is a small difference between the pros and cons of each absorbent. However, amine-based carbon capture technology is currently more advanced. Therefore, the primary technique for reducing CO_2 can be an amine solution carbon capture device. According to a life cycle study, reducing the running energy usage of a carbon capture system can greatly increase the total environmental benefits of the whole system.

3.1.1.5.4. Disadvantages and limitations.

Accuracy of results

Although the CCS system has attracted much attention in recent years, its application has been greatly hindered due to the constraints of cost and economy, the legal and regulatory framework, social acceptability, uncertainty, and scalability. The application popularity of CCS overall technology is extremely low, among which the application of amine solution carbon capture systems is less popular, which leads to the very limited data required. The enterprise application of amine solution carbon capture systems is only to reduce CO_2 emissions and pay little attention to other data collection related to the environment, resulting in extremely low accuracy of the required data. Because the required data is very limited and the accuracy is low, the LCA analysis of the amine solution carbon capture system often uses the average value and makes a series of assumptions, resulting in inaccurate LCA results.

Interdisciplinary and large-scale implementation assessment

At present, most of the research on CCS systems focuses on the analysis of applications. Few researchers have studied the potential impact of CCS systems on the environment, and there are few studies on the CCS system (the amine solution carbon capture system). The amine solution carbon capture system employs both the LCA and the technical-economic assessment (TEA) methods for CCS evaluation (Wang et al., 2022). In this section, the LCA of an amine solution carbon capture system is carried out, but it is not combined with TEA or other methods for a comprehensive evaluation. It is limited to the study of a single discipline, which makes the evaluation results unreasonable. At present, there is no mature integrated method for the comprehensive evaluation of an amine solution carbon capture system, and even the comprehensive evaluation method for a CCS system is not mature. Therefore, the large-scale deployment of amine solution carbon capture systems is normally carried out without comprehensive evaluation of their economic and environmental benefits. Future research on amine solution carbon capture systems should focus on the interdisciplinary evaluation of environmental impact, economic cost, and geographical factors. A high level of evaluation combined with a variety of effective disciplines is conducive to better decision-making by decision-makers and helps make decisions more convincing and credible.

3.1.2. Ionic liquids in CO_2 capture

Ionic liquids (ILs), a class of room temperature molten salt composed of cations and anions, have been intensively investigated as novel solvents and soft functional materials for CO_2 capture, owing to their low vapour pressure, high thermal stability, superior solvation ability and designable structures (Gao et al., 2020). Brennecke et al. (Blanchard et al., 1999) first reported that CO_2 has a high solubility in ILs. Subsequently, research demonstrated the application possibility of ILs in CO_2 absorption at room temperature. Classification of ILs apart from the hybrid ILs can be broadly done, as indicated in the diagram (Fig. 3.4**)**. In this part, we mainly review novel IL-based materials and hybrid ILs-based materials for CO_2 capture.

Although the CO_2 solubility in traditional ILs is relatively low compared to amine-based absorbents, the ILs properties can be improved by functionalization of cations or anions to increase the physical and chemical interactions between ILs and CO_2. Effects of CO_2 solubility in ILs have been widely investigated to increase CO_2 capture performance, and the factors affecting CO_2 capture through ILs are listed in Fig. 3.5. The longer alkyl chains on cation and fluorinated anions are profitable to facilitate the CO_2 capture process (Almantariotis et al., 2010; Zheng et al., 2020). The hydrophobic nature of the cation or anion can enhance the interaction between ILs and CO_2. Water content in ILs also has a positive effect on fluidity and CO_2 absorption (Hu et al., 2014). From the viewpoint of industrial practice, the high viscosity of ILs is one of the main reasons that cause slow gas diffusion (Hussain et al., 2021). In addition, ILs can be combined with numerous types of materials to form hybrid materials. However, doping an excessive amount of ILs may cause pore-blocking, there could be detrimental for immobilized ILs to capture CO_2 (Lian et al., 2021).

3.1.2.1. Amino ILs. On the basis of the chemical reaction of CO_2 with the amino group, a large number of amino functionalized ionic liquids were developed as absorbents. Studies have found that more amino groups in ILs lead to higher CO_2 absorption capacity, and water content has a great influence on CO_2 absorption capacity. When the moisture content increased from 0 % to 40 %, the absorption capacity of poly-amino-based ionic liquids [TETAH][BF_4] increased from 0.96 mol CO_2/mol IL to 2.04 mol CO_2/mol IL (Hu et al., 2014). A bifunctional ionic liquid [APmim][Gly] consisting of amine and amino acid has the advantages of high efficiency and high CO_2 capacity, which was as high as 1.23 mol CO_2/mol IL (Lv et al., 2016a). A polyamine functionalized ionic liquid [APmim][Lys] by introducing amine and lysine functionalization groups into imidazole ILs was reported and its absorption load was 1.80 mol CO_2/mol IL (Zhou et al., 2016). A novel hydrophilic amino acid ILs ([C_2OHmim][Gly]) was designed and the level of capture capacity reached 0.575 mol CO_2/mol IL (Lv et al., 2016b), which makes it has great potential to make up for the deficiency of water-based MEA and is beneficial to industrial application.

However, the formation of intermolecular hydrogen bonds in ILs-CO_2 complex may lead to a sharp increase in viscosity after absorbing CO_2, thus affecting mass transfer performance and limiting the application of amine ILs (Cui et al., 2016). Bhattacharyya and Shah (2016) synthesized the ether functionalized choline amino acid ILs [$N_{1,1,6,2O4}$][Lys] with low viscosity and high CO_2 sorption capacity. Luo et al. (Luo et al., 2016) introduced hydrogen receptors such as N or O atoms into amino-functionalized ILs, and showed that ILs such as [P_{66614}][4NH_2-NC], [P_{66614}][Ac-Gly], [P_{66614}][Me-Gly], [P_{66614}][Ac-PhO] and [P_{66614}] [MA-Tetz] have two active sites for CO_2 on an amine group through the formation of intramolecular hydrogen bonds and proton transfer processes, and the viscosity of these amino-functionalized ILs slightly increased or even decreased during CO_2 capture.

In order to achieve low regenerative energy consumption and low viscosity, a novel CO_2 capture method for [TEPAH][2-MI] combined with organic solvents was proposed (Liu et al., 2020). The absorption load of [TEPAH][2-MI]/N-propanol/ethylene glycol was 1.72 mol CO_2/mol IL, which was much higher than MEA/water. The regeneration

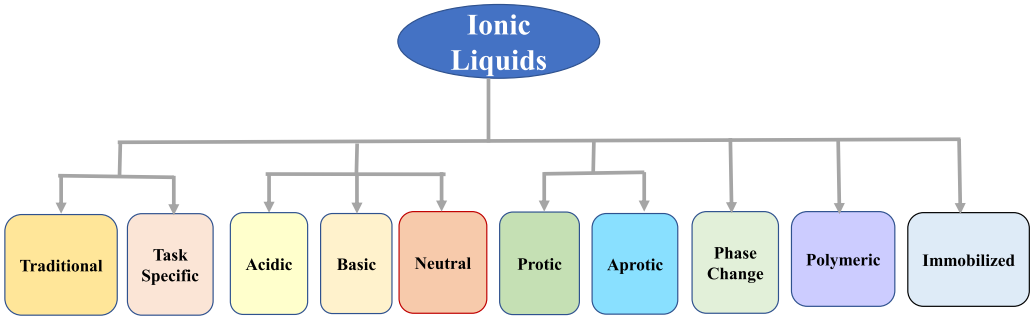

Fig. 3.4. Classification of ILs. (For interpretation of the references to color in this figure legend, the reader is referred to the web version of this article.)

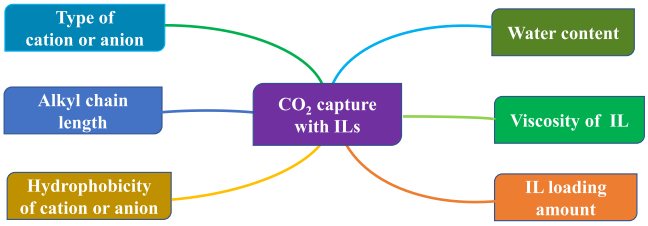

Fig. 3.5. Factors affecting the CO_2 absorption with ILs. (For interpretation of the references to color in this figure legend, the reader is referred to the web version of this article.)

efficiency remained at 90.7 % after the fifth regeneration cycle, and the viscosity of the solution before and after absorption was only 3.66 and 7.65 mPa s.

3.1.2.2. Protic ILs. Protic Ionic Liquids (PILs) generally include proton donor and proton acceptor, and a hydrogen bond network can be formed in the structure with strong polarity (Cohen et al., 2019; Er et al., 2019; Sun et al., 2014), which not only has typical ILs properties, but also builds the hydrogen bond network due to the proton that can migrate in its structure. In general, PILs have high viscosity, which is a result of strong interactions between the ions through, mainly, the hydrogen bonds of hydroxyl groups and protic ion-ion interactions. Therefore, when PILs are used to absorb CO_2, it is generally mixed with water, methanol, ethanol and other solvents and then used in its two-phase system.

The viscosity of PILs is an important property in studying its application range. The structure of anions in PILs has a great influence on the viscosity, and the anions such as F $(HF)_n^-$, N $(CN)_2^-$, N $(CN_3)^-$ have relatively low viscosity (Ignat'ev et al., 2015; Seki et al., 2010). Weak intermolecular interactions (such as van der Waals forces and hydrogen bonds) have a certain effect on the viscosity of PILs. The stronger the intermolecular interaction, the greater the viscosity of PILs. Delocalization of charges on anions in PILs (e.g. fluorination) can weaken hydrogen bond interactions and reduce viscosity.

Zheng et al. (2017) determined the solubility of CO_2 in the cation PILs 3- (dimethyl amino) -1-propylamine (DMAPA) and different anions, and the results showed that the solubility of CO_2 in [DMAPAH][F] aqueous solution reached 3.62 mol/kg at 0.1 MPa and 35.2 °C. A series of etoxyacetic anionic PILs containing three different amine cations were designed (Wei et al., 2020), and the CO_2 solubility in [3-(dimethylamino)-1-propylamine][ethanol amine] ([DMAPAH][EOAc]) was as high as 2.44 mol/kg. An anionic functionalized PIL synthesized by superbase 1,8-diazabicyclo [5.4.0]-undec-7-ene (DBU) and imidazole was synthesized (Zhu et al., 2017), which can reversibly capture CO_2 with a capacity of 1 mol CO_2/mol IL. In addition, there are many studies on fluorine substituents. Dimethyl-1,3-malon-2,3,5-difluorophenol salt ([DMAPAH][3,5F-PhO]) was synthesized, and its optimal absorption capacity was 3.99 mol CO_2/kg IL (0.86 mol CO_2/mol IL) (Zhao et al., 2018).

As for the influence of cations and anions of PILs on CO_2 absorption, other researchers have given their own ideas. Ma et al. (2021) found that the absorption path by the anion of dimethylethylenediamine 4-fluorophenolate ([DMEDAH][4-F-Pho]) was favourable in kinetics, while the absorption path by the cation was thermodynamically beneficial. Moreover, dimethylethylenediamine acetate ([DMEDAH][OAc]) only showed the possibility of cation absorption.

For the application of PILs in CO_2 capture, in addition to their CO_2 absorption performance, selectivity should also be considered as an important performance. Alcantara et al. (2018) measured the phase equilibria data of low viscous diethylammonium butanoate [Bu] with CO_2, CH_4 and N_2 from 30 °C to 60 °C and up to 20 MPa. The results were shown that this PIL presented moderate to low CO_2 solubility, but it would display higher CO_2/CH_4 selectivity than most ILs studied at high pressures. Swati et al. (2021) synthesized several ionic liquids, namely, 1-butylsulfonate-3-methylimidazolium P-toluene sulfonate ([BSmim][tos]), 1-butylsulfonate pyridine P-toluene sulfonate ([BSmpy][tos]), 1-butyl-3-methylimidazolium chloride ([Bmim]Cl) and 1-butylpyridine chloride ([Bpy]Cl) for the separation of CO_2/N_2 and CO_2/CH_4 by supported ionic liquid membranes (SILMs). It was found that the presence of sulfonic group in proton ionic liquid would increase Lewis acid-base force and enhance the affinity of CO_2 to ILs, resulting in PILs having certain advantages in selectivity. The selectivity of [BSmim][tos] and [BSmpy][tos] to pure CO_2/CH_4 was 47.4 and 40.7, respectively.

3.1.2.3. Phase change ILs. CO_2 capture using phase change ILs has attracted increased interest for the potential to reduce the cost of energy consumption. Upon CO_2 absorption, phase change ILs form a two-phase system, namely a CO_2-enriched phase and a CO_2-lean phase. The CO_2-lean phase is a liquid phase and the CO_2-enriched phase is either a liquid or solid phase. Only the CO_2-enriched liquid phase is used for solvent regeneration; thus, the heat required to regenerate the solvent is reduced. Recently, the research on PILs has been mainly focused on ionic liquid-amine composite and pure ionic liquids systems (Lv et al., 2020; Tiwari et al., 2021; Wu et al., 2019; Zalewski et al., 2021).

The blends of diethanolamine (DEA) with one of three IL, [EMIM][Tf_2N], [BMIM][Tf_2N] and [HMIM][Tf_2N], were able to form a solid phase during CO_2 absorption (Hasib-ur-Rahman and Larachi, 2013; Hasib-ur-Rahman et al., 2012; Iliuta et al., 2014). The solid products of this IL-amine composite system are mainly carbamates and alkyl carbonates, and more than 99 % are concentrated in the CO_2 rich phase. The precipitation of the carbamate product allowed CO_2 absorption to proceed beyond the equilibrium limitation exerted on a liquid phase system.

To enhance CO_2 capture capacities, some researchers investigated functionalized ILs in such phase change systems. Triethylenetetramine L-lysine ([TETAH][Lys]) was dissolved in ethanol-water solvent to form a phase change solvent, and the CO_2 capacity reached 2.35 mol CO_2/mol

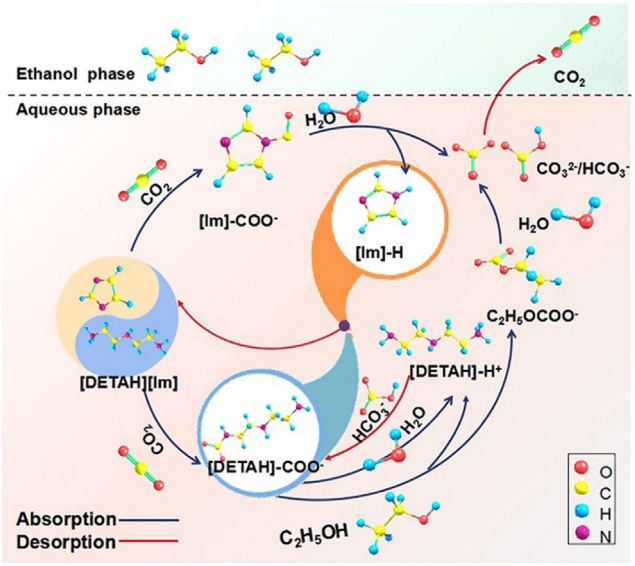

Fig. 3.6. The mechanism of CO_2 capture into [DETAH][Im]-EtOH-H_2O (Lü B, 2021). (For interpretation of the references to color in this figure legend, the reader is referred to the web version of this article.)

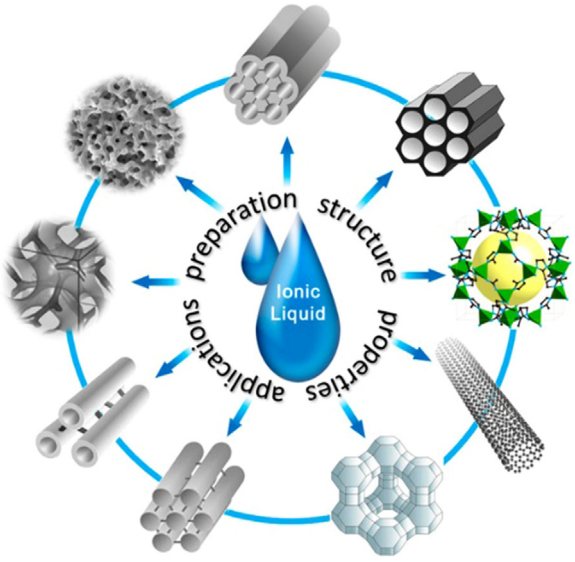

Fig. 3.7. Concept of ILs immobilized by various porous solid matrices (Zhang et al., 2017). (For interpretation of the references to color in this figure legend, the reader is referred to the web version of this article.)

IL as well as the volume ratio of the CO_2-rich phase was 66 % (Huang et al., 2018). At the same time, the regeneration energy consumption (1.29 GJ/t CO_2) and solvent loss during the regeneration process are also reduced. The CO_2 capacity of triethylenetetramine hydrobromide [TETA]Br-PMDETA-H_2O phase change system was high to 2.631 mol CO_2/L at 30 °C and 0.1 MPa, and the regeneration efficiency remained above 95 % after four cycles at 150 °C (Zhou et al., 2020).

Recently, an amino-azolyl dual-functional IL/ethanol/water system ([DETAH][Im]-CH_3CH_2OH-H_2O) for CO_2 capture was constructed via dissolution of a diethylenetriamine-imidazole functionalized ionic liquid ([DETAH][Im]) in the mixed ethanol-water solvent and the CO_2 loading was reported to be 1.548 mol CO_2/mol absorbent whereas the volume only accounted for 32 % (Lü B, 2021). As shown in Fig. 3.6, in the process of absorption, [DETAH][Im] as the main absorbent, cations can react with CO_2 to form carbamates (RN^+COO^-), while azolyl anions can react with CO_2 to form HCO_3^-/ CO_3^{2-}, which ensures the efficient CO_2 trapping ability of the system. At the same time, [Im]-H and ethanol can promote the decomposition of carbamate (RN^+COO^-) and produce easily decomposed HCO_3^-/ CO_3^{2-} and ethyl carbonate products, while leads to the high regeneration efficiency of the rich liquid.

3.1.2.4. Immobilized ILs. Supported ILs (SILs) or encapsulated or nanoconfined ILs (ENILs) are loading or incorporating ILs into the pore structure of solid matrices (Zheng et al., 2021). ENILs are new types of ILs hybrid materials with high gas-liquid contact area and a large amount of ILs is wrapped in the shell structure of the support (Silva et al., 2020). The ILs in ENILs are physically restricted by the cavity of the support, which can keep the complete molecular structure, fluidity and CO_2 affinity of the ILs (Luo and Pentzer, 2020; Santiago et al., 2018). Both SILs and ENILs improve CO_2 adsorption capacity and selectivity by introducing CO_2-philic reactive sites compared with blank porous matrices, so these improvements render SILs and ENILs with great potential for large scale application. In this section, we will provide a comprehensive review of the above two types of immobilized ILs in application in CO_2 capture, emphasizing the alternative porous matrices for supporting or encapsulating ILs (Fig. 3.7).

Porous silica and zeolite are the preferred matrices for ILs considering their porosity, nontoxicity and facile synthesis. The interaction between the pore wall and ILs plays a key role in affecting the properties of the corresponding SILs or ENILs, which depends on both silica surface properties and the functional groups of ILs. The surface of silica and zeolite mainly contains Si, Al, Si-O groups and Si-OH groups, which serve as interaction sites for the supported ILs (Wang et al., 2011; Zhang et al., 2017). For example, Zhu et al. (2018) immobilized imidazolium and phosphonium ILs into porous silica supports and suggested that the CO_2 adsorption through the porous nature of the silica dominated the adsorption behavior of the hybrid adsorbent. Pohako-Esko et al. (2016) prepared the ENILs by encapsulating chitosan containing ILs with nanoporous fumed silica. The results showed that dissolution chitosan in ILs increased the CO_2 adsorption capacity of chitosan about 10 times. In addition, functional groups usually increase the interaction between ILs and CO_2, resulting in increased CO_2 capacity. Zhang et al. (2019) prepared multi-amino functionalized IL adsorbent supported on SBA-15, which exhibited a high CO_2 capacity of 2.15 mmolCO_2/g-adsorbent under 60 °C and 0.015 MPa. Arellano et al. (2015) reported the SBA-15 supported metal-based zinc-functionalized ILs. It was shown that an excellent CO_2 capacity of 4.70 mmolCO_2/g-adsorbent was achieved under 40 °C and 0.015 MPa after incorporating EZT3 into SBA-15. As displayed in Fig. 3.8, the CO_2 capacity of EZT3@SBA-15 is 600 % and 250 % of the pristine ILs and SBA-15, owing to the creation of abundantly accessible CO_2 adsorption sites and the elimination of the viscosity-imposed limitation on mass transfer. Yu et al. (2014) applied NaY zeolite as support to encapsulate [$C_n$mim][Br] (n = 4, 6, 8, 10). It was shown that the encapsulated [$C_n$mim][Br]@NaY was more thermal stable than the neat one. Moreover, the results showed that the CO_2 capacity under 35 °C and 0.015 MPa increased with decreasing length of the side chain on the cation. Besides, immobilization methods affect the performance of the SILs a lot. Zhu et al. (2018) studied the effect of immobilization methods (impregnation and grafting) on the CO_2 selectivity of silica-supported ILs. They found that compared with the impregnated adsorbent, grafting ILs on the support surface caused a weak loss of microporosity, leading to a slight decrease in CO_2 adsorption capacity, and had better recycling. The grafted silica exhibited diffusivities faster than those of the impregnated one, indicating that excessive filling of with ILs was unfavourable for CO_2 diffusion. According to Yin's report Yin et al. (2018), the CO_2 capacity of [C_4mim][BF_4]@SBA-15 synthesized by supercritical fluid method (0.79 mmol CO_2/g-adsorbent) is higher than that of the impregnation method (0.63 mmolCO_2/g-adsorbent) under 25 °C and 0.003 MPa. The authors proposed that the supercritical fluid method

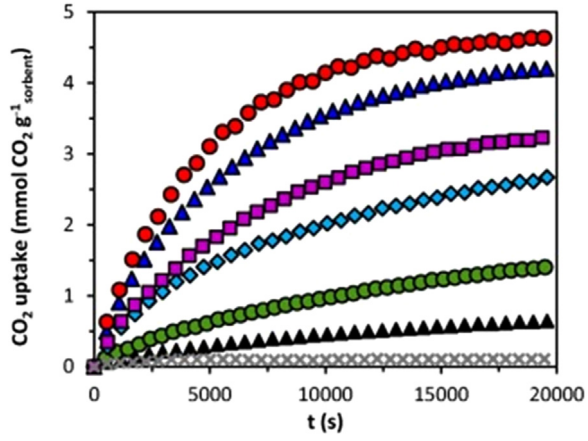

Fig. 3.8. Dynamic CO_2 uptake capacity for SBA-15 (green), nonfunctionalized IL ET (grey), EZT3 (black), and EZT3@SBA-15 with different IL loadings: 10 wt% (cyan), 25 (dark blue), 50 wt % (red), and 80 wt % (pink) (Arellano et al., 2015). (For interpretation of the references to color in this figure legend, the reader is referred to the web version of this article.)

could make ILs more homogeneously distributed on the support and increase the loading amount of ILs, resulting in the increased CO_2 adsorption capacity.

CO_2 adsorption on pristine carbon materials is physical and weak, thus, the adsorption is sensitive to the reaction temperature and CO_2 selectivity is very low (Wang et al., 2011). Immobilizing ILs on carbon materials, such as activated carbons (AC) and carbon nanotubes (CNT), is particularly interesting to overcome the drawbacks of both pristine carbon materials and ILs, and combine their respective advantages. CNTs are investigated the most since their initially empty channel could spontaneously be filled with surrounding ILs in the container to achieve a saturated state. Fig. 3.9 displays one of the typical ENILs, where the $[Me_3NC_2H_4OH][ZnCl_3]$ is encapsulated inside CNTs with different diameters (Chen, S. et al., 2009). Maurya and Singh (2019) compared the CO_2 adsorption capacity of MOFs (InOF-1, UiO-66 and ZIF-8), COFs (COF-108 and COF-300) and carbon based materials (single-wall carbon nanotube SWCNT), and the results showed that SWCNT had the highest CO_2 adsorption capacity. Moreover, the CO_2 adsorption capacity and selectivity further improved by impregnating with ILs. Zeng et al. (2018) synthesized a series of ENILs using carbon nantube (CNT) as shell material, including $[C_4mim][PF_6]$@CNT, $[C_4mim][SCN]$@CNT and $[C_4mim][Tf_2N]$@CNT, to study the effect of anions on the ENILs for CO_2 capture. The results showed that $[C_4mim][PF_6]$@CNT exhibited the highest CO_2 capacity of 1.30 $mmolCO_2$/g-adsorbent under 30 °C and 0.1 MPa, because $[PF_6]^-$ had a stronger interaction with CO_2 than $[SCN]^-$ and $[]Tf_2N]^-$. As a consequence of the reduced pore volume by the larger anion inside CNT, $[C_4mim][Tf_2N]$@CNT showed the low CO_2 capacity. In general, the CO_2 selectivity of SILs and ENILs synthesized by impregnation method is higher than that of the grafting method.

He et al. Wang et al. (2019a) incorporated the phosphonium ILs $[(EtO)_3SiP_{8883}][Tf_2N]$ into activated carbon (AC) by the grafting method and the impregnation method, respectively. The results showed that the CO_2/N_2 selectivity of the adsorbent synthesized by the impregnation method is higher than that of the grafted one. This is because the thin film of ILs formed on the support after impregnation is beneficial for permitting the entry of CO_2 but blocking N_2 (Wang et al., 2019a; Zhu et al., 2018). Besides, Karousos et al. (2016) found that the CO_2/SO_2 selectivity of the AC-impregnated $[C_2mim][OAc]$ is much higher than that of the AC-grafted one under 50 °C and 0.1 MPa. The similar conclusions for other supports (SBA-15 and MOF-177) were also obtained. Graphene oxide was also reported to construct ILs-based solid CO_2 adsorbent. For example, Huang et al. (2019) synthesized the encapsulated imidazolium-based ILs with alkylated graphene oxide as the shell with ILs loading of 80 wt%. The shell material was permeable to CO_2 and allowed CO_2 to reach the inner IL core effectively, resulting in the increased CO_2 adsorption rate. As shown in Fig. 3.10, the time to reach CO_2 adsorption equilibrium for encapsulated ILs was shortened from 271 to 97 min compared with the agitated ILs. This result proves that the encapsulating ILs in special structure can increase the gas-liquid contact area and improves the mass transfer.

Metal-Organic Frameworks (MOFs) are constructed from transition metal ions and bridging organic ligands, which are a new family of porous materials. Impregnation of ILs on MOFs has been proposed as a promising alternative to traditional ILs, because they are non-volatile, non-flammable and thermal stable and therefore are categorized as green adsorbents. Fig. 3.11 shows the schematics of $[C_2mim][SCN]$ incorporated into Cu-BTC. Silva et al. (2015) proposed MOF-supported ILs for CO_2 capture and proved that the incorporation of $[C_4mim][PF_6]$ to Cu-BTC enhanced the CO_2 adsorption capacity compared with pristine MOFs. However, the CO_2 adsorption capacity of $[C_4mim][PF_6]$@Cu-BTC with 5 wt% ILs loading (1.2 mmol CO_2/g-adsorbent) under 25 °C and 0.025 MPa was lower than pure Cu-BTC (1.3 $mmolCO_2$/g-adsorbent). Besides, a further decrease in CO_2 adsorption capacity was observed as the ILs loading increased. This might be caused by channel jam after the incorporation of excessive ILs. Although loading conventional ILs suppressed the CO_2 adsorption capacity of MOFs, it is worth noting that the conventional ILs have a positive effect on CO_2 selectivity (Vicent-Luna et al., 2018). Kinik et al. (2016) incorporated $[C_4mim][PF_6]$ into zeolitic imidazolate frameworks-8 (ZIF-8) and found that the CO_2 adsorption capacity of $[C_4mim][PF_6]$@ZIF-8 (0.10 $mmolCO_2$/g-adsorbent) was twice as high as that of the pristine ZIF-8 under 25 °C and 0.00065 MPa. Furthermore, CO_2 selectivity in CO_2/CH_4 and CO_2/N_2 was improved. Ferreira et al. (2019) found that incorporating $[C_{10}mim][Tf_2N]$@ZIF-8 onto ZIF-8 enhanced the CO_2/CH_4 selectivity of 3.1 under 0.05 MPa, which increased by 35 % compared with the blank ZIF-8. Besides, the nonpolar and long side chain of $[C_{10}mim][Tf_2N]$ strengthened its interaction with CO_2, making $[C_{10}mim][Tf_2N]$@ZIF-8 show better CO_2 separation performance than other ILs@ZIF-8. The functional groups, like amino group and carboxyl group, also play a key role in CO_2 adsorption, considering their interaction with CO_2. For instance, Mohamedali et al. (2018) incorporated the acetate-based ILs into ZIF-8, which enhanced the CO_2 capacity and CO_2/N_2 selectivity. In comparison with the pristine ZIF-8, the CO_2 uptake of $[C_4mim][OAc]$@ZIF-8 was increased by more than seven times, and the CO_2/N_2 selectivity reached 18 times. By increasing the ILs loading to 83.04 wt%, Wang et al. (2019) prepared a $[C_4Py][Tf_2N]$@ZIF-8 adsorbent with 1.36 $mmolCO_2$/g-adsorbent under 30 °C and 1.8 MPa, which increased by 24 % compared with pristine ILs. Mohamed et al. (2019) investigated six ENILs with different ILs and the same ZIF-8 support via Monte Carlo simulations. The results showed that the encapsulation of $[C_4mim][B(CN)_4]$ and $[C_4mim][TCM]$ into ZIF-8 can achieve higher CO_2/N_2 and CO_2/CH_4 selectivity than that of $[C_4mim][Tf_2N]$@ZIF-8. For explanation, the authors proposed that more ILs pairs in ZIF-8 cages provided more CO_2 adsorption sites, consequently the higher CO_2 selectivity.

In addition to the intensively studied rigid inorganic matrices, ILs could also be confined into organic polymer matrices. The application of polymers as porous hosts for ILs gives rise to the easy and convenient formation of flexible membranes, although this system often experiences a loss of mechanical when the loading of immobilized ILs is too high. Polymer-immobilized ILs are usually prepared by either in situ polymerization of monomers in ILs (Guyomard-Lack et al., 2015) or a solvent casting method (Tang et al., 2015; Yang et al., 2015). Several polymers have been explored for supporting ILs, such as polymethyl methacrylate (PMMA) (Uehara et al., 2018; Wang et al., 2013), fluorinated copolymer poly- (vinylidene fluoride-co-chlorotrifluoroethylene) (P (VDF-CTFE)) (Yang et al., 2015), biopolymers (Guyomard-Lack et al., 2015; Trivedi et al., 2015), and

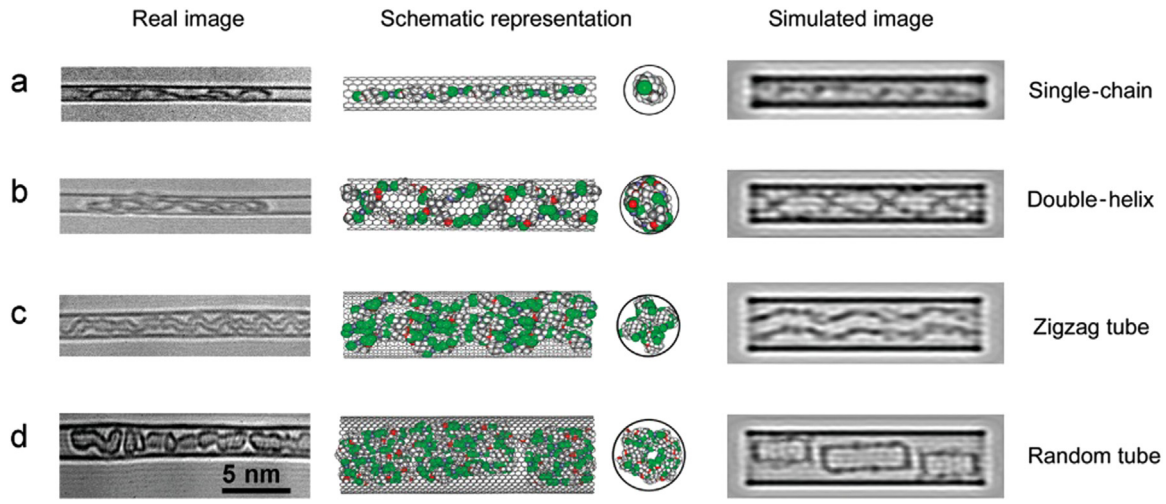

Fig. 3.9. Images of $[Me_3NC_2H_4OH][ZnCl_3]$ encapsulated inside SWCNTs with different diameters (Chen et al., 2009). (For interpretation of the references to color in this figure legend, the reader is referred to the web version of this article.)

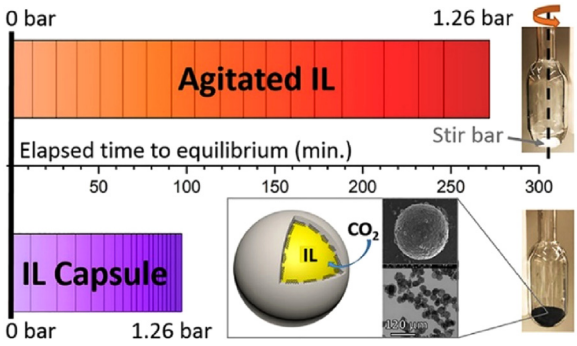

Fig. 3.10. The elapsed time to reach CO_2 adsorption equilibrium and schematic of encapsulated $[C_2mim][Tf_2N]$ (Huang et al., 2019). (For interpretation of the references to color in this figure legend, the reader is referred to the web version of this article.)

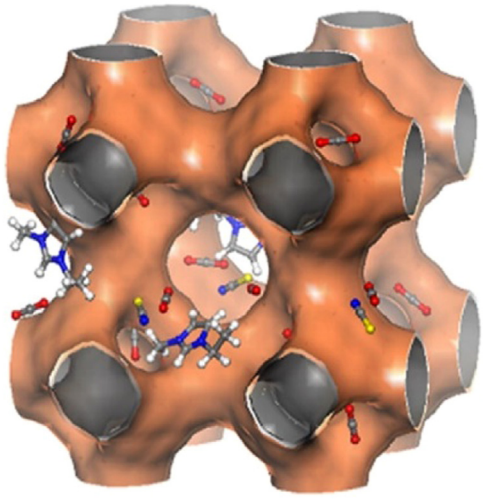

Fig. 3.11. Schematics of $[C_2mim][SCN]$@Cu-BTC (Manuel Vicent-Luna et al., 2013). (For interpretation of the references to color in this figure legend, the reader is referred to the web version of this article.)

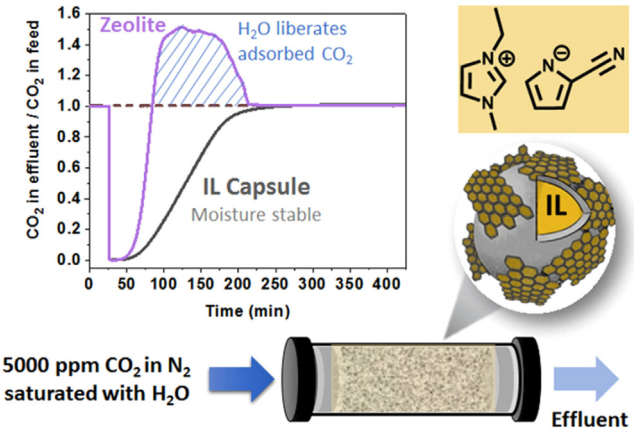

Fig. 3.12. Schematics of encapsulated $[C_2mim][2\text{-}CNpyr]$ with polyurethane and graphene oxide nanosheet shells (Lee et al., 2020). (For interpretation of the references to color in this figure legend, the reader is referred to the web version of this article.)

epoxy resins (Matsumoto and Endo, 2008). Ren et al. (2018) synthesized a series of SILs by impregnating tetramethylammonium glycinate ($[N_{1111}][Gly]$) into four supports, including polymethyl methacrylate (PMMA), titanium oxide (P25), MCM-41 and silica gel (SG). Among them, PMMA-$[N_{1111}][Gly]$ displayed the best CO_2 adsorption behavior in terms of adsorption capacity and rate. The CO_2 adsorption capacity reached up to 2.14 $mmolCO_2$/g-adsorbent at 35 °C. Pristine ILs and supported ILs might exhibit opposite behavior. For instance, Uehara et al. (2018) synthesized a series of polymethyl methacrylate (PMMA) supported ILs, including $[C_2mim][Lys]$@PMMA, $[C_2mim]$ @PMMA, $[C_2mim][Gly]$@PMMA, $[P_{4444}][Lys]$@PMMA, $[P_{4444}]$ @PMMA and $[P_{4444}][Gly]$@PMMA. It was found that $[Lys]^-$ exhibited higher CO_2 capacity than $[Gly]^-$. However, the CO_2 capacity was the opposite when these ILs were supported on PMMA. The $[C_2mim][Gly]$@PMMA had a higher CO_2 capacity (0.88 $mmolCO_2$/g-adsorbent) than $[C_2mim]$ @PMMA (0.63 $mmolCO_2$/g-adsorbent) under 30 °C and 0.0023 MPa. This was because the side chains with amino groups blocked the pore structure of PMMA, which inhibited the entry of CO_2 and thus reduced CO_2 capacity. Lee et al. (2020) combined [C2mim][2-CNpyr] with polyurethane and graphene oxide nanosheet shells to prepare the reactive ENILs. As shown in Fig. 3.12, the CO_2 capacity of this adsorbent was 1.30 $mmolCO_2$/g-adsorbent under 25 °C and 0.0005 MPa. In comparison with the most advanced zeolite 13X, these ENILs had better stability, recyclability and higher CO_2 capacity. Kaviani et al. (2018) investigated the feasibility of ILs encapsulation within a polymeric shell and

Table 3.3
Qualitative comparison between amines and ammonia as CO_2 absorbers.

Characteristics	Amines	Ammonia
CO_2 capture capacity	0.5 mol- CO_2/mol-MEA	1.0 mol- CO_2 /mol-NH_3
Regeneration energy (GJ/t_{CO2})	4.2 (MEA)	< 2.5
Absorption rate	Fast	Slow
Corrosiveness	Severe	Mild
Volatility	Low	High
Absorbent cost	Expensive	Cheap
Advantages	Fast reaction kinetics and high absorption capacity	Absorption at high loading, low corrosion, and degradation, easy regeneration
Disadvantages	High regeneration energy, high corrosion rate, easily oxidized and degraded	Ammonia escape, secondary pollution

evaluated the hybrid adsorbent in CO_2 absorption. The proper choice of chemistry for the polymeric matrix allows the ENILs to outperform the pristine ILs. The improvement was ascribed to the synergistic effect between the fluorine-containing polymer and ILs on the CO_2 adsorption of the ENILs.

3.1.3. New ammonia-based CO_2 capture

As the most feasible post-combustion CO_2 capture technology, the chemical absorption method shows great prospects for industrial applications. Currently, the main industrial method is alcohol-amine solution-ethanolamine (MEA) absorption. However, there are many problems in the practical application, such as high regeneration energy consumption, serious equipment corrosion, and easy solvent volatilization and decomposition (Liang et al., 2016a). Therefore, ammonia-based carbon capture technology may become the main theme of CO_2 capture technology, but its ammonia escape problem is serious. The advent of additives brings a turnaround, and ammonia and additives can promote each other to some extent to improve the CO_2 absorption rate of ammonia. Ethanol as an additive excels in all aspects, and a new ammonia-based carbon capture technology (ammonia-ethanol hybrid absorber) (Zhang et al., 2019) was born. Due to the high corrosiveness of MEA and regeneration problems, ammonia-based CO_2 capture is a viable carbon capture technology over conventional amine-based CO_2 capture technology, technically and economically.

3.1.3.1. Ammonia-based CO_2 capture technology. Reliable absorbents for low concentration CO_2 capture are amine- and amino-based CO_2 capture technologies. The thermochemistry of CO_2-NH_3-H_2O systems with ammonia as an alternative to amine-based absorbers is reasonably well understood, including vapour-liquid-solid equilibria, species formation, absorption heat, reaction kinetics, and thermodynamic model development. Many thermodynamic models based on CO_2-NH_3-H_2O systems were developed by Thomsen and Rasmussen (1999), and Que and Chen (2011), which accurately predicted the gas-liquid-solid phase equilibrium. Fig. 3.13 shows the typical post-combustion ammonia carbon capture system and the proportion of electricity consumption of each part of the process. The existing typical processes of this technology are as follows: Alstom refrigerated ammonia process, Powerspan ECO$_2$ process, CSIRO ammonia process of Australian Federal Science and Industry Commission, RIST ammonia process of Korea Industrial Science and Technology Research Center, etc.

During CO_2 capture, ammonia reacts with carbon dioxide (aq) to form carbamate, which is immediately deprotonated to give carbamate. Due to the reversal of the equilibrium as the pH changes with continued CO_2 uptake, the carbamate eventually decomposes to produce protonated ammonia and bicarbonate. The carbamate equilibrium constant of MEA is much higher than that of ammonia, indicating that the yield of ammonia-derived carbamate is lower than that of the equivalent monoethanolic ammonium carbamate ammonia possesses a higher CO_2 capture capacity compared to MEA. Based on equilibrium calculations (Darde et al., 2009), the cold ammonia method resulted in significantly lower energy consumption in the regeneration step than the amine-based method. Table 3.3 shows a qualitative comparison between amine and ammonia as CO_2 capture absorbents. Ammonia-based CO_2 capture technology outperforms conventional amine-based CO_2 capture technology in terms of technical and economic advantages, with high CO_2 absorption capacity, low heat of absorption reaction, and less susceptibility to downgrading by O_2 in the flue gas, low corrosiveness, and low feedstock prices (Darde et al., 2009; Pellegrini et al., 2010).

3.1.3.2. Ammonia escape. While ammonia solution as a CO_2 absorber has the above-mentioned significant advantages, there are also common shortcomings and deficiencies in the current application.

1) Low CO_2 absorption rate, the reaction rate of CO_2 absorption by ammonia at the same temperature is about an order of magnitude lower than that of MEA.
2) Serious ammonia escape, the concentration of escaped ammonia during CO_2 absorption can be as high as 2 vol.%, and the concentration of escaped ammonia during rich liquid regeneration reach 10–20 vol.%; with 14 % ammonia, for example, the total ammonia loss is as high as 43.1 % (Jilvero et al., 2015).
3) High energy consumption for desorption and regeneration and up to 4-4.2 MJ/kgCO_2 for regeneration in the pilot experiment of ammonia decarbonization (Yu, 2018).

The main drawbacks of ammonia-based CO_2 capture technology are slower absorption kinetics and higher volatility than amine solutions. The ammonia escape mechanism is shown in Fig. 3.14, and the ammonia escape problem is becoming one of the most critical technical and economic challenges in the commercial application of ammonia-based CO_2 capture technology. A high NH_3 escape rate also reduces the concentration of NH_3 in the solution, thus reducing the CO_2 uptake capacity (Wang et al., 2018). In addition, ammonia can leak into the air, thus causing serious secondary pollution. Therefore, it is imperative to develop effective methods to suppress ammonia leakage or recover the leaked ammonia. Optimizing process parameters through acid and aqueous washing, membrane technology, additives and accelerators, and applying cold ammonia processes and mixed salts are common strategies to control ammonia escapes.

3.1.3.3. Ammonia-ethanol mixture absorber. To solve the ammonia escape problem, many scholars have proposed the modification of CO_2 absorption by ammonia solutions using additives, which inhibit not only NH_3 escape but also improve CO_2 absorption performance. Table 3.4 provides the results of studies on CO_2 capture by ammonia additive in the last five years. Gao et al. (2015), Zhang et al. (2019) have shown significant advantages of using ethanol as an additive in various aspects. Ammonia and ethanol can promote each other to improve the CO_2 absorption rate of ammonia (Yang et al., 2014). However, there is a slight contradiction between the hybrid absorber increasing the absorption rate and inhibiting ammonia escape (Ma et al., 2016). The additive mainly binds the free ammonia in the ammonia solution through hydrogen bonding. It thus inhibits ammonia escape, but when the hybrid absorber absorbs CO_2, the additive does not achieve effective ammonia

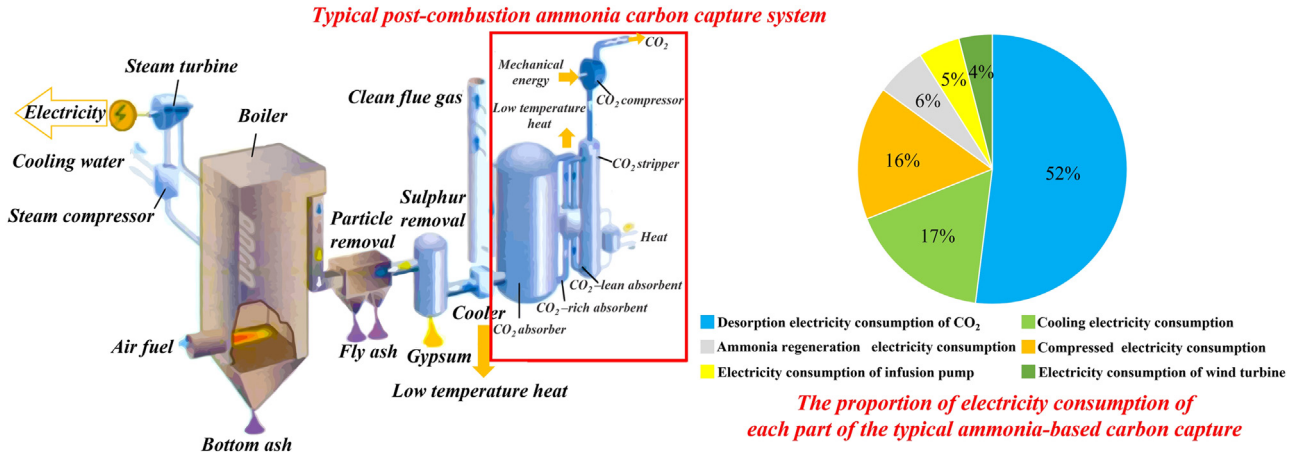

Fig. 3.13. Typical post-combustion ammonia-based carbon capture system and the proportion of electricity consumption of each part of the process diagram (Yu and Wang, 2015). (For interpretation of the references to color in this figure legend, the reader is referred to the web version of this article.)

Table 3.4
Comparison of ammonia CO_2 capture performance with different additives.

Parameters	Additives	CO_2 loading (mol/mol)	CO_2 removal efficiency	Reference
8.22 mol NH_3/kg H_2O, T = 27 °C	1.5 mol K_2CO_3/kg H_2O	0.4	90 %	(Pachitsas and Bonalumi, 2022)
6.31 mol NH_3/kg H_2O, T = 27 °C	1.0 mol K_2CO_3/kg H_2O	0.3	90 %	
4 M NH_3, T = 25 °C, CO_2 = 12 vol%	0.25 mol Piperazine /kg H_2O	0.43	85.0 %	(Jiang et al., 2018)
2.5 M NH_3, T = 25 °C	1.50 M K_2CO_3	0.35	>90 %	(Lillia et al., 2019)
0.85 mol/L NH_3, T = 20 °C	Ethanol	-	1.64 kg/kg	(Gao et al., 2015)
3 mol/L NH_3, T = 26 °C	Capacitive deionization	0.24	87.0 %	(Ullah et al., 2017)
3.6 wt.% NH_3, T = 25 °C	20 mL microalgae	-	76.8 %	(Song et al., 2019a)
5 wt.% NH_3, T = 20 °C, CO_2 = 15 vol %	0.1 mol/L Piperazine /kg H_2O	-	60.0 %	(Xu et al., 2019)
247 mg/L NH_3, T = 25 °C, CO_2 = 5 vol %	423 mg/L microalgae	17 mg/L	87.0 %	(Song et al., 2019c)

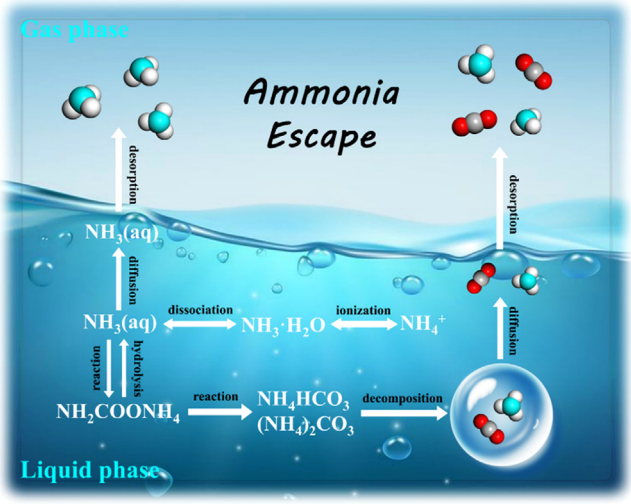

Fig. 3.14. Schematic diagram of ammonia escape. (For interpretation of the references to color in this figure legend, the reader is referred to the web version of this article.)

release, thus decreasing the liquid-phase partial pressure of free ammonia, which adversely affects the absorption process. Ethanol as an additive does not show significant differences in this regard. In addition, Pellegrini et al. (2010) pointed out that partial replacement of water in chemical absorbents by ethanol solvents with a smaller specific heat can significantly reduce the regeneration energy consumption (the specific heat of anhydrous ethanol is 2.4×10^3 J/ (kg- °C), which is only 57 % of that of water, i.e., the same mass of solvent can save nearly 40 % of the heat by increasing the same temperature), which shows that "ammonia-ethanol mixture (i.e., the same mass of solvent can save nearly 40 % of the heat by increasing the same temperature), which shows that the "ammonia-ethanol mixture" has significant advantages for CO_2 absorption and capture (Zhang et al., 2019).

The solubility of the products in the reaction process of CO_2 absorption by ammonia is known. Ammonium carbamate is soluble in water and soluble in ethanol, and ammonium bicarbonate is soluble in water-insoluble in ethanol. As reported (Gao et al., 2015; Zhang et al., 2019), the ammonia carbon capture process could be controlled to a low carbonation degree (<0.5) (Fig. 3.15) to ensure the efficient carbon capture rate of the system and adopted a new decarbonization and regeneration process of "ammonia-ethanol mixed absorption leading to solvation crystallization and crystal regeneration instead of rich liquid regeneration." It has been proved that the ammonia-ethanol liquid-phase mixed absorption of the CO_2 dissolution crystallization process is mainly precipitated by NH_4HCO_3 crystals.

The regeneration tower only needs to heat the NH_4HCO_3 crystal products, indicated in Fig. 3.16. NH_4HCO_3 crystals could be decomposed into CO_2, NH_3, and H_2O above 36 °C and completely decompose at 60 °C. This can greatly reduce the system's energy consumption by eliminating the energy consumed by heating and vapourizing the solvent during conventional liquid-rich desorption.

3.1.3.4. Applications and outlook. The mainstream CO_2 liquid-phase chemical absorption method is difficult to avoid high regeneration energy consumption, degradation problems, and high corrosiveness. The discovery of ethanol additives has further improved the techno-economic of the amino CO_2 absorption system. The new ammonia carbon capture technology ("ammonia-ethanol hybrid absorber") shows great potential in carbon capture. With the rapid development of CO_2 solid-phase adsorption technology, biochar is considered the most promising solid CO_2 adsorbent for application (Creamer et al., 2014). Suppose biochar particles are used as modified materials to enhance the liquid-phase mass transfer characteristics. In that case, their stronger

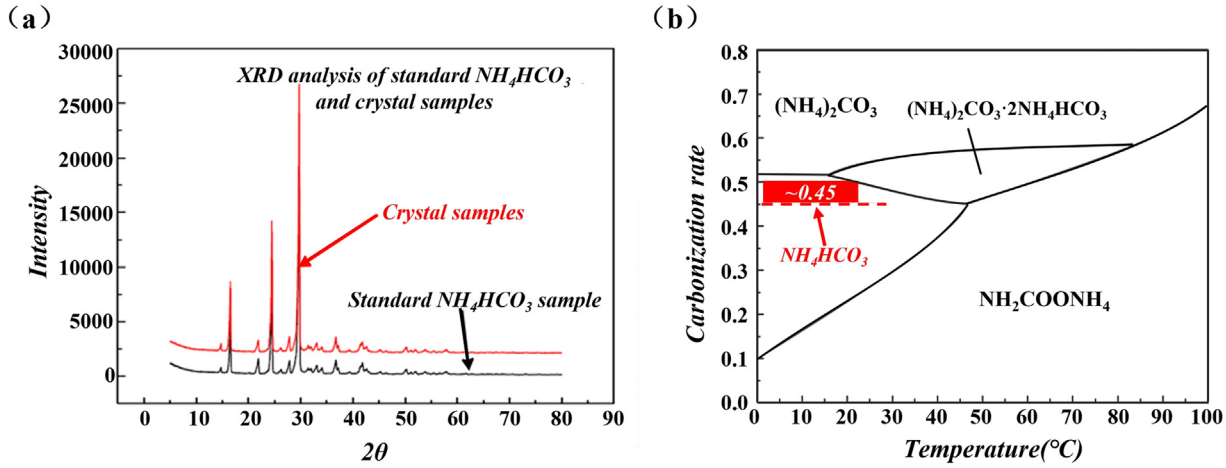

Fig. 3.15. (a) Crystal and standard NH_4HCO_3 sample analysed by X-ray diffractometer (b) The effect of carbonization rate on the "carbon balance" of ammonia-based carbon capture system (Gao et al., 2015). (For interpretation of the references to color in this figure legend, the reader is referred to the web version of this article.)

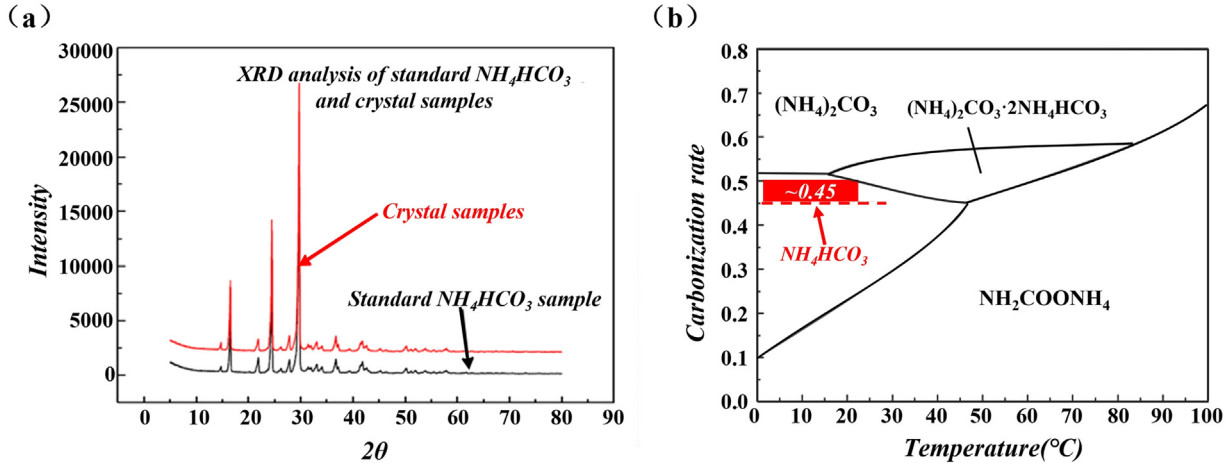

Fig. 3.16. The crystal sample after reaction (Gao et al., 2015). (For interpretation of the references to color in this figure legend, the reader is referred to the web version of this article.)

CO_2 diffusion characteristics can be fully utilized to improve the overall carbon-negative degree and CO_2 capture rate of the CO_2 capture system, enhance the solid-liquid two-phase mass transfer enhancement and suppress ammonia escape (Zhang, et al., 2022). The high-quality rice husk nano-pore carbon was prepared using agricultural waste rice husk, combined with the new ammonia CO_2 capture technology to improve the overall performance of carbon dioxide capture. In addition, the intermediate product NH_4HCO_3 from the new ammonia CO_2 capture and the intermediate product K_2SiO_3 from the preparation of rice husk nano-pore carbon were used to prepare nanoscale silica through process regulation, which significantly solved the problems of CO_2 capture product dissipation, agricultural waste pollution, and high-value product preparation. The production of high-value products - rice husk nano-pore carbon and nano-grade silica - also helps form an integrated system of energy and product laddering and integrated removal of various pollutants, which provides a new idea for a CO_2 capture system.

3.2. Low-temperature solid sorbents

3.2.1. Cyclic adsorption processes for carbon capture

Advanced sorbents, process design and swing technologies are the fundamentals for adsorptive carbon capture technologies. The adsorbents and their shaping and pellet sizes have been demonstrated to have a significant impact on the separation performances (Hedin et al., 2013; Zapata Ballesteros et al., 2022). Bed design such as multilayer packing has been employed to selectively pre-remove minor impurities including SO_x, NO_x and H_2O, with part of the adsorbents being replaced by activated alumina, silica gel or zeolites (Hefti and Mazzotti, 2018).

One of the most challenging tasks in adsorption is the ranking of the performances of different adsorbents, in which isotherm based selectivity and working capacity are often unsatisfying (Khurana and Farooq, 2016a). Simplified cycles have been used for adsorbent screening, which provides rapid (seconds to minutes) solutions to pre-select suitable adsorbents for various functions (Ajenifuja et al., 2020; Gutierrez-Ortega et al., 2022; Maring and Webley, 2013b; Rajagopalan et al., 2016; Subramanian Balashankar et al., 2019; Wang, Jiajun et al., 2021). Moreover, efficient engineering processes are the key to the development of operable and economical adsorption technologies. The fine-tuning of both adsorbents and processes is crucial to commercializing adsorption technologies (Zanco et al., 2017).

Almost all adsorbents appear to have a strong affinity to CO_2 over other major components, i.e., N_2 and O_2, due to the large quadrupole moment and high polarizability of CO_2, which means CO_2 is always the heavy component that is adsorbed and regenerated from adsorbents. CO_2 selective adsorbents are also favoured due to the low concentration of CO_2 in carbon capture applications, e.g. confined space (0.7 %) (Zhan et al., 2020), air (0.04 %), flue gas in natural gas fired (3–5 %) and coal

fired (10–15 %) power plants. The target of these cycles is to recover the heavy product at high purities.

CO_2 capture using adsorption can be classified as temperature swing adsorption (TSA) and pressure swing adsorption (PSA) based on their dominant regeneration mechanism, i.e. increase in temperature or decrease in pressure (Webley, 2014). Other effects must also be taken into account, such as heat and mass transfer, pressure drop, and energy consumption, and there is still no straightforward way to design regenerative cycles for adsorption processes (Subramanian Balashankar et al., 2019).

3.2.1.1. Pressure/vacuum swing adsorption (P/VSA). P/VSA cycles have been developed over the last several decades through various applications, reported by Skarstrom (1960) for gas mixture separation, Sircar and Kratz (1988) for hydrogen purification, Grande et al. (2010) for propane/propylene separation. P/VSA is the most frequently studied for the adsorptive carbon capture process, with multiple pilot scale demonstrations reported (Cho et al., 2004; Krishnamurthy et al., 2014b; Wang et al., 2013a,b). PSA cycles are the most suitable for precombustion conditions as the feed gas is often at high pressures, while VSA is more often used for post-combustion, where vacuum evacuation is employed for the regeneration of adsorbents. Adsorption at high pressure and regeneration under vacuum may also be considered to enhance the working capacity of adsorbents. A typical P/VSA cycle includes two necessary steps: adsorption at high pressure and desorption at low pressure, with a few modifications available to improve separation performances and process efficiencies, such as depressurization, purge, pressure equalization, repressurization.

The high flexibility of PSA makes it possible to meet the specifications of feed conditions and desired separation targets, through one or multiple stages. However, it seems a single stage PSA struggles to reach the > 95 % CO_2 purity target with > 90 % recovery from a 15 % feed gas, which often requires extremely low vacuum conditions (Khurana and Farooq, 2016b; Ntiamoah et al., 2015; Yan et al., 2016). Another concern regarding P/VSA is that the energy consumption is often underestimated as high grade energy (electricity) must be used for pressure variation (Zhao et al., 2017b), where a thermal energy conversion is necessary to compare its performance with the benchmark amine processes fairly.

Dual reflux pressure swing adsorption (DR-PSA), also known as duplex PSA, is a special format of PSA in which the feed position is not constrained to the end of an adsorption column. An adsorption column can then be divided into a rectifying section and an enriching section, and two high purity product streams can be achieved simultaneously (Diagne et al., 1994; Leavitt, 1992). DR-PSA cycles consist of four fundamental steps, i.e., adsorption/feed, pressurization, purge and blowdown. It can be applied via four basic configurations, i.e., DR-PL-A, DR-PH-A, DR-PL-B and DR-PH-B, depending on the feed position and purged streams (Guo et al., 2021; Kearns and Webley, 2006a,b). Here, PL and PH refer to the feed injected into the high- and low-pressure column, respectively; A and B denote the types of the purged gas, adsorbate (heavy component) and less adsorbed component, respectively.

DR-PSA has been a rapidly developing process in the past two decades, with many researchers dedicated to providing process optimization methods, such as the Triangular Operating Zone (TOZ) (Rossi et al., 2020), Capacity Ratio (ℂ) (May et al., 2017) and feed position (z_{feed}) analysis (Guo et al., 2021). Zhang et al. achieved 99 % CO_2 purity with 99 % recovery from a 15 % feed gas in a simulated work (Li et al., 2016). In a pilot investigation, Wawrzyńczak et al. compared a 9-step DR-PSA with an 8-step PVSA cycle with a 4-bed system using 540 kg activated carbon as adsorbents (Wawrzyńczak et al., 2019). The DR-PSA cycle showed a 14 % higher CO_2 purity and 28 % higher energy costs, 29 % lower CO_2 recovery and 30 % lower productivity. This may be due to the cycles are not fully optimized, such as feed position, pressure ratio and purged quantity (Bhatt et al., 2017, 2018).

3.2.1.2. Temperature swing adsorption (TSA). TSA cycles regenerate the adsorbents via lifting the column temperature. The packed adsorption column also serves as a heat exchanger packed with adsorbents (Masuda et al., 2021). Researchers have explored multiple ways to heat the entire column to the desired temperature, via direct or indirect heating. TSA has drawn great interest in carbon capture from power plants, given that available waste heat reuse is an advantage. For example, the temperature of low grade heat in power plants, such as waste steam and flue gases, can be over 300 °C, which perfectly suits the regeneration of adsorbents (Leppänen et al., 2014; Zanco et al., 2017).

Direct heating often refers to the adsorbents in direct contact with heating media such as hot steam, air or CO_2. As direct heating using nonadsorbing gases leads to the dilution of CO_2 products, hot steam or CO_2 product are preferred to serve as the heating sources (Ntiamoah et al., 2016). Indirect heating does not incur the dilution problem and refers to heating sources such as heating/cooling jacket and inner heating/cooling pipes, which often requires a less adsorbing sweep gas (N_2, air or flue gases) to recover the desorbed CO_2.

The basic step sequence of a TSA cycle is adsorption, heating and regeneration, and cooling, where CO_2 product purity can rarely reach the 95 % target in carbon capture applications. Several novel design concepts have been employed to achieve better separation performances. For example, a purge using feed prior to adsorption can push the regenerated CO_2 out of bed to enhance recovery; a purge step using the CO_2 product prior to the heating and regeneration step can push the free gas out of bed to increase the product purity; other internal purge steps can also be used to integrate the heat and reduce energy consumptions, e.g., a novel 5-step cycle consists of adsorption, heavy reflux using the light purged gas stream, desorption/heating, light purge, cooling (Joss et al., 2017). Mazzotti et al. compared four TSA cycles and concluded that the cycle with purge and recycle steps outperformed others, reaching the DOE target of 95 % CO_2 purity with 90 % recovery from flue gases containing 12 % CO_2 (Joss et al., 2017; Peh et al., 2022). The major issue with TSA is the long time required for heating and cooling, resulting in the long cycle time ranging from minutes to days. Hence, the number of columns and the time schedule of TSA cycles are crucial in assessing their separation performances.

3.2.1.3. Pressure temperature swing adsorption (PTSA). Separation performance is extremely sensitive to the regeneration temperature and evacuation pressure, which is dependent on the properties of adsorbents (Plaza and Rubiera, 2019; Zhan et al., 2021) The productivity of conventional PSA cycles is often reduced due to the exothermic nature of adsorption, i.e., high bed temperature during adsorption and low bed temperature during desorption (Plaza and Rubiera, 2019). Hybrid cycles by combining the effects of temperature and pressure, i.e., pressure temperature swing adsorption (PTSA), may be capable of solving this problem and allowing for milder regeneration conditions which are easier to achieve for large scale CO_2 capture plants, i.e., lower regeneration temperature compared with TSA and higher desorption pressure than PSA (Wang et al., 2012; Wurzbacher et al., 2011). Such lower temperature is easier to be integrated with waste heat in power plants than conventional TSA. Hence, PTSA possibly requires lower energy consumption and achieves higher process efficiency/productivity, although with higher cycle complexity (Su and Lu, 2012).

A simple PTSA process consists of the following steps: adsorption, heating and depressurization or evacuation, cooling and/or pressurization (Wang, et al., 2021). More complex cycles are also reported, such as a 7-step cycle, including adsorption, pressure equalization, depressurization, vacuum heating, vacuum cooling, pressure equalization, and pressurization (Zhan et al., 2021). Cooling water may also be introduced to maintain the column temperature during the adsorption step to avoid the capacity drop due to the released heat of adsorption. Tsutsumi et al. reported a 40 % energy penalty reduction via energy recovery measures such as pressure recovery through an expander and adsorption heat recovery through a chemical heat transformer (Song et al., 2016). Plaza

and Rubiera simulated a PTSA carbon capture process in an 820 MWe power plant using a desorption temperature of 80 °C and pressure of 5 kPa. Results showed the energy penalty is 2.41 MJ (heating)/kg CO_2 and 1.15 MJ (evacuation)/kg CO_2, which is mainly due to the extremely low desorption pressure (Plaza and Rubiera, 2019).

3.2.1.4. Electric swing adsorption (ESA). ESA has been reported as commercially viable for volatile organic compounds (VOC) removal (Subrenat and Le Cloirec, 2006). Adsorptive carbon capture using ESA aims to solve the lengthy heating time issue related to conventional TSA and improve the overall productivity of adsorbents (Zhao et al., 2019), in which rapid and homogeneous heating can be achieved via electrification by Joule effect (or Ohmic heating). The temperatures of adsorbents can be raised to 70 °C in 22 s at a potential of 24 V (Mendes et al., 2021) or 10 V (Pereira et al., 2022), 101 °C in 90 s at a potential of 60.5 V (Zhao et al., 2019), and 150 °C in less than 30 s at a potential of 8 V (Verougstraete et al., 2022). Even though the electric power for ESA is of a higher exergetic energy format than thermal energy required by TSA, such low voltage requirements in ESA cycles offer an opportunity to integrate with renewable electricity.

A simple operational ESA cycle consists of the following steps: adsorption, electrification, rinse/purge or evacuation, and cooling. More complex cycles have also been demonstrated for high CO_2 purity and recovery, with extra internal rinse, purge and depressurization steps (Grande et al., 2009); 89.7 % purity and 72.0 % recovery were achieved from 3.5 % CO_2 flue gases.

ESA cycles require that adsorbents must be conductive, such as activated carbons, hybrid adsorbents combining zeolite and activated carbon, and uniform adsorbents to allow heat to be transferred homogeneously (Zhao et al., 2018). Uneven heating may lead to hot spots and damage the adsorbents due to partial overheat. Three-dimensional (3D) printing is an ideal methodology to replace conventional pelleting, which shows lower pressure drop, no fluidization and better heat transfer. This also provides a pathway to create hybrid adsorbents, which may combine the best properties of multiple adsorbents, CO_2 uptake capacity, CO_2/N_2 selectivity and mass transfer coefficient. It should be noted that the cooling step still requires quite a significant time, which may be a major hurdle for its application. According to Grande et al., electric heating only accounts for 1.5 % of the cycle time (2225 s) (Lillia et al., 2018), with enormous time put into the cooling of adsorbents.

3.2.1.5. Rapid pressure or temperature swing adsorption (RPSA/RTSA). A 600 MWe coal power plant emits 500 m^3/s of flue gas with 13 % CO_2 (Merkel, et al., 2010). Hence, it is critical to develop economical CO_2 separation technologies to handle flue gases with massive flow rates. Rapid swing adsorption shows its superiority as CO_2 capture from flue gases is often at a very large scale, and the structuring of adsorbents becomes crucial to allow a high flow rate and avoid sorbent pulverization. The cycle sequence in rapid swing adsorption is similar to conventional ones, with modifications in different aspects. In a reported rapid pressure swing adsorption process, the total cycle time is 18 s, which employs the same cycle as conventional PSA, i.e., adsorption (8 s), desorption (8 s), purge (1 s) and repressurization (1 s) (Luberti et al., 2017). The superficial velocity is as high as 1.6 m/s, which is much higher than conventional PSA cycles (0.1–0.5 m/s), resulting in a significant pressure drop of 16 kPa at the column length to diameter ratio of 1:1.

Rapid temperature swing adsorption (RTSA) can be achieved via direct heating using hot steam, which involves quick heating through the latent heat and adsorption competition between water vapour and CO_2. A hot air stream is essential to remove the condensed steam right after CO_2 regeneration (prior cooling) to avoid a significant capacity drop. The cycle time can also be reduced to 20–330 s, which is much lower than conventional TSA cycles (≥15 min) (Verougstraete et al., 2020). RTSA may also be achieved using hybrid materials, which employ a hollow fiber embedded with porous adsorbents, as demonstrated by Lively et al. (2009). Such hollow fiber adsorbent performs as both a heat exchanger and gas contactor (or "adsorbing heat exchangers" (Lively et al., 2010)), for which 90 % adsorption occurs within the first 2 s (Lively et al., 2012), and thermal equilibrium can also be achieved within seconds. A high linear velocity of 1.6 m/s was also tested (Lively et al., 2012). This setup also enables internal cooling during adsorption so the adsorption enthalpy can be quickly removed to maintain a high CO_2 uptake capacity. The hollow fiber RTSA cycles have also been extended to air separation by integrating LiX zeolites on thermally stable polymers (Sujan et al., 2018).

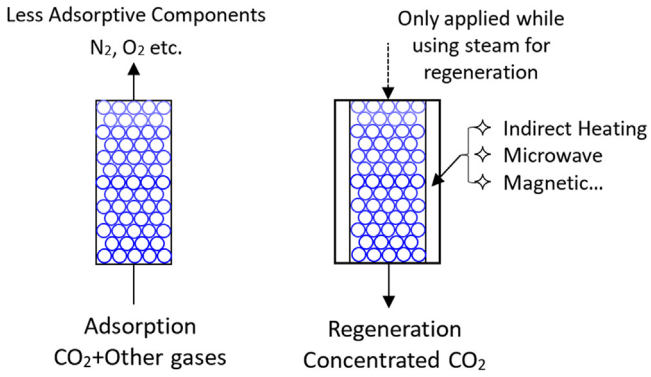

Fig. 3.17. A simplified schematic adsorptive cycle. Adsorption occurs at high pressure and/or low temperatures. Regeneration occurs at low pressure and/or high temperatures, where the heating can be achieved by heat conduction, Joule effect, magnetic effect, microwave etc. (For interpretation of the references to color in this figure legend, the reader is referred to the web version of this article.)

Other novel design concepts are also seen in literature such as the rotary adsorption system for MOF based carbon capture systems (Lin et al., 2021), fin coil heat exchangers filled with an adsorbent that allows internal heating and cooling (Masuda et al., 2021, 2022) and structured honeycomb carbon monolith adsorbents which can tolerate high linear velocities of flue gases as high as 3.4 m/s (Verougstraete et al., 2020).

3.2.1.6. Other swing concepts. Hybrid cycles combining two or more of the above mentioned swing technologies have been widely investigated, such as those combining ESA and VSA, namely VESA (Zhao et al., 2019); ESA and TSA, namely TESA (Lillia et al., 2018); ESA ad VSA, namely VESA (Zhao et al., 2019). Different adsorption column configurations are also considered including fixed beds, fluidized beds, moving beds and simulated moving beds to improve the separation performances (Yi et al., 2007). Fixed beds are still the most commonly used configuration due to their simplicity and low requirement in the mechanical strength of adsorbents.

Novel swing concepts are continuously proposed to improve the energy efficiency and separation performances of adsorptive carbon capture technologies. Microwave, commonly interpreted by three mechanisms, i.e. ionic conduction, dipolar rotation of polar molecules and dielectric polarization (Lee et al., 2019), has been applied to the regeneration of adsorbents using a hybrid adsorbent of graphene oxide and MIL-91 (Muschi et al., 2021), in which desorption occurred faster and under lower temperature, i.e. 50 °C for 150 s using microwave versus 80 °C for 215 s using conventional electrical heating. High microwave absorption allows temperature increases through energy dissipation. Sound assisted adsorption/desorption is reported to enhance kinetics and cut overall energy consumption (Ammendola et al., 2015; Raganati et al., 2020). Magnetic induction swing adsorption (MISA) has also attracted interest due to its high energy efficiency (Bellusci et al., 2021; Li et al., 2016a). However, these concepts are rather immature and needs more exploration.

In summary, adsorptive swing technologies can be as simple as shown in Fig. 3.17, which consists of an adsorption and a desorption step. The adsorption step occurs at high pressure and/or low temper-

atures. Regeneration occurs at low pressure and/or high temperatures. Any form of radiation may be used for adsorbents regeneration as long as the adsorbents can absorb the form of radiation, such as evacuation (PVSA), heating (TSA), Joule effect (ESA), magnetic effect (MSA), microwave (MCSA) etc. However, efficient processes, which can heavily impact the performance of cyclic adsorption processes, are much more complicated than the two-step cycles. There is yet no best way to design and optimize such processes.

3.2.2. MOF-based materials for CO_2 capture

Metal organic frameworks (MOFs) are deened to be the most promising materials for CO_2 adsorption due to their high porosity, large specific surface area, designability, tunability, rich spatial topology, and unsaturated metal sites. Zn (BDC) became the first reported MOFs material for CO_2 adsorption (Li et al., 1998), and then Yaghi synthesized a series of MOFs to systematically investigate the effects of structural and porous attributes on CO_2 adsorption performance (Millward and Yaghi, 2005). The results showed that the higher pressure and larger specific surface area were favourable for CO_2 adsorption, which opened the door to explore MOFs in the field of CO_2 adsorption capture and separation. Several MOFs have been prepared and commercialized on a large scale, such as MOF-177, HKUST-1, ZIF-8, UIO-66, and MIL-127 (Gargiulo et al., 2020).

3.2.2.1. Influence of pressure on CO_2 capture. The adsorption of gases can be divided into high and low pressure. For high pressure condition, CO_2 adsorption is generally related to the specific surface area and pore volume of MOFs. Hu et al. (Hu et al., 2013) studied the behavior of ZIF-8 for high pressure CO_2 adsorption using situ FTIR spectroscopy, the results showed that the chemical and mechanical robustness of the framework formed by the relatively stiffer metal centered tetrahedrons as joints but with flexible linkers makes ZIF-8 a promising agent for the storage of CO_2 at high pressure conditions. Arstad et al. (2008) synthesized USO-2 using Ni $(NO_3)_2$ as a metal ion source and 1,4-phenylene terephthalic acid (1,4-H_2BDC) as a ligand, which increased CO_2 adsorption at 25 atm compared to atmospheric pressure adsorption by 46 %. Qasem et al. (2018) prepared MOF-177, which has excellent storage capacity at high pressure (≥10 bar) and gradually increases its adsorption capacity with increasing external pressure, from 0.07 kg kg^{-1} at 5 bar to 1.58 kg kg^{-1} at 30 bar, with a 22-fold increase in its adsorption capacity. Llewellyn et al. (2008) prepared mesoporous MIL-101 and found a high adsorption capacity of 40 mmol g^{-1} by activating it with ethanol and KF at 5 MPa and 303 K. To further increase the surface area of the adsorbent material, Farha et al. (2010)) designed a new MOF material (NU-100) with Cu^{2+} as the metal center and hexatopic carboxylate as the organic ligand through calculation and simulation, and successfully prepared it through experiments. The MOF has a super high surface area of 6143 m^2 g^{-1} and the total pore volume is 2.82 cm^3 g^{-1}, and its CO_2 adsorption capacity reaches 2315 mg g^{-1} at 40 bar and 298 K. Furukawa et al. (2010) synthesized MOFs using Zn^{2+} as the metal center and various carboxylate organic ligands, among which MOF-210 has a larger surface area (6240 m^2 g^{-1}) and a large pore volume (3.6 cm^3 g^{-1}), so that its adsorption capacity also reaches an impressive values of 2870 mg g^{-1} at 50 bar and 298 K. In addition to the selection of ligands with longer molecular chains, the surface area of MOFs can also be increased by introducing defects. Wu et al. (2013) adjusted the degree of defects by adding different concentrations of acetic acid to the UIO-66 system and setting different reaction times, and the porosity of UIO-66 increased dramatically with increasing dosage and longer reaction times, which results in an increase in pore volume from 0.44 cm^3 g^{-1} to 1 cm^3 g^{-1} and an increase in surface area from 1000 m^2 g^{-1} to 1600 m^2 g^{-1}. Moreover, the hydroxyl group on the surface of UIO-66 was found to contribute to the adsorption of CO_2 due to the presence of the Columbic interactions between the negatively charged O (of CO_2) and the positively charged H (of the -OH group), making the CO_2 uptake in the hydroxylated MOF (2.50 mmol g^{-1}) at 300 K and 1 bar is more than 50 % higher than that in the dehydroxylated MOF (1.60 mmol g^{-1}).

Compared with high-pressure adsorption, low-pressure adsorption is more common in industrial production and is mainly used to capture CO_2 from combustion exhaust gases. Low-pressure adsorption is mainly related to the heat of CO_2 adsorption, which can be improved by introducing unsaturated metal sites, ligand group modification, and introducing defects.

(i) Introduction of coordinated unsaturated metal sites and ion doping. During the preparation of MOFs, solvent molecules will be coordinated with metal sites, and the unsaturated metal sites are obtained by removing solvent molecules through the solvent exchange, vacuum heating, and freeze-drying to enhance the adsorption capacity of MOFs. MOF-74 is a common low-pressure CO_2 adsorption material, which is prepared from divalent metal ions (Fe^{2+}, Co^{2+}, Ni^{2+}, Mg^{2+}, Zn^{2+}, etc.) and 2,5-dihydroxyterephthalic acid, where Mg-MOF-74 has excellent low-pressure CO_2 adsorption (8.6 mmol g^{-1}) at 100 kPa and 298 K. This is due to the high density of open metal sites in MOF-74 and the presence of Mg–O bonds that improve the CO_2 adsorption capacity relative to the chemical bonds formed by other metal ions (Bahamon and Vega, 2016; Caskey et al., 2008). In addition to this, HKUST-1 is also a common material for low-pressure CO_2 adsorption, due to the high charge density of Cu^{2+}, which allows a strong interaction with CO_2 (Hamon et al., 2010; Yazaydin et al., 2009). After treatment with ethanol and NH_4Cl at 338 K, it also has a high adsorption capacity (11.6 mmol g^{-1}) at 1 atm and 273 K (Yan et al., 2014). To further improve the adsorption performance, bimetals can be introduced to the MOF framework as metal sites and optimal results have been obtained by adjusting the ratios, Gao et al. (2021) prepared $Zn_{0.75}Mg_{0.25}$-MOF-74 by one-step hydrothermal synthesis (Fig. 3.18a), due to the large surface area (667.6 m^2 g^{-1}) and affinity for CO_2, its CO_2 adsorption capacity of 128.3 cm^3 g^{-1} at 1 bar and 273 K. Also, due to the multiple active sites of the unsaturated metal centers as active Lewis acid sites and O atoms from Zn–O and Mg–O as Lewis basic sites, conferring excellent catalytic properties. Kadi et al. (2020) prepared $Cu_{1.5}Mg_{1.5}$ $(BTC)_2$ with a molar ratio of Cu to Mg of 1:1, and this MOF maintained the original crystalline shape of HKUST-1. The substitution of Cu of atomic radius 128 pm by larger ions of Mg of atomic radius 173 pm may lead to electrostatic unbalance in the surface of the MOF, which enhance the adsorption efficiency due to the created synergetic phenomenon, resulting in a significant increase in adsorption to 23.85 mmol g^{-1}, which is much higher than Cu-BTC (5.95 mmol g^{-1}) and Mg-BTC (4.57 mmol g^{-1}). In addition to this, unsaturated alkali metal ions can be introduced into the framework of MOF to enhance the adsorption performance, for example, K^+ can be immobilized in NKU-521 through a tetrazole based motif and are effectively embedded in a trinuclear Co^{2+}-tetrazole coordination motif (Fig. 3.18b), resulting in a 24 % increase in isosteric heat for CO_2, with a CO_2 adsorption capacity of 139 cm^3 g^{-1} at 273 K and 1 atm (Li et al., 2019). Bae et al. (2011) introduced Li^+ into Zn-MOF using different methods to enhance the adsorption performance, and after experimental analysis, it is known that the chain structure can be replaced and the pore capacity can be reduced by the chemical reduction method leading to improved adsorption, while the ion exchange method is due to the stronger interaction of the desolvated Li^+ with CO_2 (Fig. 3.18c).

(ii) Organic ligand selection and group modification. Since the acid-base and dipole-quadrupole interactions between N atoms and CO_2 molecules induce dispersion and electrostatic forces between CO_2 and MOFs, thus enhancing the adsorption capacity of MOFs, the current chemical modifications are mainly based on the selection of organic ligands containing N elements or the

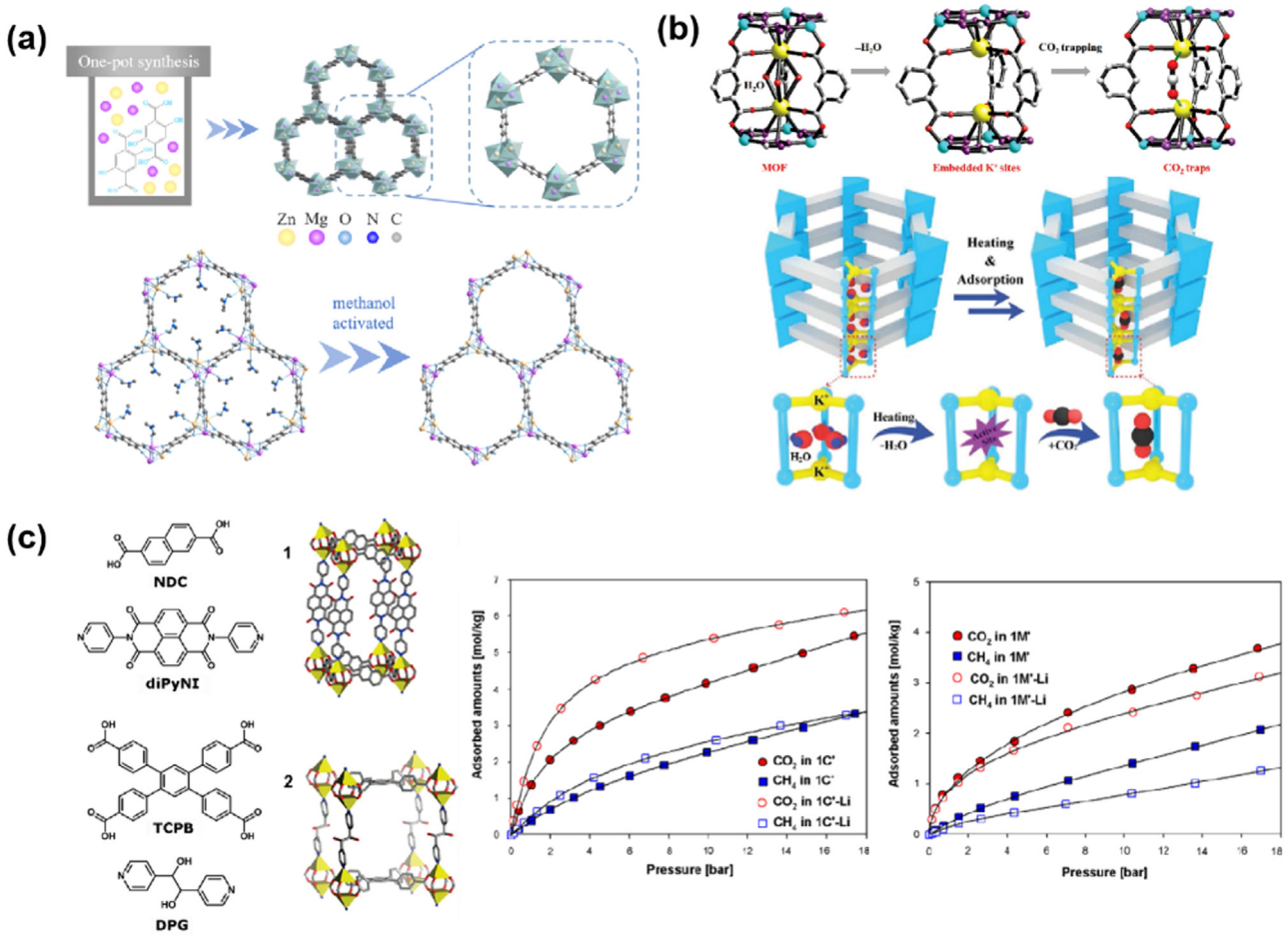

Fig. 3.18. (a) facile one-pot method to synthesize bimetallic Zn/Mg-MOF-74, and 2D structure of original and methanol-activated Zn/Mg-MOF-74 (Gao et al., 2021); (b) the structures of the framework of NKU-521 and Co-K MBB, and schematic illustration of the MOF featuring novel K^+ binding sites for CO_2 (Li et al., 2019); (c) chemical structures of ligands, the crystal structure of MOFs and effect of chemical reduction on the CO_2 and CH_4 isotherms in 1C and 1M at 298 K (Bae et al., 2011). (For interpretation of the references to color in this figure legend, the reader is referred to the web version of this article.)

introduction of Lewis bases. The direct selection of ligands containing N element can eliminate the complex preparation process, such as nitrogen heterocycles, aromatic amines, adenine, triazole and so on. Hong et al. (2017) used 4- (2-hydroxy-3-methoxy-benzyli-dene-hydrazinocarbonyl)-N-pyridin-4-yl- (benzamide) compounds as organic ligands for the synthesis of Cd-MOF, which has a heat of adsorption of 26 kJ mol^{-1} and an adsorption capacity of 1.5 mmol g^{-1} at 273 K and 1 bar. Maity et al. (2019) chose Cu^{2+} and Zn^{2+} with adenine and terephthalic acid as organic ligands for the preparation of IISEPR-MOF26 and IISEPR-MOF27, which exhibited excellent cyclic stability with CO_2 adsorption amounts of 4.3 mmol g^{-1} and 3.8 mmol g^{-1} at 273 K and 1 atm, respectively, due to the lower heat of adsorption and thus ease of desorption. In addition, the synthesized MOFs also have excellent water stability with no decay of adsorption properties in water as well as exposure to water vapour for more than 24 h. The above synthesized MOFs can be seen to only rely on nitrogen-containing ligands for CO_2 adsorption, which has a low adsorption capacity. Therefore, post-modification of the MOFs by introducing Lewis bases (amino acids, alkyl amines, etc.) is needed to further enhance the adsorption performance. Khan et al. (2018) synthesized ZIF-8 nanoparticles with n_{Zn2+}:n_{Hmim} = 1:8. At the same time, a small amount of triethylamine was added to the synthesis process. Due to the introduction of N-H group, it helped to improve the adsorption capacity of CO_2, reaching 22.43 mmol g^{-1}. Li et al. (2016b), Li et al. (2019) used Brønsted Acid-Base Reaction and solvent effect to access alkylamines to Cr-MIL-101 (Fig. 3.19a), and the use of low-polar cyclohexane as dispersant could make higher chemical potential of alkylamine and enhanced driving force from cyclohexane to MOF, allowing for introduce more amino groups into the MOF and enhancing the adsorption capacity of CO_2, which was 4.21 mmol g^{-1} at 150 mbar and 298 K. Yoo and Jhung (2022) used aminosilanes for UIO-67 modification and by choosing different types and amounts of aminosilanes (Fig. 3.19b), the heat of adsorption after treatment was found to be between 35–50 kJ mol^{-1}, due to the formation of a carbamate via the interaction between primary/secondary amino groups and CO_2, resulting in good adsorption of amino acids on CO_2 at 298 K and 15 kPa, the highest adsorption capacity can reach 0.58 mmol g^{-1}. In addition, the experimental analysis revealed no major difference in the adsorption of CO_2 between primary and secondary amino groups. Yang et al. (2011) investigated the effect of different group modifications on the adsorption properties by means of simulated calculations (Fig. 3.19c), and the heat of adsorption increased with increasing group polarity: -SO_3H>-CO_2H>- NH_2 > -OH > -NO_2 > -Br > -CF_3. Although the polarity of the -CF_3 group is the lowest, the strongest CO_2 adsorption mainly results from the highest confinement caused by the significant decrease of the accessible pore volume.

(iii) Pore size tuning. The molecular size of CO_2 is between 0.3–0.4 nm, so tuning the pore size of MOFs and using the size effect

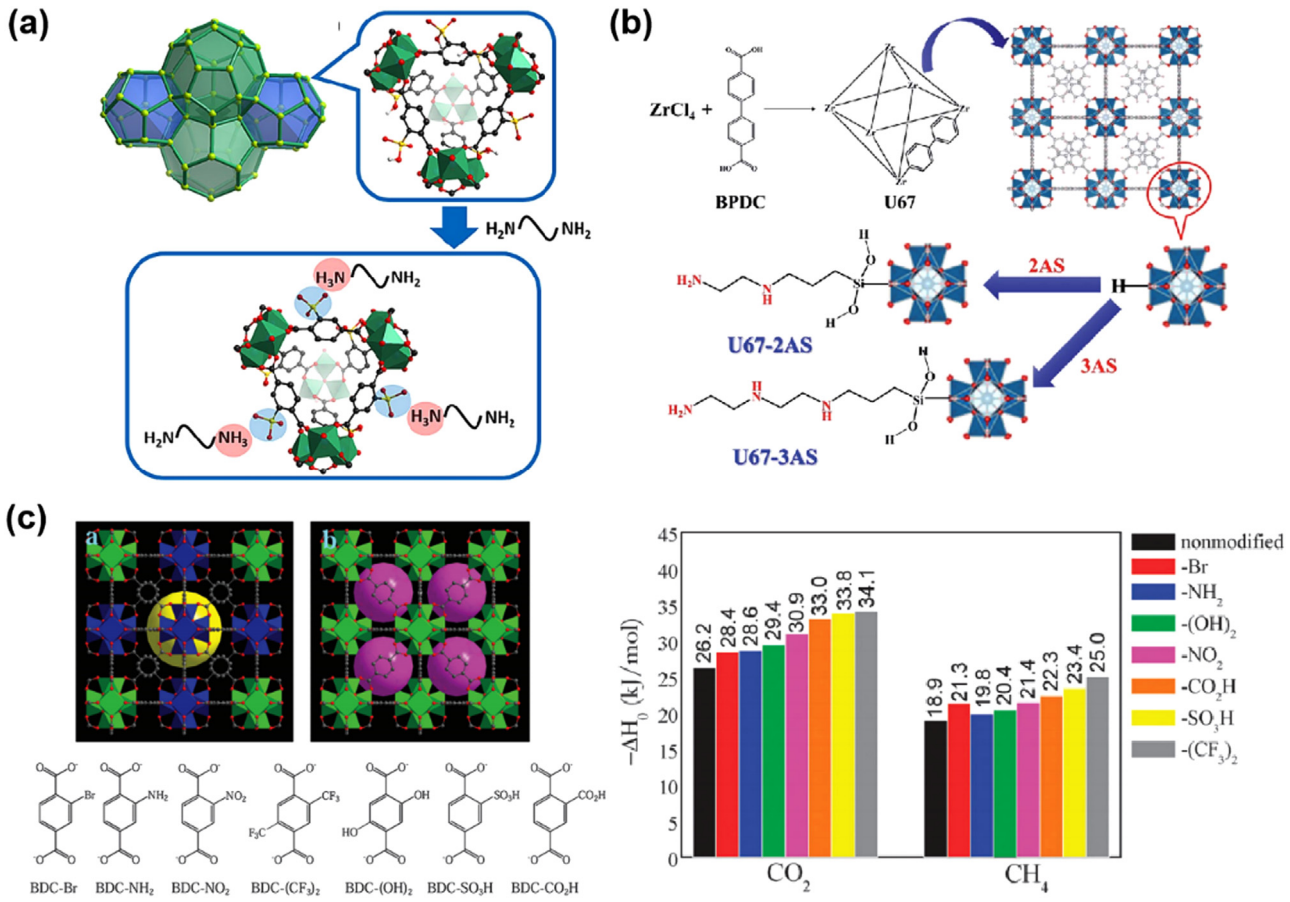

Fig. 3.19. (a) Cr-MIL-101-SO_3H topology and illustration of electrostatic interaction between sulfonate groups and ammonium groups (Li et al., 2016b); (b) a scheme to introduce amino groups on the U67 MOF (Yoo and Jhung, 2022); (c) illustration of the UIO-66 (Zr) crystalline structure, including: octahedral cages, tetrahedral cages and functionalized ligands, calculated low-coverage adsorption enthalpies of pure CO_2 and CH_4 gases in the non-modified UIO-66 (Zr) and its functionalized derivatives at 303 K (Yang et al., 2011). (For interpretation of the references to color in this figure legend, the reader is referred to the web version of this article.)

for adsorption is also an effective way. Jiang et al. (2018) synthesized highly symmetric NJU-Bai35 with Cu^{2+} as metal sites and isonicotinic acid and $[Cu(IN)_2]_\infty$ as dual ligands (Fig. 3.20a). Its internal space has homogeneous dimensions in the a, b, and c axis with dimensions of 3.6*3.6, 3.4*3.4, and 3.6*3.6 $Å^2$, respectively, which are close to those of CO_2, resulting in CO_2 adsorption up to 7.2 wt.% at 298 K and 0.15 bar. Bao et al. (2015) used biphenylcarboxylic acid derivatives as ligands to synthesize $[Zn_2L_2]$·2DMF (Fig. 3.20b), which has a high heat of adsorption (33 kJ mol^{-1}) and a high adsorption capacity of 79.9 cm^3 cm^{-3} at 298 K and 100 kPa due to the presence of N elements in the structure and a one-dimensional nanochannel with a diameter of 3.6 Å. By fine design of the pore size structure of MOFs, a size matching CO_2 can be obtained. However, the more complicated preparation process and the screening of organic ligands are not suitable for large-scale applications. Compared with directly designing MOFs with the size matching CO_2, the intercalated structure is a more convenient method. Yao et al. (2012) synthesized three SUMOFs with intercalated structures using Zn_4O clusters and rigid dicarboxylate anions (Fig. 3.20c), all of which have two different types of small pores and high pore volumes. Among them, MOF synthesized with terephthalic acid as a ligand has a structure closer to the molecular size of CO_2 (5.9 Å and 7.7 Å). In addition, with the aid of interpenetration in these MOFs, the electric field gradients in the small pores are increased, and therefore enhancing the interaction between CO_2 and the host framework. At 273 K and 100 kPa, The three MOFs synthesized have high low-pressure adsorption properties of 4.26, 3.44 and 3.6 mmol g^{-1}, respectively. Pal et al. (2017) added a flexible N-containing donor to the Zn^{2+} and sulfonyldibenzoic acid system and synthesized $\{[Co_2(SDB)_2(L)]\cdot(H_2O)_4\cdot(DMF)\}_n$ with a double interpenetrating structure by hydrothermal method. The MOF material has a rhombic channel with a size of 3.4*5.0 Å inside, and its adsorption heat is 23 kJ mol^{-1}, the CO_2 adsorption capacity is 50.6 cm^3 g^{-1} at 273 K and 1 bar.

Due to the structural limitations, MOFs suitable for high-pressure adsorption have low CO_2 adsorption performance under low pressure environment due to the larger pore size, which reduces the potential energy superposition between the pore walls and the interaction between CO_2 molecules and the material (Mason et al., 2011). MOFs suitable for low-pressure adsorption have lower surface area, which limits the performance of CO_2 adsorption. In contrast, MIL-53 has a unique double-cage structure that allows it to have a "breathing effect", which can achieve low-pressure adsorption in the internal small frame and high-pressure adsorption in the external large frame, giving the desired adsorption performance of CO_2 at different air pressures. Finsy et al. (2009) synthesized MIL-53 using Al^{3+} as the metal site and found that at pressures below 5 bar, CO_2 adsorption led to the contraction of the framework and the formation of a narrow pore, while at high pressures, further adsorption of CO_2 reopened the framework, leading to a sudden increase in adsorption above 6 bar. Mahdipoor et al. (2021) synthesized three MOFs (Fe-MIL-53, Fe-MIL-101, Fe-MIL-101-NH_2) and investigated the adsorption capacity of CO_2 at different pressures (0-40 bar), compared to the other two, Fe-MIL-101-NH_2 has a larger specific surface area (915 m^2 g^{-1}) and pore volume (0.4 cm^3 g^{-1}) with heat of adsorption of 46.7 kJ

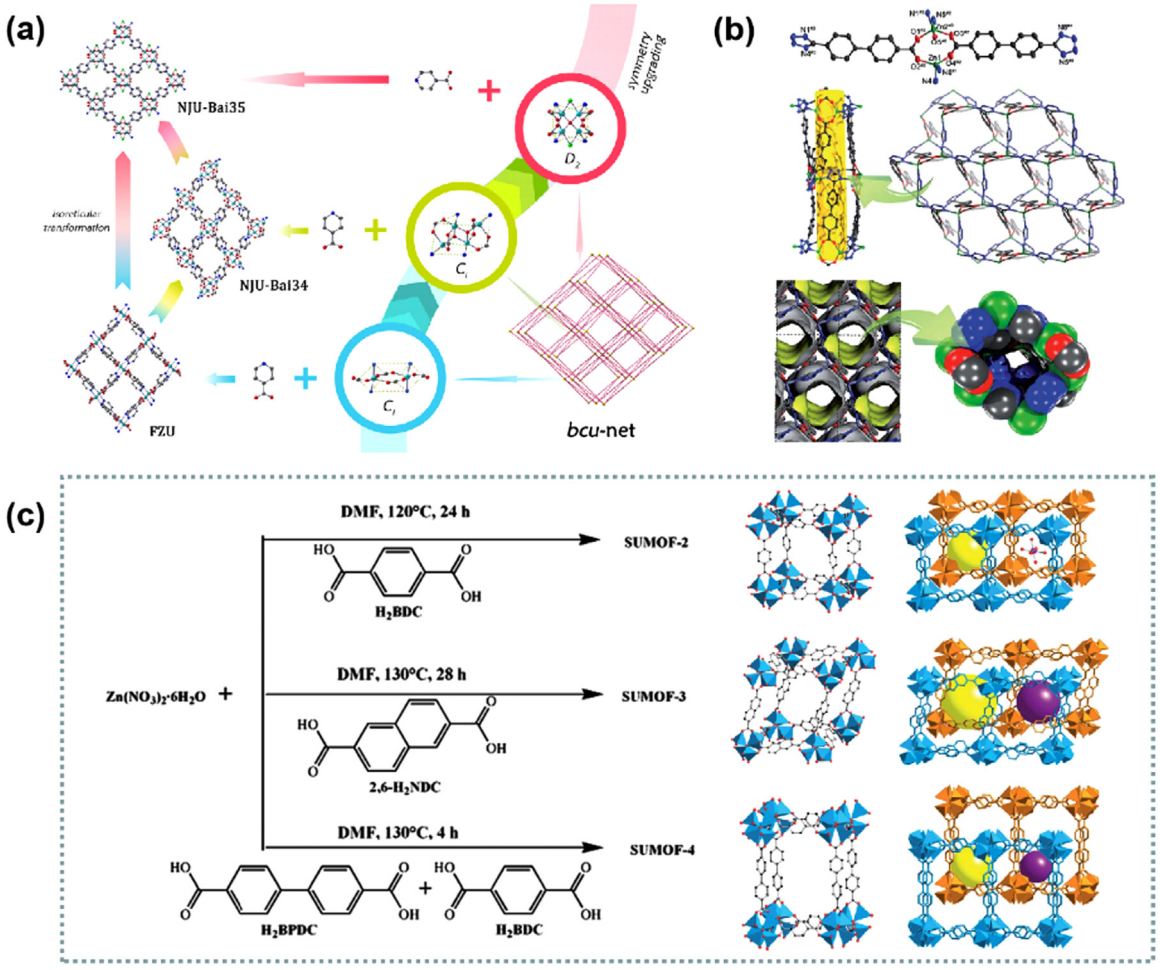

Fig. 3.20. (a) isoreticular transformation of bcu-type MOF by symmetry-upgrading inorganic clusters (Jiang et al., 2018); (b) the structure of NENU-520 obtained by Pore size design (Bao et al., 2015); (c) synthesis of the SUMOFs, non-interpenetrated models and crystal structures of the doubly interpenetrated frameworks (Yao et al., 2012). (For interpretation of the references to color in this figure legend, the reader is referred to the web version of this article.)

mol^{-1}. Moreover, the adsorption capacity increased sharply between 15–20 bar, and finally reached 13 mmol g^{-1} at 298 K and 40 bar.

In addition, MOF materials are often combined with other materials to enhance the adsorption effect. Policicchio et al. (2014) investigated the adsorption performance of urea-modified graphene oxide with Cu-BTC for CO_2 at different temperatures and pressures, and the surface area and total pore volume of the composites were 1367 m^2 g^{-1} and 0.663 cm^3 g^{-1}, respectively. Compared to MOF, the surface area and total pore volume of the composites were 1367 m^2 g^{-1} and 0.663 cm^3 g^{-1}, which were improved by 53.25 % and 54.91 %, respectively, and the heat of adsorption reached 30 kJ mol^{-1} with 7.27 mmol g^{-1} at low pressure (0.1 MPa) and 15 mmol g^{-1} at high pressure (1.5 MPa) at 277 K. In addition, it also has a fully reversible adsorption process to recover its CO_2 adsorption capacity without heat treatment. Chakraborty and Maji (2014) prepared composites for CO_2 adsorption at room temperature by immobilizing nanocrystals of Mg-MOF-74 in the mesopores of SBA-15 rods by in situ growth, and the CO_2 adsorption capacity was 88 ml g^{-1} at 293 K and P/P_o, the heat of adsorption was 30.3 kJ mol^{-1}. Ghahramaninezhad et al. (2018) synthesized Li^+-doped polyoxometalate ({Mo132})-coated ZIF-8 with a surface area of 237 m^2 g^{-1} and a CO_2 adsorption of 16 mmol g^{-1} at 298 K and 10 bar, and the composite also has excellent water stability. After being exposed to humid air for 7 months, the adsorption capacity of CO_2 has not changed significantly. Qasem et al. (2017) modified multi-walled carbon nanotubes with HNO_3 and grew Cr-MIL-101 in situ on their surface. Compared with Cr-MIL-101, the surface area and pore volume of the prepared composites were 4004 m^2 g^{-1} and 2.07 cc g^{-1}, which were increased by 6.92 % and 4.62 %, respectively. At 298 K and 20 kPa, the maximum adsorption capacity was 1.2 mmol g^{-1}.

3.2.2.2. Surface chemistry of MOFs based CO_2 capture. The intrinsic capacity for CO_2 uptake by MOFs is influenced thorough either structural or functional routes.

(i) Structural route: it involves reducing the size of micropores in the 0.5-1.2 nm range by penetration or intercalation to encourage intermolecular interactions and achieve molecular sieving (Han et al., 2013). IRMOF-9, 13, and 15 have an interpenetrated MOF-5 scaffolding, however, it has less pore size than its parent framework (Eddaoudi et al., 2002). Transition metal interpenetrated Co_2 $(ndc)_2$ (bipym) having pore cross-section of 4.4 × 3.4 Å is another example of such strategy (Choi et al., 2004; Lee et al., 2003).

(ii) Functional route: it involves the creation of frameworks with coordinatively unsaturated metal sites acting like charge-binding sites for adsorption. These could be obtained by dissolving the material in a vacuum or at high temperatures (Bae et al., 2008; Moon et al., 2006). One of the examples of such material is [M_2 (DOBDC) $(EG)_2$] (M = Mg, Co, Ni) frameworks, with open Mg (II), Co (II), and Ni (II) sites offering zero-loading enthalpies as 44.0, 35.0 and 62 kJ/mol, respectively (Kim et al., 2019).

Apart from the above two approaches, MOFs can also be modified post-synthesis through heterogeneous chemical transformations of metal groups and ligands without disturbing the overall geometry of the structure (Demessence et al., 2009; Hoskins and Robson, 1990; Jones and Bauer, 2009; Wang and Cohen, 2007). Some MOFs have been post-synthetic functionalized with alkylamines like HCu[$(Cu_4Cl)_3$ $(BTTri)_8$] (H_3BTTri = 1,3,5-tris (1*H*-1,2,3-triazol-4-yl)benzene) and diamines like *N,N'*-dimethylenediamine (McDonald, 2011). Few MOFs undergoing this approach are ethylenediamine modified Mg_2 (dobdc) having unsaturated sites of Mg (II) (Choi et al., 2012), Mg_2 (dobpdc), and Zn_2 (dobpdc) (McDonald et al., 2012). The functionalization with ethylenediamine not only enhances the CO_2 uptake capacity, but also improves the material regenerability. ZIF-68, -69, and -70 show excellent adsorption and CO_2/CO separation capacities after modification with alkaline/polar charges and N-functionalization with 4&5-azabenzimidazolate and purinate ligands (Bastin et al., 2008; Chen et al., 2008; Liu and Smit, 2010; McCarthy et al., 2010). Apart from this, ZIF-related compounds like Zn (bdc) $(4,4'\text{-bipy})_{0.5}$ showed improved CO_2 separation from CO_2/N_2 and $CO_2/CH_4/N_2$ gas mixtures (Bastin et al., 2008).

Unsaturated metal sites can also be created in MOFs via post-synthesis treatment. One of the example is impregnated [Zn_3 $(tcpt)_2$ $(HCOO)$][NH_2 $(CH_3)_2$] with Li^+, Mg^{2+}, Ca^{2+}, Co^{2+}, and Ni^{2+} cations. This in return results in increased zero-loading CO_2 uptake isosteric heat from 29.3 to 34.5-37.4 kJ mol^{-1} in [Zn_3 $(tcpt)_2$ $(HCOO)$][NH_2 $(CH_3)_2$] and cation-doped compounds, respectively (Park and Suh, 2013).

3.2.2.3. Effect of water on CO_2 adsorption. Contrary to zeolites, the adsorption capacity of MOFs can be highly affected by water due to weak metal-ligand bonds, which sometimes may result in structure collapse. Steam stability routs have been reported for MOFs over wide range of temperatures (Park and Suh, 2013). The most common example to hydrothermally unstable MOF is MOF-5. IRMOF series with Zn carboxylate clusters are also less hydrothermally stable due to quick hydrolysis of Zn-carboxylate bonds (Kaye et al., 2007; Li and Yang, 2007; Schröck et al., 2008). MIL family compounds show the highest hydrothermal stability, especially robust MIL-100 and M101 having clusters of Cr (III) (Férey et al., 2005, 2004; Küsgens et al., 2009), Zr (IV)-MOFs (i.e., Zr_6O_4 $(OH)_4$ $(CO_2)_{12}$ (UiO-66) (Cavka et al., 2008), and Ni_3 $(btp)_2$-based on azolate linkers (Colombo et al., 2011).

Apart from hydrothermal stability, water also plays an important role in identifying CO_2 over other gases and improve adsorption capacity. Half pore blockage by H_2O upon CO_2 adsorption is also reported in rigid MOFs. Mg_2 (dobdc) shows a sturdy deactivation when H_2O is adsorbed via reduction of CO_2 binding energy (Yu and Balbuena, 2013). However, Co_2dobdc) and Ni_2 (dobdc) performed better after H_2O exposure and kept a stable CO_2 adsorption (Kizzie et al., 2011; Liu et al., 2011). KHUST-1 impregnated with unsaturated Cu (II) showed reduction in CO_2 capacity after two H_2O molecule coordinated at Cu sites (Liu et al., 2010). However, when one H_2O molecules coordinated, the framework showed a major improvement in CO_2 adsorption. This is due to the presence of selective electrostatic interactions among coordinated H_2O molecule and CO_2 molecule (Yazaydın et al., 2009). On the other hand, in hydrated MIL-101, the terminal H_2O molecules act as an extra binding set for CO_2 adsorption.

A very special type of property has been observed in flexible MOFs (such as the MIL-53 family) where H_2O can promote reversible structural changes. Flexible MOFs can perform adsorption/desorption cycles but become less stable over time (Cheng et al., 2009). In pure MIL-53 (Al)-NH_2, water improves the stability of narrow pores and provides an excellent material for membrane design (Bureekaew et al., 2008). Since the flue gas contains 5-15 % of water, the evaluation of MOF-based membranes in humid environment, and ternary breakthroughs tests for the mixture of CO_2, N_2, and H_2O are needed. MOF adsorbents, particularly those with unoccupied Lewis acid sites, generally have reduced CO_2 adsorption capabilities when exposed to moisture due to the higher affinity of H_2O compared to CO_2. For instance, Mason et al. (Mason et al., 2015) proposed 83 % decrease in total CO_2 adsorption (from 5.87 mmol g^{-1} (Hu et al., 2017b) to 1 mmol g^{-1}) for Mg-MOF-74 under wet condition. In the case of MOFs with small apertures, the same trend is followed as in the case of opt-UiO-66 (Zr)- $(OH)_2$, which shows 90 % (from 2.47 mmol g^{-1} to 0.7 mmol g^{-1}) reduction in CO_2 adsorption capacity (Nguyen et al., 2014). The water-repellent characteristics of MOFs can be improved by either doping chemical functions like alkyl amines, or by boosting the hydrophobicity. For example, doping with hydrazine (N_2H_4), N,N′-dimethylethylenediamine (mmen), and 2,2-dimethyl-1,3-diaminopropane (dmpn) can result in 100 % retention of CO_2 uptake. Nguyen et al. (2014) developed a hydrophobic chabazite-type ZIF-300, capable of upholding constant CO_2 uptake capacity within 80 % relative humidity. Furthermore, Hu et al. (2017a) synthesized a triphasic hydrothermal approach for introducing ligands into parental UiO-66 structures and demonstrated that UiO-66 (Zr)-NH_2-F_4-0.53 show a loss of only 30 % in CO_2 capture capacity under 70 % relative humidity and CO_2 (15)/N_2 (85) mixture.

In summary, it can be seen that MOFs have made a big breakthrough in CO_2 adsorption due to their advantages such as designable chemical structure, adjustable pore size, and high chemisorption capacity. However, there are still problems that need to be solved. Firstly, we should continue to improve the adsorption capacity of MOFs, especially under atmospheric pressure, and conduct in-depth research on the adsorption mechanism; secondly, we should improve the environmental stability of MOFs, so that they have high thermal stability, water stability, and high selective adsorption; thirdly, the current research mainly focuses on the adsorption of CO_2, and in the future, we can focus on the desorption, enrichment, and conversion of CO_2; fourthly, the ligands used in MOFs are mainly derived from chemical materials, which is not conducive to sustainable development, the use of biomass materials (e.g., lignin derivatives, furandicarboxylic acid, etc.) as ligands and their structure and adsorption properties can be explored.

3.2.3. Carbon materials (biochar and activated carbon) for CO_2 capture

3.2.3.1. Biochar for CO_2 adsorption.

3.2.3.1.1. Introduction of biochar and its properties. Biochar is an eco-friendly adsorbent that is produced from different kinds of biomass and organic wastes. Although many carbon-based porous materials are available on the market, biomass-derived adsorbents seem attractive for biomass and waste management. Biochars and activated biochars might be used as adsorbents for carbon dioxide capturing thanks to their developed porous structure, noticeable carbon dioxide adsorption capacities (Singh et al., 2019) and also high thermal, chemical and mechanical resistance (Amer et al., 2022). Biochars are also about ten times cheaper than other CO_2 adsorbents due to the wide availability of biomass on the market and relatively simple and cheap synthesis methods. Additionally, to minimize the cost of the adsorbent, waste materials are used as a raw feedstock in a pure state or as a mixture with biomass, usually woody or lignocellulosic (Ibrahim et al., 2022; Igalavithana et al., 2020; Liu, 2019; Xu et al., 2016).

The physicochemical properties of biochar are greatly affected by the pyrolysis operating parameters (e.g., temperature, retention time, carrier gas flow rate, and heating rate) (Foong et al., 2020). For instance, slow pyrolysis was reported to produce biochar with a larger pore volume and surface area. This is because a longer reaction time/slow heating rate enhanced the release of volatile organic matter from the feedstock, thus creating a more porous structure on the surface of biochar (Foong et al., 2020).

Pristine biochar obtained through pyrolysis was reported to have a low total pore volume (0.016–0.083 cm^3/g) and surface area (8–132 m^2/g). The pore size of the pristine biochar is contributed mainly by micropores (12.1–58.0 %) and mesopores (18.9–31.7 %), which is within pore size of < 50 nm (Leng et al., 2021). Sajjadi et al. (2019a) also reported that cellulose-rich biomass produces highly microporous biochar while lignin-rich biomass produces highly macroporous

biochar. Besides that, high pyrolysis temperature and activation temperature enhanced the formation of larger surface area and pore size on the biochar (Feng et al., 2017; Lam et al., 2018). However, micropores are highly desired in CO_2 capture for sorption and storage of the gas molecules via the micropores' diffusional activation energy (Ghanbari and Kamath, 2019; Lahijani et al., 2018). Thus, pyrolysis or activation at lower temperatures is preferable to avoid excess widening of the pores that lead to a decrease in CO_2 adsorption capacities.

The physicochemical properties of biochar have been shown to affect CO_2 adsorption capacities. These properties include microporosity, total pore volume, specific surface area, surface chemistry, and pore size. Microporosity and specific surface area are interrelated. A high volume of micropores contributes to a larger surface area, which in turn promotes CO_2 adsorption capacities (Durá et al., 2016; Serafin et al., 2017). Besides that, the CO_2 adsorption capacity in micropores is dependent on the adsorption pressure and temperature. The CO_2 adsorption at temperature and pressure of 0 °C and < 0.1 bar as well as 25 °C and < 1 bar is governed by the pore size of < 0.7 nm (ultra-micropore) and < 1 nm (micropore), respectively (Adeniran and Mokaya, 2016; Presser et al., 2011).

Surface chemistry plays an important role in CO_2 capture. For instance, an increase in the N-containing functional group (e.g., amino group) on the biochar surface facilitates the adsorption of CO_2 *via* interactions such as H-bonding, dipole-dipole interaction, and covalent bonding (Shafeeyan et al., 2010). The presence of O-containing functional groups (e.g., phenols, carboxylic acids, carbonyl) on the biochar surface was shown to affect CO_2 adsorption as most of them are acidic. The O-containing functional group and N-containing functional group are removed *via* pyrolysis at a temperature higher than 100 °C and 400 °C, respectively (Sajjadi et al., 2019a). S-doped on biochar surfaces also plays an important role in CO_2 adsorption. The S-containing functional group present on the biochar surface is basic in nature, thus facilitating the adsorption of weak acidic CO_2 *via* acid-base interaction (Seema et al., 2014). A strong pole-pole interaction is also present between the polar sites of S functional groups and the large quadrupole moment of CO_2 thus enhancing the adsorption of CO_2 onto the biochar surface (Xia et al., 2012).

Hydrophobicity and polarity of biochar were reported to influence the CO_2 capture performance. It can be determined through the content of oxygen (O), hydrogen (H), nitrogen (N), and sulphur (S) as well as the aromaticity of the biochar. Low content of O, H, the ratio of (O + N)/C and (O + N + S)/C contributed to high hydrophobicity and low polarity, thus limiting the adsorption of polar molecules (e.g., H_2O) and enhancing the adsorption of non-polar molecules (e.g., CO_2) (Shafawi et al., 2021; Shen et al., 2016). The presence of alkali (e.g., K, Na) and alkaline earth metals (e.g., Ca, Mg) in the biochar was also reported to affect the CO_2 adsorption through chemisorption, as the presence of metal can improve the basicity of biochar (Xu, X. et al., 2016). For instance, Lahijani et al. (2018) reported that the introduction of Mg to biochar (82.0 mg/g) improved the CO_2 adsorption capacities as compared to pristine biochar (72.6 mg/g) due to the enhancement of basicity of the modified biochar. In another research, Xu, X. et al. (2016) reported that biochar prepared from pig manure is highly basic (pH = 10.4), which showed high CO_2 adsorption capacities (23.5 mg/g) as compared to biochar prepared from sewage sludge (18.2 mg/g) with lower pH (pH = 8.44).

Over the few decades, various types of activation methods and advanced pyrolysis techniques have been introduced to improve the porous characteristics of biochar used in CO_2 capture. The activation methods include chemical activation (e.g., KOH, NaOH, HCl) (Liew et al., 2018; Sakhiya et al., 2021) and physical activation (e.g. CO_2, steam) (Sangon et al., 2018), while advanced pyrolysis techniques include microwave pyrolysis (Huang et al., 2015), catalytic pyrolysis (Jalalabadi et al., 2019), CO_2 pyrolysis (Kwon et al., 2019), and co-pyrolysis (Igalavithana et al., 2020a). These methods were introduced to resolve the limitation of pristine biochar in CO_2 adsorption as pristine biochar possesses low surface area, porosity, limited surface functional group, and low basicity (Shafawi et al., 2021). Pristine biochar is tuned via these methods to produce "engineered biochar" with optimum characteristics for CO_2 capture (high basicity, surface area, pore volume, pore size, and high hydrophobicity).

Among them, co-pyrolysis shows the potential to produce biochar with higher CO_2 adsorption capacities, as shown in Table 3.5. Besides that, the ratio of feedstock selected during co-pyrolysis plays an important role as it may change the surface chemistry and porous structure of the biochar produced, which in turn affects the CO_2 adsorption capacities. As reported by Igalavithana et al. (2020a), an increased ratio of food waste during co-pyrolysis produced biochar with reduced amounts of N%, S%, and C%, as well as micropores on the surface, thus lowering the CO_2 adsorption capacities. Interestingly, there is positive synergy by adding wood waste to the co-pyrolysis, as it can help to reduce the moisture content contributed by the food waste in the gasifier and increase the C% in the biochar produced. Igalavithana et al. (2020a) also modified the co-pyrolyzed biochar from food and wood waste with KOH and reported an increase in microporous structure, thus increasing the CO_2 adsorption (148 mg/g) compared to that without activation (115 mg/g). Another research by Liu and Huang (2018) converted coffee ground into biochar via pyrolysis, then performed ammoxidation, followed by KOH activation to produce engineered biochar with higher surface area ranging from 990 m^2/g to 1684 m^2/g compared to those without KOH activation (0.8 – 402 m^2/g) and pristine biochar (34 m^2/g). The CO_2 adsorption capacities of the engineered biochar is higher (89.8 – 117.5 mg/g) compared to biochar without KOH activation (18.0 – 37.4 mg/g) and pristine biochar (6.2 mg/g). The research reported that N-doped ammoxidation and KOH activation had significant effects on CO_2 adsorption by improving the biochar basicity and amount of microporosity. Although previous research reported promising result on using biochar in CCT, however, limited research is performed for optimization of different methods as well as combination of these methods, where the synergy presence in the processes still remain unknown. CO_2 adsorption test should also be performed with larger scale or in real industry to identify the feasibility of using biochar for CO_2 capture. Table 3.5 summarizes the production of biochar from various techniques.

3.2.3.1.2. Biochar activation. Activated carbons are obtained through several processes, starting from carbonization under inert atmosphere. Initially, the raw biochar product does not have a developed porous structure; therefore, its activation is carried out through physical processes such as high-temperature carbon dioxide or steam gasification or by chemical treatment. A general concept of biochar and activated carbon synthesis is presented in Fig. 3.21.

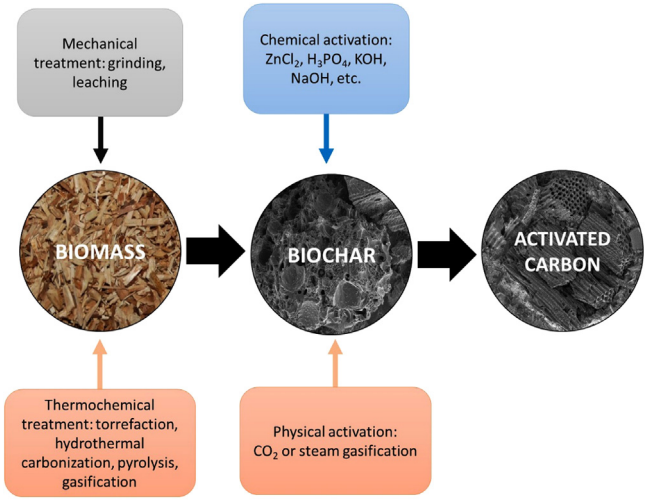

Fig. 3.21. Biochar and activated carbon synthesis methods, based on (Karimi et al., 2022). (For interpretation of the references to color in this figure legend, the reader is referred to the web version of this article.)

Table 3.5
Summary of biochar as CO_2 adsorbent.

Feedstock	Preparation and modification of biochar	Biochar porous characteristic			CO_2 adsorption capacity (mg/g) (adsorption temperature)	Ref.
		BET surface area (m^2/g)	Total pore volume (cm^3/g)	Average pore width (nm)		
Taihu blue algae	Conventional pyrolysis Temp: 500 °C	29.18	0.02	18.8	89.8 (0 °C) 62.9 (25 °C)	(Wang et al., 2021)
Rice straw	Microwave pyrolysis Power: 200 W Temp: 300 °C Time: 20 min	122.2	0.08	5.0	86.2 (20 °C)	(Huang et al., 2015)
Chicken manure	CO_2 pyrolysis Temp: 700 °C	13.59	-	9.3	-	(Kwon et al., 2019)
Sewage sludge	Slow pyrolysis Temp: 500 °C Time: 4 h	10.12	0.02	-	18.2 (25 °C)	(Xu et al., 2016)
Pig manure	Slow pyrolysis Temp: 500 °C Time: 4 h	31.57	0.04	-	23.5 (25 °C)	(Xu et al., 2016)
Walnut shell	Slow pyrolysis Temp: 900 °C Time: 90 min Modification: Mg	292.0	0.16	2.15	82.0 (25 °C)	(Lahijani et al., 2018)
Coffee ground	Fast pyrolysis Temp: 400 °C Time: 60 min	34.0	0.18	-	6.2 (35 °C)	(Liu and Huang, 2018)
Coffee ground	Fast pyrolysis Temp: 400 °C Time: 60 min Modification: Ammoxidation	0.8 – 402	0.01 – 0.22	-	18.0 – 37.4 (35 °C)	(Liu and Huang, 2018)
Coffee ground	Fast pyrolysis Temp: 400 °C Time: 60 min Modification: Ammoxidation followed by KOH activation	990 - 1684	0.55 – 0.94	-	89.8 – 117.5 (35 °C)	(Liu and Huang, 2018)
Food waste (20 %) + wood waste (80 %)	Gasification Temp: 800-1000 °C	294.7	0.05	2.3	115.1 (25 °C)	(Igalavithana et al., 2020a)
Food waste (40 %) + wood waste (60 %)	Gasification Temp: 800-1000 °C Activation: KOH	841.3	0.36	2.9	148.0 (25 °C)	(Igalavithana et al., 2020a)

"Temp" denoted temperature.

Several modification methods were also implemented to enhance the adsorption properties of the biochar-derived activated carbons (Dissanayake et al., 2020). In terms of gaseous species, adsorption capacity and selectivity of the carbonaceous material are important factors (Ben Petrovic, 2022) for CO_2 adsorption selectivity toward nitrogen, and the presence of steam is another key factor (Manya et al., 2018). Specific properties of the materials are adjusted to the end-user requirements by proper modifications of production method and process conditions, raw material kind, its properties and additional post modifications (impregnation, doping etc.) (Xie et al., 2022). In addition, CO_2 adsorption using biochar-based materials is favourable at low-temperature adsorption; normally, its adsorption capacity increases with a temperature decrease (Cao et al., 2022).

The physical and chemical properties of biochars depend on the origin of biomass. Lignocellulosic biomass cell walls (e.g. woody, agriculture, food waste) are composed of three main components: two polysaccharides (hemicellulose - $(C_5H_8O_4)_m$, cellulose - $(C_6H_{10}O_5)_n$) and an aromatic polymer (lignin -$[C_9H_{10}O_3\ (OCH_3)_{0.9-1.7}]_x$) and also other organic components (with acetyl groups, phenolic compounds) and mineral matter (Ashokkumar et al., 2022; Nahak et al., 2022). The content of each fiber component in biomass feedstocks is different: 6 – 38 % of hemicellulose, 10–50 % of cellulose, and 6-46 % of lignin (Saravanan et al., 2022). Cellulose is a polymer built with glucose monomers connected by glycosidic bonds, whereas hemicellulose is not a homogeneous polymer. It consists of glucose, mannose, arabinose, rhamnose, and other sugars. Because of their similar structure and nature, cellulose and hemicellulose make the stability of the matrix of biomass cell walls (Nagarajan et al., 2017). Lignin is a hydrophobic polymer built by aliphatic and aromatic hydrocarbons with a developed structure. Lignin plays the binding role between cellulose and hemicellulose, providing strong mechanical support to increase the recalcitrance of lignocellulosic biomass (Afzal et al., 2022). On the other side, lignin has a negative impact on cellulose conversion during conversion of thermochemical conversion of biomass (Zoghlami and Paes, 2019). It should be emphasised that lignocellulosic biomass was found as a good feedstock for biochar and activated carbon (AC) production (Duan et al., 2021; Kiełbasa et al., 2022). For biochar and AC production, the content of particular fiber components and mineral content are crucial because they determine the properties of obtained products. H. Tian et al. found that biochar derived from the highest content of lignin in biomass characterized the highest reactivity, whereas cellulose biochar had a rich porous structure (Tian et al., 2022). The literature revealed that cellulose could be obtained the activated carbon with a surface area of more than 1000 m^2/g (Suhas et al., 2016). Cellulose can also be used to produce nanofibrils and cellulose nanocrystals, which after modification, have a large surface area and high selectivity towards CO_2 and high CO_2 capacity (Ho and Leo, 2021).

The most suitable activated carbon synthesis method in the case of biomass is thermochemical treatment and chemical activation. Biochars obtained from pyrolysis or hydrothermal carbonisation of lignocellulosic biomass can be successfully activated to produce active carbon with a very high specific area (Shen et al., 2021). Cao et al. (2022) proved that high adsorbent properties for CO_2 capture and good reusability characterised biochar produced from woody and straw biomass. As well as biochar from palm biochar is a porous carbon-based material with high CO_2 adsorption capacity through physisorption and chemisorption

processes (Ben Salem et al., 2021a), whereas biochar from rice straw produced by using microwave pyrolysis was characterised by CO_2 adsorption ability (Huang et al., 2015). Pyrolysis and further chemical activation using KOH of carbonaceous material of sugar cane bagasse resulted in the formation of phenolic and carboxylic functional groups with high affinity to CO_2 (Peres et al., 2022). During biochar synthesis, a pyrolysis process temperature favours the development of porous structure, which directly affects the CO_2 adsorption capacity of the material (Mukherjee et al., 2021). The development of the microporous structure of biochar is directly associated with the adsorption capacity of the carbonaceous material at low pressures in the range of 5–15 kPa (Manya et al., 2020). The main mechanism of CO_2 adsorption with biochar is a physical method (physisorption) through van der Waals forces which adsorb CO_2 molecules (Zhang et al., 2022). According to the literature, specific surface area and pore size are the main factors affecting the process of CO_2 physical adsorption (Majchrzak-Kuceba and Soltysik, 2020; Xu, X.Y. et al., 2016).

Synthesis of adsorbents from biowaste is an important challenge nowadays. Constant economic progress, urbanization and industrialization are leading to a significant increase of the amount of municipal waste, food waste, bio-waste and sewage sludge. Therefore, the most important challenges for people are related to the reduction of waste generation and waste utilization in the circular economy concept bringing effective solutions (where re-materials generation, which can be returned into production processes) and environmental benefits for humans. One of the possibilities to reduce the use of natural resources is, in line with the waste management hierarchy, the use of waste to produce new products through material or energy recovery. The use of waste fuels, such as industrial non-hazardous waste, municipal waste, sewage sludge or the solid fraction after anaerobic digestion of the organic fraction of municipal waste in thermal conversion processes enables the production of valuable products, including gaseous energy carriers and solid products used in adsorption processes. The results presented by M. Karimi et al. in Karimi et al. (2020) show that compost from municipal solid wastes might be a valuable resource for adsorbent synthesis through chemical activation using sulfuric acid and activation at 800 °C. The results of carbon dioxide capture were comparable to those obtained for commercial samples (Karimi et al., 2020). Biowaste, as a mixture of food waste and wood waste, was also a potential material for microporous activated carbon synthesis through gasification; combining with chemical activation using KOH gives better results of porosity of the material (Igalavithana et al., 2020).

A mixture of sewage sludge and leucaena wood was tested as a precursor of biochar synthesis through microwave co-torrefaction. The results show that the adsorption capacity of pure leucaena wood biochar was almost four times higher than that of pure sewage sludge biochar (Huang, Y.F. et al., 2019). Biochar-derived carbons prepared from coffee grounds were studied by Liu and Huang (2018). The activated carbons were obtained through carbonisation, ammoxidation and KOH activation. A highly developed microporous structure resulted in high CO_2 adsorption capacity. Peanut shells were tested as a potential raw material for the synthesis of biochar through catalytic pyrolysis in the molten salt of $ZnCl_2$, giving a high capacity of CO_2 and selectivity over other gases. It was reported by Manya et al. (2018) that chemical activation of vine shoots results in 20–30 % higher CO_2 adsorption capacity of produced biochars compared with physical activation with CO_2.

Due to the chemical reactions of mineral matter components to form carbonates, an enhanced process of CO_2 adsorption was observed. Mineral matter components, especially Mg, Al, Fe, Ni and Ca promote the chemical sorption of carbon dioxide. Additionally, high temperature and water vapour content in the gas stream enhance chemisorption (Xu et al., 2016). Mineral matter also influences the activation process and gases released during the process. For example, during the activation process of chicken manure, which is a fuel rich in $CaCO_3$, an enhanced generation of CO and suppressed dehydrogenation was observed (Kwon et al., 2019).

3.2.3.1.3. Modifications enhancing carbon dioxide capture. To enhance the CO_2 adsorption capacity of carbonaceous materials, it is possible to introduce different modifications, increasing the role of the chemisorption mechanism in the process of adsorption. An overview of modification methods to enhance the porous structure and enhance the adsorption capacity of biochar towards carbon dioxide adsorption, using both chemical and physical methods, is presented in Fig. 3.22.

It was proved that the adsorption capacity of biochar towards CO_2 might be enhanced by increasing the alkalinity of the material surface (Dissanayake et al., 2020). It is possible to enhance CO_2 adsorption on carbon-based material by incorporating chemisorption and modifying biochar with metal oxides and amine-containing materials (Ben Salem et al., 2021a). Especially in the case of waste materials, such modifications are implemented, as organic waste usually contains smaller amounts of carbon, which directly affects the material's adsorption capacity. More advanced procedures are implemented and described in the literature to enhance biochars' adsorption capacity, for both physically and chemically activated samples. For example, A. Igalavithana et al. defined modification of biochars through hetero atoms doping as a promising strategy to further increase CO_2 adsorption (Igalavithana et al., 2020). A nitrogen doped biochar derived from chicken manure possessed a well-developed porous structure of above 300 m^2/g, resulting in very high adsorption capacity and selectivity (Nguyen and Lee, 2016). Anaerobic digestion solid residue might also be a raw material for biochar-based sorbent synthesis. It was observed that nitrogen-functionalised porous carbon synthesised in a one-step process using urea seems to be effective in improving the uptake of CO_2 (Qiao et al., 2020). However, modifications before the chemical treatment of sawdust biochar by a simple impregnation method resulted in pores clogging and reduction of sample adsorption capacity (Madzaki et al., 2016). Pore blockage was also observed after K_2CO_3 impregnation of conocarpus biochar (Al-Wabel et al., 2019).

A biochar dedicated to biogas treatment and capturing CO_2 and H_2S was produced from sawdust biochar treated with urea phosphate to improve the porosity and surface N-containing functional groups of biochars (Ma et al., 2021). An enhanced adsorption process of CO_2 was observed on metalized-biochar in the sequence of metals: Mg > Al > Fe > Ni > Ca (Lahijani et al., 2018), due to a change of physical mechanism to the chemical reaction between e.g., iron oxyhydroxides and carbon dioxide (Xu et al., 2020). Sorption properties might also be enhanced using mechanical treatment e.g. using ball mining (Xu et al., 2020).

Biochars, on the example of coconut shell biochar, might be used for a simultaneous NO/CO_2 removal system which uses biochar and calcined limestone in the calcium looping process (Zhang et al., 2020b). To further enhance adsorption properties, Cu-modification of biochar was proposed together with CaO in the carbonation stage of calcium looping (Zhang et al., 2020a).

In Table 3.6, the review of adsorption capacities toward carbon dioxide of biomass-derived adsorbents was shown. Biochars are produced from a wide range of feedstocks characterizing different CO_2 adsorption capacities.

3.2.3.2. Sewage sludge char for CO_2 adsorption.

3.2.3.2.1. Composition and main characteristics of sewage sludge derived biochar. The biochar product of sewage sludge pyrolysis is a carbon-like material that contains sulphur, nitrogen and oxygen-containing compounds, polycyclic aromatic hydrocarbons, valuable nutrients for the soil (e.g. N, P, K, Ca, Fe, Mg, Cu, Zn) and heavy metals (e.g. As, Cd, Cr, Ni, Pb, Se). Depending on the raw material and the reaction parameters, the yield of biochar is usually between 20 and 70 % (Table 3.7). The amount of ash, fixed carbon and volatile compounds is 29–86 %, 7–64 %, 1–39 %, respectively (Chen et al., 2021; Hossain et al., 2011; Moško et al., 2021; Stylianou et al., 2020; Tong et al., 2021). It is also known, that the ash content of sewage sludge derived biochar is generally higher, than that of based on biomass, which can be attributed

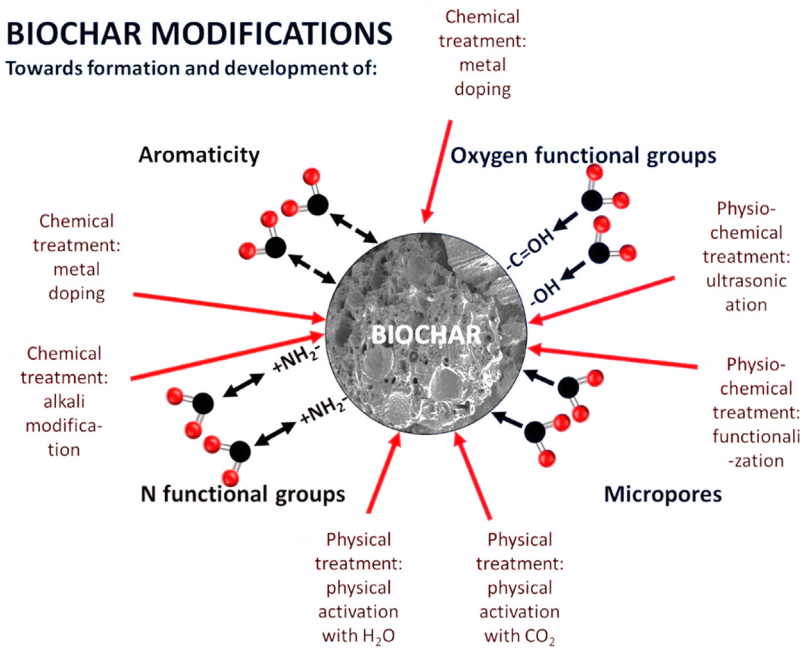

Fig. 3.22. Biochar modification methods towards enhanced CO_2 adsorption capacity, based on (Kumar et al., 2022; Shafawi et al., 2021). (For interpretation of the references to color in this figure legend, the reader is referred to the web version of this article.)

Table 3.6
CO_2 adsorption capacities of biomass-derived adsorbents.

No.	Sample	CO_2 adsorption capacity, mmol/g	Adsorption process parameters	Reference
1	Biochar-derived carbons from coffee grounds	2.04 - 2.67	Ambient pressure, 35 °C	(Liu and Huang, 2018)
2	Biochar from compost from municipal solid wastes	2.5	2.5 bar and 40 °C	(Karimi et al., 2020)
3	Biochar prepared by catalytic pyrolysis of waste roasted peanut shell in the molten salt of $ZnCl_2$	3.8	100 kPa and 0 °C	(Guo et al., 2018)
4	Carbonaceous material of sugar cane bagasse	1.22	Ambient pressure, 25 °C	(Peres et al., 2022)
5	Biochar derived from chicken manure chemically treated with HNO_3 and NH_3 at 450 °C	10.15	Ambient pressure (1 bar), 20 °C	(Nguyen and Lee, 2016)
6	Leucaena wood biochar	1.20	Ambient pressure (1 bar)	(Huang et al., 2019)
7	Vine shoots-derived biochar using both chemical and physical methods	0.92-2.42	15 kPa, 0 °C	(Manya et al., 2018)
8	pine cone biochars activated with KOH	3.64	1 bar, 25 °C	(Kaya and Uzun, 2021)
9	Pecan nut shell biochar obtained through microwave pyrolysis	2.5 (2.0)	1 bar, 0 °C (25 °C)	(Duran-Jimenez et al., 2021)
10	Vine shoots biochar obtained at 600 °C and activated with CO_2 (at 0.1 MPa and 800 °C	2.35-2.67	1 bar, 25 °C	(Manya et al., 2020)
11	Wheat straw biochar obtained at 500 and activated with CO_2 (at 0.1 MPa and 800 °C)	2.44-2.63	1 bar, 25 °C	(Manya et al., 2020)
12	Sawdust biochar activated using urea phosphate at 700 °C	2.42	1 bar, 25 °C	(Ma et al., 2021)
13	Bamboo chips biochar modified by ZIF-8 grafting	1.8	1 bar, 30 °C	(Zhang et al., 2022)
14	Anaerobic digestion solid residue biochar modified by urea	1.22	1 bar, 25 °C	(Qiao et al., 2020)
15	Lignin impregnated with sodium lignosulfonate	2.34	1 bar, 25 °C	(Zhang et al., 2022)
16	Rape straw, soybean straw, corn stalk, wheat straw, walnut shell, hickory wood, and pine wood biochar obtained at 600 °C	0.69-1.02	1 bar, 25 °C	(Cao et al., 2022)
17	Conocarpus biochar obtained at 400 °C	4.47	1 bar, 25 °C	(Al-Wabel et al., 2019)
18	Date palm waste biochar obtained at 500 °C	0.38	1 bar, 25 °C	(Ben Salem et al., 2021b)
19	Biocarbon	0.6	30 mbar, 30 °C	(Majchrzak-Kuceba and Soltysik, 2020)
20	Walnut shell biochar (Mg metalized)	1.65 (1.86)	Ambient pressure, 25 °C	(Lahijani et al., 2018)
21	biochar/Fe oxyhydroxide composite	3.63	Ambient pressure, 25 °C	(Xu et al., 2020)
22	Spent coffee grounds obtained at 600 °C	2.8	1 bar, 25 °C	(Mukherjee et al., 2021)
23	Pig manure biochar obtained at 500 °C	0.53	1 bar, 25 °C	(Xu et al., 2016)
24	Wheat straw biochar obtained at 500 °C	0.78	1 bar, 25 °C	(Xu et al., 2016)
25	Peanut shell derived activated carbon with KOH	7.06 (4.61)	1 bar, 0 °C (25 °C)	(Deng et al., 2015)
26	Rambutan peel-derived KOH-activated hydrochar using KOH:HC ratio of 2:1 at 850 °C for 120 min with the involvement of water-soaking pretreatment	2.78	1 bar, 30 °C	(Zubbri et al., 2021)
27	Sugarcane bagasse biochar produced at 600 °C	1.67	1 bar, 25 °C	(Creamer et al., 2014)
28	Argan fruits shells obtained through dry physical mixing with KOH	5.63	1 bar, 25 °C	(Boujibar et al., 2018)
29	Rice straw biochar produced by microwave pyrolysis (200 W and 300 °C)	1.75	1 bar, 20 °C	(Huang et al., 2015)
30	Rambutan peel biochar impregnated with magnesium nitrate (raw biochar)	1.71 (1.56)	1 bar, 30 °C	(Zubbri et al., 2020)

Table 3.7
Yields, composition and main characteristics of biochar products of sewage sludge pyrolysis.

Raw material	Pyrolysis conditions	Biochar yield,%	Properties, elemental composition, %								Other properties				Ref.
			Ash	Volatile compounds	Fixed carbon	C	H	N	S	O	HHV, MJ/kg	BET surface area, m^2/g	Pore volume, cm^3/g	Average pore diameter, nm	
Sewage sludge (100 g)	T = 400-800 °C, τ = 2 h, He atmosphere (150 ml/min) quartz reactor	46.3-61.7	67.9-80.8	0.9-21.5	10.6-18.3	17.2-23.1	0.3-1.6	0.9-3.0	0.8-0.8	<3.6	8.0-9.5	14.9-85.7	<0.1	-	(Moško et al., 2021)
Sewage sludge (10 g)	T = 300-500 °C, 10 °C/min heating rate, N_2 atmosphere (100 ml/perc), quartz reactor	55-68	50.7-62.5	24.4-39.0	9.9-13.1	21.5-29.6	1.4-5.3	2.8-5.1	0.6-1.3	12.3-24.4	8.2-12.5	-	-	-	(Chen et al., 2021)
Sewage sludge + rice husk (5 g)	Hydrothermal treatment, T = 600 °C, τ = 0,5 h, $N_{2\ atmosphere}$ (200 ml/min) high pressure autoclave	24.4-62.4	28.8-86.1	5.6-9.5	8.2-63.6	2.5-62.1	0.9-2.2	0.7-0.8	0.1-0.2	6.2-8.4	3.9-23.0	13.7-211.9	0.1-0.3	2.5-17.5	(Tong et al., 2021)
Sewage sludge (kb. 250 g)	T = 300-700 °C, $N_{2\ atmosphere}$ (50 ml/min) Horizontal fixed-bed reactor	52.4-72.3	52.8-72.5	15.8-33.8	6.8-9.1	20.2-25.6	0.5-2.6	1.2-3.3	-	<8.3	-	-	-	-	(Hossain et al., 2011)
Sewage sludge, cattle manure, used coffee grounds (20-24 kg)	T = 550 °C, $N_{2\ atmosphere}$, τ = 1.5 h	21.2-41.6	-	-	-	28.5-87.4	0.9-2.4	1.6-5.7	0.3-0.5	-	-	1.5-14.0	<0.1	3.9-60.4	(Stylianou et al., 2020)

to the higher mineral content of sewage sludge (Li et al., 2018). The properties of biomass and sewage sludge derived bio-carbons should be different depending on the composition of raw materials and process parameters (Li et al., 2018; Zhang et al., 2019).

The sewage sludge derived biochar can be used for many purposes, e.g. as a sorbent, catalyst and soil amendment. The application is determined by the physico-chemical properties (e.g. specific surface area, pore volume, average pore diameter), the relative proportions of volatile compounds, fixed carbon and ash in the biochar (Yuan et al., 2015). Biochar obtained at higher pyrolysis temperature (T > 450 °C) has higher specific surface area and increased adsorption capacity (Peng et al., 2011; Yuan et al., 2015). As it was mentioned earlier, sewage sludge derived biochar also contains heavy metals, that accumulate in the carbonaceous residue; e.g. Pb, Zn, Ni, Cd, As, Cu or Cr. Their concentrations should be significant (>5000 ppm) and it can be increased as function of temperature (Cao and Harris, 2010; Xiong et al., 2021; Yin et al., 2021; Zheng et al., 2013).

For sequestering CO_2, many technologies (e.g. absorption, adsorption, membrane separation, chemical or Ca looping, pre- and post-combustion and oxy-fuel) have been developed (Osman et al., 2021). Among the variety of routes, adsorption technologies seem to be the most promising. Based on this fact, different types of porous solid sorbents such as synthetic or natural zeolites, mesoporous silica, metal organic frameworks, active carbon, etc. have already been studied for CO_2 removal (Creamer et al., 2014; Lahijani et al., 2018; McEwen et al., 2013). Although the listed sorbents have high adsorption capacity, the application of metal organic frameworks and zeolites is limited (Ahmed et al., 2016). In case of metal organic frameworks, the instability should be mentioned (Guo et al., 2022), and in the case of zeolites, the fast deactivation, the irreversible adsorption, the steric hindrance of the heavy compounds and the high regeneration temperature are the main disadvantages (Perot and Guisnet, 1990). Biochar can also be an excellent CO_2 sequestering sorbent (Singh et al., 2022). However, before its usage, it is inevitable to create the appropriate pore structure, alkalinity and surface functional groups with different modification methods (Guo et al., 2022; Miricioiu et al., 2021).

3.2.3.2.2. Modification of sewage sludge derived biochar for CO_2 reduction. In order to create the appropriate pore structure, alkalinity and surface functional groups, physical, chemical, physical-chemical modification of the biochar and co-pyrolysis of sewage sludge and biomass have been proposed in the literature (Shafawi et al., 2021; Xiao et al., 2022). The reason for the latter is that biomass also contains alkali elements and alkali earth metals and thus enabling the alkalinity and CO_2 adsorption capacity of the produced biochar to be increased (Huang et al., 2017).

The modification processes have three types. One of them is physical modification, which involves two steps: (i) carbonization carried out at low temperature (T = 400–750 °C) in the presence of physical agents, heat, gases (e.g. CO_2/He/N_2) or steam and (ii) activation in gas atmosphere at a relatively high temperature (T = 800–1200 °C) in order to further increase the porosity (Singh et al., 2020). The process that takes place is slow oxidation, which leads not only to the formation of new pores, but also to an increase in the diameter of the existing pores (Wang et al., 2017).

Physical treatment has already been studied by several research groups, especially in the case of biomass derived bio-carbons (González et al., 2013; Plaza et al., 2011, 2010; Shahkarami et al., 2015; Xiong et al., 2013). In these cases, a CO_2 adsorption capacity of even more than 100 mg/g can be achieved. In an interesting way, considerably less information is available about physical modification of sewage sludge derived bio-carbons. Despite the fact, that Tinnirello and co-workers (Tinnirello et al., 2020) observed a CO_2 adsorption capacity of 103 mg/g (temperature = 600 °C, dwell time = 2 h, nitrogen flow rate = 300 Nml/min) when they studied the physical activation of the anaerobically digested sewage sludge derived biochar. It is important to note that the reported value (2.3 mmol/g) is consistent with the adsorption capacity of activated carbon (2.6 mmol/g) (Siriwardane et al., 2001).

In addition to nitrogen, steam and CO_2 can also be used for biochar activation. According to Pallarés et al. (2018) CO_2 activation is more beneficial than steam modification, because CO_2 activation allows the formation of the desired micropores. The beneficial temperature of CO_2 activation is about 600–650 °C and the resulting biochar has basic/alkaline character. In those cases, when nitrogen is used as activating agent the temperature should be around 700 °C or even higher (Gao et al., 2014).

To increase the CO_2 sequestration capacity, chemical modification can also be used. This type of modification can be done in two ways: (i) impregnation of sewage sludge or biomass sample with the chemical agent and thermal treatment, (ii) impregnation of sewage sludge or biomass based biochar with the chemical reagent and thermal treatment (Ahmed et al., 2016; Sajjadi et al., 2019b). Increasing the CO_2 adsorption capacity, it may be beneficial to create nitrogen-containing functional groups (e.g. amide, imide, nitriles, etc.) on the surface of the biochar. For this purpose, ammonia, amines and nitric acid are the most widely used compounds (Shen and Fan, 2013). In case of ammonia treatment/ammonification the most commonly used temperature is between 600 and 900 °C, where ammonia first decomposes to free NH_2, NH radicals, atomic hydrogen and nitrogen and then the nitrogen containing functional groups are formed from the reaction of the resulting radicals and the carbon (Stöhr et al., 1991). Between the functional groups and the ammonification temperature correlations have been observed (Mangun et al., 2001). It was found that amides, imides, imines, amines and nitriles are the most dominating functional groups below 600 °C, while the thermally stable aromatic rings-like functionalities are dominated at higher temperatures (Plaza et al., 2009; Shafeeyan et al., 2010). It was also reported, that C–N and C=N chemical groups had been introduced into the char surface, by the using of 200–1000 °C ammonification temperature till 2 h (Przepiórski et al., 2004). In another study (Zhang et al., 2016) soybean straw derived biochar and 500–900 °C ammonification temperature was applied before the CO_2 adsorption capacity was determined. The resulting biochar had a micropore surface area of 311–461 m^2/g and the adsorption capacities changed between 48 and 74 mg/g (CO_2 adsorption temperature = 30 °C). It was found that increasing the temperature is beneficial from the point of view of micropore production, but the ammonification temperature has a maximum (T = 800 °C) and above this value both the surface area and the adsorption capacity decreased.

The chemical treatment can also be conducted using alkaline solutions such as KOH and NaOH (Jin et al., 2014), but impregnation of biochar with metal salt solution can also be a promising option. In case of KOH and NaOH activation O-containing functional groups (e.g. carboxyl, hydroxyl etc.) are formed on the surface of the biochar and enhance the adsorption capacity for CO_2. The reason for this is that carboxyl and hydroxyl groups led to intermolecular forces and dipole-dipole interaction with the molecule of CO_2 (Shafawi et al., 2021; Shafeeyan et al., 2012). As a result of this, the CO_2 adsorption capacity can be higher than 70 mg/g at ambient conditions, but in some cases it can be over 100 mg/g (Du et al., 2020; Manyà et al., 2018; Quan et al., 2020).

The literature results are also promising in the case of metal or metal oxide modification. In this case, aluminium chloride, magnesium chloride and iron chloride are the most widely used metal salts to impregnate the biochar. The first step is impregnation, which is followed by a thermal treatment, where the metal salts are converted into metal oxides (Ahmed et al., 2016; Jung and Ahn, 2016). Lahijani et al. (2018) studied more individual metals (Mg, Al, Fe, Ni, Ca, Na) for the activation of biochar. It was found that Mg derived compounds have the highest CO_2 adsorption capacity (82 mg/g) and Na derived compounds are the least suitable for sequestering CO_2. The latter had an even lower adsorption capacity than raw biochar. In Table 3.8 some of the results of chemical

Table 3.8
Results of chemical modification of sewage sludge derived bio-carbons.

Raw material	Conditions for biochar production	Chemical activation	BET surface area, m^2/g	Micropore volume, cm^3/g	Adsorption temperature (°C) and pressure	CO_2 adsorption capacity, mg/g (mmol/g)	Ref.
Chicken manure	400 °C	KOH, activation under N_2 at 700 °C for 1 h	22	N/A	25.1 bar	76.8	(Huang et al., 2017)
Chicken manure	400 °C	HCl, activation under N_2 at 700 °C for 1 h	137	N/A	25.1 bar	85.7	(Huang et al., 2017)
Sewage sludge	400 °C	KOH, activation under N_2 in the temperature range of 500-900 °C for 30 min	984	0.6	-	-	(Hunsom and Autthanit, 2013)

modification are summarized, particularly focusing on sewage sludge based bio-carbons.

3.2.3.2.3. Mechanism of adsorption. The CO_2 reduction should be taken by physical and chemical adsorption at low temperature or even by chemical looping at high temperatures (Igalavithana et al., 2020b; Jung et al., 2019; Shafawi et al., 2021). The adsorption properties of biochar obtained from sewage sludge pyrolysis are based on the surface characteristics of the solid particle. The adsorption ability is greatly influenced not only by the pore size or surface area of the macropores and microporous, but also by their chemical properties. Micropores have a significant role in the physical aspects of adsorption, while the surface groups can affect rather the formation of chemical relationships (Igalavithana et al., 2020b; Jung et al., 2019). When carbon dioxide is adsorbed, the groups containing nitrogen or oxygen usually form chemical linkage through acid-base (Lewis-acid and Lewis-base) reactions, while the groups containing aromatics form chemical linkage through van der Waals bonds (Igalavithana et al., 2020b; Jung et al., 2019). As a result of activation and surface modifications carried out in different ways, the relative ratio of before discussed chemical groups can be changed. This can also change the adsorption ability significantly. However during desorption, the strong chemical linkage is disadvantageous in many cases, because it does not exclude the fully removal of the adsorbed components (Igalavithana et al., 2020b; Jung et al., 2019; Shafawi et al., 2021).

3.2.3.3. Chitosan for CO_2 capture. Chitosan is a deacetylated-derivative of chitin (abundantly available biopolymer after cellulose) that has been used in various fields, including cosmetics, food industry, pharmaceuticals, biomedicine, agricultural and wastewater treatment (Pakizeh et al., 2021). Chitin can be extracted from various sources, including crustaceans, mollusks, insect shells, and cell walls of fungi (Said Al Hoqani et al., 2020; Sayari et al., 2016; Soetemans et al., 2020). Similar to biochar, chitosan possesses excellent properties that are suitable for CCT, which are biodegradability, non-toxicity, functionality, biocompatibility, and high adsorption capacity (El Knidri et al., 2016). The quality of chitosan is characterized by molecular weight (Mw) and degree of deacetylation (DD%), where commercial chitosan has a DD% ranging from 70 to 95 % and Mw ranging from 50 kDa to 200 kDa (Sun et al., 2009). In general, chitosan with high Mw (>1000 kDa) exhibits better mechanical properties (suitable to use as an adsorbent), while medium (100–1000 kDa) to low (<100 kDa) Mw exhibit better biological properties (suitable for pharmaceutical applications) (Gonçalves et al., 2021; Kou et al., 2021).

Chitosan as an adsorbent/precursor for CO_2 capture has recently caught the attention of researchers owing to the natural basicity of chitosan, where the free amino group in the chitosan structure can provide basic sites for CO_2 adsorption. Other advantages of chitosan as an adsorbent/precursor include high thermal stability, chemically inert, tunable surface functional group, minimal energy for recovery, and it is inexpensive due to the ability of mass production from chitin sources (Kamran and Park, 2020). Previous studies applied chitosan-based adsorbents in CO_2 capture and revealed that CO_2 could be adsorbed on the adsorbent surface and converted into ammonium carbamates at room temperature, then released as CO_2 from the adsorbent upon heating (Ababneh and Hameed, 2021). However, pure chitosan possesses low CO_2 adsorption and therefore, modification of the surface properties of chitosan is required to improve or maximize its adsorption efficiency toward CO_2 (Kumar et al., 2018; Peng et al., 2019). The chitosan adsorbent can be prepared via thermochemical technology such as hydrothermal carbonization, or surface functionalization with chemicals or structural modification.

Hydrothermal carbonization (HTC) operated at a temperature ranging from 180 to 260 °C with the presence of water and autogenous pressure, is a promising method for preparing chitosan-based adsorbent. It is a simple, low-cost process without the use of a catalyst or organic solvents. Thus, it has been introduced as a greener approach for the synthesis of functionalized chitosan and improving its CO_2 adsorption efficiency (Titirici and Antonietti, 2010). Research by Chagas et al. (2020) reported an outstanding performance of HTC chitosan adsorbent where the CO_2 uptake is 4-fold higher than the pure chitosan. The HTC of chitosan has been shown to increase the carbon content, and reduce the oxygen content but does not significantly change the amount of nitrogen in chitosan. Interestingly, the structural characterization of chitosan revealed the production of more aromatic amines at a longer HTC reaction time, hence causing lower basicity of chitosan, but showed a higher CO_2 adsorption capacity, suggesting that aromatic structure in HTC chitosan exposed the N atom for CO_2 adsorption (Chagas et al., 2020). Modification of the chitosan into a spherical structure via HTC was an alternative to improve the CO_2 adsorption efficiency of chitosan due to the carbon sphere providing properties such as a large contact area, adjustable surface chemistry, and open-pore structure for adsorption reactions. For instance, Wu et al. (2019) have reported that the chitosan sphere (3.28 mmol/g) has a higher BET surface area (462 m^2/g), with up to 85.5 % of micropore structure and ultra-micropore (<0.9 nm) able to enhance CO_2 capture compared to rod-structure (1.36 mmol/g) and 2D sheet structure (2.61 mmol/g) of chitosan. However, chitosan hydrochar still possesses low CO_2 adsorption efficiency and thus HTC combined with a different technique such as chemical impregnation is required to modify the surface chemistry to enhance the CO_2 capture performance.

Physical activation such as steam activation usually requires a long reaction time to achieve a high temperature, which may lead to high energy consumption (Yek et al., 2020). In contrast, chemical activation requires chemical reagents to carbonize and develop the porosity of the chitosan under low-temperature conditions and short reaction time, thus reducing energy consumption (Wang et al., 2021). In particular, NaOH, KOH, and K_2CO_3 have been discovered as effective chemical activation agents that can enhance the development of porosity in carbonaceous materials (Liew et al., 2018, 2019). For instance, Wang et al. (2021) reported on the use of mild KOH as an activation agent to enhance the porosity of chitosan hydrochar, resulting in the production of a high surface area of chitosan hydrochar (up to 2547 m^2/g). Chitosan hydrochar produced at a temperature of 600 °C exhibited the highest CO_2 capture capacity (4.41 mmol/g) compared to the other carbon produced under different precursors (e.g., walnut shell) and activating agents (e.g., $NaNH_2$), which only possessed CO_2 uptake of

Table 3.9
Summary of chitosan as CO_2 adsorbent.

Sample	Biochar porous characteristic			N content (wt%)	CO_2 adsorption capacity (mg/g) (adsorption temperature)	Ref.
	BET surface area (m^2/g)	Total pore volume (cm^3/g)	Average pore width (nm)			
Chitosan hydrochar	2.6	N/A	N/A	7.5	19.8 (25 °C)	(Chagas et al., 2020)
Carbon sphere	462	0.27	2.04	4.6	142 (25 °C)	(Wu et al., 2019)
Carbon sphere	384	0.27	N/A	11.6	154 (0 °C)	(Primo et al., 2012)
Chitosan hydrochar	1249	0.67	N/A	7.6	304 (0 °C) 194 (25 °C)	(Wang et al., 2021)
N,P-co-doped chitosan	895	0.73	6.56	N/A	234 (25 °C)	(Xiao et al., 2022)
KOH activated N-doped chitosan	1928	0.72	N/A	4.1	172 (25 °C)	(Li et al., 2022)
KAc activated N-doped chitosan	1273	0.46	N/A	5.4	156 (25 °C)	(Li et al., 2022)
K_2CO_3 activated N-doped chitosan	1147	0.42	N/A	5.3	155 (25 °C)	(Li et al., 2022)
$KHCO_3$ activated N-doped chitosan	1054	0.38	N/A	8.4	146 (25 °C)	(Li et al., 2022)
K_2CO_3 activated chitosan	1673	0.73	0.60	5.3	169 (25 °C)	(Fan et al., 2013)
$NaNH_2$ modified chitosan	1740	0.98	N/A	5.1	278 (0 °C)	(Yang et al., 2022)

3.06 mmol/g (Yang et al., 2019). This suggests the potential of chitosan hydrochar as a desirable precursor and KOH as an effective activation agent in producing carbon with high porosity as an adsorbent for CO_2 uptake.

Other than alkalis, acids can also be used as an alternative activation agent. Xiao et al. (2022) introduced phytic acid into the carbon network of chitosan gel to fabricate N, P-co-doped porous carbon materials (NPPCs). The surface area of NPPCs (690–1010 m^2/g) was lower than carbon produced using alkali but exhibited a higher CO_2 uptake (5.31 mmol/g) as compared to chitosan hydrochar in the previous study (2547 m^2/g and 4.41 mmol/g, respectively) (Wang et al., 2021), thus showing the better potential of NPPC to be used as a CO_2 capture. The effects of different chemical activators for chitosan activation were performed by Li et al. (2022) using KOH, potassium acetate (KAc), potassium carbonate ($KHCO_3$), and potassium bicarbonate (K_2CO_3). The research revealed that activation via KOH produces a chitosan-based adsorbent with a high surface area (1928 m^2/g) and high CO_2 adsorption capacity (3.91 mmol/g). However, KOH is highly corrosive, and an alternative has been provided by the author by using KAc activation that produced a chitosan-based adsorbent with comparable surface area (1273 m^2/g) and CO_2 adsorption capacity (3.52 mmol/g).

Physical impregnation has emerged as a new research area for the synthesis of chitosan-based adsorbents for CO_2 adsorption. For instance, Peng et al. (2019) synthesized an amine-impregnated adsorbent by impregnating chitosan-derived adsorbent with a pentaethylenehexamine (PEHA), which was inspired by conventional CO_2 adsorption using liquid amine. Chitosan loaded with PEHA showed higher CO_2 (3.72 mmol/g) uptake compared to pure chitosan-derived adsorbent (0.21 mmol/g) at 100 °C, thus implying the effectiveness of amines-impregnated carbon to capture CO_2. Besides that, Yang et al. (2022) developed N-doped porous carbon via mixing and ball-milled chitosan and $NaNH_2$. The use of $NaNH_2$ as the source of nitrogen and porogen during carbonization has increased the surface area and pore structures of the N-doped porous carbon. N-doped carbon material showed a high surface area (2398 m^2/g) and high CO_2 adsorption capacity (6.33 mmol/g), showing better CO_2 adsorption performance compared to carbon-based adsorbent produced using $ZnCl_2$ (2.62 mmol/g) (Xu et al., 2020). Although much research has been carried out to modify the physicochemical properties of chitosan to be used in CO_2 adsorption, there are many research gaps to be filled as compared to biochar as CO_2 adsorbents, such as the optimization of carbonization parameters, utilization of suitable activator and the CO_2 adsorption temperature and pressure. It is worth noting that chitosan has a more desirable properties such as high surface N-functional group in nature, low cost, biodegradable and non-toxic as compared to biochar, thus, novel and optimize research for chitosan-based adsorbent for CCT should be performed. Table 3.9 summarizes the synthesis techniques of chitosan-based adsorbent for CO_2 capture.

The CO_2 adsorption mechanism of biochar and chitosan are similar as both carbon materials have N-containing functional group on the surface, and pore structure that facilitates the adsorption processes. Studies have indicated that CO_2 adsorption to the adsorbent occurs *via* physisorption and chemisorption. Physisorption of CO_2 is dominated by the pore structure and surface area, where micropore sizes of 0.3–0.8 nm are preferable, and < 0.5 nm are optimum for CO_2 adsorption (Igalavithana et al., 2020c). Physisorption is mainly induced by van der Waals and micropore-filling effects (Shafawi et al., 2021). The chemisorption of CO_2 is dominated by Lewis acid-base interaction and hydrogen bond interaction. The hydrogen bond is formed between CO_2 and O-containing functional groups. In general, O-containing functional groups are acidic, which may hinder the adsorption of acidic CO_2. Interestingly, some studies revealed that hydroxyl (-OH) and carboxyl group (-COOH) enhance the hydrogen bond interaction. This is attributed to the electronegativity different of H atom (2.1) and O atom (3.5), causing the H atom from -COOH and -OH having high electropositivity to interact with the O atom from CO_2 *via* hydrogen bond (Liu and Wilcox, 2012). However, this hydrogen bond is weak and the presence of H_2O molecules would hinder the formation of the hydrogen bond. This is because the presence of H_2O molecules created a strong dipole moment on the adsorbent surface compared to the weak quadrupole moment of CO_2 (Liu and Wilcox, 2012). Thus, H_2O molecules are selected for hydrogen bonding instead of CO_2 with the adsorbent.

Lewis acid-based interaction occurs between N-containing functional group on the adsorbent surface and the CO_2 molecule. Generally, the N atom is electron-rich, attributed to the presence of a lone pair of electrons, thus it facilitates the adsorption of CO_2. Other than lewis acid-based interaction, some N-containing functional groups can form hydrogen bonds with CO_2 molecules owing to their naturally high electropositivity (Lim et al., 2016; Liu et al., 2013). Thus, CO_2 can form hydrogen bonds with the N-containing functional group on the adsorbent. For instance, Fan et al. (2013) reported that a major of pyridone was present in the chitosan-derived CO_2 adsorbent, and contributed mainly to CO_2 adsorption. The presence of -OH adjacent to the N atom resulted in a p-π conjugation effect (from -OH) with the π bond, thus increasing the adsorbent's electron density and improving its Lewis basicity. Fig. 3.23 shows the possible reaction that occurs during CO_2 adsorption to biochar/chitosan adsorbent. Although many studies have been carried out to identify the possible reaction mechanism for CO_2 adsorption

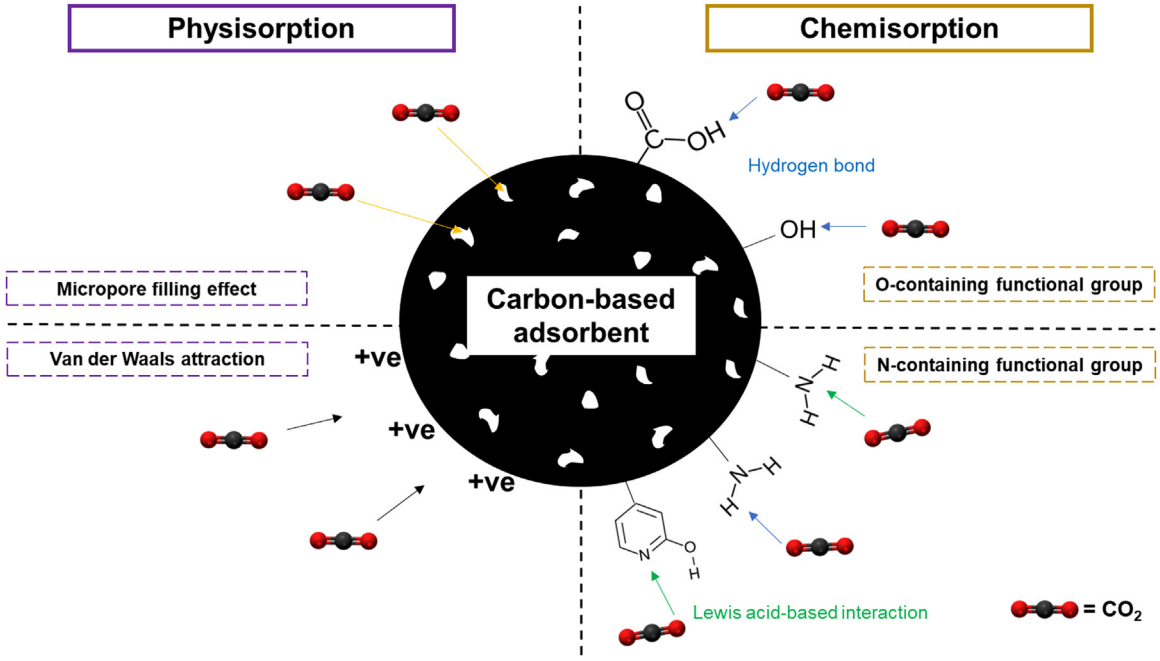

Fig. 3.23. Possible reaction mechanism of CO_2 adsorption on carbon-based adsorbent. (For interpretation of the references to color in this figure legend, the reader is referred to the web version of this article.)

on the carbon-based adsorbent, the variation of feedstock types can significantly affect the functional groups of the adsorbent, thus affecting the adsorption efficiency of CO_2.

3.2.4. Solid amine-based sorbent

Amine-based adsorbents have the advantages of high adsorption capacity, thermal stability, and good regeneration performance in comparison with granular solid adsorbents (Raganati et al., 2021). By means of the addition of amine functional groups, it could evenly disperse in solid adsorbents, providing alkaline sites for the adsorption of acid gas (CO_2). Porous solid supports, such as porous silica, alumina, porous carbons, zeolites, polymers, and metal organic frameworks (MOFs), always have large pore volumes and specific area. CO_2 adsorption performances of diverse amino-solids are discussed in the following sections.

3.2.4.1. Reaction mechanism. Solid amine-based sorbents are the functional combination of aqueous amine and porous solid adsorbents. As for existing amines, tethered amines onto solid adsorbents could substantially reduce energy requirements to liberate captured CO_2 from the relatively dilute amine solutions, and avoid equipment corrosion occurring during the amine scrubbing process. Conceivably, the interaction between amino groups is strengthened within the constrained space of porous solid material. From the perspective of porous solid adsorbents, the incorporated amine will dramatically improve CO_2 capacity and selectivity via chemical adsorption even at low pressure, but might increase mass transfer resistance of adsorbate to contact amine groups within microporous materials. Therefore, the performance of solid amine-based sorbents reflects a compromise on the advantages and disadvantages between aqueous amine and porous solid adsorbents. To deeply uncover adsorption-desorption mechanism, the structure of amines and their reaction routes with adsorbate, the texture of different solid supports and their physisorption properties, as well as the interaction between amines and solid supports, should be taken complete account. Three aspects i.e. reaction mechanism of CO_2 with amines, adsorption thermodynamics and kinetics, and the deactivation mechanism, are discussed.

3.2.4.1.1. Adsorption mechanism. CO_2 adsorption mechanism of solid amine-based sorbents is analogous to one that occurs by absorption of amine solutions via acid-base interaction, which is confirmed by numerous in situ spectroscopic studies using solution- and solid-state nuclear magnetic resonance (SSNMR) and infrared (IR) spectroscopy combined with theoretical calculations (Chen et al., 2018; Forse and Milner, 2020). Under dry conditions, the formation of carbamate is achieved by substituting hydrogen of amine with CO_2, which means only H-containing amines, i.e. primary and secondary amines are available. According to Reaction 3.3, two amidogens are necessitated to capture one molecule of CO_2. Whereas the introduction of moisture, which exits widely in various sources for CO_2 capture, could improve amine efficiency by one fold via the formation of bicarbonate or carbonate compared with that without moisture. In Reaction 3.4, water attributes a hydroxide to CO_2 molecule. Therefore, it is suitable for all primary, secondary and tertiary amines. Obviously, amine-based adsorbents could achieve higher CO_2 adsorption under humid conditions, while moisture is deleterious on the CO_2 adsorption capacity of porous zeolites and MOFs owing to their hydrophilic nature over exposed metal ions. It should be noted that the amine efficiency is limited to 0.5-1 under humid conditions because of kinetically controlled bicarbonate formation (Serna-Guerrero, 2008).

$$2RNH_2 + CO_2 \rightleftharpoons RNHCOO^{-}RNH_3^{+} \tag{3.3}$$

$$RNH_2 + CO_2 + H_2O \rightleftharpoons RNH_3^{+}HCO_3^{-} \tag{3.4}$$

Said et al. (2020) proposed a unified approach to CO_2-amine reaction mechanism in Fig. 3.24. At high amine loading under dry conditions, nucleophilic attack of CO_2 by amines is primarily assisted by a neighbouring amine (X = N, Y = N), which leads to a 1,n-zwitterion (n > 3) or to alkylammonium carbamate, and it depends on whether two amines involved are linked or separated. At low amine loading, nucleophilic attack of CO_2 by isolated amines may be assisted by hydroxyl groups (X = N, Y = O), leading to carbamic acid or hydronium carbamate. Under humid conditions, water may assist nucleophilic attack of CO_2 by amines (X = N, Y = O) to form hydronium carbamate or play a role of a nucleophile assisted by amines to form ammonium bicarbonate (X = O, Y = N) at the expense of carbamate. The latter mechanism applies for tertiary and hindered amines, regardless of surface density.

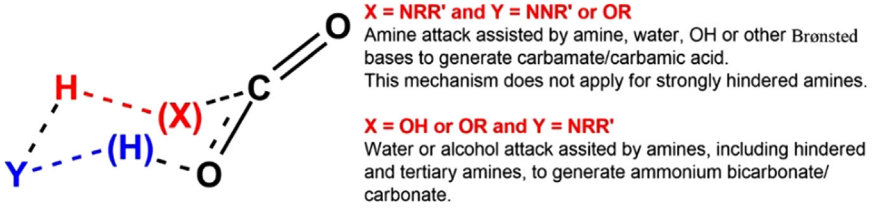

Fig. 3.24. The unified schematic mechanism for CO_2-amine-water interactions (Said et al., 2020). (For interpretation of the references to color in this figure legend, the reader is referred to the web version of this article.)

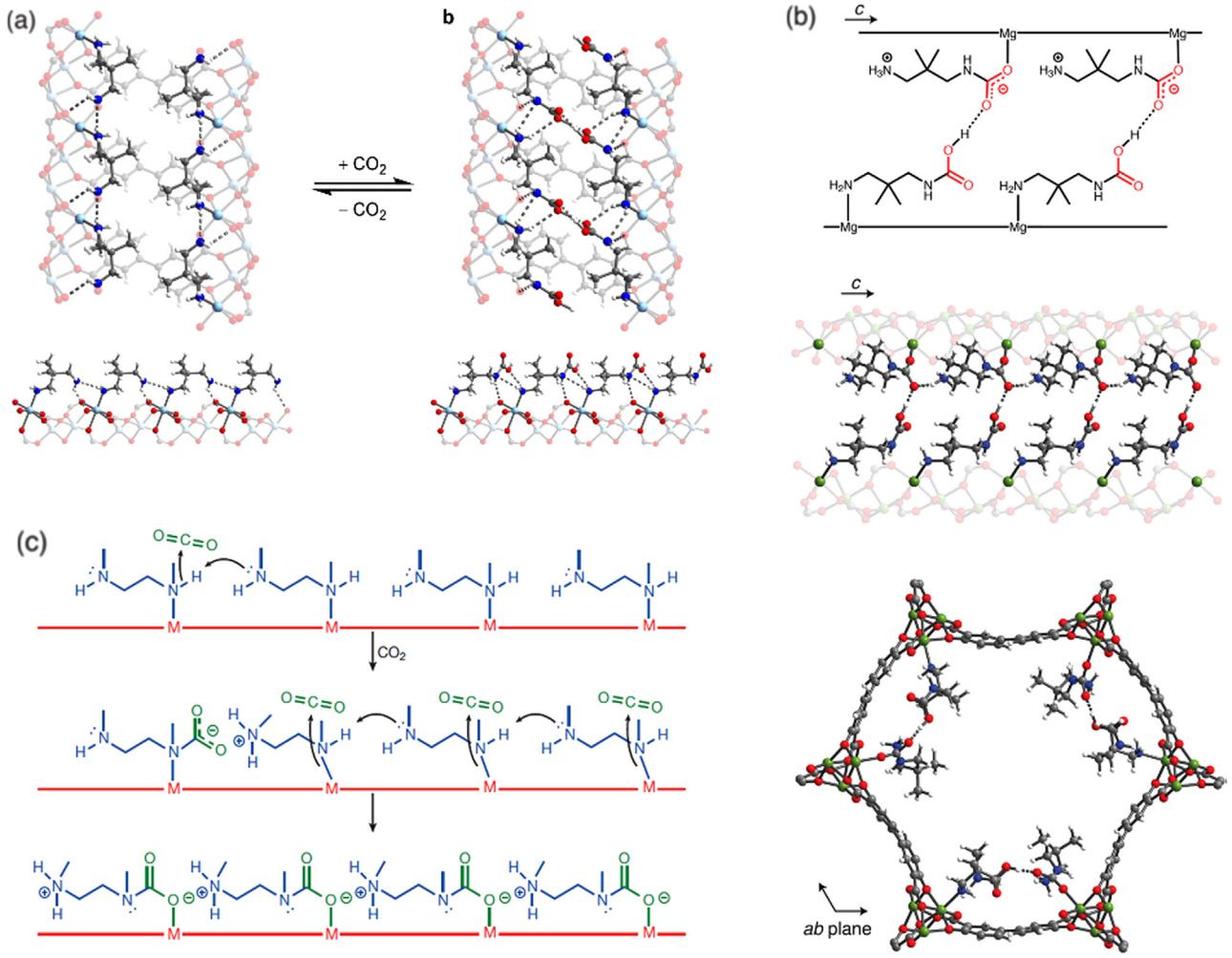

Fig. 3.25. The cooperative mechanism over amine-functionalized MOFs sorbents (a) The formation of carbamic acid pairs over dmpn-Zn_2 (dobpdc) (Milner et al., 2017); (b) Mixed chemisorption structure with ammonium carbamate and carbamic acid in a 1:1 ratio for dmpn–Mg_2 (dobpdc) (Forse et al., 2018); (c) The formation of carbamic acids and mixed ammonium carbamates/carbamic acids over mmen-M_2 (dobpdc) (mmen = N,N9-dimethylethylene diamine, M = Mg, Mn, Fe, Co, Zn) (McDonald et al., 2015). (For interpretation of the references to color in this figure legend, the reader is referred to the web version of this article.)

Initially, amine-based silica sorbents are widely investigated. Therefore, classical preparation methods, referring to impregnation and grafting by silane linkage, are derived from amine-silica adsorbents. Meanwhile, the proposed reaction mechanism above is based on aminosilicas. In the last decade, thriving porous materials such as MOFs, covalent organic polymers (COPs), and their amine functionalized adsorbents have drawn more attention. New reaction pathways beyond the traditional formation of ammonium carbamates are then proposed (Forse and Milner, 2020). Long et al. proposed a unique cooperative mechanism of CO_2 adsorption involving the formation of ammonium carbamate chains (Milner et al., 2017; Siegelman et al., 2017), and firstly demonstrated the feasible formation of carbamic acid pair to compete with ammonium carbamate chain during CO_2 adsorption over dmpn-Zn_2 (dobpdc) (dmpn= 2,2-dimethyl-1,3-diaminopropane) (Fig. 3.25a) (Milner et al., 2017). Later, they elucidated a new chemisorption mechanism using dmpn-Mg_2 (dobpdc), which involved the formation of a 1:1 mixture of ammonium carbamate and carbamic acid (Fig. 3.25b) (Forse et al., 2018). Also, a cooperative mechanism, the formation oxygen-bound carbamate chains by CO_2 inserting into the metal-N bonds, given rise to unusual step-shaped CO_2 adsorption (Fig. 3.25c) (Kim, 2020; McDonald et al., 2015). It was anticipated that coordination forms of amine and porous material with different structure could give rise to a spectacular mechanism in the future.

3.2.4.1.2. Adsorption thermodynamics & kinetics. Equilibrium adsorption capacity, reaction heat, and kinetics are key parameters for overall evaluation. These parameters could be obtained by adsorption isotherms. The distinction caused by amine functionalization is principally summarised. As for amine-functionalized solid sorbents,

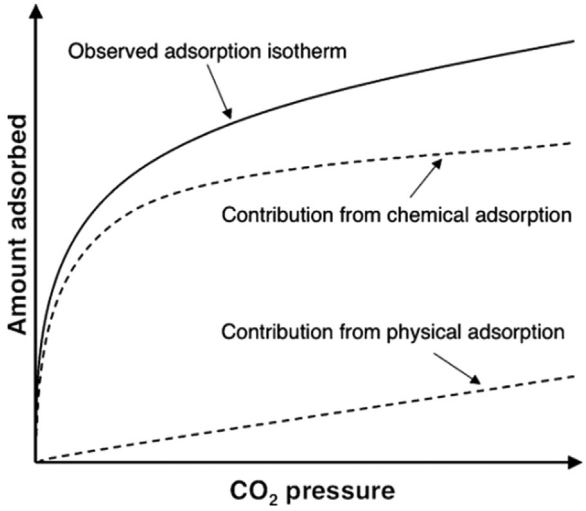

Fig. 3.26. Schematic representation of CO_2 adsorption on amine-functionalized mesoporous adsorbents (Serna-Guerrero et al., 2010). (For interpretation of the references to color in this figure legend, the reader is referred to the web version of this article.)

CO_2 adsorption is implemented via two independent mechanisms, i.e. chemisorption with amine-functionalized groups and physisorption on surface of solid adsorbent. In Fig. 3.26, chemical adsorption contributes to a high initial CO_2 uptake at the lower partial pressure while physisorption is enhanced with the increasing partial pressure. Langmuir isotherm model and Freundlich isotherm model, suitable for both chemisorption and physisorption processes, are widely adopted for describing the adsorption behaviour of amine functionalized adsorbent. However, Serna-Guerrero et al. (2010) pointed out that these two isotherm models were acceptable for describing adsorption profiles at low concentrations of CO_2 but less reliable at higher pressures. Therefore, they adapted a semi-empirical two-site Toth isotherm model, including two parts to represent chemisorption and physisorption, respectively. The model was successfully employed on different amine-functionalized materials with various adsorbates (Bollini et al., 2012a; Gebald et al., 2014).

Adsorption heat can be calculated from the adsorption isosteric curve by applying Clausius–Clapeyron. Generally, adsorption heat lower than 50 kJ/mol indicates weak physical adsorption, while that higher than 50 kJ/mol indicates the effects of chemical adsorption or reaction (Gelles et al., 2019; Siriwardane et al., 2005). High adsorption heat demonstrates strong interaction between CO_2 and amine, and further improves CO_2 selectivity, however, will increase the temperature of the process. Higher temperatures can decrease the adsorption capacity of the adsorbents, meanwhile resulting in higher desorption energy demands. To reduce energy consumption, two approaches are listed as follows:

1) Tuning the structure of solid support material and its interaction with suitable amine types through a new reaction mechanism. For instance, the distinct adsorption route of dmpn-Mg_2 (dobpdc) to CO_2, i.e. the formation of both ammonium carbamates and carbamic acids, results in high entropy penalty (-74 kJ/mol) coupled with a large entropic penalty (-204 J/mol/K). It can reduce the temperature required to desorb CO_2 in a temperature-swing adsorption process to lower than 100 °C (Milner et al., 2017). Long et al. prepared serials of diamine-appended MOFs, which could behave as 'phase-change' adsorbents with unusual step-shaped CO_2 adsorption isotherms (McDonald et al., 2015). As shown in Fig. 3.27, adsorption isotherm shifts markedly with temperature, resulting that a large working capacity can be achieved with only a small increase in temperature. Besides, they demonstrated tetraamine-appended MOFs with two-step cooperative CO_2 adsorption that could use low-temperature steam for the desorption process (Kim, 2020).
2) System analysis and optimization of the whole reaction process. Zhang et al. (Zhang et al., 2016) systematically evaluated the effect of significant parameters, i.e. adsorbent property, adsorption heat, specific capacity, working capacity, moisture adsorption, swing temperature difference and heat recovery degree. The calculated regeneration heat for PEI/silica adsorbent was 2.47 GJ/tCO_2, while this value was 3.9 and 3.3 GJ/tCO_2 for a typical aqueous and an advanced MEA system, respectively.

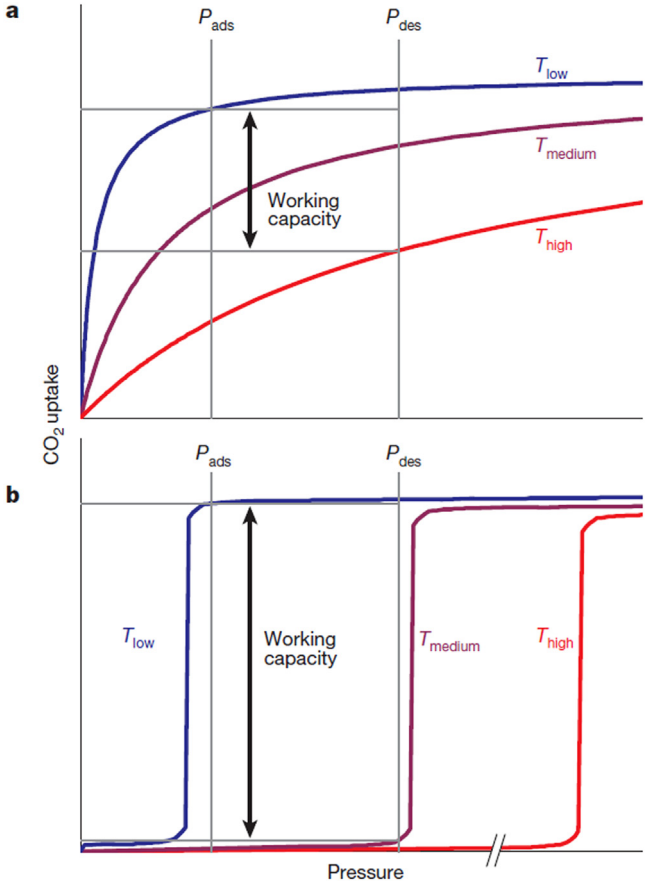

Fig. 3.27. Variation in the idealized adsorption isotherm behaviour with temperature for a classical microporous adsorbent (a) The usual Langmuir-type isotherm shape, compared with that of a phase-change adsorbent (b) Step-shaped (sometimes referred to as 'S-shaped') isotherms (Kim, 2020). (For interpretation of the references to color in this figure legend, the reader is referred to the web version of this article.)

Similar to porous adsorbents, kinetics for amine-functionalized adsorbents can be modelled by pseudo-first order law, pseudo-second order law, Elovich equation, Avrami model, and film diffusion model, among which pseudo-first order and pseudo-second order models are the simplest to understand the interaction mechanism of gas-solid adsorption (Syeda Saba Fatima, 2021). In Fig. 3.28, compared with benchmark adsorbent, the dynamic adsorption breakthrough curve of CO_2 over amine-functionalized adsorbents displayed a relatively sharp trend followed by a long tail. The sharp trend inferred favourable interactions between CO_2 and amine groups, while long tails signified large mass transfer resistance because of diffusion hindrance of amine groups (Bollini et al., 2012a, b). It has been well established that the adsorption behaviour of CO_2 onto benchmark adsorbent was driven by thermodynamic effects, while an opposing trend for amine functionalized adsorbent was controlled by kinetic effects. It is of significance to balance the thermodynamic and kinetic effects of CO_2 adsorption. Besides, adsorp-

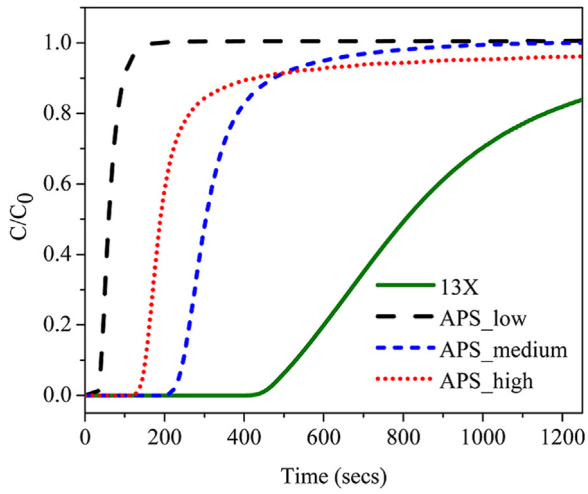

Fig. 3.28. APS-functionalized silica adsorbents at three different amine loadings compared to the benchmark zeolite 13X at 25 °C (Bollini et al., 2012a, b). (For interpretation of the references to color in this figure legend, the reader is referred to the web version of this article.)

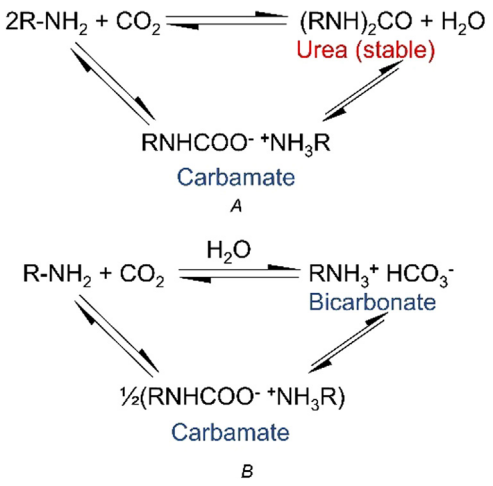

Fig. 3.29. (A) Schematic representation of urea formation under dry adsorption conditions, and (B) Inhibition thereof in the presence of added water vapour (Belmabkhout, 2010). (For interpretation of the references to color in this figure legend, the reader is referred to the web version of this article.)

tion kinetics are largely influenced by the process temperature, amine type, amine loading, and support material, which have been widely discussed in previous literature.

3.2.4.1.3. Deactivation mechanism. Stabilities of amine-functionalized CO_2 adsorbents during multiple adsorption-desorption cycles are the prerequisite for its industrial applications. A robust adsorbent should withstand many adverse effects including physical and chemical properties, feed gas composition and characteristics, and operational parameters. More detailed reviews have been summarized by Jahandar Lashaki et al. (2019) and Fan and Jia (2022). Herein, chemical deactivation associated with the interaction between amines and different gas compositions is focused, such as O_2, SO_x, NO_x and CO_2.

Due to the existence of oxygen in the feeding gas, such as 3-15 % from power plant flue gas (Siegelman et al., 2021), 21 % in the air, oxidative degradation of adsorbents has to be concerned. Akin to gas-liquid absorption systems, amine in adsorbents is prone to be oxidized to imine, imide, amide or nitrone groups when exposed to high O_2 concentration, elevated temperature and metal ions (Heydari-Gorji et al., 2011a). Amine structure obviously affects its oxidative degradation, which indicates that single secondary amines and mixed amines readily degrade to oxygen-containing gas mixtures at high temperatures (Bali et al., 2013). Though strategies such as conversing primary amines into secondary/tertiary amines (Choi et al., 2016; Zhang et al., 2012), chelating ppm-level metal impurities of PEI (Min et al., 2018), and using longer linkers between amine groups in amino-polymers (Pang et al., 2018) could mitigate the adverse effect of oxygen, the mechanism of oxidative degradation is still unclear.

CO_2-induced deactivation refers to the formation of stable urea between amine and CO_2. In Fig. 3.29, urea groups may form readily by direct interaction between amine species and CO_2 at high temperature under dry conditions. When moisture-containing gases are employed, urea formation can be strongly inhibited, even at a relatively low humidity (Belmabkhout, 2010; Li et al., 2016). Sayari et al. (2012) investigated the interaction between CO_2 and amines-containing mesoporous silica under dry condition, and proposed different reaction pathways depending on the structure and nature of amine-containing species (Fig. 3.30). As for primary amines, CO_2-induced deactivation undergoes through intermediacy of isocyanate followed by reaction with primary or secondary amine into di- and trisubstituted open-chain urea or N-substituted imidazolidinones. As for materials containing ethylenediamine units with secondary amines, formation of the corresponding N,N′-disubstituted imidazolidinones takes place through the dehydration of ammonium carbamate or carbamic acid. Also, they pointed out that all or some CO_2-deactivated materials may be regenerated via urea hydrolysis using a humidified inert gas under relatively high temperature (100–200 °C). Furthermore, Jung et al. (2017) found that the conversion of primary into secondary amines in different oligomers and polymers via functionalization with 1,2-alkylepoxide, 1,3-butadiene diepoxide and epichlorohydrin could effectively inhibit the formation of urea linkages.

Generally, SO_x and NO_x in the flue gases potentially cause adsorbent deactivation by competing adsorption with CO_2, resulting from adsorption reversibility on amines in the order of $CO_2 > SO_2 > NO_2$ (A. Diaf, 1994). Since SO_2 is a stronger Lewis acid, SO_2 can interact strongly with all amines, including tertiary amines, through Reaction 3.5 under dry conditions and Reaction 3.6 under humid conditions, respectively. Nevertheless, Tailor and Sayari (Heldebrant et al., 2010; Tailor and Sayari, 2016; Yang et al., 2013) found that SO_2 could react with tertiary amines by Reaction 3.7 and Reaction 3.8 to form non-covalent charge transfer complexes, leading to adsorbent deactivation.

$$2RNH_2 + SO_2 \rightleftharpoons RNH_2^+SO_2^- \quad (3.5)$$

$$RNH_2 + SO_2 + H_2O \rightleftharpoons RNH_3^+HSO_3^- \quad (3.6)$$

$$R\,(CH_2CH_2OH)_2N + SO_2 \leftrightarrow R\,(CH_2CH_2OH)_2N \cdots SO_2 \quad (3.7)$$

$$R\,(CH_2CH_2OH)_2N + SO_2 + H_2O \leftrightarrow R\,(CH_2CH_2OH)_2NH^+HSO_3^- \quad (3.8)$$

3.2.4.2. Modification of different adsorbents.

3.2.4.2.1. Description of three subclasses (I, II, III class). Considering bond structures and preparation methods, amine-based adsorbents could be divided into three subclasses in Fig. 3.31. Class I materials are prepared by physical impregnation with monomeric or polymeric within the pore of the supports, bonding through hydrogen bonds and/or dipole interactions. Class II materials are obtained by covalently grafting the targeted amines with relatively low molecule weight onto the surface of the support. As for Class III materials, they are prepared via in-situ polymerization of amine-containing monomers. Also, Class I materials are considered as promising candidates for industrial CO_2 capture because of high CO_2 adsorption capacity under the condition of low CO_2 concentration. However, shorter chained amines are preferable for the formulation of class II or class III adsorbents due to lower activation energies which aid in the facilitation of tethering (Bollini et al., 2011).

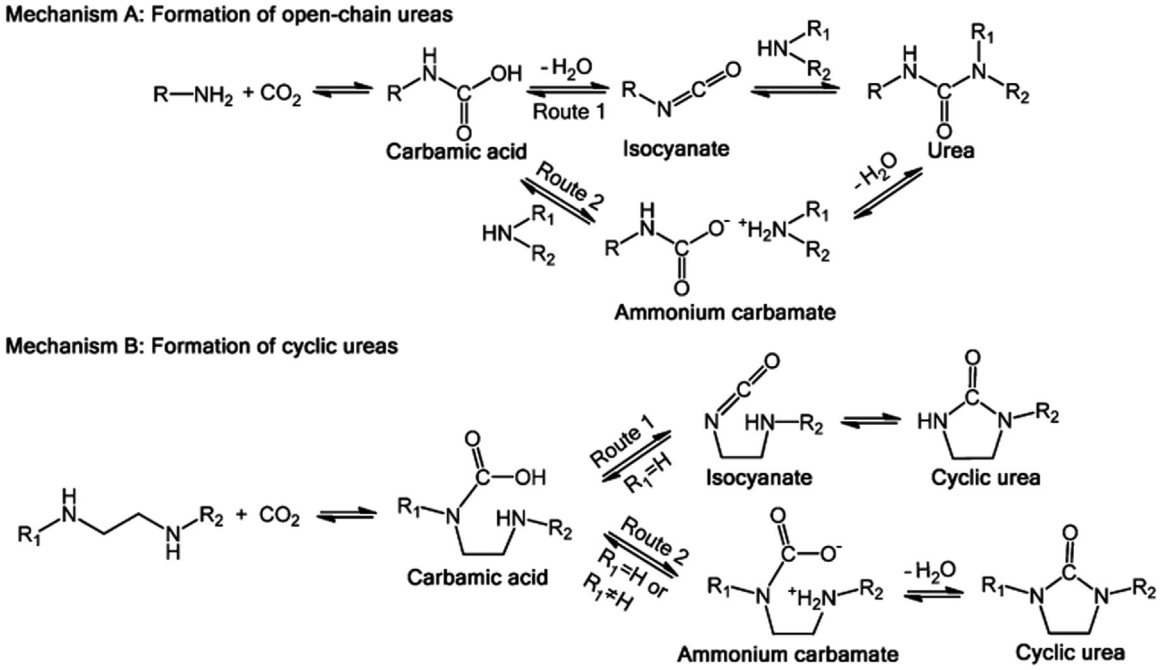

Fig. 3.30. Mechanisms of CO_2-induced degradation of supported amines (Sayari et al., 2012). (For interpretation of the references to color in this figure legend, the reader is referred to the web version of this article.)

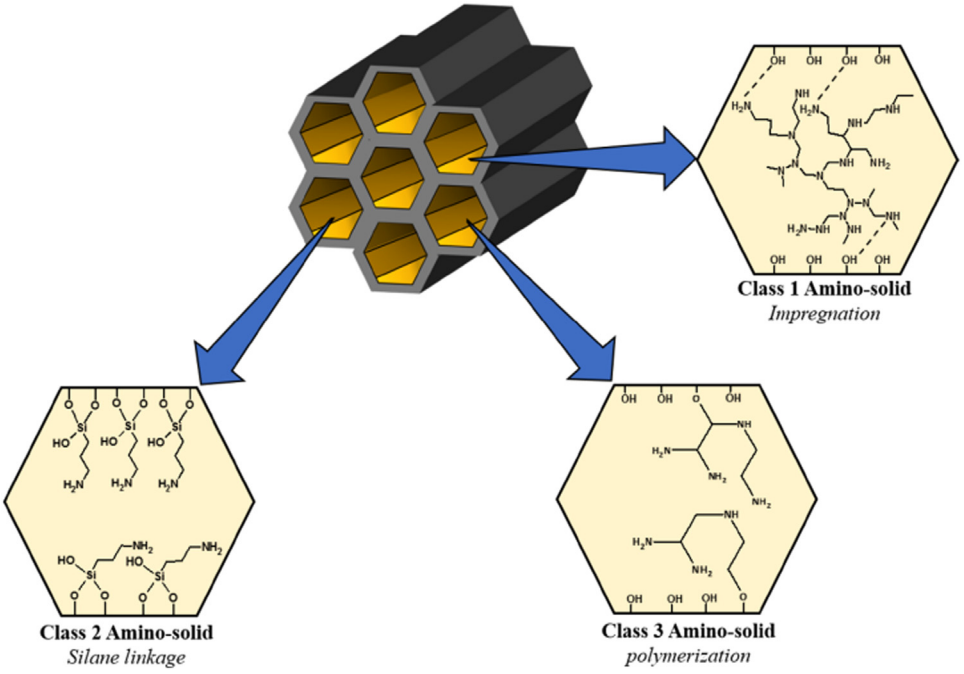

Fig. 3.31. Amino-solids based on preparation methods (Didas et al., 2015). (For interpretation of the references to color in this figure legend, the reader is referred to the web version of this article.)

3.2.4.2.2. Porous silica supports (I, II, III). As one of the important porous materials, porous silica is a chemically and thermally stable material with turntable textural and surface properties, e.g. pore size, pore distribution, surface area, and surface hydroxyl groups (Gawande et al., 2015; K, 1979; Verma et al., 2020). These features make it versatile and used in various technological or industrial applications, e.g. adsorption, medical, energy, catalyst and support materials (Liang et al., 2017). Thus, a variety of porous silica materials functionalized with amine have been synthesized and characterized to chemisorb CO_2 from different gas streams. For three classes of supported amine adsorbents, recent advances in porous silica support are summarized and discussed in this section.

Class 1: Amine-impregnated silica

The first ever literature reported in the field of amines impregnated silica was reported in 2002 (Xu, 2002), and the authors used a high surface area mesoporous silica MCM-41 as the support material for PEI loading, and the resulting adsorbent was termed as “molecular basket”. With PEI loading amount of 75 wt%, the highest CO_2 adsorption capacity of 3.02 mmol/g was achieved at a pure CO_2 atmosphere and 75 °C. The pore structure of porous silica was an important factor that affected the distribution of PEI. Son et al. (2008) further synthesized mesoporous silica with different pore structures and impregnated it with the same amount of PEI (50 wt%). CO_2 uptake capacity was in the order of KIT-6 (3D) > SBA-15 (1D) ~ SBA-16 (3D) > MCM-48 (3D) > MCM-41 (1D). The highest CO_2 adsorption capacity achieved by KIT-6 was mainly attributed to the large pore size and 3D structure. To further investigate

Table 3.10
Amine-porous silica CO_2 adsorbent prepared by physical impregnation method.

Support material	Amine type	Temperature (°C)	CO_2 partial pressure (atm)	Adsorption capacity (mg/g, dry CO_2)	Ref.
MCM-41	PEI	75	0.15	89	(Xu, 2005)
Pore expanded MCM-41	PEI	75	1	210	(Heydari-Gorji et al., 2011b)
SBA-15	PEI	75	0.15	105	(Yan et al., 2011b)
As-syn SBA-15		75	1	173	(Yue et al., 2006)
	Tetraethylenepentamine				
HMS	PEI	75	1	184	(Chen et al., 2010)
KIT-6	PEI	75	1	135	(Son et al., 2008)
As-syn KIT-6	PEI	75	1	139	(Kishor and Ghoshal, 2016)
Silica monolith	PEI	75	1	210	(Chen et al., 2009)
Mesocellular silica foam	PEI	75	0.15	152	(Yan et al., 2011a)
MSU-F silica		50	1	260	(Goeppert et al., 2011)
	Tetraethylenepentamine/diethanolamine				
Fumed silica	PEI	25	0.0004	52	(Goeppert et al., 2011)
CARiACT G10 silica	PEI	80	1	123	(Ebner et al., 2011)
Mesoporous silica nanotubes	PEI	85	0.6	121	(Niu et al., 2016)
Rice husk derived silica	PEI	75	0.15	159	(Zeng and Bai, 2015)
TUD-1 mesoporous sponge	PEI	75	0.15	116	(Wang et al., 2014)
Hollow silica microspheres	PEI	25	1	149	(Cecilia et al., 2016)

the influence of the pore structure of silica on CO_2 adsorption, Yan et al. (2011b) investigated PEI impregnated SBA-15 with different pore structures, and found that CO_2 adsorption amount increased proportionally with the total pore volume of SBA-15 support. However, pore size was not the main factor influencing CO_2 adsorption capacity. Besides, roles of micropores in SBA-15 were found not obvious as they have been blocked by amine (Yan et al., 2013). Overall, the ideal silica support would have high pore volume, which can load a high amount of amines and it should leave the voids in the pores for CO_2 diffusion. Thus, extensive research on the amine-impregnated porous silica for CO_2 capture have been reported. Some typically porous silica supports used for amine impregnation are summarized and given in Table 3.10.

Class 2: Amine-containing silane modified silica

The grafted amines on silica often have better thermal stability up to 200–250 °C when compared with physically impregnated silica (Sayari, 2006). Hydroxyl groups of silica supports played an important role because covalent bonds will be formed between hydroxyl groups and amino-silanes. Thus, available hydroxyl groups determine the content of amines grafted. Similar to the amine physically impregnated silica, the CO_2 adsorption capacity of amine containing silane modified silica was also affected by the pore structure of the silica support. Fayaz et al. (Fayaz and Sayari, 2017) found that P10 silica with a pore size of 21 nm exhibited a high CO_2 adsorption capacity of 86 mg/g after 3-[2- (2-aminoethylamino)ethylamino] propyltrimethoxysilane grafted. Jahandar Lashaki et al. (2017) synthesized SBA-15 with different pore structures, and functionalized them with 3-[2- (2-Aminoethylamino) ethylamino] propyltrimethoxysilane for CO_2 adsorption. Results indicated that amine-silane grafted SBA-15 with larger pore size exhibited a higher CO_2 adsorption capacity. The CO_2 capture performance of aminesilane-modified silica is included in Table 3.11.

Class 3: In situ polymerized amine on silica

Class 3 adsorbents bind amines covalently to hydroxyl groups of the support, which is similar to class 2 sorbents. However, the densities of amine groups are similar to class 1. Thus, Jones et al. defined class 3 as a combination of class 1 and 2 (Sanz-Perez et al., 2016a). Usually, the adsorption capacities of Class 3 sorbents are higher than that of Class 2 adsorbents due to their high amine loading amounts, and they also have good reusability in successive runs. Porous silica support has a large surface area, pore volume and plenty of surface -OH groups, which facilitate the grafting of the amines. Thus, different kinds of silica materials have attracted considerable research interest since 2000s (Acosta et al., 2004; Chaikittisilp et al., 2011; Lunn and Shantz, 2009). A summary of the CO_2 adsorption capacity of grafting amines by in-situ polymerization onto porous silica is given in Table 3.12.

3.2.4.2.3. Polymer supports (I, II, III). Polymers can refer to inorganic polymers (e.g. geopolymer, clay etc.), organic polymers (i.e. porous organic polymers, POPs) and inorganic-organic coordination polymers (e.g. MOFs). Since geopolymer, MOFs and their amine-tethered adsorbents have been introduced in other sections, amine-tethered POPs adsorbents are especially focused. Amine adsorbent known as HSC+, which was applied by NASA to regeneratively remove CO_2 from space shuttle in 20 years ago, belongs to the amine-tethered polymer adsorbents (Satyapal et al., 2001). This proprietary material bonds polyethyleneimine (PEI) to solid polymethyl methacrylate polymeric support, with poly (ethylene glycol) (PEG), to enhance CO_2 adsorption and desorption rates. POPs with ultrahigh surface areas, tunable pore structure and adjustable chemical properties can be synthesized diversely from organic molecular building blocks (Cooper, 2009; Dawson et al., 2012), and are ideal supports for amine functionalization because of their chemically inert, high stability, and low production cost (Slater and Cooper, 2015). Amine modification can improve POPs not only for CO_2 adsorption capacity, but also for CO_2 selectivity (Lu et al., 2012). For example, amine e.g. EDA DETA, TETA, TAEA, AA, PEI and 2.5-dibromoaniline anchored onto PPN-6, CMP-1, polymethylmethacrylate (PMMA) could increase CO_2 uptake when compared with corresponding pristine supports (Gelles et al., 2019; Han et al., 2015; Hu, Xiayi et al., 2020; Jahandar Lashaki et al., 2019; Jiang et al., 2013; Mukhtar et al., 2020). A detailed list of amine-modified POPs and their CO_2 adsorptive properties can be found in a recent review (Zou et al., 2017).

For amine-loaded polymers, researchers have focused on amine selection and polymer preparation. Jafari et al. (2017) synthesized mesoporous polydivinylbenzene (PDVB) materials using 2, 2′-Azobis (2-methylpropionitrile) (AIBN) as the initiator through microwave-assisted polymerization and then impregnated the material with the amine-rich co-monomers of vinylimidazole (VI) and vinyl triazole (VT). With more active sites, VT-modified PDVB had a maximum CO_2 adsorption of 2.65 mmol/g at 0 °C under 100 kPa, while the adsorption capacity of VI-modified PDVB was 2.35 mmol/g under the same conditions. Liu F. et al. (2017) prepared PDVB through one-pot, timsolvothermal polymerization and impregnated them with PEI. The optimum formulation was 58 wt% PEI (to the adsorbent) impregnated PDVB (0.58PEI@PDVB) with maximum adsorption capacities of 3.76 and 3.00 mmol/g under pure CO_2 and 10 % CO_2, respectively, at 75 °C. The stability under both conditions was maintained after ten adsorption cycles under both dry

Table 3.11
Amine-porous silica CO_2 adsorbent prepared by the amine-silane grafting method.

Support material	Amine type	Temperature (°C)	CO_2 partial pressure (atm)	adsorption capacity (mg/g, dry CO_2)	Ref.
Pore-expanded MCM-41	N- (3-trimethoxysilylpropyl) diethylenetriamine	75	0.2	92	(Loganathan and Ghoshal, 2017)
MCM-48	2-[2- (3-trimethoxysilylpropylamino) ethylamino]ethylamine	25	0.15	70	(Nigar et al., 2016)
SBA-15	3-[2- (2-Aminoethylamino) ethylamino] propyltrimethoxysilane	25	0.05	83	(Jahandar Lashaki et al., 2017)
HMS	Aminopropyltrimethoxysilane	20	0.9	53	(Knowles and Chaffee, 2016)
P10 silica	3-[2- (2-Aminoethylamino)ethylamino] propyltrimethoxysilane	50	0.05	86	(Fayaz and Sayari, 2017)
Amorphous silica	[3- (methylamino)propyl]trimethoxysilane	30	0.17	60	(Park et al., 2016)
SBA-16	N- (2-Aminoethyl)-3-aminopropyltrimethoxysilane	60	0.15	32	(Wei et al., 2008)
SBA-12	3-Aminopropyltrimethoxysilane	25	0.1	46	(Zelenak et al., 2008)
MSU-F silica	3-[2- (2-Aminoethylamino)ethylamino] propyltrimethoxysilane	45	0.3	72	(Lee et al., 2011)
Silica gel	3-Aminopropyltrimethoxysilane	27	1	18	(Leal, 1995)
Fumed silica	3-[2- (2-Aminoethylamino) ethylamino]propyltrimethoxysilane	25	1	41	(Czaun et al., 2013)
SiO_2 aerogel	3-Aminopropyltrimethoxysilane	25	0.1	86	(Cui et al., 2011)
Double-walled silica nanotube	3-[2- (2-Aminoethylamino)ethylamino] propyl trimethoxysilane	25	1	98	(Ko et al., 2013)

Table 3.12
Amine-porous silica CO_2 adsorbent prepared by the in-situ polymerization method.

Support material	Amine type	Temperature (°C)	CO_2 partial pressure (atm)	adsorption capacity (mg/g, dry CO_2)	Ref.
Pore-expanded -MCM-41	3-[2- (2-aminoethylamino)ethylamino]propyl trimethoxysilane	25	0.05	62	(Sayari, 2006)
SBA-15	3-aminopropyltrimethoxysilane	25	0.1	50	(Chaikittisilp et al., 2011)
Mesoporous Silica	Polyethenimine	75	0.15	124	(Klinthong et al., 2016)
Silica spheres	Trimethoxy [3- (methylamino)propyl]silane	50	0.1	44	(Hahn et al., 2016)
Silsesquioxane aerogel	(3-Aminopropyl) triethoxysilane	50	0.01	134	(Kong et al., 2016)
Precipitated silica	(3-Aminopropyl) triethoxysilane	50	0.14	45	(Quang et al., 2017)
Silica monolith	tetraethylenpentamine	75	1	171	(Wen et al., 2010)
SiO_2 aerogel	3-Aminopropyltriethoxysilane	25	0.1	86	(Cui, Sheng et al., 2011)

and wet conditions. Zheng et al. (2019) synthesized an N-abundant and mesopores-rich POPs by solvothermal copolymerization of divinylbenzene (DVB) and 1-vinylimidazole (VI) without the use of any templates. It was found that PEHA-impregnated P (DVB-VI) adsorbents displayed CO_2 capacities as high as 4.56 mmol/g at 75 °C and atmospheric pressure, together with excellent CO_2/N_2 selectivity and good recycling stability.

To reduce the cost of material development, a simplified preparation route and utilization of existing polymers have drawn more attention. Wang et al. (2022) reported a novel synthesis method by in situ ring-opening grafting copolymerization of aziridine with the polyHIPE (HIPE = high internal phase emulsion). The adsorption capacity of 2.40 and 3.25 mmol/g could be achieved under dry and humid conditions at 0.1 atm partial pressure of CO_2, respectively. Further, they fabricated 4.0PEI70k@polyHIPE adsorbent by one-step method (Fig. 3.32), which indicated a maximum adsorption capacity of 4.18 mmol/g at 20 °C under humid conditions (Wang et al., 2021). Stiernet et al. (2022) combined Radziszewski's multicomponent reaction and high internal phase emulsion (HIPE) polymerization in a one-pot manner (Fig. 3.32). The bifunctional amine/imidazolium foams revealed superior CO_2 capture performances when compared to their monofunctional counterparts, indicating the synergy between functional groups. Yang et al. (2019) developed a facile strategy that converted a cost-effective porous organic polymer, which was synthesized by Friedel-Crafts alkylation reaction of dichloro-p-xylene, into outstanding CO_2 adsorbents through one-step post-synthesis functionalization with polyamines. Adsorbents showed good CO_2 uptake capacity, fast adsorption-desorption kinetics and excellent stability toward both water vapour and regeneration cycles under dynamic flow conditions. As for existing polymers, Meng et al. (2021) found that tethering PEI onto conventional porous supports HP20 could achieve superior adsorption properties with above 4 mmol/g and cyclic stability with around 1 % loss after 30 cycles, which were rather than ones synthesized through complex approaches.

3.2.4.2.4. Zeolite supports (I, II, III). Zeolites, possessing the merit of tunable textural properties, variable pore sizes, and interconnecting channels and cavities, have been widely used in CO_2 via their steric effect, kinetic effect, equilibrium effect and trapdoor effect (Bai et al., 2022; Yue et al., 2022). However, hydrophilic nature and physical adsorption behavior incapacitate zeolites for CO_2 separation under the conditions of humidity, high temperature (>30 °C), and low pressure (<2 bar). Amine-functionalized zeolites have been demonstrated to empower CO_2 capture from humid streams and improve selectivity (Chen et al., 2015; Kim et al., 2016; Kolle et al., 2021; Jadhav, 2007; Su et al., 2010). Two kinds of amine-functionalized zeolites, prepared by impregnation and grafting, are discussed as follows respectively. (Fig. 3.33)

Class I: Physical impregnation of monomeric and polymeric amines.

Impregnation is a cost-effective method for the preparation of amine-functionalized zeolites. However, two issues should be addressed. Firstly, microporous zeolite is prone to be blocked by impregnated amines, resulting in the decrease of adsorption capacity. Murge et al. (2019) found that the adsorption capacity of in-house-synthesized zeolites decreased with increasing TEPA loading. Meanwhile, the decrease in physisorption capacity was several times higher than the expected increase in chemisorption capacity. However, commercial zeolites had an optimal amine loading 2.5 %. On the contrary to high amine loading up to 70 %, Panda et al. (2019) synthesized a binder-containing zeolite 4A bodies (IBA-Z4A) modified with 0.3 % iso-butylamine, which

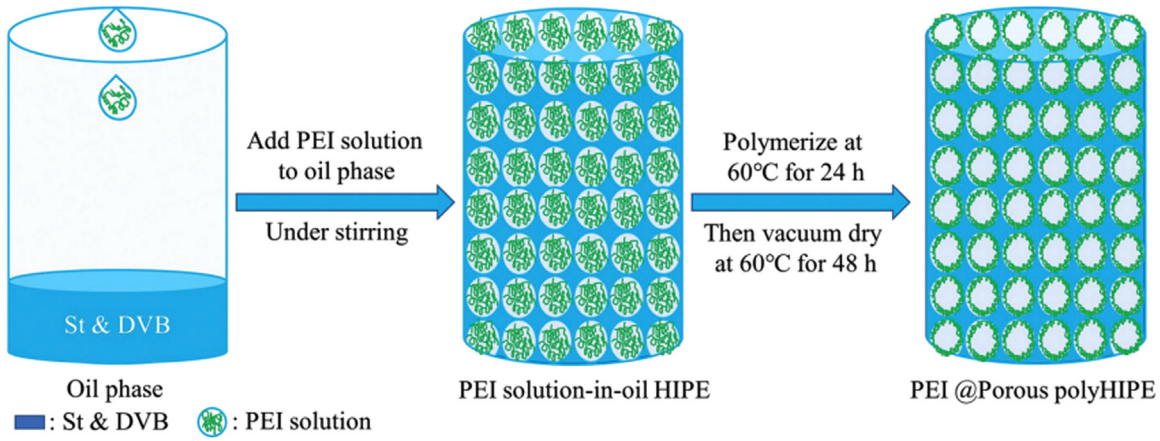

Fig. 3.32. Synthetic procedure for PEI functionalized polyHIPE (Wang et al., 2021). (For interpretation of the references to color in this figure legend, the reader is referred to the web version of this article.)

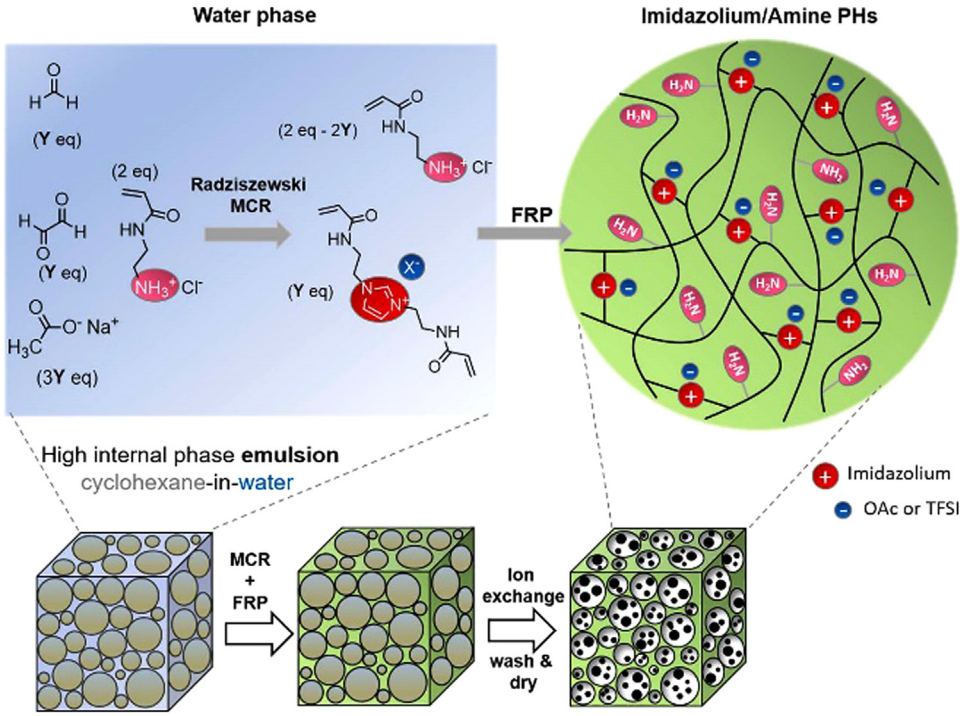

Fig. 3.33. Imidazolium/amine polyHIPEs synthesis combining Radziszewski MCR and emulsion templating polymerization (Stiernet et al., 2022). (For interpretation of the references to color in this figure legend, the reader is referred to the web version of this article.)

exhibited excellent CO_2 adsorption performance with adsorption capacity of 2.56 mmol/g and remarkably high CO_2/N_2 selectivity of 335 at 25 °C and 1 bar. Whereas CO_2/N_2 selectivity of pristine binder-containing zeolite 4A bodies was only 24. The other issue is that the impregnated amines is liable to evapourate at elevated temperature, especially for small-molecular amines. It remarkably affects adsorption thermal stability. To hinder the amine loss, Yu et al. (2014) proposed a ship-in-a-bottle method to prepare NaY zeolites loaded with amine functionalized ionic liquids (Fig. 3.34) by employing unique cage structures of microporous zeolites. The trick of this method lay in the in-situ synthesis of large molecular ionic liquid, 1-aminopropyl-3-methylimidazolium bromide ([APMIM]Br) within super cage using the smaller precursors (e. g. N-methylimidazole and 3-bromopropylamine) that can diffuse through zeolite windows. Whereas the formed target guest ([APMIM]Br) is too big to cross the windows. These host-guest systems exhibited superb adsorption capacity up to 4.94 mmol/g and good cyclic ability with 5 % decreasing adsorption capacity after 20 working cycles.

Heat consumption and cost should be taken into account for industrial applications. Kalantarifard et al. Cheng et al. (2021b) synthesized EDA impregnated ZSM-5 for CO_2 adsorption, with the highest CO_2 adsorption capacity of 6.13 mmol/g in the presence of water at 75 °C. Microwave heating was employed for the desorption process, and the fastest desorption time was 9 min for 70 % EDA loaded ZSM-5. Recently, Cheng et al. (2021a) tethered monoethanolamine (MEA) and hydroxyethyl ethylenediamine (AEEA) onto HZSM-5 zeolites via wet impregnation method, respectively. The result indicated that MEA and AEEA fixed HZSM-5 zeolites had good CO_2 adsorption capacities, with maximum values of 4.27 and 4.44 mmol/g, respectively. Notably, the CO_2 desorption process of AEEA loaded HZSM-5 exhibited a low activation energy of 54.27 kJ/mol. HZSM-5 zeolite provided a large number of free H^+ ions to directly participate in carbamate breakdown, and metal atoms (Al) that attached to N atom of carbamate, thereby stretching the C–N bond and promoting decomposition. To further reduce the cost of adsorbents, Thakkar et al. (2017) prepared ZSM-5, zeolite-Y and SAPO-34 from kaolin clay and modified them with TEPA for capturing CO_2 from

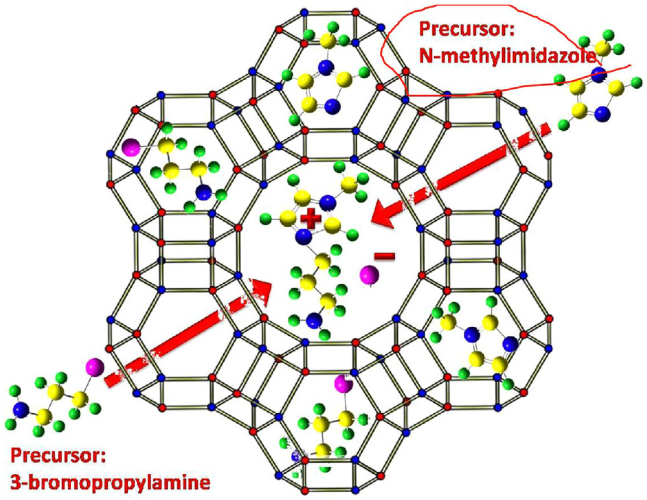

Fig. 3.34. Schematic illustration of ship in a bottle synthesis of [APMIM]Br@NaY (Liu F. et al., 2017). (For interpretation of the references to color in this figure legend, the reader is referred to the web version of this article.)

the air. The best adsorption capacity was 1.12 mmol/g for the TEPA-loaded ZY at 25 °C using 5000 ppm CO_2 in nitrogen.

Class II: Grafting.

Similar to the impregnated amine onto zeolites, the grafted amine can reduce adsorption capacity, but improve the selectivity over other gas and amine stability. Kim et al. (2013) functionalized SAPO-34 with 3-aminopropyltrimethoxysilane (APMS). It demonstrated that the functionalized mesoporous SAPO-34 (NH_2-SAPO (M)-34) had a lower CO_2 adsorption capacity than its pristine counterparts. However, it exhibited improved CO_2/N_2 selectivity. Bezerra et al. (2014) found that increasing amine grafted to zeolite 13X adsorbent tended to reduce micropore volume of the resulting adsorbents by pore blocking with MEA. Liu F. et al. (2017) synthesized an ethylenediamine-grafted Y zeolite with working capacities higher than 1.1 mmol/g over 20 temperature swing adsorption (TSA) cycles, and reported that the strongly co-adsorbed H_2O within the hydrophilic zeolite micropores suppressed urea formation under desorption conditions according to Le Chatelier's principle. Yang et al. (2012) concluded that CO_2 adsorption capacity varied in the sequence of MCM-22 (2.09) > NH_2-ITQ-2 (1.73) > ITQ-2 (1.64) > NH_2-MCM-22 (1.52) > MCM-36 (1.32) > NH_2-MCM-36 (1.20) > Fe-MCM-22 (1.20 mmol/g) at 298 K, but NH_2-ITQ-2 showed exceptionally high CO_2/N_2 selectivity of 10.8.

To further boost the stability of APTES grafted zeolite β, Liu et al. (2020) proposed an alkyl-functionalization method for the stoichiometric conversion of primary amines to secondary amines. Alkyl-functionalized-APTES zeolite exhibited the adsorption capacity of 1.44 mmol/g of 15 % CO_2 at 90 °C and a very high sorption rate ($t_{1/2}$ = 0.69 min of over 90 % of total sorption capacity within 5 min). Also, long-term stability after 20 cycles in a TSA operation with above 0.9 mmol/g at pure CO_2 regeneration was observed.

Recently, another zeolite-like adsorbent, geopolymer, was adopted as efficient amine support. Chen et al. (2022) grafted APTES onto the geopolymer treated with nitric acid and achieved a high grafting amount of 3.5 mmol N/g due to the large specific surface area of 412 m^2/g and superior silanol density of 4.25 mmol/g. The as-prepared amine functionalized solid sorbent showed a remarkable adsorption capacity of 1.82 mmol/g with fast adsorption kinetics and low energy requirement for regeneration.

Class III

Liang et al. (2022) immobilized monoethanolamine (MEA) and ethylenediamine (ED) via ionic bond to the zeolite Y framework to overcome amine degradation. The elemental analysis demonstrated that ED had successfully grafted almost twice as many amino groups as MEA within the same solvent concentration. It indicated that 20 % ED@HY had the highest CO_2 adsorption capacity of 1.76 mmol/g at 90 °C with superior performance in cyclic thermal stability in the condition of the adsorption temperature of 90 °C and the desorption temperature of 150 °C. Wahono et al. (2021) deposited a solid-state amine adsorbent on natural mordenite-clinoptilolite zeolite through a simple plasma polymerization. The plasma deposition of amine polymer under certain conditions resulted in a significant increase in surface area-weighted CO_2 adsorption capacity and weakened the strength of the interaction between CO_2 and the adsorbent.

Post-synthetic functionalization by organic molecules has been proposed as an effective strategy to tailor the adsorption properties of zeolites (Nik et al., 2011). Small amine molecules can be chemisorbed onto micropore walls via conjugate acid-base formation between the Brønsted acid sites of the zeolite and the basic N atoms. Kwon et al. (2022) adopted this method to covalently attached various functional groups (-$PhNH_2$, -$PhCH_2NH_2$, -PhCOOH, -PhOH, -Ph) onto the micropore walls of beta zeolites to modify their adsorption properties. The results conducted that the benzylamine functionalized β zeolite exhibited higher CO_2 adsorption than its pristine counterpart under flue gas conditions with 10.5 % CO_2, 5 % H_2O and 84.5 % N_2, which might be attributed to the synergistic effect of the hydrophobic benzene and basic amine moieties in the benzylamine group.

Hierarchical microporous and amorphous is another strategy for improving the properties of amine functionalized zeolite (Ge et al., 2021; Jia et al., 2022). Liu et al. (2016) fabricated a series of 5A zeolite-based hybrids with a shell of mesoporous silica-supported-amine (5A@MSAs) to dynamically hinder the diffusion of water molecules into the zeolite core. 5A@MSA-30 was demonstrated to be the best candidate for CO_2 capture with the CO_2 uptake as high as 5.05 mmol/g at 298 K and 10 cyclic stable adsorption/desorption operation.

3.2.4.2.5. MOF supports (I, II, III). MOFs as porous crystalline materials are composed of metal nodes that are combined with organic linkers. In view of their well-ordered porous structures, such as high specific surface area, pore volume and easily adjustable composition and pore structure, MOFs have been viewed as promising candidates for CO_2 capture technology. Over the last two decades, research on MOFs and MOFs-amine composites has been the study button and widely studied. However, the crystalline or microcrystalline form factor has limited the development of MOFs for commercialization application (Sanz-Perez et al., 2016a). Therefore, the modification of MOFs by amines has been sought in an effort to advance the utility of MOFs.

Class I

Class I amine-modified MOFs are common in adsorption applications because large pore volume allows the loading of high amine contents, which results in physisorption and chemisorption conducted at the same time. Therefore, Class I amino-MOFs always show high CO_2 adsorption capacity. However, unlike traditional mesoporous amine-based adsorbents, MOFs are microporous materials. The bulky amino polymers have the possibility to block the pores during the impregnation process and even decompose the structure (Gelles et al., 2019). A majority of Class I amino-MOFs select MIL-101 as support in view of its chemical stability, which could prevent pore degradation as a result of unintended side reactions (Gelles et al., 2019). For example, the impregnation of PEI onto MIL-101 was first reported in 2013. The results demonstrated an increase in CO_2 adsorption capacity, reaching 5.1 mmol/g at 25 °C, 1.75 bar when the amine loading is 100 % (Lin et al., 2013). Also, Uio-66 was impregnated with PEI and achieved a CO_2 adsorption capacity of 1.65 mmol/g and 2.41 mmol/g under the condition of a dry and humid environment. After several adsorption and regeneration experiments, the composite could recover the capture performance completely (Xian et al., 2015a). Typical class I amino-MOFs are summarized in Table 3.13.

Class II

Class II amine-MOFs CO_2 adsorbents are rarely reported due to the lack of functionalized sites, which are suitable for silane attachment.

Table 3.13
CO_2 adsorption capacity of class I amine-MOFs CO_2 adsorbent.

Support material	Amine type	Temperature (°C)	CO_2 partial pressure (kPa)	Adsorption capacity (mmol/g, dry CO_2)	Reference
MIL-101	PEI	25	175	5.10	(Lin et al., 2013)
MIL-101	PEI	25	100	3.30	(Xian et al., 2015a)
MIL-101 (Cr)	PEI	25	10	1.30	(Yan et al., 2013)
MIL-101 (Cr)	DETA	23	100	3.56	(Hu et al., 2014)
MIL-101 (Fe)	DETA	25	100	1.82	(Mutyala et al., 2019b)
MIL-101 (Cr,Mg)	PEI	25	100	3.04	(Gaikwad et al., 2019)
MIL-101 (Cr)	PEI	75	100	3.81	(Mutyala et al., 2019a)
MIL-101	TREN	25	0.04	2.60	(Darunte et al., 2016)
MIL-53	TEPA	45	500	1.40	(Martínez et al., 2016)
Uio-66	PEI	65	100	1.65	(Xian et al., 2015a)
Uio-66	PEI	35	10	0.75	(Xian et al., 2015a)
Cu_3 $(BTC)_2$	PEI	25	100	10.0	(Aarti et al., 2016)
HKUST-1	TEPA	45	500	2.3	(Martínez et al., 2016)
ZIF-8	TEPA	45	500	2.0	(Martínez et al., 2016)
ZIF-8	PEI	35	10	1.4	(Yang et al., 2022)
ZIF-8	PEI	65	100	1.61	(Xian et al., 2015b)
Zn/Co ZIF	PEI	25	100	1.82	(Cheng et al., 2019)
MOF-177	DETA	25	100	2.83	(Gaikwad et al., 2021)
MOF-177	TEPA	25	100	3.82	(Gaikwad et al., 2021)
MOF-177	TEPA	55	100	4.6	(Gaikwad et al., 2021)
Mg-MOF-74	TEPA	25	100	5.68	(Su et al., 2017)

Pokhrel et al. (2018) grafted APTES onto ZIF-8, and the results suggested CO_2 adsorption capacity of 0.8 mmol·g^{-1} was achieved under the condition of 1 bar dry CO_2 atmosphere at 25 °C. Also, the capture performance of class II amino-ZIF didn't change (0.8 mmol/g) under 10 % RH humid condition and humidified stability was improved. Also, deprotonated MEA was grafted onto UiO-66, which reveals a CO_2 capacity of 0.8 mmol·g^{-1} at 0.15 bar CO_2 and 298 K, and it could maintain the adsorption performance even at high relative humidity (82 %) (Li et al., 2015). When it comes to adsorption performance, markedly improvement was not observed between class II and class III amino-MOFs. Therefore, considering the inefficient synthesis procedure of preparation of amino-MOFs, class II amino-MOFs prepared by the grafting method are not suitable for scaled applications (Gelles et al., 2019).

Class III

As for class III amine-MOFs CO_2 adsorbents, less energy is required for amine-tethering in comparison with the energy used for silane attachment of class II amino-MOFs making them attractive candidates for capture application. As for class III materials, ED was first incorporated into ZIF-8, and the experimental results demonstrated the potential for stable CO_2 adsorption. At 1 bar, the composite showed a CO_2 adsorption capacity of 0.68 mmol/g (Pokhrel et al., 2018). Since then, various supports have been selected for amine modification with different amines. For example, MIL-101 was grafted with PEHA and TEPA, and increased CO_2 adsorption capacities were observed, with the highest adsorption capacity up to 3.1 mmol/g at 25 °C, 1 bar (Huang et al., 2016). Similarly, a number of attempts have been conducted for Mg_2/DOPDC and Mg_2 (dobpdc). And class III amino-MOF adsorbents are listed in Table 3.14 (Gelles et al., 2019).

3.2.4.2.6. Carbon supports (I, II, III). Carbonaceous adsorbents are utilized widely in the field of gas adsorption and separation processes due to high surface area, large pore volume, high stability and relatively low adsorption/desorption temperatures (Lee et al., 2015). Amine-modified carbonaceous materials, such as activated carbon (AC), carbon nanotubes (CNTs) and porous carbon supports, could perform similar CO_2 adsorption performance as amine-modified porous silica because of their stable structural pores. Among various carbonaceous materials, cost-effective ACs are the most common in practical applications. ACs supports always use lignocellulose and coal, e.g. coconut shell, bamboo and coke, as raw materials. After the physical or chemical activation process, pore structures of ACs are improved. The high surface area of ACs allows for subsequent amine modification. After surface amine modification, ACs display higher affinities towards CO_2, which could then improve CO_2 adsorption capacity. As advanced materials, CNTs have been investigated widely in recent years in light of their high thermal and chemical stability as well as their unique physiochemical properties. Additionally, CNTs exhibit similar CO_2 adsorption performance as functionalized high surface area ACs (Lawson et al., 2018).

Class I

Class I materials have been widely investigated due to the simplicity of the physical impregnation method. Gholidoust et al. impregnated DEA onto oil sands coke-based ACs and reported the highest CO_2 adsorption capacity of 5.63 mmol/g at 50 °C. The results suggested a 75 % improvement in comparison with commercial zeolite 13X (Gholidoust et al., 2017). Moreover, the effects of different amines, including DEA, MDEA and TEPA were investigated. The results indicated that ACs impregnated with secondary amines (DEA) have a more profound reaction with CO_2 than tertiary amines (MDEA), which agreed with CO_2 and amine reactivity: order primary > secondary>tertiary (Gholidoust et al., 2017). Also, the stimulatory effect of water was proven by MDEA@AC, increasing from 0.58 mmol/g to 1.70 mmol/g at 20 % RH. Gibson physically impregnated EDA and TETA onto microporous and mesoporous ACs. The results demonstrated that microporous ACs were not suitable for amine-impregnation because the filling of the external channel leaded to the blockage of pores and then restrained further diffusion into the inner pores (Gibson et al., 2015). For CNTs, Zhou compared the CO_2 capture capacity of two types PEI-modified CNTs (L-PEI and B-PEI). The results suggested that although lower CO_2 adsorption capacity was achieved by L-PEI-impregnated CNT when compared with CNT modified by B-PEI, it exhibited lower desorption and better stability, which allowed for practical application for a long time (Zhou et al., 2017). CO_2 adsorption capacity of class I amine-carbon materials are shown in Table 3.15.

Class II

Class II amino-carbon materials are always focused on CNTs supports rather than ACs supports because covalent functionalization on the CNTs interface does not compromise the structural integrity of the supports (Gelles et al., 2019). By means of covalently bonding PEI onto functionalized-single wall CNTs (SWCNTs), enhanced CO_2 adsorption capacity could reach 1.77 mmol/g at 75 °C, 1 bar (Eoghan, 2008). Similarly, increased CO_2 uptake was also observed by APTES-modified multi-wall CNTs (MWCNTs), reaching 1.25 mmol/g 60 °C and 0.15 bar with 5 wt% APTES loading. Also, in the presence of water, CO_2 capture capacity increased with the increase of water content. Under the same condition of temperature, pressure and amine loading, CO_2 uptake increased from 1.25 mmol/g to 1.53 mmol/g at 35 % RH (Su et al., 2009). What's more, due to the combined adsorption capacities of chemisorp-

Table 3.14
CO_2 adsorption capacity of class III amine-MOFs CO_2 adsorbent.

Support material	Amine Type	Temperature (°C)	CO_2 partial pressure (kPa)	Adsorption capacity (mmol/g, dry CO_2)	Reference
ZIF-8	ED	25	100	0.68	(Pokhrel et al., 2018)
ZIF-8	ED	25	2500	10.0	(Zhang et al., 2013)
ZIF-8	ED	35	1000	4.8	(Thompson et al., 2013)
MIL-101	PEHA	25	100	1.3	(Anbia and Hoseini, 2012)
NH_2-MIL-101	TEPA	25	100	3.1	(Huang et al., 2016)
MIL-101 (Cr)	TEPA	25	100	2.75	(Wang et al., 2012)
Mg_2/DOPDC	m-2	25-120	100	5.0	(Siegelman et al., 2017)
Mg_2/DOPDC	mm-2	25-120	100	5.1	(Siegelman et al., 2017)
Mg_2/DOPDC	mmen	25-120	100	5.0	(Siegelman et al., 2017)
Mg_2/DOPDC	i-2	25-120	100	4.9	(Siegelman et al., 2017)
Mg_2/DOPDC	ii-2	25-120	100	5.1	(Siegelman et al., 2017)
Mg_2/DOPDC	e-2	25-120	100	4.5	(Siegelman et al., 2017)
Mg_2/DOPDC	ee-2	25-120	100	4.4	(Siegelman et al., 2017)
Mg_2/DOPDC	e-2-e	25-120	100	4.6	(Siegelman et al., 2017)
Mg_2 (dobpdc)	dmen	40	100	4.34	(Lee et al., 2015)
Mg/DOBDC	ED	25	100	4.5	(Lee et al., 2015)
Mg/DOBDC	ED	25	0.04	1.6	(Choi et al., 2012)
Mg/DOBDC	mmen	25-75	100	4.0	(McDonald et al., 2015)
Mg_2 (dobpdc)	pn	40	100	4.6	(Milner et al., 2017)
Mg_2 (dobpdc)	mpn	40	100	3.8	(Milner et al., 2017)
Mg_2 (dobpdc)	dmpn	40	100	4.2	(Milner et al., 2017)
Co/DOBDC	mmen	25-75	100	3.9	(McDonald et al., 2015)
Fe/DOBDC	mmen	25-75	100	3.5	(McDonald et al., 2015)
Mn/DOBDC	mmen	25-75	100	3.5	(McDonald et al., 2015)
Ni/DOBDC	mmen	25-75	100	3.9	(McDonald et al., 2015)
Zn/DOBDC	mmen	25-75	100	3.0	(McDonald et al., 2015)

Table 3.15
CO_2 adsorption capacity of class I amine-carbon materials CO_2 adsorbent.

Support material	Amine type	Temperature (°C)	CO_2 partial pressure (kPa)	Adsorption capacity (mmol/g, dry CO_2)	Ref.
Oil sands coke-based AC	DEA	50	66	5.63	(Gholidoust et al., 2017)
Oil sands coke-based AC	MDEA	50	66	0.58	(Gholidoust et al., 2017)
Oil sands coke-based AC	TEPA	50	66	0.90	(Gholidoust et al., 2017)
AC	MEA	75	10	1.70	(Bezerra et al., 2011)
AC	TEA	75	10	0.27	(Bezerra et al., 2011)
Palm shell-based AC	AMP	25	30	1.50	(Lee et al., 2013)
Palm shell-based AC	AMPD	25	30	1.20	(Lee et al., 2013)
AC	AMP	26	15	0.77	(Khalil et al., 2012)
AC	MEA	25	15	1.11	(Khalil et al., 2012)
Mesoporous AC	BPEI	25	0.04	2.25	(Wang et al., 2015)
Mesoporous AC	BPEI	25	0.5	3.34	(Wang et al., 2015)
Nanoporous carbon	PEI	75	100	0.26	(Tang et al., 2013)
Nanoporous carbon	PEI	75	100	1.01	(Tang et al., 2013)
Nanoporous carbon	PEI	75	10	0.23	(Tang et al., 2013)

Table 3.16
CO_2 adsorption capacity of class II amine-carbon materials CO_2 adsorbent.

Support material	Amine type	Temperature (°C)	CO_2 partial pressure (kPa)	Adsorption capacity (mmol/g, dry CO_2)	Reference
SWCNT	PEI	75	100	1.77	(Eoghan et al., 2008)
MWCNT	APTES	60	15	1.25	(Su et al., 2009)
MWCNT	APTES	50	15	1.95	(Su et al., 2011)
MWCNT	PEI	70	20	0.98	(Zhou et al., 2018)
CNTs	APTS	25	10	0.93	(Chungsying Lu, 2008)
CNTs	APTS	25	50	2.19	(Chungsying Lu, 2008)
Granular AC	APTS	25	50	1.81	(Chungsying Lu, 2008)
CNTs	APTS	20	15	0.98	(Su et al., 2009)

tion and physisorption for amine-based CNTs, CO_2 adsorption capacity enhanced with the increase of amine loading amounts. The investigation of PEI-modified MWCNTs demonstrated the steam and resultant suitability for CO_2 capture in post-combustion process after eleven working cycles (Zhou et al., 2018). Class II amine-carbon adsorbents are listed in Table 3.16.

Class III

CO_2 adsorption capacities of Class III amine-carbon materials have also been investigated widely, especially for ACs. Firstly, after anchoring TETA onto the surface of carbonaceous material, the highest CO_2 adsorption performance was 1.90 mmol/g with 10 wt% TAEA loadings at 70 °C and 1 bar, and CO_2/N_2 selectivity also increased. Zhao et al. (2010) modified graphene oxide with ED, DETA and TETA. In particular, ED modified graphene oxide showed the highest CO_2 adsorption capacity in the presence of a longer amine chain and enhanced N content, reaching 1.06 mmol/g with 50 wt% ED loadings (Zhao et al., 2012). Houshand et al. grafted ED and DETA onto AC. The results suggested that the inclusion of toluene in the solvent resulted in increased active sites (Lee, C.S. et al., 2013). The CO_2 adsorption capacity of class III amine-carbon materials is summarized in Table 3.17.

Table 3.17
CO_2 adsorption capacity of class III amine-carbon materials CO_2 adsorbent.

Support material	Amine type	temperature (°C)	CO_2 partial pressure (kPa)	Adsorption capacity (mmol/g, dry CO_2)	Ref.
Carbonaceous material	TAEA	70	100	1.90	(Zhao et al., 2010)
Graphene oxide	ED	30	100	1.06	(Zhao et al., 2012)
Palm shell-based AC	MMEA	25	30	1.00	(Lee et al., 2013)
Mesoporous carbon	PEI	30	100	3.80	(Wang et al., 2013)

3.2.5. Other low-temperature solid adsorbents

3.2.5.1. COF-based materials for CO_2 capture. Covalent organic frameworks (COFs), a newly emerging class of porous crystalline materials, have been regarded as a promising alternative for CO_2 capture due to their easy pore surface engineering, ordered pore distribution, structural tenability endow them with excellent CO_2 selectivity, good stability, and low energy requirement for regeneration even under moist conditions (Cote et al., 2005; El-Kaderi et al., 2007; Tilford et al., 2006). COFs are constructed by strong organic covalent bonds in a periodic arrangement entirely from light elements such as C–C, C–N, C–O, B–O, C=N, and C–Si (Biswal et al., 2013; Wan et al., 2008). Since the first pioneering work of CO_2 adsorption of COFs in 2009, great efforts have been devoted to improving the CO_2 capture performance of COFs, including Boron-based COFs, Triazine-Based COFs, and Imine-Based COFs (Aksu et al., 2022; Van Der Jagt et al., 2021; Zeng et al., 2016).

Boron-based COFs. According to the structural dimensionality and corresponding pore size, the boron-based COFs can be classified into three groups: Group 1 consists of 2D structures with 1D small pores (9 Å for each of COF-1 and COF-6), group 2 includes 2D structures with large 1D pores (27, 16, and 32 Å for COF-5, COF-8, and COF-10, respectively), and group 3 is comprised of 3D structures with 3D medium-sized pores (12 Å for each of COF-102 and COF-103) (Fig. 3.35) (Furukawa and Yaghi, 2009; Modak and Jana, 2019). As previously reported, Ar adsorption isotherm of COFs follows the sequence of BET surface area, COF-102 (3620–3530 $m^2\ g^{-1}$) > COF-10 (1760 $m^2\ g^{-1}$) > COF-5 (1670 $m^2\ g^{-1}$) > COF-8 (1350 $m^2\ g^{-1}$) > COF-1 and COF-6 (750 $m^2\ g^{-1}$). However, CO_2 uptake capacity at 273 K and 1 bar decreased in the order of COF-6 > COF-1 > COF-103 > COF-102 > COF-8 > COF-5 > COF-10, that is, group 1 > group 3 > group 2 COFs. COF-6 with a 9 Å pore diameter can adsorb CO_2 as high as 85 $cm^3\ g^{-1}$ at 273 K and 1 bar, outperforming the other six COFs despite its lowest BET surface area of (750 $m^2\ g^{-1}$), indicating that the low-pressure CO_2 uptake mainly depends on the pore width of COFs rather than the BET surface area and pore volume. The adsorbed amount of CO_2 at 298 K and 55 bar follows the order of COF-102 (611 $cm^3\ g^{-1}$) > COF-103 (606 $cm^3\ g^{-1}$) > COF-10 (514 $cm^3\ g^{-1}$) > COF-5 (443 $cm^3\ g^{-1}$) > COF-8 (321 $cm^3\ g^{-1}$) > COF-6 (158 $cm^3\ g^{-1}$) > COF-1 (117 $cm^3\ g^{-1}$), that is group 3 > group 2 > group 1 COFs, revealing that the high-pressure CO_2 uptake capacities are dominantly determined by pore volumes and BET surface area of COFs (Olajire, 2017).

Triazine-based COFs. Compared to boron-based COFs, triazine-based COFs exhibit excellent thermal and chemical stability, high CO_2 capacity, and selectivity even in water vapour, making them ideal candidates for CO_2 capture (Bhunia et al., 2013; Katekomol et al., 2013). The first triazine-based COF (CTF-1), possessing a hexagonal structure with 1D pore channels and a BET surface area of 1000 $m^2\ g^{-1}$, was synthesized by Thomas and co-workers via the ionothermal synthesis method (Kuhn et al., 2008). They constructed CTF-1 by cyclotrimerization of 1,4-dicyanobenzene in the presence of $ZnCl_2$ at 400 °C. As previously reported, perfluorinated alkanes not only exhibit more hydrophobic and lipophobic characteristics than their corresponding hydrocarbons but also show an extraordinary affinity to CO_2 molecules. Han et al. designed and synthesized a perfluorinated triazine-based COF (FCFT-1) for selective CO_2 capture (Zhao et al., 2013). It was found that the CO_2 capture capacity of FCTF-1 was as high as 1.76 mmol g^{-1} at 273 K and 0.1 bar due to the enhanced CO_2 electrostatic interaction caused by the high electronegativity of F. In addition, FCTF-1 exhibited an exceptional CO_2–N_2 selectivity of 77 under kinetic flow conditions in mixed-gas breakthrough experiments because the incorporation of F groups produced a significant amount of ultra-micropores (<0.5 nm). Moreover, FCTF-1 proved to be tolerant to water and its CO_2 capture performance remained excellent when there was moisture in the gas mixture, due to the hydrophobic nature of the C–F bonds. Because only a few triazine-based COFs exhibit crystallinity to some extent and their performance greatly depends on the synthetic conditions, the abovementioned drawbacks are inevitable issues during their further development (Ren et al., 2012).

Imine-based COFs. Another class of COFs is the imine-based COFs, first developed by Yaghi and co-workers using the strategy of dynamic covalent chemistry (Uribe-Romo et al., 2009). Compared with the CTFs, the imine-based COFs have much better crystallinity and structural regularity, which are beneficial to tuning the order of pore size (Kandambeth et al., 2013; Kandambeth et al., 2015). Imine-based COFs are divided into two types based on the covalent formation of distinct -C=N- bonds. One is the “Schiff base” type formed by the co-condensation of aldehydes and amines, and the other is the “hydrazine” type built by the co-condensation of aldehydes and hydrazides (Uribe-Romo et al., 2011). The first application of imine-based COFs in CO_2 adsorption was reported by Banerjee et al. in 2012 (Kandambeth et al., 2012). They reported two chemically stable (acid and base) 2D COFs (TpPa-1 and TpPa-2) through reversible and irreversible routes, which were constructed from 1,3,5-triformylphloroglucinol (Tp) with p-phenylenediamine (Pa-1) and 2,5-dimethylp-phenylenediamine (Pa-2), respectively. The CO_2 uptake of TpPa-1 and TpPa-2 was measured to be 78 and 64 $cm^3\ g^{-1}$ at 273 K and 1 bar, respectively. More COFs were prepared using similar building blocks with different functional groups (Chandra et al., 2013). The order of CO_2 capacity at 273 K and 1 bar is TpPa-1 > TpPa-NO_2 (73 $cm^3\ g^{-1}$) > TpPa-2 (64 $cm^3\ g^{-1}$) > TpBD-$(NO_2)_2$ (52 $cm^3\ g^{-1}$) > TpBD (40 $cm^3\ g^{-1}$) > TpBDMe$_2$ (37 $cm^3\ g^{-1}$) > TpPa-F_4 (35 $cm^3\ g^{-1}$) > TpBD- $(OMe)_2$ (27 $cm^3\ g^{-1}$). Interestingly, these water and chemically stable COFs can be delaminated using the mechanical grinding route to transform into covalent organic nanosheets that were characterized via transmission electron microscopy and atomic force microscopy. The stability of COFs is a central issue before any applications, and the stability of imine-based COFs in most organic solvents and water, when compared with boron-based COFs, has motivated researchers to incorporate several polar groups in the pore walls of imine-based COFs for enhanced CO_2 capture. More importantly, the good water and chemical stabilities of some imine-based COFs also favour their regeneration without loss of their CO_2 uptake performance. All these merits of imine-based COFs coupled with high CO_2 selectivity, large CO_2 capacity, and moderate heat of adsorption will provide a powerful platform for designing functional materials for CO_2 capture.

Surface chemistry of COF based CO_2 capture

El-Mahdy et al. (2018) in 2018 conducted an experiment to synthesize and adsorb CO_2 on triphenylamine COFs (TPA-3NH_2) and (triphenyltriazine COFs) (TPT-3NH_2). Various triacrylaldehydes were used in the synthesis of COFs. These varied in planarity, nitrogen concentrations, and symmetry. Through monitoring the monomer symmetry and planarity, specific crystalline COFs can be prepared targeting particular applications.

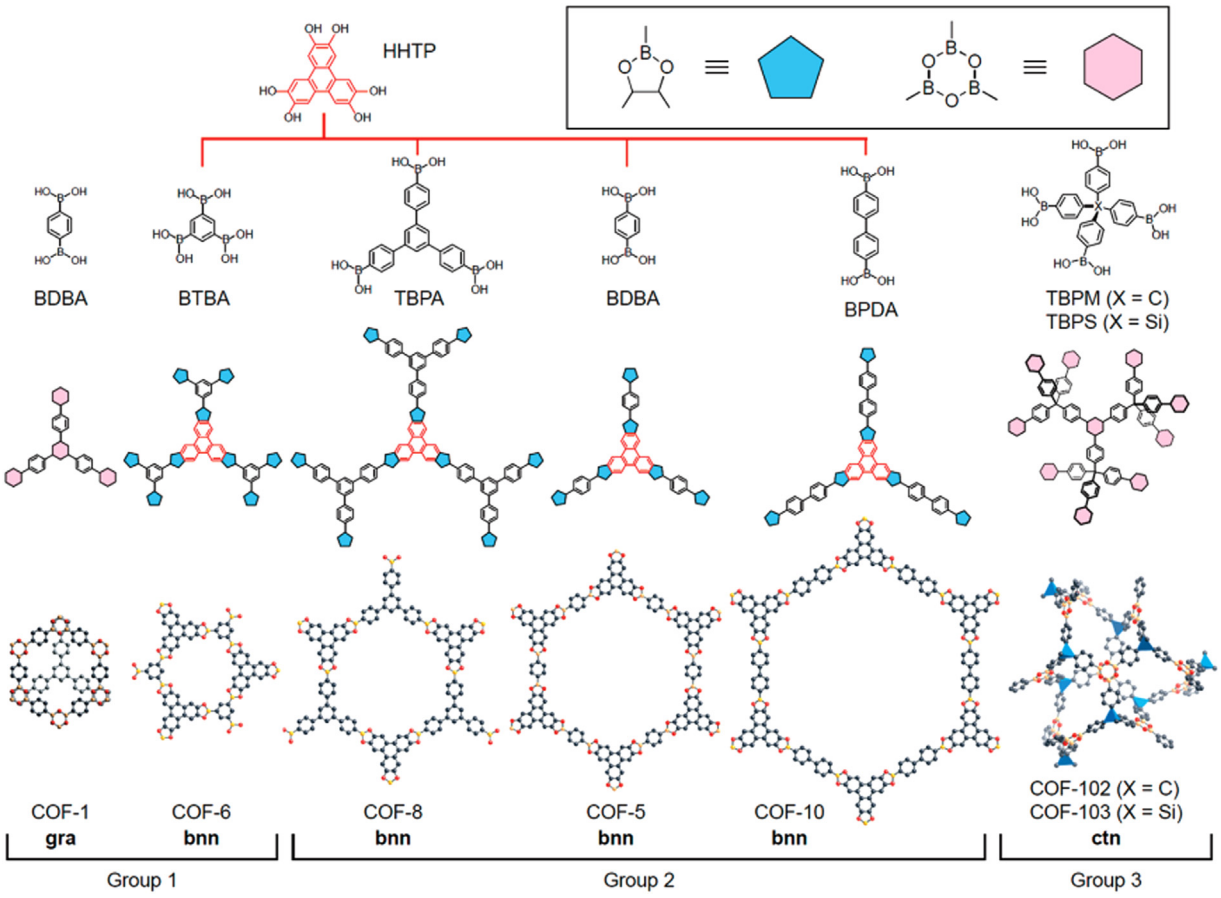

Fig. 3.35. Condensation reactions of boronic acids and HHTP are used to produce COFs (top) and resulting fragments of COFs (middle). Atomic connectivity and structures of crystalline 2D and 3D COFs (bottom). The topology and the group classification number are indicated for each COF. Inset: the C_2O_2B (blue) and the B_3O_3 (pink) rings are formed by condensation reactions (Furukawa and Yaghi, 2009). (For interpretation of the references to color in this figure legend, the reader is referred to the web version of this article.)

Symmetrical monomers were also used in many studies (Gao et al., 2018; Haase et al., 2017; Zhai et al., 2017), but none showed good gas storage properties. El-Mahdy et al. (2018) thought to control the fluctuation in the crystallinity of COFs and study its effect on CO_2 adsorption. The XRD confirmed the crystallinity of the material, which increased with increasing monomers. The surface area of TPT-COF-6 synthesized from most planar and symmetrical linkers came out to be 1535 m^2g^{-1} (calculated with BET). Although, another material (TPT-COF-5) reported a surface area of 1747 m^2g^{-1}, the highest CO_2 uptake capacity was still shown by TPT-COF-6. The study concluded that planarity and symmetry were the two most important factors to vary the total surface area of COFs.

Very few numbers of research have been seen about synthetic routes which can affect the structural variations of COFs. Gao et al. (2018) discovered that the combination of tetraphenylethane (Ascherl et al., 2016; Pang et al., 2016) will give [4 + 4] TPE-COF-I and [2 + 4] TPE-COF-I upon heating in o-dichlorobenzene and n-butanol solvents, respectively. Keeping it as a basis, the new TPE-COF-II was prepared. It showed surprisingly high CO_2 uptake of 23.2 wt% at 1 bar and 273 K, whereas TPE-COF-I showed only 13.4 wt% CO_2 adsorption. TPE-COF-I and TPE-COF-II displayed a BET surface area of 1535 m^2g^{-1} and 2168 m^2g^{-1}, respectively.

Effect of water on CO_2 adsorption using COF

While many COFs have shown good future for CO_2 capture, the industrial implementation of COFs is affected by their intolerance towards harsh conditions like water (Li et al., 2018; Uribe-Romo et al., 2011; Zhang et al., 2018). The crystal structure of COFs depends on the reversible reactions in synthesis process. In the reactions, the amorphous products first dominate the structure, but slowly the formation of low energy products take place, making COF crystals as major products (Zhu and Zhang, 2017). The reactions with which may COFs are synthesized are generally reversible and thus the crystals suffer degradation in mild aqueous surroundings (Spitler et al., 2011). Due to all these complications of reversible reactions, it is emphasized to prepare MOFs from non-reversible reactions. It is a very challenging task, but effective if possible. For the first time, Kandambeth et al. (2012) prepared COF (TpPa-1 and TpPa-2) from an irreversible reaction. The developed technique was a two-step method; first is reversible Schiff base reactions, and the second is an irreversible keto-enol tautomerization. The CO_2 adsorption capacity of TpPa-1 at 273K was 153 $mg.g^{-1}$. This capacity is in relation to COF-6 (Furukawa and Yaghi, 2009), but with high stability. To further test the material, COFs were immersed in water for 7 days and various analysis were carried. There was no change in the pXRD peaks, and no new peaks were noticed in FTIR testing. Furthermore, the TpPa-2 did not show any change in surface area, FTIR, and XRD analysis even after soaking in NaOH for 7 days. This exceptional stability is due to the irreversible keto-enol tautomerization reaction.

Abdelnaby et al. (2018) prepared amine-functionalized crosslinked porous polymer (KFUPM-1) using 1,4-benzenediamine, formaldehyde, and pyrrole with HCl as the catalyst. High concentration of primary and secondary amines in the framework offered very high selectivity for CO_2 over N_2 (i.e. 14 at 298 K) with CO_2 uptake of 15.1 cm^3g^{-1} in wet conditions. The material also exhibited stale activity for 45 cycles with similar selectivity. Later, Abdelnaby et al. (2019) prepared another

novel crosslinked microporous organic polymer (KFUPM-2) via Frieldel-Crafts alkylation between pyrrole and phenothiazine, crosslinked by paraformaldehyde. The material processed 39.1 cm^3g^{-1} CO_2 uptake at 273 K with CO_2/N_2 selectivity value of 51. Another polymer KFUPM-4 developed from different monomer exhibited superior CO_2 uptake in wet conditions. The presence of aniline and pyrrole monomers dispenses CO_2-philic properties to the material. It also offers high CO_2/N_2 selectivity of 79 and CO_2/CH_4 selectivity of 16. It was also reported that the existence of water vapours in feed improves the CO_2 uptake capacity, which is due to the strong solubility of CO_2 in the presence of water (Alloush et al., 2020).

3.2.5.2. Conjugated microporous polymers (CMPs) for CO_2 capture. CMPs (Conjugated Microporous Polymers), represent another class of amorphous covalent organic polymers with a considerable conjugated skeletal structure. These polymers are constructed using π-π conjugated rigid structural units, resulting in a rigid framework that can achieve complete conjugation system through tautomerism involving single, double, and triple bonds. The covalent bonds connecting the structural elements ensure the stability of CMPs even at elevated temperatures, making them highly suitable for CO_2 adsorption applications. CMPs have attract great attention as a versatile platform for CO_2 adsorption, primarily owing to their remarkably high specific surface area (BET), total volume (V_{total}), and exceptional thermal stability. Through manipulating the structural design and synthetic approach, CMPs are then allowed for tuning their CO_2 adsorption capacity and selectivity.

For example, Su et al. (Xu et al., 2019) synthesized two distinct porphyrin-contained CMPs, namely Porp-TPE-CMP and Porp-Py-CMP, using a $FeCl_3$-catalyzed coupling reaction. The specific surface area of Porp-TPE-CMP measured at 547 m^2 g^{-1} exceeded that of Porp-Py-CMP registered at 31 m^2 g^{-1}. This considerable higher BET values of Porp-TPE-CMP is indicative of the substantially higher CO_2 adsorption capacity (88.75 mg g^{-1}) when compared to Porp-Py-CMP (54.41 mg g^{-1}) under conditions of 273 K and 0.1 MPa. Furthermore, the selectivity ratios for CO_2/N_2 and CO_2/CH_4 between Porp-TPE-CMP and Porp-Py-CMP were evaluated and found to be 55.3 and 40.8, as well as 4.1 and 5.1, respectively.

CMPs are typically prepared through various reactions and by employing different monomers, leading to the fabrication of polymers with diverse CO_2 adsorption properties attributed to variations in porosity and functional groups. Hu and his group (Zhou et al., 2019) synthesized three distinct CMPs using cationic cyclization polymerization, employing monomers with multiple enediyne moieties. The specific surface area measurements for CMP1, CMP2, and CMP3 were found to be 767, 624, and 780 m^2 g^{-1}, respectively. Moreover, the values for specific microporous surface area (Smicro) and micropore volume (V_{micro}) for CMP1 were notably higher, at 481 m^2 g^{-1} and 0.19 cm^3 g^{-1}, than those of CMP2 (302 m^2 g^{-1} and 0.12 cm^3 g^{-1}) and CMP3 (134 m^2 g^{-1} and 0.02 cm^3 g^{-1}). This enhanced Smicro and Vmicro of CMP1 contribute to its excellent CO^2 adsorption performance, registering at 129.60 mg g^{-1} under conditions of 273 K and 0.1 MPa. Porphyrin-based polymers are widely recognized for their structural stability and inherent porosity. When doped with metal ions, these polymers exhibit increased activity at active sites, thereby improving their performance in gas adsorption applications.

3.2.5.3. Aerogels for CO_2 capture. Aerogel have received extensive attention due to well-developed pore structure. There is a wide variety of aerogel materials and numerous synthetic procedures for obtaining aerogel materials. The most common method of synthesizing aerogel is the sol-gel followed by drying. The drying procedures determine the final state of the aerogel. An ambient drying will destroy the structure due to capillary forces. Freeze drying eliminates the capillary forces during the solvent evapouration process. However, during the freezing process, the structure may be slightly damaged. Through supercritical drying, the structure can be preserved completely. After drying, a great number of mesopores and macropores can be obtained, which can provide abundant active sites for gas adsorption (Vinayakumar et al., 2022a; Wu et al., 2022). Competitive adsorption of coexisting gas components often has an adverse effect on the adsorption of target gases. Therefore, most of the research work in recent years has focused on modifying aerogels to improve their adsorption capacity or selectivity for target gases (Ho and Leo, 2021; Keshavarz et al., 2021; Maleki, 2016; Vinayakumar et al., 2022a). In terms of CO_2 adsorption and capture, for SiO_2 aerogels (Cui et al., 2011; Cui et al., 2017; Lin et al., 2013; Zhou et al., 2021), SiC aerogels (Cui et al., 2017; Guo et al., 2018; Han et al., 2014), graphene aerogels (Pruna et al., 2021) and other new aerogels (Wang et al., 2019b). At present, basic active centers are mainly introduced by amino functionalization, nitrogen doping, etc. (Jeon et al., 2015; Li et al., 2020; Tian et al., 2021; Wormeyer et al., 2012; Wormeyer and Smirnova, 2013; Xu et al., 2021). Chemisorption can also improve the adsorption capacity and selectivity of CO_2 by aerogels. For aerogels, the specific surface area and micropores can be further increased by activation, which also plays a key role in CO_2 adsorption at the same time. The CO_2 adsorption capacity of a few common aerogels is shown in Fig. 3.36.

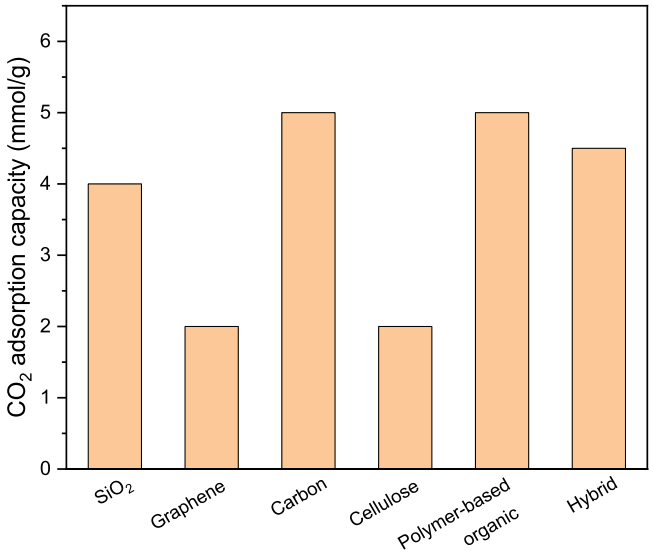

Fig. 3.36. The approximate adsorption capacity of CO_2 (Keshavarz et al., 2021; Kong et al., 2017; Lee and Park, 2020; Shao et al., 2018; Vinayakumar et al., 2022b; Wang et al., 2020; Wu et al., 2022; Yay and Gizli, 2019; Zhang et al., 2020; Zhu et al., 2020). (For interpretation of the references to color in this figure legend, the reader is referred to the web version of this article.)

SiO_2 aerogel. As an adsorption material, SiO_2 aerogel has the advantages of high adsorption efficiency, convenient desorption, and stable performance. It is the most studied and mature aerogel material, and was first applied to the field of gas adsorption and purification. The current research work focuses on amino functionalization or hydrophobic modification of SiO_2 aerogel to further improve its adsorption performance for CO_2. There are two main modification methods: one is grafting, and impregnation after the formation of wet gel or after supercritical drying (Fang et al., 2020; Linneen et al., 2014). The other method is to functionalize the surface of SiO_2 aerogel, which is to introduce functionalized precursors in the sol-gel reaction process, and use a mixed silicon source to endow SiO_2 aerogel with specific properties through in-situ polymerization (Liu et al., 2021; Xu et al., 2018). Amino functionalization of SiO_2 aerogels is currently the main method to improve its selectivity to CO_2, increase the saturated adsorption capacity and accelerate the CO_2 adsorption rate. The presence of an appropriate amount of water vapour in the mixed gas can significantly improve the adsorption capacity of CO_2 by aerogels.

Carbon aerogel. Activation is a common method to control the pore structure of porous carbon materials. During the activation, the microporous structure can be introduced into the mesoporous pores of carbon aerogels, increasing the specific surface area further. Therefore, it is beneficial to the application of carbon aerogels as CO_2 adsorption materials. Similar to SiO_2 aerogels, the adsorption performance of carbon aerogels for CO_2 can also be improved by means of amino functionalization, nitrogen doping, and the introduction of active metals (Geng et al., 2020; Li et al., 2019; Marques et al., 2013; Robertson and Mokaya, 2013; Xie et al., 2017; Zhuo et al., 2016).

Graphene aerogel. Graphene sheet layers stacked on top of each other can form graphene aerogels with three-dimensional porous network structures, which have not only the characteristics of fast graphene electron transport rate, but also rich surface oxygen groups, large aerogel specific surface area, high porosity, and easy for further modification (Pruna et al., 2021; Ren et al., 2020).

Metal oxides aerogel. Metal oxide aerogel is a type of inorganic aerogel. Whether it is the preparation of one-component or multi-component metal oxide aerogels, the metal salts are first dissolved in organic solvents or water, and the reaction reagents can be added after adjusting the concentration and pH value of the solution to form a gel. Metal oxide aerogels are rich in surface active sites such as metal centers, active hydroxyl groups, etc., which have high chemical adsorption capacity and selectivity. (Li et al., 2019)

Polymer-based organic aerogels. Polymer-based organic aerogels are polymer molecules passed with glue, and the body particles are formed by combining hydrogen bonds or van der Waals forces organic compounds with porous network structures. Compared to conventional inorganic aerogels, the performance of organic aerogels depends mainly on the type of polymer. Therefore, the polymer based organic aerogels offer flexible design and performance adjustability. Assemble synth-based organic aerogels mainly include polyurethane (PU), polyurea (PUA), polyimide (PI), etc (Kong et al., 2015; Li et al., 2019).

3.2.5.4. Zeolites materials for CO_2 capture. Zeolites have been widely used as CO_2 adsorbents due to the large surface area, high stability, and tunable physiochemical properties. Zeolites are porous aluminosilicates with three-dimensional rigid frameworks consisting of corner-sharing SiO_4 and AlO_4 tetrahedra through shared oxygen atoms. The framework of zeolites contains the periodic arrangement of cages and channels with molecular dimensions (3-15 Å in diameter). According to the number of oxygen atoms forming the largest pore aperture, zeolites can be divided into small-pore zeolites (8-membered ring), medium-pore zeolites (10-membered ring), large-pore zeolites (12-membered ring) and extra-large-pore zeolites (≥14-membered ring). The frameworks of pure silica zeolite are electrically neutral. The isomorphous replacement of Si^{4+} by Al^{3+} in the lattice will induce negative charges on the framework, which require extra-framework cations for charge balance. The physicochemical properties of zeolites can be tuned by incorporating extra-framework cations via ion exchange or impregnation methods. Zeolites with desired properties can be achieved for target applications by tuning the topology of zeolites (Fig. 3.37), and the type and density of extra-framework cations.

Zeolites show outstanding CO_2 adsorption performance in terms of high CO_2 capacity and selectivity, and excellent regenerability, which highly rely on the properties of zeolites. Generally, materials with large surface areas show high adsorption capacities. However, the high surface area with non-specific nature benefits the adsorption of both target and unwanted adsorbates, which is not enough when the selectivity is considered. The selectivity on the other hand is governed by the distinct adsorbent/adsorbate interaction, which relates to the type of the adsorption sites (e.g., extra-framework cations, functional groups etc.). In the case of CO_2 separation, a higher affinity of zeolite towards CO_2 over other accompanying species is desired, such as N_2 and CH_4 in flue gas and biogas/natural gas, respectively. However, an overly strong gas-host interaction requires a high energy consumption during the regeneration process. CO_2 adsorption on various zeolites is reviewed aiming to provide references for its utilization in industrial processes.

Separating molecules with similar sizes (e.g., CO_2, 3.3 Å; N_2, 3.6 Å; CH_4, 3.8 Å) is challenging through the sieving effect due to the difficulty in preciously adjusting the pore size locating just in between the sizes of molecules. (Shang et al., 2012, 2013) Small-pore zeolites are effective and highly selective adsorbents for CO_2 capture due to the similar sizes of the window aperture (3~5 Å) and the kinetic diameters of adsorbates (CO_2, 3.3 Å; N_2, 3.6 Å; CH_4, 3.8 Å), which enables the separation through size sieving and "molecular trapdoor" mechanism. (Shang et al., 2012) In addition, the high thermal and mechanical stability make small-pore zeolites attractive in industrial processes. Shang *et al.* have studied the CO_2 and N_2 adsorption on alkali metal ion-exchanged chabazite (CHA) zeolites (Si/Al of 1~50). (Shang et al., 2012, 2013) They achieved ultra-high selectivity for CO_2/N_2 (325, 20 kPa, 273 K) and CO_2/CH_4 (98, 100 kPa, 233 K) by Cs^+CHA (Si/Al = 2.2) and K^+CHA (Si/Al = 2.2), respectively. The high selectivity was attributed to the temperature-dependent "molecular trapdoor" mechanism (Fig. 3.38), which describes the different capability of gas molecules to deviate the cation from the center of the 8-ring windows to enter the pores of zeolites. Molecules such as CO_2 with high polarizability can interact with the "door-keeping" cation (e.g., Cs^+ and K^+) strongly and need to pay lower energy toll than the "weak molecules" (e.g., CH_4 and N_2). In terms of the zeolites, the key factors for realizing this mechanism are the cations with proper size, and the proper Al distribution on the pore aperture providing enough electronegativity for cations to coordinate to large extent for the effective blockage. The kinetics on the other hand is an important parameter to evaluate the CO_2 capture performance, especially during the industrial processes, which is determined by the energy barrier for cation deviation. The cation with smaller size or a weaker cation-window interaction strength requires lower energy for deviation, which can help in improving the kinetics. Further tunings among the zeolites topology, the Si/Al ratio and the type of cations are required for developing CO_2 adsorbents with both high selectivity and promising kinetics.

Typically, high selectivity and high regenerability cannot be attained simultaneously. Highly selective materials tend to consume lots of energy for the completed regeneration, and conventional physisorption-driven adsorbents with easy regeneration always feature low selectivity. To address this contradiction, Sun *et al.* prepared transition metal (Co, Ni, Zn, Fe, Cu, Ag, La, and Ce) ion-exchanged SSZ-13 zeolites (CHA type, Si/Al = 12) for flue gas (CO_2/N_2:15/85) separation. (Sun et al., 2019) The selectivity of Co^{2+}SSZ-13 and Ni^{2+}SSZ-13 reached above 50 at 273 K, which was higher than the alkali metal ion-exchanged SSZ-13 zeolites (23–36). (Bower et al., 2018) The improvement was attributed to the Pi-complexation interaction (Fig. 3.39) formed between CO_2 and the transition metal ions, which is with moderate interaction strength between those of physisorption and chemisorption. The isosteric heat of adsorption of CO_2 is 30~60 kJ/mol, much lower than that of chemisorption (>80 kJ/mol), which enables regeneration under mild conditions.

Considering the higher polarizability and quadrupole moment of CO_2 than the unwanted gases (N_2 or CH_4) in the mixture, cations with strong polarizing power are highly desired, which can improve the affinity of adsorbents towards CO_2. Researchers have studied the CO_2 adsorption behavior on alkali metal (Li, Na, K, Rb, Cs) ion-exchanged FAU (X and Y) and MFI (ZSM-5) zeolites. (Dunne et al., 1996; Katoh et al., 2000; Walton et al., 2006; Wirawan and Creaser, 2006a, b; Yamazaki et al., 1993) Generally, the CO_2 capacity is reduced in the order of LiZ > NaZ > KZ > RbZ > CsZ (Z representing zeolite), which is coincident with the order of increasing ionic radius. For the ions with the same valance state, those with smaller ionic radius feature higher polarizing power: Cs^+ (3.3 Å) < Rb^+ (2.9 Å) < K^+ (2.7 Å) < Na^+ (1.9 Å) < Li^+ (1.4 Å). The result indicates the interaction of CO_2 with alkali metal is electrostatic interaction dominated. The consistent results were also demonstrated on alkali metal ion-exchanged X zeolite through density functional theory calculations. (Plant et al., 2006) The CO_2 adsorption

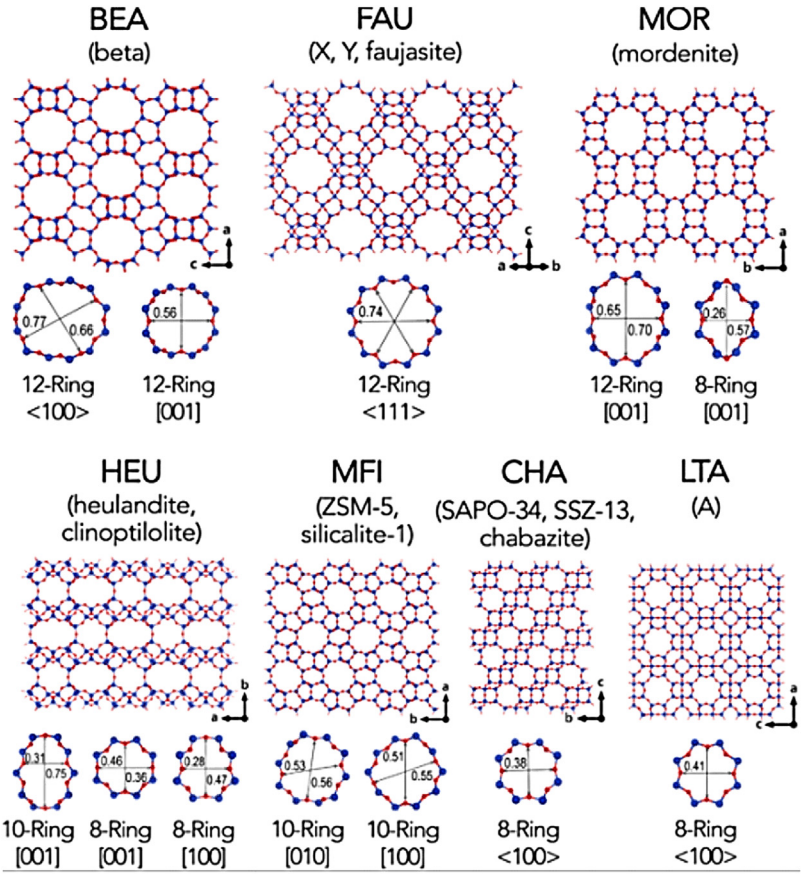

Fig. 3.37. Selected widely applied zeolite frameworks. The three-letter code relates to the type of framework, assigned by the International Zeolite Association (IZA) (in bold). The size of the pore window and the ball-stick atomic model are given. Blue and red spheres represent T atoms and oxygen atoms, respectively (Li et al., 2017). (For interpretation of the references to color in this figure legend, the reader is referred to the web version of this article.)

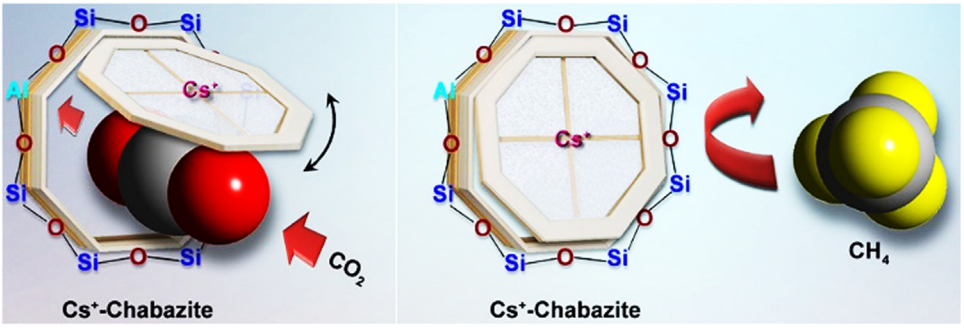

Fig. 3.38. Illustration of the "molecular trapdoor" mechanism in discriminative gas separation: Cs^+ locating in the middle of 8MR acts as a door keeping cation, which can only be deviated by strong gas molecules (e.g., CO_2), but not by weak molecules (e.g., CH_4) at certain temperature (Shang et al., 2012). (For interpretation of the references to color in this figure legend, the reader is referred to the web version of this article.)

enthalpies at low coverages vary from 33.20 to 17.17 kJ/mol, decreasing with the increase of the ionic radius. The smaller cations are with higher affinity towards CO_2, which was also evidenced by the shorter distance between the oxygen of carbon dioxide and the cations with smaller sizes.

The presence of moisture is unavoidable in the gas separation process, which is another challenge when adopting zeolites as adsorbents due to the extremely hydrophilic nature. Featuring high polarizability, H_2O is indeed a main inhibitor for CO_2 adsorption even when the water is at a low concentration, by forming a favourable interaction with the adsorption sites, especially the extra-framework cations in the cationic forms of zeolites, which can dramatically reduce the CO_2 capacity. (Brandani and Ruthven, 2004) Grafting amine functional groups in zeolites was found as a powerful approach for CO_2 capture under wet conditions. (Kim et al., 2016) Kim *et al.* prepared ethylenediamine (ED)-modified Y zeolite prepared via the gas-phase titration method and tested the CO_2 capture performance in wet flue gas (Kim et al., 2016). CO_2 was effectively captured through interacting with the amine groups, and H_2O was co-adsorbed in the micropores of zeolites without forming urea. The CO_2 working capacity was maintained at a stable level (> 1.1 mmol/g) during 20 temperature swing adsorption (TSA) cycles. The ED-modified Y zeolite features a high H_2O tolerance and remarkable resistance against the urea formation simultaneously.

In the industrial separation process, the energy lost due to the undesirable pressure drop in the fixed bed needs additional blower power to maintain the constant flow. Fabricating zeolite powder into monoliths with desired channel sizes, wall thicknesses, and high mechanical properties by 3D printing is a promising strategy to tackle this issue. Wang *et al.* prepared mechanically robust binder-free 3D printing zeolite monoliths (ZM-BF) as a superior configuration for CO_2 capture (Wang et al., 2019). Halloysite nanotubes (HNTs) with high strength were used as printing ink additives, which benefited the formation of robust interfacial "HNTs-bridges" for individual zeolite crystals. ZM-BF showed a promising equilibrium CO_2 capacity of 5.58 mmol/g (298 K, 1 bar), which is higher than other reported 3D-printed CO_2 adsorbents. Compared with the commercial benchmark NaX zeolites, ZM-BF showed

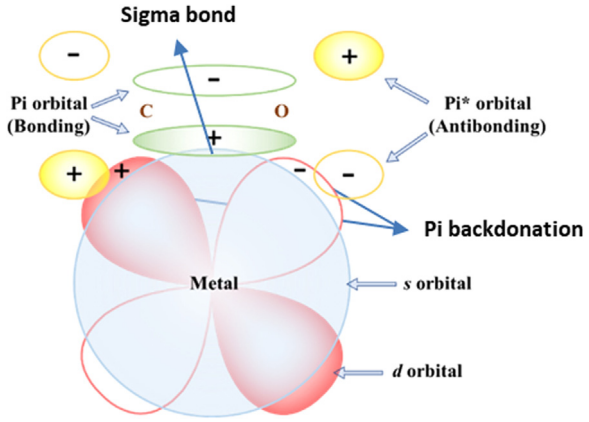

Fig. 3.39. Pi-complexation interaction formed between Pi-structured molecules and transition metal ion (Sun et al., 2019). (For interpretation of the references to color in this figure legend, the reader is referred to the web version of this article.)

superiority in dynamic adsorption breakthrough tests in terms of dynamic, CO_2 capture capacity and selectivity. In addition, the binder-free ZM-BF shows outstanding mechanical properties (with a robust compressive strength of up to 5.24 MPa), higher than most of the reported monoliths with binders. The "3D printing and zeolite soldering" strategy developed in this study afforded a promising approach for precisely fabricating monoliths with desirable configurations, which may provide references for other related applications, such as catalysis and sensoring.

The zeolite topology and the type/density of adsorption sites in zeolites are the essential factors for CO_2 adsorption on zeolite materials. The CO_2 capacity can be affected by the type/density of adsorption sites and the surface area of zeolites, as well as the presence of high-affinity components (e.g., H_2O) in the gas mixture. The high selectivity can be attained by introducing the adsorption sites with high CO_2 affinity, as well as through the "molecular trapdoor" mechanism. However, it still requires efforts to achieve easy regeneration and fast kinetics simultaneously. Thus, tuning the physiochemical properties of zeolites together with optimizing the experimental conditions are required for approaching effective CO_2 capture in industries.

3.3. Photo-responsive adsorbents for low-energy CO_2 capture and release

For post combustion CO_2 capture techniques to achieve widespread feasibility, energy cost must be substantially reduced. Traditional CO_2 liberation technologies highly relied on pressure (pressure swing adsorption, PSA), temperature (temperature swing adsorption, TSA), vacuum (vacuum swing adsorption, VSA), or any combination of them (Li and Hill, 2017). Both VSA and PSA are in demand of large amounts of electrical energy to alter the pressure for driving the CO_2 to be liberated from adsorbents (Mason et al., 2011). Although waste heat can be exploited in the TSA method, some adsorbents are so thermally insulating that these methods cannot be applied on a large scale unless the heating transformation distance can be designed into the gas adsorbent contactor (Labreche et al., 2015). Apart from that, the long cycle time and the demand for high vapour to heat the column also resist the development of the TSA method (Qiao et al., 2022). Considering that the traditional triggers for the liberation of adsorbed CO_2, such as high temperature and vacuum, are so energy consuming (Lyndon et al., 2013), it's necessary to establish new stimuli that are more naturally abundant and renewable resources such as solar light. In this case, the adsorbents with maximum CO_2 uptake capacity and further reduced energy will obtain a more prospective and wide application (Huang et al., 2022).

Light, particularly concentrated solar light, as a naturally abundant, renewable resource, is an extremely appealing trigger for regenerating the adsorbents. Compared to traditional technologies, light can be regarded as the most energy-efficient method (Li and Hill, 2017). When the adsorbents show strong light absorption, combined with the large amounts of CO_2 desorption, much energy cost could be saved (Jiang et al., 2019). Therefore, through the different directions of adsorbents functionalization, light triggered different applications can be developed.

3.3.1. Photo responsive porous polymer adsorbents for CO_2 switching capture

Recently, porous materials have been reported as attractive light responsive candidates for low energy CO_2 capture (Heinke and Wöll, 2019). Because of their large surface area, structural variety and easy functionalization ability, high CO_2 adsorption performance and the potential for integration with light responsive photochromic units in the pore channels can be realized. Such light triggered CO_2 release performance of porous materials can be achieved by the functionalization of photochromic units into the structural molecules of porous materials (Huang and Wu, 2022). Such photochromic organic molecules can undergo a reversible photoisomerization process, and then change the electronic state and molecular structures under light irradiation. Up until now, azobenzene (AB), diarylethene (DET) and spiropyran (SP) are the most reported photochromic units that were successfully reported to be incorporated into porous materials (Fig. 3.40) (Jones et al., 2016). Among them, azobenzene can transition between the trans/cis state through different wavelength number of light irradiation, and DET can undergo a structural transition through ring-open/close reaction while SP molecules can switch between the zwitterionic merocyanine counterpart upon light exposure (Bigdeli et al., 2020). These photo switchable compounds can be either integrated into the backbones or side chain of porous materials or directly loaded as the guest to pore channels (Haldar et al., 2019). Therefore, the light triggered photoisomerization transition of these materials can finally contribute to a remote light controlled CO_2 capture and release recycle.

3.3.1.1. Photo responsive MOFs for CO_2 switching. Photo switching MOFs are the most widely reported porous materials for low energy CO_2 capture owing to their high uptake capacity, crystallinity and adjustable structures (Mukhopadhyay et al., 2014). For photoswitching MOFs, azobenzene functionalized photo switching MOFs were widely reported because of the easy functionalization method. For example, azobenzene based PCN-123 can switch the conformation upon UV light irradiation and lateral thermal heating (Park et al., 2012). Such material was fabricated by the introduction of azobenzene pendants to the organic linkage. After UV light irradiation, a release of 54 %, from 22.9 cm^3/g to 10.5 cm^3/g, in CO_2 uptake capacity could be realized. In addition, the CO_2 uptake ability could also be recovered by thermal heating. Apart from functionalization as linkage pendants, azobenzene groups could also be incorporated as backbones of MOF materials. Matthew et al. Lyndon et al. (2013) reported an azobenzene based Zn (AzDC) $(4,4'\text{-BPE})_{0.5}$ by directly incorporating the azobenzene units into the backbone of the framework. The switching of CO_2 uptake capacity was found to be tremendously strong, with up to 64 % changes under dynamic light switch on/off conditions. In addition, azobenzene molecules were also reported to be directly loaded as a guest in MOF materials. Matthew et al. Lyndon et al. (2015b) also reported Mg-MOF-74 materials. Through methyl red loading, such MOF exhibited 84 % tailored CO_2 uptake changes after visible light irradiation.

DET and SP based MOFs are also other promising alternatives for low energy CO_2 capture. For example, a photochromic diarylethene linkage was utilized to fabricate a photo responsive DMOF material (Luo et al., 2014). The local photoisomerization reactions induced by UV and lateral visible light irradiation in DMOF frameworks contributed to a 76 % desorption of CO_2 capacity. Apart from that, Deanna et al. (Healey et al., 2016) also reported a photoactive spiropyran based MOF-808-SP adsorbent through a post-synthetic modification strategy. Such MOF material suggested both photo responsive BET surface area and light trig-

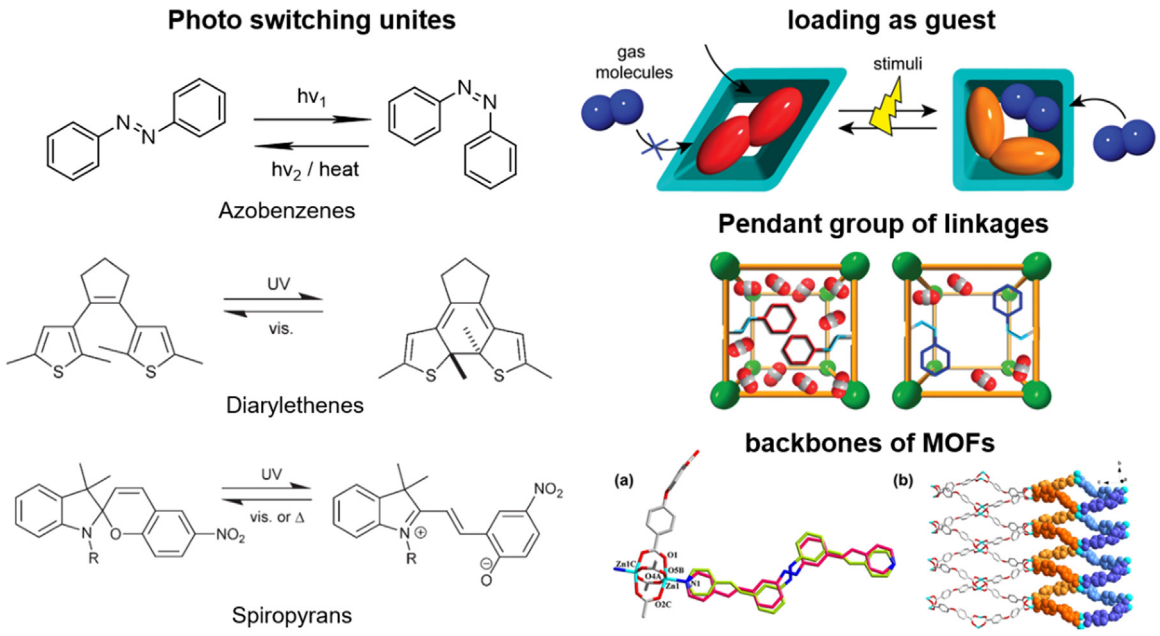

Fig. 3.40. A schematic representation of different strategy to integrate photo switchable components into a metal–organic framework (MOF) (Jones et al., 2016). (For interpretation of the references to color in this figure legend, the reader is referred to the web version of this article.)

gered tailorable CO_2 capture performance, which provides a promising, remote light controlled, low energy cost gas separation and storage method.

3.3.1.2. Other photo responsive porous polymer adsorbents for CO_2 switching. Considering the structural tunability, some other porous materials are also promising candidates for fabricating the light responsive adsorbents for tailorable carbon capture. For instance, porous organic polymers are one of the most developed adsorbents for carbon capture, which possess many similar inherent properties as MOFs, such as high porosity and gas uptake capacity. Bradley et al. (Lyndon et al., 2015a) fabricated a diarylethene based porous aromatic framework-1 materials. Such DArE@PAF-1 material exhibited an up to 26 wt.% desorption capacity of CO_2 at the 50 wt.% DArE guest molecules loading. The photo responsive ability could also be modulated by different guest loading content, which provided greatly controlling for carbon capture and release for industrial applications.

Zhang et al. Zhu and Zhang (2014) also reported the first example of azobenzene based porous organic polymer. Under UV light irradiation and, consequently thermal heating, both the pore size distribution and the CO_2 uptake ability could be reversibly changed. In contrast to most reported azobenzene based MOFs, the trans to cis isomerization in this material suggested increasing adsorption of CO_2 because of the enhanced dipole-quadrupole interactions between CO_2 molecules and cis isomer pendants. In detail, the UCBA-1 showed a dramatic increase in CO_2 adsorption capacity, up to 29 %, which could complement the most reported photo responsive MOF materials so far.

3.3.1.3. Photo responsive chemicals for CO_2 switching. Fabian et al. Wilm et al. (2022) first fabricated photo responsive superbases containing the photochromic DET units. The reported N-heterocyclic imines can undergo a reversible electronic isomerization under UV light exposure and lateral visible light irradiation, with multiple cycles. The transition between ring opening and ring closing states was accompanied by a remarkable pK_a shift (up to 8.7 units). The ring closing isomers of these imines are effectively basic to act as CO_2 capture sites via the production of zwitterionic bases, which enable the light triggered CO_2 capture and release cycles. Such light stimulated basicity alterations provided guidance for developing new photo switching transformations in a variety of fields of research.

3.2.2. Photothermal conversion applied in low light-triggered temperature of CO_2 adsorbents regeneration

Endowing the adsorbents with photothermal conversion capability is also another alternative way to utilize the sunlight for CO_2 adsorbent regeneration. Through combining photothermal conversion ability, thermos sensitivity with the high density of amino sites with CO_2 affinity, an energy saved light triggered high capacity of CO_2 capture and release process can be achieved. He et al. Lu et al. (2022) synthesized solar energy triggered cellulose nanofiber based thermos responsive fiber adsorbents. The contained poly (N-isopropylacrylamide), graphene oxide and polyethyleneimine served as thermos responsive switchers, photothermal conversion switchers and CO_2 uptake sites. Therefore, the prepared CNF-TBFA fiber adsorbents exhibited a high CO_2 uptake capacity of up to 6.52 mmol/g, and low regeneration temperature (60 °C) at the same time. These provide a great promising strategy for energy saved CO_2 adsorbents regeneration method.

Since noble metal crystals such as Ag and Au can effectively absorb sunlight photons and convert them to thermal energy, Paolo et al. (Li, Haiqing et al., 2016) utilized Ag nanocrystals as “nanoheaters” to form silver incorporated Ag/UiO-66 composites. Considering the low-cost and high CO_2 adsorption performance of UiO-66 MOF, such composites are an ideal adsorbent for remote light triggered CO_2 low energy CO_2 capture and release. Under visible light irradiation, 90.5 % captured CO_2 in Ag/UiO-66 composites can be released out, which demonstrates a promising energy saved method for remotely regenerating the MOF adsorbents under the natural abundant light resources.

3.3. Medium temperature solid sorbents

3.3.1. MgO-based materials for CO_2 capture

Depending on the origin of the CO_2-containing gas stream, e.g. a combustion process, it may be more efficient thermodynamically to operate the CO_2 process at elevated temperature, instead of cooling the gas stream to near-ambient temperatures prior to CO_2 removal. Sections 3.3 – 3.4 review recent developments of CO_2 capture processes with

Table 3.18
Overview of properties of binary alkali metal oxide/carbonate pairs for CO_2 capture applications.

Alkali metal oxide /carbonate pair ($MeO/MeCO_3$)	Reaction enthalpy in kJ/mol_{MeO} (at 298 K)	Melting temperature in °C of $MeO/MeCO_3$	CO_2 uptake capacity in g_{CO2}/g_{MeO} ($mmol_{CO2}/g_{MeO}$)	Equilibrium temperature in °C for $p_{CO2} = 1$ bar *	Potential applications
$MgO/MgCO_3$	±101	2825/990	1.094 (24.86)	395	Pre-combustion CO_2 capture, Sorption enhanced conversion reactions
$CaO/CaCO_3$	±178	2900/1330	0.786 (17.86)	885	Pre-combustion CO_2 capture, Post-combustion CO_2 capture, Sorption enhanced conversion reactions, Thermochemical energy storage
$SrO/SrCO_3$	±241	2530/1495	0.426 (9.68)	1225	Thermochemical energy storage
$BaO/BaCO_3$	±272	1973/1555	0.288 (6.54)	1560	Thermochemical energy storage

* Below the equilibrium temperature CO_2 sorption and the formation of $MeCO_3$ are favored thermodynamically, whereas above the equilibrium temperature CO_2 release and the formation of MeO are favored for a given partial pressure of CO_2, p_{CO2}, in the gas environment.

solid sorbents at medium (>250 °C) and high (>500 °C) temperatures, respectively. To this end, mostly alkali or alkaline earth metal oxides have been used as sorbents, often mixed with other metal oxides that themselves are not active for CO_2 sorption. Such "inactive" metal oxides function as support materials, or structural stabilizers, for binary oxides to mitigate the cyclic decay in CO_2 sorption activity that all alkali or alkaline earth metal oxides have in common due to the rather low melting temperatures of the carbonates formed (Dunstan et al., 2021); they also can play an important role in the carbonation mechanism of ternary oxide sorbents. The formation of carbonate phases, rather than adsorbed carbonate species upon exposure to CO_2, is one of the most significant differences of medium- to high temperature solids sorbents when compared to low temperature solid sorbents, and influences the overall process design appreciably. Table 3.18 provides an overview of binary alkali metal oxide/carbonate pairs that have been investigated frequently for CO_2 capture.

3.3.1.1. Introduction of MgO-based sorbents. Thermodynamically, MgO-based sorbents are suitable materials for CO_2 capture ($MgO + CO_2 \rightarrow MgCO_3$, $\Delta H_{298K} = -100.9\ kJ \cdot mol^{-1}$) at intermediate temperatures, with CO_2 sorption being feasible up to ~ 400 °C when the partial pressure of CO_2 is 1 bar. MgO-based materials have a lower energy penalty associated with the decomposition of the carbonate phase (i.e. the regeneration of the metal oxide phase) than other alkali metal oxide/carbonate pairs (e.g. $CaO/CaCO_3$, Table 3.18) due to their lower reaction enthalpy and the lower regeneration temperatures (<500 °C). Further, they possess a high theoretical CO_2 sorption capacity (1.09 g_{CO2}/g_{MgO} – the highest among the alkali earth metals) (Chi et al., 2014). Mg-containing minerals are abundant (the earth crust contains ca. 2 mol. % of Mg) (Goff and Lackner, 1998), environmentally benign and are less extensively used in other industries, e.g. building and construction, than limestone, such that there is less competition for raw materials with these industries compared to $CaO/CaCO_3$.

3.3.1.2. CO_2 capture capacity and kinetics of MgO-based sorbents. Despite the promising theoretical characteristics, there has been only little interest in using MgO-based sorbents for CO_2 capture applications due to their slow CO_2 sorption (i.e. carbonation) kinetics, resulting in low actual CO_2 uptakes (typically less than 0.02 g_{CO2}/g_{MgO} when using commercial MgO). Two reasons for the poor carbonation performance are (i) the formation of a CO_2-impermeable mono-dentate surface carbonate layer (Harada and Hatton, 2015; Harada et al., 2015), and (ii) the high lattice enthalpy of crystalline MgO (Glasser and Jenkins, 2000; Zhang et al., 2014). Several ways have been suggested to improve the carbonation performance of MgO, including (i) the synthesis of high surface area MgO (in particular for low temperature CO_2 adsorption) (Bhagiyalakshmi et al., 2010; Ruminski et al., 2011), (ii) the synthesis of MgO supported by e.g. ZrO_2, TiO_2, Al_2O_3 or C to improve also its structural stability (Han et al., 2014; Hiremath et al., 2019; Jeon et al., 2012; Li et al., 2017; Liu et al., 2008; Liu et al., 2013), or (iii) the promotion of MgO with molten alkali metal salts (AMS, predominantly nitrates) (Dunstan et al., 2021; Hu et al., 2019). The first two approaches have led only to limited improvement of the CO_2 uptake, typically up to 0.1–0.3 g_{CO2}/g_{MgO} both at low and medium temperatures (Hu et al., 2019). The maximum CO_2 uptake of these sorbents scales with their surface area and is reached within several minutes of exposure to CO_2 when the surface is saturated with carbonates. No crystalline $MgCO_3$ is formed upon exposure of unpromoted MgO to CO_2 (Wang et al., 2014). Modification of MgO with molten AMS, however, enables the rapid formation of crystalline $MgCO_3$ and leads to a significant improvement in the carbonation performance. With AMS promotion, the conversion of MgO into $MgCO_3$ proceeds through a nucleation and growth mechanism (Bork et al., 2021), with the type of the AMS influencing the number of nucleation sites (Jo et al., 2017) and the solubility of CO_2 and MgO in the salt (Dal Pozzo et al., 2019).

3.3.1.3. Chemical composition of MgO-based sorbents. The discovery that the addition of AMS to MgO enhances its CO_2 sorption rate (Zhang et al., 2013) appreciably has led to the research community focusing on two broad aspects: The optimization of the sorbent's CO_2 capture performance (largely by trial and error) (Harada and Hatton, 2015; Harada et al., 2015; Hu et al., 2019), and the understanding of the promotion mechanism by the AMS (Bork et al., 2021; Gao et al., 2021; Lin et al., 2021; Harada et al., 2015; Jo et al., 2017; Landuyt et al., 2022; Zhang et al., 2014).

The former includes the optimization of the carbonation conditions (Harada and Hatton, 2015), the amount of the AMS promoter (Dal Pozzo et al., 2019; Harada and Hatton, 2015; Harada et al., 2015), the selection of various synthesis routes for MgO production (Zhao et al., 2018) and, most predominantly, the variation and optimization of the promoter's composition (Dal Pozzo et al., 2019; Huang et al., 2017; Qiao et al., 2017). The promoters investigated range from the single nitrates ($LiNO_3$, $NaNO_3$ or KNO_3) to their binary and ternary mixtures with lower melting points. Furthermore, the addition of alkali nitrites, such as $NaNO_2$, was shown to improve the carbonation performance of sorbents. Some reports, however, have shown that $NaNO_2$ itself is not stable and transforms into $NaNO_3$ and Na_2CO_3 upon cyclic operation (Gao et al., 2021; Gao, Wanlin et al., 2021; Gao et al., 2018).

The beneficial effect of the addition of carbonates (e.g. Na_2CO_3 or $CaCO_3$) on the carbonation performance of alkali nitrate-promoted MgO has been demonstrated relatively early on (Zhang et al., 2015). Furthermore, it was shown that the presence of residual amounts of $MgCO_3$ (obtained by partial regeneration of the sorbent) also has led to an improved carbonation performance in the following reaction cycle (Prashar et al., 2016). Some carbonate additives readily form double carbonates with magnesium, e.g. $Na_2Mg(CO_3)_2$, $K_2Mg(CO_3)_2$

(Wang et al., 2017) and CaMg $(CO_3)_2$ (Cui et al., 2020, 2018; Dong et al., 2022; Hu et al., 2019; Papalas et al., 2021), whereas others do not, e.g. $SrCO_3$ (Jo et al., 2017). It was suggested that the addition of carbonates enhances the CO_2 sorption performance of alkali nitrate-promoted MgO further by (i) acting as stabilizers (or spacers), preventing the sintering of MgO (Cui et al., 2020), (ii) being dissolved in the molten alkali nitrate promoter increasing the concentration of carbonate ions (Wang et al., 2017) that act as "CO_2 carrier" (Vu et al., 2016), or (iii) acting as nucleation seeds for the $MgCO_3$ nucleation (Jo et al., 2017).

3.3.1.4. Regeneration and cyclic stability of MgO-based sorbents. The major factors governing the long-term stability of other solid sorbents (e.g. CaO) and their CO_2 uptake rate are the available surface area, the sorbent's porosity and the average crystallite size (Alvarez and Abanades, 2005; Sun et al., 2007). The formation of $MgCO_3$ in AMS-promoted MgO proceeds via a nucleation and growth mechanism (Bork et al., 2021; Harada and Hatton, 2015; Jo et al., 2017); therefore, the stability of the sorbent is influenced by a larger number of parameters, including the properties of MgO, of the promoters and the interaction between them. Importantly, after promotion with AMS, the available surface area of MgO has a much lesser influence on the overall CO_2 uptake capacity than without AMS (Dal Pozzo et al., 2019; Rekhtina et al., 2020; Zhao et al., 2018). Still, other surface properties of MgO (e.g. surface defects and secondary phases acting as nucleation points) area play an important role in the cyclic stability of the sorbent since $MgCO_3$ is formed via a nucleation mechanism. An in-depth understanding of how these surface parameters evolve upon cycling between carbonation and calcination, and how they correlate with the carbonation performance is yet to be obtained. The cyclic evolution of AMS is another important and, thus far, largely under-investigated factor influencing the cyclic performance of sorbent. It has been proposed that the segregation of the molten salt from the MgO surface can lead to a decrease in the cyclic CO_2 uptake performance of sorbent (Dal Pozzo et al., 2019; Jo et al., 2017). Yet, these conclusions were drawn based on ex-situ contact angle measurements between the salt and the MgO surface, and do not represent the distribution of the molten promoter in the sorbent under operation conditions. Furthermore, the thermal stability of the molten promoter and its effect on the overall performance must be considered in greater detail (Chen et al., 2021; Gao et al., 2021), since the thermal decomposition temperatures of many nitrates, e.g. $LiNO_3$ or $NaNO_3$, are below or equal to the typical sorbent regeneration temperature of 450 °C (Hoshino et al., 1981; Qiao et al., 2017).

3.3.1.5. Effect of the gas composition. Flue gas contains, besides CO_2, a variety of compounds in different concentrations depending on the preceding process, and they all can potentially affect the CO_2 sorption performance of alkali metal oxide-based sorbents (Aaron and Tsouris, 2005). The presence of water vapour in the CO_2-containing gas stream was observed to improve the carbonation performance of both pristine (Fagerlund et al., 2012) and promoted MgO-based sorbents (Jin et al., 2017; Vu et al., 2016; Yang, Xinfang et al., 2016; Zarghami et al., 2015). It was suggested that the MgO is hydrated partially, forming reaction intermediates (e.g. Mg $(OH)_2$) that have an intrinsically higher reactivity with CO_2, and also that the presence of steam alters the morphology of the sorbent such that the surface area is increased (Béarat et al., 2002; Zarghami et al., 2015). Furthermore, it has been shown that the addition of liquid water to a used MgO-$NaNO_3$ sorbent, followed by calcination, is effective in regenerating its activity, because the water helps to distribute the $NaNO_3$ promoter on the surface of MgO and to decrease the average crystallite size of MgO (Dal Pozzo et al., 2019).

MgO can theoretically react with SO_2 and O_2 to form $MgSO_4$, which is thermodynamically stable at typical regeneration temperatures of sorbents (< 600 °C) (Scheidema and Taskinen, 2011). The accumulation of $MgSO_4$ in the sorbent with time would lead to a loss of MgO for CO_2 capture, and hence to a gradual reduction of the CO_2 uptake capacity. However, the formation of $MgSO_4$ does not occur on pristine MgO at a fast rate at typical carbonation temperatures such that the presence of SO_2 may practically not impair the CO_2 sorption performance of MgO (Bakhshi Ani et al., 2021). Thus far, it remains unclear whether molten salts promote the formation of $MgSO_4$ at lower temperatures, similar to their promoting effect on the formation of $MgCO_3$.

3.3.1.6. CO_2 capture applications. MgO-based sorbents, even when promoted with AMS, require high CO_2 partial pressures (≫ 1 bar) for fast CO_2 sorption rates and high theoretical CO_2 capture efficiencies (i.e. the thermodynamic limit of the fraction of CO_2 that can be removed from a gas stream) (Donat and Müller, 2022). Therefore, they are much more suitable for pre-combustion CO_2 capture than post-combustion CO_2 capture in which CO_2 partial pressures are rather low (usually between 3 and 10 vol.% in a flue gas stream). Experimental studies using MgO-based sorbents in packed bed reactors have demonstrated the efficient removal of CO_2 from high-pressure coal gas (Abbasi et al., 2014; Zarghami et al., 2015) or water-gas shift processes (Hu et al., 2019; Sikarwar et al., 2022) (sorption enhanced water-gas shift reaction, SEWGS).

3.3.2. Hydrotalcites for CO_2 adsorption

Hydrotalcite (HTL) compounds have attracted much attention in the context of CO_2 capture due to their potential application for the CO_2 capture from flue gas (Ding and Alpay, 2001; Ram Reddy et al., 2006) and in particular sorption enhanced reactions (SER) for H_2 production (Bassani et al., 2019; Fang et al., 2019; Gil et al., 2018; Halabi et al., 2012; Qi et al., 2018; Reijers et al., 2006; Yong and Rodrigues, 2002). They exhibit beneficial features including low cost, a wide range of preparation variables, high specific surface area, good regenerability, and high selectivity towards adsorption of CO_2 over gases like CH_4, CO, N_2 and steam at medium temperature, i.e. 200–500 °C (Baskaran et al., 2015; Cavani et al., 1991; Hufton et al., 1999; Lee et al., 2007; Vaccari, 1998).

Hydrotalcites, which belong to the class of layered double hydroxides (LDH, also known as anionic clays), are naturally occurring minerals (Vaccari, 1998). Since their natural occurrence is limited, the HTLs in use today are prepared by chemical companies (e.g. BASF, Sigma-Aldrich, SASOL, Clariant, Kisuma, Chemicals, or Sakei Chemicals) that sell tons of synthetic hydrotalcite-like compounds yearly (Forano et al., 2013). Synthetic hydrotalcites can be prepared via co-precipitation, urea hydrolysis, hydrothermal, sol-gel, microwave irradiation, steam activation, or solvothermal routes, as detailed in recent reviews (Forano et al., 2013; Othman et al., 2009). Furthermore, Mg-Al hydrotalcites can be prepared even from waste products, for example, using coal fly ash from coal-fired power plants (Muriithi et al., 2017; Yong and Rodrigues, 2002), and hazardous aluminum waste from the aluminum industry (Bui et al., 2018; Galindo et al., 2015; Gil et al., 2018).

HTLs are described by the general formula $[M^{2+}_{1-x}M^{3+}_{x}(OH)_2][A^{n-}_{x/n}\cdot mH_2O]$ or $[M^{+}_{1-x}M^{3+}_{x}(OH)_2][A^{n-}_{(2x-1)/n}\cdot mH_2O]$, where the metal cations M^+ = Li, M^{2+} = Mg, Ni, CO, Zn, and M^{3+} = Al, Cr, Fe, and usually, x has a value between 0.25 and 0.33 for the most widely used HTLs with M^{2+} and M^3+ (Vaccari, 1998). The metal cations together with the hydroxide form a di-metal hydroxide layer, and A^{n-} denotes anions which, together with the molecules of water, constitute the anionic layer. The hydrotalcite structure can accommodate a plethora of anions including inorganic (e.g. CO_3^{2-}, NO_3^{2-}), organic (e.g. oxalate, citrate, tartrate), and complex anions (e.g. Fe-, Cr-, porphyrin complexes). A comprehensive list of anions used in the hydrotalcite-like compounds can be found in the review by Baskaran et al. (2015). The structural flexibility of hydrotalcite-like compounds to accommodate a high variety of metals and anions is reflected by their use in a wide range of applications (Corma et al., 1992; Kagunya et al., 1996; Kung and Ko, 1996; Laycock et al., 1991; Orthman et al., 2003; Reichle, 1985; Salam et al., 2020; Takuo et al., 1979).

3.3.2.1. CO_2 adsorption capacity and kinetics of Mg-Al hydrotalcite compounds. Among the considered HTLs, the Mg-Al hydrotalcite, where M^{2+} is magnesium and M^{3+} is aluminum, has received the most attention for CO_2 sorption at medium temperature due to the highest CO_2 capture performance (Ding and Alpay, 2000; Lee et al., 2010; Oliveira et al., 2008; Yong et al., 2001; Yong and Rodrigues, 2002). HTLs can adsorb CO_2 at higher temperature (200–500 °C), compared to other adsorbents that capture CO_2 below 200 °C such as zeolites, supported amines, or metal organic frameworks (Dunstan et al., 2021). The adsorption capacity is typically <1 mmol per g sorbent, which is low in comparison with alkali metal oxide solid sorbents (Table 3.18) and is a major challenge for their practical applications (Choi et al., 2009; Ding and Alpay, 2000). For example, Ding and Alpay (2000) observed equilibrium adsorption capacities of 0.65 and 0.58 mmol g^{-1} during isothermal measurements at 400 and 480 °C, respectively. Generally, the saturation capacity increases with an increase in pressure. Interestingly, Reddy et al. (Ram Reddy et al., 2008) found that diluting the concentration of CO_2 (from 14 % at atmospheric pressure) in the gas feed by almost seven times did not affect the CO_2 sorption capacity. Most of the tested HTLs are powder samples with particle sizes ranging from nanometer to micrometer. Recently, Veerabhadrappa et al. (2021) produced pelletized (2 mm) exfoliated LDH-based nanosheets to investigate whether they can be used in industrial-scale applications. The best sample displayed a high surface area (264 m^2/g) and a CO_2 sorption capacity of 1.4 mmol/g at 200 °C and 86 % CO_2 at 1 bar.

The use of alkali metal impregnation has been used widely to increase the HTL's basicity and thereby improve its CO_2 sorption capacity. When Mg-Al hydrotalcites are impregnated with K_2CO_3 (commonly referred to as K-promoted HTL), an optimum of 20 wt.% offers the maximum adsorption capacity (Choi et al., 2009; Hutson and Attwood, 2008; Yang and Kim, 2006; Yong and Rodrigues, 2002). Also, it has been found that the CO_2 sorption capacity depends more strongly on the basicity of the surface of the modified HTL than the associated changes in the surface area (Hutson and Attwood, 2008).

There is some debate in the literature about how to best describe and accurately model the kinetics of CO_2 uptake by HTLs (Ebner et al., 2006, 2007; Lee et al., 2007; Singh et al., 2009). Considering K-promoted HTL, the reaction has been described as a diffusion limited reaction similar to a physical adsorption process (Ding and Alpay, 2000, 2001). Comparing the values of the fitted mass-transfer coefficients, as determined by a diffusion limited reaction model, show large differences suggesting that the adsorption mechanism is more complex, as pointed out by Ebner et al. (2007). For example, mass transfer coefficients for adsorption have been determined as low as 0.0058 s^{-1} for K_2CO_3 promoted Mg-Al hydrotalcites (Ding and Alpay, 2000). In contrast, other works have shown steep break-through curves for the same type of HTL, suggesting fast kinetics and a high mass transfer coefficient with a fitted value of 0.0151 s^{-1} (Soares et al., 2005). Ebner et al. (2006, 2007) observed that the CO_2 uptake reached equilibrium saturation only after a very long adsorption time (700 min). To describe this behavior, the authors developed a non-equilibrium model consisting of three reversible reactions and four phases which had a better fit throughout the slow adsorption process. However, the discrepancies in interpretation and modelling can to a large extent, be related to preparation of the HTL, variations in composition, impregnation degree and coverage, pressure range, and temperature range (Halabi et al., 2012). Recent kinetic studies were able to accurately model the CO_2 adsorption kinetics between 300 and 500 °C in dry and wet conditions, where there is competitive adsorption of H_2O and CO_2 (Coenen et al., 2019).

3.3.2.2. Chemical composition of hydrotalcites. There have been several efforts towards modifying the chemistry of HTLs to improve their CO_2 adsorption capacity and kinetics (Aschenbrenner et al., 2011; Oliveira et al., 2008; Yang and Kim, 2006; Yong et al., 2001). Yong et al. considered different combinations of di- and trivalent cations, including Ni-Al, Co-Al, Cu-Al, Zn-Al, and Mg-Al, and found that the latter showed the best performance (Yong and Rodrigues, 2002). Further optimizing the ratio of Mg and Al affects the number of basic sites and capacity. A high content of Al increases the charge density, providing a higher number of basic sites, but at the same time decreases the interlayer spacing and void space, thereby accommodating less CO_2 molecules (Baskaran et al., 2015; Choi et al., 2009). Increasing the Mg content provides more basic sites, which suggests that there exists an optimal ratio of Mg and Al for highest CO_2 adsorption capacity (Yang and Kim, 2006; Yong et al., 2001). For K-promoted Mg-Al HTL, with 20 wt.% of K_2CO_3 impregnation, an optimum ratio of Mg/Al = 2 provided the highest CO_2 adsorption capacity (0.77 mmol/g) at 450 °C and 1 bar (Yang and Kim, 2006). While an optimum ratio of Mg/Al = 2 was found specifically for K-promoted HTL under those conditions, a large variation in the optimum ratios of Mg/Al between 1 and 3 has been reported depending on the type of interlayer anion, whether other metal cations were used, the synthesis procedure, and which conditions they have been tested under (Baskaran et al., 2015; Choi et al., 2009).

The HTL composition changes with temperature and gas atmosphere, exhibiting hydroxylation, decomposition of carbonate and formation of oxides (mixed metal oxide, MMO). The decomposition occurs in four steps: (i) The desorption of interlayer water molecules at 100–200 °C, (ii) the loss of OH^- groups bonded to Al^{3+} at 200–300 °C, (iii) the loss of OH^- groups bonded to Mg^{2+} at 250–450 °C, and (iv) the loss of carbonates at 400–600 °C (León et al., 2010; Othman et al., 2009). The calcination temperature to achieve the highest CO_2 adsorption capacity has generally been reported as 400 °C, providing an optimum balance between surface area and basic sites (Ram Reddy et al., 2006). Under reaction conditions for sorption enhanced water gas shift (SEWGS), 400 °C and 5 bar, the layered clay structure decomposes and the material can be described as a mixed magnesium aluminum oxide with basic adsorption properties, and the basicity is further enhanced by the addition of potassium carbonate (van Dijk et al., 2011).

3.3.2.3. Regeneration of hydrotalcites. Hydrotalcites possess good capabilities for regeneration as measured by a small loss in the successive adsorption/desorption CO_2 capacity. For example, Halabi et al. (2012) assessed the regenerability of K-promoted HTL over 30 cycles at 400 °C and 1.5 bar. The sorbent displayed an uptake of 0.96 mmol g^{-1} in the first cycle, which decreased to 0.89 mmol g^{-1} in the second cycle and remained stable afterwards. The synthesis route also affects the ability to regenerate the HTLs. León et al. (2010) studied the adsorption/desorption mechanism and regenerability of hydrotalcites prepared by different methods. They observed that co-precipitation led to 86 % regenerability (with a low CO_2 adsorption capacity of 0.72 mmol g^{-1} at 100 °C and 1 bar) opposed to only 67 % for sonication (with a higher initial CO_2 adsorption capacity of 0.84 mmol g^{-1} at 100 °C and 1 bar). The reason for the differences was attributed to the bonding strength of the basic sites. The HTL prepared by sonication conditions had the strongest basic sites due to the formation of unidentate CO_2-adsorbent species causing irreversibility. On the other hand, co-precipitation produced materials with weaker basic sites with the formation of bidentate and surface bicarbonates causing highly reversible adsorption (León et al., 2010).

3.3.2.4. Effect of the gas composition. The impact of gas composition including H_2O and impurities such as H_2S, SO_2 have been investigated with respect to the CO_2 adsorption capacity. Generally, steam enhances both the CO_2 adsorption capacity and the cyclic stability of hydrotalcites (Ding and Alpay, 2000, 2001; Hufton et al., 1999; León et al., 2010; Ram Reddy et al., 2008). Ding et al. measured a 10 % increase in the CO_2 adsorption capacity under humid conditions compared to dry conditions at 480 °C (Ding and Alpay, 2000). They also found no further increase in the CO_2 adsorption capacity when the partial pressure of steam was increased from 0.03 to 2.45 bar, similar to what has been observed for $CaO/CaCO_3$ where only low partial pressures of steam have a positive impact on the CO_2 sorption capacity (Donat et al., 2012). The reason for the CO_2 sorption enhancement of Mg-Al HTLs, measured in the range

of 300–480 °C, has been attributed to the formation of magnesium and aluminum hydroxides, a higher hydroxyl concentration of the surface, and/or avoiding coke deposition (Choi et al., 2009; Ding and Alpay, 2000). Due to the independence of the water concentration in the CO_2 sorption step, it has also been suggested that new adsorption sites are created through the surface coverage of water (Ram Reddy et al., 2008). Furthermore, performing the regeneration of the HTL with steam has proven to be more effective in maintaining a high regenerability than with N_2, demonstrated by 30–40 % higher CO_2 recovery in the presence of steam at 300 °C and 1 bar (Ding and Alpay, 2001).

Hydrotalcites promoted with K_2CO_3 are able to reversibly capture both H_2S and CO_2 with high selectivity. With up to 2000 ppm of H_2S, the CO_2 sorption capacity is not affected compared to the sulphur-free conditions (van Dijk et al., 2011). The high selectivity and reversibility suggest that SEWGS can eliminate CO_2 and H_2S simultaneously from the syngas, and an almost CO_2 and H_2S-free H_2 stream and a separate CO_2 and H_2S stream can be produced (Bassani et al., 2019; van Dijk et al., 2011). On the other hand, SO_x has a severe negative impact on the CO_2 adsorption capacity of HTLs, as the adsorbents deactivate rapidly due to irreversible SO_x adsorption. Also, the adsorption of SO_x is favoured over CO_2 due to strong acid-base interactions, such that a desulfurization unit upstream of CO_2 capture unit is necessary on a process scale (Ram Reddy et al., 2008).

3.3.2.5. CO_2 capture applications. Similar to MgO-based sorbents, at medium temperatures HTLs are most suitable for pre-combustion CO_2 capture when CO_2 partial pressures are high. Recent European Horizon 2020 projects (e.g. STEPWISE or FReSMe) have demonstrated the large potential of SEWGS using HTLs to reduce CO_2 emissions from the iron and steel industry (Cobden et al., 2018; Gazzani et al., 2015; Manzolini et al., 2020; Sebastiani et al., 2021). Here, the sorbent is operated through a pressure swing adsorption approach (CO_2 sorption at >20 bar, and CO_2 removal from the sorbent at ~1 bar) (Gentile et al., 2022).

3.3.3. Alkali-metal-based carbonates

Among the various solid sorbents, dry alkali-metal-based solid sorbents are considered promising candidates for post combustion CO_2 capture, which are expected to be cost-effective and energy-efficient (Dong et al., 2015; Rodríguez-Mosqueda et al., 2018). Alkali-metal carbonates, such as K_2CO_3 and Na_2CO_3, can react with CO_2 to form alkali hydrogen carbonates in the presence of H_2O at low temperatures (60–80 °C) as displayed in Reaction 3.9, which can be easily regenerated at 120–200 °C via the reverse reaction of Reaction 3.9 (Qin et al., 2014). By comparison, K_2CO_3 has been revealed to give better performance than Na_2CO_3 in terms of both CO_2 adsorption capacity and kinetics, and thus most attention has been diverted to the former (Jaiboon et al., 2013). Nevertheless, the employment of pure K_2CO_3 is mainly restricted by their low conversion and poor reaction kinetics, which has been proven to be limited by the adsorption, instead of chemical reaction. Furthermore, pure K_2CO_3 is a deliquescent substance with a compact structure and a relatively low surface area, leading to its inferior CO_2 adsorption capacity (Bararpour et al., 2019; Zeng et al., 2022). It has been reported that the hydration of K_2CO_3 (Reaction 3.10) generally occurs as a competing reversible reaction in parallel with Reaction 3.9 during the carbonation process in the presence of a high amount of moisture in the inlet gas, which converts the active adsorption sites to hydrated by products with poor CO_2 capture capacity (Fig. 3.41) (Bararpour et al., 2020; Gomez et al., 2016). Therefore, the modification of K_2CO_3 sorbents is required to enhance their CO_2 capture capacity and durability before use for cyclic carbonization and regeneration operations.

$$M_2CO_3 + H_2O + CO_2 \leftrightharpoons 2MHCO_3 \ (M=Na, K) \quad (3.9)$$

$$K_2CO_3 + 1.5H_2O \leftrightharpoons K_2CO_3 \cdot 1.5H_2O \quad (3.10)$$

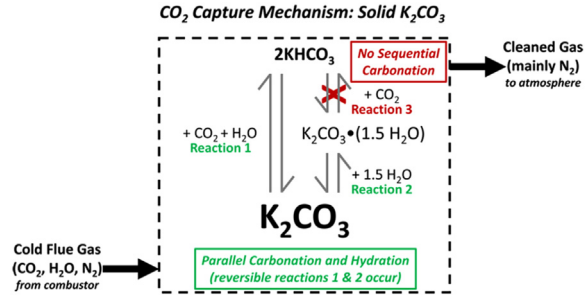

Fig. 3.41. Reaction mechanism of solid K_2CO_3 for CO_2 capture (Gomez et al., 2016). (For interpretation of the references to color in this figure legend, the reader is referred to the web version of this article.)

The most extensively studied method is to support K_2CO_3 by a stable and porous material, which contributes to better contact between the sorbent and CO_2 and hence increases the overall carbonation rate. The commonly used supports include activated carbon (AC), TiO_2, CaO, MgO, ZrO_2, silica gel, zeolites and Al_2O_3 (Li et al., 2011). Al_2O_3 and MgO are the most widely employed supports because of their excellent CO_2 capture capacity. However, the main drawback of Al_2O_3 and MgO supported K_2CO_3 sorbents is their easy deactivation because of the generation of undesirable by products, such as KAl $(CO_3)_2$ $(OH)_2$, K_2Mg $(CO_3)_2$, and K_2Mg $(CO_3)_2 \cdot 4$ (H_2O), which could not be completely regenerated to the original K_2CO_3 phase (Lee et al., 2008; Qin et al., 2018). For example, Lee et al. (2014), Lee et al. (2013) investigated the phase of Al_2O_3 on the CO_2 capture performance of supported K_2CO_3 sorbents by calcining Al_2O_3 at various temperatures of 300, 600 (γ-Al_2O_3), 950 (δ-Al_2O_3) and 1200 °C (α-Al_2O_3). They demonstrated that the regeneration capacity of the sorbents increased with elevating the calcination temperature due to the production of less inactive KAl $(CO_3)_2$ $(OH)_2$ byproducts, in spite of the decreased surface area of the sorbents at higher calcination temperature. In this case, the regeneration capacity of the sorbents was more dependent on the structure properties of alumina, rather than the texture properties. In comparison, AC and TiO_2 supported K_2CO_3 sorbents are more promising in retaining the CO_2 capture capacity with the formation of mainly $KHCO_3$ in the carbonation process (Lee et al., 2008; Qin et al., 2018).

It has been proven that the nature and physiochemical properties of the support, such as the surface area, pore structure, and surface property, play a significant role in determining the CO_2 capture capacity of supported K_2CO_3 sorbents. For instance, Qin et al. (2014) discovered that for K_2CO_3 sorbents supported by various materials (fly ash, Portland cement, clay, Al_2O_3, and calcium aluminate cement), K_2CO_3/Al_2O_3 displayed the highest CO_2 capture capacity of 71 mg CO_2/g sorbent, which was stable in 10 cycles. The reason could be explained by the developed mesoporous structure and high surface area of K_2CO_3/Al_2O_3 sorbents. Similar results have been reported by Wang et al. that among various Al_2O_3-based supports (i.e., activated alumina (Al_2O_3), Bayer aluminum hydroxide (Bah), kaolinite clay (KC) and calcium aluminate cement (CA)), Bah supported K_2CO_3 displayed the highest CO_2 sorption capacity of 1.85 mmol CO_2/g, which might be ascribed to its loose surface and well-developed pore structure, as well as its highest surface area and pore volume (Fig. 3.42) (Wang et al., 2019). In addition, Masoud et al. (2021) studied the role of surface oxygen groups on the carbon supports (i.e. polarities of the support) in CO_2 capture by K_2CO_3 sorbents. The result showed that the apolar carbon support was more favourable to CO_2 capture, since an apolar support accelerated the adsorption of apolar CO_2 molecules while decreasing the local concentration of polar H_2O on the sorbent, contributing to a higher carbonation degree. On the contrary, a polar support was expected to promote the hydrate formation by attracting more polar H_2O molecules on the K_2CO_3 sorbent, which thereby limited the carbonation reaction.

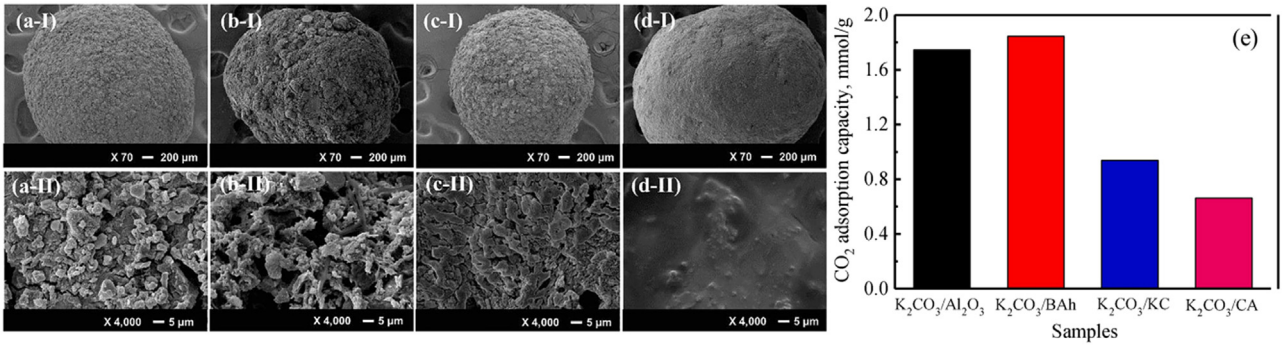

Fig. 3.42. SEM images of K_2CO_3-based sorbents supported by (a) Al_2O_3; (b) BAh; (c) KC and (d) CA, and (e) CO_2 adsorption capacities of K_2CO_3-based sorbents with different supports (Wang et al., 2019). (For interpretation of the references to color in this figure legend, the reader is referred to the web version of this article.)

In addition to the support properties, the loading amount of K_2CO_3 on the support is another important parameter affecting the CO_2 capture performance of the composite sorbents. It has been proven that a proper K_2CO_3 loading favours the achievement of well-developed pore structures and surface morphology with active components uniformly distributed on the support, contributing to the enhancement of CO_2 capture performance. On the contrary, excessive K_2CO_3 loading will result in the agglomeration of K_2CO_3 crystallites and hence the coverage and blocking of the surface and pores of the sorbents, which could be responsible for the deteriorated CO_2 capture capacity (Wang et al., 2019). Guo et al. (2018) evaluated the CO_2 sorption capacity of silica aerogel supported K_2CO_3 sorbents with various K_2CO_3 loadings of 0–30 wt%. The maximum CO_2 capture capacity of 1.32 mmol CO_2/g was achieved at a K_2CO_3 loading of 20 wt%, which should be attributed to its best particle morphology with a uniform dispersion of K_2CO_3 and small pores. Zeng et al. (2022) also varied the content of K_2CO_3 on Al_2O_3 support from 20 to 60 wt% and discovered a decrease of the surface area and pore volume with increasing the K_2CO_3 content. In spite of the relatively inferior texture properties of K30Al to that of K20Al, K30Al achieved the highest CO_2 capture capacity because of its higher amount of active K_2CO_3. With the further increase of K_2CO_3 content to 40–60 wt%, the CO_2 capture capacity decreased sharply due to the blockage of the pores, leading to the increase of the internal diffusion resistance of CO_2.

The synthesis method is another crucial factor influencing the physiochemical properties of the sorbents. In recent years, various methods have been developed for the preparation of K_2CO_3-based sorbent, in order to enhance its CO_2 capture performance. For example, Sengupta et al. (2015) compared the performance of K_2CO_3/Al_2O_3 sorbents synthesized by single- and multi-step impregnation (SI and MI) methods. They found that the sorbent synthesized by the MI method was more promising than that synthesized by the SI method in terms of CO_2 adsorption capacity and regeneration efficiency. The reason could be the more uniform dispersion of K_2CO_3 in the broad macropores without the blockage of narrower mesopores of Al_2O_3 in the sorbent synthesized by the MI method, which enabled a higher loading of accessible K_2CO_3 for CO_2 adsorption. On the contrary, the blockage of narrower mesopores by large K_2CO_3 aggregates could be obviously observed in the sorbent synthesized by the SI method, which limited the accessibility of CO_2 towards active K_2CO_3 species. In order to eliminate the adverse effect of H_2O on the CO_2 capture performance of supported K_2CO_3 sorbent, Bararpour et al. (2020) synthesized a core-shell structured support with γ-alumina as the core and TiO_2 as the shell. The result showed that the CO_2 capture performance of K_2CO_3/γ-alumina was significantly enhanced after shelling the support with TiO_2, due to the low hydrophilicity of the sorbent, which restricted the occurrence of reaction (2). The effect of calcination temperature on the CO_2 adsorption performance of Al_2O_3-supported K_2CO_3 pellets synthesized by graphite-casting method (Fig. 3.43 (a)) has also been investigated in a previous study (Zeng et al., 2022). Although it is widely accepted that a high calcination temperature will lead to a less developed microstructure and hence an inferior CO_2 adsorption capacity because of the aggregation of active components at higher temperatures, the K_2CO_3-based pellets calcinated at 900 °C displayed a 2.5 times higher CO_2 adsorption capacity than that of the sorbent calcinated at 300 °C (Fig. 3.43 (b) and (c)).The reason could be explained by that the residual graphite coating on the sorbent surface calcinated at 300 °C supressed the diffusion of H_2O to K_2CO_3 because of the hydrophobicity of graphite.

On account of the relatively poorer CO_2 adsorption rate of Na_2CO_3 than that of K_2CO_3, the studies on CO_2 capture using Na_2CO_3-based sorbents are limited. However, the primary advantages of using Na_2CO_3 over K_2CO_3 are its easier accessibility, lower regeneration temperature, and lower CO_2 capture costs (Wu et al., 2020). If the reaction kinetics of CO_2 capture could be dramatically improved via proper modifications of Na_2CO_3-based sorbents, their applications in large-scale CO_2 capture could be significantly broadened. Therefore, the understanding of the rate-limiting steps of CO_2 capture by Na_2CO_3 is critical to systematically improving the kinetics. Cai et al. (2019) employed first-principles density functional theory (DFT) to study the structural, mechanistic, and energetic properties of CO_2 adsorption on the low-index (001) and high-index (−402) surfaces of unmodified Na_2CO_3 sorbent, in order to clarify the actual reason of the slow kinetics. They discovered that the reaction barriers for bicarbonate formation on the above two facets were comparable with that on K_2CO_3 surfaces. However, on account of the much lower overall kinetics of CO_2 capture by Na_2CO_3 observed by experiments, they assumed that the kinetics of CO_2 captured on Na_2CO_3 was controlled by surface diffusion, rather than by surface carbonation reaction as that observed for K_2CO_3.

In order to enhance the reaction kinetics of CO_2 capture on Na_2CO_3, the dispersion of Na_2CO_3 on various supports is considered as the most dominant strategy, where the support effect and Na_2CO_3 loading are important factors in developing efficient Na_2CO_3-based sorbents (Cai et al., 2020; Luo and Kanoh, 2017). It is well accepted that the textural properties of the support play a crucial role in determining the CO_2 capture performance of the sorbent. Kazemi et al. (2020) tried to improve the specific surface area and pore volume of γ-Al_2O_3-supported Na_2CO_3 sorbent using a modified sol-gel process with the addition of polyethylene glycol (PEG). They demonstrated that the surface area and pore volume of the modified sorbent were around 38 % and 340 % higher than that of the sorbent synthesized without the addition PEG. As a result, the CO_2 capture capacity of the sorbent increased by 34 %. In addition to the texture properties such as surface area and pore structure, the morphology and distribution of Na_2CO_3 have also been confirmed to affect the CO_2 capture performance. As observed by Cai et al. (2020), the morphology of Na_2CO_3/γ-AlOOH sorbent could be changed by varying the loading amount of Na_2CO_3, which thereby influences the CO_2 capture capacity significantly. At lower Na_2CO_3 loadings of <17 wt%, Na_2CO_3

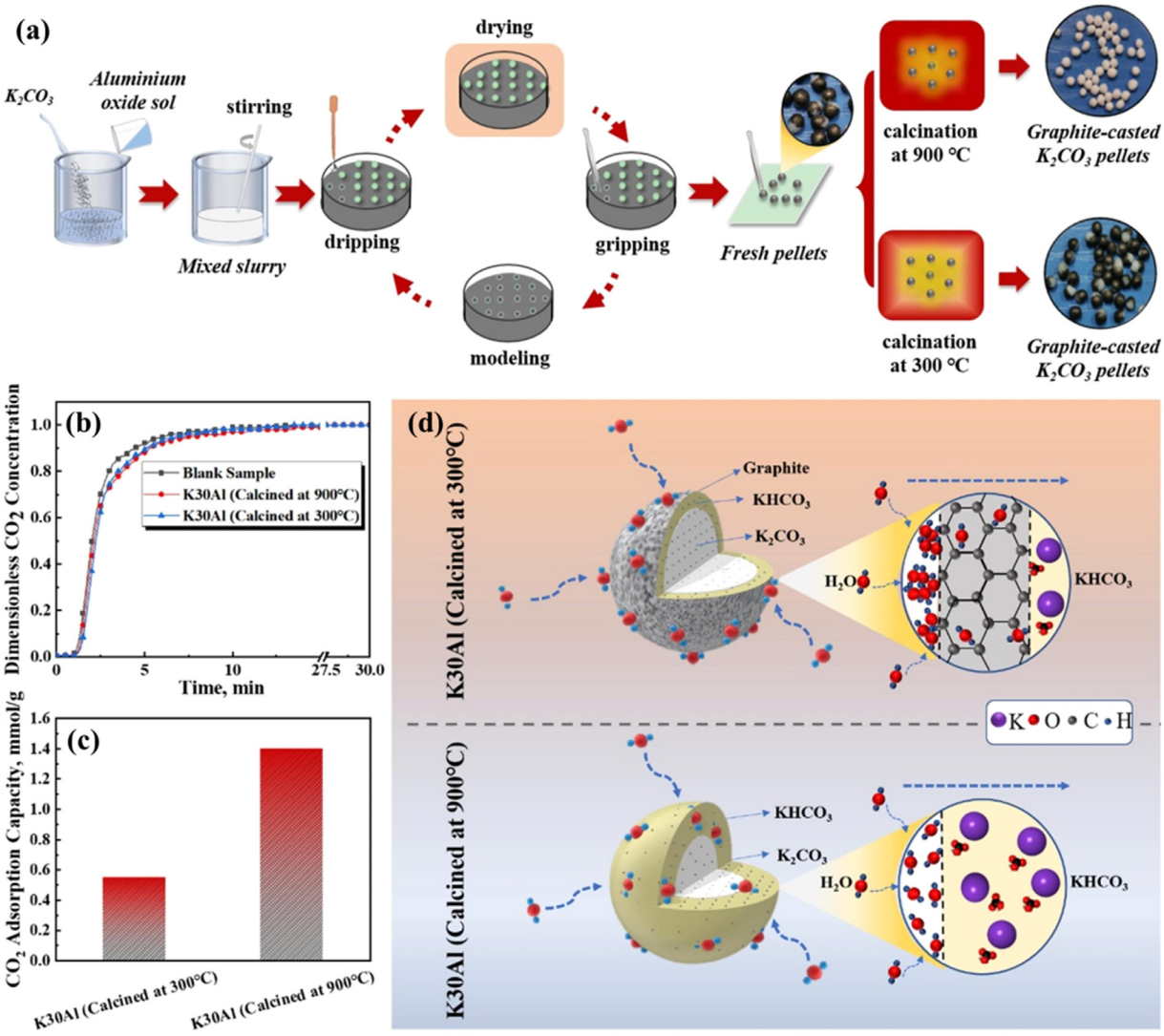

Fig. 3.43. (a) Scheme for the preparation of graphite-casted K_2CO_3 pellets, (b) breakthrough curves of CO_2 adsorption, (c) CO_2 adsorption capacity of K30Al calcined at 300 and 900 °C, and (d) mechanism of the adverse effect of residual graphite coating on CO_2 adsorption (Zeng et al., 2022). (For interpretation of the references to color in this figure legend, the reader is referred to the web version of this article.)

was uniformly dispersed on γ-AlOOH surface sites as a monolayer amorphous form. With the increase of Na_2CO_3 loading up to 23–29 wt%, the Na_2CO_3 crystallites grew uniformly to form nanoparticles on the inner surface of γ-AlOOH, contributing to the exposure of more high-index facets of Na_2CO_3 (such as (1 1 2) and (−4 0 2) facets) and hence the enhancement of the CO_2 capture capacity.

In summary, alkali-metal-based carbonates of K_2CO_3 and Na_2CO_3 are proven as promising candidates for CO_2 capture, while the practical applications of pure carbonates were restricted by their poor capacities and kinetics. As a result, the proper design of efficient K_2CO_3- and Na_2CO_3-based sorbents is of significant importance in broadening their application prospects. The most potential method for modification of K_2CO_3 and Na_2CO_3 is to load them on a porous support, where the optimization of the support materials, K_2CO_3/Na_2CO_3 loading amounts, and preparation methods are expected to improve the texture properties and surface morphology, enhance the dispersion of active K_2CO_3/Na_2CO_3, and hence accelerate the CO_2 adsorption. In spite of the extensive studies on this topic, the influence of the abundant impurities in flue gases, such as sulphur- and chlorine-containing species, on the CO_2 capture performance of alkali-metal-based sorbents was rarely studied systematically, which is critical in evaluating their durability and regeneration efficiency in practical applications.

3.4. High-temperature solid sorbents

3.4.1. CaO for CO_2 capture

Among the alkali earth metal oxides CaO, SrO, and BaO, CaO has been studied most thoroughly for CO_2 sorption applications at high temperatures (Kierzkowska et al., 2013; Krödel et al., 2020; Omodolor et al., 2020; Yu et al., 2012). Many of the early studies in the 1990s and 2000s benefitted from experience with CaO-based sorbents in the context of flue gas desulfurization, when SO_2 was considered more problematic than CO_2 (Dunstan et al., 2021). The CO_2 capture process using CaO-based sorbents, also referred to as calcium looping (CaL), utilizes the reversible reaction between CaO and CO_2 at elevated temperatures, viz Reaction 3.11:

$$CaO + CO_2 \rightarrow CaCO_3 \ (\Delta H^0_{298K} = -178 \text{ kJ mol}^{-1}) \quad (3.11)$$

The operational windows for the carbonation and the calcination reactions are defined by the reaction equilibrium, i.e. the equilibrium partial pressure of CO_2 at a given temperature (Samanta et al., 2012). In sorbent research, calcination is commonly conducted at 800–950 °C in air, N_2 or pure CO_2; at the process level, the calcination reaction would have to be carried out in (almost) pure CO_2 to process the CO_2 released

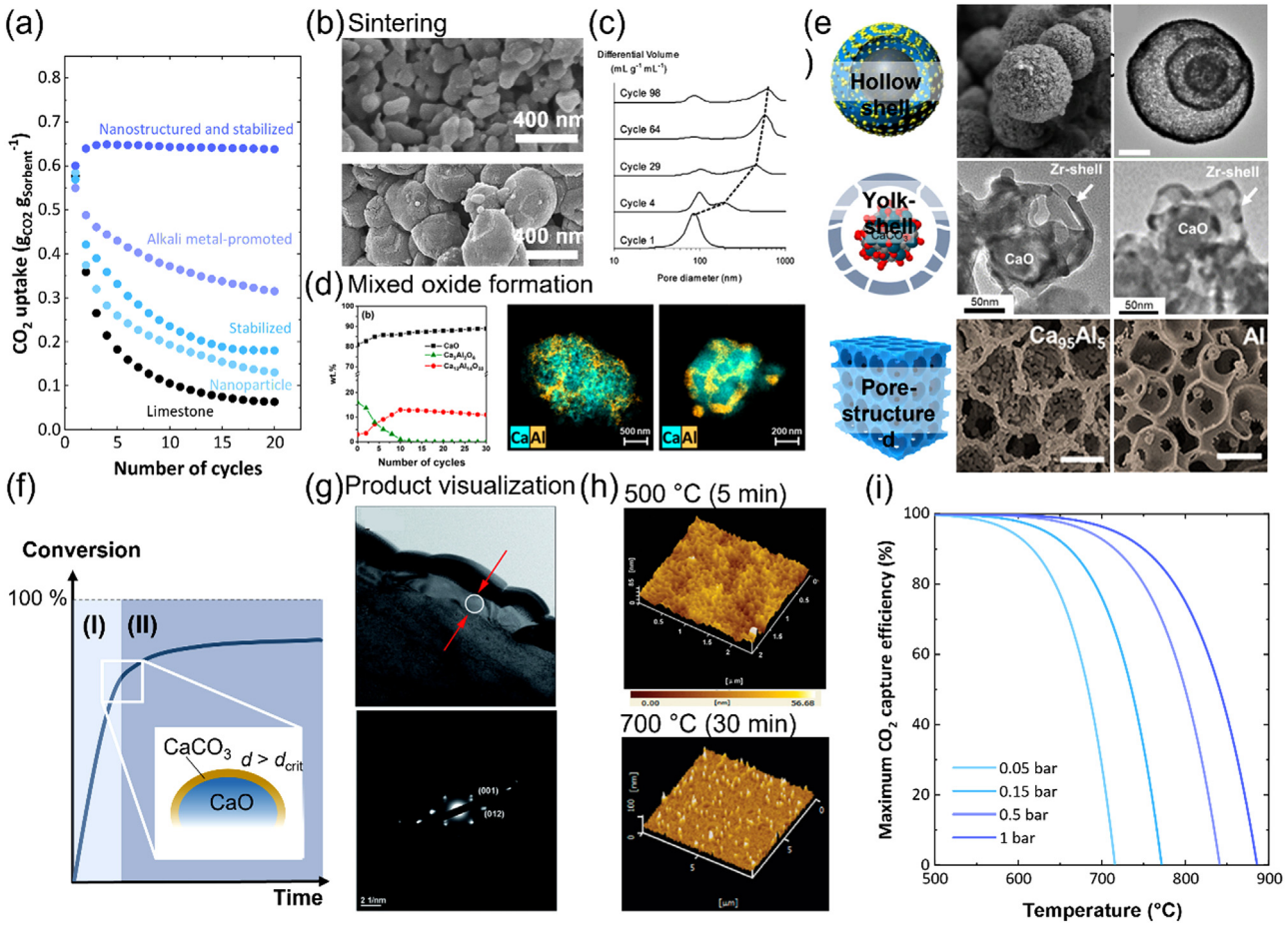

Fig. 3.44. (a) Typical cyclic CO_2 uptake of selected CaO-based sorbents over 20 carbonation-regeneration cycles, illustrating the performance improvement compared to bare limestone via stabilization, promotion or nanostructuring of the sorbent. (b) SEM micrographs of limestone after the 1st calcination (top) and after 10 cycles (bottom) (Naeem et al., 2018). (c) Evolution of the pore volume of La Blanca limestone measured via Hg intrusion porosimetry over 98 carbonation-calcination cycles (Alvarez and Abanades, 2005). (d) Changes in the phase composition of a $Ca_3Al_2O_6$-stabilized CaO-based sorbent over carbonation-regeneration cycling derived from in situ XRD using Rietveld analysis (Kim et al., 2018). (e) Electron micrographs of a nanostructured hollow multishell CaO-based sorbent reported by Naeem et al. (Naeem et al., 2018), a yolk-shell-type CaO-based sorbent reported by Krödel et al. (Krödel et al., 2022), and pore-structured (via a sacrificial template) CaO-based sorbent reported by Kim et al. (Kim et al., 2019) (f) Conversion over time curve for CaO-based sorbents exhibiting the two typically observed regimes: (I) a kinetically-controlled regime and (II) a diffusion-controlled regime. (g) Visualization of the $CaCO_3$ product on CaO via TEM and SAED (Sun et al., 2019). (h) AFM plots of the $CaCO_3$ product formation on a CaO single crystal at two different carbonation temperatures and after varying carbonation times (Li et al., 2012). (i) Maximum CO_2 capture efficiency for CaO-based sorbents as a function of temperature and the partial pressure of CO_2 in the gas stream. (For interpretation of the references to color in this figure legend, the reader is referred to the web version of this article.)

from the sorbent further (e.g. compression and storage) and avoiding additional downstream gas purification. Typically investigated carbonation conditions range between 550 °C and 700 °C as well as 10–15 vol.% CO_2 in air or N_2 to reflect CO_2 concentrations in off-gases from (coal) combustion processes. During the carbonation reaction, two reaction regimes are observed: (Bhatia and Perlmutter, 1983; Cai et al., 2017). A fast, kinetically-controlled regime and a slow, diffusion-controlled regime, see Fig. 3.44f. The CO_2 uptake in the kinetically-controlled regime correlates directly with the initially available surface area of the CaO-based sorbent, which is usually supplied by pores with diameters smaller than 100 nm (Alvarez and Abanades, 2005; Alvarez and Abanades, 2005; Bhatia and Perlmutter, 1983). The shift between the two reaction regimes is often explained with the $CaCO_3$ product layer reaching a critical thickness, estimated at 30–50 nm at which the reaction becomes limited by CO_2 diffusion through $CaCO_3$ (Fig. 3.44g and h).

For practical CO_2 capture applications at high temperature, CaO-based sorbents need to be repeatedly cycled between their oxide and carbonate states, making the cyclic CO_2 uptake an important metric for the CO_2 capture costs (Hanak et al., 2015a). Generally, the cyclic CO_2 uptake should be as close as possible to the theoretical maximum CO_2 uptake capacity of 0.78 g_{CO2}/g_{CaO} and stable over ideally thousands of cycles. In reality, the cyclic CO_2 uptake of sorbents derived from natural limestones decreases rapidly with cycling, as shown exemplarily in Fig. 3.44a. The deactivation of the sorbent is a result of material sintering (Fig. 3.44b and c), which (i) reduces the surface area of the regenerated CaO available for the reaction with CO_2, and (ii) increases the diffusional resistance of CO_2 into the bulk sorbent, such that both the rate and the extent of CO_2 uptake during the carbonation step are reduced (Barker, 2007; Li et al., 2006; Wang et al., 2014). To mitigate the sintering-induced deactivation, research efforts have focused on either reactivating the sorbents, e.g. using a steam treatment at high temperatures, or stabilizing and promoting the sorbent using non-alkali metal oxides and alkali metal salts, respectively (Salaudeen et al., 2018).

3.4.1.1. Synthetic stabilized and promoted sorbents. The cyclic CO_2 uptake performance of CaO-based sorbents can be stabilized using metal oxides with high Tammann temperatures such as Al_2O_3, ZrO_2 or MgO (Kierzkowska et al., 2013; Krödel et al., 2020; Naeem et al., 2017; Radfarnia and Iliuta, 2013; Salaudeen et al., 2018). These stabilizers

are mixed into the CaO matrix in contents of typically 5–20 wt.%, e.g. through ball-milling, co-precipitation, sol-gel or more advanced techniques like atomic layer deposition, and they are assumed to act as physical barriers against the sintering of CaO particles (Kim et al., 2018; Kurlov et al., 2020a; Kurlov et al., 2016; Liu et al., 2010). Stabilizers effectively reduce the cyclic decrease of the surface area and pore volume of the sorbents, thereby improving their cyclic CO_2 uptake. For example, Kim et al. reported a $Ca_3Al_2O_6$-stabilized CaO-based sorbent showing a CO_2 uptake of 0.38 $g_{CO2}/g_{Sorbent}$ after 30 cycles, an increase of 300 % compared to the benchmark limestone (Kim et al., 2018). Other materials utilizing ZrO_2, MgO or SiO_2 showed similar CO_2 uptakes of up to 0.37, 0.31 or 0.39 $g_{CO2}/g_{Sorbent}$ after 10 cycles, respectively (Kurlov et al., 2016; Sanchez-Jimenez et al., 2014; Zhao et al., 2014). Despite these improvements, even stabilized materials deactivate with cycling via mixed phase formation with CaO, viz. a loss of the reactive phase for CO_2 sorption, or the agglomeration of the stabilizing phase as surface-segregated particles, reducing the effectiveness of the stabilizer as a physical barrier against sintering of CaO grains/particles (Fig. 3.44d) (Kim et al., 2018; Kurlov et al., 2016). Hence, optimizing both the distribution and the mobility of the stabilizer phase in the material are crucial aspects for the design of stabilized, long-lasting CaO-based sorbents. Works by Naeem et al. (2018) and Armutlulu et al. (2017) have employed means of stabilization as well as morphological design techniques to derive sorbents with even more stable cyclic CO_2 uptakes (Fig. 3.44e). For example, one of the best performing sorbents to date consists of a double shell structure of a CaO-MgO nanocrystalline matrix. This material exhibited a CO_2 uptake of 0.65 $g_{CO2}/g_{Sorbent}$ after 10 cycles, which equals 93 % of the theoretical maximum CO_2 uptake of a sorbent containing 10 wt.% MgO.

The promotion of CaO-based sorbents using alkali metal salts (AMS), e.g. Na_2CO_3, NaCl, K_2CO_3 or KCl, is another approach to improve their cyclic CO_2 uptake (González et al., 2011; Kurlov et al., 2020b; Lee et al., 2018; Xu, Yongqing et al., 2018). Added in relatively large amounts (>5 wt.%), these low Tammann-temperature promoters increase the sintering of the sorbents, thereby reducing the cyclic CO_2 uptake performance significantly compared to benchmark materials without AMS (Krödel et al., 2020). In addition, some alkali metals form low-melting mixed phases with CaO that tend to form either large surface-segregated particles or a layer around the bulk CaO particles (Kurlov et al., 2020b). For example, Kurlov et al. reported the formation of $Na_2Ca(CO_3)_2$ coatings around Na_2CO_3-modified CaO particles due to the melting of the mixed phase under calcination conditions (900 °C, 100 vol.% CO_2), negatively affecting the accessibility of CaO for reaction with CO_2. On the other hand, low AMS contents of < 1 wt.% have been reported to have a positive effect on both the carbonation and calcination reaction, therefore increasing the cyclic CO_2 uptake (Xu et al., 2023; Xu et al., 2017; Yang et al., 2018). The best reported sorbents to achieve CO_2 uptakes of up to 0.5 $g_{CO2}/g_{Sorbent}$ after 10 cycles with < 1 wt.% of promoter added. In nature, various alkali metals are found in the structure of $CaCO_3$, which may explain the large differences in the cyclic CO_2 uptake of limestone-derived sorbents of different origin/geographical location (Fennell et al., 2007; Grasa and Abanades, 2006; Valverde et al., 2015; Yoshimura et al., 2017). Similarly, researchers have proposed that alkali metal promoters may be incorporated into the structure of the $CaCO_3$ product forming during carbonation (Leukel et al., 2018). This could positively affect the rate of carbonation, e.g. by enhancing CO_2 diffusion through $CaCO_3$, but evidence for this mechanism is still lacking. It has been reported that AMS affects the transition temperature between CaO and $CaCO_3$, leading to the onset of the decomposition of $CaCO_3$ at lower temperatures which may be interesting from a process perspective. For the CaL process to be implemented at industrially relevant scales, also the mechanical stability of sorbent particles is important, and maintaining a high stability with cycling is currently an active area of sorbent research (Pi et al., 2019; Sun et al., 2019; Sun et al., 2015).

3.4.1.2. Effect of the gas composition. Unburnt fuel gases (e.g. CO, H_2, CH_4) hardly affect the rate of the carbonation or calcination reaction of CaO-based sorbents (Dunstan et al., 2021); under conditions that favour the reverse water-gas shift reaction, H_2 was observed to react with CO_2 released from the $CaCO_3$, thereby accelerating its decomposition. The presence of SO_2 and steam is more influential, and affects the sorbent behavior during both the carbonation and calcination reaction.

SO_2 forms $CaSO_4$ with CaO in the presence of oxygen, a reaction that has been utilized for high-temperature flue gas desulfurization (He et al., 2021). As the decomposition of $CaSO_4$ does not proceed rapidly below ~ 1200 °C (viz. at temperatures much higher than typical decomposition temperatures of $CaCO_3$) (Tian et al., 2008), the presence of SO_2 in a flue gas stream is problematic and with time reduces the amount of CaO that is available for CO_2 to form $CaCO_3$ (Grasa et al., 2008). The carbonation reaction is faster at typical carbonation conditions (15 vol.% CO_2, 550–700 °C) than the sulfation reaction, but sulfation rates increase with rising temperatures. The $CaSO_4$ product also has an approximately 25 % higher molar volume than $CaCO_3$, increasing the diffusional resistance for CO_2 further, which shifts the transition between the kinetically-controlled regime and the diffusion-controlled regime to lower CO_2 uptakes, and also negatively affects the CO_2 uptake in the diffusion-controlled regime (Borgwardt et al., 1987).

Contrarily, the presence of steam usually enhances both the rate and extent of CO_2 uptake, mainly in the diffusion-controlled regime (Arias et al., 2012; Dong et al., 2020; Li et al., 2016). It has been shown both experimentally and computationally that steam concentrations <1 vol.% are sufficient to achieve this effect. From a morphological point of view, the presence of steam has a positive effect on the surface area and pore volume for pores with diameters < 100 nm, enhancing the rate of carbonation (Dong et al., 2020; Wang et al., 2014). It has also been reported that the presence of steam lowers the driving forces ($p_{CO2} - p_{CO2,\,eq}$) for the carbonation reaction to commence at a fast rate (Blamey et al., 2015). Structurally, it has been proposed that the presence of steam may lead to the formation of $Ca(OH)_2$ as an intermediate product. However, bulk $Ca(OH)_2$ is not thermodynamically stable under typical carbonation conditions (600–700 °C).

3.4.1.3. CO_2 capture applications using CaO-based sorbents. CaO-based sorbents can be used for a range of applications involving CO_2 capture, and thus far, post-combustion CO_2 capture has most frequently been investigated. Different from MgO-based sorbents, relatively high CO_2 capture efficiencies can be realized with CaO-based sorbents even at low CO_2 partial pressures as in flue gases from combustion processes. Several pilot-scale reactor units, typically operated as interconnected fluidized bed reactors involving the transfer of CaO-based sorbents between them, have shown CO_2 capture efficiencies of 90 % or higher with steam present, close to the thermodynamic limit (Fig. 3.44i) (Dieter et al., 2013; Duelli et al., 2015; Hanak et al., 2015a). Large demonstration plants at the MW scale have demonstrated the feasibility of the CaL process for post-combustion CO_2 capture (Chang et al., 2014; Diego and Arias, 2020; Hilz et al., 2017; Ströhle et al., 2020), yet there are currently no industrial units in operation.

Closer to the industrial application may be CaO-based CO_2 capture processes that offer, besides the removal or the elimination of CO_2 emissions, additional economic value, e.g. hydrogen through sorption-enhanced reforming or water-gas shift reactions (Chirone et al., 2022; Di Giuliano and Gallucci, 2018; Harrison, 2008; Ma et al., 2021; Masoudi Soltani et al., 2021; Zhang et al., 2022; Zhu et al., 2020) or thermal energy (Arcenegui-Troya et al., 2020; Medina-Carrasco and Valverde, 2022; Perejón et al., 2016).

3.4.2. Challenges and emerging technologies: a life cycle thinking

Compared with other alternative technologies, calcium looping is expected to substitute amine looping in dealing with fuel gas with low CO_2 concentration ranging from 5–15 %. But successful installation and

operation of calcium looping should be relied on techno-economically competitiveness. High CO_2 concentration is obviously the main advantage for calcium looping. In addition, this CO_2 from post-combustion unit then only needs to be conditioned and dehydrated prior to compression, transport and commercial purposes. However, despite of the simple chemistry and efficient recycling involved in calcium looping, the following challenges are believed to hinder wider applications of such technology for CO_2 capture.

1) The net efficiency of tail-end configuration is reduced by integrating cryogenic air separation unit (Plaza et al., 2020; Yang et al., 2021).
2) The combustion temperature must be controlled to avoid hot spots in the combustion zone that would enhance NO_x production in the boiler (Chen et al., 2020; Hu et al., 2020).
3) Fast catalyst deactivation and poor reaction engineering technologies for optimum operations.

Those challenges could be addressed by applying advanced reaction technologies. However, those solutions should be proposed based on techno-economic thinking. (Colelli et al., 2022; Galusnyak et al., 2022; Kong et al., 2022; Moore et al., 2022) From a perspective of process development, the overall techno-economic advantages or disadvantages should be quantitatively assessed to evaluate the feasibility prior to practical implementation. The following aspects have been the main R&D focus in the past five years.

Emerging technologies from a life cycle assessment

(1) Combinatory processes with H_2 generation technologies

The combinatory technologies involving CO_2 capture and in-situ transformation could be a most promising solution to enhance environmental sustainability and technological viable. (Han et al., 2022; Hashemi et al., 2022; Li et al., 2022) Researchers have been proposing a variety of combinatory processes to integrate calcium looping with advanced H_2 generation techniques.

The commercial technologies based on the fuels reforming and gasification processes involve the production of syngas (H_2, CO, CO_2, and some CH_4 and hydrocarbons). (Han et al., 2022; Madejski et al., 2022; Yang et al., 2021) Downstream applications of molecular H_2 usually demand high purity with 99.99 % and CO-free composition. This purpose has been achieved through water gas shift reaction (WGS), where CO reacts with water vapour to produce additional H_2 and CO_2. However, this reaction (Reaction 3.12) is equilibrium-limited, but if CO_2 is continuously removed, the reaction will be shifted in favour of increased H_2 production.

$$CO(g) + H_2O(g) \leftrightarrow CO_2(g) + H_2(g)\ \Delta H_r^o = 41\ kJ/mol \quad (3.12)$$

Consequently, the syngas produced during the reforming or gasification (>600 °C) is upgraded in an independent WGS reactor (250–500 °C). The capture of CO_2 generated in-situ during the reforming and gasification processes, or syngas upgrade in a separate reactor, can favourably shift the thermodynamic equilibrium of the above-mentioned reactions toward a higher efficiency of H_2 production.

Another advanced energy efficient technique is called sorption-enhanced steam reforming. CaO is incorporated in this process in sorbents and immobilized with active metallic catalytic materials to enhance the overall the economics of CO_2 capture. Ni-based reforming catalysts, synergistically working with trance amounts of noble Rh, Pt, Pd and Ru have better performances in coke resistance for converting natural gas into highly purified molecular H_2. The flow scheme is present in Fig. 3.45, where reformer/shift reactors are working with calciner in a synchronizing fashion, coupled with pressure swing adsorption (PSA) for producing high quality H_2. Life cycle assessment has confirmed that, such novel combination could lower the H_2 production cost by 3–5 % comparatively with no capture conventional reforming (approximately $40/MWh capacity).

(2) Solar thermal calcium looping

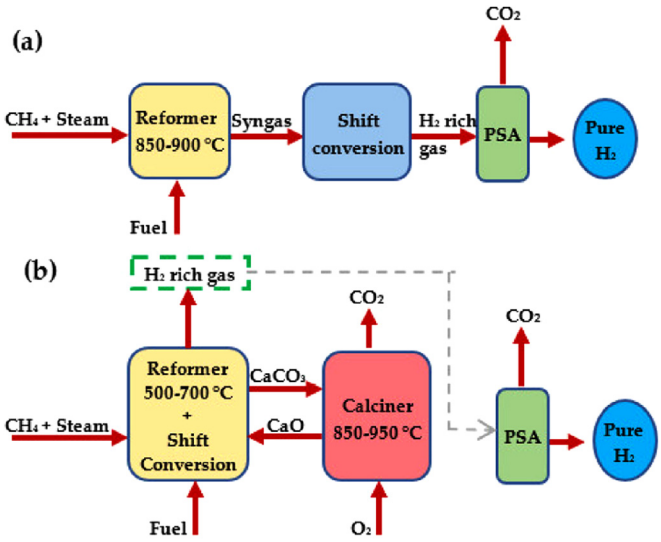

Fig. 3.45. Flow diagram of (a) steam methane reforming and (b) sorption-enhanced steam methane reforming ($CaCO_3$ as sorbent). (For interpretation of the references to color in this figure legend, the reader is referred to the web version of this article.)

Grey H_2 production from natural gas conversion, or dry reforming of CH_4 and CO_2 could enhance the overall sustainability of CO_2 capture processes. However, carbon footprint analysis shows that, using solar energy as primary source could potentially reduce process cost by almost 12–25 %, simply using solar heat as energy carrier. (Khosa et al., 2019; Salaudeen et al., 2018; Valverde, 2018)

An earlier version of solar thermal-assisted calcium looping has been involving compressed CO_2 and high-pressure air in carbonation stage. It assumed that CO_2 was completely converted in the carbonator, and then only high-temperature and high-pressure air was sent to the turbine to generate work. The power generation efficiency of the system was maximum, as high as 40–43 %. It is worth mentioning that the complete consumption of CO_2 in the carbonator is an ideal situation.

Heat storage would favour the efficiency enhancement for calcium looping. An indirect integration of the steam Rankine cycle in calcium looping can be optimized from both energy and economic aspects, which determined the size and operating conditions of the main components. A complete exergy analysis show that, exergy loss occurs in the solar receiver (about 37 %), the calcination section (26 %), and the steam Rankine cycle (about 21 %). (Erans et al., 2016; Perejon et al., 2016) In sharp contrast, the exergy loss that occurred in the carbonation section was relatively small, lower than 5 %. The improved solar thermal-assisted calcium looping (shown in Fig. 3.46) leads to a much higher process efficiency of 51 %. (Ortiz et al., 2019; Tregambi et al., 2021)

(3) Nanomaterials

The use of functionalized materials not only could reduce the carbon footprint by combining H_2 generation technologies with calcium looping, in addition, nanomaterials with high surface areas would significantly enhance heat transfer in carbonation and calcination, leading to lowered loss of exergy. Experimental studies have suggested that the coupling of a solid looping cycle, for example, Fe/FeO and Cu/CuO, can deliver the heat required in the calcination step in a faster way. The improvement is achieved by the exothermic oxidation of the Fe (Cu) to FeO (CuO) with air, which took place in the same fixed bed reactor as the calcination. (Santos and Hanak, 2022)

Nanostructured CaO and $CaCO_3$ materials could also slow sorbent and catalyst deactivation during high temperature looping. In earlier stages of looping operation, reactions occur in a kinetic controlled regime. In this stage, catalyst size is small thus reactions are consid-

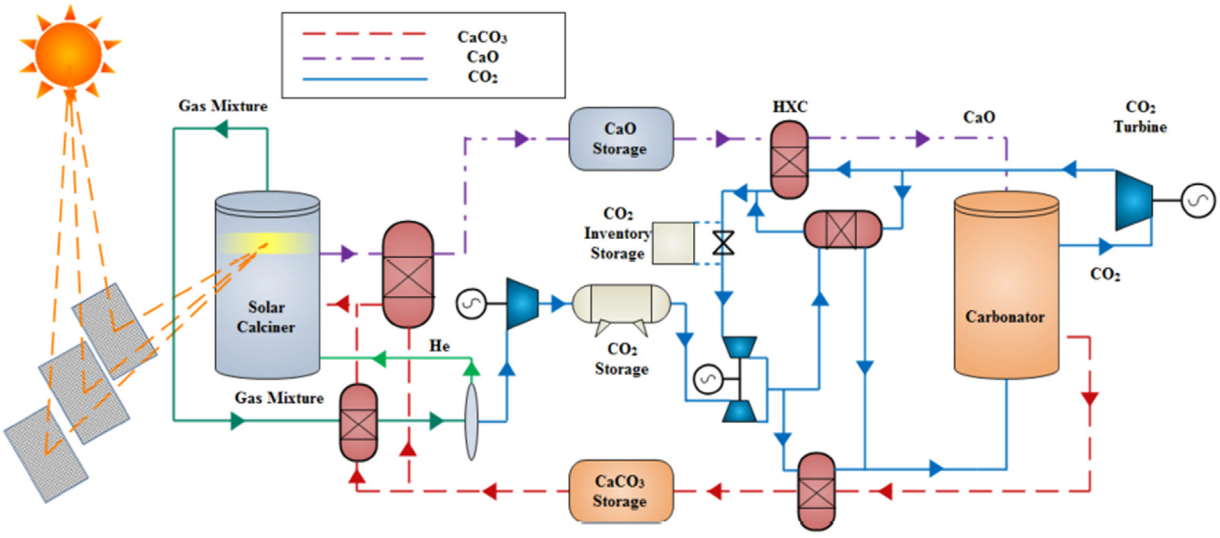

Fig. 3.46. Solar thermal calcium looping (Chacartegui et al., 2016). (For interpretation of the references to color in this figure legend, the reader is referred to the web version of this article.)

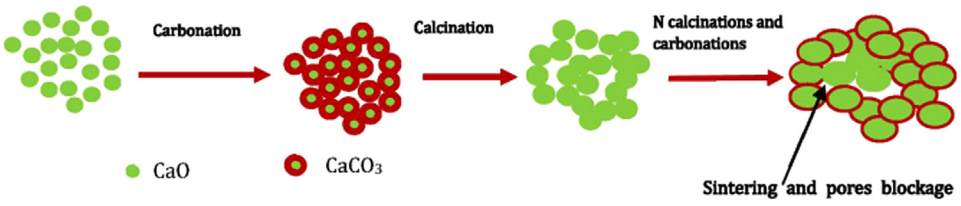

Fig. 3.47. Particle sintering during carbonation-calcination cycles (Teixeira et al., 2022). (For interpretation of the references to color in this figure legend, the reader is referred to the web version of this article.)

ered as rate limiting step. However, catalyst size has been enhanced significantly after several cycles, leading to poor surface area and loss of sorbent reactivity by particle sintering and pore blockage (Fig. 3.47).

Recent experimental studies have demonstrated the advantages of using nano-sized CaO and $CaCO_3$ materials in calcium looping. Unfortunately, no life cycle assessment has been conducted to quantitatively evaluate the environmental impact of preparation steps on the overall sustainability in calcium looping. (Li et al., 2022; Xu et al., 2021)

3.4.3. Li-, Na-, Sr-, and Ba-based sorbents

Unlike $MgCO_3$ and $CaCO_3$, other carbonates of alkali metal or alkaline earth metals, e.g., Li_2CO_3, Na_2CO_3, $SrCO_3$ and $BaCO_3$, are hard to decompose in practically achievable conditions, making them unsuitable for reversible CO_2 capture in their monometallic forms. To address this issue, transition metals and/or semi-metals are often incorporated into oxides of Li, Na, Sr and Ba to form ternary oxide sorbents. The incorporation of the transition metals modifies the basicity of the oxides, thus rendering their regenerability over CO_2 capture cycles. This section discusses some developments in Li, Na, Sr and Ba based CO_2 sorbents. Table 3.19 summarises the stoichiometric CO_2 capacities and experimental CO_2 uptakes of these sorbents.

3.4.3.1. Li-based sorbents.

3.4.3.1.1. Lithium silicates. Lithium silicates, including Li_4SiO_4 and Li_8SiO_6, are the most often studied lithium based sorbents. Li_4SiO_4 reacts with CO_2 between 450 and 700 °C with a stoichiometric CO_2 capacity of 36.7 wt.%:

$$Li_4SiO_4(s) + CO_2(g) \rightleftharpoons Li_2CO_3(s) + Li_2SiO_3(s) \quad (3.13)$$

The carbonation mechanism of these ternary oxides is different from simple oxides like CaO or MgO, because more than one solid phase will be produced. The two solid products, Li_2CO_3 and Li_2SiO_3, form an outer shell and an inner shell surrounding the unreacted Li_4SiO_4 core, respectively, generating a double-shell structure, as shown in 8 (Yang et al., 2016b).

The subsequent carbonation requires the transport of CO_2 through the Li_2CO_3 layer, and the migration of Li^+ and O_2^- ions out of the Li_2SiO_3 layer. As the shells grow thicker during carbonation, the diffusion resistances of both CO_2 and ions will increase, slowing down the carbonation. It is believed that the rate limiting step is the CO_2 gas diffusion through the Li_2CO_3 layer. Owing to these product layer diffusion resistances, the experimental CO_2 uptake capacity of Li_4SiO_4 is always lower than the stoichiometric value. Increasing the surface area of the chemically unmodified lithium silicates is one of the most effective means to enhance the CO_2 uptake performance of Li_4SiO_4.

Li_8SiO_6, as a CO_2 sorbent with higher Li contents than Li_4SiO_4, also has a higher theoretical CO_2 uptake of 98 wt.%. The process of Li_8SiO_6 carbonation consists of 3 steps (Cova et al., 2019). Steps 1 and 2 involve the CO_2 adsorption on the surface and in bulk:

$$Li_8SiO_6(s) + 2CO_2(g) \rightleftharpoons 2Li_2CO_3\ (s) + Li_4SiO_4\ (s) \quad (3.14)$$

Step 3 involves the reaction between CO_2 and the formed Li_4SiO_4:

$$Li_4SiO_4(s) + CO_2(g) \rightleftharpoons Li_2CO_3(s) + Li_2SiO_3(s) \quad (3.15)$$

Lithium silicates can be synthesised by mechanically mixing solid particles of lithium and silicon precursors at stoichiometric ratios, followed by drying and calcination. Commonly used lithium precursors include Li_2CO_3 (Chen, X. et al., 2016; Wang, Haiyang et al., 2018), Li_2O (Lara-García et al., 2019), and $LiNO_3$ (Wang, K. et al., 2019), while the silicon precursor is almost always SiO_2. However, the lithium silicates obtained by solid-state reactions typically have low surface areas (<1 m^2/g) and low experimental CO_2 uptakes (28–35 wt.% for Li_4SiO_4 (Chen, X. et al., 2016; Wang, Haiyang et al., 2018) and 42 wt.% for Li_8SiO_6) (Cova et al., 2019). Additionally, the poor sintering resistance of the Li_2SiO_3 results in a rapid decrease in CO_2 capture capacity over carbonation cycles (Chen, X. et al., 2016; Yang et al., 2016b).

Table 3.19
Stoichiometric CO_2 capacities and experimental CO_2 uptakes of Li, Na, Sr and Ba based sorbents.

Sorbent	Stoichiometric CO_2 capacity [wt.%]	Experimental CO_2 uptake [wt.%]	Carbonation Temperature [°C]	Calcination Temperature [°C]	Carbonation CO_2 partial pressure [bar]	Calcination CO_2 partial pressure [bar]	Max No. of Cycles	Ref
Li_4SiO_4	36.7	1.8-36.0	RT-700*	550-900	0.04-1.0	0	250	(Chen et al., 2016; Lara-García et al., 2019; Seggiani et al., 2018; yang et al., 2018; Wang et al., 2019; Yang et al., 2016a, b)
Li_8SiO_6	98.0	0-42.0	25-776*	-	1.5	-	-	(Cova et al., 2019)
Li_2ZrO_3	28.7	0.01-23.0	500-575	600-700	0.10-2.0	0-0.585	30	(Gómez-Garduño and Pfeiffer, 2019; Peltzer et al., 2019; Peltzer et al., 2018)
Li_6WO_6	41.1	3.6-25.9	30-710*	730-760	0.60	0	4	(Gaultois et al., 2018)
Li_6CoO_4	80.0	5.0-76.4	300-700	700-750	0.20-1.0	0	10	(Bernabé-Pablo et al., 2020)
Li_3BO_3	69.1	0-47.2	500-650	650	0.20-1.0	0	10	(Harada and Hatton, 2017)
Li_2CuO_2	40.2	3.6-37.4	30-750*	750-850	1.0-5.0	0	-	(Martínez-Cruz et al., 2020; Yañez-Aulestia et al., 2020)
Li_5FeO_4	71.2	0-62.0	30-700*	-	1.0	-	-	(Blanco et al., 2018)
Li_4TiO_4	47.3	0-42.0	300-856	-	1.0	-	-	(Togashi et al., 2007)
Na_4SiO_4	23.9	7.7-19.2	50-840*	-	0.80	-	-	(Liu et al., 2019)
Na_2ZrO_3	23.8	4.5-23.8	150-800	680-900	0.025-1.0	0	70	(Ji et al., 2017; Martínez-dlCruz and Pfeiffer, 2012; Munro et al., 2020; Zhao et al., 2007)
$NaCoO_2$	15.0	3.3-11.1	100-800	-	0.050-1.0	-	-	(Vera et al., 2019)
SrO	42.5	3.0-37.1	1100-1200	1100-1200	0.30-0.50	0	10	(Miccio et al., 2016)
$La_{0.1}Sr_{0.9}Co_{0.5}Fe_{0.5}O_{3-\delta}$	20.7	0-17.3	600-800	-	0.10-1.0	-	-	(Yang and Lin, 2006)
$Sr_xCa_{1-x}Fe_{0.5}Co_{0.5}O_{3-\delta}$	15.1	0.4-17.0	RT-950*	-	1.0	-	-	(Homonnay et al., 2002; Juhasz et al., 2001; Nomura et al., 1996)
$SrCo_{1-2x}$ $(Fe,Nb)_xO_{3-\delta}$	11.6	0-13.1	925	-	0.75	-	-	(Lu et al., 2011)
$Li_2SrTa_2O_7$	5.1	0-4.9	140	700	-	-	6	(Galven et al., 2010)
$Ba_{0.95}Ca_{0.05}Co_{1-x}Fe_xO_{3-\delta}$	9.3	2.8-12.0	850	-	0.10	-	-	(Nomura et al., 1996)
$Ba_{0.5}Sr_{0.5}Co_{0.8}Fe_{0.2}O_{3-\delta}$	10.1	0-14.9	RT-950*	-	1.0	-	-	(Lu et al., 2011)
$Ba_2Fe_2O_5$	9.4	0-9.4	1000	1000	1.0	0	-	(Fujishiro et al., 2011; Yi et al., 2013)
$BaCe_{0.9}Y_{0.1}O_{2.95}$	13.8	0-13.1	600-1000	-	1.0	-	-	(Sneha and Thangadurai, 2007)
$Ba_4Sb_2O_9$	14.1	9.5-14.0	650-750	950	0.42	1	100	(Dunstan et al., 2013)

* indicates temperature programmed CO_2 capture experiments in a TGA.

To overcome the product layer diffusion resistances during carbonation, wet chemistry methods (e.g., impregnation suspension) are applied to synthesise Li_4SiO_4 with high surface areas (Yang et al., 2016a, b). With improved specific surface areas (1.65-2.09 m^2/g), Li_4SiO_4 prepared by impregnation suspension afforded higher CO_2 uptake (up to 37 wt.%) and better cyclability (over 40 cycles) than those prepared by solid-state reactions (Yang et al., 2016b).

The CO_2 capture performance of Li_4SiO_4 can also be improved by metal doping. Low melting-point dopants, e.g. Na_2CO_3, K_2CO_3, $NaNO_3$ and KNO_3, can accelerate the migration of CO_2 through the Li_2CO_3 product layer (Seggiani et al., 2018; Wang, K. et al., 2019; Yang et al., 2016a). Alternatively, redox-active dopants, such as salts containing Fe^{3+}, are able to promote the transport of O^{2-} through the Li_2SiO_3 shell (Lara-García et al., 2019). Some practical methods to introduce the dopants into Li_4SiO_4 sorbents include adding dopant precursors during the solid-state reactions (Chen, X. et al., 2016; Wang, Haiyang et al., 2018), impregnating the solid-state synthesised Li_4SiO_4 with soluble dopants, and conducting further solid-state synthesis between Li_4SiO_4 particles and the dopant precursors (Lara-García et al., 2019). Wang et al. (2018) chose acid-leached blast furnace slag, which contains TiO_2, Fe_2O_3, Al_2O_3, CaO and K_2O, as an economic and sustainable alternative for silicon precursor of Li_4SiO_4 (Wang, Haiyang et al., 2018). In many cases, doped Li_4SiO_4 showed many improvements, including higher specific surface area, enhanced CO_2 uptake (up to 35 wt.%) (Chen et al., 2016), improved cyclic stability (for up to 250 cycles) (Seggiani et al., 2018) and faster carbonation rate at lower temperatures and/or in lower CO_2 concentrations (Lara-García et al., 2019).

3.4.3.1.2. Other Li-based sorbents. Lithium zirconate (Li_2ZrO_3) is the second most studied Li based sorbent. It has a stoichiometric CO_2 capacity of 28.7 wt.% when used within a temperature range of 450–650 °C:

$$Li_2ZrO_3(s) + CO_2(g) \rightleftharpoons Li_2CO_3(s) + ZrO_2\ (s) \quad (3.16)$$

Like lithium silicates, the carbonated Li_2ZrO_3 also exhibit a double-shell structure, with ZrO_2 and Li_2CO_3 forming the inner layer and the outer layer, respectively. Similarly, the CO_2 diffusion through the Li_2CO_3 layer is believed to be rate limiting. Li_2ZrO_3 can be prepared by a solid-state reaction between Li_2CO_3 and ZrO_2. However, solid-state synthesised Li_2ZrO_3 shows relatively slow carbonation and low capacities (5.9 - 10 wt.%) (Gómez-Garduño and Pfeiffer, 2019; Peltzer et al., 2018). Likewise, metal doping methods e.g. (i) doping low-melting point salts (Peltzer et al., 2018) (ii) doping redox-active Fe^{3+} chemicals (Gómez-Garduño and Pfeiffer, 2019), and (iii) impregnation suspension method (Peltzer et al., 2019) have been adopted to improve the performance of Li_2ZrO_3 sorbents. Both (i) and (iii) could effectively improve CO_2 uptake (20 - 22 wt.%), whereas the Fe-doping method gives marginal enhancements (7.0 - 9.2 wt.%).

Other Li-based ternary oxide phases have also been studied for CO_2 capture (Bernabé-Pablo et al., 2020; Blanco et al., 2018; Gaultois et al., 2018; Martínez-Cruz et al., 2020; Togashi et al., 2007; Yañez-Aulestia et al., 2020). Among these ternary oxides, Li_6CoO_4 shows the highest stoichiometric CO_2 capacity and experimental uptake of 80.0 and 74.5 wt.%, respectively (Bernabé-Pablo et al., 2020). Li_6CoO_4 reacts with CO_2 according to:

$$Li_6CoO_4(s) + 3CO_2(g) \rightleftharpoons 3Li_2CO_3(s) + CoO\ (s) \quad (3.17)$$

However, the CO_2 capture uptake of Li_6CoO_4 decreases quickly over cycles in the presence of O_2, reaching 30.5 wt.% after 10 cycles. This deterioration is attributed to the irreversible oxidation of Co^{2+} to Co^{3+} (Bernabé-Pablo et al., 2020). In contrast, for Li_5FeO_4, O_2 appears to accelerate the ion diffusion through the $LiFeO_2$ layer, improving its CO_2

capture performance (Lara-García et al., 2019). Similar to lithium silicates and lithium zirconates, doping is an effective strategy to enhance the CO_2 capture performance of lithium-transition metal oxides. Several dopants, including second transition metal salts (e.g. Mn, Fe or Ni) (Martínez-Cruz et al., 2020) or alkali metal nitrates (MNO_3, M = Li, Na, K) (Yañez-Aulestia et al., 2020), were found to increase the CO_2 uptake and cyclic stability of Li_2CuO_2. Recently, Li_6WO_6 nanowires were developed and showed the capability to capture CO_2 at ambient temperatures in the presence of moisture, owing to the hydration and activation of Li_6WO_6, which promoted the carbonation kinetics. At 30 °C and with a relative humidity = 58 ± 3 %, Li_6WO_6 was able to achieve a CO_2 uptake of 7.6 wt.% within 1 min (Bernabé-Pablo et al., 2020).

$$4Li_3BO_3 + 3CO_2 \rightleftharpoons 3Li_2CO_3 + Li_6B_4O_9 \quad (3.18)$$

Lastly, Li_3BO_3, with a stoichiometric CO_2 uptake capacity of Li_3BO_3 of 41.4 wt.% has shown an experimental CO_2 uptake of 35.4 wt.% (Harada and Hatton, 2017), through Reaction 3.17. However, the cyclic stability of Li_3BO_3 is inferior. Doping with $NaNO_2$ or KNO_2, which facilitates the formation of a molten layer, could accelerate product layer diffusion and the carbonation of Li_3BO_3. Interestingly, adding 10 mol % (Na-K)NO_2 achieved an experimental uptake of 47.2 wt.%, exceeding the stoichiometric capacity. The enhanced CO_2 uptake may have originated from the deeper carbonation, which was induced by the incorporation of alkali metal nitrites. Accordingly, Reactions 3.18 and 3.19 corresponds to improved stoichiometric uptake capacities of 69.1 and 55.4 wt.%, respectively.

$$4Li_3BO_3 + 5CO_2 \rightleftharpoons 5Li_2CO_3 + Li_2B_4O_7 \quad (3.19)$$

$$Li_3BO_3 + CO_2 \rightleftharpoons Li_2CO_3 + LiBO_2 \quad (3.20)$$

3.4.3.2. Na-based sorbents. Na-based sorbents share similar chemical formulae with Li based ones. On one hand, Na-based sorbents are cheaper as Na is more earth abundant. On the other hand, Na based sorbents generally have lower stoichiometric CO_2 capacities than the Li equivalents in terms of weight percentage because Na is a heavier element. Experimentally, Na_4SiO_4, Na_2ZrO_3 and other Na based ternary oxides have shown promising CO_2 capture performance up to 850 °C:

$$Na_4SiO_4 + CO_2 \rightleftharpoons Na_2CO_3 + Na_2SiO_3 \quad (3.21)$$

$$Na_2ZrO_3 + CO_2 \rightleftharpoons Na_2CO_3 + ZrO_2 \quad (3.22)$$

Similarly, Na based sorbents can be obtained by either solid-state reactions or wet-chemistry methods, e.g., sol-gel synthesis (Ji et al., 2017; Zhao et al., 2007), using several combinations of precursors, e.g. Na_2SiO_3 + NaOH (Liu et al., 2019), $Na_2CO_3 + ZrO_2$ (Martínez-dlCruz and Pfeiffer, 2012), and $Na_2CO_3 + CoCO_3$ (Vera et al., 2019). Na_4SiO_4 has a stoichiometric capacity of 23.9 wt.%, an experimental uptake of 19.2 wt.% at 840 °C, and a generally good performance above 750 °C (Liu et al., 2019). To improve the capture performance of Na_4SiO_4 at lower temperatures (< 700 °C), modification with alkali carbonates (M_2CO_3, M = Li, Na, K) could be a good choice, because the molten can accelerate the diffusion of O_2^- through the product layer (Liu et al., 2019). In particular, K_2CO_3-doped Na_4SiO_4 has shown a CO_2 uptake of 4.7 wt.% at 300 °C, doubling that of undoped Na_4SiO_4.

Unlike the silicates, the gas permeability through the product layer during the carbonation of Na_2ZrO_3 is higher. Therefore, the Na_2ZrO_3 sorbents do not appear to encounter serious product layer diffusion resistance, as shown in Fig. 3.48 (a) and (b). Ji et al. prepared Na_2ZrO_3 by a sol-gel method, and achieved an experimental uptake of 22.6 wt.%, (stoichiometric uptake = 23.8 wt.%), which lasted over 5 cycles (Ji et al., 2017). The authors attributed the high performance of Na_2ZrO_3 to the partly sintered product layer, which could form channels to facilitate fast sodium diffusion, as illustrated in Fig. 3.49c. For $NaCoO_2$, partially doping the Co sites with Fe could increase the CO_2 capture performance by enhancing the redox activity and ionic conductivity of the sorbent. For instance, $NaCo_{0.7}Fe_{0.3}O_2$ showed increased uptake of 10.6 wt.% in 20 % CO_2 at 700 °C, while undoped $NaCoO_2$ could only achieve 3.3 wt.% (Vera et al., 2019). (Fig. 3.49)

3.4.3.3. Sr-based sorbents. SrO itself can be directly used as a CO_2 sorbent, functioning at temperatures > 1000 °C. Miccio et al. (2016) synthesised coarse SrO particles by calcining $SrCO_3$ and fine SrO particles by wet-granulation method (Fig. 3.50). Both SrO sorbents showed relatively high initial CO_2 uptakes of 37.1 and 30.5 wt.%, respectively. On the other hand, the capture capacities dramatically dropped after 5 cycles due to severe sintering. To increase the cyclic durability, it could be helpful to load SrO onto Al_2O_3 to form the thermally stable $Sr_3Al_2O_6$ and/or $SrAl_2O_4$ sorbents.

In fact, Sr-containing CO_2 sorbents are more often perovskite structured, where Sr occupies the A sites in the ABO_3 lattice. The CO_2 capture performance of the perovskites are greatly affected by both A and B site metals, which can be adjusted by changing the compositions of precursors during the sol-gel synthesis (Yang and Lin, 2006). For example, $La_{0.1}Sr_{0.9}Co_{0.5}Fe_{0.5}O_{3-\delta}$ is able to adsorb more CO_2 (17.3 wt.%) than $Sr_{0.95}Ca_{0.05}Fe_{0.5}Co_{0.5}O_{3-\delta}$ (4.37 - 8 wt.%) (Homonnay et al., 2002; Juhasz et al., 2001). Further changing Sr:Ca ratio to $Sr_{0.5}Ca_{0.5}Fe_{0.5}Co_{0.5}O_{3-\delta}$ could improve the uptake to 17 wt.% (Juhasz et al., 2001), owing to the formation of more ordered oxygen vacancies, which is considered to be helpful for CO_2 uptake (Homonnay et al., 2002; Nomura et al., 1996):

$$2(Sr,\ Ca)(Fe,\ Co)O_{2.5} + CO_2 \rightleftharpoons (Sr,\ Ca)CO_3 + (Sr,\ Ca)(Fe,\ Co)_2O_4 \quad (3.23)$$

Lu et al. (2011) studied the effects of B-site occupancies for Sr based, perovskite structures. They prepared $SrCo_{1-2x}(Fe,Nb)_xO_{3-\delta}$ with equimolar Fe and Nb. The fresh $SrCo_{1-2x}(Fe,Nb)_xO_{3-\delta}$ sorbents had CO_2 uptake of 13.1 wt.% and 11.1 wt.%, when $x = 0.05$ and 0.10 respectively. The increased Nb occupancy of the B sites would reduce the carbonation activity due the weakened basicity of the perovskite (Yi et al., 2010). Besides the perovskite-structured Sr-based sorbents, a $Li_2SrTa_2O_7$ sorbent having a Ruddlesden–Popper (RP) phase ($A'_2[A_{n-1}B_nO_{3n+1}]$) was reported by Galven et al. (2010) to achieve 4.90 wt.% experimental uptake (with a stoichiometric capacity of 5.11 wt.%) at 140 °C, 30 bar. Additionally, the $Li_2SrTa_2O_7$ sorbent exhibited good cyclability after 5 carbonation-regeneration cycles.

$$Li_2SrTa_2O_7 + 0.5CO_2 + 0.5H_2O \rightleftharpoons LiHSrTa_2 + 0.5Li_2CO_3 \quad (3.24)$$

3.4.3.4. Ba-based sorbents. Similar to Sr based sorbents, most Ba based sorbents are perovskite-structured oxides with Ba occupying the A sites. These sorbents can be prepared by either state reactions (Sneha and Thangadurai, 2007) or sol-gel synthesis (Nomura et al., 1996). The capture performance of the Ba based perovskites also depends on the metal site occupancies. For example, Nomura et al. (1996) discovered that if the Fe contents in $(Ba_{0.95}Ca_{0.05})(Co_{1-x}Fe_x)O_{3-\delta}$ is increased from 0.2 to 0.9, the CO_2 uptake will drop from 10.0 wt.% to 8.7 wt.%. The $BaFeO_{3-\delta}$ ($0 < \delta < 0.5$) structures could switch phases between perovskite (ABO_3) and brownmillerite ($A_2B_2O_5$), representing oxygen uptake and release. It is believed that these phase changes are beneficial to the CO_2 capture performance. For instance, the thermal decomposition of perovskite structured $Ba_{0.95}Ca_{0.05}Co_{0.8}Fe_{0.2}O_{3-\delta}$ to brownmillerite in the absence of O_2 would improve CO_2 uptake of 12 wt.%; this phenomenon is in line with the findings of Lu et al. (2011) and Fujishiro et al. (2011) Like Sr based perovskites, doping B-sites with Nb will hinder the carbonation of Ba based perovskites as well. Yi et al. (2013) reported low CO_2 uptake (0 – 1.3 wt.%) of the Nb-doped $BaFeO_{3-\delta}$. It is possible that the reduced performance may be related to the electron-donating behaviour of Nb dopant, which makes the perovskite sorbents more thermodynamically inert towards CO_2.

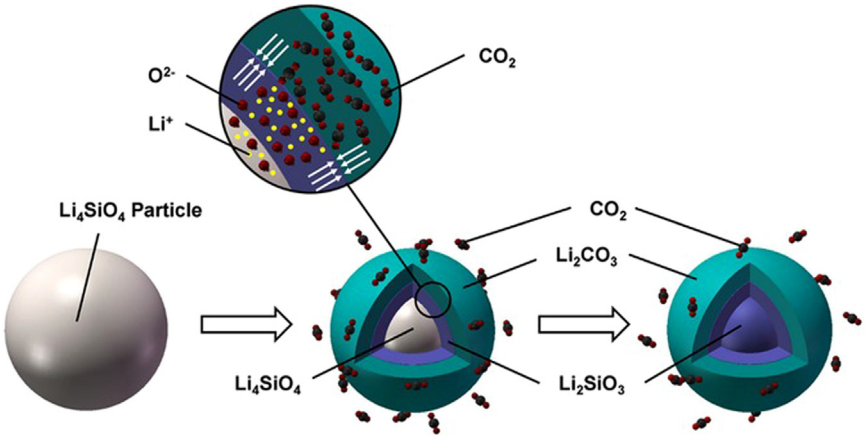

Fig. 3.48. Schematic illustration of the "double shell" model describing Li_4SiO_4 carbonation. Reprinted with permission (Yang et al., 2016b). (For interpretation of the references to color in this figure legend, the reader is referred to the web version of this article.)

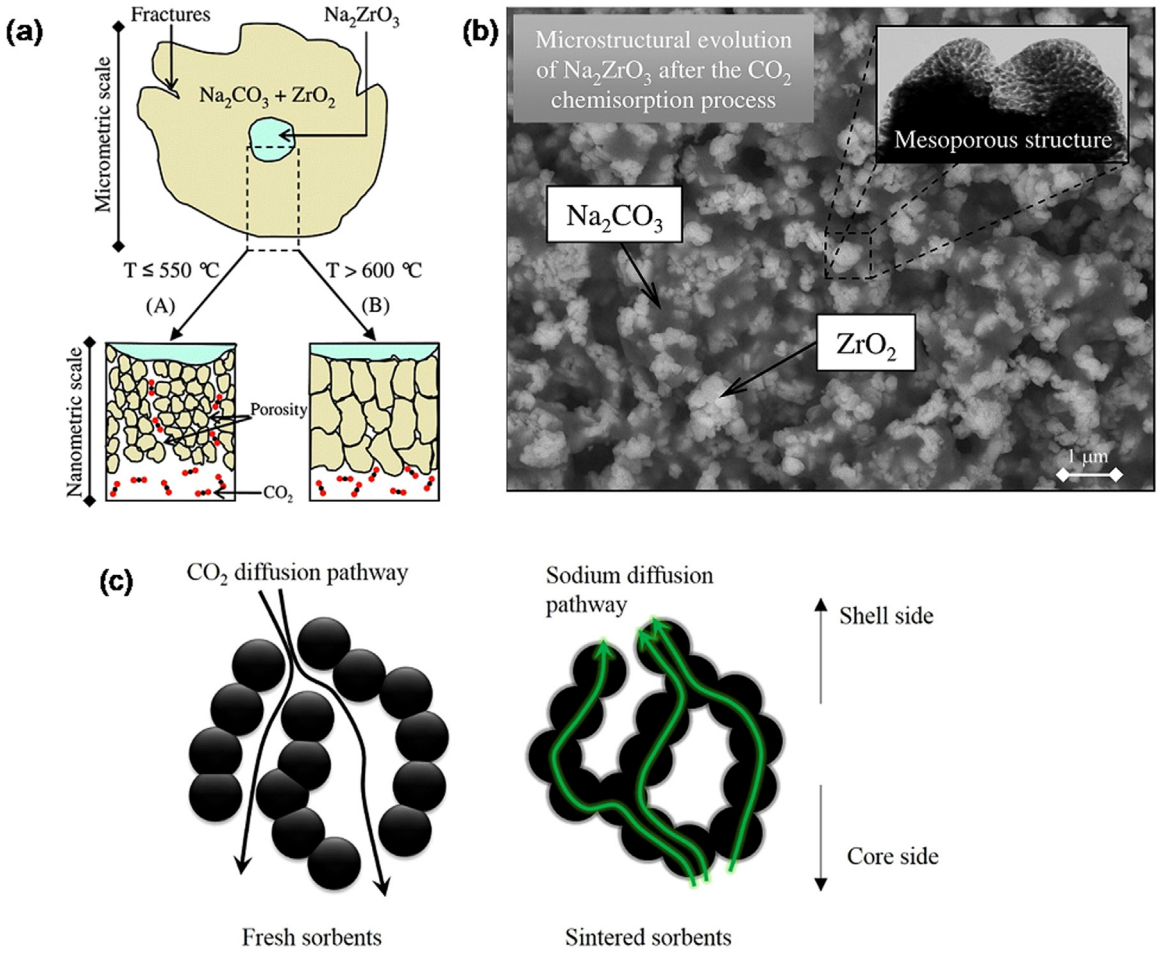

Fig. 3.49. (a) Scheme of the carbonation of Na_2ZrO_3 at different temperatures. Reprinted with permission (Martínez-dlCruz and Pfeiffer, 2012) (b) SEM image of growth of ZrO_2 and Na_2CO_3 after the carbonation of Na_2ZrO_3. Reprinted with permission (Martínez-dlCruz and Pfeiffer, 2012) (c) Scheme of the CO_2 and Na^+ diffusion in fresh and sintered Na_2ZrO_3 sorbents. Reprinted with permission (Ji et al., 2017). (For interpretation of the references to color in this figure legend, the reader is referred to the web version of this article.)

The most outstanding Ba based sorbent so far is probably be the 6H-perovskite $Ba_4Sb_2O_9$ reported by Dunstan et al. (2013) $Ba_4Sb_2O_9$ has a stoichiometric capacity of 14.1 wt.%:

$$Ba_4Sb_2O_9 + 3CO_2 \rightleftharpoons BaSb_2O_6 + 3BaCO_3 \quad (3.25)$$

Experimentally, a near-stoichiometric CO_2 uptake of 13.8 wt.% was achieved at 750 °C. During cyclic carbonation-regeneration, $Ba_4Sb_2O_9$ exhibited >10 wt.% CO_2 uptake over 100 cycles (Fig. 3.51a). The excellent cyclic stability of $Ba_4Sb_2O_9$ was attributed to its outstanding regenerability: its pore structure could be fully recovered after calcination in each cycle (Fig. 3.51b). The authors also discovered that $Ba_4Nb_{2-x}Ta_xO_9$

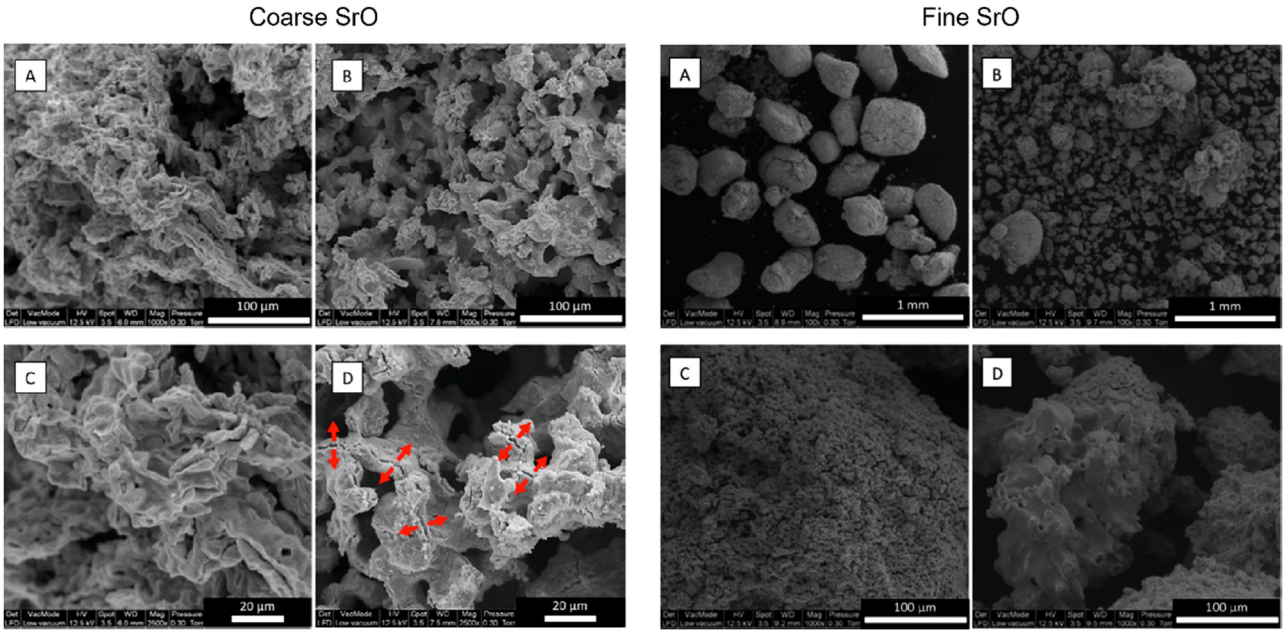

Fig. 3.50. SEM images of coarse and fine SrO particles before (A & C) and after (B & D) five cycles of carbonation–calcination at 1100 °C. Reprinted with permission (Miccio et al., 2016). (For interpretation of the references to color in this figure legend, the reader is referred to the web version of this article.)

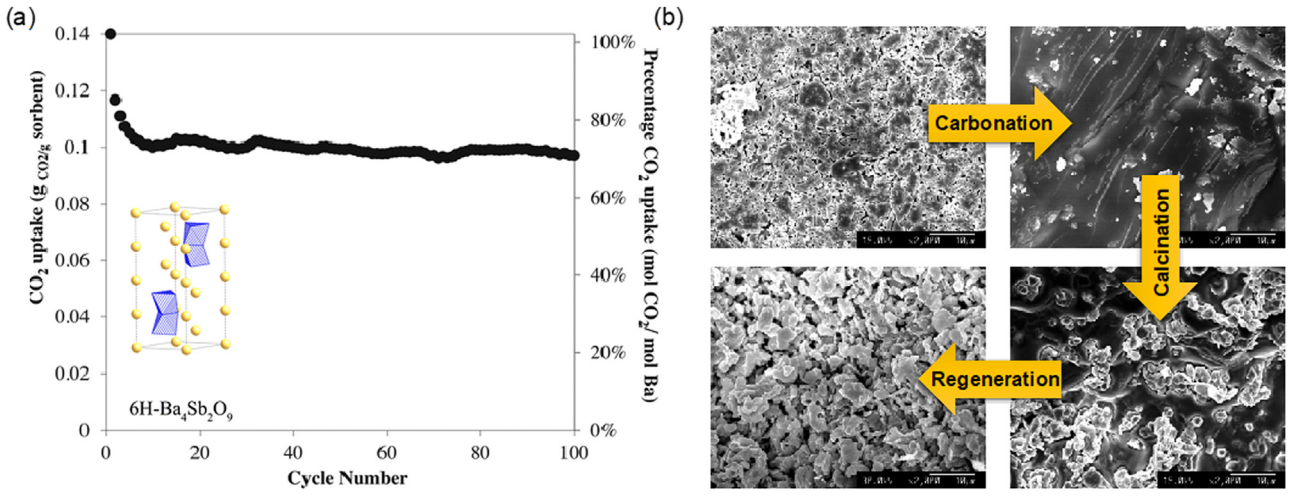

Fig. 3.51. (a) CO_2 uptake by 6H perovskite $Ba_4Sb_2O_9$ over 100 carbonation-calcination cycles in at TGA. (b) surface morphology $Ba_4Sb_2O_9$ as it evolves over carbonation-calcination cycles. Reprinted with permission (Dunstan et al., 2013). (For interpretation of the references to color in this figure legend, the reader is referred to the web version of this article.)

is a poor CO_2 sorbent, with only <0.07 wt.% in 100 % CO_2 at 1000 °C (Dunstan et al., 2011).

4. Membrane based CO_2 capture

4.1. Polymeric membranes

4.1.1. Introduction for polymeric membranes CO_2 capture

Membrane technology (a thin interface that acts as a permselective for two-phase separation, typically in a range of 100 nm to a few micrometers) has emerged as one of the promising alternative technologies in CO_2 capture compared to the conventional gas-liquid contractors, due to their inherent attribution such as smaller footprint, simpler setup, and operation, energy-saving and do not involve in phase transformation (Fujikawa et al., 2020; Ramasubramanian et al., 2013). But still, the highly permeable membrane is a big challenge for efficient CO_2 capture. Thanks to the unique architectural properties of polymeric chemistry, it has great potential to design a versatile membrane with outstanding properties for gas separation, especially for CO_2 capture (Robeson et al., 2009; Wang et al., 2016). Polymeric membrane technology has been used widely for CO_2 capture and is considered a next-generation technology for CO_2 capture due to its inherent properties such as cost-effectiveness, efficiency, separation performance, mechanical stability, and applicability for large scale-manufacturing (Feron and Jansen, 2002). Over the past decade, an extensive research quest has been devoted to the polymeric membrane with unprecedented transport properties for CO_2 capture from post-combustion (CO_2/N_2), syngas processing (CO_2/H_2), and natural gas sweetening (CO_2/CH_4).

One of the major challenges associated with the commercialization of membrane technology is the permeability and selectivity trade-off, i.e., high permeability is achieved always at the cost of lower selectivity and vice versa, for a specific component of the mixture. Robeson's proposed the empirical upper bounds limit in 1991 and updated the upper bounds in 2008 to explain such a limiting behavior (Robeson, 1991;

Table 4.1
Physical properties of CO_2, N_2, and CH_4

Gas	Kinetic diameter/nm	Critical temperature/K
CO_2	0.330	304.1
N_2	0.364	126.2
CH_4	0.380	190.6

Robeson, 2008). The paradigm shift is desirable in developing a new polymer-based membrane to outreach the Robeson's upper bounds limit along with long-term stability to be able to mitigate a massive volume of CO_2 emission.

In this section, we will review the recent efforts of the membrane's main research theme to surpass Robeson's upper bond limit focusing on polymeric materials. The unique structural properties of polymeric materials exhibit high permeability of CO_2 with sufficient selectivity. We categorized polymeric-based membranes into two categories based on the transport mechanism, 1) solution-diffusion membranes, including polyethylene oxide (PEO) (copolymer membranes, blend membranes, crosslinking membranes), perfluoro polymers, polymers of intrinsic microporosity, thermally rearrange polymers; and 2) facilitated transport membranes, including Amin based membranes, RTIL and other carriers for facilitated transport membranes.

4.1.2. Solution - diffusion transport mechanism

The driving force in membrane separation is pressure or concentration gradient. Firstly, the gas molecules dissolve in the dense polymeric membrane at the higher-pressure side for non-reactive polymer, then diffuse across the membrane and desorb at the lower-pressure side. This simple approach to gas transportation is known as the solution diffusion transport mechanism. This mechanism can be expressed as a product of the solubility coefficient (S_x) and diffusion coefficient (D_x) term as permeability coefficient (P_x) (Doong et al., 1995).

$$P_x = S_x \times D_x \tag{4.1}$$

The permeability is commonly expressed in terms of Barrer, whereas 1 Barrer = 1 Barrer = 1×10^{-10} cm^3 $(_{STP)}cm{\cdot}cm^{-2}\cdot s^{-1}\cdot$ (cm Hg) $^{-1}$. The permeability is an inherent property of polymeric materials, as solubility is the thermodynamic affinity of materials toward gas and diffusivity is dependent upon the morphology of the material and the size of gas molecules. The separation performance of the membrane can be expressed in terms of the permeability of the membrane divided by the thickness of the membrane.

The separation efficiency of the membrane is described by selectivity. The selectivity of the membrane is termed as the ability of a membrane to separate one component from another component of the mixture. The ideal selectivity is the ratio of two gas (x, y) permeability as shown in the equation below, which can further be extended in terms of solubility selectivity and diffusivity selectivity as:

$$\alpha x_{/y} = \frac{S_x}{S_y} \times \frac{D_x}{D_y} \tag{4.2}$$

The perm selectivity is deeply rooted in the solubility or diffusivity of gas molecules into the polymeric membrane. The solubility selectivity is enthalpy driven, dependent upon the condensability (increase with the increasing critical temperature) of penetrant gas molecules in the polymer and the affinity of penetrant gas toward the polymeric membrane (Frisch, 1970; Zydney, 1995). The solubility of CO_2 is higher as compared to other gases due to its significantly high critical temperature, $T_{c,\ CO2} = 304.1$ K shown in Table 4.1 (*Bondar et al., 2000*). The diffusivity selectivity kinetic diameter of penetrant gas molecules is dependent, and the gas molecules migrate through the free voids of polymer, which is the inherent characteristic of the polymer. The diffusivity selectivity of CO_2 is also higher as compared to other gases due to its smallest kinetic diameter, $d_k = 0.330$ nm. The less packing density and chain to chain spacing allows penetrant molecules to diffuse. Typically, the diffusivity increases with the decreasing in the kinetic diameter of gas molecules as well as increasing in free voids.

The fractional free volume (FFV) plays a vital role in the gas transport phenomenon in glassy polymeric membranes. Free volume is obtained during the condensation, as the less packing density leads to a more void not occupied by the polymer chain. Contrary to glassy polymer in rubbery polymer, solubility selectivity is more favourable (Lee, 1980). But the aging and plasticization of the membrane limit the fractional free volume and decrease the performance of the membrane (Du et al., 2011). It is required to mitigate such a challenge to fabricate an efficient and long-term durable membrane to move forward toward commercial applications.

4.1.2.1. PEO based polymeric membrane. Poly (ethylene oxide) (PEO) containing polymers have been extensively studied and shown a great potential to capture CO_2 due to their outstanding affinity toward CO_2 attributed to its dipole- quadrupole interaction between ethylene oxide (EO) group and CO_2 (Rindfleisch et al., 1996). Due to the inherent property of polar ether linkage (-c-c-o-) in PEO (rubbery polymer), it has a reasonable separation performance of CO_2 from other light gases. However, the limitation of PEO is its tendency toward crystallinity and film-forming ability due to its polar oxygen atoms, which are prone to reduce the free volume leading to the poor separation performance of CO_2, poor mechanical strength, and ultimately hampering their commercial applications (Sangroniz et al., 2021). Therefore the current effort of the researchers is to overcome the crystallinity constrain by cross-linking to form a highly branched polymeric network, copolymerization with the hard segment, and blending with the low MW polymer PEG, to enhance the separation performance as well as the thermal stability of the PEO based membrane. The PEO based membranes have been widely investigated via different synthesis approaches and some examples are summarized in Table 4.2.

PEO based copolymeric membrane. To overcome the limitation of crystallinity in the PEO based membrane is the copolymerization approach with the different rigid segments (Han and Ho, 2018). The transport properties of these membranes are controlled by altering the PEO phase and the unit length of soft and rigid segments (Yave et al., 2010). Luo et al. investigated the copolymer membranes of commercial polyether amines, pentiptycene-based diamine, and 6FDA, which exhibited high CO_2 gas permeability of 39 Barrer with CO_2/H_2 selectivity of 4.1 and CO_2/N_2 of 46 (Luo et al., 2016). The supramolecular chain threading and interlocking induced by the pentipytcene structures, effectively minimize the inherent crystallization ability of PEO, leading to an amorphous structure. Jankowski et al. synthesized a series of PEO based copolyimides with varying hard segment structures and found OPDA-ODA-PEO is the best copolyimide, with CO_2 permeability of 52 Barrer with CO_2/N_2 selectivity of 63 (Jankowski et al., 2021). A CO_2 selective copolymer based on aromatic poly ethers tethered with flexible PEO side chains was synthesized via polycondensation by Loannidi et al. showing maximum CO_2 permeability of 11.2 Barrer along with CO_2/H_2 and CO_2/CH_4 ideal selectivity of 9.6 and 68 respectively surpassing the upper bond limit for H_2 (Ioannidi et al., 2021). An asymmetric TF-MMM with ZIF-8 in the copolymer of PVI-POEM was synthesized by Lee et al. observed high CO_2 performance of 4474 GPU with high CO_2/N_2 and CO_2/CH_4 ideal selectivity of 32 and 12.4, respectively (Lee et al., 2022).

PEO based crosslinked membrane. The crosslinking approach is also the best alternative to overcome the crystallinity limitation of PEO based membranes. The crosslinking strategy is the transformation to a highly branched polymer by the free radical polymerization of ethylene oxide monomers and oligomers. At the incipient, the crosslinked PEO based polymers were designed by the free radical polymerization of different methyl acrylate monomers. Another noticeable building block for designing of PEO crosslink network is the addition reaction of amino and epoxy groups shows a high separation performance as well as thermal stability (Lin et al., 2006). Zhang et al. explored the crosslinking of PEO with nitrogen-rich polyamines network (PAN-NH_2) to synthesized CO_2-

Table 4.2
Examples of polymeric-based membranes with their performances (solution diffusion mechanism).

Material	p (CO_2)/atm	T/°C	P (CO_2)/Barrer	α (CO_2/N_2)	α (CO_2/CH_4)	References
PEO based polymeric membrane						
$HPEO_2$-800	30 psig	35	540	43	14	(Zhang and Tran et al., 2022)
PAN-NH_2/PEO	5bar	35	1160	73	19.7	(Zhang et al., 2022)
DME240-45	3bar	35	1400	45	-	(Guo et al., 2022)
STA-PEO	0.5MPa	35	1294	50	-	(Li et al., 2022)
PEO/PDMS-PEGBEM	1 bar	35	240	34.6	12.2	(Kang et al., 2021b)
PEO/PEGDEI 37	1 bar	35	201.1	49.3	15.7	(Min et al., 2021)
OPDA-ODA-PEO	6 bar	30	52	63		(Jankowski et al., 2021)
PEGDME-500			2281.1	48.1		(Li et al., 2019)
XLPP3-30	5 bar	25	92	92		(Motahari and Raisi, 2020)
PEO/PGP-POEM	1 bar	35	120.9	44.9	14.5	(Kim et al., 2020)
XLPEO/C6-60	30 psig	35	1340	48		(Huang et al., 2020)
1-GEF-M	4 bar	35	460	57	18	(Liu, et al., 2022)
PVI-POEM -PZ-50	1bar	30	4474	32	12.4	(Lee et al., 2022)
PEO/PTMSP EFCM	0.3MPa	25	281	32.94		(Zheng et al., 2022)
XLPEO		35	761.9	40.3	11.5	(Cheng et al., 2020a)
Perfluoro based polymeric membrane						
Teflon AF1600	*1000kPa*	*35*	489		12	(Scholes et al., 2016)
Poly (PFMMD-co-CTFE)	*50psig*	22	44.3		49	(Fang et al., 2018)
PEBAXs 2533	*350kpa*	*35*	*1860*	22		(Scofield et al., 2016b)
F-SPEEK/Matrimid	*10 bar*	*25*	33.2	51.11	47.45	(Asghar et al., 2018)
PEBAX 1657/P1 (60 wt%)	*350kpa*	*35*	226	39		(Scofield et al., 2016a)
PIM-COOH-360h		*30*	96.43	53.6	25.2	(Jeon et al., 2017)
PIM−1/SNW−1	*2 bar*	*30*	7553	22.7	13.5	(Wu et al., 2017)
PIM-1/PEG-POSS-10	*1 bar*	*30*	1300	*31*	30	(Yang et al., 2017)
PIM-TMN-Trip		*31*	16,500	*11*		(Stanovsky et al., 2020)
PIM-SBI-Trip	*1bar*	*25*	35 600	15.4	7.74	(Bezzu et al., 2021)
PIM-1/SBI-Trip	*1bar*	*25*	24 410	18.8	9.69	(Wang et al., 2017)
PAO-PIM-1/NH_2-UiO-66 (30 %)	*1bar*	*35*	8425	27.5	23.0	(Wang et al., 2017)
3-SCPIM-6/24	*1 atm*	*25*	4008	58.1	40.9	(Zhou et al., 2020b)
PIM-BM-70	*50psi*	*25*	48.3	30.1	43.9	(Chen et al., 2020)
PIM-MP-TB	*1 bar*	*25*	633	29.6	24.4	(Williams et al., 2018)
PIM-1-450	*3.5 atm*	*35*	40	40	110	(He et al., 2020)
AOPIM-1-9	*1 atm*	*35*	2483.6	31.2	30.1	(Wang et al., 2020)
PIM-1/sPPSU-3.5 (98:2)	*3.5 atm*	*35*	3003	22.9	18.0	(Kammakakam et al., 2021)
TR polymeric based membrane						
Im-PBOIonene] + [2-IL]	*2 atm*	*20*	44.7	34.1	51.9	(Kammakakam et al., 2021)
TR400-0	*76 cmhg*	*25*	184	26	63	(Suzuki, 2021)
6F-AP-450	*100 psi*	*35*	200.3		28	(Suzuki, 2021)
TR-coated PBOA	*0.5 Mpa*	*25*	24.0 gpu	18.9	18.2	(Ye et al., 2021)
ODA/APAF (3:7)			127.4	*20.6*	34.2	(Jia et al., 2022)
PIOAc30	*3 bars*	*30*	1036	*23*	28	(Aguilar-Lugo et al., 2021)
XTR-PBOI	*3 bars*	*75*	400 GPU	*20*		(Lee et al., 2017)
TR-PBOI-AD5		*25*	481 GPU	*17.7*		(Woo et al., 2016a)
XTR425	*1 atm*	*35*	271	*20*		(Lee et al., 2019)
TR-PBOI-375			560 GPU	*16.8*		(Woo et al., 2016b)
2D-diXTR	*3 bar*	*35*	4,590 GPU	*18.0*		(Lee, Jongmyeong et al., 2020)
6F-TM-Ac-425	*1 bar*	*35*	205	*25*	33	(Hu, Xiaofan et al., 2020)
rGO–PBOI	*1 atm*	*25*	1784 GPU	17.7	32.4	(Kim et al., 2018)

philic mixed matrix membrane, showing the excellent separation performance of CO_2 1160 Barrer along with CO_2/N_2, CO_2/CH_4 selectivity of 73, 19.7 respectively, surpassing the Robeson's upper bond (2019) limit (Zhang et al., 2022). Recently, a highway built up in PEO based membrane via a solvothermal annealing approach, offered a superior CO_2 permeability of 1299 Barrer with CO_2/N_2 selectivity of 50 along with long-term stability of 110 h, beyond the Robeson's upper bond line (Li et al., 2022). The solvothermal annealing approach enhances the flexibility of PEO chain and rearranges the side chain, which is an essential tuning permanent to boost the membrane performance, opening a new dimension for PEO based membrane for CO_2 capture towards industrialization.

PEO based blended membrane. The blending approach with a low molecular weight (100–200) polymer like PEG is also a suitable strategy not only to circumvent the limitations of crystallinity but also to obtain superior separation performance and thermal stability (Chen et al., 2016b). The introduction of low MW polymer in the backbone of PEO leads the crystalline PEO to the amorphous materials with outstanding separation performance. In addition it provides another tuning parameter to reduce the strong hydrogen bonding among the ether groups. Kang et al. synthesized an amphiphilic combo copolymer PDMS-PEGBEM via free radical polymerization and incorporated it into commercially available polymer PEO, resulting in extremely enhanced selectivity of CO_2/N_2 and CO_2/CH_4 from 0.78 and 0.71 to 41.7 and 13.3 respectively (Kang et al., 2021a)

4.1.2.2. Perfluoro based polymeric membrane. Perfluoro polymers are a fluorinated polymeric family, which attracted the most attention because of its mostly or all hydrogen atoms are replaced by fluorine atoms. The enrichment in strong C–F and C–C covalent bonds, transformed the per fluoropolymers to extremely thermally and chemically stable, which is the beneficial trait of this class of polymer to be a prospective candidate for commercial application (Merkel et al. 2006) Although it has a low tendency toward swelling because of its insolubility in many organic compounds and its semi-crystalline nature, it limits the applicability of perfluoro polymer in membrane advancement for gas separation (Prabhakar and Freeman, 2002). Since 1980, a new family of perfluoro polymers like Teflon AF, Hyflon AD, and Cytop polymers have been de-

signed for gas separation. The bulky dioxole monomer as a copolymer or cyclic homopolymer in these polymers reduces the chain mobility and crystallinity, leading to an amorphous polymer with exponential FFV, which renders the superior gas separation performance (Hellums et al., 1989; Tanaka et al., 1992). Fang et al. reported a new class of amorphous perfluorinated polymeric membranes to exhibit tuneable transport properties, which showed excellent separation performance for important gas pairs including CO_2/CH_4 (Wang et al., 2019). The summarized membrane performance mentioned is in Table 4.2.

4.1.2.3. Polymer of intrinsic microporosity-based membrane. In 2004 Budd and McKeown et al. introduced a new family of glassy polymers with a unique backbone feature having rigid ladder-like and contorted macromolecular structures, which are called polymers of intrinsic microporosity (PIMs) (Budd et al., 2004). The restricted chain rotation due to the absence of a single bonded chain in the backbone, kink chain, and their three-dimensional contorted conformation due to the tetrahedral carbon atom interaction with five-membered carbon rings, inhibit the macromolecules to effectively compact packing leads to the higher fractional free volume of typically 20 % FFV (McKeown, 2012; Rose et al., 2017). Therefore, PIM exhibits unprecedented permeability with moderate selectivity of CO_2 in a CO_2/N_2 and CO_2/CH_4 mixture. These versatile features of PIM attract the attention of researchers to focus on the designing of highly permeable and selective membranes. In recent years many efforts have been employed to enhance the CO_2 selectivity of PIM-based membranes. Some are summarized in Table 4.2. Bezzu et al. synthesized polymer of intrinsic microporosity (PIMs) by blending with rigid and bulky triptycene to the spirobisindane (SBI) and showed excellent permselective for the CO_2/CH_4 and CO_2/N_2 gas pairs (Bezzu et al., 2021). A hybrid mixed matrix membrane of PIM with the metal-organic framework synthesized by Wang et al., 2021 exhibited excellent performance with CO_2 permeability of 8425 Barrer and CO_2/N_2 and CO_2/CH_4 selectivity of 27.5 and 23, respectively, surpassing the 2008 Robeson's upper bound (Bandehali et al., 2021). Recently, thermally self-crosslinked Bromo alkylated PIM-based membranes were constructed by Xiuling Chen and co-workers and treated for gas separation, indicating superior CO_2 permeability of 48.3 Barrer along with CO_2/CH_4 selectivity of 43.9 (Halder et al., 2018). Jeon et al. reported, highly carboxylate functionalized PIMs (HCPIMs), due to their smaller interchain distance and CO_2 affinity exhibited high separation performance for CO_2 separation with a selectivity of 53.6 for CO_2/N_2 separation (Zhou et al., 2019).

4.1.2.4. Thermally rearranged (TR) polymeric-based membrane. Park et al. first introduced a new concept of more rigid and planer macromolecules from ortho-functionalized polyimides or polyamides by thermal rearrangement, named thermally rearranged (TR) polymer (Park et al., 2007). The TR polymer engineered with an unprecedented inherent feature of bimodal narrow cavity distribution (3-10 Å) and structural rigidity led to a high free volume, which was attributed to the excellent gas separation performance of TR-based polymeric membranes (Chern et al., 1983; Zhuang et al., 2015). Several examples TR based polymeric membranes are listed in Table 4.2 with their transport properties for lighter gas pairs. The ortho-position hydroxy group of polyimides or polyamides thermally rearranged via polycondensation reaction and formed twisted rigid-rod structure with a uniform microporosity, i.e., Poly benzoxazole (PBO) or polybenzimidazole (PBI) (Calle et al., 2015; Kim and Lee, 2015). The intrinsic uniform and small size micropores, result in the TR polymer to outstanding rapid gas transportation along with high selectivity for lighter gas pairs (Budd and McKeown, 2010). These inherent properties of TR polymer can further modify by tuning the thermal treatment protocol to surpass Robeson's upper bound along with the major bottleneck of TR polymer such as fragility and brittleness for gas separation.

Many research endeavours have been done due to the unprecedented intrinsic property of TR polymer. Recently, a new TR polymer incorporation of ionic components to obtain a novel imidazolium mediated poly benzoxazole by Kammakakam et al. in order to enhance the gas separation performance (Kammakakam et al., 2021). Suzuki et al. synthesized a novel TR-PBI-silica hybrid membrane and found an outstanding gas separation performance for CO_2/CH_4 due to the enlargement in the FFV and d-spacing with size-selective CO_2/CH_4 free volume holes at polymer-silica interfacial region (Suzuki, 2021). Lugo et al. synthesized mixed matrix membrane (TROH and TROAc-MMMs), notably increasing the permeation of CO_2 with 1036 Barrer CO_2/N_2 and CO_2/CH_4 surpassing the 2008 Robison's upper bound limit, with a selectivity of 28 for CO_2/CH_4 bit lower than the pristine TR-PBO membrane (Aguilar-Lugo et al., 2021). The thermal densification of the skin layer in the hollow fiber membrane of TR polymer hindered the permeance, and Lee et al. exploited this limitation by ultrathin skin layer. The crosslinking thermally rearranged diXTR hollow fiber, exhibits remarkable permeance of 4600 GPU with CO_2/N_2 selectivity of 18 (Lee et al., 2020).

4.1.3. Facilitated transport mechanism

Contrary to the solution-diffusion transport mechanism, membranes with a reactive carrier (amino group, -NH_2) which enhanced the reversible reaction between CO_2 and reactive carriers, refer to facilitated transport membranes (Schultz et al., 1974; Tong et al., 2017). The reactive carriers either be chemically embedded onto a backbone (fixed site carrier) or in the form of mobile carriers (mobile carriers) in a polymer matrix (Noble, 1990). Initially, CO_2 diffused into the polymer metrics, herein CO_2 reacts with the carrier and forms a CO_2-carrier complex at the high-pressure side, as due to the concentration gradient, it transports towards the low-pressure side by intramolecular diffusion (fixed-site carrier) or intermolecular diffusion (mobile carrier) where it released CO_2 and the reactive-carrier been regenerated back (Meldon et al., 1982).

While on the other hand, the small magnitude of inert gas molecules to the carrier transports through the membrane by the phenomenon of solution-diffusion mechanism. Worth noticeable that in the facilitated transport mechanism, the solution-diffusion mechanism is important. In general, the total CO_2 flux through the membrane is the combination of facilitated transport and solution diffusion transport mechanism, which can be represented by the following equation:

$$J_{CO_2} = \frac{D_{CO_2}}{l}\left(\Delta C_{CO_2}\right) + \frac{D_{Carrier+CO_2}}{l}\left(\Delta C_{Carrier+CO_2}\right) \quad (4.3)$$

Where, D_{CO2} and $D_{carrier+CO2}$ are the diffusion coefficient of Fick's diffusion (solution-diffusion) and carrier-CO_2 complex diffusion (facilitated diffusion), respectively. The thickness of the membrane is represented as *l*. The above equation clearly shows that the reactive carrier can drastically increase the total flux in addition to the solution diffusion, which can be attributed to the outstanding performance of facilitated transport-based membranes. However, the strong interaction between carrier and CO_2 hindered the desorption of CO_2 at permeate side. Contrary to this weak interaction between carrier and CO_2, it induced additional CO_2 partial pressure due to the CO_2 saturation in the membrane, consequently having an adverse effect on the performance of the membrane. Therefore, it is required to optimize reaction kinetics and CO_2 loading capacity for the outstanding separation performance of facilitated transport-based membranes.

4.1.3.1. Amine-based polymeric membranes. The most investigated reactive carrier in the facilitated transport of CO_2 captures is amines. The inherent features of amines provide structural versatility with tuneable of fast reaction kinetics and the extraordinary capacity of CO_2 loading (Perinu et al., 2017). The chemistry of CO_2 and amines is shortly explained in this section. Primary and secondary amine (electron-rich) acts as a nucleophile and attacks the electron-deficient carbonyl group CO_2 from zwitterion as shown in the below Equation (Caplow, 1968). The immediate proton transformation of another amine zwitterions transforms to a stable carbamate and ammonium ion as shown in Reactions 4.1, 4.2 and 4.3, in the nutshell 2 mol of amines are required for 1 mol

Table 4.3
Examples of polymeric based membranes with their performances (facilitated transport mechanism).

Material	p (CO_2)/atm	T/°C	P (CO_2)/Barrer	α (CO_2/N_2)	α (CO_2/CH_4)	Reference
Amine-based polymeric membranes						
65/35 PG/PVAm	1.5 psig	57	1100 GPU	200		(Chen et al., 2016a)
TFC-a-Tertiary amine	0.11 Mpa feed pressure	70	173 GPU	70	37	(Yu et al., 2010)
PEBAX/AFS-15	2 bar	25	145		28	(Isanejad and Mohammadi, 2018)
PAA-C3H7/PVA	2 atm F	110	308.6	346.9		(Zhao and Ho, 2012)
zeolite Y/Biomax PES	1 atm	57	745 GPU	25.4		(Zhaoet al., 2016)
PVAm/PG		57	1100 GPU	140		(Chen, Y. and Ho, W.W. 2016)
poly (N-methyl-N-vinylamine)	1 atm	102	6804	350		(Tong and Ho, 2017)
PES	4 atm	67	1451 GPU	165		(Han et al., 2019c)
HMMP-1	0.2 MPa	298 K	1544 GPU	252		(Yuan et al., 2021)

of CO_2 (Danckwerts, 1979). Hydrolysis of carbamate ions can occur at low PH to produce bicarbonate regenerating free amine. However, it is not favourable due to the stability of carbamate, as shown in the below Equation.

$$CO_2 + R - NH_2 \rightarrow R - NH_2 - COO^- \rightarrow R - NH - COOH$$

(Reaction 4.1)

$$R - NH - COOH + R - NH_2 \rightarrow R - NH - COO^- + R - NH_3^+$$

(Reaction 4.2)

$$R - NH - COO^- + H_2O \rightarrow HCO_3^- + R - NH_2$$

(Reaction 4.3)

The sterically hindered amino group effectively contributes to fasting reaction kinetics with CO_2, leading to an equimolar stoichiometry between CO_2 and amine. Consequently, it increases the CO_2 loading capacity of amine (Sartori et al., 1983). The sterically hindered destabilized the carbamate intermediate by restricting the C-N bond in carbamate. As the carbamate is destabilized by the bulky substituted amino group, it forms bicarbonate, releasing the free amine as shown in the Reactions 4.4, 4.5 and 4.6.

$$CO_2 + R_1 - NH - R_2 \rightarrow R_1R_2 - NH^+ - COO^- \rightarrow R_1R_2 - N - COOH$$

(Reaction 4.4)

$$R_1R_2 - N - COOH \rightarrow R_1 - NH - R_2 \rightarrow R_1R_2 - N - COO^- + R_1R_2 - NH_2^+$$

(Reaction 4.5)

$$R_1R_2 - N - COO^- + H_2O \rightarrow HCO_3^- + R_1 - NH_2 - R_2$$

(Reaction 4.6)

A common polymer matrix that attracted much attention from a researcher is poly (vinyl alcohol) (PVA), polyvinyl amine (PVAm), and polyallylamine (PAA) for facilitated-based membranes. Some examples are summarized in Table 4.3. Chen et al. synthesized a polyvinyl amine (PVAm) based membrane featuring the fixed-site carrier also with different amino acid salts mobile carries for CO_2 facilitated transport, demonstrated a CO_2 permeance of 1100 GPU and selectivity of 200 for CO_2/N_2 (Chen et al., 2016b). Zhao et al. studied the steric hindrance effect on amine and observed that it has a great advantage to enhance CO_2 transport (Zhao and Winston Ho, 2012). A hindered polyamines cross-linked with polyvinyl alcohol and obtained polymeric membrane of the fixed-site carrier, which exhibits an outstanding transport property of 440 % enhancement in CO_2 permeability along with 311 % increment in CO_2/N_2 selectivity. The same group studied again a sterically hindered polyvinyl amine effect more comprehensively by Tong et al. (2017b) the modified poly (N-methyl-N-vinylamine) demonstrated superior performance of CO_2 permeability of 6804 Barrer with a selectivity of 350 for CO_2/N_2 and 162 for CO_2/H_2 (Tong and Ho 2017b). Polyvinyl amine/piperazine glycinate membrane is fabricated by Chen and coworkers, consequently achieving the excellent performance of about 1100 GPU of CO_2 permeability and selectivity of 140 for CO_2/N_2 mixture, such high performance is attributed to the PVAm fixed-site-carrier whereas piperazine glycinate mobile carrier (Chen and Ho, 2016).

4.1.3.2. RTIL and other carrier based facilitated polymeric membranes. The designer solvent, room temperature ionic liquids (RTIL), nowadays are highly investigated as a potential candidate to replace other conventional materials, especially in CO_2 capture, due to its extraordinary features, such as low vapour pressure, high CO_2 uptake capacity, task-specific tuneable features, high thermally and chemical stability (Gan et al., 2011). These unique features supported ionic liquid-based membranes (SILMs) attracted much attention from a researcher for light gas separation. For instance, supported ionic liquid-based membranes have been investigated by Scovazzo et al. and exhibited an excellent separation with CO_2 permeability of 1000 Barrer along with the selectivity of 22 for CO_2/N_2. The major challenges for SILMs are the leaching of ionic liquids at the low-pressure difference from the polymer matrix due to its weak interactions limiting their mechanical stability (Tomé and Marrucho, 2016). To minimize these limitations, different approaches have been applied such as poly (ionic liquids) PIL by direct polymerization of IL monomers, embedding of IL into a compatible polymer matrix, and ion-gel membranes showing robust mechanical stability along with outstanding separation performance. For instance, Mannan et al. reported polyether sulfone/emim (Tf2N) ionic liquid polymeric membrane, observed 124-fold enhancement than the neat PES membrane, CO_2 permeability of 298.84 Barrer with 57.53 (3.6-fold enhancement) selectivity of CO_2/CH_4 (Mannan et al., 2016).

A small molecule of diamine and polyamine-based ionic liquid is used by Dai et al. to cross-link PEG diglycidyl ether (PEGDE) to obtain poly (ethylene glycol)-based epoxy-amine networks, exhibiting good separation performance due to CO_2-phillic ionic liquids along with robust mechanical strength due to the cross-linking. Moghadam et al. fabricated an interesting double-network ion-gel membrane of triethyl (2-methoxymethyl) phosphonium indazole ([P222 (101)] [Inda]), displaying an excellent CO_2 separation performance and excellent mechanical strength. By tuning the cross-linking loading, the impact of CO_2 separation performance significantly increases such as 4 mol% loading showing CO_2 permeability of 2254 Barrer with 210 selectivity of CO_2/N_2 (Moghadam et al., 2017). Ionic liquid based epoxy-amine ion gel membrane designed by M.McDanel et al. for fixed-site-carrier facilitated transport of CO_2 (Kasahara et al., 2014). The CO_2-phillic free RTIL carrier in membranes enhances the CO_2/N_2 separation performance of epoxy-amine ion-gel membrane drastically and surpasses the 2008 Robeson's upper bound limit. Ionic liquids featured with highly CO_2-philic functional groups make them more interesting alternatives for CO_2 separation. Its CO_2-philic functional groups lead it to a highly facilitated transport for CO_2 as well as also provide a solution-diffusion transport effect. Zhang et al. first introduced diamine-monocarboxylate-based protic ionic liquids (PILs) as a supported ionic liquid membrane

(SILMs), exhibit an excellent separation performance of CO_2 permeability of 3028 Barrer with ideal selectivity of CO_2/N_2 and CO_2/CH_4 is 151 and 72 respectively (Zhang et al., 2017a). A series of imidazolium based phenolate ionic liquid feature with dual sites of interaction with CO_2 reported by Zhang et al. The outstanding separation performance of CO_2 permeability of 2540 Barrer with ideal selectivity of CO_2/N_2 of 127, such an excellent performance is attributed to facilitated transport of CO_2 from carbene to phenolated anion based on theoretical calculations (Zhang et al., 2019).

Beyond the amine and RTIL, many other carriers also have been widely investigated for CO_2 separation and show a vibrant separation performance with mechanically stable such as nanotube, GO, nanoparticles, etc. A novel nanotube-reinforced facilitated transport membrane is fabricated by Han et al., a selective layer of 170 nm coated on the polyether sulfone substrate demonstrates a CO_2 permeance of 975 GPU along with a CO_2/N_2 ideal selectivity of 140 (Han et al., 2018). This excellent separation performance is attributed to the amino group bound to the polymer backbone acting as a fixed-site carrier and 2-(1-piperazinyl) ethylamine as a mobile carrier. Zhang et al. reported a mixed matrix membrane (MMMs) by introducing amino silane functionalized graphene oxides (f-GO) nanosheet into the Pebax polymer matrix, demonstrating a high CO_2 permeability of 934.3 Barrer along with CO_2/CH_4 and CO_2/N_2 ideal selectivity of 40.9 and 71.1 respectively (Zhang et al., 2019b). The amino groups on graphene oxides introduce facilitated transport effects in the MMMs, leading to surpassing Robeson's upper bound limit. An interesting hollow fiber thin film composite membrane with a three-phase hybrid facilitated transport effect (host polymeric matrix feature with fixed-site carriers, 2D-GO filler, CO_2-reactive mobile carrier) is investigated by Janakiram, showed a CO_2 permeance of 825 GPU with CO_2/N_2 and CO_2/CH_4 separation factor of 31 and 20 respectively (Janakiram et al., 2020).

Although much research focus has been made to explore the efficient membrane for CO_2 separation still far to make it applicable for industrial applications. In view of the exponential increment of carbon dioxide levels in the atmosphere, a high efficiency, low cost, energy effective, and stable membrane is required urgency.

4.2. Mixed matrix membranes

Although polymeric membranes have been extensively investigated for gas separation due to their inherent features such as low costs, mechanical stability and easy processability, they are hindered due to their trade-off relationship between selectivity and permeability for industrial application (Sanders et al., 2013). Many researchers have devoted an effort to the advancement of polymeric materials like thermally rearranged polymer (TR) (Meis et al., 2022) and polymer of intrinsic microporosity (PIMs) (Zhou et al., 2020a) as discussed in the above section, proved its potential to surpass Robeson's upper bound.

However, in the past few decades, mixed matrix membranes (MMMs) gained much attention from researchers due to their outstanding property to surpass Robeson's upper bound limit (Katare et al., 2023). In 1970, Paul and Kemp reported MMMs of zeolite 5 Å into polydimethylsiloxane (PDMS) for the first time (Paul and Kemp, 1973). MMMs generally comprise inorganic fillers dispersed into a polymeric matrix that exhibit excellent permeability and selectivity for gas separation (Zornoza et al., 2015). MMMs featured with the dispersed phase (inorganic-fillers) provide the selectivity and continuous phase (polymer matrix) enhanced permeability and mechanical strength. MMMs are potential alternatives to a conventional polymeric membrane to overcome the trade-off between permeability and selectivity for gas separation.

Generally, the transport behaviour of small gas molecules through membranes depends upon the pore size of the porous membrane and solubility or reactivity in the case of the dense membrane, as explained in the above section (Kanehashi and Nagai, 2005). However, the transport property of MMMs is dependent upon many factors such as the compatibility of filler and polymer matrix, loading of filler, size, and shape of filler, etc. Maxwell model is a well-known model for the prediction of the transport mechanism of gas through MMMs for low loading and good compatibility between polymer and filler (Kanehashi et al., 2015). For higher loading and ideal morphology, Lewis-Nielsen models are more appropriate (Lewis and Nielsen, 1970). Many inorganic fillers such as carbon molecular sieves (CMS) (Rafizah and Ismail, 2008), graphene oxides (GOs) (Li et al., 2015), zeolite imidazolate framework (ZIfs) (Yuan et al., 2017), metal-organic framework (MOFs) (Fu et al., 2016), covalent organic framework (COFs) (Fan et al., 2021) are investigated as filler into a polymeric matrix for gas separation. Recently, Fan et al. reported an interesting approach to enhance MOF/polymer interaction. However, it affects the permeability and selectivity of MMMs (Fan et al., 2022b). Deng et al. reported the effect of the morphology of filler (ZIfs 0D, ZIFs 1D, and ZIFs 2D) on the performance of MMMs (Deng et al., 2020a). Zhang et al. investigated 2D MFI nanosheet as a filler in Pebax polymeric matrix showing an excellent CO_2 permeability of 159.1 Barrer with a selectivity of 27.4 for CO_2/CH_4 (Zhang et al., 2021b). Yoo et al. studied defects in metal-organic frameworks, a highly porous defect-engineered UiO-66 incorporated into PEGDA exhibit superior CO_2 permeability of 470 Barrer with CO_2/N_2 selectivity of 41 (Lee et al., 2021b). Although by incorporating different and effective fillers into an appropriate polymer matrix we can achieve high separation performance, the defects exist at the polymer and filler interface. Therefore, evenly dispersion of fillers and appropriate fillers are still existing challenges for the researchers.

The separation of H_2/CO_2 is extremely difficult due to its kinetic diameters (Zhu, L et al., 2019). However, the exponential separation performance, sieving effects, high thermal, chemical, and mechanical stability of MMMs is extensively investigated for H_2/CO_2 or CO_2/H_2 separation. In this section, we discussed the pre-combustion and post-combustion CO_2 capture through MMMs.

4.2.1. Mixed matrix membranes for pre-combustion CO_2 capture

The separation of CO_2 or H_2 before the combustion is an effective strategy to limit the CO_2 concentration level in the atmosphere, generally termed pre-combustion CO_2 capture (Babu et al., 2016). After the water gas shift reaction, a mixture of CO_2/H_2 is obtained with high temperature and high pressure from the IGCC system (Kanniche et al., 2010). Membrane technology is a promising alternative to the conventional separation technologies such as cryogenic distillation, chemical absorption, and physical sorption. Membrane materials must be considered especially for pre-combustion separation. MMMs have the potential to sustain such extreme conditions due to their thermal and mechanical stability. For precombustion CO_2 capture, the membrane must either be H_2 selective or CO_2 selective (Al-Rowaili et al., 2023). We categorized MMMs as H_2 selective and CO_2 selective. H_2 selective membranes have been investigated mostly, which might be due to the increasing demand for pure hydrogen fuel. Among the polymer classes polybenzimidazole (PBI) exhibit excellent H_2/CO_2 selectivity. However, permeation is not significant (Zhu et al., 2017). MMMs provide an interesting window for such a polymer to enhance the permeability along with reasonable selectivity by incorporation of suitable fillers. For example, recently, Etxeberria-Benavides et al. studied the effect of zeolitic-imidazolate framework (ZIF-8) filler into the polybenzimidazole (PBI) matrix, found superior H_2 permeance of 65 GPU to 170 GPU with ideal selectivity of 18 for H_2/CO_2 at 150 °C and 7 bar (Etxeberria-Benavides et al., 2020). Asymmetric PBI/ZIF-8 MMMs with 1 µm skin layer designed by Sanchez-Lainez et al. exhibit unprecedented H_2 permeability of 20.3 GPU and H_2/CO_2 ideal selectivity of 35.6 at 250 °C and 6 bar (Sánchez-Laínez et al., 2018). Cheng et al. work on Zn/CO zeolitic imidazolate framework filler into a PEBAX polymer matric to fabricate CO_2 selective MMMs showing CO_2 permeability of 102.5 Barrer along with 9.4 CO_2/H_2 selectivity (Cheng et al., 2020b).

Metal-organic frameworks (MOFs) are also emerging material that has been reported as filler due to their pour size and functional groups giving superior gas transportation property (Lin et al., 2018). Friebe

et al. fabricated NH_2-MIL-125 MOF layer MMMs for shown enhanced selectivity and H_2 permeability (Friebe et al., 2016). The morphology of fillers is also a good tuning property to enhance the separation performance of MMMs. Kang et al. reported an effect of filler morphology on membrane performance. PBI/[Cu_2 (ndc)$_2$ (dabci)]n MMMs with different morphology (bulk crystal (BC), nanocube (NC), and nanosheet (NS)), stacking orientation of NS MOF in MMMs provide a CO_2 barrier and enhance the H_2/CO_2 selectivity of 26.7 along with the H_2 permeability of 6.13 Barrer (Kang et al., 2015). Ashtiani et al. demonstrated defect-free CO_2 selective MMMs by dispersing UiO-66-NH_2 (MOF) into a polyethyleneimine (PEI) (Ashtiani et al., 2021). Interestingly polymer-filler interfacial interaction enhanced by covalently bounding polyvinylpyrrolidone (PVP) with polymer and filler, exhibit CO_2 permeability of 394 Barrer along with a 12.7 separation factor. Ma et al. demonstrated ZIF-7@PI MMMs as a superior H_2 performance of 3.0×10^{-7} $molm^{-2}s^{-1}Pa^{-1}$ with 128.4 of separation factor for H_2/CO_2 and 91.5 for H_2/CH_4 due to the high channelling effects of ZIF-7 (Ma et al., 2019). Mei et al. modified the ZIF-8/Polysulfone MMMs with polydopamine, which enhanced the performance of MMMs showing H_2 permeability of 23.3 along with the selectivity of 9.3 for H_2/CO_2 (Mei et al., 2020). MMMs can thus be considered as a next-generation membrane for pre-combustion and post-combustion CO_2 capture due to their potential for industrial application. The novel design of inorganic fillers, such as MOFs, COFs, GOs, ZIFs, etc., makes this area more attractive.

4.2.2. Mixed matrix membranes (MMMs) for post-combustion carbon capture

MMMs containing dispersed inorganic fillers in continuous polymer matrices have emerged as an effective and versatile platform to obtain superior CO_2/N_2 separation properties for post-combustion carbon capture (Buddin and Ahmad, 2021; Hu et al., 2022b). The addition of nanofillers may also improve physical and chemical stabilities against plasticization and aging (Ahmad et al., 2020; Chi et al., 2019; Smith et al., 2020; Zhao et al., 2019). More importantly, the diversity of polymers and fillers offers enormous possibilities for designing membranes with desirable properties (Budhathoki et al., 2019).

A variety of functional polymers have been used as polymer matrice to construct MMMs to achieve superior CO_2/N_2 separation properties (Han and Ho, 2020; Hu et al., 2022b; Hu et al., 2018; Lee and Gurkan, 2021), including glassy polymers such as PIMs (Chen et al., 2021; Fan et al., 2022a; Shen et al., 2019) and polyimides (Hu et al., 2020; Jiang et al., 2021; Wang, Hongliang et al., 2018), and rubbery polymers such as Pebax (Nadeali et al., 2019; Sanaeepur et al., 2019; Thankamony et al., 2019), Polyactive (Rahman et al., 2018; Sabetghadam et al., 2019), and polyethers (Alebrahim et al., 2022; Hu et al., 2018; Liu et al., 2020). Polymers containing fixed CO_2 carrier sites, including poly (vinyl alcohol) (PVA) (Cao et al., 2019; Gao et al., 2018; Jia et al., 2020) and poly (ionic liquid)s (PILs) (Dunn et al., 2019; Lee and Gurkan, 2021; Yang et al., 2022) were also used to realize facilitated transport for CO_2, but not for N_2.

Porous or non-porous fillers can be used to create MMMs, while most studies focus on porous nanofillers with well-designed pores, such as metal-organic frameworks (MOFs) (Hu et al., 2018; Knebel et al., 2020), metal-organic polyhedra (MOPs) (Guo et al., 2021; Liu et al., 2020), porous organic frameworks (POFs) (Duan et al., 2019; Zhang et al., 2022), and two-dimensional (2D) nanosheets (Shi et al., 2021; X X Li et al., 2019). These porous fillers have high porosities that can tremendously improve gas diffusivity and solubility or well-controlled pore sizes that exhibit precise cut-off between CO_2 and N_2. Non-porous fillers with affinities towards CO_2 have also been used to improve CO_2 solubility and CO_2/N_2 solubility selectivity (Matteucci et al., 2008; Zhu, L et al., 2019). Additionally, non-porous fillers might disrupt polymer chain packing, increasing free volume and thus gas diffusivity (Hu et al., 2020; Merkel et al., 2002). Typical non-porous fillers include silica (SiO_2) (Aghaei et al., 2018; Hu et al., 2020), metal oxide (MO_x) (Qiu et al., 2022; Sanaeepur et al., 2019), and polyhedral oligomeric silsesquioxane (POSS) (Kanezashi et al., 2019; Ren et al., 2019).

In addition to the rapid growth of advanced materials, various empirical models are employed to describe gas transport properties in MMMs, such as the Maxwell model, modified Maxwell model, Lewis-Nielson model, and Kang-Jones-Nair model (Hoang and Kaliaguine, 2013; Monsalve-Bravo and Bhatia, 2018). Computational simulations have also been applied to predict the structure/property relationship in MMMs, such as molecular dynamics simulation (Erucar and Keskin, 2016), Monte Carlo simulation (Harami et al., 2019), computational fluid dynamics calculation (Kattula et al., 2015; Safaei et al., 2021), and artificial neural network model (Rezakazemi and Mohammadi, 2013; Rostamizadeh et al., 2013).

Despite tremendous progresses made in the last decades, the MMMs are faced with key challenges for practical applications, including particle agglomeration, interfacial incompatibility, brittleness, and poor thin-film formability. This section will highlight various strategies to address these challenges for the MMMs containing porous nanofillers, as well as the improvement of CO_2/N_2 separation properties. Tables 4.4 and 4.5 record separation properties for the key materials and thin-film composite (TFC) membranes developed, respectively.

4.2.2.1. MOF-based MMMs. MOFs have well-controlled apertures with sizes similar to gas molecules, such as ZIF-8 (3.4 Å) (Hu et al., 2018) and ZIF-90 (3.5 Å) (Huang et al., 2010). However, MOFs have flexible structures and show "gate-opening" behavior, leading to lower intrinsic CO_2/N_2 selectivity than most polymers (Bondorf et al., 2022; Ryder et al., 2014). Consequently, the MOF-based MMMs confine to the trade-off between CO_2 permeability and CO_2/N_2 selectivity, though their separation properties can still be described by empirical models such as the Maxwell model. Additionally, polymers (particularly glass polymers) do not have affinities towards MOFs, generating interfacial defects that can degrade separation performance and mechanical properties.

Compared to the blending of polymers and MOFs to form MMMs, *in-situ* growth of MOF nanoparticles (NPs) in polymers or *in-situ* polymerization of polymers provides an effective approach to improve interfacial compatibility by wetting the NPs with the polymers or precursors (Hu et al., 2022a; Park et al., 2020). Moreover, *in-situ* growth of the NPs can effectively control the NP sizes and avoid their aggregation (Ma et al., 2019). The NP sizes and shapes (or dimensions) can also be optimized to improve gas separation performance. Interestingly, low loadings of the NPs with optimized morphologies were reported to unexpectedly increase gas permeability because of the percolation networks formed by the highly porous NPs (Ashtiani et al., 2021; Chi et al., 2019).

Creating strong interactions between MOFs and polymers can efficiently enhance interfacial compatibility (Hu et al., 2022b). Specifically, the surface of the MOF NPs can be modified to exert affinities towards the polymer phase (Guo et al., 2019; Jiang et al., 2021; Lee, Jooyeon et al., 2020). For example, Fig. 4.1a shows that the ZIF-8 was modified using dopamine (a bio-inspired adhesive) before mixing. The addition of ZIF-8-DA substantially increased gas permeability without reducing selectivity (Fig. 4.1b,c), breaking the permeability/selectivity trade-off.

The surface of the ZIF-67 NPs was functionalized with N-heterocyclic carbene ligands to achieve excellent mechanical and separation properties (Knebel et al., 2020). Polymer chains can also be grafted onto the MOF surface, acting as brushes and generating favourable interactions with the polymer (Wang et al., 2018). Compatibilizers like ionic liquids (ILs) were also used to modify the MOF surface (Lu et al., 2021). Additionally, the MOF was even used to cross-link polymers to improve both interfacial compatibility and size-sieving ability. For example, UiO-66 NPs were functionalized with nitrile groups and then covalently bonded to PIM-1 by thermal treatment (Yu et al., 2019). The cross-linking with 20 wt% UiO-66 increased CO_2 permeability by 4 times to 12,000 Barrer and CO_2/N_2 selectivity by 2 times to 54 at 25 °C.

Table 4.4
CO_2/N_2 separation performance of representative MMMs.

MMMs			T (°C)	CO_2 permeability (Barrer)	CO_2/N_2 selectivity	Ref.
Polymers	Fillers	Loading (wt.%)				
PEGDA-*co*-PEGMEA	-	0	35	424	33	(Ma et al., 2019)
	ZIF-8	49.7		910	33	
	ZIF-7	34.3		1084	38	
XLPEGDA	-	0	35	130	50	(Hu et al., 2018)
	ZIF-8	50		1300	33	
6FDA-DAM	-	0	35	970	18	(Chi et al., 2019)
	HKUST-1	30		2360	16	
sPIM-1	-	0	25	5929	24	(Yu et al., 2019)
	UiO-66-CN	20		12063	54	
XLPEO	UiO-66-H	30	35	70	49	(Lee et al., 2020)
	UiO-66-Vinyl	30		110	47	
	UiO-66-NO_2	30		115	44	
	UiO-66-Naph	30		82	47	
ODPA-DAM	-	0	35	65	17	(Wang et al., 2018)
	UiO-66-NH_2@PI	27		142	27	
PIM-1	-	0	20	7062	10	(Lu et al., 2021)
	UiO-66-NH_2@IL	10		8283	23	
XLPEGDA	-	0	35	110	55	(Liu et al., 2020)
	MOP-3	50		480	42	
XLPDXLA	-	0		190	70	
	MOP-3	30		580	62	
XLPEO	-	0	35	440	35	(Zhang et al., 2022)
	COF	6-9.6		804	61	
6FDA-DAM	-	0	25	812	25	(Cheng et al., 2019)
	COF300	7		1205	33	
	COF@PEI	10		1154	49	
PIM-1	-	0	35	4500	14	(Li et al., 2019)
	Azo-COP-2	15		10,500	12	
Pebax®1657	-	0	20	53	51	(Thankamony et al., 2019)
	CTPP	0.025		73	79	
PTMSP	-	0	-	43,000	7	(Smith et al., 2020)
	p-DCX	-		42,000	12	
Pebax®1657	-	0	25	94	32	(He et al., 2019)
	POP-PGO	2		233	81	
Pebax®1657/	-	0	35	590	43	(Shin et al., 2019)
PEGMEA	GO	0.3		610	56	
Pebax®1657	-	0	25	125	65	(Shamsabadi et al., 2017)
	AS-TiO_2	3		189	85	
	CMC-TiO_2	3		195	82	
ODPA-TFMB	-	0	35	67	28	(Hu et al., 2020)
	SiO_2-NH_2	20		210	31	
XLPEO	-	0	35	520	52	(Alebrahim et al., 2022)
	$LiClO_4$	2		710	53	
Pebax®1657	-	0	RT	71	30	(Deng et al., 2020b)
	ZIF-C	20		387	47	
Pebax®1657	-	0	35	96	39	(Zhang et al., 2019a)
	f-GO	0.9		934	71	

Table 4.5
CO_2/N_2 separation performance of representative TFC membranes based on MMMs.

MMMs				Gutter layer	T (°C)	CO_2 permeance (GPU)	CO_2/N_2 selectivity	Ref.
Polymers	Fillers	Loading (wt.%)	Thickness (μm)					
Pebax 1657	ZIF-8	30	~1.5	PTMSP	25	350	31	(Sutrisna et al.,
	ZIF-7	30	1–1.5			300	48	2017; Sutrisna et al.,
	UiO66-NH_2	50	1–1.5			340	57	2018)
PEGDME	NH_2-MIL-53	47.4	4.9	None	35	560	35	(Xie et al., 2018)
PIM-1	MOF-74-Ni	10	0.65	PDMS@aMOF	35	1200	30	(Liu et al., 2020)
PGMA-co-POEM	UiO-66-NH_2	28.6	<0.1	PTMSP	25	1300	31	(Kim et al., 2019)
PEGDMA	EG3-MOP	5	~0.29	PDMS	35	300	16	(Sohail et al., 2021)
Pebax 1657	GO/IL	0.05	~0.1	PTMSP	25	900	45	(Huang et al., 2018)
Pebax 1657	MXene	0.05	0.07	PTMSP	25	1360	31	(Shamsabadi et al., 2019)
PSF	Montmorillonite	NA[c]	0.1	None	50	800	125	(Qiao et al., 2016)
PA	MIL-101 (Cr)	NA	0.2	PDMS	NA	930	220	(Wang et al., 2020)
PIL-IL	GO	~1	0.9	None	22	3090	1180	(Lee and Gurkan, 2021)
PVAm	PEI-g-ZIF-8	16.7	0.33	None	30	2000	80	(Gao et al., 2018)
PVAm	HMP (F)	NA	~0.3	PDMS/PVA	25	1800	65	(Wang et al., 2020)

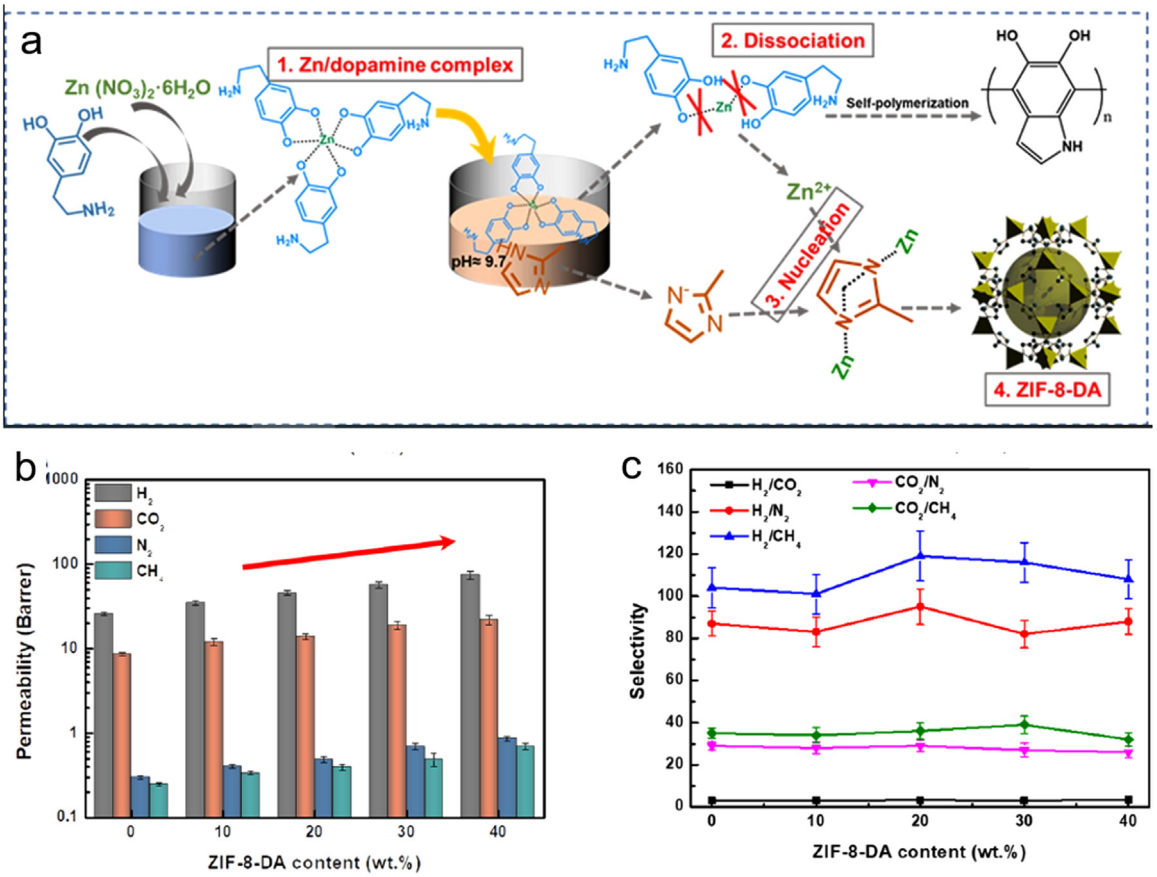

Fig. 4.1. (a) Illustration of the dopamine-modulated synthesis process of ZIF-8-DA. Effect of the ZIF-8-DA loading in Matrimid on (b) gas permeability and (c) selectivity (Jiang et al., 2021). (For interpretation of the references to color in this figure legend, the reader is referred to the web version of this article.)

2D MOF nanosheets (NSs), especially ZIF, have been widely used to form MMMs (Bi et al., 2020; Feng et al., 2020). For instance, metal-tetrakis (4-carboxyphenyl) porphyrin (M-TCPP) NSs have open metal sites and affinities towards polymer chains and CO_2, increasing CO_2 solubility and interfacial compatibility (Wang et al., 2019; X Li, 2019; Zhao et al., 2017; Zhao et al., 2018). In addition, the M-TCPP NSs have intrinsic micropores and interlayer spacing near 1 nm, which can be utilized to enhance gas separation properties (Lee et al., 2021a; X Li, 2019).

4.2.2.2. MOP- and POF-based MMMs. MOPs are highly porous molecular cages formed via the self-assembly of metal ions and organic ligands, similar to MOFs. However, MOPs are discrete cages of 1–5 nm, which can be dissolved in solvents and easily processed into TFC membranes, as shown in Fig. 4.2a (Fulong et al., 2018). MOPs were incorporated in glassy or rubbery polymers to improve CO_2/N_2 separation properties (Fulong et al., 2018; Liu et al., 2020; Liu et al., 2018). In particular, the metal ions on the MOPs can have favourable interactions with polymers such as polyethers, enhancing interfacial compatibility. For instance, MOP-3 NPs have a uniform size of ≈5 nm (Fig. 4.2b) with aperture sizes of 1.1 and 0.89 nm. Fig. 4.2c shows a photo of a freestanding film containing 50 % MOP-3, and the SEM photo confirmed the well-dispersed NPs in the polymer (Fig. 4.2d). The introduction of 50 % MOPs in the polyether increased CO_2 permeability from 190 to 580 Barrer while retaining high CO_2/N_2 selectivity of 62 (Fig. 4.2e). Interestingly, low loadings of MOPs can also significantly increase CO_2 permeability and retain CO_2/N_2 selectivity because of the percolation networks derived from the MOP NPs (Hosono et al., 2019).

Unlike MOFs and MOPs containing metal atoms, POFs are assembled by pure organic compounds and can be categorized as covalent organic frameworks (COFs), covalent organic polymers (COPs), and porous aromatic frameworks (PAFs). Due to their high crystallinity and well-defined porous structures, COFs have been intensively investigated for gas separations. However, most COFs have pore sizes far larger than gas molecules, increasing gas permeability but decreasing selectivity (Zhang, Yahui et al., 2022). Several approaches have been adopted to reduce COF pore sizes to increase the size-sieving ability (Fan et al., 2018; Yang et al., 2019). For instance, 3D COF-300 NPs were constructed from 2D COF layers to attain pore sizes of 4 Å, and the incorporation of the NPs in Pebax increased both CO_2 permeability and CO_2/N_2 selectivity (Cheng et al., 2019). One of the challenges in using COFs for MMMs is their hydrophobicity, leading to poor interactions with polymers. To mitigate this problem, the COFs are often functionalized with ions or hydrophilic groups to enhance interfacial compatibility (Cheng et al., 2018; Liu et al., 2021). Additionally, the hydrophilic groups, such as PEO and polyethylenimine (PEI), can have affinities towards CO_2, further improving CO_2/N_2 separation properties (Liu et al., 2021).

POFs can also be further functionalized with N_2-phobic groups, such as azo groups (–N=N–), decreasing N_2 solubility and increasing CO_2/N_2 solubility selectivity (Patel et al., 2013). For example, the addition of 15 % azo-COP-2 in polysulfone increased CO_2/N_2 solubility selectivity by ~ 90 % (Li, Siyao et al., 2019). Other POFs have also been developed and used in MMMs to improve CO_2/N_2 separation properties, such as PAFs (Smith et al., 2020, 2019) and covalent triazine piperazine polymer (CTPP) (Thankamony et al., 2019; Zhang, Yahui et al., 2022).

4.2.2.3. MMMs containing 2D nanomaterials. 2D nanomaterials with tunable channels are another popular type of porous fillers used to con-

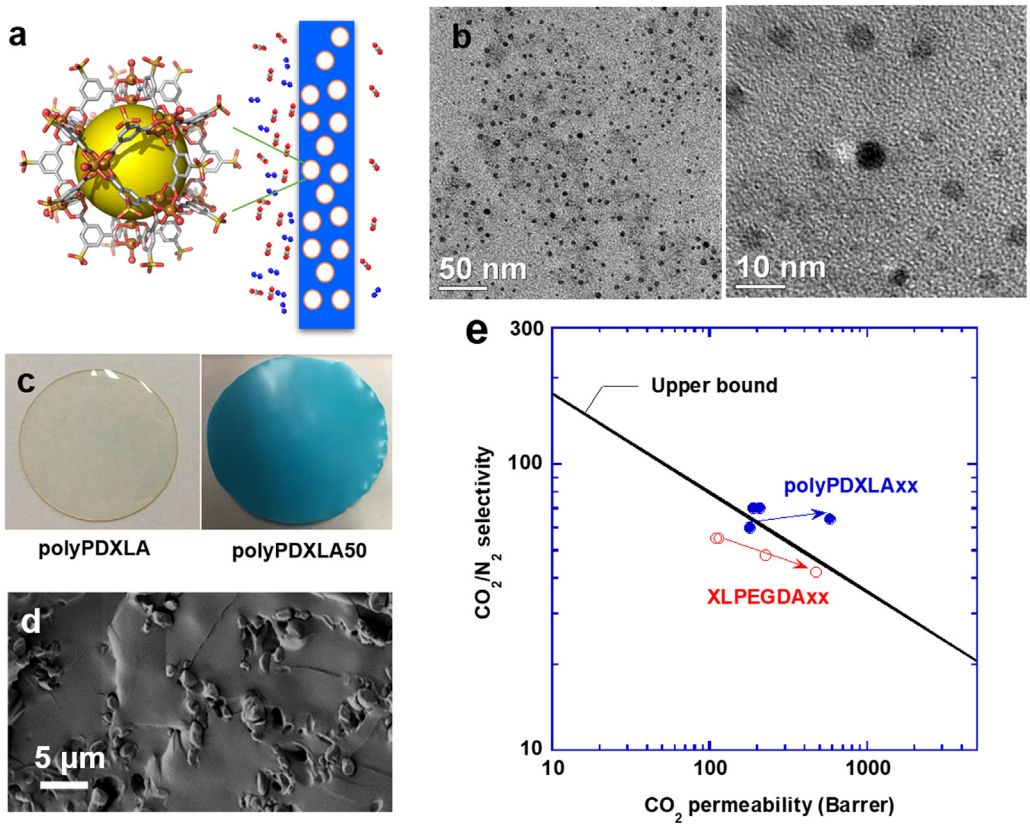

Fig. 4.2. (a) Schematic of the MOP-based MMMs for CO_2/N_2 separation. (b) TEM images of MOP-3 NPs. (c) Photos of polyPDXLA and polyPDXLA50 (containing 50 mass% MOP-3). (d) Cross-sectional SEM image of the XLPEGDA30. (e) CO_2/N_2 separation performance of XLPEGDAxx and polyPDXLAxx in 2008 upper bound (Liu et al., 2020). (For interpretation of the references to color in this figure legend, the reader is referred to the web version of this article.)

struct MMMs, such as 2D COF and MOFs, graphene-based NSs, and MXene NSs (Shi et al., 2021). For instance, porous graphene was demonstrated with the potential to achieve CO_2 permeance of 100,000 GPU and CO_2/N_2 selectivity of ~ 300 (Liu et al., 2013). Graphene oxide (GO) NSs have high aspect ratios and can be stacked to form sub-nm channels for gas molecular sieving. Furthermore, GO NSs can be chemically modified by grafting or blending to enhance interfacial compatibility with polymers and affinity toward CO_2 (He et al., 2019; Li et al., 2015). For example, the addition of 0.3 wt% GO NSs in Pebax/PEGMEA increased CO_2/N_2 selectivity from 42 to 56 with enhanced stability against physical aging (Shin et al., 2019).

MXenes contain metal carbides and carbonitrides and have a large surface area and hydrophilicity (Huang et al., 2021). MXene nanosheets can be stacked to attain interlayer spacings near gas molecule sizes, thus achieving a strong size-sieving ability for CO_2/N_2 separation. For example, $Ti_3C_2T_x$ NSs showed an interlayer spacing of 3.5 Å, larger than CO_2 but smaller than N_2 (Shamsabadi et al., 2019), and the addition of 0.1 wt% $Ti_3C_2T_x$ in Pebax increased CO_2/N_2 selectivity by 41 % to 43 and CO_2 permeability by 83 % to 1810 Barrer because of the disrupted polymer chain packing and increased free volume.

4.2.2.4. Facilitated transport MMMs. MMMs with facilitated CO_2 transport have also been investigated to obtain superior CO_2/N_2 separation properties, and typical polymers can be poly (vinyl amine) (PVAm) and PolyILs (Cao et al., 2019; Lee and Gurkan, 2021). For example, MMMs were prepared by self-assembly of PVAm and modified MIL-101 (Cr) (MKP) (Wang et al., 2020), and a TFC membrane with 200-nm MKP/PVAm exhibited CO_2 permeance of 823 GPU and CO_2/N_2 selectivity of 242 in the presence of water vapour.

Nanofillers can also be functionalized with CO_2 carrier groups to achieve facilitated CO_2 transport (Deng et al., 2020b; Zhang et al., 2019a). Fig. 4.3 presents the structure and properties of the MMMs containing ZIF NSs in Pebax (Deng et al., 2020b). The ZIF NSs showed good dispersion in MMMs (Fig. 4.3b). Increasing the relative humidity (RH) generally improves the CO_2/N_2 separation properties due to the facilitated CO_2 transport. An MMM film containing 20 wt% NSs exhibited high CO_2 permeability of 390 Barrer and CO_2/N_2 selectivity of 47 in the presence of saturated water vapour (Fig. 4.3c,d).

4.3. Inorganic membranes for CO_2 capture

Polymeric inorganic membranes (PIMs) are still at the initial stage of research; they display prospective characteristics for pre- and post-combustion CO_2 capture. These membranes offer high permeabilities, thus reducing the total investment as compared to polymeric membranes. Moreover, PIMs can be operated in a continuous operation and can withstand high flow rates.

The market of inorganic membranes is very small and is expected to rise in the near future. Inorganic membranes like zeolites, porous glass, microporous beryllium oxide, silicon nitride, carbon, and silica are quite popular because of their characteristic of high permeability and selectivity (Ogieglo et al., 2019; Sazali et al., 2021; Shi et al., 2020). The phenomenon of high permeability and selectivity is known as the upper bound trade-off curve, first introduced by Robeson (1991) in 1991 and later updated in 2008 (Robeson, 2008). The phenomenon describes an inverse dependency of selectivity and permeability for gas separation of membranes. For example, as the gas selectivity decreases, the permeability decreases, and vice versa. For this reason, inorganic membranes have superior performance as compared to glassy mem-

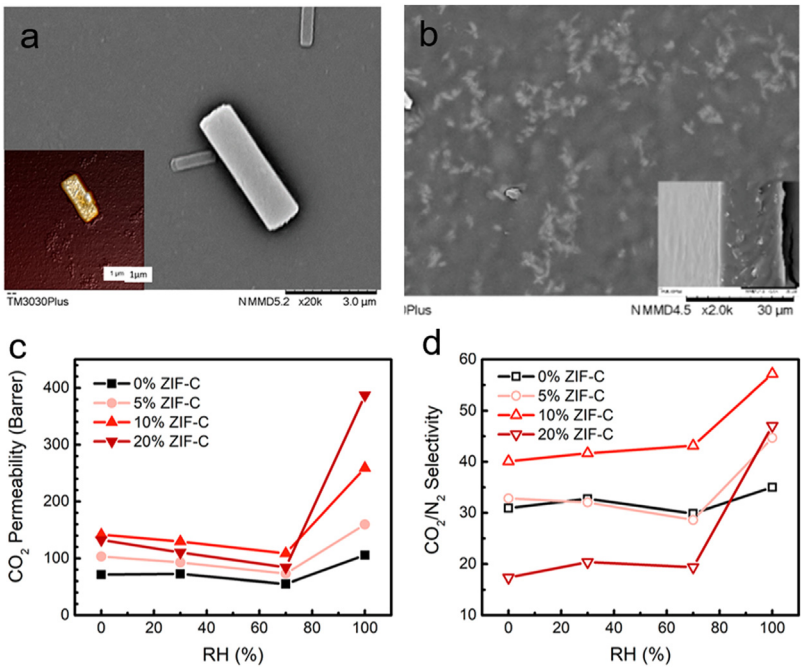

Fig. 4.3. Morphology of (a) ZIF-C 85–124 NS and (b) MMM with 10 wt% ZIF-C 85–124 NS. (c) CO_2 permeability and (d) CO_2/N_2 selectivity of MMMs as a function of relative humidity (Deng et al., 2020b). (For interpretation of the references to color in this figure legend, the reader is referred to the web version of this article.)

branes. J.W. McBain introduced the first ever inorganic polymeric membrane in 1930s. This membrane was initially utilized as a molecular sieve material and surprisingly displayed excellent selectivity (McBain, 2002). Apart from the processes of permeability and selectivity, membrane properties play another important role in carbon capture and separation. Primarily, the support material for any membrane is selected based on the requirements of mechanical strength, chemical resistance, and durability (Lee et al., 2016). In most cases, the support material is porous in nature to experience minimal gas/water transport resistance. Porous inorganic membranes contain either contain porous metal or ceramic support structures, with additional porous layers on top with different structures and morphologies. Inorganic membranes have different pore shapes like (i) straight pores of equal diameter extending from end to end of the membrane, and (ii) conical pores smaller at the bottom and a larger diameter at the surface of the membrane.

In addition to the general advantages of the PIM, new generation hybrid materials of zeolites, silica, and organometallic frameworks (MOFs) offer an abundance of opportunities to produce new membranes with selective functional groups for carbon recovery (Ding et al., 2019; Shi et al., 2020). Recent reviews of CO_2 capture on hybrid membranes have provided only brief insights into membrane design for CO_2 and H_2 separation.

4.3.1. *Zeolite based inorganic membrane*

Zeolites, also known as semi-stable silicates or alumina silicates, with a uniform topology, giving an intracrystalline network of voids and channels. They also have an abundant surface chemistry that varies with the Si/Al ratio, amount, and type of exchangeable cations. Cations in zeolites sometimes act as Lewis acids, while the framework oxide ions nearby cations may act as Bronsted/Lewis bases. Furthermore, the silanol groups might act as Brönsted acids. The CO_2 adsorption capacity of zeolites are highly affected by their topology, modelling the energy interactions, segregating, and clustering effects. The dependence of zeolites on topology is not always precise as most of the zeolites are very complex to prepare in pure silica form or in proper Si/Al ratios. Noteworthy exceptions to this statement are silicate-1 (Tawalbeh et al., 2021; Zhu et al., 2006), clathrasil DD3R (Himeno et al., 2007; Van Den Bergh et al., 2010), CHA (Debost et al., 2020; Miyamoto et al., 2012), and ITQ-29 (Palomino et al., 2010). Silicalite-1 composite membranes with thin zeolite layers, prepared by Wirawan et al. (2011) provided a simulated results of 9.8 and 4.0 mol/ (m^2s) for CO_2/H_2 separation factor and CO_2 flux, respectively. Faujasite (FAU)-type zeolites with low Si/Al ratio often provide the highest adsorption selectivity for CO_2. Study by Krishna and van Baten (2010). proposed that FAU-type membrane can achieve a selectivity of 500 and permeability of 10000 Barrer for CO_2/N_2 separation. The presence of aluminum in the silicon-aluminum framework creates a negative charge that must be neutralized by the metal cations in the pores. The most observed configurations involve the presence of Na^+ ions as counterions, termed NaX and NaY. Compared to N_2, CO_2 exhibits a stronger interaction with the electric field of the micropores, influenced by the number and type of cations present. NaX, which has a lower Si/Al ratio than NaY and contains more cations, exhibits higher selectivity for CO_2 over N_2, despite having a smaller pore volume than NaY (Maurin et al., 2005). White et al. (2010) developed a zeolite Y membrane on alumina, which gave CO_2 permeance of 300 GPU and more than 500 selectivity factors for CO_2/N_2.

4.3.1.1. Surface chemistry. The Si/Al ratio in zeolite surface is highly responsible for influencing its ability to adsorb CO_2 by pitching the number and setting of exchangeable cations, including the acid-base character of zeolite topology. Among the most famous zeolite structures, faujasites provide the highest CO_2 uptake capacity of 5-10 mmol CO_2/g at 101 kPa and 303 K. The CO_2 affinity follows the order of NaA > NaX > NaY. This trend can be explained by decreasing pore size and the presence of a high number of type III cations at the starting of super-cage structure, leading to preferential interaction with CO_2 (Li and Pidko, 2019). The CO_2 uptake in ITQ-29 dramatically increase with Si/Al ratio (Fig. 4.4). This property is exceptional for membrane design as it enables preferential separation of CO_2 by precisely modulating the polarity and surface science of LTA scaffold in specific separations. In the case of Aluminosilicate-based zeolites, CO_2 adsorption Henry's coefficients are 1-2 orders greater than corresponding N_2 and CH_4. This difference is attributed to the high heat of adsorption of CO_2 as compared to N_2 and CH_4.

The zeolite basicity increases with Al content and cation electropositivity (Barthomeuf, 2003; Verdoliva et al., 2019). Ward and Habgood (1966) supported the hypothesis of chemical interactions among

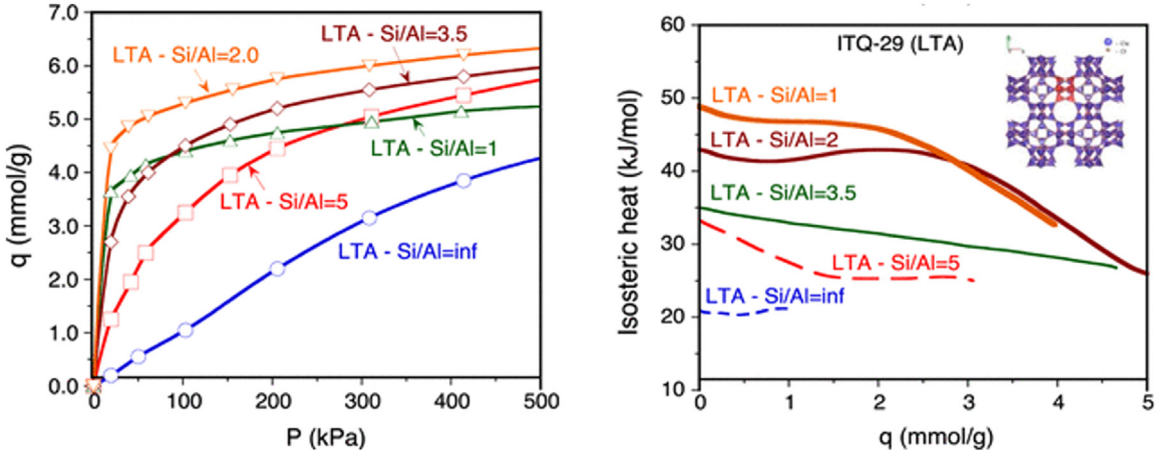

Fig. 4.4. Effect of the Si/Al ratio on the isosteric heat of CO_2 adsorption for a series of ITQ-29 zeolites displaying the LTA (Pera-Titus, 2014). (For interpretation of the references to color in this figure legend, the reader is referred to the web version of this article.)

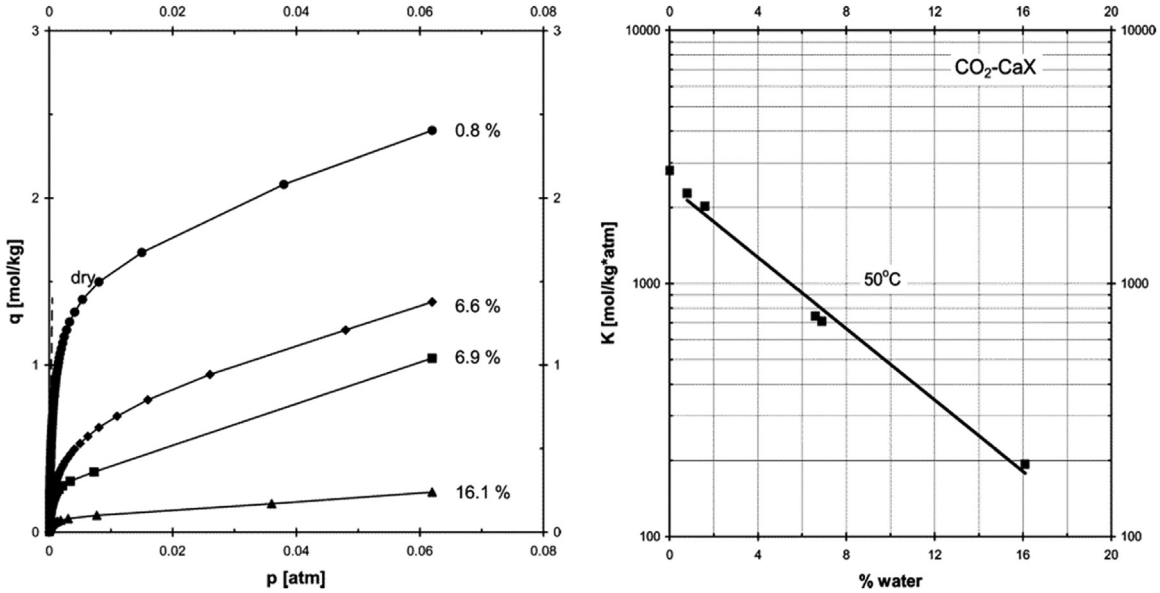

Fig. 4.5. CO_2 adsorption isotherms (left) and Henry's constants (right) on CaX at 323 K for different pre-adsorbed water loadings (Brandani and Ruthven, 2004). (For interpretation of the references to color in this figure legend, the reader is referred to the web version of this article.)

adsorbed CO_2 and alkaline cations. They reported the characteristic IR bands of carbonates for CO_2 adsorption in KX, NaX, and LiX zeolites. Heavy cations (Rb and Cs) compensate for the strong basicity with electrostatic interactions of cation and quadrupole (Walton et al., 2006). The basicity of zeolite structure can further be devised by incorporating amine groups, resulting in phase alteration of zeolite, and the formation of Si-N-Si moieties (Han et al., 2005).

4.3.1.2. Effect of water on CO_2 adsorption. Water is studied as a simple molecule to increase the CO_2 adsorption of zeolites. The CO_2 uptake can be highly influenced by high water partial pressure as CO_2 and H_2O molecules compete for the sorbent sites (Kolle et al., 2021). H_2O favourably adsorb on exchangeable cations, lessening the electrical field on zeolite cavities. For instance, as reported by Brandani and Ruthven (2004), the CO_2 uptake in CaX-zeolite at 0.06 bar and 323 K decreases between 2.5 and 0.1 mmol/g on increasing H_2O concentration from 0.8 wt% to 0.1 wt% (Fig. 4.5). Meanwhile, in case of CO_2 concentration less than 300 ppm, H_2O pre-adsorption may promote CO_2 adsorption capacity by forming surface bicarbonate species. This improvement automatically normalises CO_2 uptake as the CO_2 concentration reaches 1000 ppm, stating that CO_2 loadings are higher for dry adsorption.

In zeolites with high Si/Al ratios, the H_2O isotherm deviates from the characteristic type-I trend (i.e., Langmuir type), as noticed in LTA and FAU zeolites. The H_2O adsorption proceeds through the formation of clusters in MFI channels, resulting in the reduction of CO_2 uptake capacity (Ahunbay, 2011; Cailliez et al., 2008; Trzpit et al., 2007). The deviation from Langmuir-type is generally known as type-II behaviour. Introducing germanium in the MFI structure also improves hydrophobic properties. Fig. 4.6 represents water adsorption on MFI zeolite improved with Al, B, and Ge species.

MFI membranes have yielded comparatively low amounts of CO_2/N_2 separation factors. However, their use for the separation of CO_2/N_2 mixtures is still being investigated because of their low Al content. This gives the membranes better reproducibility and chemical stability. Ando et al. (Ando et al., 1998) reported a separation factor of 25.5 at a CO_2 permeance of 6.6×10^{-7} mol/(m^2 s Pa). The MFI membranes synthesized by Guo et al. (2006) show CO_2/N_2 separation of about 65 μmol·m^{-2}·s^{-1}·Pa^{-1} at room temperature with equimolar CO_2/N_2 mixtures under Wicke–Lallenbach conditions. In addition, the

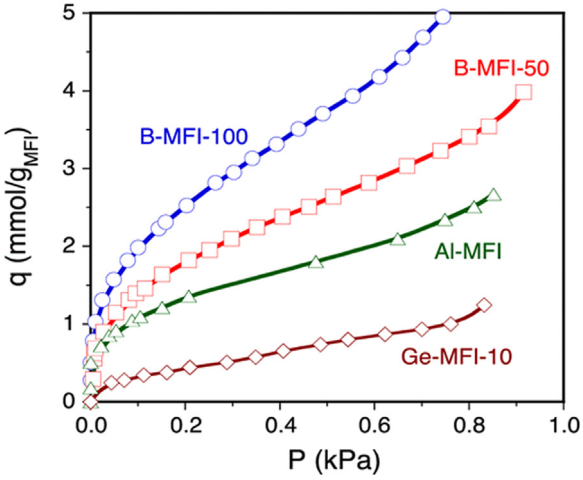

Fig. 4.6. Water adsorption at 303 K on crushed Al-MFI (Si/Al = 30), B-MFI-100 (Si/B = 100), B-MFI-50 (Si/B = 50), and Ge-MFI-10 (Si/Ge = 10) (Nicolas and Pera-Titus, 2012). (For interpretation of the references to color in this figure legend, the reader is referred to the web version of this article.)

CO_2 molecules were seen to pass at the rate of 0.7 μmol·m^{-2}·s−1·Pa^{-1} through the membrane. These factors were better than the pre-recorded values for silicate-1, BaZSM-5, B-NaZSM-5, and BHZSM-5. The isomorphous substitution of Si (IV) in place of B (III) results in materials with comparable CO_2 permeation, but with better stability. Sublet et al. (2012) reported the post-combustion separation of CO_2/N_2 using α-supported MFI zeolite membrane. At higher water concentrations, MFI membranes show static reduction of gas permeance of 40 % for water concentration. The insertion of water improves CO_2/N_2 separation due to the development of (bi)carbonate stable intermediates. In addition, the MFI membranes like HZSM-5 (Guo et al., 2006) and NaZSM-5 (Shin et al., 2005) show a good perspective for CO_2/N_2 separation in the presence of water. These two membranes compete with the best reported NaY membranes in terms of CO_2/N_2 separation, CO_2 permeances, and permeabilities. Shin et al. (2005) proposed an increased membrane selectivity of ZSM-5 for the separation of an equimolar CO_2/N_2 mixture saturated with moisture. At room temperature, the separation factor for the dry mixture was 50, while it was 60 for the wet mixture. Due to the higher ration of Si/Al in ZSM-5, these membranes can be a potential candidate for future membranes in CO_2 separation technologies.

4.4. Carbon molecular sieve membranes for post-combustion carbon capture

4.4.1. Introduction for carbon molecular sieve membranes

The rapid increase of greenhouse gas emissions causes global climate change (Hoegh-Guldberg et al., 2019; Malhi et al., 2021), and CO_2 capture, utilization and storage (CCUS) is becoming one of the most attractive solutions for the reduction of CO_2 emissions (Figueroa et al., 2008; Hassanlouei et al., 2013). Different technologies such as chemical absorption, adsorption, membranes, and cryogenic distillation, have been developed for CO_2 capture (Araújo et al., 2022; Shah et al., 2020). Among them, membrane-based gas separation technology is one of the most promising strategies due to its high adaptability and reliability, energy-saving, and being environmentally friendly (Agaton and Karl, 2018; Araújo et al., 2022; He et al., 2022; Kunalan and Palanivelu, 2022; Rodrigues et al., 2019). Various membrane materials have been investigated for CO_2 capture (Kunalan and Palanivelu, 2022; Lei et al., 2020; Liu et al., 2022; Shah et al., 2020), such as polymer membranes (Meixia Shan et al., 2018; Zhu et al., 2018), mixed matrix membranes (MMMs) (Guo et al., 2022; Voon et al., 2022; Zhang et al., 2021a), fixed-site-carrier (FSC) membranes (Hägg et al., 2017; He et al., 2017b), two-dimensional (2D) nanosheets (Achari et al., 2016; Cacho-Bailo et al., 2017; Ding et al., 2018; Ying et al., 2018; Yu et al., 2011) and carbon molecular sieve membranes (CMSMs) (Araujo et al., 2020; Cao et al., 2019; Karousos et al., 2020; Lei et al., 2021; Sazali et al., 2021; Tseng et al., 2016). Among them, CMSMs are considered the next-generation gas separation membranes due to their high separation performance, and thermal and chemical stability, which shows great potential for pre- and post-combustion carbon capture (Koros and Zhang, 2017; Lei et al., 2020). Importantly, the development of flexible carbon hollow fiber membranes (CHFMs) is expected to produce practical membrane modules with a low cost and a high packing density (Liu et al., 2016). In this section, a systematic review of CMSMs for CO_2 capture or removal related to both material and process performances will be conducted.

4.4.2. Carbon membrane structure and gas transport mechanisms

Under inert purge gas or vacuum conditions, CMSMs are prepared by pyrolysis of precursors at high temperatures. During the pyrolysis process, the polymeric precursors are transformed to ordered carbon plates, which usually results in a bimodal structure with ultramicropores (3–7 Å) and micropores (7–20 Å) (Ma et al., 2019; Qiu et al., 2019; Rungta et al., 2017; Zhang and Koros, 2017). Fig. 1 illustrates the proposed pyrolysis mechanism from a cellulosic precursor to CMSMs (Lei et al., 2020). The polymeric precursors start aromatization and fragmentation with temperature ramping and afterwards transform into rigidly aromatic carbon strands (Fig. 4.7 (i) & (ii)). Next, the rigid carbon strands align and form carbon “plates” due to higher entropy to the system (Fig. 1 (iii)). The final CMSMs usually result in a microstructure with imperfectly packed plates due to the kinetic restrictions (limited time at high temperature) (Fig. 4.7 (iv)). In the end cooling stage, the micropore “cells” are stacked to form a cellular structure (Fig. 4.7 (v)) in which the ultra-micropores share the “walls” between micropores.

There are four different mechanisms related to mass transfer of gas through a porous carbon membrane: Poiseuille flow; Knudsen diffusion; partial condensation/capillary diffusion/selective adsorption and molecular sieving, as it is shown in Fig. 4.8 (Hamm et al., 2017). The dominating mechanism will be dependent on the membrane properties, the permeated gases and the operating conditions such as feed temperature and pressure (Anne Julbe, 2001), and quite often more than one mechanism will contribute to the gas separation performance together. Carbon membranes with a selective surface flow mechanism (with micropores of < 20 Å) may be applied to the separation of heavy hydrocarbons (HHCs) in the petroleum industry, while carbon molecular sieve membranes with ultramicropores (3–7 Å) can potentially be used for the separation of small gas molecules that are alike in size such as CO_2-N_2, and CO_2-O_2 (i.e., post-combustion carbon capture) (Kumakiri, 2020).

4.4.3. Carbon membranes for CO_2/N_2 separation

Carbon membranes for pre-combustion carbon capture and CO_2 removal from biogas and natural gas have been critically reviewed in the previous work (Lei et al., 2020). Therefore, the main focus in this section is to discuss the status and challenges of applying carbon membranes for post-combustion carbon capture. The low feed pressure (~1 bar), the low CO_2 concentration and similar sizes like CO_2, O_2 and N_2 in the flue gas are the main challenges for post-combustion CO_2 capture. Development of high performance CMSMs with high CO_2/N_2 selectivity is of emerging interest in this application. Fig. 4.9 summarizes the gas separation performances of CMSMs for CO_2 /N_2, which clearly surpass the Robeson upper bound. To improve the separation performance of CMSMs, the pore size and distribution of CMSMs can be finely tuned by the chemical deposition method. Tseng and Itta (2012) selected poly (propylene oxide) (PPO) polymers as the segment-forming agent, and applied the self-deposition method to adjust the pore structure of CMSMs, The modified PPO/polyimide (PI)-derived CMSMs presented CO_2 permeability of 1318.2 ± 37.6 Barrer and a CO_2/N_2 selectivity of 156.4, respectively.

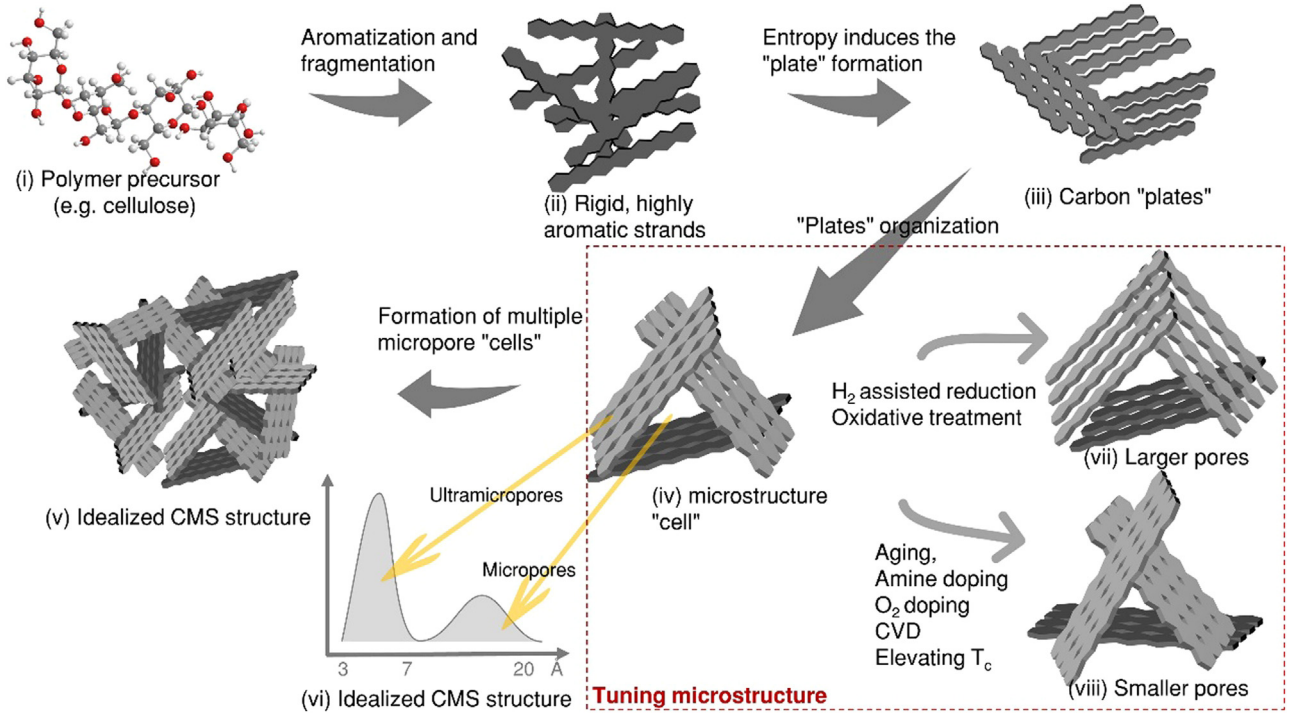

Fig. 4.7. Illustration of pyrolysis mechanism from a cellulosic precursor to CMSMs (Lei et al., 2020). (For interpretation of the references to color in this figure legend, the reader is referred to the web version of this article.)

The porous N-doped carbon as an advanced adsorbent has been investigated for CO_2 separation as the polar N-doped sites within the carbonaceous framework provide a strong and selective dipole-quadrupole interaction with CO_2 molecules. Zhu et al. (2013) prepared polymeric membranes through superacid-based method using the trimerization of aromatic nitriles with a superacid catalyst (trifluoromethanesulfonic acid, CF_3SO_3H), and the obtained precursors were further used to synthesize the N-doped CMSMs. The final carbon membranes showed a CO_2 permeability of 1149.3 Barrer and a CO_2/N_2 selectivity of 43.2, respectively. Moreover, the resorcinol–formaldehyde (RF) with high char yield and thermal stability, can be applied as nanoporous carbon membranes (NCMs). Zhang et al. prepared NCMs through pyrolysis of thermosetting RF resin blending with thermally labile F-127 in the presence of a basic catalyst. The RF resin/F-127-based NCMs have CO_2 permeabilities of 4862 ± 350.8 Barrer and CO_2/N_2 selectivity of 85.9, respectively (Zhang et al., 2014). To enhance gas separation performance of CO_2/N_2, the introduction of functional materials to the pore of CMSMs has been proven to be a versatile strategy (Hou, 2016). Ionic liquids (ILs) are promising candidates for CO_2 capture and separation due to their low vapour pressure, high thermal stability, good mechanical stability, non-toxic nature, non-flammable, designability and high CO_2 affinity (Patil et al., 2022; Tome and Marrucho, 2016). Guo et al. prepared the IL/CMS hybrid membrane spin-coating IL dissolved in ethanol at different concentrations on Matrimid®-derived CMSMs with CO_2 permeability of 675 Barrer and CO_2/N_2 selectivity of 53, respectively (Guo et al., 2020). Interestingly, the covalent triazine frameworks (CTFs)-derived materials with fluorine functional groups have been proved to significantly enhance the CO_2 sorption properties. Yang et al. reported fluorinated CMS hybrid membrane has CO_2 permeability of 2140 Barrer and CO_2/N_2 selectivity of 36, respectively (Yang et al., 2020).

Although some previous work reported the evolution mechanism of polyimide-based precursors to carbon membranes, the design and synthesis of novel polyimide precursors are still required to fabricate high-performance carbon membranes for gas separation due to the complicated rearrangement of the pyrolytic aromatic fragments of the decomposed precursors (Hazazi et al., 2019; Ngamou et al., 2019; Ogieglo et al., 2019; Pérez-Francisco et al., 2020). Deng et al. synthesized new binaphthol-6FDA polyimide precursors and pyrolyzed into the CMS membranes. The binaphthol-6FDA polyimide-derived CMSMs have CO_2 permeability of 2674 Barrer and CO_2/N_2 selectivity of 37.1, respectively (Deng et al., 2021). It is well-known that the gas separation performance of CMSMs is highly dependent on the intrinsic property of polymer precursors, so the pyrolysis of polymeric precursors comprising thermally-stable microporous fillers has been promising as a sample approach to improve gas separation performance of CMSMs (Li et al., 2019). Chuah et al. (2021) fabricated mixed matrix carbon membranes (MMCMs) including SAPO-34 zeolites have CO_2 permeabilities of 2248 ± 4 Barrer and CO_2/N_2 selectivity of 33.2 ± 0.7, respectively. Moreover, the MMCMs with activated carbon (YP-50F) presented a high CO_2 permeability of 1833 Barrer and a CO_2/N_2 selectivity of 30.4, respectively (Chuah and Lee et al., 2021). Yang et al. prepared polyimide/sepiolite derived MMCMs have CO_2 permeability of 6711.5 Barrer and a CO_2/N_2 selectivity of 30.4, respectively (Yang et al., 2021). Overall, it can be found that CMS membranes have been proven attractive for post-combustion carbon capture due to their rigid, typical tunable and bimodal pore structure, which could effectively transport CO_2 molecules.

4.4.4. Techno-economic feasibility of CMSMs for post-combustion carbon capture

The current and fairly established technology (such as chemical absorption) allows for effective CO_2 capture from flue gas with a low concentration at low temperatures, but it is expensive owing to the large size of columns and equipment installation. Additionally, thermal efficiency is also reduced. Utilizing membrane separation units could be a different approach. A carbon membrane separation unit was designed to be integrated into typical post-combustion power plants, as it was previously described (He et al., 2009). To ensure a significant reduction in emissions and to reduce the future costs for compression and transport, the criteria of purity and recovery of CO_2 from flue gas are highly required, generally higher than 90 % (Yang et al., 2009). The CO_2 content in flue gas is low (10–20 %), rendering it difficult to

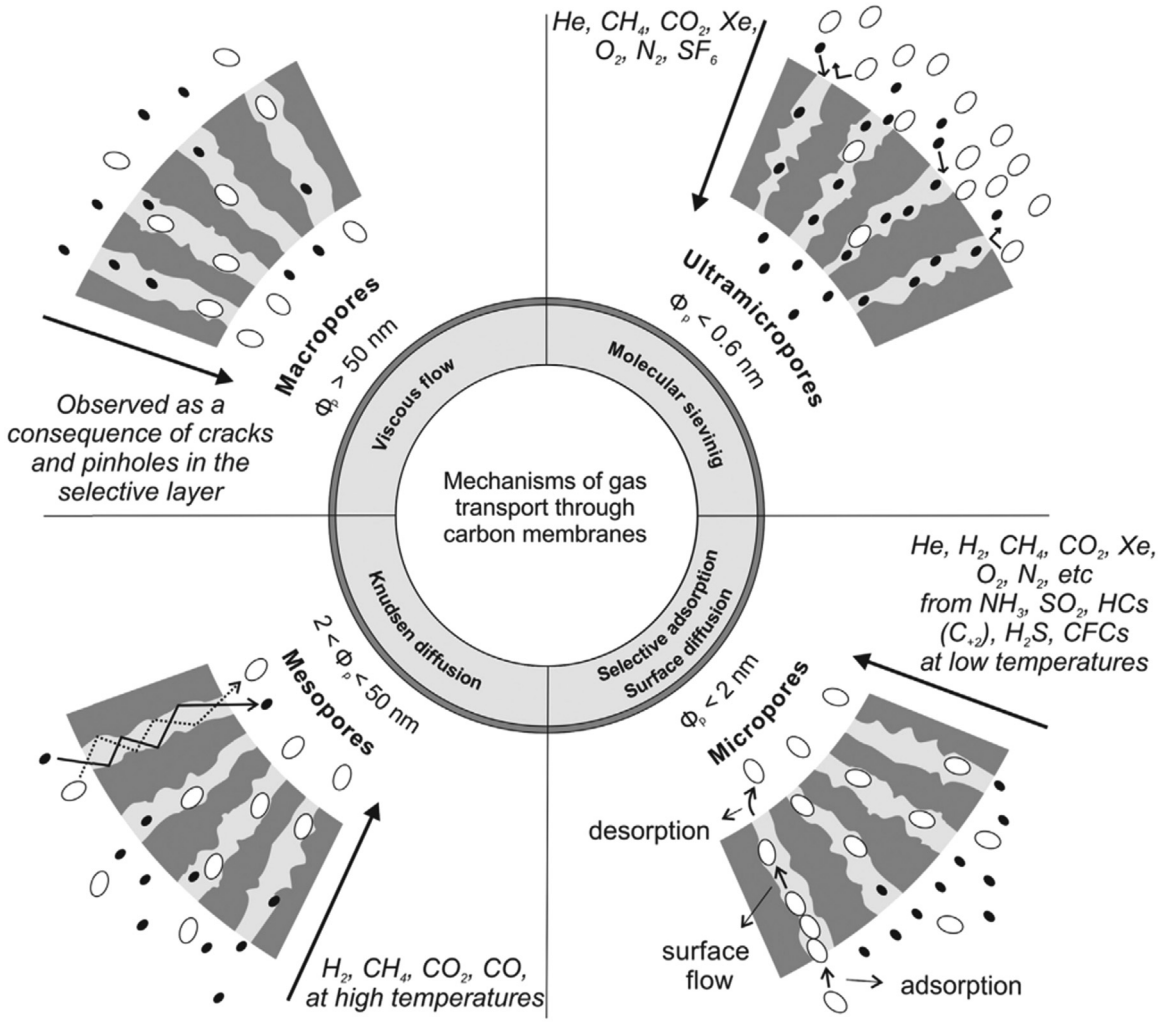

Fig. 4.8. Different mechanisms of gas transport through carbon membranes (Hamm et al., 2017). (For interpretation of the references to color in this figure legend, the reader is referred to the web version of this article.)

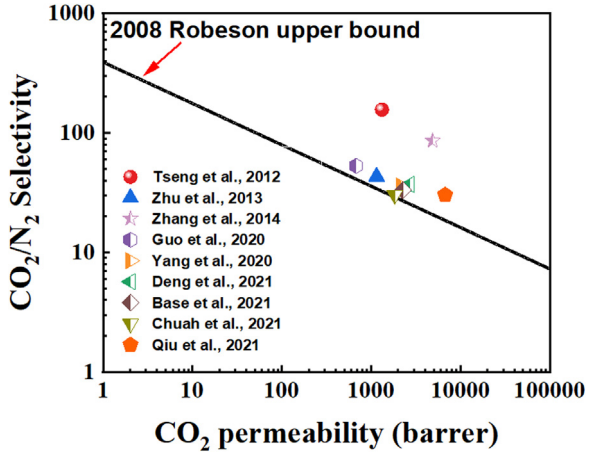

Fig. 4.9. The CO_2 /N_2 separation performances of different CMSMs. (For interpretation of the references to color in this figure legend, the reader is referred to the web version of this article.)

accomplish through a single-stage membrane technique. Consequently, implementing a multi-stage membrane arrangement becomes necessary, and two-stage membrane systems have been reported to be the effective configuration to achieve the separation target (Xu et al., 2019; Yang et al., 2009). For the purpose of creating a driving force for CO_2 diffusion, several studies on the techno-economic feasibility analysis of a process by combining the feed compression with the vacuum suction on the permeate side (Merkel et al., 2010; Yang et al., 2009). The operating conditions (e.g., feed temperature, feed and permeate pressures), membrane properties (CO_2 permeance, selectivity, membrane lifetime), and corresponding costs were typically reported along with representative parameters such as specific area [m^2/ ($kgCO_2$/s)], specific energy [MJ/$kgCO_2$], and CO_2 capture cost [$/ton$CO_2$] (energy cost and capital cost for membranes, pumps, compressors, etc.).

Favre et al. outlined the major difficulties in applying membranes for post-combustion capture and indicated the ranges of operating conditions within which the membrane process can compete with cutting-edge absorption technology (Favre, 2007). Due to the significant energy consumption of the compression step, it has been claimed that the membrane process with feed compression can only be competitive when the inlet CO_2 content is more than 20 %. Benchmarking was performed by Roussanaly et al. to determine the required CO_2 permeance and membrane selectivity to ensure the membrane process is competitive with absorption technology (Roussanaly et al., 2016). It was revealed that simple membrane process configurations and more sophisticated configurations, including recycling or sweep could be economically competitive with the absorption technology. He et al. explored the techno-economic feasibility of hollow fiber carbon membranes which is based

on the carbonization of deacetylated cellulose acetate (He and Hägg, 2011). It was reported that the CO_2 recovery of 67 % and the CO_2 purity of 88 % could be achieved with a total required membrane area of 1.62×10^7 m^2 and a total compressor duty of 1.37×10^5 kW [1]. In addition, He et al. also contrasted the feasibility of single-stage membrane process and two-stage cascade membrane process. It was indicated that the single stage membrane process cannot achieve high CO_2 purity and CO_2 recovery simultaneously employing such hollow fiber carbon membrane whereas the two-stage cascade membrane technology can be economically competitive with the chemical absorption method (He and Hägg, 2011).

4.4.5. Future perspectives

Although carbon membrane technology is considered one of the energy-efficient processes for CO_2 separation, the application of CMSMs for post-combustion CO_2 capture is still challenging: (1) the relatively low CO_2 permeance compared to polymeric membranes, which requires a large carbon membrane area and thus increases the membrane unit cost significantly; (2) many CMSMs are sensitive to water vapour existing in flue gas, which may reduce the membrane durability and lifetime; (3) difficult in the flat-sheet carbon membrane upscaling and production cost as well as the brittleness of carbon structure. To address these challenges, the development of hydrophilic, ultra-thin supported carbon membranes or flexible asymmetric CHFMs should be pursued in future work. It should be noted the advantage of its strong mechanical strength may direct the operation of carbon membranes for CO_2 capture at a relatively higher feed pressure, but the optimal operating conditions should be identified based on cost minimization by balancing capital expenditure and operation cost.

4.5. Facilitated transport membranes

In facilitated transport (FT) membranes, the transport of CO_2 molecules can be enhanced through specific reversible reactions (Li et al., 2015). Many studies have shown that the transport of CO_2 occurs in the form of carbamate and bicarbonate in FT membranes (Caplow, 1968). In most cases, water is required in FT processes (Chiwaye et al., 2021). The reaction equations for primary amine, secondary amine, and tertiary amine with CO_2 are given in Reaction 4.7-4.11 below.

$$RNH_2 + \frac{1}{2}CO_2 \leftrightarrow RNHCOO^- + RNH_3^+ \quad \text{(Reaction 4.7)}$$

$$RNH_2 + H_2O + CO_2 \leftrightarrow HCO_3^- + RNH_3^+ \quad \text{(Reaction 4.8)}$$

$$R_2NH + \frac{1}{2}CO_2 \leftrightarrow R_2NCOO^- + R_2NH_2^+ \quad \text{(Reaction 4.9)}$$

$$R_2NH + H_2O + CO_2 \leftrightarrow HCO_3^- + R_2NH_2^+ \quad \text{(Reaction 4.10)}$$

$$R_3N + H_2O + CO_2 \leftrightarrow HCO_3^- + R_3NH^+ \quad \text{(Reaction 4.11)}$$

The scheme of FT processes is illustrated in Fig. 4.10. In comparison to conventional polymeric membranes, where gas is transported through the membrane via a solution-diffusion model, gas transport in FT membranes involves a reversible reaction, which is depicted in Eq. (4.4) (Kim et al., 2013).

$$J_A = \frac{D_A}{l}(c_{A,o} - c_{A,l}) + \frac{D_{A,B}}{l}(c_{AB,o} - c_{AB,l}) \quad (4.4)$$

Compared to solution-diffusion based membranes, FT membranes can achieve much higher CO_2 fluxes at relatively low CO_2 concentration conditions by utilizing reversible reactions between CO_2 and carriers, as shown in Fig. 4.11. This property makes FT membranes ideal for flue gas CO_2 capture, as flue gas is usually present in large amounts and at low pressures (Chao et al., 2021; Kárászová et al., 2020). However, the phenomenon of 'carrier saturation' (Han and Ho, 2022; Li et al., 2015)

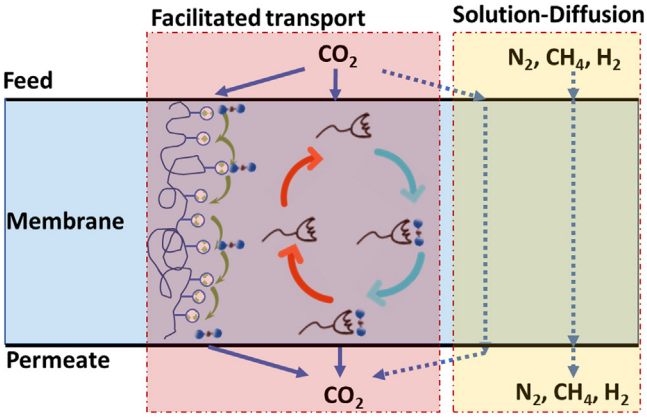

Fig. 4.10. Gas transport through the facilitated transport membrane.

causes a gradual reduction in CO_2 permeance as the CO_2 partial pressure increases in the feed. As a result, the CO_2 separation performance of FT membranes is sensitive to the CO_2 partial pressure.

4.5.1. Mobile carrier

Mobile carriers have been intensively studied for CO_2 separation purposes, with representative examples including alkaline solutions (e.g., KOH) (Ansaloni et al., 2015), amino acid salts (e.g., GlyK, ProK) (Dai et al., 2019a; Dai et al., 2019b), small amine molecules (e.g., MEA, DEA) (Teramoto et al., 1996), and ionic liquids (ILs) (Klemm et al., 2020) (Fig. 4.12). In the early stage of FT membrane research, these mobile carriers were incorporated into supported liquid membranes (SLMs) (Bao and Trachtenberg, 2006; Peng et al., 2022; Teramoto et al., 1997), which exhibited rather high intrinsic CO_2 separation performance for CO_2/N_2, CO_2/CH_4, and CO_2/H_2 separations. However, the stability of SLMs is always a serious issue, especially under high operational pressure conditions. Additionally, reducing the thickness of an SLM to ensure a feasible CO_2 flux across the membrane is difficult. As a result, mobile carrier-based SLMs are less competitive in practical CO_2 separation applications.

On the other hand, mobile carriers are also widely used in TFC membranes for CO_2 separation applications (Tong and Ho, 2017a). Exceptional separation performances have been obtained for many of these materials. However, similar to SLMs, long-term stability is always an issue, as the small molecules may easily leach out of the membrane, especially if there is water vapour condensation on the surface of the membranes.

4.5.2. Fixed site carrier

Fixed site carrier (FSC) membranes are a group of polymers with functional groups that can undergo reversible reactions with CO_2 to facilitate its transport (Deng et al., 2009; He et al., 2017a). Normally these materials contain different kinds of amine groups, including primary amine, secondary amine, and tertiary amine (Fig. 4.13). In some cases, -COOH group can also function as an effective carrier for CO_2 transport (Zhao et al., 2006). Compared to mobile carrier FT membranes, FSC membranes typically exhibit better stability. On the other hand, since many FSC membranes contain a large amount of amine groups, they can be rather brittle in the dry state due to strong hydrogen bonding, and their mechanical strength is not good. Therefore, in many cases, a second polymer is blended with the FSC polymer to improve its mechanical strength and sometimes to promote water uptake as well (Han et al., 2020; Han and Ho, 2021a; Han et al., 2018).

Fig. 4.13 presents a few representative FSC polymers. In principle, for primary and secondary amines, with the help of water vapour, one mole of amine could react with more than one mole of CO_2, thus making it a very promising option for CO_2 separation. However, it has been found that tertiary amines only react with one mole of CO_2, even with

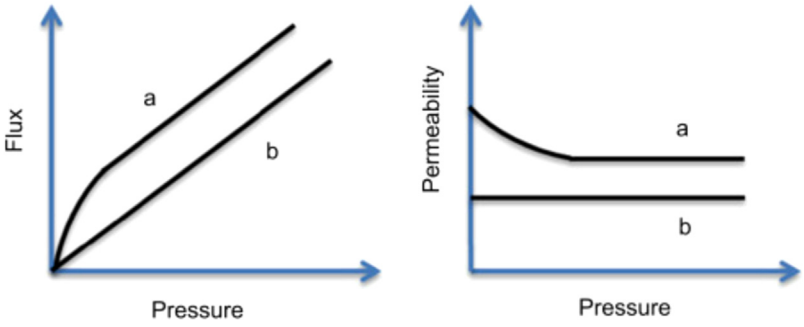

Fig. 4.11. FT membrane presents higher CO_2 flux at lower CO_2 partial pressure conditions but the CO_2 permeance gradually reduces due to carrier saturation. (For interpretation of the references to color in this figure legend, the reader is referred to the web version of this article.)

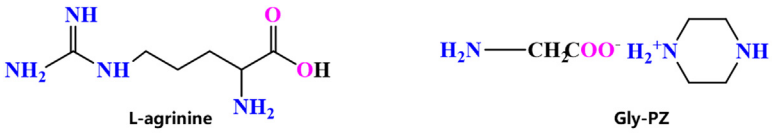

Fig. 4.12. Typical mobile carrier used in FT membranes, reproduced from (Zhang et al., 2021). (For interpretation of the references to color in this figure legend, the reader is referred to the web version of this article.)

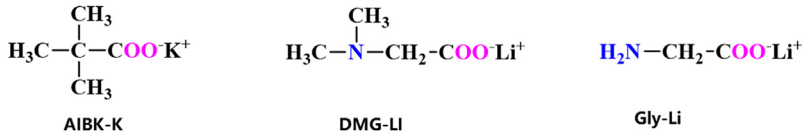

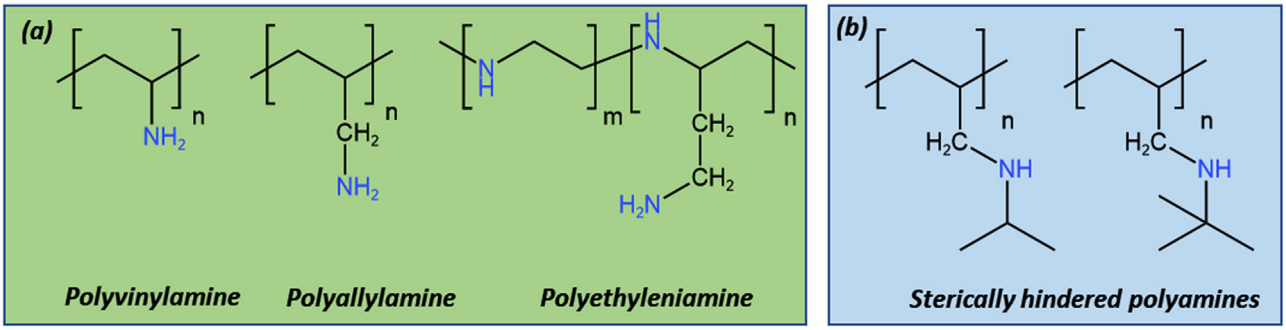

Fig. 4.13. **(a)**Typical fixed site carrier materials used in FT membranes, (b) sterically hindered membranes exhibited higher CO_2 separation performances, reproduced from (Han et al., 2020). (For interpretation of the references to color in this figure legend, the reader is referred to the web version of this article.)

one mole of tertiary amine. In some cases, if the amine is sterically hindered, it can be more effective than primary and secondary amines (Tong and Ho, 2017b). There have been several reviews discussing this topic (He, 2021; Rafiq et al., 2016; Tong and Ho, 2017a).

4.5.3. *Hybrid membranes*

Compared to the pure mobile carrier or fixed site FT membranes, in many cases, both mobile carrier and fixed site carrier can be employed in FT membranes. The polymeric phase works as a hosting matrix for mobile carriers (Han and Ho, 2021b). In addition, to improve the mechanical strength of the membrane, the hosting matrix is sometimes crosslinked (Deng and Hägg, 2015; Han et al., 2019b). Another category of facilitated transport hybrid membranes includes those membranes containing functionalized nanoadditives (Nithin Mithra and Ahankari, 2022). Compared to conventional mixed matrix membranes (MMMs), which are fabricated by blending nanoadditives and polymer phases together, facilitated transport membranes contain nanoparticles with amine-functionalized groups. Representative nanofillers include MOFs (Kim, Jiyoung et al., 2016; Wu et al., 2014), GO (Dong et al., 2016), and CNT (Ansaloni et al., 2015; Saeed et al., 2017). Additionally, hybrid membranes containing three different components are also being studied (Guo et al., 2019), which typically consist of a liquid phase, a polymer phase, and a solid phase. The liquid phase works as both facilitated transport carriers and fillers for the non-selective voids between the polymer phase and solid additives (Kalantari et al., 2020).

Many facilitated transport membranes are made using thick films with a thickness in the range of dozens of micrometers, while others have been fabricated as thin-film-composite (TFC) membranes with feasible CO_2 permeances. Dip-coating is the most commonly used method to fabricate FT TFC membranes, with both flat-sheet and hollow fiber geometries (Dai et al., 2016). Other methods, such as interfacial polymerization (Zhao et al., 2006), knife casting (Pate et al., 2022), and spin-coating (Zhang et al., 2018) have also been reported. The thickness of TFC membranes varies a lot. In principle, the thickness of the selective layer should be as thin as possible to ensure a high CO_2 flux across the membrane. Interestingly, for facilitated transport membranes, as there is a need for a proper carrier in the selective layer, it is sometimes found that membranes with thinner selective layers present lower CO_2 permeances (Kim et al., 2004), which is different from conventional membranes based on solution-diffusion model.

The CO_2/CH_4 separation performances of FT membranes developed in the past few years are listed in Fig. 4.14. As can be seen from the figure, many FT membranes showed very promising CO_2 separation performances, which are far above the Upper Bound. Meanwhile, for FT TFC membranes, both high CO_2 permeance and high CO_2/CH_4 selectivity have also been documented, indicating that FT membranes are very competitive materials in CO_2 capture.

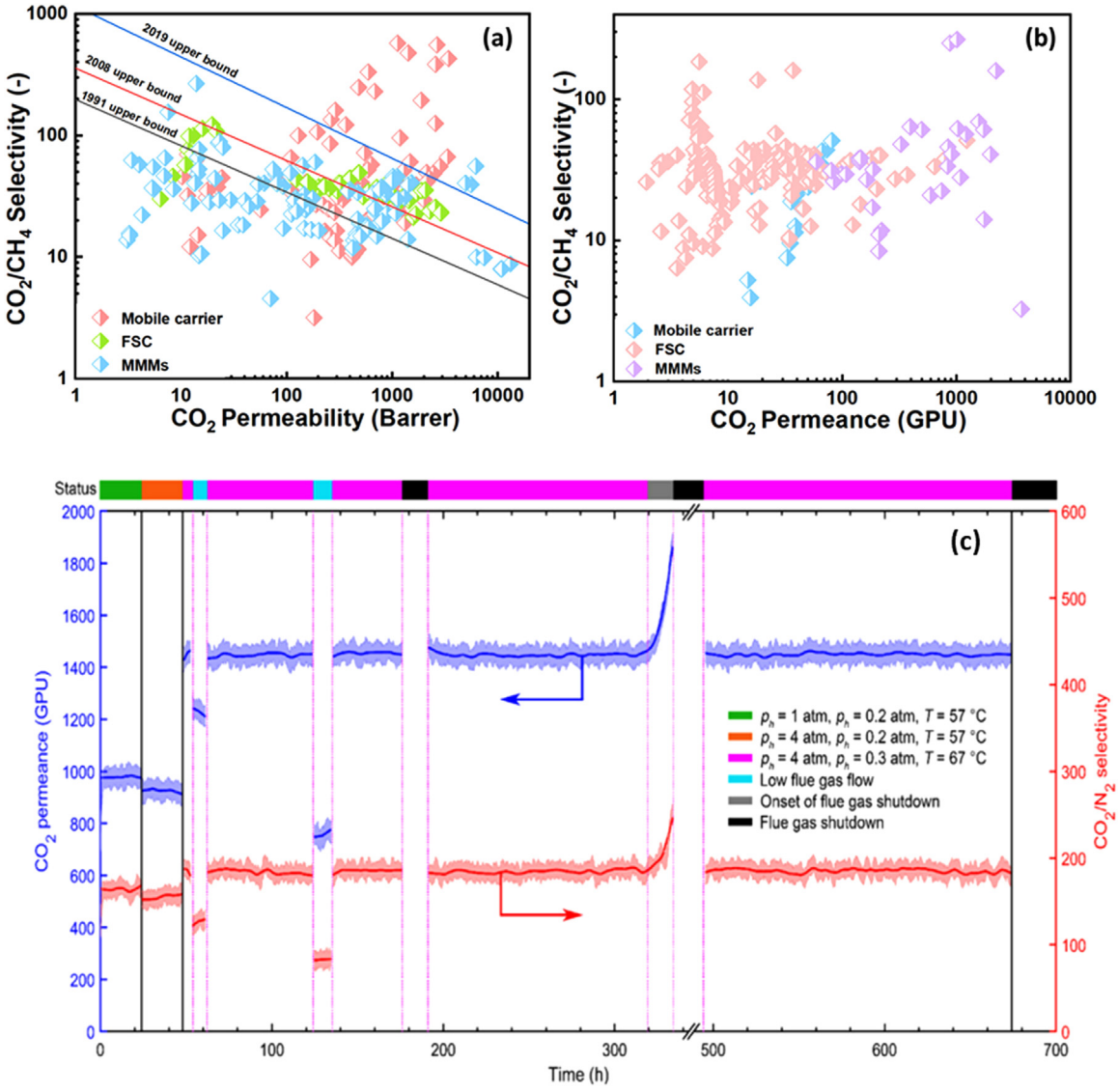

Fig. 4.14. Comparison of CO_2 separation performances of the thick film (a) and TFC FT membranes (b). Data obtained from ref (Aframehr et al., 2022; Alkhouzaam et al., 2016; Chen et al., 2012; Guo et al., 2015; Hanioka et al., 2008; Iarikov et al., 2011; Isanejad and Mohammadi, 2018; Li et al., 2010; Li et al., 2020; Liu et al., 2021; Liu et al., 2014; Mashhadikhan et al., 2020; Mubashir et al., 2018; Murugiah et al., 2018; Park et al., 2009; Peng et al., 2017; Pu et al., 2022; Qu et al., 2020; Regmi et al., 2022; Sasikumar et al., 2021; Shahkaramipour et al., 2014; Shamair et al., 2020; Swati et al., 2021; Tu et al., 2021a; Tu et al., 2021b; Wang et al., 2020; Wang et al., 2021; Wu et al., 2014; Yu et al., 2020; Zhang et al., 2021; Zhang et al., 2018; Zhang et al., 2017b; Zhang et al., 2022). (c) long-term stability performances of FT membranes tested under industrial conditions. Reproduced from ref (Han et al., 2019a). (For interpretation of the references to color in this figure legend, the reader is referred to the web version of this article.)

The long-term stability of the FT membrane has also been investigated. Unlike conventional glassy polymeric membranes, which suffer from physical aging problems (Brunetti et al., 2017; Merrick et al., 2020; Xu et al., 2014), there are few reports about physical aging of FT membranes. In addition, though the presence of impurities in the feed (e.g., SO_x and NO_x) may negatively affect the CO_2 separation performances of FT membranes, as long as the impurities are removed from the feed, the CO_2 separation performances will gradually recover to the original value (Liao et al., 2014). Ho et.al. also investigated the separation performances of FT membranes under industrial conditions and concluded that the FT membrane demonstrated excellent stability over the testing period (Han et al., 2019a).

Overall, FT membranes are promising CO_2 capture membrane materials showing exceptionally high CO_2 separation performances. Future research can be carried out to develop more efficient carriers for CO_2 transport, which could work under high CO_2 partial conditions. On the other hand, developing novel FT membranes with good RH variation tolerance can also be useful for practical CO_2 capture applications.

5. Other CO_2 capture technologies

5.1. Oxy-fuel combustion

5.1.1. Oxygen production technologies (OPTs)

This section aims to analyse oxygen production Technologies (OPTs) that are most widely utilized for oxygen production. Fig. 5.1 shows the technologies that are discussed in this work and divided into conventional OPTs: Cryogenic Distillation and Pressure Swing Adsorption, and novel OPTs: Membranes, Chemical Looping Air Separation and electrochemical water splitting technologies.

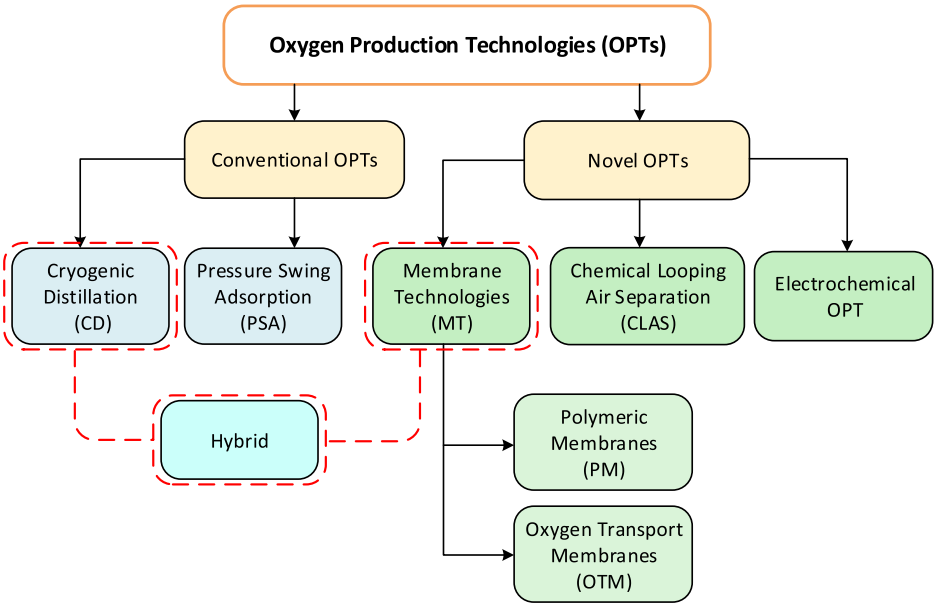

Fig. 5.1. Main oxygen production technologies for oxyfuel combustion process. (For interpretation of the references to color in this figure legend, the reader is referred to the web version of this article.)

Table 5.1
Main advantages and disadvantages of CD (Agrawal and Herron, 2000; Cao et al., 2016; Chen and Yu, 2021; Smith and Klosek, 2001; Zhu et al., 2006).

Advantages	Disadvantages
Mature and reliable technology suitable for large-scale air separation with high O_2 volume production	The air compression and fractional distillation of its constituents are very energy-intensive, accounting for around 85 % of the total energy consumption in the ASU (Zhu et al., 2006)
Cryogenic air separation units produce oxygen with a purity of 99.5 % by volume at an oxygen recovery rate of 97.85 % (Agrawal and Herron, 2000)	The technique results in a 3–4 % energy penalty and the capital investment for the CAS technique contributes to around 14 % of the overall oxy-fuel plant cost (Cao et al., 2016)
Cryogenic technology can also produce high-purity nitrogen as a useful byproduct stream at a relatively low incremental cost (Smith and Klosek, 2001)	Inappropriate for processes requiring fast startup and shutdowns
Established technology	large units with a large physical footprint
	Not profitable for processes that consume small amounts of oxygen (Chen and Yu, 2021)
	Requires moisture pre-removal

5.1.1.1. Cryogenic distillation. The cryogenic air separation (ASU) is a traditional process for producing large quantities of oxygen, nitrogen, and argon as gaseous or liquid. The technology is considered one of the most developed (Wu et al., 2018) and feasible methods for high-volume oxygen production that is required for the oxyfuel combustion process (Yadav and Mondal, 2022). The idea behind the technology is to use fractional distillation at low pressure and temperature to separate oxygen (with a purity of 99.5 %) from air elements based on their different boiling temperatures. The most important design parameters of the distillation column are the number of stages, feed stage, and reflux ratio. These parameters are selected based on distillation requirements. Table 5.1 shows the main advantages and disadvantages of the cryogenic air separation method. One added benefit is that cryogenic air separation is specifically suitable for oxyfuel technology due to the high O_2 volume production. Oxy-combustion requires high O_2 production capacity; for example, a 500 MWe coal-fired oxy-combustion power plant requires 9000 - 10,000 tO_2/d (Chorowski and Gizicki, 2015; Higginbotham et al., 2011). On the other hand, one of the main drawbacks of the cryogenic air separation unit is high energy intensity, as mentioned earlier. The energy demand for the system oxygen production is about 240 kWh/tO_2 resulting in an overall efficiency drop of a power plant of around 8–10 % (Davison, 2007). CD ASU at lower oxygen product purities, the separation of oxygen and nitrogen is only required, which is relatively easier than the separation of oxygen and argon. Fig. 5.2 illustrates that the rapid decrease in separation energy required takes place as the product oxygen purity is decreased from 99.5 % to 97.5 %, corresponding to the

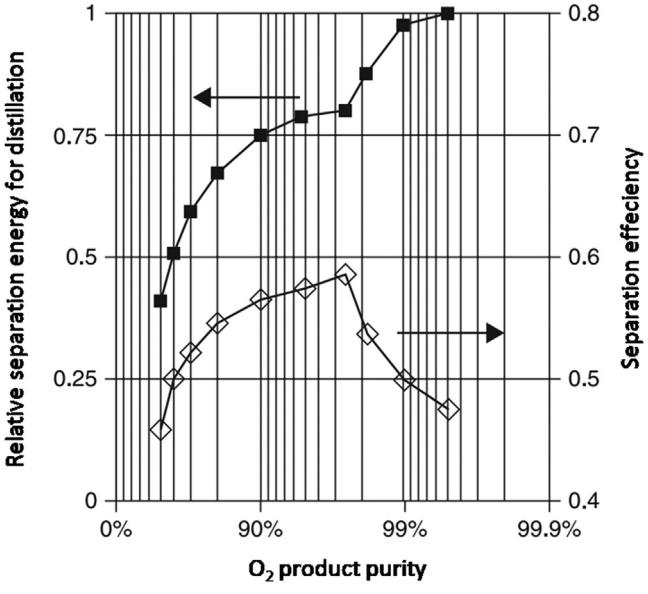

Fig. 5.2. Effect of oxygen purity on ASU separation energy (Prosser and Shah, 2011). (For interpretation of the references to color in this figure legend, the reader is referred to the web version of this article.)

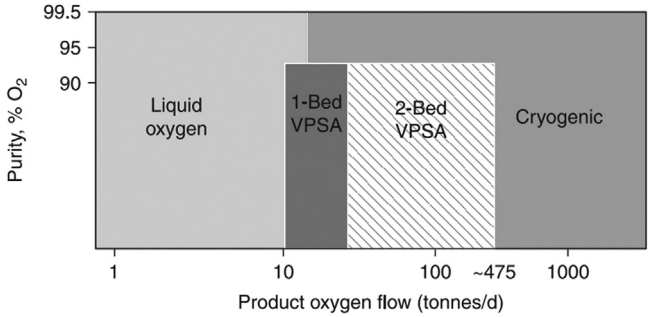

Fig. 5.3. PSA Oxygen supply system typical economic ranges (Prosser and Shah, 2011). (For interpretation of the references to color in this figure legend, the reader is referred to the web version of this article.)

change from oxygen–argon separation to an oxygen-nitrogen separation and the switch to an improved low purity oxygen process (Shash, 2011).

Cryogenic technology has greatly contributed to scientific research, specifically for oxyfuel combustion (Scaccabarozzi et al., 2016; Xiong et al., 2011, 2012; Ziółkowski et al., 2013). Beysel G. found that the energy consumption to produce O_2 with a purity of 95 % instead of 99 %, can reduce the energy consumption from 245 to 175 kWh/ton (Beysel). Tranier J. et al. reported that if the oxygen purity up to 95 % is acceptable, then the auxiliary power consumption of oxygen production can be reduced from 350 to 200 kWh/ton of oxygen (Tranier et al., 2011). Šulc and Ditl (2021) obtained a relation between energy consumption per ton of oxygen and cryogenic plant capacity and reported that the specific energy consumption per ton of oxygen remains constant up to a value of 200 kWh/t of oxygen. Overall, the power consumption of the cryogenic air separation unit to produce O_2 of 95 % purity varies between 184 and 260 kWh/tO_2 (Chorowski and Gizicki, 2015; Skorek-Osikowska et al., 2015; Ströhle et al., 2009).

Despite the widespread of cryogenic air separation units in industrial use and their major benefits, the high energy demands of cryogenic distillation commonly contribute to over 50 % of plant operating costs reported by Li and Bai (2012a). And S. García-Luna reported that cryogenic distillation is responsible for 54.42 % of the total power consumption of plant net electric power of 242.24 MWe to provide the required amount of oxygen with 95 % purity (García-Luna et al., 2022). However, R. López, based on techno-economic analysis, found that the use of cryogenic ASU makes oxy-coal fired plants unattractive for inversion due to its high total equipment plant cost (López et al., 2016).

5.1.1.2. Pressure swing adsorption (PSA). Pressure swing adsorption (PSA) is a separation method that is much newer as compared to cryogenic ASU. The first PSA technology for oxygen enrichment using nitrogen-selective zeolite was designed by Skarstrom and Attorney (1958). PSA devices take atmospheric air into a pressurized tank, a sorbent that is filled inside the tank. Zeolites are typically used and can selectively adsorb nitrogen while allowing oxygen gas to pass depending on the chosen sorbent dipole that has been created under high pressure (Ruthven and Farooq, 1990). After a certain volume of air has been separated, the adsorption sorbent will become saturated and eventually require regeneration. The adsorbent is regenerated by blowdown and a low-pressure purge using a part of the oxygen that was produced. The PSA has found use in medium and small-scale productions including industrial and health care. The performance of the adsorption system depends highly on the properties of adsorbents including: sorbent selectivity, adsorption capacities, sorption and desorption kinetics, and regeneration method (Yang et al., 2002).

One of the main drawbacks of PSA is the low oxygen purity, as shown in Fig. 5.3. Whereas PSA devices are best suited for processes that do not require extremely high purities of oxygen. Since the output of oxygen is largely controlled by the bed size, costs will rise drastically when higher volumes of oxygen are required. In addition, the installation of multiple volume PSA plants is generally required for higher capacities, as shown in Fig. 5.3. However, due to economies of scale, there is a practical limit above which cryogenic supply becomes more economically attractive.

Table 5.2
Main advantages and disadvantages of PSA (Banaszkiewicz et al., 2014; Cao et al., 2016; Smith and Klosek, 2001; Zhao et al., 2015)

Advantages	Disadvantages
Oxygen production, typically approximately 300 ton/day (Banaszkiewicz et al., 2014)	Limited scalability
Quick installation and start-up (minutes)	Not profitable for processes that consume small amounts of oxygen (Chen and Yu, 2021)
Low capital investment	Low Oxygen purity is typically 93–95 vol. % (Smith and Klosek, 2001)
	Energy penalty for large-scale applications is considerably high (Zhao et al., 2015)
Established technology	Pretreatment is required to maintain the performance of the major adsorbents in the system, which makes process design more complicated
Low waste generation, due to adsorbent recycling	It is not possible to obtain other separation products (nitrogen, argon)

Another disadvantage of this method is that it has limited adsorbent capacity for large-scale applications (Prosser and Shah, 2011). The rest main advantages and disadvantages of PSA are summarized in Table 5.2. The reported literature shows that from an energy consumption perspective, the oxygen production for a small unit using the vacuum-pressure-temperature swing adsorption technology is between 500–888 kWh/ton of oxygen (Banaszkiewicz and Chorowski, 2018).

5.1.1.3. Membrane technology for oxygen production. Membrane separation is simpler than the cryogenic separation method. One such alternative approach is to use polymeric membranes or ion transport membranes (ITM). The difference between these two techniques is that polymer membranes are used for applications at ambient temperature, while for high-temperature applications, inorganic solid-oxide ceramic materials are mainly used [23]. The differences between the two approaches are shown in Table 5.3. Membrane technology has quick start-up times and operates at near ambient conditions. In contrast, capital costs with membrane systems increase linearly with the output volume desired. However, compared to cryogenic distillation and PSA, they are less complicated since they do not require regenerative steps (Murali et al., 2013).

A general polymeric membrane-based air separation is the feed gas that is passed across the membrane surface under a pressure driving force. The permeate is the gas that penetrates through the membrane and comes out as the low-pressure stream. The retentate is the remaining gas that exits as the high-pressure stream (Wijmans and Baker, 1995). Both permeate and retentate can be used if they meet the desired product purities (Murali et al., 2013). Polymeric membranes have received the most attention due to their advantages: high selectivity between gases, good mechanical properties, and economical processing capability. Polymeric membranes are often preferred to inorganic or ceramic membranes as they have a low environmental impact, are easy to incorporate into large-scale modules, and have the lowest capital costs among the different membranes [35]

Polymeric membranes are characterised by two factors: permeability and selectivity. The higher the permeability, the lower the selectivity, and vice versa (tradeoff) (Freeman, 1999). Consequently, the tradeoff between permeability and selectivity limits the use of polymeric membranes in large-scale applications (Robeson et al., 2015). A purity of 90 % with one stage polymer membrane system is not practically achievable currently. A purity of 90 % O_2 can be achieved by using two and three stages, depending on the type of membrane that is used

Table 5.3
Main advantages and disadvantages of MT (Bai et al., 2021b; Hofs et al., 2011; Hosseini et al., 2015; Sidhikku Kandath Valappil et al., 2021).

Membrane separation technology	Advantages	Disadvantages
Polymeric	Lowest capital costs among the different membranes (Hosseini et al., 2015) Low environmental impact They can easily be modified and fabricated according to the specified requirements (Hofs et al., 2011) have competitive selectivity and permeability with ceramic and metallic counterparts	less competitive in improving oxygen purity in large-scale production compared with other conventional technologies Low oxygen purity ~ 40 % (Sidhikku Kandath Valappil et al., 2021)
OTM	High chemical, mechanical and thermal stabilities can obtain 99.99 % high purity oxygen (Bai et al., 2021b)	Very Brittle More expensive than organic polymer materials (Sidhikku Kandath Valappil et al., 2021)

(Adhikari et al., 2021). Up-to-date large-scale oxy-fuel combustion process, the feed stream is composed of an oxygen concentration higher than 21 % but lesser than 40 % in the best cases (Kianfar and Cao, 2021; Sidhikku Kandath Valappil et al., 2021).

Oxygen Transport membrane OTM or ion transport membrane (ITM) is an inorganic oxide ceramic material that is solid at the molecular level and acts as a membrane by allowing oxygen ions to pass through the ceramic crystalline structure. To conduct oxygen, the temperature of the OTM must be maintained above 800 °C and an oxygen partial pressure gradient must be applied across the membrane (Boot-Handford et al., 2014). The significant advantage of this approach is the potential reduction of capital cost and energy demand (Rastogi and Nayak, 2011).

Several studies (Engels et al., 2010; Stadler et al., 2011) have been conducted to reduce the energy consumption of the ASU by investigating the use of high-temperature OTM technology for oxygen production as an alternative to conventional cryogenic distillation methods. Reported literature shows that the OTM approach can be integrated into the front-end of combustion equipment, which results in the effective energy demand reduction to 147 kWh/ton of oxygen (Bai et al., 2021b). Normally, the conventional process has an associated consumption of 201.38 kWh/ton O (Dillon et al., 2005), whereas literature estimated a decrease in power consumption ranging between 85–362 kWh/ton of oxygen (Dillon et al., 2005; Shin and Kang, 2018). While some researchers maintain that OTM technology may replace cryogenic ASU in the long term because this alternative achieves energy and economic savings of 0.5–9 and 10.5–17.5 % (Portillo et al., 2019). Compared to cryogenic ASUs, a small-scale OTM unit consumes 60 % less energy and costs 35 % less to produce 500 kg O_2/day (Bernardo et al., 2009).

Integration of membrane and cryogenic technologies has recently attracted attention (Chen and Yu, 2021; Janusz-Szymańska and Dryjańska, 2015), as many researchers tried to evaluate the feasibility of oxy-combustion-based plants utilizing air separation units (ASUs) via cryogenic or membrane technology (Castillo, 2011; Pfaff and Kather, 2009; Skorek-Osikowska et al., 2015). Considering the implementation of a hybrid membrane-cryogenic ASU for further power reduction, Szymanska et al. (Janusz-Szymańska and Dryjańska, 2015) Demonstrated that the cryogenic ASU's reduced power usage for 99.8 % oxygen purity was 179 kWh/tO_2. In addition, Skorek-Osikowska et al. (2015) reported that the hybrid membrane cryogenic oxygen separation method has a 1.1 % higher net efficiency than the conventional cryogenic ASU.

5.1.1.4. Chemical looping. Chemical Looping Air Separation (CLAS) is based on the oxidative and reductive reactions of two interconnected reactors: air reactor and fuel reactor, which are oxidized to CO_2 and water vapour. The reduced oxygen carrier (typically metal oxide) is then transported to the air reactor where it reacts with the oxygen to reform the original metal oxide for recirculation back to the fluidized reactor (Mattisson, 2013). CLAS has been developed from chemical looping combustion (CLC), which has several challenges including the used material, mechanical stability and oxygen transfer rates, the temperature at which the oxygen carrier is active, reactor capacity, and solid handling (Shah et al., 2015; Wu et al., 2018). Yet, on the other hand, CLAS is considered a promising approach capable of reducing the cost of oxygen production required for oxyfuel combustion technology (Cormos, 2020; Zhou et al., 2015b).

Shah et al. (2013) studied the integrated chemical looping air separation (ICLAS) modes with oxy-fuel coal-fired power plants. The results show that the specific energy required to produce oxygen in an ICLAS using flue gas (ICLAS[FG]) is 71 kWh/ton (CH integration) and 69 kWh/ton (solar integration) and in an ICLAS using steam (ICLAS[S]) and solar integration of 64 kWh/ton (without NSC) and 43 kWh/ton (with NSC). While in a conventional cryogenic ASU of 415 kWh/ton (99 % purity) and 330 kWh/ton (95 % purity), in an advanced cryogenic-based ASU (CASU) of 250 kWh/ton (99 % purity) and 200 (95 % purity). Zhou et al. (2015a) reported that by replacing a CASU with an ICLAS unit, the average reduction in the ASU power demand was up to 47 % and 76 %, respectively, for ICLAS[S] and ICLAS[FG]. Similarly, the average thermal efficiency penalty associated with the CASU, the ICLAS[S] and ICLAS[FG] units was found to be about 9.5 %, 7.5 %, and 5 %, respectively, indicating that the ICLAS[FG] unit is the most energy-efficient option for oxy-fuel plants. The levelized cost of electricity associated with the cryogenic and the ICLAS[S] and ICLAS[FG] units for the NSW fleet of coal-fired power plants were found to be about 118, 105, and 95 $/MWh, respectively.

Cai et al. (2022) developed a one-dimensional packed bed model using perovskite sorbent to investigate the CLAS operation. The power consumption was 115 kWh/ton and 161 kWh/ton at 90 % and 95 % oxygen purities, respectively, while for a 5-step cycle configuration, the power consumption was 118 kWh/ton at 95 %. Cormos (2020) demonstrated that by using manganese-based CLAS, the energy efficiency was higher than the cryogenic process by 2–3.5 net percentage points. However, it was approved that the utilization of the CLAS system in coal and lignite-based oxy-combustion and gasification power plants significantly reduce the capital investment by about 12–18 % (Cormos, 2018), and the ICLAS offers between 40–70 % lower operational expenses as compared to conventional O_2 production technologies (Zhou et al., 2016).

5.1.1.5. Electrochemical water splitting. Electrochemical separation of hydrogen and oxygen using the electrolysis process dissociate water molecule by means of oxidation-reduction reactions taking place in two electrodes: cathode and anode, and separated by a medium (electrolyte) through which the ionic species transfers from one electrode to another (Bailera et al., 2020). Lately, the interest in the promotion of hydrogen energy to decarbonize the current energy system has strongly increased and is based on the Renewable Energy Roadmap (REmap) analysis. Hydrogen share will be increased by 6 % of total final energy consumption by 2050 (Gielen et al., 2019). Fig. 5.4 shows a schematic structure of the four types of electrolysis available in the market based on the difference in the operating temperature range and the ions exchange. These types include high temperature operation as; (a) solid-oxide steam

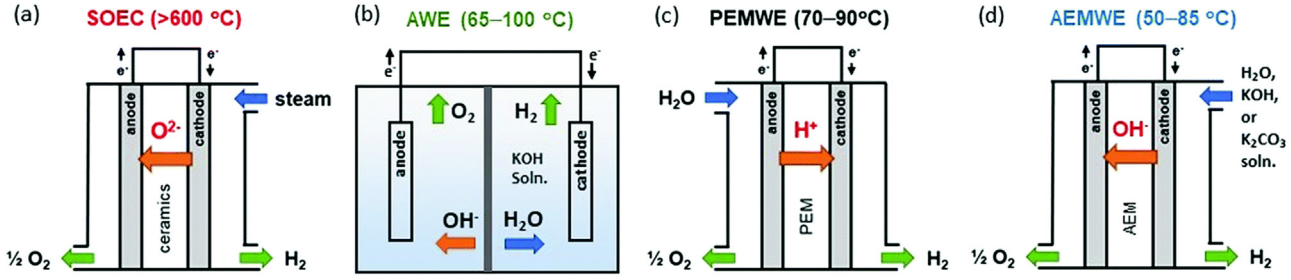

Fig. 5.4. Types of electrolysis technologies (Li et al., 2021). (For interpretation of the references to color in this figure legend, the reader is referred to the web version of this article.)

electrolyzer (SOEC) and low temperature operation as; (b) Alkaline water electrolyzer (AWE), (c) Proton exchange membrane water electrlyzer (PEMWE) and (d) Anion exchange membrane water electrolyzer (AEMWE).

Very limited publications regarding considering the potential of co-production of the energy free oxygen supplied from renewable base electrolysis for oxy-fuel combustion plants. As a reason, the high-power demand of such a process makes this option less competitive with other oxygen production methods. Yet, the efficiency of this process can be improved by using the co-product hydrogen to generate the power required for electrolysis (Iora and Chiesa, 2009).

Bailera et al. reported in different studies on hybrid power-to-gas oxy-combustion power plants where the co-product of oxygen in the water electrolysis for hydrogen production was used for the combustion (Bailera et al., 2015, 2016, 2021). The simulation of an electrolyser using Aspen Plus software that consumed 4.3–4.9 kWh/Nm^3 to produce hydrogen with integration with methanation results in an increase in the overall efficiency from 55.9 % to 67.5 % since the OPT is avoided in the oxy-coal combustion. Kezibri and Bouallou (2017) demonstrated a conceptual model of a 200 MW power supply to the electrolysis process that leads to a corresponding 155 MW of Synthetic Natural Gas (SNG) produced in a thermally integrated methanation process with an efficiency of 83.1 %. And found that by producing and storing enough amount of SNG and oxygen, an oxy-combustion power plant can be subsequently used to recover up to 480 MW of electric power as well as to produce CO_2 rich gas with an overall efficiency of 51.8 %.

5.1.2. Allam cycle

Oxy fuel combustion utilizes a pure stream of oxygen (generally > 95 %) as the oxidant for fuel combustion to achieve a product stream consisting solely of CO_2 and water vapour. The N_2 from air functions as a temperature regulator in conventional combustion; an oxidant stream devoid of N_2 can result in high flame temperatures, and this is controlled by recycling a part of the CO_2 flue gas back to the combustor. The difference in the two diluting gases (CO_2 and N_2) causes significant differences such as the density of the flue gas, heat capacity, diffusivity of oxygen and radiative properties of the furnace gases (Wall et al., 2009b). A process flow diagram of a general oxy-fuel combustion plant is shown in Fig. 5.5.

The Allam cycle, also known as the NET Power cycle or Allam-Fetvedt cycle, is an oxy-fuel based cycle which uses trans-critical CO_2 used as the thermal fluid (Allam et al., 2013a). The schematic of the cycle, as proposed by the original inventors, is shown in Fig. 5.6. The combustion chamber (6) operating at 300 bar is fed with pressurized gaseous fuel (3) and an oxidant mixture (4) of recycled supercritical CO_2 and pure O_2 from an Air Separation Unit (ASU) (27). The products (7) consisting of CO_2 and water vapour are expanded at an approximate pressure ratio of 10 in a gas turbine (9), co-fed with a bypassed coolant flow (8) of recycled supercritical CO_2 to avoid critical damage to the turbomachinery blades due to the high turbine inlet temperature. The gases (10) exiting the turbine are recuperated in a multi-stream heat exchanger (11) where the extracted heat is transferred to the incoming supercritical streams (32, 23 & 24). The cooled flue gas (12) is sent through a condenser where water (13) is eliminated, and a portion of the remaining pure CO_2 (15) stream is exported to a CO_2 processing unit (CPU) for capture, sequestration, or utilization. The rest (~95 %) is recycled (16) by compressing, cooling, and pumping to supercritical conditions. A split stream (25) is drawn to be mixed with the pure oxygen (29) from the ASU (27), forming the oxidant feed (30) to the combustion zone. The second split stream (21) is further divided (23 & 24) to form the cooling media (5 & 8) to the combustion chamber and the gas turbine, respectively.

The cycle developers evaluated the process efficiency (LHV basis) to be 58.9 % for natural gas (simulated using pure methane) and 51.4 % for coal (Allam et al., 2017). The extremely high efficiency was attributed to the difference in the thermodynamic properties of the working fluid, i.e., supercritical CO_2, which enables more energy recovery by eliminating losses typically encountered in Rankine cycles due to the phase changes (Allam et al., 2013b). While the cycle was initially developed for natural gas, it was adopted for solid fuel such as coal with some minor changes to the layout, such as the addition of a gasifier and ash filtration system upstream of the combustion chamber and flue gas desulphurization, deNO_x, and particulate removal units downstream. In addition to the high target efficiencies, the cycle claims a small plant footprint owing to the use of only a single turbine. For a power supply of 25 MW, the sCO_2 turbine is 90 % smaller than an equivalent steam turbine (Service, 2017). The Allam cycle offers 100 % carbon capture with the resulting CO_2 gas pressurized at pipeline conditions for sequestration, EOR and storage. The capital costs are expected to be lower than conventional plants without carbon capture due to the simplicity of operation (Allam et al., 2017).

The inventors have partnered with Toshiba Corporation to design the sCO_2 turbine and the oxyfuel combustor for use in the 50 MW demo plant at La Porte facility in Texas, USA, where the first run was conducted in May 2018. Planned commercialization in collaboration with multiple industrial partners has resulted in NET Power, the business venture of 8 Rivers, the inventors of the Allam cycle, announcing multiple 280 + MW scale plants at various locations across the United States and United Kingdom. With a goal of net zero emissions by 2050, each plant is capable of avoiding 1 million tons of CO_2 emissions annually.

There are, however, many challenges associated with the design components of this cycle. One such part is the heat recuperator section which handles multiple hot and cold streams. There is a large pressure gradient between the various streams, the required heat transfer area is large and the hot side may corrode the equipment as it contains CO_2 and condensing water (Scaccabarozzi et al., 2016). It is also noted that there is a significant imbalance between the heat requirement by the high pressure recycle streams and the heat supplied by the low pressure turbine exhaust, which can be corrected by adding external heat either from the ASU air compressors or the CO_2 recycle compressors into the recuperator (Allam et al., 2017). This adds to the complexity of the whole process and reduces the novelty of flexible operation. While there are several ways to provide pure oxygen to the process, the most mature technology is the cryogenic distillation of air. This is integrated

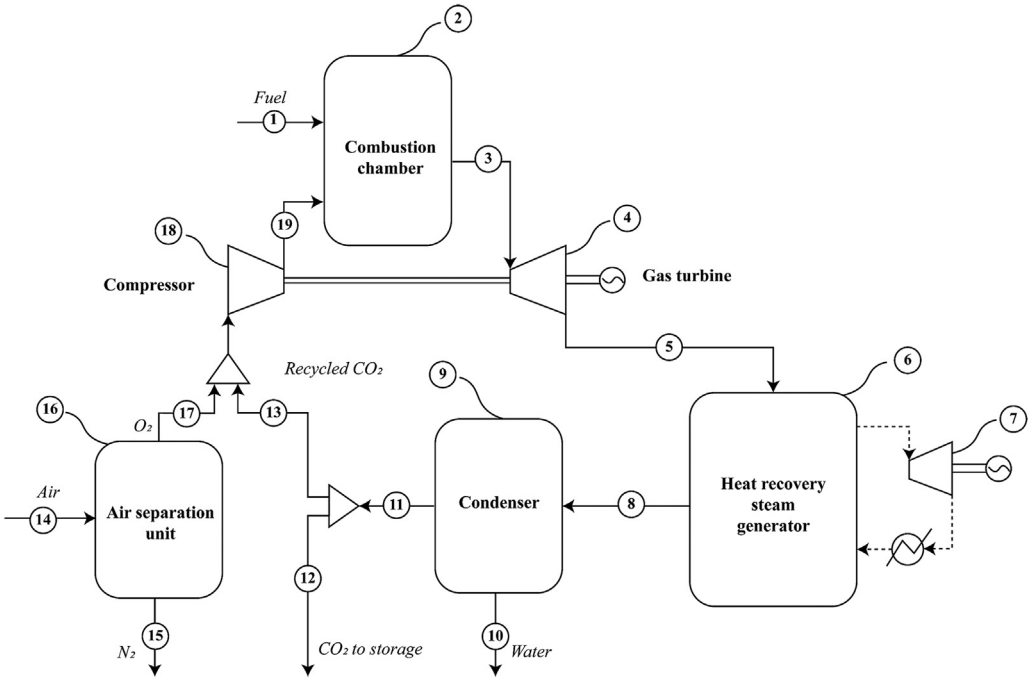

Fig. 5.5. Schematic of the general combined cycle oxy-fuel combustion process. (For interpretation of the references to color in this figure legend, the reader is referred to the web version of this article.)

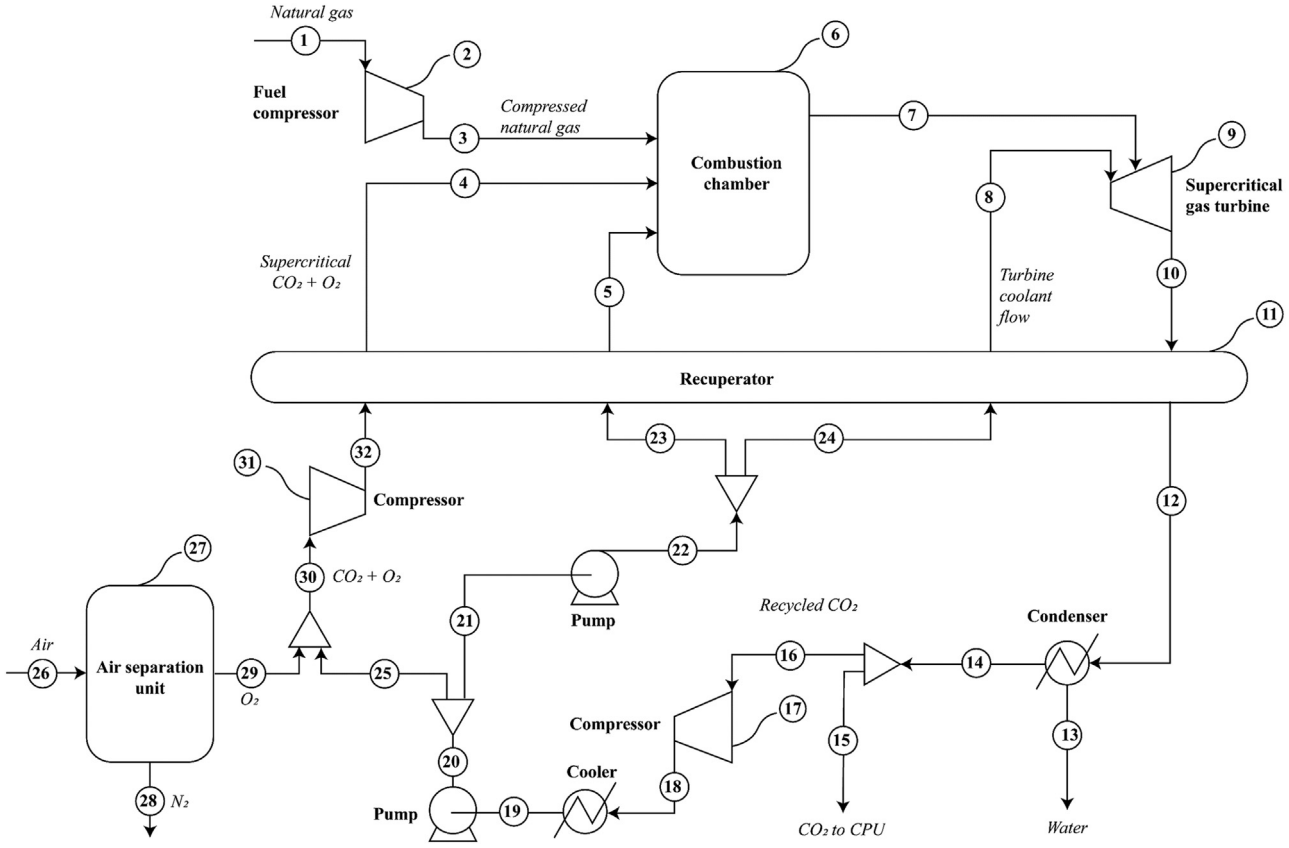

Fig. 5.6. Schematic of the natural gas fueled Allam power cycle (Allam et al., 2013b).

into the Allam cycle as a standalone unit operation. However, the compression and air separation units impose an energy penalty on the Allam cycle; when combined, they account for one-third of the gross turbine power production. Several potential modifications have been proposed in the literature to reduce this power consumption and further increase the performance of the Allam cycle.

Scaccabarozzi et al. (2016) performed a thorough thermodynamic analysis and optimization of the Allam cycle. Their study indicates the existence of an optimal range where the cycle efficiency is maximum for the turbine inlet pressure between 260 and 300 bar and turbine inlet temperature between 1100 and 1200 °C. The turbine backpressure of the cycle was increased by Zhu et al. (2019a) to keep the turbine outlet gases at near supercritical value so that all gas compressors can be eliminated and replaced by pumps, thus increasing the performance by 2.15 % at a turbine inlet temperature (TIT) of 700 °C and 2.96 % at a TIT of 900 °C. This modified process, also known as the Allam-Z cycle, also introduced the utilization of cold energy of liquified natural gas (LNG) and liquid O_2 into the cycle, but the performance enhancement was subject to the TIT not being higher than 900 °C. While the substitution of multi-stage adiabatic compression with centrifugal pumps does decrease power consumption, it also requires extreme cooling and liquefaction of the flue gas. Chan et al. (2021) proposed to do this by utilising the cold energy of LNG through a series of condensers and chillers. This, however, leads to the demand for an excessive amount of LNG (87.5 kg/s), far beyond the actual amount required for combustion (2 kg/s). Accordingly, the authors propose to send the regasified natural gas (85.5 kg/s) to other potential end users. A secondary source of power output was included as a natural gas expander, which could raise the overall efficiency to 65.7 %, much higher than the efficiency of the basic Allam cycle design, with the assumption that the cold energy associated with LNG regasification is freely available and does not constitute energy usage. A similar LNG heat sink concept, with a dual pressure Allam cycle for the cascade utilization of LNG cold energy, was proposed by Li et al. (2021); they suggested that their process could achieve 70.56 % electricity efficiency at its optimal operation point. On the other hand, an optimization study to determine the best configuration to utilize the LNG cold energy suggests that it may be difficult to justify the additional capital cost associated with employing a standalone organic Rankine cycle to recover additional energy, because the performance of the modified Allam cycle only marginally increases (Yu et al., 2021).

Some design changes have been proposed by Allam and co-workers, e.g. the introduction of a low-pressure reheat loop with a two-turbine system, which was found to afford a 57.5 % net efficiency (Allam et al., 2014). The authors also suggested that, in comparison to a single loop system, the net power output could increase by 2.5 times. Recently, Chan et al. (2020) described a reheating configuration for the Allam cycle. They added a low-pressure turbine and decoupled the ASU from the heat exchange network of the power island, at the expense of an increase the capital cost owing to the extra turbomachinery, a potentially more hazardous operation associated with the reheating of fuel and oxygen mixture and a decline in net efficiency.

The concept of Allam cycle is not limited to the combustion of natural gas, as its original designers also considered the efficient utilization of gasified coal. In fact, studies of coal-fired Allam cycle have also been conducted as part of the effort to develop clean-coal technologies. An analysis of the type of gasifiers and coal feedstock was conducted to determine the optimal performance by the Allam cycle using solid fuels (Lu et al., 2016). The key finding of the study validated the original hypothesis that a coal-fired Allam cycle could perform at higher efficiencies than the state-of-the-art integrated gasification combined cycle (IGCC) processes without carbon capture. While it was found that the different feedstock quality does not have a significant impact on cycle performance, emphasis is given to the future development of DeSNOx (de-sulphurisation and nitrogen oxide removal) processes, heavy metal removal, fouling prevention and corrosion prevention, all of which are important considerations for developing truly clean coal technologies, which are less commonly studied in the context of Allam cycle. A detailed exergy analysis of a coal-fueled Allam cycle, by Luo et al. (2021) revealed that 50 % of the exergy destruction comes from just three components, the gasifier, the turbine and the combustion chamber. These insights are important for determining the focus of further R&D efforts to improve the performance of the Allam cycle systems.

Zhu et al., who proposed the Allam-Z cycle (Zhu et al., 2019a), also proposed a similar scheme for coal-fired Allam cycle, denoted as the Allam-ZC cycle (Zhu et al., 2019b). In the Allam-ZC cycle, supercritical water coal gasification technology was employed to produce a syngas which can be directly sent to the Allam cycle with a higher turbine backpressure. As such, there is no need to add costly syngas cleaning procedures as supercritical water gasification ensures the complete conversion of contaminating elements such as N, S, P and Hg to inorganic salts and deposits. Even though a lower net efficiency of 47.3 % was reported (c.f. the original Allam coal cycle efficiency of 51.4 %), the authors argued that the Allam-ZC is still superior over the state-of-the-art to IGCC and other coal-fired plants without carbon capture.

An economic evaluation of the Allam cycle found it has a levelized cost of electricity of 91.7 €/MWh, which is higher than that of a typical natural gas CCGT (62.5 €/MWh) (Rodríguez Hervás and Petrakopoulou, 2019). Indeed, Allam cycle remains a relative new power generation technology with relatively few dedicated studies and analyses. The economic viability of the Allam cycle would also depend heavily on the CAPEX of highly specialized equipment, such as a supercritical CO_2 turbine, the cost of which may be far from being commercially competitive at its current state of development. The shortage of comprehensive experimental data in the open domain also imposes great uncertainties in validating the performance and cost-effectiveness of the Allam cycle and its various process variations (Haseli, 2021). In addition, the energy efficiency of the ASU units and their integration with the thermal power cycle would further impact the net efficiency of the Allam cycle. Optimistically, future near-commercial scale demonstration projects will provide the research community with more data validating the practical performance of the Allam cycle, highlighting the needs for further R&D and encouraging more research efforts to improve its competitiveness, e.g. by exploring integrating and hybridizing Allam cycles with other cryogenic, thermal and/or chemicals processes, under a variety of operating scenarios, including the use of gasified solid fuels.

5.1.3. O_2/CO_2 and O_2/H_2O oxy-fuel combustion

Oxy-fuel combustion is considered one of the technologies applied to capture and sequester CO_2 in coal-fired power plants, and three generations of combustion technology have been developed so far. The circulating flue gas in the first-generation oxy-fuel combustion technology is about 70 %, and flue gas recirculation (FGR) results in exergy losses and additional auxiliary loads (Gopan et al., 2020). The air separation unit (ASU) and the CO_2 purification unit (CPU) will cause about 8 % carbon capture efficiency loss. The second-generation and third-generation combustion technologies are the main development targets. According to the combustion atmosphere, they are divided into O_2/CO_2 and O_2/H_2O combustion. Combustion pressure develops towards higher, making the entire technology economically competitive.

5.1.3.1. Characteristics of O_2/CO_2 combustion. The reactive gases in O_2/CO_2 combustion are O_2 and recycled flue gas. Pure oxygen and partially recovered flue gas produced in the ASU control the flame temperature and supplement the missing N_2 volume to transfer heat to the boiler (Stanger et al., 2015). Compared with air combustion, replacing N_2 with CO_2 will significantly reduce the combustion gas temperature (Khatami et al., 2012), but the combustion temperature of O_2/CO_2 can match the air combustion temperature curve when the O_2 concentration exceeds 30 % (Scheffknecht et al., 2011).

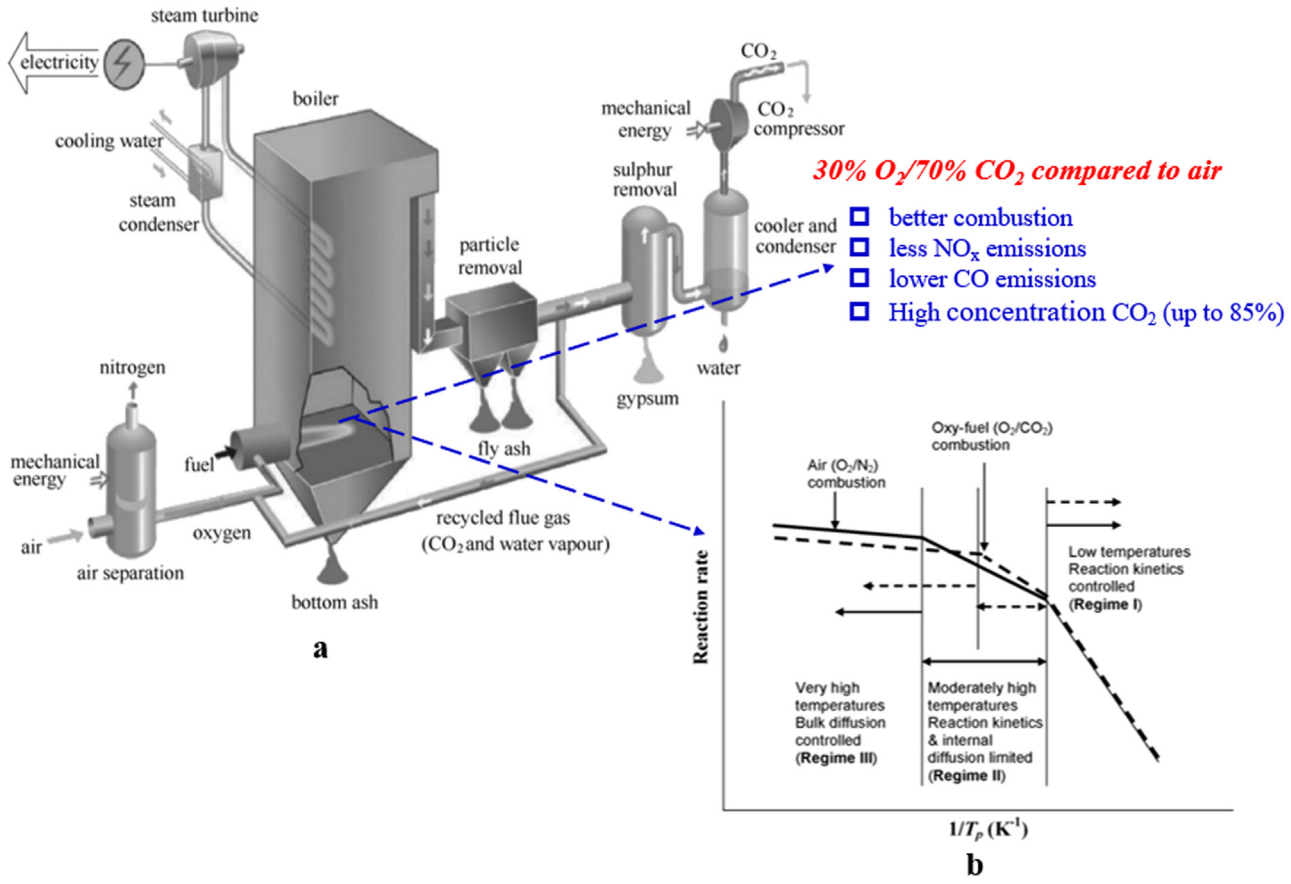

Fig. 5.7. a: technical route of oxy-fuel combustion (Horn and Steinberg, 1982), b: schematic diagram of control stage in air and O_2/CO_2 atmosphere (Wall et al., 2009a), comparison of char combustion characteristics in 30 % O_2/70 % CO_2 and air combustion (Stanger et al., 2015; Toftegaard et al., 2010).

The comparison of the characteristics between the second-generation oxy-fuel combustion technology and air combustion and its technical schematic diagram is shown in Fig. 5.7. O_2/CO_2 combustion has advantages in combustion characteristics and is conducive to CO_2 capture compared with air combustion. However, the flue gas circulation will enhance the coupling of the boiler, making it difficult to start and stop (Toftegaard et al., 2010), and cause pollutant accumulation and air leakage, which will increase the cost of CO_2 capture (Croiset and Thambimuthu, 2001). Chen et al. (2012) systematically reviewed the research on combustion thermodynamics, ignition, kinetics, pollutant emissions, combustion stability, and CFD simulation design of O_2/CO_2 before 2011. However, the research on pressurized oxy-fuel combustion has not been thoroughly analysed.

5.1.3.2. Pressurized O_2/CO_2 combustion. The ASU and CPU in the traditional oxy-fuel combustion system are carried out under high pressure, but the working pressure of the fuel combustion unit (pulverized coal boiler or fluidized bed) is normal. The pressure conversion process in the system results in a reduction in power generation efficiency of around 10 % (Tranier et al., 2011). Therefore, the concept of pressurized oxy-fuel combustion (POFC) was proposed to overcome the energy loss by increasing the pressure of the combustion unit. In addition, pressurized oxy-fuel combustion has the following advantages:

1) The size of boiler equipment is reduced, and the cost of infrastructure is reduced;
2) More latent heat of steam in flue gas can be recovered;
3) Avoid system air leakage and reduce CPU energy consumption;
4) Convective heat transfer is improved at the same speed.

Current research shows that the optimal working pressure of pressurized fluidized bed combustion is around 1 MPa (Shi et al., 2019; Ying et al., 2016). Studies on pressurized oxy-fuel combustion systems have shown that the elevated pressure of the combustion unit can improve the power plant system's net power efficiency (LHV), reduce pollutant emissions, and obtain high concentrations of CO_2 (Soundararajan and Gundersen, 2013). Chen et al. (2019) analysed the 600 MW pressurized fluidized bed oxy-fuel combustion power plant and found that more phase change heat in the flue gas can be recovered under pressurized conditions, which can increase the net power efficiency by 36.83 %. Hong et al. (2009,2010) and Gopan et al. (2014) reported that the net power plant cycle efficiency increased by 3 %–6 % when the pressure was increased beyond 1 MPa. Shi et al. (2019) showed that circulating compression work on pressurized circulating fluidized bed (PCFB) systems are negligible at a lower pressure than PC boilers. The higher combustion pressure is beneficial to the oxy-fuel circulating fluidized bed combustion, the net efficiency is increased from 27.2 % to 30.5 %, and the mole fraction of CO_2 can reach 92 %.

The research on a laboratory-scale oxy-fuel-PFBC platform found that elevated pressure can improve pulverized coal combustion performance, thereby reducing CO, NO_x, and SO_2 emissions (Duan et al., 2019; Lasek et al., 2013; Wu et al., 2011). Zhang, W.D. et al. (2020) studied the O_2/CO_2 thermal conversion characteristics of bituminous coal at 1273 K using a pressurized drop tube furnace (PDTF) and found that the char yield decreased from 59.18 % to 44.47 % when the CO_2 partial pressure was increased from 0 to 0.45 MPa. Axelbaum et al. (2017) proposed a staged pressurized oxy-combustion (SPOC) process and successfully operated it at 1.5 MPa and ~100 kW of pilot scale. The results show that the system can capture more than 90 % of CO_2 with high efficiency and

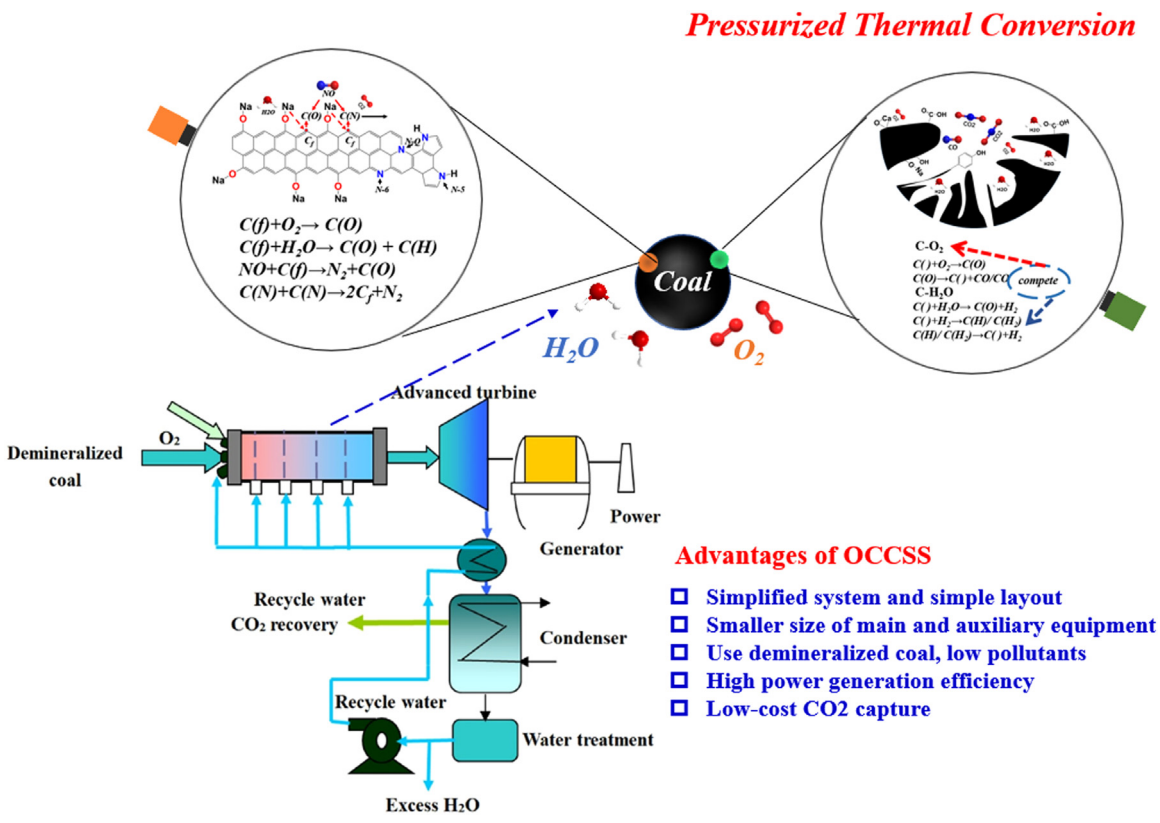

Fig. 5.8. OCCSS system diagram and technical advantages (Deng et al., 2021a, b; Zhao et al., 2019).

Table 5.4
Comparison of air combustion, O_2/CO_2 and O_2/H_2O combustion technologies (Deng et al., 2022).

	Air combustion	O_2/CO_2 combustion	O_2/H_2O combustion
Flame temperature	low	high	low
Combustion rate	low	high	high
Smoke volume	high	low	
System layout		complex	simplify
Pollutant emissions		low	low
CO_2 capture	low	high (<90 %)	high (>95 %)
Cost		higher	high

affordable cost, and the efficiency is at least 3.5 % higher than that of traditional oxy-fuel combustion devices (Yang et al., 2021).

The oxy-fuel combustion of pulverized coal mixed with biomass for power generation to reduce carbon emissions has also attracted widespread interest. Long et al. (Spiegl et al., 2021) performed a series of works on the oxy-fuel combustion of pulverized coal mixed with biomass using a laboratory-scale fluidized bed reactor, demonstrating the feasibility of mixed fuel blending. Zhong et al. (Liu et al., 2022) used a pressurized fluidized bed to achieve stable combustion of the mixed fuel, but the working pressure was only 0.1–0.3 MPa and found that the increased pressure can increase the combustion efficiency and facilitate CO_2 enrichment.

5.1.3.3. Characteristics of O_2/H_2O combustion. The O_2/H_2O combustion technique was originally proposed by Carlos et al. Salvador (2007), Seepana and Jayanti (2010), which was called steam-moderated oxy-fuel combustion (SMOC). The CANMET Energy Technology Center in Canada proposed a zero-emission power generation system based on O_2/H_2O combustion. The system uses steam to adjust the flame temperature, reducing the size of the power generation system by 2/5, and the energy consumption is greatly reduced compared with the second-generation oxy-fuel combustion technology (Zou et al., 2014b).

The O_2/H_2O combustion system eliminates the flue gas circulation system. And the flue gas condensed water is heated by the residual heat of the flue gas into steam, which is injected into the furnace to adjust the temperature. This series of processes improves the heat utilization rate of the system and removes the impurity gas in the water through the condensation and vapourization of steam, which is beneficial to the later CO_2 purification [30] (Cai et al., 2015). Deng et al. (2022) compared the characteristics of air combustion, O_2/CO_2, and O_2/H_2O combustion in the review of O_2/H_2O combustion of pulverized coal, as shown in Table 5.4.

5.1.3.4. Atmospheric pressure O_2/H_2O combustion. The H_2O concentration in O_2/H_2O atmosphere under oxygen-enriched conditions is between 25 % and 35 % (Hecht et al., 2012), which affects the ignition mode of char. Zou et al. (2015b) studied the ignition behavior of pulverized coal particles in an O_2/H_2O atmosphere (reaction temperature of 1373K, H_2O concentration of 50–79 %) and found that the addition of steam promoted the formation of a large amount of CO and H_2 on the char surface. Under the same oxygen concentration, pulverized coal ignites earlier in O_2/H_2O atmosphere than in O_2/N_2 atmosphere (Zou et al., 2014a). The high concentration of steam strengthens the reactions of $C + H_2O \rightarrow CO + H_2$ and $CO + H_2O \rightarrow CO_2 + H_2$. A large amount of H_2 and CO in the char particle boundary layer will affect the heterogeneous

Table 5.5
Economic comparison of different CO_2 emission reduction system technologies.

Power generation method	CES (Marin, 2003)	Hydroxy-fuel	OCCSS	IGCC wCO$_2$ (EPRI, 2000)	USC Oxy-fuel (Dillon, 2005)
Thermal Efficiency	50.7	35	53.4	39	35.4
CO_2 emissions (Kg/MWh)	0	0	0	83	83.7
Equipment cost (US$/kW)	1210	–	–	1642	1857
Electricity price ($/kWh)	0.054	–	–	0.069	0.062

reaction of char, making the char combustion mode change to joint ignition (Moors, 1999; Zou et al., 2015a). Blackwood et al. (1958) found that the CO_2 generated around the particles in O_2/H_2O atmosphere was mainly attributed to the homogeneous reaction ($CO + H_2O \rightarrow CO_2 + H_2$).

A high concentration of H_2O affects the combustion mode of char. The enhanced gasification reaction and the thermal effect significantly affect the combustion process of char. Therefore, many scholars quantitatively analyse the consumption of char in the H_2O gasification reaction to study the effect of H_2O concentration on the combustion characteristics of char. Hecht et al. (2012) found that the H_2O gasification reaction of char in the wet flue gas cycle of oxy-fuel combustion contributed 8.7 % to the overall char consumption. The gasification reaction accounted for about 20 % of the carbon consumption under low oxygen conditions. Zhang and Prationo et al. (2015) studied the char gasification-combustion model and found that under 31 % O_2/CO_2-18 % H_2O atmosphere (reaction temperature is 1373K), the char- H_2O gasification reaction contributed 26.2 % to the char consumption. Chen et al. (2022) found that the contribution of gasification reaction to carbon consumption in the O_2/H_2O atmosphere increased with the increase in temperature and H_2O concentration. Increasing the H_2O concentration from 5 % to 15 % increased the gasification reaction's contribution to carbon consumption by 1.96 at 1373 K.

5.1.3.5. Pressurized O_2/H_2O combustion. The research on O_2/H_2O combustion technology is still at the laboratory scale. Due to the complexity and high requirements of the experimental equipment, the understanding of the combustion characteristics of pulverized coal pressurized O_2/H_2O is still in its infancy. As shown in Fig. 5.8, Sun et al. (Zhao et al., 2019) proposed the concept of an oxy-coal combustion steam system of near-zero emissions (OCCSS).

The fuel of the system in the O_2/H_2O atmosphere is demineralized coal, and the high temperature and pressure mixed gas (the final steam concentration is about 90 %, and the rest is mainly CO_2) drives the advanced turbine to work. Then the exhaust gas is condensed to obtain high concentrations of CO_2. The economic comparison between this system and other different CO_2 emission reduction systems is shown in Table 5.5. The CES (based on coal gasification technology) and OCCSS show absolute advantages over IGCC and USC (ultra-supercritical) oxy-fuel combustion power generation systems.

Macneil and Basu (1998) found that when the oxygen concentration was constant, the combustion rate of char first increased and then decreased with the elevated pressure. The experimental work on pressurized O_2/H_2O combustion of pulverized coal is currently being carried out by Harbin Institute of Technology (Bai et al., 2022; Deng et al., 2021a, b) and Southeast University (Zan et al., 2020). Fig. 5.9 (Deng et al., 2021a, b) summarizes the char thermal conversion process of demineralized coal in the context of OCCSS under different pressure conditions, H_2O concentration, and temperature. The increase of pyrolysis pressure helps increase the yield of pyrolysis char, and the increase of pressure and H_2O concentration can both promote the combustion of char. Under pressurized conditions, the temperature exceeds 1173K, and the thermal transformation of char is significantly promoted. At equal intervals of the reaction time, the char is transformed linearly.

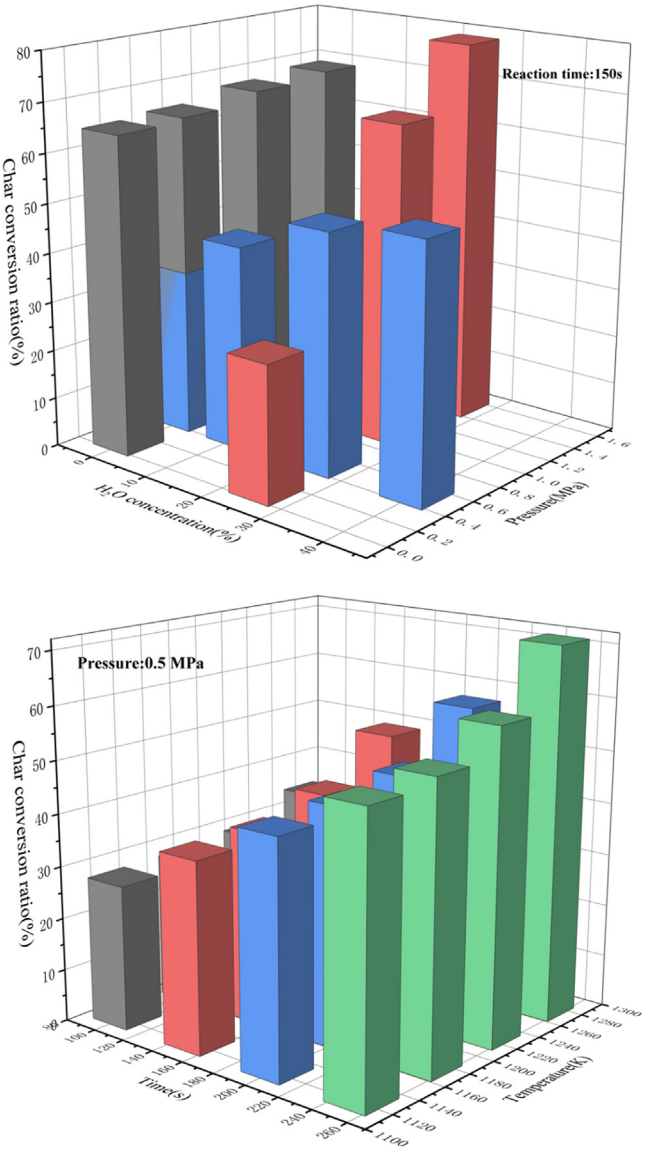

Fig. 5.9. Char conversion rate of demineralized char under different pressure, H_2O concentration and temperature, data adapted from (Deng et al., 2021a, b). (For interpretation of the references to color in this figure legend, the reader is referred to the web version of this article.)

The chemical kinetics in the pressurization stage is the rate-limiting reaction, and the pore diffusion becomes the rate-limiting reaction at high pressure (Turnbull et al., 1984). The char-H_2O reaction fully develops the micropore surface area, and pore development is achieved by consuming 5–10 % of the char (Jasieńko-Hałat and Kędzior, 2005).

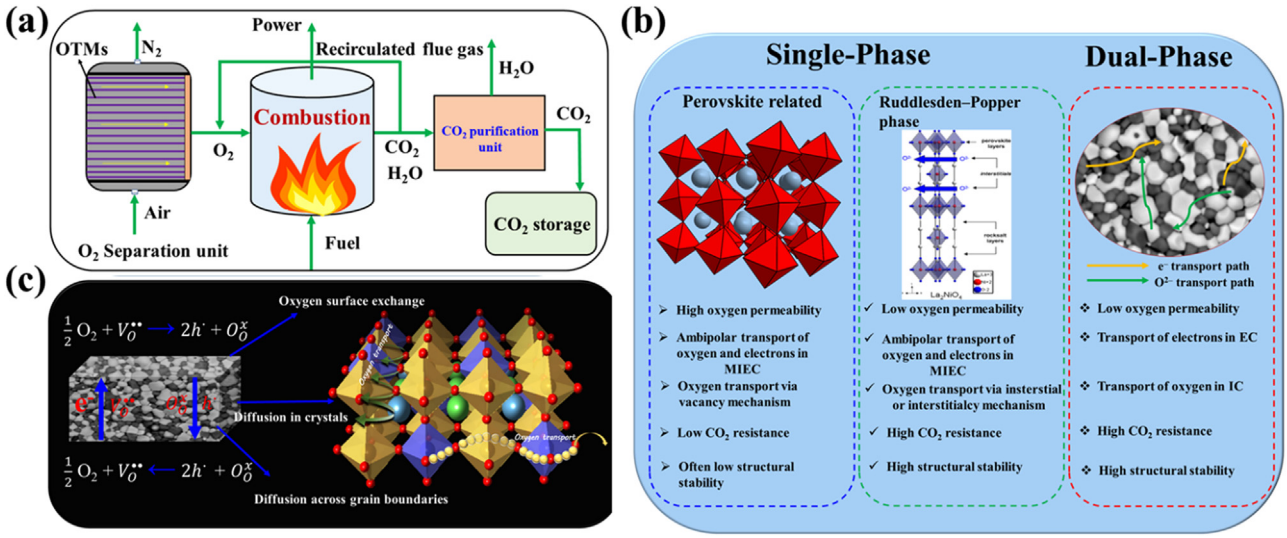

Fig. 5.10. (a) Schematic representation of using OTMs reactors for oxy-fuel combustion (b) the most common types of OTMs used for oxygen permeation and (c) a diagram of the oxygen transport mechanism (Chen et al., 2022). (For interpretation of the references to color in this figure legend, the reader is referred to the web version of this article.)

Therefore, under pressurized O_2/H_2O conditions, the change of char pore structure strongly affects its combustion process. Deng et al. (Deng et al., 2021a, b) studied the effect of H_2O concentration and pressure on char pores and found that the development of char pore structure increases first and then decreases with the increase of H_2O and pressure. When the H_2O concentration is 25 %, and the pressure is 1MPa, the specific surface area of the char is the largest.

Therefore, pressure can inhibit NO production is consistent, but the optimal pressure is not unified. Zan et al. (2020) found that increased system pressure significantly suppressed NO emissions, and H_2O suppressed the formation of NO and N_2O. Bai et al. (2022) found that pressure affects NO emission, and the lowest relative migration of char-N to NO is 0.4 MPa. In summary, the application of pressurized oxy-fuel combustion technology to coal-fired power plants has great potential to achieve CO_2 emission reduction, especially to improve the combustion efficiency of pulverized coal and reduce pollutant emissions.

5.1.4. Oxygen transport membranes for oxy-fuel combustion

5.1.4.1. Status. To meet expanding global energy demand, the power generation sectors have integrated carbon capture and sequestration technology (CCS) into their current infrastructures in order to reduce combustion emissions while maximizing process efficiency (Li et al., 2022; Shaw and Mukherjee, 2022). Directly capturing CO_2 emissions from power plants is a potential route and oxyfuel combustion technology using pure oxygen for fuel combustion has gained increasing interest from many researchers and governments since it is easy to be integrated into current power generation facilities. The massive amounts of oxygen can be obtained by incorporating oxygen transport membrane (OTMs) reactors that filter pure oxygen directly from air (Fig. 5.10 (a)), with the required heat for the oxygen permeation reaction provided by the combustion process itself. The oxygen transport membrane reactors can also be used in many other industrial sectors, such as iron and glass factories, to capture enormous quantities of CO_2 emissions. Academic and industrial communities are becoming increasingly interested in OTMs. In theory, these oxygen permeable membranes can separate oxygen with 100 % permeation selectivity and provide a cost-effective and simplified method for producing O_2. In comparison to current cryogenic technology, the revolutionary method based on OTMs can save 60 % of energy consumption and reduce production costs by 35 % (Chen et al., 2022, 2015; Kiebach et al., 2022). Another appealing advantage of OTMs is the ability to directly implement oxygen separation units into high-temperature processes such as oxy-fuel combustion. Recently, OTMs are also becoming increasingly appealing for use in membrane reactors for chemical and fuel production, in addition to O_2 separation (Chen et al., 2022; Plazaola et al., 2019).

5.1.4.2. Transport mechanism of OTMs. OTMs for oxygen separation have been extensively researched in recent decades and are broadly classified into two types, as shown in Fig. 5.10 (b): single-phase and dual-phase. The selective permeability of oxygen from the high oxygen partial pressure side to the low oxygen partial pressure side can be realized based on a driving force created by oxygen partial pressure difference on the two sides of the dense OTMs. The oxygen ionic transfer in one direction and the simultaneous electronic transfer in the opposite direction allow oxygen to permeate through dense OTMs membranes at high temperatures. The oxygen transport process is generally comprised of the following steps (Bai et al., 2021a; Garcia-Fayos et al., 2020; Kiebach et al., 2022):

1) Diffusion of oxygen from the feed stream to the OTMs surface
2) Adsorption of O_2 on the surface of the OTMs
3) The adsorbed oxygen on the OTMs surface undergoes dissociation surface exchange reaction:

$$\frac{1}{2}O_2 + V_O^{\bullet\bullet} \rightarrow O_O^x + 2h^{\bullet}$$

where $V_O^{\bullet\bullet}$ represents oxygen vacancies, O_O^x represents lattice oxygen and $h^{\bullet}$ represents electron holes.

1) Oxygen ion incorporation into membrane crystal lattice to form lattice oxygen.
2) Lattice oxygen diffusion and electrons diffusion via electron bands inside OTMs.
3) Lattice oxygen undergoes charge transfer on the OTMs surface to create chemisorbed oxygen.
4) Recombination surface exchange reaction:

$$O_O^x + 2h^{\bullet} \rightarrow \frac{1}{2}O_2 + V_O^{\bullet\bullet}$$

5) O_2 molecule desorption from the OTMs surface

The oxygen permeation process involves a number of physical and chemical processes that are primarily controlled jointly by surface exchange and bulk diffusion in most cases. It is important to note that

the rate-limiting steps are determined by several parameters, including membrane material, operating conditions, and membrane geometry. To obtain accurate prediction of the oxygen permeation fluxes for various limiting cases, intensive efforts have been devoted to developing empirical equations or models that integrate surface exchange and bulk diffusion reactions. More detailed descriptions of the existing oxygen permeation flux models on the basic assumptions and transport mechanism of OTMs can be found in the previous excellent reviews (Li et al., 2018; Sunarso et al., 2008).

5.1.4.3. Performance overview of different types of OTMs. Single-phase perovskite-type OTMs materials with a general formula of $A'_xA''_{1-x}B'_yB''_{1-y}O_{3-\delta}$ are among the most studied and promising candidates for oxygen separation since they exhibit high mixed ionic and electronic conductivity, which allow transporting the oxygen ions sustainably. An ion is typically an alkaline-earth metal like Ba^{2+} or/and Sr^{2+}, whereas B ion is generally a transition metal like Fe^{3+} or/and Co^{3+}. Based on the literature (Chen et al., 2022; Han et al., 2022; Widenmeyer et al., 2020), the chemical compound combinations $Ba_xSr_{1-x}Co_yFe_{1-y}O_{3-\delta}$ (BSCF) appear to be the best candidates with the highest oxygen permeation flux, which is generally more than 1 mL min^{-1} cm^{-2} for a 1 mm-thick membrane at 950 °C and can even reach to more than 10 mL min^{-1} cm^{-2} for an ultra-thin BSCF membrane at 1000 °C (Zhang et al., 2017). Despite exhibiting good performances for oxygen separation, the low chemical stability of BSCF membranes in CO_2-containing atmospheres resulted in oxygen permeation flux deterioration because of the formation of strontium or barium carbonates, which limits their applicability for oxy-fuel combustion. In addition, the high thermal expansion arising from the phase transition in the OTMs operating temperature range will lead to mechanical instability. Based on the reported studies, several major approaches have been taken to improve the chemical stability of perovskite-based OTMs towards CO_2 (Chen et al., 2022; Chen et al., 2019; Zhang et al., 2017):

(a) Partially substituting the transition metal components in the B-site with more stable or acidic metal components.
(b) Reducing the Co content in the B-site;
(c) Using a rare earth metal cation as the A-site cation (e.g. La or Pr);

Although the proposed approaches (partial substitution of A- and B-site cations) can enhance the CO_2 resistance of perovskite-type OTMs, performance degradation is unavoidable due to the formation of an alkaline-earth carbonate layer over time when exposed to CO_2-containing atmospheres.

An attractive alternative to perovskite is the Ruddlesden–Popper single-phase membrane material with a general formula $A_{n+1}B_nO_{3n+1}$ (A is an alkaline earth or lanthanide and B is a transition metal; n = 1, 2, 3, 4….). One of the most studied examples is Ln_2NiO_{4+d} (Ln is referred to rare earth metals such as Nd, Pr or La), which has been proved to be totally CO_2 tolerant during long-term oxygen permeation test in a CO_2 atmosphere (Chen et al., 2019; Xue et al., 2015). However, when compared to perovskite-type OTMs, the oxygen permeability of Ruddlesden-Popper single-phase membrane is significantly lower. Furthermore, it is reported that the presence of a small amount of SO_2 was sufficient to damage the Ruddlesden–Popper phase membranes because of the formation of sulphur containing products (Kiebach et al., 2022), which instantaneously blocks the active sites of the membranes for oxygen transport.

Dual-phase membranes, which are composed of an electronic phase and an ionic phase, have a high potential for oxygen separation and can address the issues of low chemical stability of single-phase OTMs (Bai et al., 2021a; Chen et al., 2021; Fang et al., 2015; Garcia-Fayos et al., 2020). Ideally, they combine the best properties of the electronic and ionic conductors to achieve both good oxygen permeation fluxes and satisficed chemical and mechanical stability in harsh operating conditions (for example, CO_2 and SO_2) at high temperatures. The successful materials for dual-phase membranes should meet the basic requirements: (a) no reactions between these two phases at working temperature; (b) the creation of good percolation paths for the diffusion of electrons and ions; (c) a proper ratio between these two phases; (d) high electrical conductivities of both electronic and ionic conductors. Noble metals such Ag or Pd were used as electronic conductors in early approaches. More recently, conductive oxide phases were selected as the electronic conductor. It is well accepted that the incorporation and release of oxygen are restricted to triple-phase boundaries (gas phase / electronic conductor / ionic conductor). The concept of combining two mixed ionic-electronic conductors in the dual phase OTMs is a promising route to overcome this limitation, where one shows superior electronic conductivity while the other has excellent ionic conductivity. Although dual-phase membranes also exhibit high CO_2 resistance after long-term CO_2 exposure, their oxygen permeability is lower than that of perovskite-type single-phase OTMs, similar to ruddlesden–popper single-phase membranes. To sum up, there is a trade-off between oxygen permeability and CO_2 tolerance. It is difficult to achieve high oxygen permeation flux while maintaining excellent chemical stability for the designed OTMs. Often, improving one property comes at the expense of sacrificing another. Reduced membrane thickness or optimization of OTMs geometry are two alternatives that do not induce such a trade-off. Since oxygen flux and membrane thickness are inversely related, reducing membrane thickness generally increases the oxygen permeation flux of the membrane. This is true up to a certain thickness known as characteristic thickness, after which the predominant bulk diffusion is limited by the oxygen surface exchange at gas/solid interfaces.

5.1.4.4. Membrane geometry and strategies for improving CO_2 resistance and oxygen permeability. At present, three shaped membrane configurations of OTMs have been widely studied: disk, tubular, and hollow fiber membranes. Despite being relatively simple to fabricate, the oxygen permeation performance of disk and tubular membranes is constrained by their small surface area, thick wall, sealing, and connection issues. The hollow fiber membranes have been considered as the most promising and practical one to improve O_2 permeation flux, which solves the problems faced by disk and tubular membranes. It is important to note that when the thickness of the membrane is reduced in order to achieve high oxygen permeability, the mechanical strength of the membrane decreases. A promising method for simultaneously obtaining high oxygen permeability and satisfied mechanical strength was an asymmetric structure membrane supported by a porous substrate. Aside from structural and chemical modifications to improve the oxygen permeability and CO_2 resistance of the OTMs, engineering approaches are effective methods to be applied. Coating the membrane surface with a porous CO_2 resistant layer is currently used as an effective approach to protect the single-phase perovskite-type membranes from CO_2 poisoning. For an ideal CO_2 protective layer material, high ionic conductivity, good chemical and mechanical stability towards CO_2 at working temperatures, and compatibility with the protected membrane are required. It is possible for the protected dense membrane and the porous protective layer to be made of the same material. If oxygen surface exchange predominates the transport process, it may be possible to increase the oxygen permeation fluxes by speeding up the surface exchange reaction rate by depositing a surface decoration (catalyst) layer on the membrane surface. Some intriguing ideas for improving oxygen permeability include using external electronic short-circuit methods to enhance the electronic conductivity of the membrane and utilizing plasma-based approaches that decouple oxygen molecule splitting and oxygen incorporation from the OTMs surface (Buck et al., 2021; Zhang et al., 2017; Zheng et al., 2022).

5.1.4.5. Existing developments for potential industrial applications of OTMs. The design of modules is a critical step in enabling OTM technology for large-scale purity oxygen production. Significant efforts are being made to improve the performance and stability of OTMs materials, and significant steps are also being taken in the design and integration of OTMs with oxy-fuel combustion systems. There are several developed

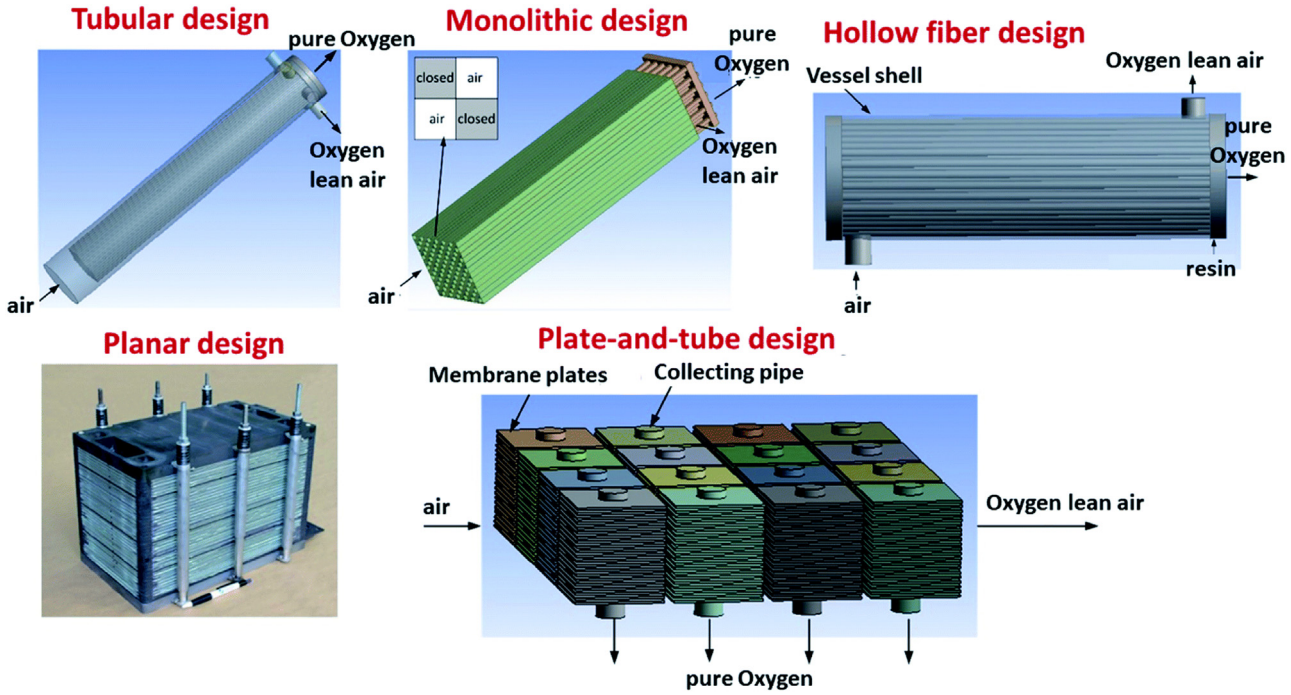

Fig. 5.11. Different design configurations for OTM modules for large-scale oxygen production. Reprinted with permission from (Kiebach et al., 2022). (For interpretation of the references to color in this figure legend, the reader is referred to the web version of this article.)

OTMs membrane modules (Fig. 5.11.) with different design configurations targeted at small and medium scale oxygen production, as recently summarized by Kiebach et al. (2022). A number of companies and academic research institutions have been working to scale up OTM concepts, developing membrane modules and successfully integrating them into industrial environments. Praxair, Inc. (now Linde plc) has made significant progress towards applications of dual-phase OTMs containing multipanel tubular reactor systems to improve the syngas produced by coal-gasification (Gupta et al., 2016). Currently, the pilot scale infrastructure is being reconfigured to connect OTM technology with steam methane reforming for blue hydrogen production by Linde. In terms of technology readiness levels and O_2 production rates, Air Products and Chemicals Inc. has made the most advanced developments. A membrane vessel with a total capacity of 2000 ton-per-day (TPD) O_2 production was developed, consisting of several 1 TPD OTM modules. However, no new information about OTM development activities was revealed, which was most likely due to a significant company restructuring in 2015 (Garcia-Fayos et al., 2020). It's also important to mention the OTM pilot module research conducted by the two Germany academic research organizations - RWTH Aachen University and Fraunhofer Institute for Ceramics Technologies and Systems (IKTS), both of which used $Ba_{0.5}Sr_{0.5}Co_{0.8}Fe_{0.2}O_{3-\delta}$ (BSCF) as the membrane material. With regard to the pilot module developed by RWTH Aachen University, a membrane module with a total of 596 tubular BSCF membranes was created and tested in a variety of environments (Nauels et al., 2019). It was possible to operate continuously for a maximum of 1800 h with an operating pressure of 10 bars and a temperature of 880 °C. The testing results demonstrated their concept is generally feasible. However, significant improvement is still needed to address the problems of breakages of membrane tubes. Since 2009, Fraunhofer IKTS has developed various OTM pilot plants with a growing oxygen production rate and a decreasing energy demand. A 18,000 h long-term oxygen permeation measurement was carried out using 93 capillaries, and the results showed the O_2 permeation flux dropped only by approximately 6 % during the last 14,000 h continuous operation (Chen et al., 2022). The pilot plant design is still being refined, and more information can be found in (Chen et al., 2022). Similarly, a perovskite membrane module made up of 889 $La_{0.6}Sr_{0.4}Co_{0.2}Fe_{0.8}O_{3-\delta}$ hollow fiber membranes has also been developed and could be operated continuously for 1067 h at about 960 °C (Tan et al., 2010).

It is worth noting that the majority of the above results were obtained in the absence of CO_2. Considered the harsh operation environments of the oxy-fuel combustion process, the membranes should deliver high stability while maintaining satisfied performance. In this context, special attention should be given to the development of dual-phase OTMs by optimizing the preparation approaches and microstructures, which have shown high resistance towards CO_2 and acceptable oxygen permeation flux. Engineering approaches such as depositing a surface decoration (catalyst) layer and designing an appropriate module should also be considered. Despite many advancements, there are still many research and technological challenges to overcome before OTMs for oxy-fuel combustion in power plants can be commercialized.

5.2. *Chemical looping related carbon capture*

In a fuel-based power generation unit, the combustion of fuels is the route for energy generation, and carbon capture and storage (CCS) technology is necessarily employed to minimize CO_2 emissions combustion reactions (Gao et al., 2022b; Song et al., 2018b). CO_2 capture can be implemented in post-, oxy- or pre-combustion, wherein post-combustion is the conventional fuel oxidation method of combining fuel and air in a single heated reactor to give power (Alalwan and Alminshid, 2021). The flue gas containing CO_2 emitted has a low CO_2 partial pressure (i.e., < 0.15 atm), which makes current CO_2 technology challenging due to difficulties in separation and absorption. Progressing toward more efficient carbon capture, oxy-combustion, as described in Section 5.1, is the alternative to improve energy efficiency for the separation of CO_2 due to using pure oxygen from separation for fuel combustion to give only CO_2 and water vapour (Figueroa et al., 2008). More importantly, the CO_2-rich stream could be obtained by condensing water vapour, which is favourable for more-energy efficient carbon capture. Similar to oxy-combustion, pre-combustion primarily aims to form synthesis gas or syn-

gas, a mixture of H_2 and CO, from gasification or reforming. Thereafter, CO_2 is produced from CO via a water-gas shift reaction to produce more H_2 for combustion to give energy (Alalwan and Alminshid, 2021). Hence CO_2 before the combustion stage is captured (i.e., pre-combustion).

In any case, combustion technologies that require either CO_2 separation or O_2 separation from the air will incur high economic and energy costs. With the desire to avail of more energy-efficient process technologies for energy and material conversions, chemical looping processes, whereby a reaction or separation is divided into at least two sub-reactions that take place in a decoupled manner, have emerged as a competitive alternative in terms of the facile intrinsic CO_2 capture ability (Zeng et al., 2018). Typically, the chemical looping process involves circulating a chemical intermediate or looping material, such as metal oxides (MeO), that oxidizes feedstocks and reduces MeO. The reduced MeO (i.e., metals; M) would be re-oxidized, typically with air, in another unit. Such process is known as Chemical Looping Full Oxidation (CLFO), or conventionally also known as Chemical Looping Combustion (CLC). Some researchers labelled CLC as a pre-combustion CO_2 capture technology or a standalone fourth technique after post-, oxy- and pre-combustion CO_2 capture (Mukherjee et al., 2015). Importantly, CLC differentiates itself from pre-combustion CO_2 capture due to much higher concentrations of CO_2 in an effluent stream (i.e., up to 100 %) compared to only 50 % in that of pre-combustion. While many carbon capture technologies are being developed (e.g., solvent scrubbing, integrated gasification combined cycle), chemical looping is the most competitive technology by means of carbon capture cost (Bhave et al., 2017; Fan et al., 2012). Presently, most of the chemical-looping technologies for carbon capture in the power generating sector are still under laboratory research development stage, with several pilot-scale setups in operation for at least 11 000 h in 46 chemical looping combustors (Lyngfelt et al., 2019).

5.2.1. Chemical looping techniques

Chemical looping concept dates back to the 19th century by Quentin and Arthur Brin for air separation, with BaO as the looping material (i.e., $BaO + 1/2O_2 \rightleftharpoons BaO_2$) (Hepworth, 1892). CLC, the most widely adopted concept for chemical looping, was first introduced and patented by Lewis and Gililand for the production of pure CO_2 using a solid oxygen carrier or any oxidizable carbon-based materials in two interconnected fluidized bed reactors. (Lewis and Gilliland, 1954) More scholars began to explore a deeper understanding of the process design (Mattisson et al., 2018, 2009), looping material selection (Tian et al., 2021; Zeng et al., 2018; Zhang, Z. et al., 2022), and the energetics of CLC, (Mukherjee et al., 2015) and expanded to a broad range of applications, depending on the nature of the recyclable reaction or looping reaction (Hu et al., 2018; Zeng et al., 2018). CLC consists of two mutually exclusive reaction steps that are performed sequentially and in a cycle with two interconnected fluidized bed reactors (i.e., fuel combustion reactor; reducer and air reactor; oxidizer) and solid oxygen carriers like metal oxides (Fig. 5.12 A1). In the first reaction step within the fuel combustion reactor, fossil fuel feedstock such as natural gas is oxidized by lattice oxygen found in MeO. Complete combustion with oxygen resulted in the formation of CO_2 and H_2O (Reaction 5.1), for which pure CO_2 can be obtained by condensation, thus doing away with costly CO_2 separation. Sequentially, in the second reactor (i.e., air reactor; oxidizer), the reduced oxygen carrier is subjected to airflow for re-oxidation (Reaction 5.2). The oxidized MeO is then circulated back to the first reactor for complete feedstock combustion.

$$(2n+m)\ Me_yO_x + C_nH_{2m} \rightleftharpoons (2n+m)\ Me_yO_{x-1} + m\ H_2O + n\ CO_2 \quad (5.1)$$

$$Me_yO_{x-1} + \tfrac{1}{2}\ O_2 \rightleftharpoons Me_yO_x \quad (5.2)$$

The reduction reaction (equation 1) is, in general, an endothermic reaction for most oxygen-carrier metal oxides, while the re-oxidation of MeO is exothermic. (Peltola et al., 2013) The heat released from equation (2) is of the same magnitude as if for complete conventional combustion of fossil fuel in the air, thus making CLC intrinsically advantageous. (Lyngfelt et al., 2001)

Chemical looping processes can be broadly classified into two groups depending on the type of looping material carriers, oxygen-carrier or non-oxygen carriers (e.g., CO_2-carrier). (Fan et al., 2012) Others may classify the different chemical looping processes as either CO_2-producing or separation is involved or not. CLC or CLFO process is one of the processes that only use oxygen carriers for energy generation (Fig. 5.12 A1), and others include partial oxidation or selective oxidation for syngas or hydrocarbons production, respectively, thus going beyond energy generation efficiency (Fig. 5.12 A2,3). Chemical looping can be extended to hydrogen production (i.e., chemical looping hydrogen production; CLH), and other forms of chemical looping, such as sorption enhanced reforming (SER) and sorption enhanced chemical looping reforming (SECLR). (Chisalita and Cormos, 2019) Regardless of the choice of looping materials (i.e., oxygen-carriers, non-oxygen-carriers, or both in tandem), chemical looping has been shown to effectively give better yields and product selectivity while having better CO_2 management, either by concentrating the CO_2 stream for capture or efficient CO_2 utilization. For example, Chisalita and co-workers conducted a techno-economic analysis of CLH with iron-based oxygen carriers for natural gas reforming to hydrogen and found that the chemical looping process is expected to have a production cost of 41.84 €/MWh, lower than 42.43 €/MWh from that of a conventional natural gas reforming without carbon capture. (Chisalita and Cormos, 2019) Furthermore, CLH allows for a very high carbon capture rate of > 99 %, the unexpected inherent advantage of using chemical looping. The techno-economic assessment was applied to the natural gas combined cycle using oxy-fuel and carbon capture technologies with and without chemical looping design. With CO_2 and H_2O splitting chemical looping that permitted CO_2 recycling, the parasitic power load was reduced and thus resulted in an increase in net energy efficiency by 7.5 % from 43.25 %. (Farooqui et al., 2018) Hence, the chemical looping process can improve economic viability for chemical processes with 100 % intended carbon capture. Fig. 5.12 briefly describes possible chemical looping processes, including more advanced hybrid chemical looping processes with three reactors for desulfurization and ammonia synthesis (Laassiri et al., 2018; Xuan et al., 2018).

5.2.2. Chemical looping materials

Ideal carriers, be it to carry oxygen or other atoms, require good reactivity with respective carrying atoms (e.g., oxidation in the air in oxidizers) or reduction with carbonaceous feed in the reducer reactor. Secondly, the carriers should have sufficient mechanical strength to minimize attrition and excellent resistance to carbon deposition, sintering, and agglomeration at high temperatures. Carriers also need to be fluidizable, and their physical and chemical properties remain robust against repeated reduction and oxidation kinetics at high temperatures. Transition metals such as Co, Ni, Cu, Fe and Mn have been investigated as oxygen carriers with their corresponding oxides CoO, NiO, CuO, Fe_2O_3 and Mn_3O_4 (Zhang, et al., 2022) .

Among the transition metals, Ni and Co are among the costlier metals, but both have good reactivity with hydrocarbons (Dewangan et al., 2019; Hu et al., 2021a; Zhou et al., 2022), making them good candidates for the chemical looping process with carbonaceous feedstock. Close to 100 % CH_4 conversions can be obtained over Ni-based oxygen carriers during a CLR process (Han et al., 2021; Huang et al., 2018). However, Ni sintering and the loss of metallic Ni, owing to partial re-oxidation into NiO, resulted in a reduction of the overall active surface area and hence catalytic performance after repetitive chemical looping cycles. Ni-based catalyst also suffers from sulfur-poisoning with the formation of nickel sulfide, Ni_3S_2. (García-Labiano et al., 2009) Co possesses high oxygen transport capacity, and readily undergoes a redox process between Co and CoO at above 900 °C (Fig. 5.13A). However,

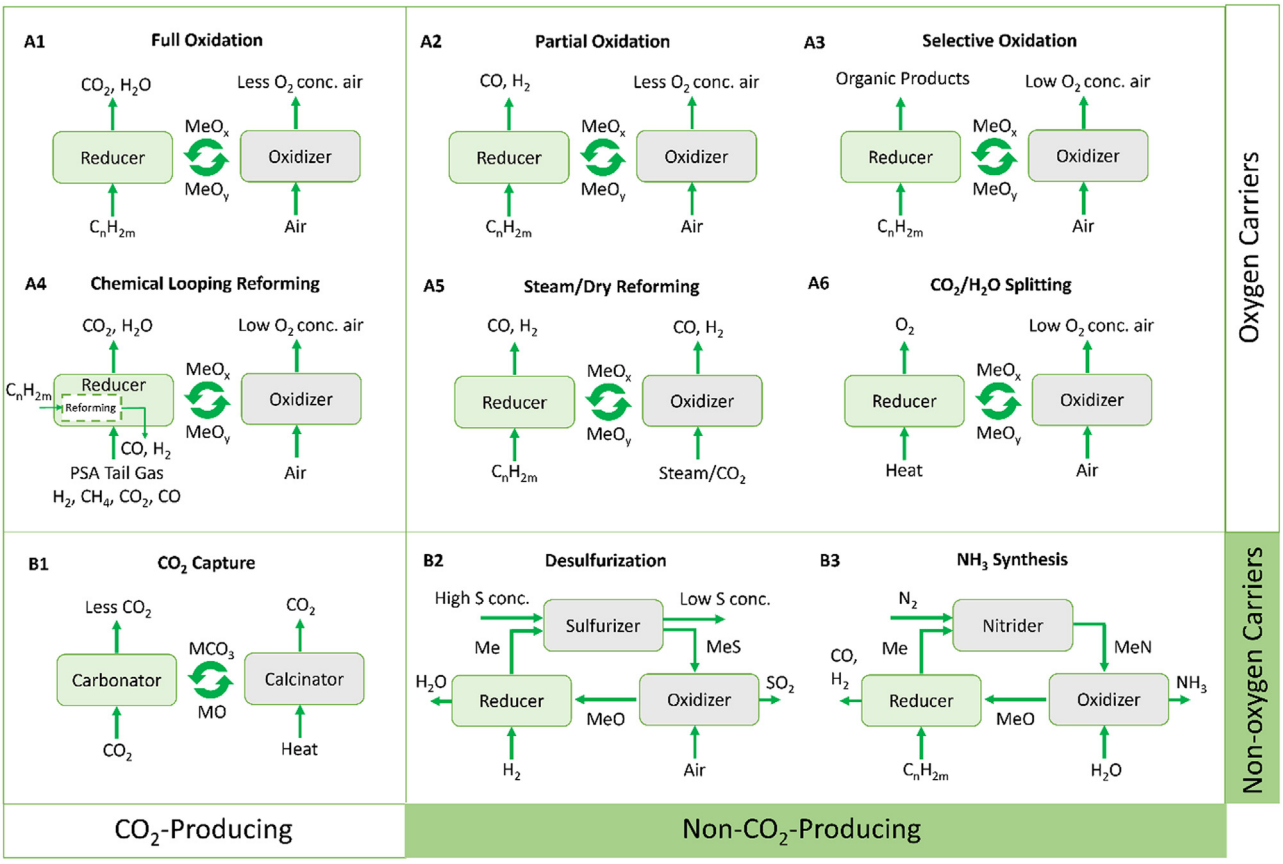

Fig. 5.12. Chemical looping techniques with different looping materials, broadly classified as either oxygen carriers (A) or non-oxygen carriers (B), and with different process designs, broadly classified as either CO_2-producing (A1, A4, B1) or non-CO_2-producing (A2, A3, A5, A6, B1-3). A1) Conventional chemical looping full oxidation (CLFO) or chemical looping combustion (CLC) (Alalwan and Alminshid, 2021). A2) Partial oxidation of carbonaceous feed to give syngas (Zhang et al., 2022). A3) Selective oxidation of carbonaceous feed affords high-value higher order hydrocarbons such as alkanes and alkenes. A4) Chemical looping reforming (CLR) with separate standalone conventional stream reforming in a reducing reactor (Luo et al., 2018). A5) Alternate chemical looping reforming (CLR) via steam or dry reforming process to convert carbonaceous feed into syngas (Hu et al., 2018; Hu et al., 2021c). A6) Thermochemical splitting chemical looping reactors for CO_2 to give CO and H_2O to give H_2 (Kim et al., 2022). B1) Carbon capture with carbonates to trap CO_2 (Zhang et al., 2022). B2) Hybrid chemical looping to carry O and S atoms for desulfurization (Xuan et al., 2018). B3) Hybrid chemical looping to carry O and N atoms for NH_3 synthesis (Laassiri et al., 2018). (For interpretation of the references to color in this figure legend, the reader is referred to the web version of this article.)

CoO has a strong affinity with common catalyst support materials like Al_2O_3, MgO, and TiO_2 to give thermally-stable and unreactive $CoAl_2O_4$, $Mg_{0.4}CO_{0.6}O$, and $CoTiO_3$ phases (Hu et al., 2018).

Cu-based catalyst has increasingly gained attention for their flexible redox ability from Cu with +2 oxidation state in CuO to +1 or 0 oxidation state in Cu_2O or Cu. Moreover, Cu is less toxic and low cost, and has a sulfur-resistant ability that Ni-based oxygen carrier lacks (Forero et al., 2010). Drawbacks of Cu include severe agglomeration at high temperatures due to its low melting point (i.e., 1085 °C) (Fig. 5.13 B), but strategies with tuning metal-support interaction to disperse Cu can overcome the limitation to give high chemical and mechanical stability (Izquierdo et al., 2021).

Fe-based oxygen carriers also face similar agglomeration problems with the formation of magnetite (Rydén et al., 2010). But, among the metals, Fe is environmentally-friendly, low cost, and possesses high mechanical strength – suitable for fluidization. While Fe falls short in the spectrum of oxygen transport capacity and reactivity towards hydrocarbons, its flexible oxidation states (i.e., Fe, FeO, Fe_2O_3, and Fe_3O_4) allow for use in different reaction systems (e.g., counter-flow moving bed reactor (Hu et al., 2020; Luo et al., 2014; Yu et al., 2019) Akin to Cu, Fe has modest resistance against H_2S poisoning, with H_2S being instead oxidized to SO_2 in the flue gas (Cabello et al., 2014), making Fe the most common versatile choice, together with Ni, for oxygen-carriers in many chemical looping processes and applications (Zhang et al., 2022).

Lastly, Mn-based catalysts as oxygen carriers are beneficial in terms of toxicity and cost, comparable with Fe, except that they boast higher oxygen transport capacity. However, Mn has flaws consisting of sulfur intolerance and the ability to form unreactive phases with Al_2O_3, SiO_2 and TiO_2 (Tian et al., 2009; Zafar et al., 2006). Fig. 5. 13 C shows a broad overview of the possible metal-based oxygen carriers, contingent on a certain desirable chemical looping process (i.e., activity, sulfur-tolerance, cost etc.) To better meet the practicality and commercial viability of chemical looping processes, strategies to improve the shortcomings in the monometallic oxygen-carriers have been reported with 1) introducing promoters (Hu et al., 2021b, 2021c; Machida et al., 2015), 2) mixed oxide or bimetallic catalysts (Hossain and de Lasa, 2007; Mungse et al., 2015), and 3) unique structures (e.g., perovskites (He et al., 2013), core-shell (Neal et al., 2015; Tian et al., 2017) etc.)

Conventional oxygen carriers generally function by 1) generating oxygen vacancies or ions and electron-hole pairs, 2) permitting bulk diffusion of the oxygen species and electron-hole pairs, and 3) providing surface sites for reactions (Fig. 5.13D). In the reduction step of the chemical looping process, where the oxygenated oxygen carriers are subjected to a reducing gas (e.g., carbonaceous feedstock, hydrogen, etc.), oxygen anions are first generated due to the exposure and absorption of thermal energy, which would diffuse from within the bulk (i.e., higher oxygen potential) to the surface (i.e., lower oxygen potential) with a concomitant counter-current flow of electrons to ensure charge neutrality. The

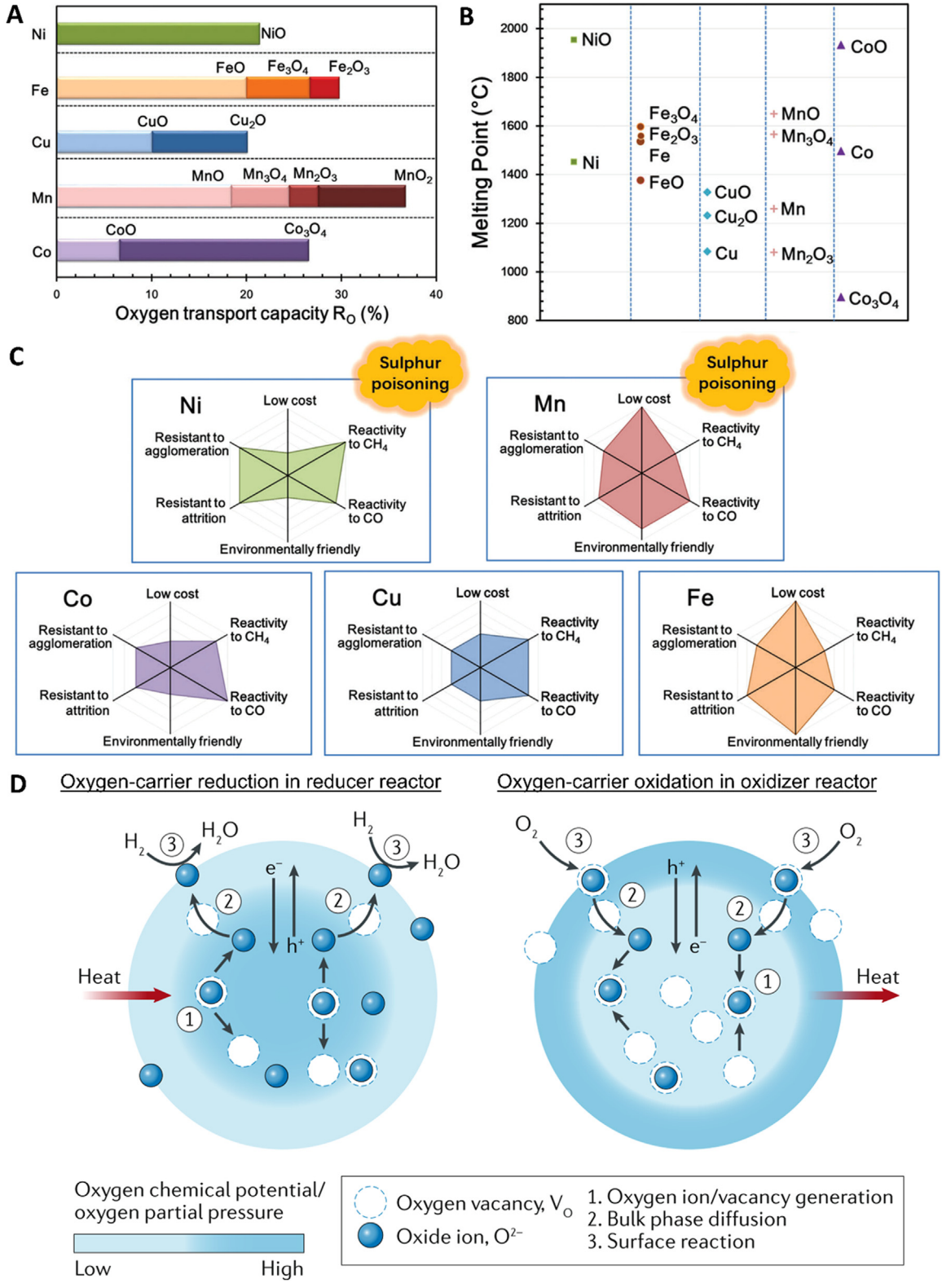

Fig. 5.13. Chemical and mechanical properties of oxygen carriers. A) Oxygen transport capacities comparison among Ni, Fe Cu, Mn and Co. B) Melting points of common metal oxides as oxygen carriers. C) Catalytic performance, cost, environmental-friendliness, agglomeration, and attrition resistance comparison (*Zhao et al., 2017*). D) Lattice oxygen generation and consumption of oxygen carriers in reducer and oxidizer segments of the chemical looping process (*Zeng et al., 2018*). (For interpretation of the references to color in this figure legend, the reader is referred to the web version of this article.)

active oxygen anions that have diffused to the surface can react and oxidize the reacting gas. On the other side, in the oxidation reactor, the oxidation of the oxygen-deficient oxygen carriers proceeds with oxygen occupying the oxygen vacancies on the surface before moving towards the bulk down an oxygen concentration gradient.

Another variant of the chemical looping process is chemical looping with oxygen uncoupling (CLOU), wherein the oxygen carriers do not just generate oxygen anions or vacancies, but rather release oxygen gas (O_2) to the gaseous phase in the reducer. The separated oxygen available for direct combustion overcomes the rate-limiting surface reaction with lattice oxygen on the typical oxygen carriers (Skulimowska et al., 2017). The common types of oxides capable of uncoupling oxygen are Cu and Mn-based, which allow the uncoupling of oxygen with sufficient oxygen partial pressures for combustion at elevated temperatures (Abián et al., 2017; Rydén et al., 2014). Interestingly, the majority of these carriers are Mn-based, either pure Mn_2O_3 or combined with other oxides (i.e., Ni, Fe, Mg, and Si) to give mixed oxides (Abián et al., 2017; Azimi et al., 2013; Shulman et al., 2009, 2011). The mixed oxides allowed higher oxygen partial pressures than pure Mn_2O_3 from between 850 to 1000 °C for combustion – a temperature range that is unsuitable for low-melting point Cu-based oxides.

Non-oxygen-carriers such as carbonates, sulfides, and nitrides for carbon capture, desulfurization, and ammonia production deviated from conventional oxygen carriers to allow novel applications (Zeng et al., 2018). Super-dry reforming is one example of hybrid chemical looping with both oxygen-carrier (e.g., Fe_3O_4) and carbon dioxide-carrier (e.g., $CaCO_3$), to convert CO_2 and CH_4 in a 3 by 1 molar ratio to H_2O in the reducer unit (Buelens et al., 2016). The work demonstrated that carriers can be used in tandem with other carriers (for a different purpose) to achieve broader applications. Also, the chemical looping concept can also be ingeniously exploited in a way without the use of an existing carrier. Hu and co-workers demonstrated that carbon deposits formed from dry reforming reaction (i.e., $CO_2 + CH_4 \rightleftharpoons 2H_2 + 2CO$) on the catalyst could serve as a transient looping material for NO reduction in a sequential step (i.e., $C + xNO \rightarrow CO_x + \frac{x}{2} N_2$) (Hu et al., 2021a). Henceforth, chemical looping technologies have high commercial-deployability value in the near future for efficient carbon capture, CO_2 utilization, or higher exergy efficiency with immediate CO_2 mitigation.

5.3. Cryogenic CO_2 capture

5.3.1. Introduction for cryogenic CO_2 capture

Cryogenic CO_2 capture refers to a physical separation process operating at sub-zero temperatures, which induces the anti-sublimation and, or liquefaction of CO_2 from process streams that require CO_2 removal, often combustion flue gases. Prior to cryogenic CO_2 capture, the flue gas should be completely de-humidified to prevent extensive frost formation in the pipeline and the process vessels. The advantages of this separation process include little or no usage of chemicals, a high rate of recovery, and high purity of the CO_2 product. In general, cryogenic CO_2 capture is considered economically viable when the feed stream is appropriately conditioned (Berstad et al., 2013), or when sufficient cold energy is available with fairly low cost.

The phase diagram for pure CO_2 is shown in Fig. 5.14. With a triple point at −56.6 °C and 5.1 bar, cooling the process stream at CO_2 partial pressures below 5.1 bar would produce dry ice, while cryogenic capture with CO_2 partial pressure above 5.1 bar would produce liquid CO_2 upon direct cooling. To decarbonise flue gases from thermal powerplants with a typical CO_2 concentration of ca. 3–14 %, depending on fuel sources, cryogenic carbon capture can be retrofitted as a post-combustion capture technology. For instance, to achieve 90 % capture rate from a coal-fired powerplant (with a typical CO_2 concentration of 13 vol %), a maximum operating temperature of −120 °C is required at 1 atmospheric pressure. To capture CO_2 from the flue gases of natural gas-fired powerplants (e.g. NGCC powerplant) that contains ~5 vol% CO_2, a maximum operation temperature of −140 °C is required to achieve 90 % capture rate.

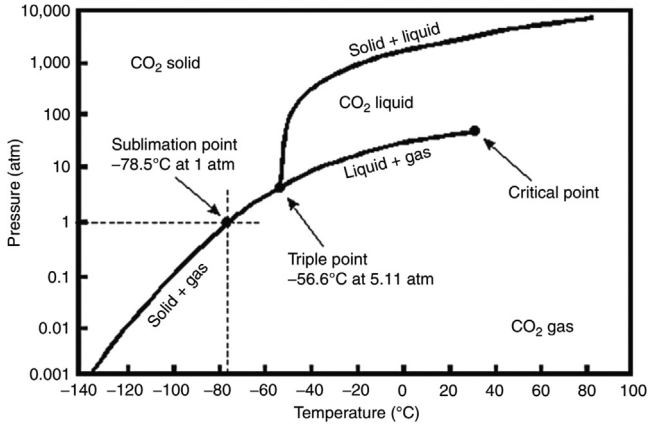

Fig. 5.14. Phase diagram for pure CO_2. Image reproduced from (McCollom, 2011). (For interpretation of the references to color in this figure legend, the reader is referred to the web version of this article.)

5.3.2. Vapour-to-liquid cryogenic separation

Distillation is the most common type of separation technique. As shown in Fig. 5.15, the traditional Ryan-Holmes process has been proposed for the purification of natural gas (Holmes and Ryan, 1982). Cryogenic distillation is a technique for separating biogas, natural gas and flue gas with careful consideration of CO_2 freezing temperature and pressure. The specific process of cryogenic distillation is as follows: The feed gas is pre-cooled and then chilled to a cryogenic temperature by a heat exchanger and enters the distillation column, which usually has a certain number of gas-liquid contact devices (e.g. trays or packing materials). After the distillation column, the raw gas is divided into two parts: the gas product at the top and the liquid product at the bottom of the column, respectively. Normally, in the biogas upgrading process, the methane after upgrading is discharged at the top of the column through a partial condenser, and the condensed CO_2 is passed through a reboiler at the bottom of the column to provide the heat required for evapouration. Eventually, the purified liquefied CO_2 is obtained through the separator.

Avoiding CO_2 freezing out during the cryogenic distillation process is an important point worth noting. Yousef et al. investigate the effect of tray temperature on CO_2 freezing by pressurizing biogas to 4.9 MPa and cooling it to −61 °C to obtain liquefied CO_2 at the bottom of the column and biomethane with 94.4 % purity at the top of the column (Yousef et al., 2018a). Although widely used in industry, cryogenic distillation is still characterized by high energy consumption, often reaching more than half of the overall operating costs (Ebrahimzadeh et al., 2016; Li and Bai, 2012b). A dual column cryogenic distillation process was proposed to use the cold energy of biomethane to pre-cool the biogas, thus reducing energy consumption to 0.236 kWh/Nm^3 CH_4, while the purity of biomethane was improved to 97.16 % (Yousef et al., 2018b). Process intensification and mixed hybrid cryogenic distillation networks were explored in Maqsood's work, and the result shows a significant reduction in energy reduction and an enhancement in purification performance (Maqsood et al., 2014a; Maqsood et al., 2014b). In addition, a number of energy-efficient methods have been applied to the distillation process, such as recompression distillation (Kazemi et al., 2016), and heat integrated distillation column (Jana, 2016). In general, studies on cryogenic distillation focus on the reduction of energy consumption and the improvement of methane purity.

The controlled freeze zone (CFZ) is a solution based on single-tower cryogenic distillation for the removal of acidic impurities from natural gas because the presence of acidic gases (CO_2 and H_2S) in natural gas has

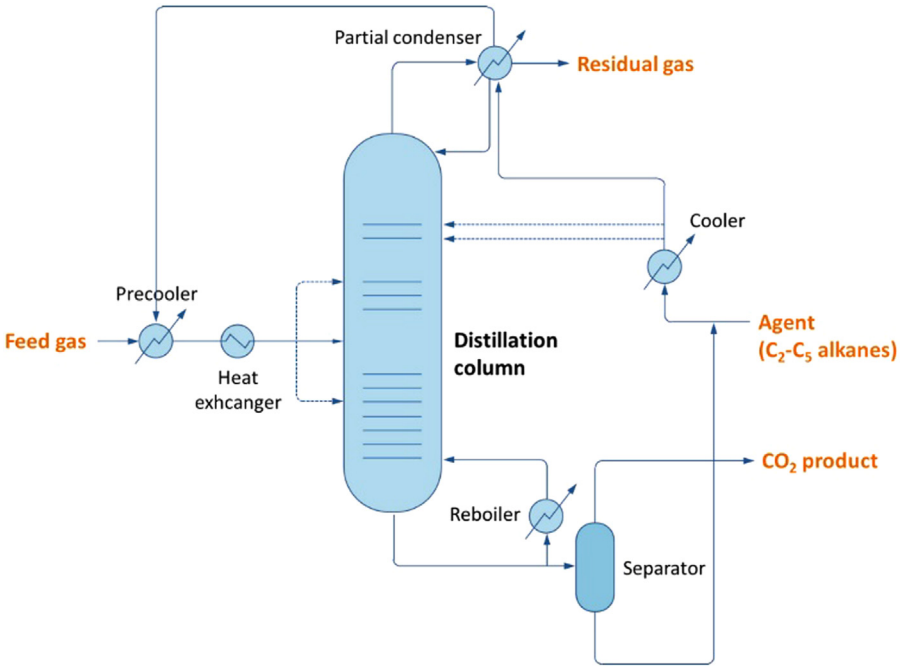

Fig. 5.15. The schematic flow diagram of Ryan Holmes process (Holmes and Ryan, 1982). (For interpretation of the references to color in this figure legend, the reader is referred to the web version of this article.)

a negative impact on both its combustion and transportation (Rufford et al., 2012). In this technology, the cryogenic distillation column consists of three parts: a controlled freezing zone, an upper distillation section and a lower distillation section. After dehydration and cooling, the feed enters the CFZ through a nozzle where the CH_4 evapourates above due to the higher temperature above than below. The solidified CO_2 is collected in the melt tray, and the temperature is kept moderately above the CO_2 solidification temperature so that CO_2 leaves at the bottom as a high concentration of liquefied CO_2 (Michael et al., 2011). The Exxon-Mobil Upstream Research Company developed this technology in 1983 and successfully demonstrated it in a commercial demonstration plant (Michael et al., 2011). The project results show that the technology has a natural gas processing capacity of 0.02 MNm^3 and a maximum operating capacity of 28.3 MN^3/day, and that most of the captured CO_2 can be used for enhanced oil recovery (EOR). However, it should be mentioned that CFZ is not economical when there is a high content of ethane or higher hydrocarbon in the feed gas (Kelley et al., 2011).

5.3.3. *Vapour-to-solid cryogenic separation*

Antisublimation carbon capture technology is a vapour-to-solid cryogenic process in which CO_2 is converted directly from the gas phase to the solid phase at atmospheric pressure (or below the three-phase point pressure). The process of antisublimation CO_2 capture can be roughly divided into five steps (Pan et al., 2013): 1) chilling of flue gas to −40 °C and removal of moisture and other impurities, 2) heat exchange between rich and poor flue gases, 3) refrigeration integrated cascade (RIC) process, 4) freezing heat exchange of CO_2, 5) recovery of CO_2.

Clodic et al. used lab-scale tests for an antisublimation carbon capture process in a 660 MW boiler under flue gas conditions of 15.47 % CO_2 concentration at 60 °C and 120 KPa, respectively (Clodic et al., 2005a, 2005b). The result shows that the energy loss in total power efficiency is controlled between 3.8 % and 7.2 %, which is a relatively low level compared to other technologies (Clodic et al., 2005a). Schach et al. performed simulations by reproducing the gas-liquid and solid-liquid phase equilibrium models, where the flue gas was chilled to 155 K at 100 KPa, and the specific electric demand was 0.286 kWh/kgCO_2 (Schach et al., 2011). In this process, the carbon capture performance is further improved by improving the compression cooling cycle, and the power consumption is further reduced to 0.193 kWh/kgCO_2, but the high equipment investment cost is a major bottleneck problem. A similar process mechanism was reported by Spitoni, where the optimized process was able to recover both liquid CO_2 and liquid biogas with an electrical power consumption of 1.093 kWh/kgCO_2, which is 23 % and 22 % lower than the energy consumption levels of the alternative processes (Spitoni et al., 2019).

The CO_2 concentration in raw biogas has a significant effect on electricity consumption, which varies from 1.093 to 1.574 kWh/kgCO_2 when the CO_2 concentration is raised from 5 % to 50 %. CO_2 concentration also affects its freezing point during flue gas carbon capture. The freezing point of pure CO_2 gas is −78.5 °C. However, it reduces to −99.3 °C when the CO_2 concentration is low to 15 % that in the flue gas condition, undoubtedly increasing the overall energy consumption (Song et al., 2014). Therefore, low CO_2 concentration and high expected capture target increase the overall energy consumption of the antisublimation process in flue gas (Clodic et al., 2005a). For the carbon capture process in biogas, even though the overall energy consumption increased and the liquid biogas revenue decreased when the feed CO_2 concentration was in the worst condition (50 % CO_2 content), the total energy cost increased up to 5 % due to 50 % increment of by-product (liquefied CO_2) (Spitoni et al., 2019).

Generally speaking, the advantage of antisublimation carbon capture is that it has lower energy requirements in certain carbon capture scenarios (Clodic et al., 2005a; Spitoni et al., 2019). Another advantage of antisublimation technology is that the CO_2 thawed on the heat exchanger surface can be used for heat recovery, providing pre-cooling (Clodic et al., 2005b; Spitoni et al., 2019). At the same time, the latent heat during melting can be used to cool the refrigerant before evapouration (Clodic et al., 2005a). However, there are some limitations with the antisublimation process. For example, the moisture in the flue gas and raw biogas must be removed to less than 5 ppm to avoid clogging and other adverse effects. In addition, the choice of heat exchanger material is crucial to the effect of heat transfer efficiency after frosting. Finally, the concentration of CO_2 in the flue gas and raw biogas plays an equally important role in the evaluation of economic technology.

Stirling coolers are specific for their small size and low refrigeration temperature and can be used in the antisublimation capture process of flue gas and biogas. Song et al. designed a Stirling-based cryogenic capture process for post-combustion flue gas (Song et al., 2012c). This

carbon capture system consists of three parts. The pre-cooling tower removes the water from the flue gas to avoid blockage. The dehydrated flue gas is continuously cooled down to −99.3 °C by cooling towers. The CO_2 in the flue gas is frosted on the storage tower, the solid CO_2 is collected by scrapers, and the remaining flue gas (the main component is N_2) is discharged to the atmosphere. The parameter analysis, energy consumption, study and energy integration of the system are also reported in the relevant articles, where the energy consumption of the simulated flue gas carbon capture at the experimental scale is controlled below 0.55 MJ/kgCO_2 (Song et al., 2012a; Song et al., 2012b; Song et al., 2017). However, the antisublimation carbon capture technology based on the Stirling cooler may be limited by the real flue gas conditions (impurities, high temperature, atmospheric volume, etc.), which is the focus of further research.

5.3.4. Heat exchangers

Heat exchangers can be utilized to cryogenically antisublimate CO_2 concentrations at atmospheric pressure for both high concentrations of CO_2 found in the flue gas of post-combustion processes (~13–15 %) and for very low concentrations of CO_2 found directly in the atmosphere (~0.04 %). While the idea of antisublimating CO_2 directly from exhaust gas streams at atmospheric pressure using a cryogenic heat exchanger has been around for around 20 years, newer studies are beginning to explore thermally capturing CO_2 directly from the atmosphere utilizing massive heat exchangers placed in arctic climates. Even though the two situations have drastically different CO_2 concentrations, the technology needed to design cryogenic heat exchangers to antisublimate CO_2 is analogous.

5.3.4.1. Heat exchangers: CO_2 cryogenic flue gas capture at atmospheric pressure. While considerable research to directly capture CO_2 from the atmosphere via chemical- and adsorption-based methods (Deng et al., 2021; Lai et al., 2021; Sanz-Perez et al., 2016b) is ongoing, due to the immaturity of the technology, questions remain on how and at what cost these techniques will scale to the gigaton level (Baxter et al., 2009; Keith et al., 2006; Lackner et al., 2012). On the other hand, cryogenic CO_2 removal is better understood, making potential faster scale-up possible. Cryogenic heat exchangers may be used for post-combustion carbon remover as well as for direct-air capture. Cryogenic CO_2 removal directly from the atmosphere or from power plant effluent is based on the thermal sublimation of CO_2 at very low temperatures, thus creating solid CO_2 for disposal. Post-combustion carbon removal from power plant exhaust streams using cryogenic heat exchangers is a mature technology that has been utilized for some time. Recently, several researchers have been exploring potential direct air capture cryogenic CO_2 heat exchanger designs for placement in Arctic and/or Antarctic climates (Boetcher et al., 2020; Perskin et al., 2022; von Hippel, 2018).

Clodic and Younes (2003) investigated the energy consumption associated with antisublimating CO_2 from flue gas using cryogenic refrigeration at atmospheric pressure. Theoretically, they determined that more than 93 % of a 15 % flue-gas CO_2 concentration could be captured at plate-heat-exchanger surface temperatures between −99 and 122 °C. Since flue gases exit at high temperatures, above 85 °C, water must first be condensed out of the mixture, then, after the CO_2 "frosts" onto the surface, it must be removed by a "defrosting process," so a multi-step process is needed cryogenically removing CO_2 from effluent at atmospheric pressure. Follow-on test-bench work by Clodic et al. (2005b) presented an experimental examination of the defrosting process. Water from flue gas, at 15 % CO_2 concentration, is first removed to equal 0.01 g of water per kg of dry flue gas, by multi-stage condensation. The flue gas is then routed to a low-temperature evapourator, where the flue gas is cooled to −120 °C, energy recovery is utilized, and an energy cost is determined by process steps. Excluding other steps, such as pre-cooling to remove condensate, the energy cost of the cryogenic process was determined to be approximately 1.12 MJ/kg CO_2, including a defrosting waste-energy recovery of around 0.26 MJ/kg CO_2.

In the process proposed by Baxter et al. (2009), the flue gas is cooled, dried, and moderately compressed before it is cryogenically formed into a solid. In their process, with a concentration of CO_2 less than 15 %, 99 % of the CO_2 is antisublimated at −135 °C. The advantage of the system proposed by Baxter et al. (2009) is that it can be easily retrofitted to existing carbon removal systems. Energy cost per mass CO_2 was not reported.

Haddad et al. (2019) modelled the frost growth and formation of CO_2 cryogenically antisublimating on a flat plate from biogas and flue gas stream utilizing simplified heat and mass transfer equations. The heat and mass transfer equations include heat and mass transfer coefficients which are determined using existing correlations in the literature. The exact starting CO_2 concentrations in the biogas and flue gas streams are unclear. Utilizing parabolic trough solar collectors to power a vapour absorption refrigeration cycle, Sateesh et al. (2021) tried to capture post-combustion CO_2. The authors assumed a flue-gas composition of 15 % CO_2, 75 % N_2, and 10 % H_2O and claimed a 100 % CO_2 capture rate at an energy penalty of 1.25 MJ/kg of CO_2.

5.3.4.2. Heat exchangers: cryogenic direct air capture of CO_2. Pure CO_2 at 1 atm pressure antisublimates (changes phase from vapour to solid) at −78.5 °C. However, for CO_2 in the atmosphere, which has partial pressures much below 1 atm, a much lower temperature is required to extract solid CO_2 from power plant streams or the air. Power plant exhaust CO_2 concentrations can reach up to 14 %. Recent measurements of the concentration of CO_2 in the atmosphere at the Muana Loa Atmospheric Baseline Observatory have reached 419 ppm (NOAA, 2022), which equals a partial pressure of 0.000419 atm, which corresponds to an antisublimation temperature of −141.5 °C. However, it should be noted that the CO_2 continues to antisublimates, and the partial pressure also decreases, which corresponds to a decrease in antisublimation temperature. Temperatures as low as −162 °C may be required to antisublimate 99 % of the CO_2 from the atmosphere. Air is primarily made up of N_2 and O_2. At 1 atm, O_2 and N_2 begin to liquefy at −181 °C and −195.8 °C, respectively. Since the partial pressures of those components in the air are less than 1 atm, the liquefication temperature will be even lower, allowing CO_2 to be cryogenically removed before liquefying O_2 or N_2.

In the last decade, due to the urgency of the global CO_2 problem, research has emerged on thermally capturing CO_2 directly from the environment via antisublimation using a cryogenically cooled plate heat exchanger. The heat exchanger would be a part of a CO_2 deposition plant placed in Antarctica. The cold-air temperatures in Antarctica allow the inlet temperature to be as low as possible and closer to the CO_2 antisublimation temperature, thus reducing the cooling the sensible load needed to reach that temperature. Another advantage of Antarctica is that at those low temperatures, the air is virtually completely dry. Agee et al. (2013) were one of the first to conceptually propose such a system, referring to it as a CO_2 "snow" maker. An initial laboratory prototype was analysed by Agee and Orton (2016). The prototype was a benchtop-scale sequestration chamber situated with an aluminum plate interfaced with LN_2. This experiment showed proof-of-concept, but the authors did not perform an in-depth energy analysis.

A systems-level energy analysis for a CO_2 deposition plant hypothetically placed in three candidate arctic climate scenarios (Snag, Yukon, Oymyakon, Russia, and Vostok Station, Antarctica) was performed by von Hippel (von Hippel, 2018). Using a simplified energy balance, von Hippel determined that CO_2 heat exchanger antisublimation in an arctic environment may be competitive with other technologies. Follow-on work, using a more sophisticated thermodynamic model and investigating more cases, including exploring pre-compression, was conducted by Boetcher et al. (2020) and Perskin et al. (2022). There, the energy performance of a waste-heat (or better, a "waste-cool") precooler heat exchanger attached to the antisublimation heat exchanger was evaluated. It was found that this type of system could theoretically antisublimate

90 % of 405 ppmv concentration (~0.04 %) atmospheric CO_2 for as low as 133 MJ/kg in an arctic environment.

5.3.5. Cryogenic liquids

In addition to heat exchangers, cryogenic liquid as a cold source can directly take away the heat of flue gas containing CO_2, resulting in the solidification of CO_2. Then, the mixture liquid slurry of CO_2 and the cryogenic liquid goes through a filter to produce a CO_2-rich product (Jensen et al., 2015). Generally, the vapour pressures of cryogenic liquids should be low in order to reduce losses during evapouration. Fazlollahi et al. have chosen isopentane to prevent CO_2 solidification on the surfaces, which would end the process (Fazlollahi et al., 2015). In Jesen's work, the heat duty is provided by an internal CF_4 refrigeration and an external cooling loop of CH_4, and the result shows that the parasite power loading is about 15 % (82.6 MW_e) and the energy consumption is 0.74 $MJ_e/kgCO_2$ (Jensen et al., 2015).

In most carbon capture processes, the biggest challenge is the high energy consumption. For the cryogenic carbon capture process, the waste cold energy like LNG (liquefied natural gas) is a promising approach to reduce the energy consumption by a thermal process, an inertial carbon extraction system or an external cooling loop. A hybrid cryogenic carbon capture process with an external cooling loop (CCCECL) was proposed (Baxter et al., 2009; Jensen et al., 2015). Briefly, the CCCECL system concludes: 1) dehydrated and cooled flue gas was sent from the system to the CCCECL process, 2) the flue gas was compressed and chilled to a temperature above the solidification of CO_2, 3) the gas was expanded to be further chilled, 4) an amount of CO_2 was precipitated, 5) the CO_2 was pressured and reheated via the inlet gases, 6) the liquid CO_2 product was achieved for further utilization and the N_2-rich exhausted gas was discharged. Some configurations of the CCCECL process can store energy as LNG (Jensen et al., 2015). In such system, the refrigerant was regenerated during low-demand periods, and then it was used to drive the cryogenic carbon capture process during peak demand periods. As a result, the parasitic load to the grid reduces. Besides, renewable intermittent power sources could be integrated with conventional power generation systems via CCCECL, resulting in a low energy intensive compared to the conventional capture process (0.98 $MJ_e/kgCO_2$) (Safdarnejad et al., 2015).

5.3.6. Packed beds

Packed beds have been worked as a heat transfer surface for the cryogenic carbon capture process that is usually filled with cold bed materials like steel monolith structure (Tuinier et al., 2011b). The capture process follows the steps: 1) chilled N_2 stream is sent to precool bed material, 2) the N_2 steam is stopped, and the flue gas is sent to cryogenic packed bed, 3) CO_2 frost on the surface of bed materials till saturation, 4) a CO_2 frost front happen through the column, 5) a regeneration step is required when the packed column is saturated. The advantages of a cryogenic packed bed are that both CO_2 and H_2O can be separated from flue gas simultaneously via the difference of their dew and solidification points and the cold energy can be provided by LNG (Tuinier et al., 2010). Tuinier proposed a dynamically cryogenic packed bed, and the results show that the low volume fraction of frosted CO_2 leads to a low requirement of the elevated pressure value (Tuinier et al., 2011b). This indicated that the pressure drop and clogging phenomenon are mitigated in the cryogenic packed bed process. Apart from the carbon capture process in flue gas, cryogenic packing is also applied to the biogas upgrading process (Tuinier and van Sint Annaland, 2012). A novel cryogenic packed bed has been proposed for biogas treatment, and the result shows that the purity and recovery of biomethane products are higher. Meanwhile, the bed capacity is much higher (350.2 kg CH_4 h^{-1} m^{-3} packing), and the energy consumption is lower (2.9 $MJ/kgCH_4$), compared to the conventional vacuum pressure swing adsorption process (Tuinier and van Sint Annaland, 2012). Moreover, the removal of H_2S content in raw biogas can be simultaneously achieved when the initial cryogenic packed bed temperature as low as −150 °C (Abatzoglou and Boivin, 2009). However, this may lead to an augment in operating cost on required cold energy. Fortunately, the cold energy required in the cryogenic packed beds process may be provided by LNG, making it competitive (Abatzoglou and Boivin, 2009). Moreover, the thermal insulation of cryogenic packed bed is another challenge that should be taken into consideration to reduce latent heat loss.

5.3.7. Compression

Compression is an important part in the cryogenic carbon capture process. The vapour-to-liquid and vapour-to-solid routes are determined by the pressure and cryogenic temperature of the carbon capture process. In Baxter's work, flue gas was compressed to 5–7 bar before cooling and chilled and then was expanded to form CO_2 solidification, which was called cryogenic carbon capture with compressed flue gas (CCCCFG) (Baxter et al., 2009). Similarly, in the cryogenic distillation process, the feed gas is compressed to 4.9 bar via four stage compressor and then cooled to 35 °C by water (Yousef et al., 2018a, b, 2019). Maqsood et al. compared the effect of pressure on liquid and solid formation during cryogenic separation. The result showed that the vapour-solid region decreased with the pressure (−60 to −98 °C for 20 bar and −62 to −75 °C for 40 bar) and the CH_4 purity was higher at 40 bar under the same cryogenic temperature (Maqsood et al., 2017).

The energy consumption in the cryogenic process is one of the main challenges for the scale-up application of cryogenic carbon capture processes. In the cryogenic distillation process, the power penalty for the compression process accounts for 43.1–50.9 % of the total biogas upgrading energy consumption, and the energy consumption for CO_2 capture is 1.66–1.79 $MJ/kgCO_2$ (Yousef et al., 2018a, b). Energy saving technologies have been applied to cryogenic carbon capture processes. Compared with the conventional distillation carbon capture process, more than 34 % energy reduction was observed when the multibed hybrid network was introduced into cryogenic distillation for the natural gas sweetening process (Maqsood et al., 2014c). Moreover, the energy consumption can be further reduced when the capture process is applied with intensified side mounted and integrated switch cryogenic antisublimation bed, resulting in a 69.24 % profit increment (Maqsood et al., 2017). Moreover, Pellegrini et al. compared three cryogenic purification technologies for natural gas upgrading, including the dual pressure cryogenic distillation process, Ryan-Holmes and antisublimation process (Pellegrini et al., 2018). Compared with Ryan-Holmes process, the mechanical power consumption of dual pressure cryogenic distillation is higher because the raw biogas required to be compressed to 50 and 40 bar, and for antisublimation process, 99.84 % of the energy requirement is the cooling duties consumption (Pellegrini et al., 2018). Up to now, the reduction of energy consumption in the cryogenic carbon capture processes requires further development and research to be applied in practical sceneries.

5.3.8. Life cycle assessment of cryogenic CO_2 capture

An overview of cryogenic-based carbon capture pathways and technology challenges, which mean the extreme utilization of cold energy and energy consumption barriers, is provided by Shen et al. (2022). A recent review paper by (Song et al. (2019b) focused on cryogenic carbon capture technology progress, including cryogenic system structure and optimal system parameters, which revealed that cryogenic carbon capture technology provided remarkable cost and efficiency benefits. However, most of the studies involved cryogenic carbon capture considering its energy consumption (Esfilar et al., 2018), technical feasibility (Naquash et al., 2022) and economic performance, without taking its carbon abatement and other environmental impacts into consideration (Markewitz et al., 2013). Only a few studies provided a far-reaching insight into the life-cycle environmental impacts or life-cycle cost analysis of systems combined with cryogenic technologies and other carbon capture pathways, which shows a possibility to be deployed in biogas upgrading (Hiloidhari and Kumari, 2021), air separation unit (Schreiber et al., 2013; Troy et al., 2016; Zhang et al., 2014), natural

gas purification (Rocco et al., 2019) and biomass-coal co-gasification (Esfilar et al., 2018). Herein, all selected LCAs report significant carbon capture processes with regard to cryogenic technologies. However, global warming potential (GWP) can hardly be compared, since each cryogenic LCA exhibits specific system boundary and functional unit, use different life cycle inventory source and database, such as Ecoinvent, Simapro and Gabi. The uniform and comprehensive framework principles should be further investigated and paid more attention to, including system boundaries, functional units and inventory analysis.

System boundaries: System boundaries vary to different extents for all kinds of cryogenic capture systems, but it is necessary to take some vital processes into consideration, such as raw material production and transportation, energy conversion, carbon capture and storage. Biogas-related cryogenic systems usually contain the whole supply chain of biogas from cradle to gate, which includes biomass feedstocks cultivation, harvesting and transportation processes, and bioenergy conversion processes (Florio et al., 2019). However, there are still few studies that considered the product end-use process (Adelt et al., 2011). Cryogenic air separation units are the most common forms while talking about cryogenic carbon capture, which can be deployed in steel production, liquefied natural gas (LNG) production and combined with membrane capture. Some studies have taken the whole life cycle of air separation and carbon capture processes into consideration, which included up-stream processes (O_2 production process, MDEA and membrane production), main processes (steel production and CO_2 capture), and down-stream processes (CO_2 transport and storage), but not considering the end-of-life processes of different equipment (Luca and Petrescu, 2021). More comprehensive frameworks have considered waste treatment processes in the life cycle of IGCC and oxy-fuel plants (Schreiber et al., 2013; Zhang et al., 2014).

Functional unit: Per unit of product (biogas, biomethane, electricity, heat etc.) produced (Adelt et al., 2011; Florio et al., 2019) or per unit CO_2 removal from biogas (Starr et al., 2012) are usually selected as functional units of biogas upgrading systems. Electricity or heat supply is selected to be functional units since air separation is usually connected with generation processes.

Environmental categories: Most of the LCAs of cryogenic-related systems considered ReCiPe 2016 midpoint (H), CML 2001 and Eco-indicator 99 Hierarchist as the impact assessment methods with various impact categories, among which GWP is the most cared one. Hence, it seems that there is an agreement to consider multiple environmental impact categories for the assessment of cryogenic systems.

Cryogenic carbon capture technologies have been studied for thermodynamic performance and technical feasibility with a limited understanding of overall environmental implications. Because of the lack of large-scale deployment or pilot demonstration, there is a huge knowledge gap in the availability of operation parameters and related energy/resource consumption data on cryogenic carbon capture, which is the direct reason for the shortage of LCAs about cryogenic carbon capture. This part aims to conclude the LCA of the cryogenic carbon capture situation to fully understand the environmental benefits and potential trade-offs associated with cryogenic carbon capture technologies. Based on the available body of cryogenic carbon capture LCA literature, we conclude that existing LCA results for most cryogenic technologies are not representative of cryogenic carbon capture schemes since these studies are all related to cryogenic air separation or biogas upgrading processes. However, a high-purity CO_2 product in either a compressed liquid or solid phase and utilization of organic solvents and sorbents is the main advantage of cryogenic carbon capture technologies, indicating the environmental benefit potential for ecosystems. Furthermore, due to dramatic temperature variations and high-pressure conditions, large exergy losses exist during the whole capture process. Therefore, more efficient cryogenic carbon capture option designing will be an inevitable challenge for commercial applications. In order to explore more possibilities for the application of cryogenic carbon capture technologies, life-cycle environmental or cost assessments should be deployed under comprehensive and suitable evaluation frameworks. Moreover, life cycle environmental assessment should also quantify the environmental burden shift to reveal more realistic environmental benefits connecting with various ecologic co-benefits and compare with different conventional CCS options.

5.4. Process intensification

Currently, the improvement of carbon capture efficiency generally needs high investment, including more expensive materials and increasing operating cost. This scenario has sent researchers fleeing to the application of process intensification (PI) techniques in the field of carbon capture for saving energy and decreasing consumption. For example, in the commonly alkanolamine method, the chemical reaction is fast while the efficiency of carbon capture is limited by the gas-liquid/gas-solid mass transfer in most cases. Therefore, it is promising to break through the limitation of low-speed heat and mass transfer via drastic improvement of equipment and process efficiency. According to the principle of PI (Van Gerven and Stankiewicz, 2009), the intensified strategies for carbon capture can be classified into four domains: spatial, functional, energy, and temporal. Specifically, the PI of carbon capture can be achieved by (1) developing novel structures to enhance mass transfer; (2) combining a variety of technologies to maximize the synergistic effect; (3) designing rational process to minimize the energy cost; and (4) shortening the process time to improve the whole efficiency.

5.4.1. Spatial domain: novel structure for ample transfer

With the aim to enhance mass transfer, many researchers tried to optimize the internal structure of the absorption columns, such as the geometry of aperture and baffles (Garcia-Abuin et al., 2010), the structure of packing (Smith et al., 2015), etc. and adjust the operating conditions, including gas velocity, gas-liquid ratio, and liquid height in the column (Yan et al., 2019). The experimental results of these studies showed that installing baffles and using smaller apertures, lower sorption temperature, higher regeneration temperature, and lower regeneration pressure exerted positive effects on CO_2 capture. The principle of above studies is to increase gas-liquid mass transfer coefficient by enhancing fluid turbulence or enlarge the gas-liquid contact area by changing the fluid flow patterns, including the deformation, splitting, stretching and breakup of bubbles (Yin et al., 2022).

With the idea of intensifying gas-liquid mass transfer, microchemical technology has recently attracted great attention in the field of CO_2 capture due to the various advantages including efficient mass and heat transfer, safer operation, higher integration and superior controllability. By performing the processes in the scale of sub–millimeter, microreactors can dramatically intensify the gas–liquid mass transfer. As reported, the volumetric mass transfer coefficient in the micro-reactor can be several orders of magnitude higher than that in traditional gas–liquid vessels, such as plate column, packed column and stirred tank (Ganapathy et al., 2016). For example, Yue et al. (2007) investigated the absorption of pure CO_2 in a 667 μm channel. The experimental demonstrated an enhancement in mass transfer characteristics, as compared to conventional absorption systems. A comparison of mass transfer performance among different gas–liquid contactors reveals that the gas–liquid microchannel contactor of this study can provide at least one or two orders of magnitude higher liquid side volumetric mass transfer coefficients and interfacial areas than the others. Besides, Ganapathy et al. (2015) compared a microreactor to most conventional absorption systems including packed columns, plate columns, bubble columns, tube reactors, bubble reactors and venturi reactors. The experimental results showed that the interfacial areas and liquid-side volumetric mass transfer coefficients achieved using the present reactors are between 1 and 4 orders of magnitude higher than the mentioned conventional macroscale gas–liquid absorption systems, which is considered an indication of the high level of process intensification and enhancement that can be achieved by using microreactors. The high mass transfer

efficiency of micro-reactors is bound to reduce the operating consumption of carbon capture. Shao et al. (2010) investigated the influence of channel length of micro-reactors on their absorption efficiencies of CO_2 and found that when the channel length increased by 100 %, the mass transfer coefficient was higher by 290 %, improving utilization of the absorption capacity of the amine solution for a given reactor volume.

Although microchemical technology has exhibited promising performance in carbon capture, the industrial application of this method still faces many obstacles. First, smaller diameters yield substantial enhancement in mass transfer characteristics, while the pressure drop is also considerably higher (Niu et al., 2009). For the various microchannel contactors tested, an enhanced mass transfer rate was observed for smaller microchannel contactors. The shortening of the diffusion length from channel size reduction is beneficial to achieve fast mass transfer rates, and this is the size effect of mass transfer (Ganapathy et al., 2014). However, the rapidly increasing pressure drop limits the application of micro-reactors for large handling capacity. Besides, the strong interfacial force makes it very difficult to operate counter-current at microscale, not only for absorption but also for stripping, distillation and extraction (Wang et al., 2021), which limits the design of more rational structures. Therefore, in order to better utilize the advantages of microscale to carbon capture, the micro-channel should be optimally designed to ensure the inherently higher surface area to volume ratio of these systems substantially while keeping the pressure drop at moderate levels.

5.4.2. Functional domain: hybrid techniques for maximal synergism

Apart from the optimization of reactor structures, the combination of two or more standalone CO_2 capture technologies, named as hybrid processes, has also provided novel ideas to overcome the challenges of standalone CO_2 capture technologies due to the potentially high capture efficiency and low energy requirement. The hybrid processes usually consist of two or more conventional technologies (*i.e.* absorption, adsorption, membrane, cryogenic and hydrate, *etc.*). The integration of different technologies may be superior to the standalone process and avoid their disadvantages. Currently, there are four types of hybrid carbon capture technologies, including (1) absorption-based processes, including membrane contactor (Zhao et al., 2016) and absorption-adsorption (Breault et al., 2016); (2) adsorption-based processes, including adsorption-catalysis (Marono et al., 2015) and adsorption-hydrate (Yang et al., 2014); (3) membrane-based processes, including membrane-cryogenic (Burdyny and Struchtrup, 2010), and membrane-absorption (Kundu et al., 2014); (4) low-temperature-based processes, including cryogenic-hydrate (Suroutseua et al., 2011) and low temperature-absorption (Hanak et al., 2015b).

Appropriate hybrid CO_2 capture strategy can be a potential alternative of exiting standalone processes in terms of efficiency, as screening of suitable hybrid carbon capture processes highly depends on the properties of feed gas (*e.g.* CO_2 concentration, gas temperature and pressure, *etc.*), the requirement of product (e.g. purity, *etc.*) and the availability of the capture equipment. In addition, CO_2 recovery and energy consumption are also significantly affected by the source of CO_2 emission when using different capture technologies (Song et al., 2018b). For example, Song et al. (Song et al., 2018a; Song et al., 2017) employed a membrane-cryogenic hybrid system to CO_2 capture and exhibited that compared to the standalone methods, hybrid processes showed the superiority not only in CO_2 recovery and energy penalty, but also in the installation investment.

The synergistic effect existed in the hybrid processes can no doubt lead to energy saving and consumption reduction. Liao et al. (2019) designed and optimized a hybrid membrane-cryogenic system for both pre-combustion and post-combustion carbon capture, which reduced 33 % of operating cost and 28 % of total annualized cost. Besides, Scholes et al. (2013) postulated a post combustion capture process equipped with three membrane stages and a cryogenic separation to ensure the feed burner air supply is not oxygen-deficient. By employing this strategy, \$43/ton CO_2 can be avoided, and the carbon capture cost of membrane contactor technology can be decreased to \$48/ton CO_2 with over 90 % CO_2 recovery and 97 % CO_2 purity.

Although increasing interest in the CO_2 capture by hybrid processes has been attracted in recent years and exciting results have been reported, amount of existing research is undertaken by simulation or lab-scale, because the overall cost of the hybrid process has to be taken into consideration in terms of capital costs, operating costs and maintenance costs. Most costs are very site-specific, and for a full-scale system these costs strongly depend on properties (e.g. CO_2 concentration, flow rate, temperature and pressure) of feed gas, the configuration of separation units, as well. Meanwhile, the concentration of CO_2 is limited to higher than 15 %, and the capture condition is also moderate than that in industrial emissions. In addition, the hybrid processes may result in the more stringent requirements on materials and equipment, such as cold resistance of membrane in the membrane-cryogenic system, and poison resistance of membrane in the adsorption-catalysis-membrane hybrid system etc. To overcome these problems, it is essential to understand the interactions between membranes and absorbents/solvents and develop novel membranes and green solvents for hybrid processes, which requires further investigation.

5.4.3. Energy domain: process optimization for low cost

From the perspective of energy domain, it is necessary for industrializing carbon capture technologies to design rational processes via the combination of flowsheet design and rigorous optimization, with the aim to lower the energy cost and higher the environmental performance. In order to deliver better performance in recovery rates, energy consumption and solvent slip, the design and improvement of a standalone CO_2 capture flowsheet generally follows these steps: (1) Design equilibrium-based process flowsheet to obtain process specifications; (2) Conduct sensitivity analysis on the process variables to obtain process model and variables; (3) Perform multi-objective optimization to obtain the results of energy and mass balances; (4) Calculate equipment dimension and process productivity (Sharma et al., 2016). These processes are always achieved by using commercial software packages, including Aspen Plus, HYSIS, or gPROMS, because these tools contain the required physicochemical models and can provide property databanks for numerical calculation.

Different with traditional flowsheets design, the decision makers in the current society focus more on emission reduction efficiency, energy penalty, and carbon cyclic capacity among different solvents, rather than just energy consumption (Ji et al., 2021). However, the multi-objective problem leads to a time-consuming design process because of the highly non-linear nature of the model equations and the high complexity of the processes. In this case, many researches abstracted this problem as a Mixed Integer Non-Linear Problem (MINLP) to assist them in the selection of optimal retrofitting options of CO_2 capture technologies. Take a design process for a coal-fired plant as example, post-combustion capture by monoethanolamide (MEA) scrubbing is currently the commercial technology used worldwide, while oxy-fuel combustion is still on an earlier stage of development (Zhu and Fan, 2011). Many preliminary studies have shown that the latter technology is technically and economically feasible for retrofitting existing coal-fired power plants (Hu and Yan, 2012). In order to evaluate these two techniques, Bravo et al. (2021) considered economic and environmental criteria at the early stages of the process development and conducted multi-objective optimization to address the trade-off problems between different economic and environmental indicators. The numerical results indicated that carbon capture with MEA scrubbing performs better for soft environmental limits while oxy-fuel combustion is the preferred choice when more stringent environmental limitations are considered.

However, the optimal design of carbon capture processes is always time-consuming due to the highly non-linear nature of the model equations and the high complexity of the processes. Besides, the convergence management of the process simulations limits the combined flowsheet

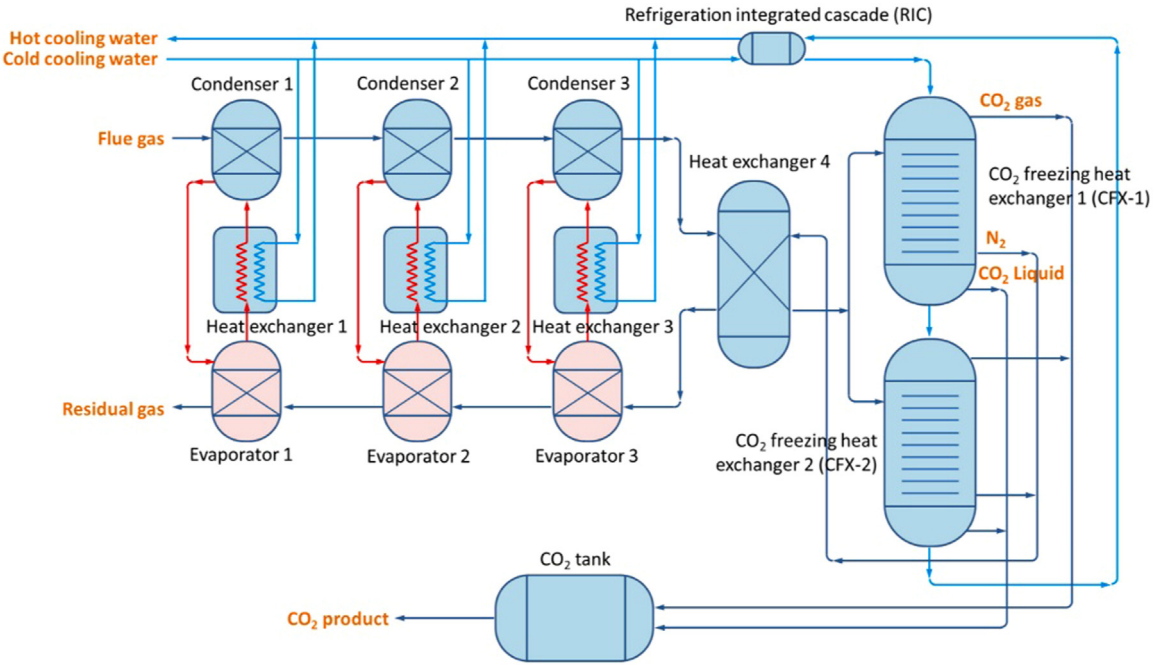

Fig. 5.16. Process flow diagram of the anti-sublimation CO_2 capture process (AnSU) (Clodic et al., 2005b). (For interpretation of the references to color in this figure legend, the reader is referred to the web version of this article.)

design. Hence, novel computing methods should be further developed for economy-environment multi-objective problems.

5.4.4. Temporal domain: external-field intensification for high efficiency

The traditional method of carbon capture suffers from severe corrosion problems, considerable energy loss, high sorbent cost, lower gas–liquid interfacial surface area, and ineffective regeneration (Bhown and Freeman, 2011). In the temporal domain, the principles of PI indicate that manipulation of the time scales may mean for instance bringing molecules under extreme temperature conditions for a very short time, which can shift the process beyond the equilibrium limitation, or it can improve heat management in multifunctional systems. For example, the regeneration of absorbents used for capture CO_2 usually employs temperature-swing adsorption (TSA) but the regeneration time usually is more prolonged due to slow heating and cooling of the adsorbent during TSA, thereby increasing the adsorbent inventory and investment costs (Leung et al., 2014). Thus, alternative (e.g., electrical) heating methods are being explored to develop an energy-efficient and rapid TSA cycle process for carbon capture. Alternative electrical heating methods for TSA include Electric Swing Adsorption (ESA), which uses the Joule Effect (Zhao et al., 2017), induction heating (Sadiq et al., 2016), and microwave heating (Li, Hong et al., 2019). These techniques could offer distinct advantages over the more traditional adsorbent regeneration techniques in terms of energy efficiency, faster heating rate, and simple and compact equipment designs.

Among the above novel heating methods, microwave heating can directly deliver energy to the targeted composition; this selective heating characteristic leads to the formation of local overheating domains in microscopic scale (called “hot spots”), which has been directly observed in the previous study (Zhao et al., 2022b). This phenomenon can be used to accelerate desorption of CO_2 absorbent. For instance, regeneration of a zeolite 13X under microwave irradiation for acetone and toluene capture resulted in higher desorption rates when compared to conductive heating regeneration (Cherbanski and Molga, 2009). Besides, Yassin et al. (2021) reported a similar result in CO_2 capture from flue gases using pelletized activated carbons. The acceleration of absorbent regeneration in the above studies can be ascribed to the formation of hot spots, inducing a much locally higher temperature over the surface of absorbents than the overall temperature in the equipment (Yang et al., 2017). Apart from the selective heating characteristic, the rapid heating rate of microwave irradiation can also lead to the atomization of liquid droplets and bubble-enhanced flow, enhancing the gas-liquid mass transfer during desorption (Liu et al., 2021; Zhao et al., 2021).

Although microwave irradiation has shown great potential to accelerate the desorption process and therefore decrease the solvents amount, the further applications of microwave irradiation to absorbent regeneration processes in industrial scale should consider the uneven heating problems caused by the inhomogeneous electromagnetic field distribution (Shen et al., 2022; Zhao et al., 2022a). Therefore, the interaction between microwaves and absorbents/solvents should be further investigated before developing microwave-assisted desorption techniques.

5.5. Bio-energy with carbon capture and storage (BECCS)

Bio-Energy with Carbon Capture and Storage (BECCS) is a special technology in CCS, which can capture and store CO_2 generated in the process of biomass combustion or conversion (Fig. 5.16) (Almena et al., 2022). The difference with traditional CCUS technology is that it can achieve negative emissions. The idea is to use plant photosynthesis to convert atmospheric CO_2 into organic matter and store it as biomass, which can be burned directly to generate heat or chemically synthesized into other high-value clean energy sources. Most climate change mitigation pathways which limit global warming to 1.5 °C or 2 °C rely on negative emission technologies, in particularly BECCS (Fajardy et al., 2021).

The development of BECCS technology can solve the problem of harmless and reduced treatment of all kinds of organic waste in urban and rural areas. If biomass waste is not effectively used, under the condition of natural decomposition, methane and other gases with stronger greenhouse effect will be released. Under the general background of comprehensively promoting the rural revitalization strategy, the future development of biomass energy will need to take a road of "agriculture-environment-energy-agriculture" green and low-carbon closed cycle development. BECCS plays an important role in both power generation and non-electricity utilization, and promotes the overall improvement of the energy structure of villages and towns. (Fig. 5.17)

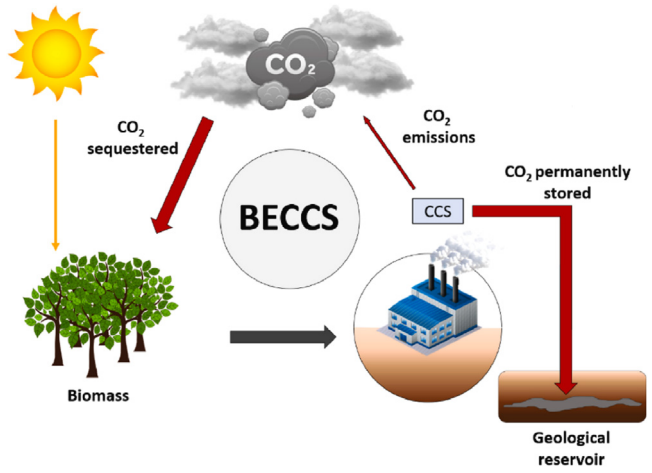

Fig. 5.17. The carbon flow of BECCS. When BECCS systems are employed, a negative carbon flow from the atmosphere into storage is created. (Almena et al., 2022). (For interpretation of the references to color in this figure legend, the reader is referred to the web version of this article.)

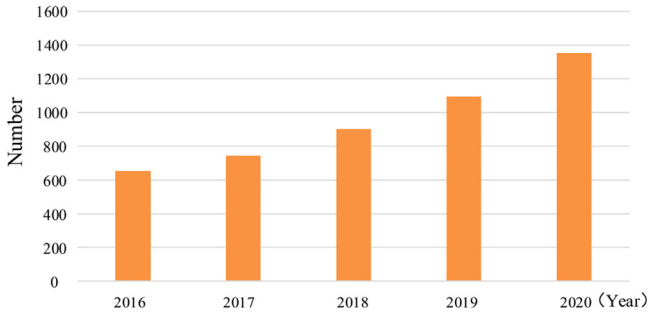

Fig. 5.18. Number of biomass power generation projects in operation (Guo et al., 2022). (For interpretation of the references to color in this figure legend, the reader is referred to the web version of this article.)

5.5.1. Biomass power generation

Biomass power generation is the largest and most mature modern biomass energy utilization technology. The number of biomass power generation projects that have been put into operation from 2016 to 2020 are shown in Fig. 5.18. China is rich in biomass resources, mainly including agricultural waste, forestry waste, livestock and poultry waste, municipal solid waste, organic wastewater and waste, etc. The total amount of biomass resources for energy is equivalent to about 460 million standard coal. Biomass power generation technology can be divided into three categories according to the working principle: direct combustion power generation technology, gasification power generation technology and coupled combustion power generation technology.

Direct combustion of biomass for power generation is very similar to coal-fired boilers in principle. It is to add biomass fuel into appropriate steam boilers for biomass combustion, convert chemical energy in biomass fuel into internal energy of high temperature and pressure steam through high temperature combustion process, convert into mechanical energy through steam power cycle. Finally, the mechanical energy is eventually converted into electricity by a generator.

Biomass gasification power generation should go through the following steps: (1) biomass gasification, after crushing and drying and other pretreated biomass pyrolysis gasification under high temperature environment, to produce gas containing combustible components such as CO, CH_4 and H_2; (2) Gas purification, the combustible gas generated in the gasification process is passed into the purification system to remove impurities such as ash, coke and tar, so as to meet the inlet requirements of downstream power generation equipment; (3) Gas combustion power generation, purified gas into the gas turbine or internal combustion engine combustion power generation, can also be passed into the boiler combustion, the use of high temperature and high pressure steam to drive steam turbine power generation.

Due to the dispersion of biomass resources, low energy density, and difficulty in collection and transportation, direct combustion of biomass for power generation is highly dependent on the sustainability and economy of fuel supply, resulting in high cost of biomass power generation. Biomass coupled power generation is a power generation method that uses biomass fuel to replace some other fuels (usually coal) for mixed firing. It can improve the flexibility of biomass fuel and reduce the consumption of coal at the same time, so as to achieve CO_2 emission reduction of coal-fired thermal power units. At present, biomass coupled power generation technology mainly includes: direct mixed combustion coupled power generation technology, indirect combustion coupled power generation technology and steam coupled power generation technology.

As we all know, biomass itself is generally considered to have zero carbon emissions. In other words, the CO_2 produced by biomass combustion or conversion is equal to the CO_2 absorbed during the growth process, so the CO_2 stored by biomass becomes negative carbon emissions after deducting the additional emissions in related processes. The life cycle assessment (LCA) method was used to evaluate CO_2 emissions from different power generation technologies. The system boundary consists of three parts: forest management (FM), collection, processing and transportation (CPT), and electricity generation with Carbon Capture and Storage (EG-CCS) through a Biomass Heat & Power Plant (BHP-CCS) (Fig. 5.19) (Briones-Hidrovo et al., 2022). The life analysis of the entire system is 25 years. As opposed to integrated coal gasification combined cycle (ICGCC), biomass integrated combined cycle (BIGCC) combined with CO_2 capture can greatly reduce CO_2 emissions.

5.5.2. Biomass liquid fuel

Biomass is the only renewable carbon resource that can be converted into liquid fuel. It has the potential to replace petroleum, provide diversified clean energy supply for transportation, and greatly reduce carbon emissions. At present, the raw materials of aviation biofuel mainly include animal and vegetable oil, lignocellulose, sugar and starch, etc. Animal and vegetable oil based jet fuel has great development potential, with its high energy density, molecular structure close to aviation biofuel, and high blending degree with fossil jet fuel (up to 50 %). It is an important source of sustainable jet fuel at present (Gnanasekaran et al., 2022).

Microalgae biosequestration technology is a process that uses microorganisms to convert a large amount of carbon dioxide into biomass. Algae cells synthesize organic matter through photosynthesis using CO_2 and light energy and release oxygen to realize photosynthetic carbon sequestration (Figueroa et al., 2008). Micrococcoid genetically engineered using tools including CRISPR-Cas9 can produce twice as much oil as its wild parent and grow at a similar rate (Ajjawi, 2017). Zhang et al. found a novel "blue light" enhancement pathway and established an induction pathway for related oil synthesis, achieving a peak productivity of triacylglycerol twice that of unmodified microalgae (Zhang et al., 2022). The advantages of microalgae carbon sequestration technology are high carbon sequestration efficiency, strong environmental adaptability, reduction of industrial carbon emissions, production of high value-added products, and creation of economic value.

5.5.3. Biomass based materials and chemical

At present, there are also many studies that use waste biomass as raw materials to generate zero-carbon plastics. By providing long-chain bio-based epoxides and innovating and efficient synthesis of CO_2 to produce polymers such as biomass polycarbonate materials, the secondary utilization of waste biomass and CO_2 brings greater emission reduction potential. Sichuan University has made a breakthrough in the efficient depolymerization of biodegradable cyclic ester copolymer to obtain its

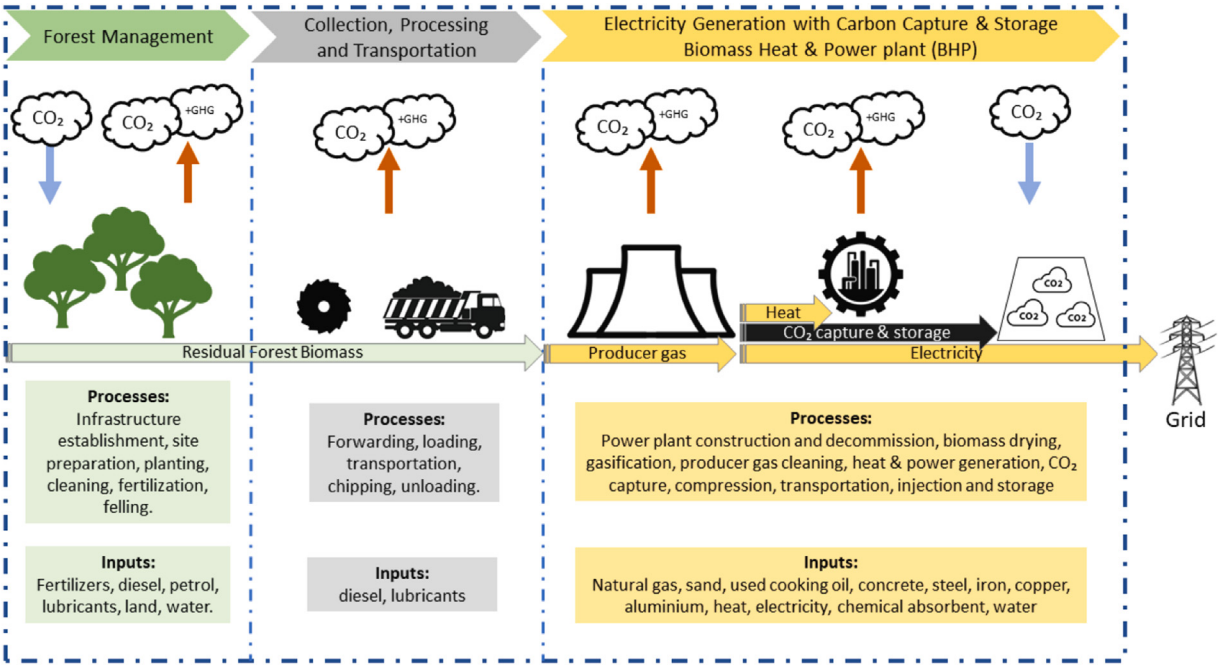

Fig. 5.19. System boundaries of the Biomass Heat and Power Plant with Carbon Capture and Storage. (Briones-Hidrovo et al., 2022). (For interpretation of the references to color in this figure legend, the reader is referred to the web version of this article.)

Table 5.6
Global BECCS project distribution.

Project title	Capture source	Capture scale / (Mt a^{-1})	CO_2 storage method
Illinois Industrial Carbon Capture	Bioethanol plant	1.0000	Saline sequestration
Arkalon CO_2 Compression Facilities	Bioethanol bioplant	0.2900	EOR
Bonanza Carbon Capture	Bioethanol plant	0.1000	EOR
Husky CO_2 Inject	Bioethanol plant	0.0900	EOR
Farnsworth Inject	Bioethanol/fertilizer plants	0.0070	EOR
Mikaua Power plant capture after combustion	Biomass power plants	0.1800	Offshore storage
Drax Power CCS	Biomass power plants	0.0003	Geological storage
Norwegian Full Process CCS	Waste-to-energy/cement	0.8000	Geological storage

Note: EOR (Enhanced Oil Recovery) refers to enhanced oil recovery or enhanced extraction.

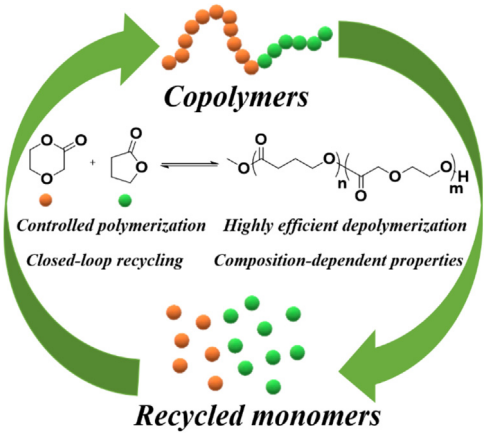

Fig. 5.20. Schematic diagram of controlled synthesis and closed loop chemical cycle of biodegradable copolymers (Yan et al., 2022). (For interpretation of the references to color in this figure legend, the reader is referred to the web version of this article.)

copolymerized cyclic ester monomer under mild conditions (no catalyst, no solvent, 120°C). Through the repolymerization of recovered monomer, a regenerated copolymer with the same structure and properties as the original depolymerization copolymer was synthesized under controlled control (Fig. 5.20). The closed-loop chemical cycle of the polymer was realized for the first time (Yan et al., 2022). Based on the characteristics of biomass unit structure, it is advisable to vigorously develop bioenergy, biochemical and biological materials, and cultivate and strengthen the biomass industry.

5.5.4. *BECCS project distribution*

The application of BECCS technology in the power industry is still in a stage of rapid development. In 2019, the UK Drax 6*660MW biomass fuel power plant started to capture CO_2, capturing 1000 kg of carbon from flue gas emissions every day. This is the first time in the world that CO_2 is captured from 100 % biomass combustion.

As of 2019, the distribution of 8 BECCS projects in the global geological sequestration is shown in Table 5.6. Five of these are already in operation, including one large-scale demonstration project and four demonstration and pilot-scale projects, with an annual CO_2 capture of about 1.5 Mt. Among them, the Illinois Industrial Carbon Capture Project in the United States is currently the largest BECCS project and the only BECCS project in operation in the world. The project captures high-purity CO_2 from maize ethanol production for geological storage in the saline aquifer on a capture scale of 1 Mt/a. The capture sources for the remaining four operating BECCS projects are small-scale ethanol production plants, all of which capture enhanced oil recovery (EOR). In addition, three BECCS geological storage projects are still being planned, with CO_2 capture sources from power plants and cement plants.

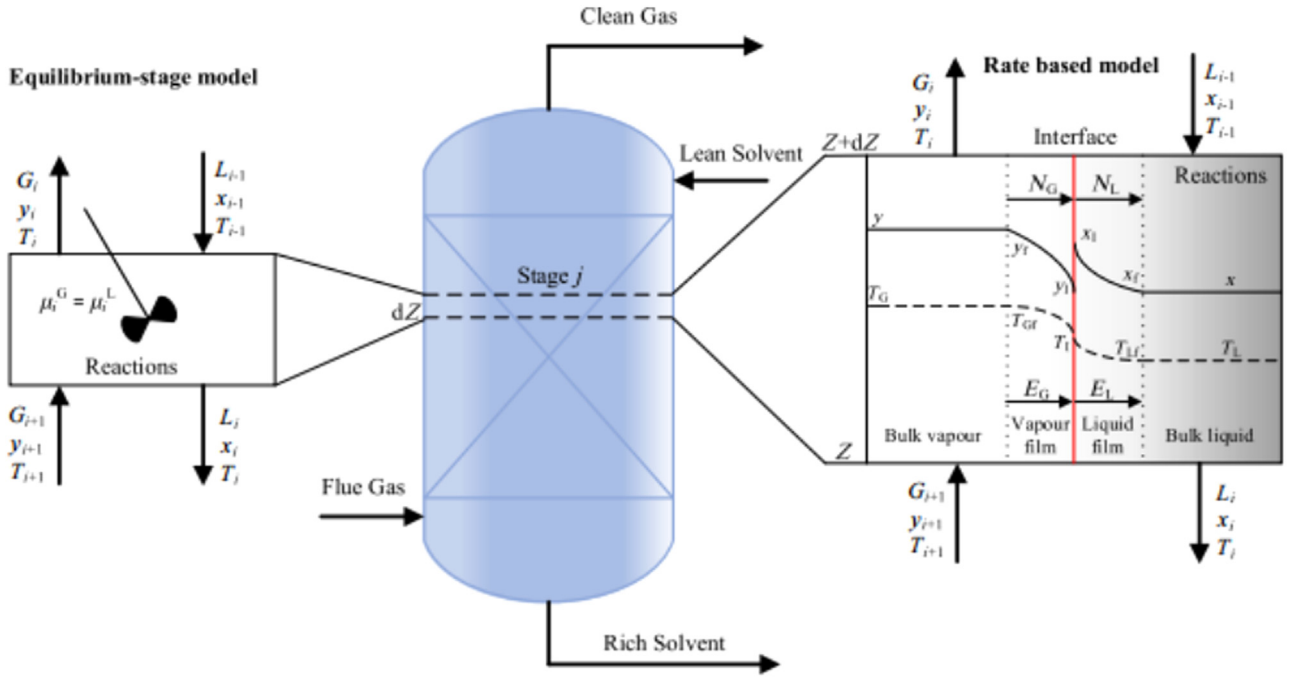

Fig. 6.1. the equilibrium-stage model and rate-based model approaches for the PCC based on chemical absorption using PB. **Adapted from** (Otitoju, 2022). (For interpretation of the references to color in this figure legend, the reader is referred to the web version of this article.)

5.5.5. BECCS development trend and potential

Biomass energy is highly integrated with fossil energy to provide electricity, gas, heat and oil in a stable and secure manner without changing the existing energy infrastructure and architecture to achieve seamless energy replacement. Moreover, in the period of adjusting the energy structure in our country, only biomass energy can cover all the energy goods of industrial civilization and assume the task of new energy transformation, which is not possessed by other renewable energy.

The influence factors of BECCS technology application potential include biomass resource quantity and biomass utilization technology maturity. Biomass resources are mainly divided into agricultural and forestry residues, solid wastes and energy crops, and the availability of resources is uncertain. It is predicted that the total biomass resources will be 17.24 EJ/a in 2050. In terms of biomass utilization technology, biomass processing, combustion, anaerobic digestion, densification technology and final products have reached the commercial level. Some advanced biomass energy utilization technologies, for example, cellulosic ethanol, F-T synthetic biofuel and biomass integrated gasification combined cycle (BIGCC) are still in the demonstration stage of development, and the future development is more uncertain.

BECCS is likely to play an important role in climate change mitigation and energy transition along with renewables, other negative emission technologies, and deep emission reduction technologies. The efficient conversion of biomass into energy, chemicals and materials to replace petrochemical based products is an important zero-carbon/negative-carbon technology to achieve the dual carbon target. Earlier deployment of BECCS greatly increases its climate change mitigation potential, suggesting that policymakers should use BECCS alongside measures for GHG abatement and carbon removal.

6. Process modelling and techno-economic analysis

6.1. Modelling, simulation and TEA for PCC based on chemical absorption using packed bed

Different mathematical models have been developed and reported in literature to describe the operation of the PCC process based on chemical absorption using packed bed (PB) column. Most of these studies have focused on steady state operation. It is imperative that the models are realistic and accurate to perform model-based application such as process design, operation and control. Investigations on the PCC process using dynamic models are required to investigate the dynamic operations such as start-up, shutdown and load following, capturing the interactions within the PCC process and the influence of the disturbances on the PCC process. Commonly used commercially available software to carry out modelling and simulation studies of the PCC-chemical absorption process using PB include Aspen Plus®, Aspen HYSYS®, gPROMS®, Aspen Custom Modeller®, Aspen Dynamics®. Amongst these software, Aspen Dynamics®, Aspen Custom Modeller®, gPROMS® are tools capable of developing efficient dynamic models that could adequately explain the process (Bui et al., 2014).

6.1.1. Modelling principles

Modelling and simulating the solvent-based PCC process is vital for the quick prediction of CO_2 capture efficiency by avoiding many expensive experimental tests (Chatziasteriou et al., 2022). PCC based on chemical absorption using a PB column involving simultaneous gas-liquid mass transfer and chemical reactions, is best described using either the equilibrium-stage or the rate-based model approach. The equilibrium-based approach assumes theoretical stages, where liquid and vapour attain equilibrium. This assumption is unrealistic and does not reflect the real stage performance of the column (Bui et al., 2014; Chatziasteriou et al., 2022). The rate-based approach, however, accounts for multicomponent mass transfer, heat transfer and chemical reactions within the column, making it more appropriate for describing the PCC process based on chemical absorption as it gives an accurate representation of the process (Lawal et al., 2009; Otitoju, 2022). In the rate-based modelling approach, the gas-liquid mass transfer can be described using different established theories such as the penetration theory (Rahimpour and Kashkooli, 2004), the surface renewal theory (Danckwerts, 1970), and the two-film theory (Biliyok et al., 2012; Lawal et al., 2009; Nittaya et al., 2014; Otitoju, 2022). The two-film theory whereby the mass transfer within the film arises from steady-state molecular diffusion, mass transfer resistance is assumed only in the vapour film and liquid film is

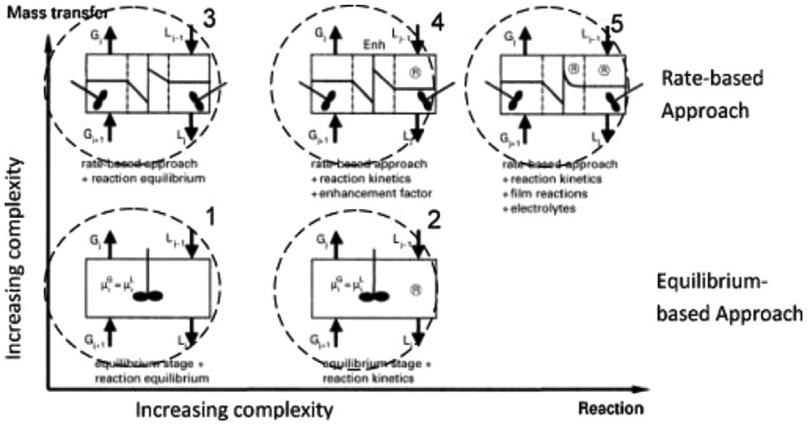

Fig. 6.2. Complexity in models for PCC based on chemical absorption using PB column. Adapted from (Kenig et al. 2001; Wang et al. 2011). (For interpretation of the references to color in this figure legend, the reader is referred to the web version of this article.)

the most widely used (Kenig et al., 2001). The Maxwell-Stefans equations are used to describe the diffusion in the film, the compositions for both bulk liquid and gas phases are assumed to be uniform.

The reaction of CO_2 with an amine in PCC based on chemical absorption using PB column is described using three reaction mechanisms: the Zwitterion mechanism, the termolecular mechanism and the base-catalysed hydration mechanism. The details of these reaction mechanisms have been extensively discussed in literature (Aboudheir et al., 2003; Littel et al., 1992). The reaction kinetics of fast-reacting solvents such as MEA and PZ can be approximated, assuming these reactions reach equilibrium. For slow-reacting solvents such as DEA and MDEA, accurate reaction kinetics is therefore needed to describe the reactions (Zhang et al., 2009). In first-principle modelling, the reaction kinetics is accounted for using the enhancement factor based on pseudo-first-order reaction kinetics. Thus, based on the level of detail required in the mass transfer and reaction kinetics, the model of the PCC process based on chemical absorption can be developed according to the level of complexities shown in Fig. 6.2. The level of accuracy increases with complexity thus, Model 5 is the most accurate as it accounts for mass transfer and reaction kinetics via the rate-based approach. Model 1 is regarded as the least accurate of all. The main assumptions in most of the models for chemical absorption process using PB column include (Koronaki et al., 2015):

- Adiabatic absorber is considered with constant pressure inside it.
- All reactions take place in the liquid film, while the liquid bulk is at chemical equilibrium.
- A plug flow model describes the movement of both gas and liquid streams into the column.
- The flowrates of gas and liquid phases are constant in the absorber.
- Axial diffusion and solvent evapouration may be ignored.
- The interface and bulk phase temperatures are equal.
- The two phases are considered as ideal.

6.1.2. Modelling, simulation and process analysis of PCC based on chemical absorption using RPB

Some studies on the modelling and simulation of the PCC process using MEA in PB have focused on the development of single components such as absorber and stripper (Kvamsdal et al., 2009; Lawal et al., 2009; Zhang et al., 2009; Ziaii et al., 2009), the whole solvent-based PCC plant (Gaspar and Cormos, 2012; Harun et al., 2011; Lawal et al., 2010), and integration of the PCC plant to CO_2 emitters such as power plants (Biliyok et al., 2012; Lawal et al., 2012). These studies have been analysed and summarized in various review papers (Bui et al., 2014; Oko et al., 2017; Wang et al., 2011). Zhang et al. (2009) presented a rate-based model for PCC using MEA solvent in Aspen Plus®. The developed model was validated against pilot plant experimental data and accurately predicted using the measurements for lean and rich CO_2 loadings, capture level and temperature profile. Khan et al. (2011) investigated the impact of various mass transfer correlations on the predictability of the rate-based model. The selection/suitability of mass transfer and hydraulic correlations depends on the type of alkanolamines, packing and flow conditions. Thus, it is important to benchmark the correlations against experiments based on various operating conditions and packing types (Gaspar and Cormos, 2012). Razi et al. (2013) investigated the impact of mass transfer coefficient correlation, kinetic models and effective interfacial area correlation on the model prediction of the pressure drop, CO_2 capture level and temperature profile in the column. The study revealed that the model prediction accuracy is dependent on the kinetic model and mass transfer correlations. MEA solvent is volatile, corrosive and requires high regeneration energy. Thus, it is imperative to focus on PCC process using alternative solvents with lower renegration energy, high reactivity with CO_2, high resistance to degradation and environmentally friendly (Zhou et al., 2010). Modelling and simulation studies of PCC process using alternative solvent such as PZ (Otitoju et al., 2021) and AMP and PZ blend (Zhang et al., 2017) solvent. For example, Otitoju et al. (2021) developed a rate-based model for the PCC process using PZ. The model was validated at pilot scale and scaled-up to treat flue gas from a 250 MWe NGCC power plant (Dillon et al., 2005"). Therefore, further modelling and simulation studies of PCC process using suitable novel solvents should be explored.

The model development of the solvent-based PCC process with process configuration modifications has received much attention because the modified process has shown better economic performance and flexibility in operation (Wu et al., 2020). Mostafavi et al. (2021) proposed combinations of process modifications such as absorber intercooling, lean vapour recompression and parallel exchanger arrangement to reduce the reboiler duty and cost of the PCC process. They found that the combination of the absorber intercooling and the lean vapour recompression resulted in an 8 % reduction in steam consumption for regeneration and consequently a significant reduction in the total costs (i.e. fixed and variable costs).

Karimi et al. (2011, 2012) developed rate-based models for five different stripper configurations of the PCC process including: standard configuration, split-stream, multi-pressure stripper, vapour recompression and compressor integration. The capital cost and CO_2 avoidance cost are calculated to evaluate the steady-state performance of different processes (Karimi et al. 2011). The dynamic performance of PCC processes with standard configuration, split-stream and vapour recompression configurations were then investigated. The simulation results showed that the standard configuration has the best dynamic behavior and is the most stable one. For the other two configurations, the vapour recompression configuration can handle disturbances better than the split-stream configuration (Karimi et al., 2012).

In the same vein, Biliyok et al. (2012) developed a dynamic model for the PCC process with inter-cooled absorber in gPROMS®. The model

was validated with dynamic experimental data and accurately predicted the behavior of the plant, especially for the trend of dynamic change. Analysis of the impact of inter-cooled solvent and flue gas moisture content on the CO_2 capture process performance was investigated using the validated model. Results revealed that the inter-cooling can slightly enhance the absorber performance when the temperature bulge is located around it. However, the moisture content in flue gas could strongly influence the temperature profile of the absorber but only had a trivial influence on the capture level. Similar study by Walters et al. (2016) using PZ solvent revealed that PZ solvent capacity could be improved by absorber intercooling.

Investigating the PCC process integrated with either a power plant or industrial process is critical to improving its operation performance. Lawal et al. (2012) integrated dynamic models for a 500MWe sub-critcal coal-fired power plant with PCC in gPROMS. The simulation results illustrated that the PCC process response was much slower than the coal–fired power plant. Olaleye et al. (2016) investigated the dynamic behaviour of a large-scale PCC model integrated with a 600 MWe supercritical coal-fired power plant on load following mode of operation of the coal-fired power plant. The simulation results showed that about 4.67 % of the maximum power of the coal-fired power plant could be quickly produced by the stripper stop mechanism, which has potential benefit for the wide-range load-varying operation of the power plant.

6.1.3. Techno-economic analysis (TEA) of PCC based on chemical absorption using PB

Several studies have focused on the model-based optimization of PCC process based on chemical absorption to establish the operating conditions that achieve the CO_2 capture targets at minimum cost. Abu-Zahra et al. (2007) investigated the minimal thermal energy duty required for MEA solvent regeneration. Studies revealed significant energy savings could be achieved by optimizing lean solvent loading, amine solvent concentration, and stripper operating pressure. A minimum thermal energy requirement of 3.0 GJ/ton CO_2 was attained at a lean MEA loading of 0.3, using 40wt% MEA and stripper operating pressure of 210 kPa compared with the base case of 3.9 GJ/ton CO_2. Comprehensive sensitivity analysis and optimization of solvent-based PCC process using MEA based on total annual cost was carried out by Arias et al. (2016). The study revealed that rich solvent, lean solvent, and flue gas temperatures are very sensitive to the total annual cost.

Further studies on TEA of the chemical absorption process focused on the process configuration modification. Dubois and Thomas (2018) presented a technical analysis of different CO_2 capture process configurations (rich solvent recycle (RSR), solvent split flow (SSF), lean/rich vapour compression (L/RVC)) using different solvents (MEA, PZ, PZ-MDEA blend). The study revealed that the configurations studied attained regeneration energy savings within 4–18 % range. The minimal regeneration energy of 2.38 GJ/ton CO_2 was obtained with PZ-MDEA blend (30 wt% PZ and 10 wt% MDEA) solvent and RVC process configuration.

Oh et al. (2020) conducted a TEA on various modified PCC processes using 30 wt% MEA. Five stripper configurations modified with two or more components of lean vapour compression (LVC), cold solvent split (CSS), and stripper overhead compression (SOC) were investigated to reduce the total equivalent work. The study revealed that the thermal energy required from the reboiler could be reduced by 8.1- 32.8 % through the modified configurations. The study suggested that for a combined configuration implementation, the total equivalent work could be up to 9.0 %, and the operating cost could be saved by up to 10.2 %. However, an increase in capital cost is attained due to the process modifications.

An investigation by Zhang et al. (2017) on the energy performance of CO_2 capture process with AMP and PZ aqueous solvent with process modifications, including intercooled absorber (ICA), lean vapour compressor (LVC) and rich solvent split (RSS) revealed that the energy demand were reduced by 6.7 %, 2.7 %, and 8.5 %, respectively. The combination of LVC + RSS, ICA + LVC and ICA + RSS modifications obtained energy savings of 9.3 %, 8.5 % and 14 % respectively. The energy demand for the combination of ICA + RSS + LVC was reduced by 15.2 %.

Otitoju et al. (2021) investigated the technical and economic performance of three different PCC process configurations using PZ solvent for 250 MWe NGCC compared with the standard process using 30 wt% MEA solvent. Results revealed that the total energy demand of the standard CO_2 capture process using 30 wt% PZ is 3.56 GJ/ton CO_2, which is 33 % less than the energy demand of the standard PCC process using 30 wt% MEA. Amongst the configurations considered, the lowest energy demand of 2.76 GJ/ton CO_2 was attained using an advanced flash stipper (AFS) using 40 wt% PZ. Results also showed that the lowest CO_2 capture cost of $34.65 per ton CO_2 was achieved using the AFS process configuration with 40 wt% PZ.

6.1.4. Summary: advantages, limitations and future prospect

Modelling and simulation of the PCC process based on chemical absorption using PB column has matured through many years of development and improvement. Many models have been developed to gain in-depth knowledge or insights into the PCC process using different solvents and configurations under steady-state and dynamic conditions. However, dynamic operating/experimental data is still insufficient to verify PCC dynamic models at different process configurations. From the validation point of view, more experimental tests should be carried out on the PCC process with different process configurations at pilot scale.

6.2. Modelling, simulation and techno-economic assessment of intensified PCC based on chemical absorption using RPB

The rotating packed bed (RPB) is the most commonly used Higee (high gravity) technology for the solvent-based PCC process. It comprises an annular packed bed connected to two disks erected on a rotating shaft. A cross-sectional view of the RPB is shown in Fig. 6.3. The RPB assembly is housed in a casing and operates in a high centrifugal field attained by rotating a cylindrical rigid bed (Cortes Garcia et al., 2017). The liquid and the vapour flow either co-currently or counter-currently in the horizontal direction. This is in opposition to the packed bed (PB) where liquid and vapour flow is vertical. Thus in RPB, the separation efficiency and capacity are determined by the rotor diameter and the axial height respectively. This is in contrast with PB where capacity is determined by the column diameter and the separation efficiency is determined by column height (see Fig. 6.4) (Cortes Garcia et al., 2017; Kiss, 2014).

Because of these fundamental structural differences, the modelling and simulation of the PB are significantly different from that of the RPB. For instance, mass transfer is considered to occur only along the packing in PB modelling whereas, mass transfer is considered to occur both along the packing and in the space between the rotor and the casing in modelling of RPB. Additionally, unlike the PB which is modelled as a straight bed with a constant cross-sectional area and constant gas and liquid velocities, the RPB is modelled as a tapered bed with a varied cross-sectional area and varied gas and liquid velocities (Cortes Garcia et al., 2017). This leads to varying gas and liquid mass transfer coefficients along the radius in RPB. The schematic of the PB and RPB, which highlights their structural and modelling differences, is shown in Fig. 6.4.

There are many research activities on the modelling and simulation of the PCC process using the RPB technology (Joel et al., 2014, 2017; Im et al., 2020; Luo et al., 2021). The majority of these studies have focused on the modelling and simulation of CO_2 capture either in the RPB absorber (Joel et al., 2014; Luo et al., 2021) or in the RPB stripper (Joel et al., 2017). The modelling and simulation of the whole intensified carbon capture process consisting of the RPB absorber, RPB stripper, heat exchanger, pumps etc. have also been reported (Im et al., 2020). Discussions on these are provided in the following subsections.

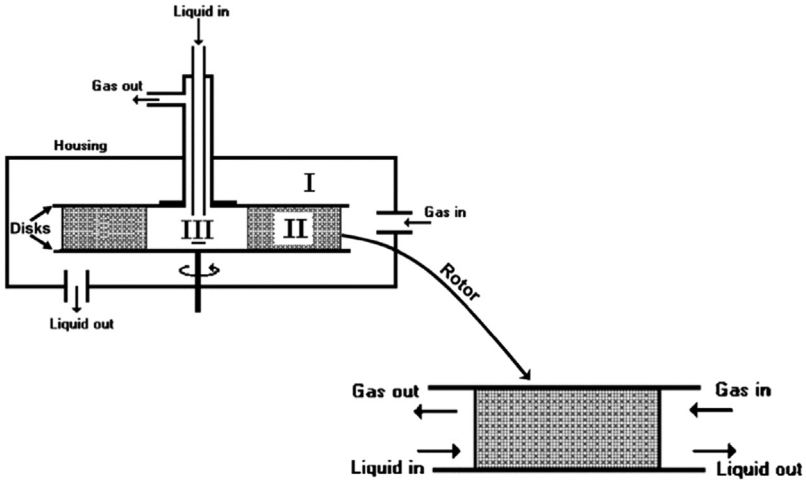

Fig. 6.3. The cross-sectional view of the RPB (Chavez and Larachi, 2009). (For interpretation of the references to color in this figure legend, the reader is referred to the web version of this article.)

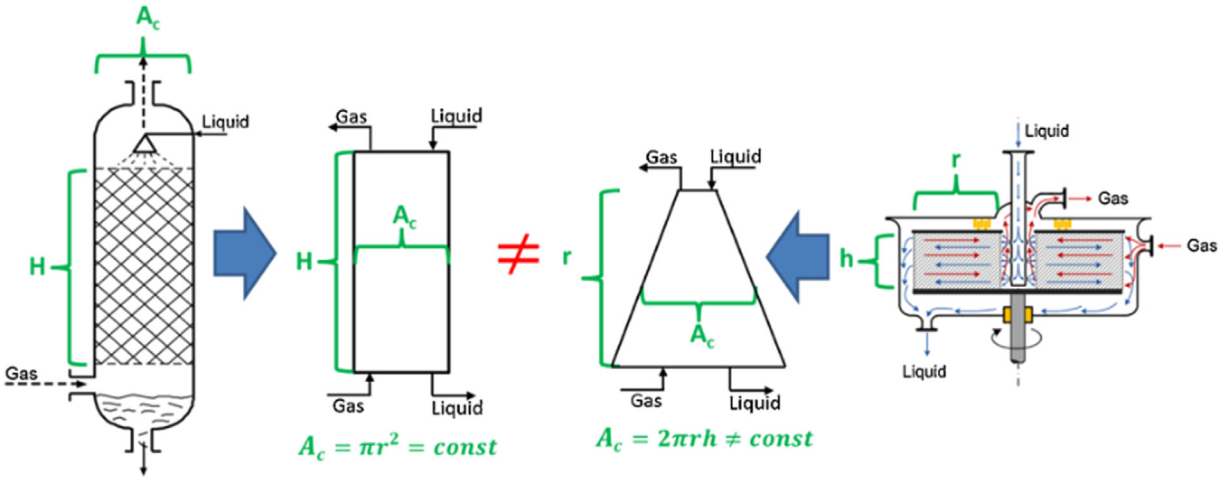

Fig. 6.4. Schematic of the PB modelling (left) vs. RPB modelling (right) (Neumann et al., 2018).

6.2.1. Modelling and simulation of CO_2 absorption in RPB absorber

Modelling and simulation of CO_2 absorption with different solvents in RPB absorbers have been reported. The absorption of CO_2 using Benfield solution (amine-promoted hot potassium carbonate) was investigated in an experimental and modelling study conducted by Yi et al. (2009). The steady-state model was developed in Matlab® based on the two-film theory and accounted for kinetics and CO_2 balance in the liquid droplets. The model was validated with experimental data collected in RPB with an inner radius of 0.040 m, outer radius of 0.10 m and axial height of 0.031 m. The model generally predicted the CO_2 mole fraction in the outlet gas and revealed the presence of an end effect zone at the inlet region of the packing where mass transfer efficiency in the RPB was the highest (Yi et al., 2009). Zhang Z., et al. (2014) developed a steady-state model of CO_2 absorption with an MDEA concentration of 10–30 wt% in a pilot-scale RPB absorber packed with multilayer stainless steel. The model was implemented in Fortran® and uses Higbie's penetration theory. The model was validated and accurately predicted the CO_2 capture level at rotating speeds less than 1100 rpm. Beyond this rotating speed, there were sharp deviations between the experimental values and model predictions. The CO_2 capture levels were generally lower than 50 % due to slow reaction and low concentration of MDEA.

More studies have focused on the modelling and simulation of CO_2 absorption with MEA in RPB absorbers. Joel et al. (2014) modified the rate-based model in Aspen Plus® to simulate a steady-state process of CO_2 absorption with MEA in an RPB absorber. The default mass transfer and hydrodynamic correlations in the rate-based model were modified by replacing the gravitational acceleration term (g) in the correlations with centrifugal acceleration ($r\omega$). The modified correlations were written in visual Fortran® and linked dynamically with the rate-based model in Aspen Plus®. The model was validated at the pilot scale and was used to investigate the effects of various operating variables on the CO_2 capture level. Process analysis showed that no temperature bulge was observed in the temperature profile of the pilot-scale RPB absorber because of the high liquid-to-gas (L/G) ratio (30 kg/kg). Furthermore, It was reported that the RPB absorber achieved a 12 times volume reduction factor compared to a PB absorber when 30 wt% MEA was used. A steady-state rate-based model of an MEA-based RPB absorber was developed by Kang et al. (2014). The model equations and the different correlations were implemented and solved in gPROMS ModelBuilder®. Their model used a modified enhancement factor which is based on the apparent reaction rate constant of Aboudheir et al. (2003) to improve the agreements between the model predictions and experimental data. Additionally, they investigated the effects of various mass transfer and liquid holdups correlations on model predictions of CO_2 mole fraction, K_Ga and CO_2 capture level. It was concluded that a combination of Onda et al. (1968) for liquid phase mass transfer coefficient and interfacial area, Burns et al. (2000) for liquid holdup and Tung and Mah (1985) for gas phase mass transfer coefficient improved model predictions and were adequate to

Table 6.1
Specifications of RPB stripper.

Institutions	Dimensions r_i, r_o, h (m)	Packing type	a_t (m^2/m^3)	ε	References
Newcastle University	0.078, 0.199, 0.02	Expamet	2132	0.76	(Jassim et al., 2007)
National Tsing Hua University, Taiwan	0.038, 0.08, 0.02	Wire mesh	803	0.96	(Cheng et al., 2013)

predict the effect of changes in liquid and gas flow rates in the RPB absorber.

Thiels et al. (2016) examined the process design for the RPB absorber to achieve varying CO_2 capture levels in Aspen Custom Modeler. They proposed a series arrangement of the RPB and PB absorbers to minimize the absorber packing volume. Borhani et al. (2018) studied the effect of different reaction models and enhancement factors on CO_2 absorption in a pilot-scale RPB absorber operated with MEA concentrations of 55 wt% to 75 wt%. In addition to this, the influence of rotor speed, lean MEA concentrations, flow rates and temperatures on CO_2 capture level was also evaluated. Oko et al. (2018) used their steady-state RPB absorber model developed in gPROMS ModelBuilder® to show that the liquid phase temperature in RPB could rise significantly and hence demonstrated the need for intercoolers in RPB absorbers. Following this, the authors proposed and investigated various intercooler design options suitable for application in RPB absorbers. In a recent study, Otitoju et al. (2023) developed, validated and scaled up a steady-state rate-based model of an RPB absorber in Aspen Custom Modeller®. The authors reported that the large-scale RPB absorber achieved a 4–13 times reduction in volume and a 3–35 % reduction in capital expenditures compared to a PB absorber. Recently Luo et al. (2021) reported the dynamic modelling and simulation of CO_2 absorption in a pilot-scale RPB absorber based on the surface renewal mass transfer theory. The RPB absorber model was developed in gPROMS ModelBuilder® and the embedded SAFT-VR EOS was used for the modelling of the thermodynamic properties. They performed steady-state process analysis to investigate the effects of key process variables such as rotating speed (300–1450 rpm), L/G ratio (2–6 kg/kg) and MEA concentrations (30–80 wt%) on the absorption performance. They also carried out dynamic simulations of the RPB absorber to study its response to changes in the flow rates of both the flue gas and the solvent. It was concluded that the RPB absorber responds quickly to process changes (Luo et al., 2021).

6.2.2. *Modelling and simulation of CO_2 desorption in RPB stripper*

Although there are many experimental studies of CO_2 desorption in RPB strippers, experimental data collected from two of those studies are commonly used to validate the model of the RPB stripper. Table 6.1 shows the specifications of the RPB used in those studies (Jassim et al., 2007; Cheng et al., 2013). There are fewer model-based studies on CO_2 desorption using an RPB stripper compared to their RPB absorber counterpart. There are only two studies in the open literature on the modelling and simulation of CO_2 desorption in RPB stripper (Joel et al., 2017). This may be due to the complexity and difficulty involved in modelling the RPB Stripper compared to the RPB absorber. The first modelling and simulation study for CO_2 desorption in a RPB stripper was reported by Joel et al. (2017). The rate-based RPB stripper model was developed using Aspen Plus® and Fortran®. Their model was validated with experimental data from Jassim et al. (2007) and Cheng et al. (2013). Model validation results were in agreement with experimental data for specific reboiler duty and lean CO_2 loading. Process analysis indicated that the regeneration efficiency increases with rotor speed, but with an increase in heat and mass transfers that subsequently resulted in a decrease in regeneration energy. The authors also reported that the RPB stripper volume was reduced by 9.692 times compared to that of a PB stripper. Borhani et al. (2019) used an equation-oriented approach to develop the model of the RPB stripper. The partial pressure, the heat of desorption and K-values were calculated from correlation developed by regression of experimental data collected for different concentrations of MEA. The model was implemented in gPROMS ModelBuilder® and was used to analyse the effect of changes in liquid flow rate, pressure, rotor speed and reboiler temperature on the regeneration energy of the RPB stripper. They concluded that the desorption energy reduces with an increase in reboiler temperature until 120 °C. Beyond this temperature, desorption energy increases.

6.2.3. *Modelling, simulation and optimization of the whole solvent-based intensified PCC process*

Modelling and simulation of the CO_2 absorption/desorption using RPB have been carried out mostly for individual RPB absorbers and RPB strippers. Only one study reported the modelling and simulation of the RPB absorber and RPB stripper as a connected system for the solvent-based PCC process at the lab scale (Im et al., 2020). In that study, the authors first developed and validated the model of the MEA-based RPB absorber and RPB stripper separately and then they developed the whole intensified PCC system by integrating the RPB absorber and RPB stripper with other process units in gPROMS ModelBuilder®. The integrated process was operated with varied MEA concentrations (30–80 wt%). Optimal design and workable operating conditions for the integrated intensified PCC process were investigated using a flue gas flow rate of 71 kg/h and design specifications including 90 % CO_2 capture level, lean solvent temperature of 40 °C, absorber and stripper pressures of 1 atm and 1.6 atm, CO_2 lean lading of 0.364 molCO_2/molMEA, flash drum temperature of 40 oC, temperature approach of 10 oC, condenser temperature of 40 °C and rotor speeds of 800 and 600 rpm for the RPB absorber and RPB stripper respectively. Steady-state optimization of the whole intensified process was performed by setting the minimization of the total energy consumption (reboiler, rotation and pumps) as the optimisation objective and parameters such as rotor speed, MEA concentration, reboiler temperature, lean solvent flow rate, condenser temperature and stripper pressure as decision variables. In addition to this, the CO_2 capture level, CO_2 purity and percentage flooding in the absorber and the stripper were chosen as constraints. The optimization results showed that the lowest total energy consumption of 4.62 GJ/ton CO_2 (3.04 GJ/ton CO_2 for reboiler duty and 1.57 GJ/ton CO_2 for rotational energy) was achieved at 90 % CO_2 capture level and 73 wt% MEA concentration. The authors concluded that although the specific reboiler duty was lower for the MEA-based PCC process using RPB its overall energy consumption could be higher than that of the MEA-based PCC process using PB due to the additional energy consumed for rotating the RPB.

6.2.4. *Scale-up of RPB for solvent-based PCC*

Unlike the solvent-based PCC process using PB as absorbers and strippers, there are not many scale-up studies on solvent-based PCC with RPB as absorbers and strippers. Hence existing studies on CO_2 capture in RPB are based on small RPB rigs with a maximum outer diameter of 0.396 m and flue gas capacity of 0.66 kg/s or less (Jassim et al., 2007). Otitoju et al. (2023) performed the first scale-up study by scaling up a validated pilot-scale model of an MEA-based RPB absorber to a large-scale MEA-based RPB absorber with capacity for flue gas flow rate (356 kg/s) from a 250 MW_e CCGT power plant. The large-scale RPB absorber was designed by estimating its basic dimensions (i.e. inner radius, outer radius, axial height and casing) using a rigorous iterative scale-up procedure developed by the authors based on the design approach of Agarwal et al. (2010). The scale-up uses the area of a transfer unit (ATU) to address the polar coordinate issue in RPBs. The results of the scale-up studies

showed that a large-scale RPB absorber operated with 55 wt% would require an inner radius of 1.48 m while the one with a 75 wt% MEA would require an inner radius of 1.47 m. According to the authors, this inner radius would be sufficient to house the liquid distributor, not lead to excessive gas velocity and allow for gas withdrawal from the RPB without causing a very high pressure drop. Furthermore, the outer radius of the large-scale RPB absorber with 55 wt% MEA and 75 wt% MEA were estimated to be 4.86 m and 4.61 m, respectively, while their axial heights were estimated to be 1.26 and 1.19 respectively. The author used the scale-up results to carry out a techno-economic assessment and quantified the size and cost of a large-scale RPB absorber operated with MEA concentration of (55–75 wt%).

6.2.5. Techno-economic assessment of the solvent-based intensified PCC process

Although there are existing techno-economic studies for systems where RPBs are used for distillation (Sudhoff et al., 2015), recovery and purification of bioethanol (Gudena et al., 2013) and absorption of aroma from a bioreactor off-gas (Lukin et al., 2020). So far only Otitoju et al. (2023) has reported on the techno-economic assessment of the solvent-based PCC process using RPB, though the study was limited to the RPB absorber only. Technical assessments of the MEA-based RPB absorber performed by Otitoju et al. (2023) included the effects of certain process variables (i.e. lean solvent CO_2 loading, lean MEA flow rate and rotor speed) on the CO_2 absorption performance. The authors reported that the RPB absorber operated with 55 wt% MEA has a 4–11 times volume reduction factor while that operated with 75 wt% MEA has a 5–13 times volume reduction factor when compared to those of the PB absorbers. Furthermore, economic assessments showed that the capital expenditure (CAPEX), operating expenditure (OPEX) and CO_2 capture cost of the RPB absorber were lower compared to that of the PB absorbers. For instance, the CAPEX was lowered by 3–53 % with the RPB absorber while the CO_2 capture cost was lowered by \$8.5/tCO_2 – \$15/tCO_2 with the RPB absorber compared to that of the PB absorbers.

6.2.6. Summary: advantages, limitations and future prospect

The RPB is the most commonly used technology in the intensified solvent-based PCC process because of its lower flooding tendency and ability to operate at higher gas and/or liquid flow rates compared to PBs. RPB is self-cleaning and can intensify the mass transfer process in the CO_2 capture process. It can reduce the process equipment footprint by reducing the size of the absorber by 5–13 times (Joel et al., 2014) and that of the stripper by 9.69 times compared to PB (Joel et al., 2017). Hence, RPB could be used in space-limited applications like ships and mobile skid plants. Furthermore, it can fulfil larger flue gas treatment than PB because mass transfer intensification in RPB could lead to a gas retention time below 1.5 s. This is significantly lower than a gas retention time of 20.4 s obtained in PBs. RPB can deal with viscous solvents and has been mostly operated with higher solvent concentrations (e.g. 55 wt% or 80 wt% MEA). The cost of the solvent-based PCC process could also be reduced by RPB technology.

Despite the many advantages of RPB, its modelling and application in the solvent-based PCC process are limited to being used separately as an absorber or as a stripper. This is due majorly to the lack of experimental data to validate the model of the whole solvent-based PCC process using RPB. Additionally, existing studies on solvent-based PCC using RPB are conducted at lab and pilot scales. To accelerate the commercial deployment of the process, there is a need for more studies involving the detailed and accurate modelling and scale-up of the whole intensified PCC process using RPB. Such studies are critical to gaining insights into the design and operation of the whole intensified process. Additionally, a detailed economic assessment of the whole process is necessary to quantify the CO_2 capture cost for the entire process. Detailed optimization studies incorporating environmental and life cycle analysis (LCA) of the intensified PCC process should be carried out and the results thereof compared with the that of solvent-based PCC process using PB.

6.3. CFD study of post-combustion carbon capture based on chemical absorption using packed bed

Packed bed (PB) has been used as multiphase contactors and reactors for post-combustion carbon capture (PCC). Like many other industry sectors, computational fluid dynamics (CFD) has been employed to design and optimize the packed bed technology for PCC. By solving a series of governing equations for fluid flows, chemical reactions, and heat and mass transfers, CFD simulation can reveal details of hydrodynamics, heat and mass transfer performance inside the packed beds.

Due to the packed bed's multi-scale nature, CFD simulation of the CO_2 capture processes in large scale PBs is still prohibitively computational expensive when the processes at the pore scale are to be resolved. In order to reduce the computational costs, two general approaches to the CFD PB simulations are employed, i.e. the micro- and macro-scale approaches. For example, the details of the flow behaviour in the PB can be investigated using the micro-scale modelling approach, whereas the overall column performance, such as the CO_2 capture rate and pressure drop, can be analysed using the macro-scale approach (Li et al., 2016). Different models, such as the element scale, corrugation scale, and column scale models, have been proposed, as illustrated in Fig. 6.5.

6.3.1. Element scale model

For mesoscale simulations, 3D representative element units (REUs) can be employed (Petre et al., 2003). The REU can be viewed as the smallest element in the PB, representing the bed dissipation mechanisms. Petre et al. (2003) utilized numerous REUs to resemble the flow at different positions in the column and they were used to simulate the gas flows over a wide range of Reynolds numbers: from pure creeping flows to fully developed turbulent flows. The overall pressure drop across the column was reconstructed based on each REU's obtained pressure loss. Furthermore, Said et al. (2011) investigated the dry pressure drop for the fully developed turbulent gas flow using two periodic REUs with different slice directions. In addition, the counter-current gas-liquid flow in the PB was studied using the VOF method based on a 3D REU, and the total liquid holdup and wetted area were estimated by Chen et al. (2009). It should be noted that although the use of the REUs can save the computing resources and time, the accuracy of the simulation results is directly related to the setting of the boundary conditions for the REUs, especially the wall effects, which may lead to an inaccurate result. It has been reported that the predicted pressure drop using REUs is usually more significant than the pressure drop measured from the experiment due to the intersection of the two adjacent flow channels (Raynal et al., 2004).

6.3.2. Corrugation scale model

The 2D corrugation scale model is usually employed to study the two-phase flow behaviours in the PB, such as the dry pressure drop, liquid holdup, and liquid film thickness using the VOF method. For example Gu et al. (2004), studied the counter-current gas-liquid flows on inclined plates using the VOF method for various packing surface microstructures, fluid properties and gas flow rates. It was concluded that the gas flow rate noticeably influenced the liquid flow pattern and film thickness. Further, the complex geometry of the structured packing in the PB was simplified as a 2D vertical cross-section channel between two neighbouring packing sheets (Raynal et al., 2004; Hosseini et al., 2012). The process of the liquid film formation on the packing surface was simulated, and the liquid film thickness and pressure drop were compared with the experimental data. In addition, Haroun et al. (2012) investigated the liquid holdup and the no-reacting mass transfer rate based on co-current gas-liquid flows in a 2D corrugation scale model. The results showed that the liquid flow rate and packing geometry mainly affected

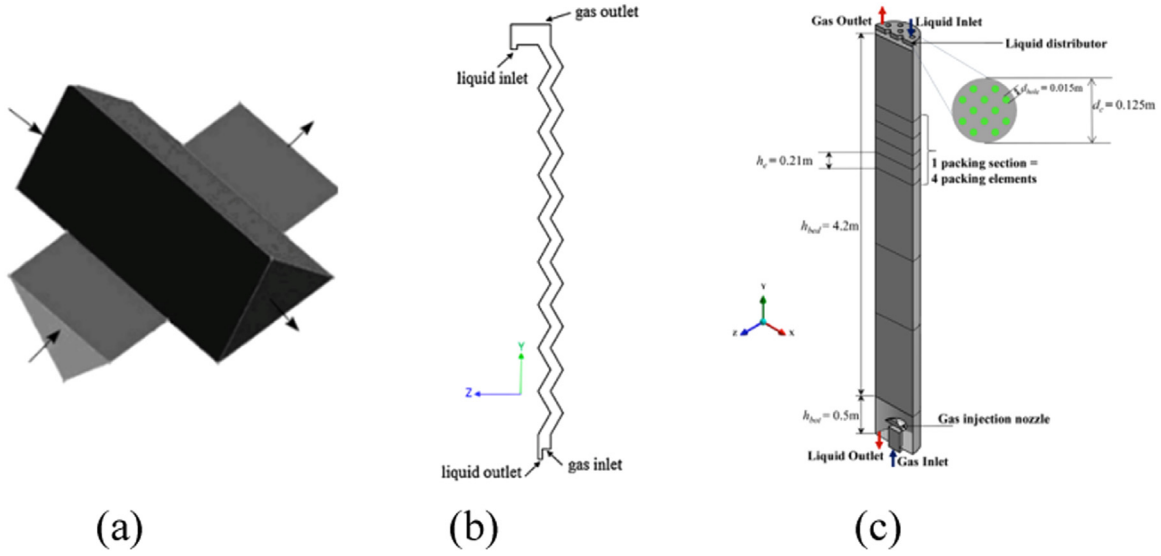

Fig. 6.5. Typical computational models employed. (a) element scale model (Chen et al., 2009); (b) corrugation scale model (Hosseini et al., 2012); (c) column scale model (Kim et al., 2016).

the mass transfer. Nevertheless, the use of the 2D geometry for the simulation of two-phase flow in the PB, although generally successful, has limitations due to the presence of highly anisotropic structured packings.

6.3.3. Column scale model

In general, the hydrodynamics and mass transfer processes have been explored in a packing column considering gas flow only or gas-liquid flows using the VOF and Eulerian methods. For the simulations of the gas flow, Wen et al. (2007) investigated the single-component (air) and two-component (air and CO_2) gas flows in a column with complex packing geometries. Then, the influence of the geometry features of the packing on the dry pressure drop was explored (Sun et al., 2021). Haghshenas Fard et al. (2007) modelled the dry and wet pressure drops in a packing column model similar to the actual geometry of the structured ceramic packing. The simulation showed that the wet pressure drop was larger than the dry pressure drop under the same gas load. This indicates that the modelling of the dry pressure drop cannot accurately describe the actual pressure drop in the packing column, where both the upward gas and downward liquid stream flows exist. Therefore, the simulations of both gas and liquid flows are essential for better understanding the flow dynamics in the packed bed.

It should be noted that the size of the column models employed in most studies such as those in the above-mentioned works, are relatively small but the required numbers of the computational mesh are still quite large. A promising approach for modelling a large-scale or industrial column is to take the packing as a porous medium without resolving the details of the packing geometry, i.e. using the Eulerian porous medium model. To utilize this approach, it is very important to accurately determine a proper resistance force model to describe the gas-liquid interfacial force and drag force from the packing (Kołodziej and Łojewska, 2009). Mirzaie et al., 2020 estimated the porous resistance using the general Ergun's equation. However, the force models employed did not consider the effect of the various geometry of the packing, which may cause an inaccurate flow behaviour prediction. As a result, various porous medium resistance force models, such as those for spherical packing (Attou et al., 1999), structured slit packing (Iliuta et al., 2004), wire gauze packing (Kołodziej and Łojewska, 2009), and tube bundle packing (Zhang and Bokil, 1997) have been proposed. These models are developed based on the packings of different types and they consider the influence of the packing geometry on the fluids across the packing region. It has been shown that the flow characteristics could be accurately predicted in the packed beds by employing these models (Fourati et al., 2013; Iliuta et al., 2014; Pham et al., 2015; Pham et al., 2015; Uwitonze et al., 2021; Zhang et al., 2017).

In addition, liquid dispersion occurs in the packed bed. Fig. 6.6 (a) shows the experimentally observed spreading of the liquid in a 3D column model with a point liquid jet source located at the top of the packing. Without considering the dispersion forces in the CFD model, the predicted liquid mal-distribution can be quite different (Tan et al., 2021).

Liquid dispersion in the packed bed may be divided into the capillary pressure induced dispersion and mechanical dispersion (Wang et al., 2013). The capillary pressure force is produced by the difference in the pressures across the fluid interface. Two main models, i.e. the Grosser model (Grosser et al., 1988) and the Attou and Ferschneider model (Attou and Ferschneider, 1999), have been widely used to model the liquid dispersion resulting from the capillary dispersion (Boyer et al., 2005; Gunjal et al., 2005; Iliuta et al., 2014; Jiang et al., 2002; Wang et al., 2013) . In Grosser's models, it was assumed that the capillary pressure force was inversely proportional only to the packing's porosity and particle diameter. It is reported that the Grosser model may fail to reproduce the steep rise in the capillary pressure as the liquid saturation approaches zero, and thus fail to catch the effect of the capillary pressure force in some packed bed models (Zhang et al., 2022).

The mechanical dispersion is caused by the complex advection of the momentum by the fluid at the pore scale (Fourati et al., 2013) or, in other words, the variation in the velocity with respect to the main flow at the macroscopic scale (Carney and Finn, 2016). The gas dispersion force is relatively small compared with the liquid dispersion force because the momentum exchange between the gas and liquid is usually small. As a result, the gas dispersion force is usually ignored (Fourati et al., 2013) in the CFD simulations. The drift velocity, which is a function of the gradient of the phase volume fraction, will lead to a driving force to cause the liquid to flow from the high liquid concentration region to the low liquid concentration region and subsequently increase the liquid holdup. Although many mechanical dispersion force models have been developed, the model proposed by Lappalainen et al. (2009) based on spherical particle packings is the most popular, and it has been employed in many works for the PB simulations (Kim et al., 2017; Lappalainen et al., 2011, 2009; Solomenko et al., 2015).

Lappalainen et al. (2009) employed their porous resistance model and dispersion force models to investigate the liquid dispersion phenomenon in a trickle bed. The results showed that the mechanical dispersion force was always larger than the capillary dispersion force under

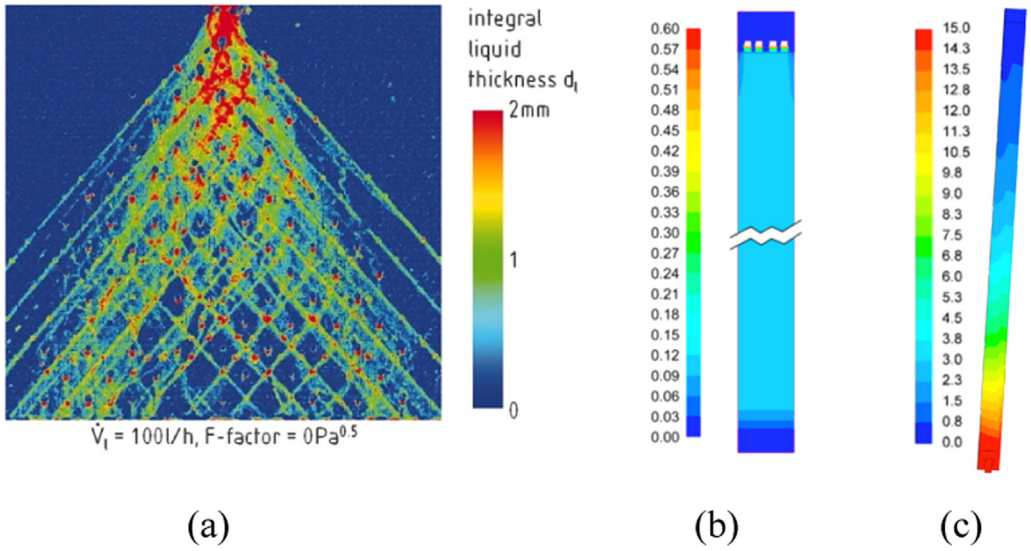

Fig. 6.6. Contours of (a) the spreading of the liquid fed from a point source (Mahr and Mewes, 2008); (b) the liquid holdup (Kim et al., 2016); and (c) CO_2 concentration (Pham et al., 2015). (For interpretation of the references to color in this figure legend, the reader is referred to the web version of this article.)

different particle sizes. Also, it was reported that the capillary dispersion force could be ignored for large particles and high packing porosity (Fourati et al., 2013). Thus, the mechanical dispersion force is the only force employed in most simulation works (Pham et al., 2015, 2015). Furthermore, Hossain et al. (2020) used the mechanical dispersion model to simulate the liquid dispersion in a structured packed bed, and the simulation results agreed with the experimental data. It was proven that the mechanical dispersion model that initially derived from the random packing was also suitable for structured packings (Fourati et al., 2013), thus indicating that this model had a wide range of adaptability to model the flow in different types of packings.

Based on the column scale models combining the porous resistance and dispersion forces, the fluid flows were investigated in randomly and structured packed beds (Pham et al., 2015a; Kim et al., 2016; Uwitonze et al., 2021). An example of the simulated liquid holdup contour is shown in Fig. 6.6 (b). By further coupling with the mass transfer model and some empirical correlations of the effective interfacial area and mass transfer coefficient, the CO_2 capture process could be successfully analysed (Gbadago et al., 2020; Pan et al., 2018). Then, the effect of the sloshing on the liquid flow mal-distribution and CO_2 capture performance (Fig. 6.6 (c)) may be investigated by using the sliding mesh method (Kim et al., 2017; Zhang et al., 2017).

6.3.4. Summary on CFD simulations of the PB

The PB's flow characteristics and mass transfer have been studied using the CFD method, mostly for small lab and pilot scale models. It has been demonstrated that employing the CFD is an efficient and effective way to simulate the carbon capture processes inside the PB, either for simulating the single or multiphase flows and for evaluating the hydrodynamics and/or mass transfer performances. Also, it can achieve much more detailed information about the processes occurring in the bed, which may not be obtained from the experimental measurements.

In order to model the gas-liquid flow and mass transfer in the PBs, different approaches have been employed. The details of the flow behaviour in the PB are usually investigated in the micro-scale model. When using this model, small and complex packing geometry can be considered and it requires a large mesh number. Some methods, such as using the REUs could be used to save computing resources and time. However, the accuracy of the simulation results is directly related to the setting of the boundary conditions and the established packing geometry. Some overall column performance parameters can be obtained using the macro scale model, such as the CO_2 capture rate and pressure drop. To make the simulation of large scale PB feasible and accurate, the Eulerian porous medium model can be used without resolving the complex geometry of the packing structure, but the sub-models for expressing the forces, including the porous resistance and dispersion forces, should be carefully considered.

6.4. CFD study of post-combustion carbon capture based on chemical absorption using rotating packed bed

The rotating packed bed (RPB) has shown great potential to capture CO_2 due to its increased effective interfacial area between the gas and liquid phases under the centrifugal force and excellent mass transfer performance. Among the studies on the RPB, CFD has been widely used to investigate the gas and liquid flows inside the 2D and 3D RPB models. For the single-phase, the gas flow behaviours, including the pressure drop and its distribution, have been studied in various RPB models. While for the gas-liquid flows, two methods, i.e. the VOF and Eulerian methods, have been employed to investigate the wet pressure drop, liquid holdup, liquid dispersion, etc., within the RPB. In addition, the mass transfer performance has been explored by using the CFD method coupled with user-defined functions (UDF).

6.4.1. Fluid flow study in the RPB

The flow characteristics, such as the gas pressure drop and liquid holdup, affect the CO_2 capture performance within the RPB and these have been investigated by using the CFD.

6.4.1.1. Single phase gas flow and pressure drop.

The distribution of the dry gas pressure and pressure drop were simulated for the gas flow passing through a 3D packing region with a complex wire mesh matrix by Liu F. et al. (2017). The influence of the liquid flow was not considered in these simulations. Liu F. et al. (2017) concluded that a considerable part of the gas pressure drop usually occurred from the gas pressure drop in the inner cavity zone of the rotating bed. Also, strong turbulence and mixing, named as the gas-side end effect, were observed in the outer packing zone of the RPB. In this study, a grid of over 90 million computational cells was used to accurately describe the gas flow by resolving at the pore scale in the wire mesh packing of a volume of just 0.009 m^3.

In addition, the packing region may be regarded as a porous medium without computationally resolving the geometry of the packing in order to reduce the required computing resources. In this way Yang et al. (2015) and Wu et al. (2018) investigated the mal-distribution of the gas pressure in the 3D RPB models. Then the optimum design of the RPB

was obtained by modifying the gas feed configurations and inserting internals or baffles in the packing region to reduce the mal-distribution and increase the gas-side mass transfer. Again, the simulations did not consider the influence of the liquid phase on the gas flow. The difference between the dry and wet pressure drops in the RPB can be pretty significant.

6.4.1.2. Characteristics of the liquid flow.

The characteristics of the liquid flow, such as the liquid holdup, liquid velocity, and liquid residence time, significantly influence the CO_2 capture in the RPB and therefore attract more attention than the gas flow. A two-phase flow model, either the VOF or the Eulerian model, must be adopted to investigate the liquid flow behaviours accurately. In particular, the VOF method has been widely used since it is well-suited for capturing the gas-liquid interface and the evolution of droplets when impacting on the packing surface, if sufficiently fine computational meshes are employed.

Using 2D VOF method, the liquid flow patterns in wire mesh and foam packings have been obtained under various operating conditions. The flow patterns can be primarily divided into three types: pore flow, droplet flow and film flow (Shi et al., 2013; Xie et al., 2017; Ouyang et al., 2018a,2018b,2019; Liu et al., 2019, 2020). In addition, the simulation investigations showed that the flow patterns varied mainly depending on the rotational speed of the RPB. The liquid distribution in the packing region became more uniform with the increased rotational speed, thus producing improved micro-mixing. Furthermore, Yang et al. (2016) and Liu et al. (2020) visually explored the liquid holdup and the liquid distribution within the packing under different operating conditions using the VOF method. The predicted liquid holdup agreed well with the correlations of Burns et al. (2000) and Yang et al. (2016).

However, the actual liquid flow in the RPB is 3D. The flow characteristics obtained under the 2D assumption are limited (Shi et al., 2013). Xie et al. (2019) analysed the gas-liquid flow by using 3D REUs of the RPB where different gravitational forces were employed in the REU to model the flow at different locations across a typical RPB, so that the overall characteristics of the liquid flow in the RPB was successfully assembled. In addition, the correlation of the effective interfacial area was proposed which has been further utilized in the work of Lu et al. (2019) and Zhang et al. (2022a, 2022b). In addition, using the VOF method, Guo et al. (2017) and Zhang et al. (2020) investigated the liquid holdup, liquid droplet size and residence time in a complete RPB model in 3D. However, the multilayer wire mesh packing was simplified as straight wires parallel to the rotor axis without considering the effect of the horizontal wire meshes. Thus, the difference of the liquid holdup obtained from the experiment, simulation and Bruns correlation was large. Therefore, it is important to model the packing geometry exactly in 3D when using VOF method. However, this would lead to a huge computational mesh.

Recently, Zhang et al. (2021) and modelled a sector of the 3D RPB model using the VOF model incorporating a periodic boundary condition. The model considered both the latitude and longitude structured wires to predict the liquid flow behaviours in the packing region accurately. Using this model, the formations of the liquid droplets when impacting on the single-layer or multi-layer wire meshes were simulated (Guo et al., 2017; Xu et al., 2019; Wei et al., 2020; Zhang et al., 2021). The results obtained were compared with the photographs recorded using high-speed cameras, as shown in Fig. 6.7. The observed liquid dispersion indicated that the gas-liquid contact area and the mixing were enhanced at the inner edge of the packing (Zhang et al., 2017). Although various liquid flow characteristics could be clearly captured by employing the VOF method in this study, it will become computationally prohibitively expensive to be used for the simulations of large/full scale RPBs (Liu Y. et al., 2017).

The Eulerian approach has shown great potential for reducing the computational cost in modelling the RPBs (Vlahostergios et al., 2020). Eulerian porous medium method has been utilized in the single-phase model to investigate the dry gas pressure drop in RPBs. When it is employed to study the liquid flow, the appropriate mathematical models need to be added to the governing momentum equations, such as the porous resistance and liquid dispersion forces. (Lu et al., 2019) proposed some beneficial mathematical models for estimating the gas-liquid interfacial force and the drag forces from the packing to be used with the two-phase Eulerian porous media model for simulating liquid flow in the RPB. These equations were derived based on the correlations originally proposed by Kołodziej and Łojewska (2009) for single-phase flow through a wire mesh. The equations have been successfully employed to investigate the gas-liquid flows in the RPBs to predict the liquid holdup and gas pressure drop. Recently, Zhang and Xie et al. (2022) further developed this model by considering the dispersion forces mentioned in Section 6.3.3, including the capillary and mechanical dispersion forces. The results showed that the predicted liquid holdup matched the experimental data after considering the liquid dispersion force, as shown in Fig. 6.8. Employing the Eulerian porous medium models and the proposed models by Lu et al. (2019) and Zhang and Ingham et al. (2022), the simulation time for a full pilot scale RPB in 3D was significantly reduced. Although the trade-off of the Eulerian porous medium model is that it does not allow a clear capture of the gas-liquid interface, it does provide a feasible and effective way to simulate the CO_2 capture process in a full-scale RPB in 3D.

6.4.2. Predicting the mass transfer performance in the RPB

As is well known, the mass transfer can be greatly enhanced in the RPB due to the centrifugal force resulting from the rotation of the packed bed. Both the VOF and the porous medium approaches have been employed in studying the mass transfer process within the RPB, especially for CO_2 capture. Guo et al. (2016) employed the VOF, together with Yang et al. (2016) investigated the oxygen absorption in the water in the packing region by employing the VOF model and Chen's liquid side mass transfer coefficient correlation via a UDF. They found that the micromixing behaviour was extreme in the 'end effect' zone due to the liquid dispersion produced by the collision between the liquid and the packing. Since the semi-empirical mass transfer correlation was used, it may not be able to accurately predict the mass transfer process in a practical RPB as the correlation was too general. As mentioned before, using VOF method requires a prohibitively large number of computational cells to model a full-scale RPB where multiple-length scales which exist in the RPB have to be resolved in order to obtain an acceptable accuracy of the CFD simulation. Therefore, the Eulerian porous medium approach is preferred.

Lu et al. (2019) developed a 2D axisymmetric Eulerian porous medium model incorporating the two-film chemical-enhanced mass transfer model to investigate the CO_2 capture in an RPB, as is illustrated in Fig. 6.9 (a). The model uses a much coarser computer mesh than that typically employed in a VOF model without resulting in significant errors in the model results. The two-film reaction-enhanced mass transfer model has shown sufficient accuracy for expressing the CO_2 mass transfer among the phases in many PB investigations (Kim et al., 2017; Pham et al., 2015). Figs. 6.9 (b) and 6.9 (c) show the predicted CO_2 capture and temperature distributions in the RPB. The results are in good agreement with the experimental observations. Using a similar approach, a complete 3D RPB model, including the packing, inner and outer cavity zones, has been simulated (Zhang et al., 2023). Fig. 6.10 shows the CO_2 and liquid temperature distributions in the RPB with a 50 % MEA concentration solvent. The simulation results showed that the CO_2 capture performance agreed well with the experimental data, indicating that the porous medium approach can accurately predict the carbon capture process within the entire RPB.

6.4.3. Summary on CFD for the RPB

The flow characteristics and mass transfer in the RPB have been successfully investigated using CFD. Unlike modelling the static packing in the PB, the RPB models usually employ multiple reference frames or

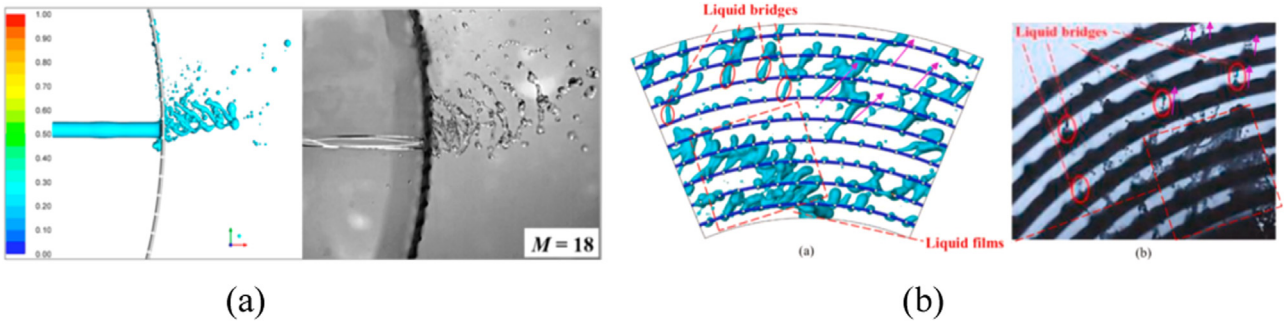

Fig. 6.7. Comparison of the simulated and visualized liquid flow across the rotating (a) single-layer wire mesh packing (Xu et al., 2019); and (b) multi-layer wire mesh packing (Zhang et al., 2021). (For interpretation of the references to color in this figure legend, the reader is referred to the web version of this article.)

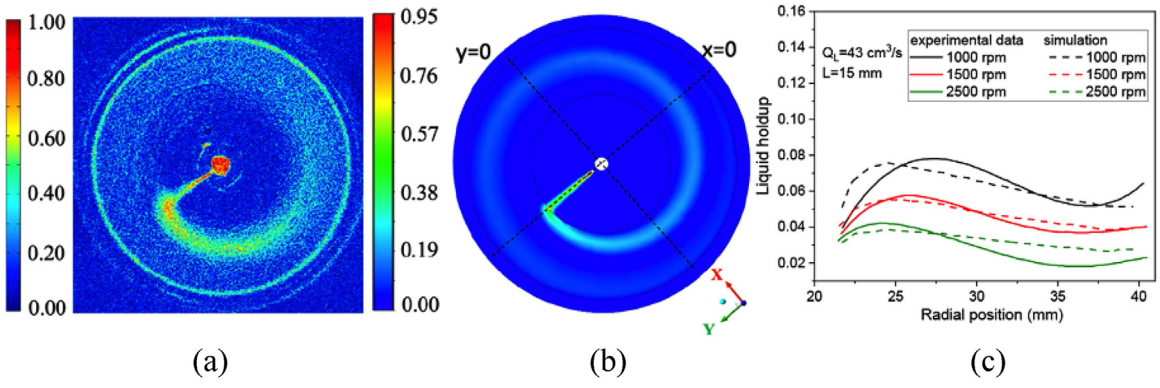

Fig. 6.8. (a) Map of the liquid holdup from the experiment (Yang et al., 2015); (b) contour of the liquid holdup from the simulation; (c) comparison of the liquid holdup along the radial position (Zhang and Ingham et al., 2022). (For interpretation of the references to color in this figure legend, the reader is referred to the web version of this article.)

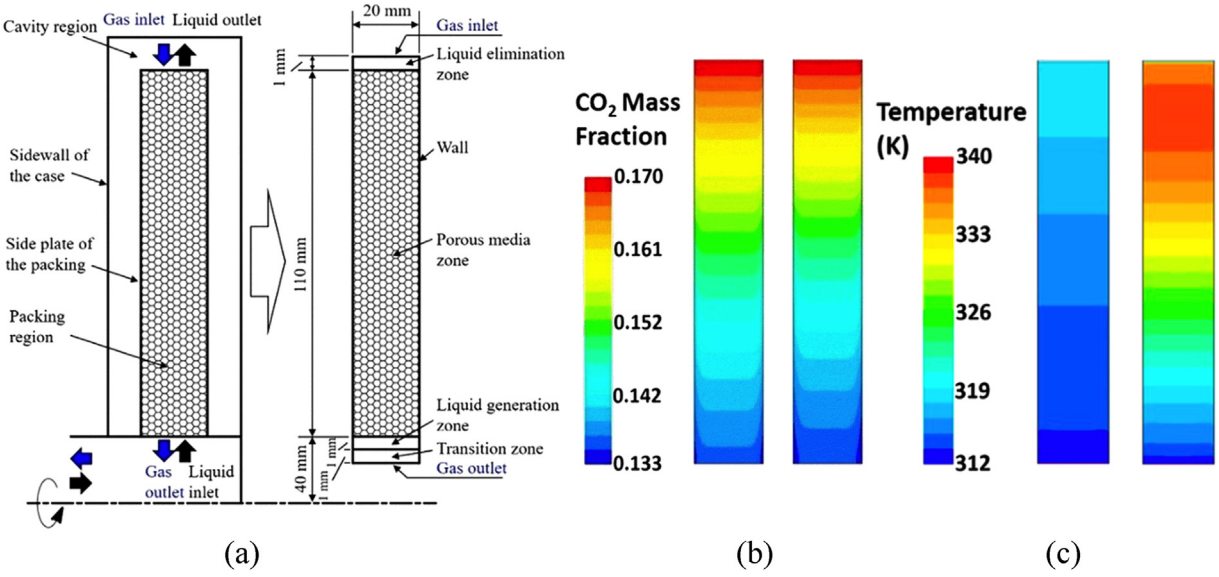

Fig. 6.9. (a) Schematic diagram of the physical 2D RPB model; contours of the (b) CO_2 mass fraction in the gas phase and (c) liquid temperature for 30 % MEA and 90 % MEA (Lu et al., 2019). (For interpretation of the references to color in this figure legend, the reader is referred to the web version of this article.)

a dynamic mesh to simulate the rotation of the packed bed. To model the gas-liquid flow and CO_2 capture in the RPBs, both the VOF and Eulerian methods have been employed. The VOF can clearly capture the gas-liquid interface and the process of droplet formation when a sufficiently fine computational mesh is employed. However, it is computationally time-consuming and can become prohibitively expensive to simulate large-scale RPBs using the VOF method. Using the Eulerian method coupled with the porous medium sub-models could save computational resources and simulation time significantly. Therefore, it has shown an excellent potential to be used to simulate large-scale RPBs for process design optimization and scaling up. Nevertheless, the model's accuracy depends on the sub-models employed, such as the porous resistance force model, effective interfacial area model, etc. Finally, as for any CFD model development, including those for both PB and RPB sim-

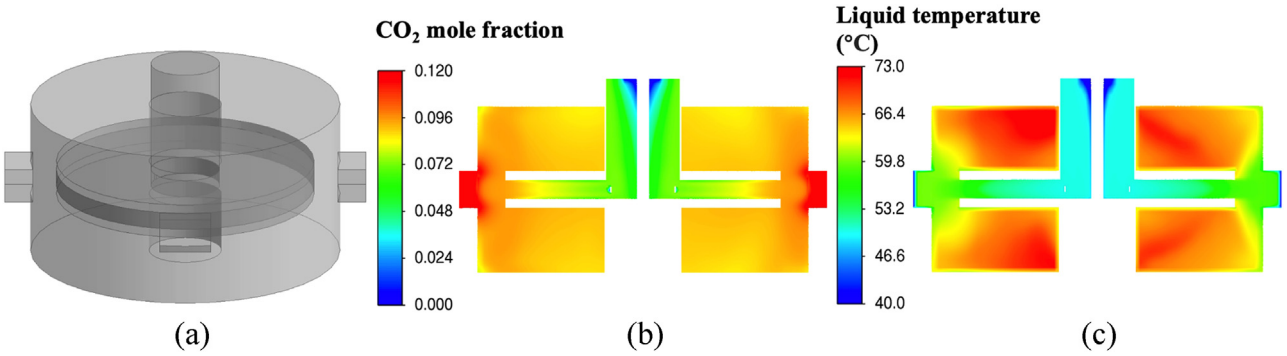

Fig. 6.10. (a) Schematic diagram of the physical 3D RPB model; contours of the (b) CO_2 mole fraction in the gas phase and (c) liquid temperature for 50 % MEA (Zhang et al., 2023). (For interpretation of the references to color in this figure legend, the reader is referred to the web version of this article.)

ulations, model validation needs to be performed before it is employed for the modelling of a specific type of packing for CO_2 capture.

6.5. Modelling, simulation and techno-economic analysis of solid adsorbent-based post combustion carbon capture (PCC)

6.5.1. Introduction for modelling, simulation and techno-economic analysis of solid adsorbent-based post combustion carbon capture (PCC)

Post combustion CO_2 adsorption is usually done in fixed bed columns (Siahpoosh et al., 2009), but it is also done in fluidized beds (Akinola et al., 2022). The design of an adsorption column based on empirical data can be expensive and time-consuming, due to the extensive experimentation required. However, predictive models that consider all important transport phenomena can be used to understand the behavior of adsorption column systems and to screen adsorbents without the need for experimentation (Maring and Webley, 2013a).

Pai et al. (2021) described three main concepts involved in modelling adsorption columns, i.e., mass transfer, heat transfer and fluid dynamics. Mathematical models that include solving coupled partial differential equations with appropriate boundary conditions are used to describe the mass and energy balance and fluid flow, to predict the behavior of the adsorption process. The models are then validated with experimental data before they are used for design, optimization, and economic analysis (Yan et al., 2016). Solving partial differential equations simultaneously can be tedious and time-consuming. Therefore, simplified models can usually be used satisfactorily by developing assumptions that simplify the representation of mainly the mass transfer phenomena within the adsorbent particles, to decrease the complexity of the model and the computational time (Shafeeyan et al., 2014). In general, mathematical models of fixed bed adsorption reflect a dynamic state, since a steady-state condition is never attained during adsorption (Valenciano et al., 2015).

6.5.2. Current status on model development of solid adsorption-based carbon capture

6.5.2.1. Fixed bed adsorption column modelling. A set of partial differential and algebraic equations derived from the conservation of mass, energy, and momentum balance are typically used in the modelling of bed columns described in the literature. These equations are used to predict the transient concentration and temperature profile in a fixed bed column. For the equations to be solved, initial conditions for a few key factors, such as concentration, temperature, and flow rate, are necessary. By using the appropriate transport rate equations and equilibrium isotherms, these conservation equations consider the restrictions imposed by the mass transfer rate and the equilibrium between the gas phase and the solid particles. Fixed-bed adsorption models differ in terms of mass transfer rate, equilibrium isotherms, thermal effect and the pressure drop equations used.

6.5.2.2. Mass balance model. Eq. (6.1) is the mathematical equation used to determine the concentration distribution of components in the gas phase along the bed. It includes the terms for: axial dispersion, convection flow, accumulation of the components in the gas phase and the mass transfer term that accounts for the adsorption process on the adsorbent particles.

$$-D_{zi}\frac{\partial^2 c_i}{\partial z^2}+\frac{\partial}{\partial z}(uc_i)+\frac{\partial c_i}{\partial t}+\left(\frac{1-\varepsilon_b}{\varepsilon_b}\right)\rho_p\frac{\partial q_i}{\partial t}=0 \tag{6.1}$$

- $D_{zi}$is the axial dispersion coefficient, which lumps together the effects that contribute to axial mixing. It can be estimated using the following correlation:

$$\frac{\varepsilon_b D_{zi}}{D_{mi}}=20+0.5ScRe \tag{6.2}$$

Where D_{mi}, Sc and Re are the molecular diffusivity of component i, the Schmidt number and the Reynolds number respectively.

- c_i is the adsorbate concentration in the gas phase; z is the distance along the bed length; u is the fluid velocity; t is the time; ε_b is the bed voidage; ρ_p is the particle density.
- q_i represents the average concentration of component i in the adsorbent particle. It is the link between the gas and solid phase mass balance equations.
- It is often assumed that there is no radial variation in concentration in both the gas and the solid phase, therefore c_i and q_i represent radial average concentrations.
- The axial mixing term, $-D_{zi}\,(\partial^2 c_i/\partial z^2)$ is often assumed to be insignificant and therefore excluded from Eq. (6.1). This assumption is reasonable for large industrial adsorption units (Simo et al., 2008).

In Eq. (6.1), $\frac{\partial q_i}{\partial t}$ is the rate of mass transfer to the solid adsorbent. It can be expressed as function of the concentration in the gas and solid phase as shown in Eq. (6.3). It is a kinetic model that describes the mass transfer mechanism within an adsorbent. There are different models for different adsorbents, which provide an accurate representation of the mass transfer mechanism (Zhao et al., 2019a).

$$\frac{\partial q_i}{\partial t}=f\left(q_i,c_i\right) \tag{6.3}$$

The main types of mass transfer kinetic models include the local equilibrium model and the mass transfer resistance model.

The local equilibrium model assumes a fast mass transfer rate between the gas and solid phase and local equilibrium is reached at every point and time in the column. The equilibrium relationship between the gas and the solid phase can be represented using equilibrium isotherms. The most common isotherms used by researchers include the Langmuir, Freundlich and Toth isotherms (Zhao et al., 2019a). An example of these models can be found in Zhao et al. (2019a), who have used various equilibrium isotherms to evaluate the performance of a PCC adsorption

system when using different adsorbents. The local equilibrium models exclude the effect of mass transfer resistance in the particle and thus do not accurately represent what is observed in adsorption columns. However, due to their simplicity, they can be used to provide an approximate representation of column behavior and they can provide valuable information about the process dynamics and the behavior of the system during the preliminary design stage of the process. Equilibrium models are also useful for designing systems in which the adsorptive selectivity depends on the difference in the equilibrium of the species in the gas mixture, but they will not be useful when the selectivity is based on kinetics when separation is achieved by the difference in the gas-adsorbent mass transfer rates between the components (Hassan et al., 1986). Therefore, a non-equilibrium model will be required to describe the behavior of such processes.

Mass transfer resistance models are based on the three potential types of resistance to diffusion into the adsorbent particles, namely: external fluid resistance and intraparticle diffusion resistance, macropore diffusion resistance, and micropore diffusion resistance. These models have been shown to predict the behavior of adsorbents in a column adequately (Mulgundmath et al., 2012). A detailed description of these models can be found in Shafeeyan et al. (2014). Although these models provide a close approximation of reality in adsorption columns, their main drawback is the complex mathematical formulation, which is difficult and time-consuming to solve, which makes them impractical for column design and optimization. In general, simplified models are adopted by applying assumptions that increase the practicability of the model without reducing its accuracy. The most used of such models is the Linear Driving Force (LDF) approximation, which suggests that the mass transfer rate of a component into the adsorbent is proportional to the linear difference between the concentration on the outer surface of the adsorbent particle and the average concentration inside the particle. The outer surface concentration is assumed to be at equilibrium with the bulk gas phase concentration. The mass transfer is therefore expressed as follows (Shafeeyan et al., 2014):

$$\frac{\partial q_i}{\partial t} = k_i\left(q_i^* - q_i\right) \tag{6.4}$$

Where q_i^* is the adsorbed-phase concentration in equilibrium with the gas phase concentration of component i, which can be obtained from various equilibrium isotherms models (Zhao et al., 2019a), an example of which is the Langmuir isotherm. This can be expressed as shown in Eq. (6.5), where: q_i^s is the saturation loading of the absorbent; K is the Langmuir isothermal equilibrium constant.

$$q_i^* = q_i^s \frac{K\,(T)P_i}{1 + K\,(T)P_i} \tag{6.5}$$

In Eq. (6.4), k_i is the effective linear driving force rate coefficient that lumps together all the resistance to mass transfer. To predict k_i accurately, many forms that have been developed can be found in the literature, with these depending on what type of mass transfer resistance is dominant. For instance, Farooq and Ruthven (1990) suggested the following model for k_i, if both macropore and micropore diffusion resistance are dominant:

$$\frac{1}{k_i} = \frac{R_p q_0}{3k_{fi}c_0} + \frac{R_p^2 q_0}{15\epsilon_p D_{pi} c_0} + \frac{R_c^2}{15D_{\mu i}} \tag{6.6}$$

Where:

- q_0 is the value of q (concentration in the solid state) at equilibrium, while c_0 is the concentration in the gas phase at feed temperature.
- D_{pi} and $D_{\mu i}$ are the effective macropore diffusivity and the micropore diffusivity respectively.
- R_p and R_c are the macropore and micropore radius.
- k_{fi} is the external film mass transfer coefficient.

6.5.2.3. Energy balance. Although there are several isothermal adsorption models that do not take the energy balance into account (Moreira et al., 2006; Shen et al., 2010), temperature variations in the adsorption column can affect adsorption equilibrium and the adsorption rate. Therefore, in order to accurately predict packed bed adsorption, the effect of heat generation due to the adsorption process must be considered. Three control volumes are usually considered - the gas, the solid and the wall of the column - and the heat transfer rate in these volumes can be modelled as follows (Shafeeyan et al., 2014):

The gas phase energy balance that is used to determine the gas temperature profile in the bed:

$$-\lambda_L \frac{\partial^2 T_g}{\partial Z^2} + \rho_g C_g \frac{\partial\left(uT_g\right)}{\partial Z} + \rho_g C_g \frac{\partial T_g}{\partial t} + \left(\frac{1-\varepsilon_b}{\varepsilon_b}\right) h_f a_s \left(T_g - T_s\right) + \frac{4h_w}{\varepsilon_b d_{int}}\left(T_g - T_w\right) = 0 \tag{6.7}$$

Where:

- T_g, T_s and T_w are the gas, solid particles, and wall temperature, respectively.
- C_g and ρ_g are the bulk heat capacity and density of the gas.
- h_f is the coefficient of the film heat transfer between the gas and the solid particles; h_w is the coefficient of the internal convective heat transfer between the gas and column wall; a_s is the ratio of the particle's external surface area to its volume; d_{int} is the internal diameter of the column; λ_L is the effective axial heat dispersion given by Grande and Rodrigues, (2005).

The solid phase energy balance:

$$\rho_p C_s \frac{\partial T_s}{\partial t} = h_f a_s \left(T_g - T_s\right) + \sum_{i=1}^{n}\left(-\Delta H_i\right)\frac{\partial q_i}{\partial t} \tag{6.8}$$

Where: $\rho_p$and C_s are the particle density and heat capacity, respectively; ΔH_i is the isosteric enthalpy of adsorption for component, which can be calculated as given in Yang et al. (1997).

The column wall energy balance:

$$\rho_w C_w \frac{\partial T_w}{\partial t} = h_w a_w \left(T_g - T_w\right) + U a_a \left(T_\infty - T_w\right) \tag{6.9}$$

Where: ρ_w and C_w are the density and the heat capacity of the wall, respectively; $a.a_w$ is the ratio of the internal surface area to the volume of the column wall; a_a is the ratio of the external surface area to the volume of the wall; U is the external overall heat transfer coefficient between the wall and the air outside the wall; T_∞ is the temperature of the outside air.

6.5.2.4. Momentum balance. The moment balance accounts for the pressure drop and the change in gas velocity in the column. Any model that estimates the pressure drop across a fixed bed can be used. The most common in the Ergun equation:

$$\frac{\partial P}{\partial Z} = -\frac{150\mu\left(1-\varepsilon_b\right)^2}{\varepsilon_b^3 d_p^2} + \frac{1.75\left(1-\varepsilon_b\right)\rho_g}{\varepsilon_b^3 d_p} u^2 \tag{6.10}$$

Where: P is the total pressure; μ is the gas viscosity; d_p is the particle diameter.

6.5.2.5. Fluidized bed adsorption modelling. When compared to fixed-bed systems, where hotspot generation is frequently unavoidable due to insufficient heat and mass transfer across the bed, fluidized-bed adsorption has the main advantage of improved adsorption due to enhanced heat and mass transfer caused by uniformity of temperature in the bed. However, modelling the behaviour of a fluidized bed is more difficult and requires the use of a complex computational method to describe the different fluidization regimes (Lee and Miller, 2013).

In addition to the gas-solid interactions phenomena that we have addressed for fixed bed column modelling (Li et al., 2022), fluidized bed adsorption modelling also requires characterization of the hydrodynamics (Jung and Lee, 2022b). Simple models that consider the important

hydrodynamic characteristics of a fluidized bed and require less computational power have been used (Akinola et al., 2022). In recent years, the use of computation fluid dynamic (CFD) has become more prevalent among researchers due to the advances in computational power (Balice et al., 2022; Cai et al., 2022; Lian and Zhong, 2022; Luo et al., 2022). According to Nikam et al. (2022), two approaches are used in these models: the Eulerian-Eulerian approach, which considers two fluid phases, i.e., the gas phase and the fluidized solid phase; the Eulerian-Lagrangian approach, which treats the solid fluidized phase as a discrete phase and keeps track of the position of individual particles in the bed. The latter approach provides a more precise description of the fluidized phase, although it requires more processing power.

6.5.3. Study of the adsorption-based carbon capture process based on process simulation

The simulation and modelling of PCC processes are usually done to screen and evaluate the performance of different adsorbent materials, and to evaluate different process configurations. According to Nikolaidis et al. (2018), the relationship between ideal process performance, operating conditions, and adsorbent properties is complicated and cannot be quantified by only considering isotherms, selectivity and data of equilibrium working capacity: detailed simulation and optimization are required. The common performance indicators used in most PCC simulations and modelling include CO_2 purity and recovery, energy efficiency, productivity, and economics (Akinola et al., 2022). Simulation and modelling packages such as gPROMS, Matlab and Aspen Adsorption are often used when evaluating these processes (Hasan et al., 2013; Leperi et al., 2019; Subraveti et al., 2019a). Several authors, including (Farmahini et al., 2018), Hasan et al. (2013), Leperi et al. (2019) and Subramanian Balashankar and Rajendran (2019) have used simulation and modelling to screen adsorbent materials. Recently, Burns et al. (2020) screened 1632 metal-organic framework (MOF) materials for PCC by integrating molecular simulation with a macroscopic process simulation of vacuum swing adsorption (VSA). They concluded that: 482 materials met the regulatory target of 95 % purity and 90 % recovery of CO_2 (95/90 CO_2 PRT); 365 of these materials had a parasitic energy requirement below that of solvent-based capture of 290 kWh per metric ton of CO_2. They also used a machine learning model to predict a given material's ability to achieve the required 95/90 CO_2 PRT.

Energy consumption is one of the important parameters, which has been extensively investigated using modelling and simulation in adsorption-based PCC and which ties up closely with process operating conditions such as feed pressurisation and blowdown pressure, plant productivity and capital cost. For instance, Haghpanah et al. (2013) did a simulation exercise in which they optimized pressure-vacuum swing adsorption (PVSA) using Zeochem zeolite 13X. They concluded that a minimum energy requirement of 149 kWh/ton of CO_2 is achievable when the process operates at low pressure, with an inlet pressure of 1 bar and a vacuum blowdown pressure of 0.02 bar to achieve a productivity of 0.49 mol of CO_2/m^3 of adsorbent corresponding to an 11 % energy penalty. They also noted that energy consumption increases with higher productivity and that a combination of feed pressurization and low blowdown pressure can reduce the plant size and the capital cost significantly. Nikolaidis et al. (2018) corroborated that energy consumption increases with increased productivity when they compared the optimized performance of zeolite 13X and modified zeolite 13X in a simulation of a single stage PVSA. In a simulation run by Subramanian Balashankar and Rajendran, (2019), more than 120 000 zeolite materials were compared, including hypothetical and existing zeolite materials. It was shown that low N_2 affinity, not high CO_2 affinity, is characteristic of a low energy consuming adsorbent. It was also shown that the best performing adsorbent materials consumed 16 % less energy than Zeolite 13X, which is considered the current benchmark for adsorbent materials.

6.5.4. Techno-economic analysis

In industrial settings, solid adsorbents have been used to remove CO_2 from hydrogen and natural gas. Unlike the flue gas from power plants, these gases are typically present at high pressure and low temperature. When the International Energy Agency (IEA) conducted a study on applying PSA to adsorption-based PCC in the early 1990s (IEA, 1992); thus, the authors concluded that this technology was not suitable for the bulk capture of CO_2 from fossil fuel power plants.

Interest in using adsorbents for CO_2 PCC only surfaced in late 2000s. Ho et al. (2008) reported the first Techno-Economic Analysis (TEA) study after the publication of the IEA 1992 report. In this study, the VSA process was compared to the PSA process, as shown in Fig. 6.11. Zeolite 13 X was selected as the adsorbent, with a capacity of 2.2 mol/kg of adsorbent, and CO_2/N_2 selectivity of 54. When the four-step Skarstrom cycle was used, the VSA showed promising results compared to PSA, with a capture cost of $51/ton of CO_2 avoided (2006 USD), close to MEA adsorption process, which is $49/ton CO_2. The CO_2 capture rate was set at 85 % in the study, but the purity of the CO_2 in the recovery stream was less than 50 %. Most of the cost comes from compression (both unit cost and energy cost), seconded by the adsorbent unit and adsorbent replacement. When a seven-step PSA cycle was applied, the capture cost was lowered to $41/ton with an improved purity of 70 %. The drawback of using the seven-setup PSA cycle is that more adsorbent is needed to compensate for the reduced CO_2 recovery rate. The authors proposed that the most cost can be reduced further if a better adsorbent is used (Ho et al., 2008). This result was very promising, as the estimated capture cost was close to that of the MEA adsorption processes.

The impact of process factors on the VSA for PCC was investigated by Zhang et al., 2008. The cost results were not comparable to those reported in previous studies since a straightforward economic assessment method was used to compare the merits of various VSA situations. However, the study did show that input CO_2 with a high concentration increases the recovery rate and purity of CO_2, which can significantly reduce the capture cost. Using a six-step VSA cycle, the study found that ordinary flue gas with a CO_2 concentration of about 12 % by volume is good for VSA, with good recovery (>70 %) and purity (>90 %). Increased purity can be attained using a nine-step VSA cycle, but the cost penalty is higher.

In their review paper, Samanta et al. (2012) evaluated the studies on PCC and noted that relatively few economic analyses were done because there was insufficient data on the performance of solid sorbents in various contactor configurations. The assessment also made it clear that the reactor and process design are crucial for the development of the PCC technology and that the sorbent is not the only important factor in the process. This assessment still holds true.

The impact of water on adsorption-based PCC was taken into consideration by Leperi et al. (2016). The study found that removing water before the PSA cycle is crucial. When moisture was eliminated during the pre-treatment phase, with zeolite 13X being used as the adsorbent, it resulted in a 90 % recovery rate with 90 % purity at a cost of $32.1/ton CO_2. Pre-treatment can cut the overall cost of capture by about 6 %.

More and more parameters can be added into the TEA as computer power and simulation models improve. Khurana and Farooq (2019) reported on an integrated optimization platform that can use a simulator based on a non-isothermal and non-isobaric linear driving force model. This platform was demonstrated using two VSA cycles: a four-step VSA cycle with light pressurization and a six-step cycle with dual reflux Fig. 6.12. The method was optimized in relation to the levelized cost of electricity (LCOE). MOF UTSA-16 was used to obtain a minimum LCOE of $114/MWh for the four-step cycle, which is less expensive than NETL's Shell Cansolv-based PCC solution. The cost of CO_2 capture is claimed to be $21.1/ton CO_2 captured and $26.3/ton CO_2 avoided, with CO_2 purity exceeding 90 % (Khurana and Farooq, 2019). This is much lower than that reported in prior research, and it meets the $40/ton CO_2 objective for second-generation PCC technologies.

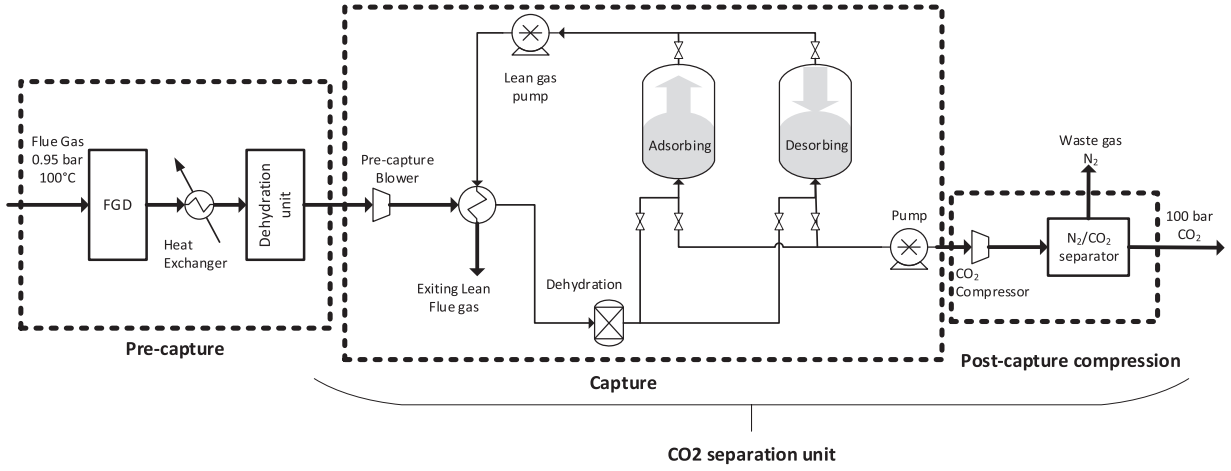

Fig. 6.11. Simplified process flow diagram for the PSA/VSA CO_2 capture process applied by Ho et al. (2008). (For interpretation of the references to color in this figure legend, the reader is referred to the web version of this article.)

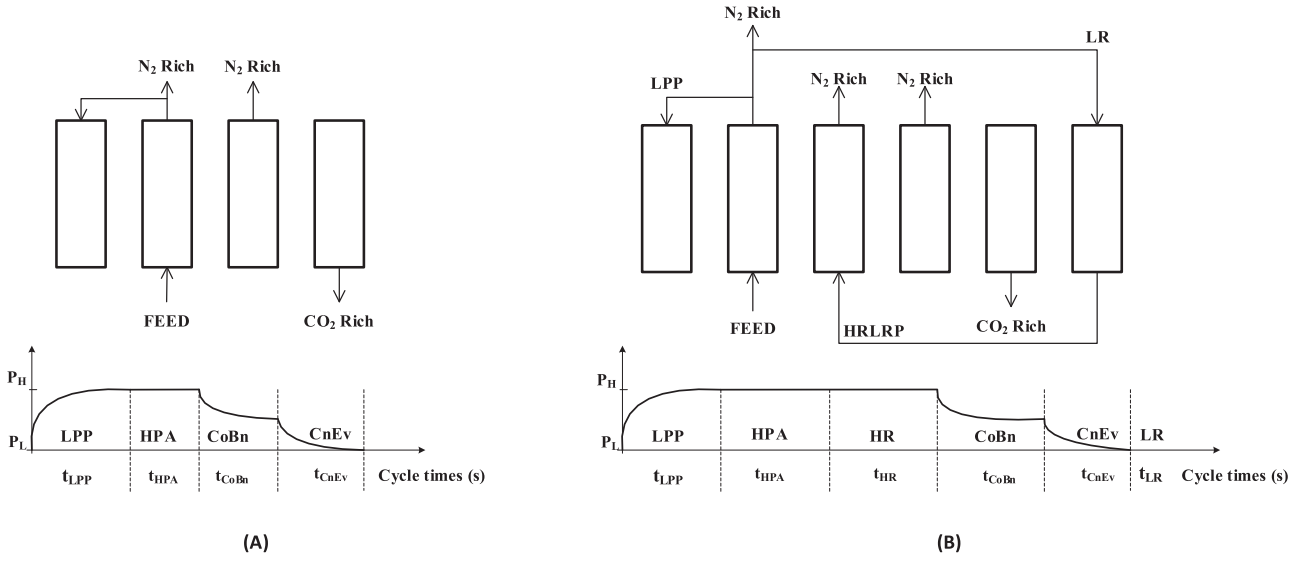

Fig. 6.12. (A) The four-step VSA cycle with LPP and (B) the six-step dual-reflux VSA cycle studied by Khurana and Farooq (2019). (For interpretation of the references to color in this figure legend, the reader is referred to the web version of this article.)

Danaci et al. (2020) created another screening tool. Twenty-two MOFs, two zeolites and activated carbon were tested against CO_2 purity, recovery rate and cost. CO_2 emissions from four sources were considered: natural gas power plants, coal-fired power plants, cement manufacture and the steel industry. UTSA-16, which is similar to zeolite 13X, was found to be the best MOF among the adsorbents examined; however, the cost of the adsorbent was higher than that of an amine-based adsorption technique. The study found that the most relevant qualities of the adsorbent are its low N_2 adsorption and moderate enthalpies of adsorption, rather than its CO_2 capacity or surface area. This work showed a new direction for adsorbent design, as well as the complexity of the PSA system.

Subraveti et al. (2021) confirmed that the cost of the VSA process when using the new proposed adsorbents Zeolite 13X and two MOFs, is still higher than that of the MEA process. The study reported that IISERP MOF 2 outperformed Zeolite 13X, which is the benchmark material for the four-step cycle process. When the CO_2 concentration in the flue gas was 20 %, the capture cost was €33.6/ton of CO_2, with a corresponding CO_2 averted cost of €73/ton, which is more than that of MEA. The study reported that optimizing the VSA process for proxy objectives, such as reducing energy used and maximizing productivity, does not automatically translate into the lowest cost. The adsorbents identified as being superior due to their high energy/productivity performance did not always result in reduced cost. The rationale offered was that the minimum cost configuration does not lay in the minimal energy vs. maximum productivity Pareto curves, due to the complexity of the VSA process scaling up. This explanation adds to the already-complex VSA process and poses a new hurdle in adsorbent screening. The study also indicated that: due to the constraint of a single VSA unit, it is difficult to profit from economies of scale; the VSA process is probably better suited to small and medium-sized operations rather than large-scale operations (Subraveti et al., 2021). It was also stated that a different strategy is required to further reduce capture costs, and the proposed solutions were to use monoliths, contact passes paired with quick cycling and using other cycles.

Jung and Lee, (2022b) claimed that the solid sorbent process outperforms the MEA process. Four processes were evaluated in their study: fluidized bed, fixed bed, moving bed and rapid thermal swing. The amine functionalized SiO_2/0.37EB-PEI powder, pellet and hollow fibre were employed as the solid sorbent. The study revealed that, except for the fluidized bed process, the proposed processes had a lower capture cost than the 30 % MEA process. The best performing process had a

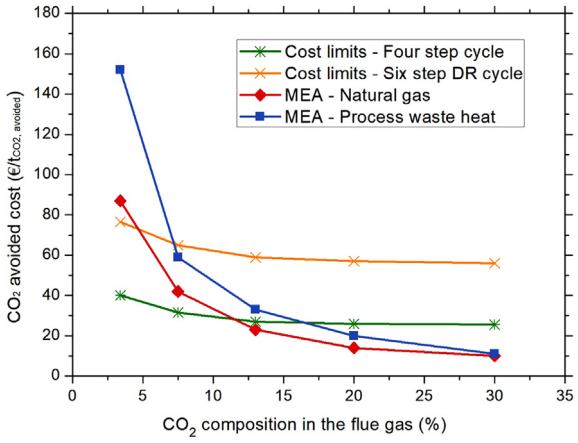

Fig. 6.13. Comparison of the cost limit of the four-step and six-step DR PVSA cycles with CO_2 avoided cost obtained using the MEA-based CO_2 capture with two streams supply scenario (Subraveti et al., 2022). (For interpretation of the references to color in this figure legend, the reader is referred to the web version of this article.)

capture cost of $48 per ton of CO_2, which was 24 % less expensive than the 30 % MEA process and only 3 % more expensive than the Water Lean Solvents method.

Subraveti et al. (2022) investigated the cost limits of the PVSA process. In this investigation, the cost of the adsorbent was adjusted to zero to determine the effect of sorbent characteristics. It was determined that the optimal adsorbent should have close to 0 % N_2 adsorption, which agrees with Danaci et al. (2020)'s conclusions, as well as linear isotherms. Based on the four-step cycle, morphological change can result in a 9–22 % lower CO_2 avoidance cost. The optimal pellet porosity and diameter was 0.42–0.76 % and 3–5 mm, respectively. When compared to the four-step cycle, the six-step DR cycle cost 15 - 42 % less. As shown in Fig. 6.13, compared to the MEA process, the four stage PVSA cycle is at least 8 % less expensive, and the six-step DR PVSA is at least 35 % less expensive for input gasses with more than 7.5 % CO_2 concentration. CO_2 averted costs ranged from €10.4 to 87.1/ton for feed gas with CO_2 concentrations ranging from 3.50 % to 30 %, while MEA costs ranged from €54.8 to €76.8, which indicates that PSA is well suited to high CO_2 concentration gas treatment.

The two most recent studies (Jung and Lee, 2022a; Subraveti et al., 2022) indicated that under certain conditions, the solid adsorbent could deliver a reduced CO_2 capture cost. It is worth noting that in the study by Subraveti et al. (2022), the optimal CO_2 adsorption isotherm varied according to the different process options and different CO_2 compositions. Examples of the CO_2 isotherms are shown in Fig. 6.14.

According to Akinola et al. (2022), although TEA research on the solid adsorbent system for PCC is still limited, the trend over the last two decades has shown that advancements in the computational capacity of available modelling and simulation tools has enabled detailed model development and simulation studies, particularly in the case of a fixed bed, which has thus far been seen as the most promising option. The detailed simulation demonstrated the difficulty of adsorbent and process screening, particularly when the best performing adsorbent does not always result in the lowest cost, and the best performing process for single unit operation does not always result in a superior large-scale setup. More creative cycle and column configurations are required to enable cost-effective PCC adsorption.

6.5.5. *Summary: advantages, limitations, and prospects*

Table 6.2 summarizes some of the important developments in PCC modelling, simulation, and economic analysis. Even though there are still few process simulations and economic evaluations, it is evident that more information on identifying the lowest-cost option has been reported thanks to increased computing capacity and model development. It is promising to see that the cost of solid-based PCC processes has decreased over the years, according to the simulation results. The second-generation PCC technologies' target cost of $40/ ton of CO_2 has been met, and additional cost reductions are possible.

Furthermore, the work done so far has indicated that the traditional way of doing materials screening, with only the CO_2 capacity and surface area being considered, was not sufficient to determine the best adsorbent. Adsorption enthalpies and N_2 adsorption both contribute significantly to reducing capture costs. The "best adsorbent" also depends on the process configuration. Various processes have different needs in terms of the optimal adsorbent. This makes material screening more changing because the best adsorbent selected for a single unit might not be the best candidate for a large-scale operation. To reduce capture cost, it would therefore be more crucial to consider different process configuration options. As recommended by Akinola et al. (2022), the key to develop more cost-effective PCC processes would lie on the development of more creative cycle and column configurations. Setting the process performance target first, understanding the process requirements for the adsorbent to reach the target, and using this as a criterion for material screening should be the philosophy for more cost-effective PCC.

6.6. *Machine learning application for modelling, simulation, optimization and control of carbon capture systems*

Carbon capture systems involve a highly nonlinear and complicated interplay of heat and mass transfer, thermodynamics and chemical reactions (Lawal et al., 2009). Accurately modelling their behaviour from the first principle is time-consuming, computationally difficult and requires advanced capabilities in process systems engineering. Data-based modelling using machine learning, which is simpler and easier to implement, has been proven to accurately model and predict the highly complex underlying relationships in carbon capture systems with reduced computational load (Li et al., 2018). Machine learning, a branch of artificial intelligence, uses empirical data to obtain models that can predict relationships and patterns. Machine learning models use algorithms, common among which are decision trees, naïve Bayes, support vector machines, random forest, AdaBoost, k-means clustering, particle swarm, genetic algorithm and artificial neural networks (Yan et al., 2021), to achieve specific tasks such as regression, classification, clustering, outlier detection and dimension reduction. The tasks are achieved by 'training' the algorithms using the selected data to 'learn' the relationships and patterns in a dataset. The methods for machine learning model training includes supervised, unsupervised and reinforcement learning (Bonetto and Latzko, 2020). Unsupervised learning algorithms use only input datasets to 'train' machine learning models to 'learn' the commonalities within a dataset, enabling clustering or association of unlabelled datasets. On the other hand, supervised and reinforcement learning uses an input-output dataset and 'trains' the machine learning model to 'learn' the input-output relationship (Bonetto and Latzko, 2020).

Supervised machine learning has been widely used in carbon capture modelling, simulation, control and optimisation due to its relative simplicity and suitability for a wide range of machine learning algorithms. Machine learning-based modelling application in carbon capture has become expedient with the growing availability of experimental and/or operating datasets of carbon capture systems as the number of test and demonstration plants commissioned worldwide continues to increase (Oko et al., 2017). State-of-the-art machine learning applications in the wider area of carbon capture storage and utilisation (CCUS) have been reported (Gupta and Li, 2022; Rahimi et al., 2021; Yan et al., 2021). Given the wide-ranging nature of the existing reviews, their discussions on machine learning applications in carbon capture are limited with no critical analysis of existing models. Therefore, this section of this review provides an in-depth critical analysis, identifies the grey areas and limitations in existing machine learning applications in carbon

Table 6.2
Summary of some of the work done on modelling, simulation, and techno-economic analysis of PCC processes and their results on capture cost and energy consumption.

Application	Authors	Method	Adsorption Type	Operation mode	Cost/ energy consumption	Software used
Adsorbent material screening	(Farmahini et al., 2018)	Molecular simulation, Equilibrium adsorption, Process simulation	Fixed bed	VSA, PSA		CySim, Platypus, Python
Adsorbent material screening	(Hasan et al., 2013)	ZEOMICS, Isotherms, Process simulation, NAPDE, NLP	Fixed bed	VSA, PSA	$23.63-$41.45 per ton CO_2	ZEOMICS
Adsorbent material screening	(Leperi et al., 2019)	Molecular Simulation, Equilibrium Isotherms, Process simulation	Fixed bed	PSA	$30-$40 per ton CO_2	Matlab-S-ODE
Adsorbent material screening	(Subramanian Balashankar and Rajendran, 2019)	BAAM, Process simulation, Equilibrium Isotherms	Fixed bed	VSA	123.21 kWh/ton CO_2	Matlab-S-PDE
Adsorbent material screening	(Burns et al., 2020)	Molecular Simulation (GCMC), Process Simulation, Machine Learning	Fixed bed	VSA	< 290 kWh/ ton CO_2	
Adsorbent material screening	(Jung and Lee, 2022a)	Process simulation	Fixed bed, Fluidized bed, Moving bed	TSA	$48.1-$75.2/ton CO_2	
Energy evaluation	(Haghpanah et al., 2013)	Process simulation -Finite Volume Method	Fixed bed	PSA, VSA, PVSA	148.96-499.65 kWh/ ton CO_2	Matlab-ode23s
Energy evaluation wet flue gas	(Krishnamurthy et al., 2014a)	Process Simulation, Equilibrium model	Fixed bed	VSA	177 kWh/ton CO_2	Matlab-ODE
Energy Evaluation	(Nikolaidis et al., 2018)	Equilibrium Isotherms, LDF	Fixed bed	P/VSA	0.89-1.08 MJ/kg CO_2	gPROMS/ gOPT
Energy Evaluation	(Jung and Lee, 2022b)	Process simulation	Fluidized bed	TSA	258.6 kWh/ton CO_2	

capture and gives recommendations to guide future research and development.

6.6.1. *Machine learning algorithm: artificial neural network*

Although a handful of machine learning algorithms have been developed for handling different tasks (Yan et al., 2021), artificial neural network (ANN) is the most widely used algorithm due to their versatility and accuracy for all task categories (Shalaby et al., 2021). ANN mimics the structure of biological neural networks and their way of encoding and decoding problems and is therefore able to identify complex underlying relationships based on input-output datasets. They include the interconnection of neurones and the basic building blocks, organised in input, hidden and output layers (Fig. 6.15). Feedforward ANN with signals flowing from the input to the output through a single hidden layer is very commonly used, although they are very likely to overfit the data and therefore have poor generalisation capability (Caruana et al., 2000). To address this limitation, NN algorithms with multiple hidden layers and recurrent networks with feedback loops are emerging. The following sections describe machine learning application in different areas of carbon capture.

6.6.2. *Machine learning for thermodynamic and physical property prediction*

The CO_2 solubility and other thermodynamic and physical property data, used for representing the vapour-liquid equilibria (VLE) in solutions of chemical solvent-CO_2, are essential for the design and modelling of the absorber and stripper in carbon capture systems. The VLE in these systems is commonly predicted using the electrolyte Non-Randon

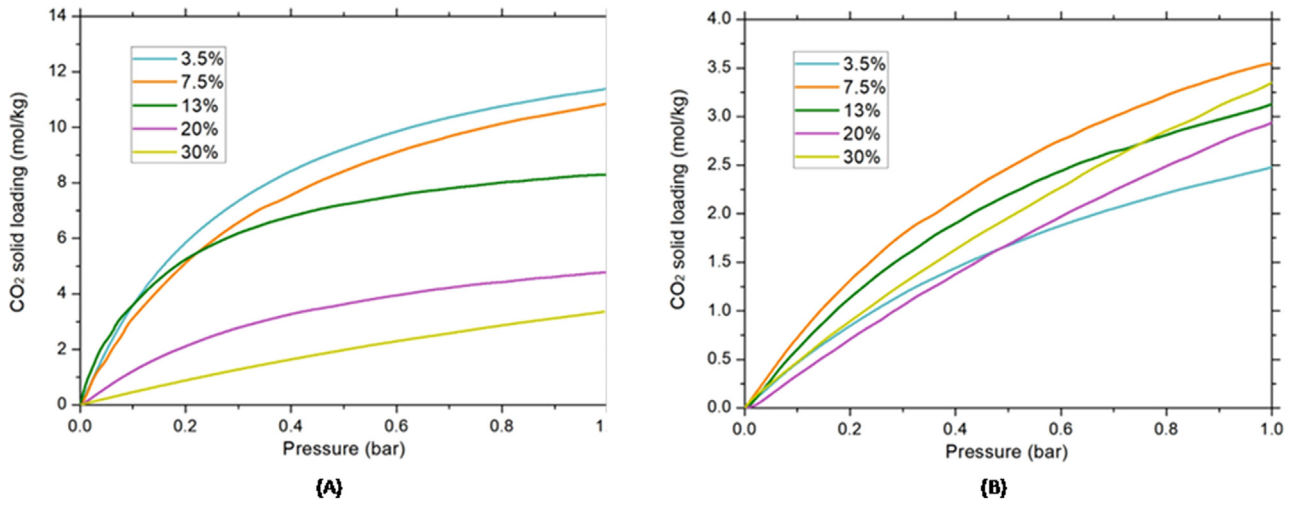

Fig. 6.14. Optimal adsorbent properties that correspond to the cost limit of (A) four-step PVSA process, and (B) six-step DR cycle with different CO_2 feed concentrations Subraveti et al. (2022). (For interpretation of the references to color in this figure legend, the reader is referred to the web version of this article.)

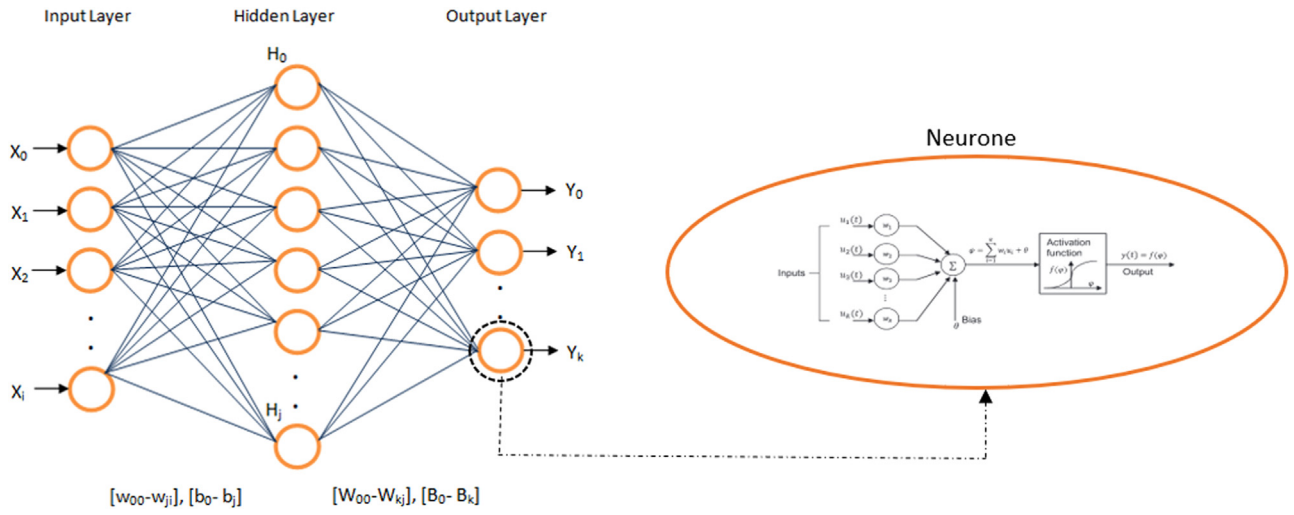

Fig. 6.15. Neural network showing the structure of the neurone (Shalaby et al., 2021). (For interpretation of the references to color in this figure legend, the reader is referred to the web version of this article.)

Two-Liquid (NRTL) or models such as the extended UNIQUAC, SAFT-VR and SAFT-γ (Aronu et al., 2011; Mac Dowell et al., 2010).The electrolyte NRTL, an activity coefficient model, is the most accurate thermodynamic equilibrium model (Austgen et al., 1989). The model predictions are based on the excess Gibbs free energy model with the Pitzer-Debye-Huckel equation used to describe the long-range interaction effects. The electrolyte NRTL model has been widely used to correlate CO_2 solubility data in 30 wt% MEA solution. Unless where these thermodynamic models are available such as in commercial simulators, developing them is non-trivial making a strong case for machine learning-based models.

ANN has proven to successfully accurately model the VLE and physical properties of solutions of the different solvents-CO_2 systems as obtained in carbon capture systems (Chen et al., 2015; Norouzbahari et al., 2015; Zhang et al., 2018). Single hidden layer back-propagation neural networks (BPNN), radial basis function neural networks (RBFNN) and general regression neural networks among others have all been shown to accurately predict the CO_2 solubility and other properties of different amine solutions (Chen et al., 2015; Zhang et al., 2018). Although BPNN show slightly better performance, these models have limited generalisation due to the one hidden-layer structure. A more robust structure, namely multiple hidden layer BPNN, showed improved accuracy (Norouzbahari et al., 2015) although this model appeared to have overfitted the data. Extreme machine learning algorithms where the input-hidden layer and hidden layer-output neurone weightings of the ANN are assigned random and via one-step regression respectively have also been shown to improve the predictive performance for CO_2 solubility and other properties (Nabipour et al., 2020). Other machine learning algorithms, namely Least Square Support Vector Machine, have comparable performance for CO_2 solubility predictions as an ANN-based model (Nabipour et al., 2020). On the other hand, ANN has also been used to predict isotherms for CO_2 capture by adsorption (Khurana and Farooq, 2019). The isotherms relate the adsorbates in the surrounding phase to the adsorbates on the adsorbent at equilibrium and constant temperature conditions and is a critical thermodynamic requirement for modelling the process. The ANN-based isotherm model can be effectively and rapidly used to screen and select adsorbents.

6.6.3. Machine learning for modelling and simulation of the CO_2 capture system

ANN model with a single hidden layer has been developed and used to evaluate carbon capture performance through chemical absorption (Wu et al., 2010). As this type of ANN model generally has poor generalisation capability beyond the training data, new solutions involving bootstrapping multiple single-layered neural networks into one network have been developed for CO_2 capture application (Li et al., 2015). Bootstrapped ANN models have a slow training process due to the increased number of calculations. The extreme learning machine algorithm, where the input-hidden layer and hidden layer-output neurone weightings are assigned randomly and via one-step regression respectively, can be employed to greatly enhanced the training speed of the bootstrapped ANN models (Li et al., 2017). Notwithstanding, the hidden single-layer nature of the bootstrapped primary networks, makes them vulnerable to accurately capturing the complicated phenomena in carbon capture systems as they may become trapped in the local optima (Dong and Li, 2012). More sophisticated deep belief networks (DBN) has been proposed to address this problem in carbon capture application (Li et al., 2018). DBN comprises multiple hidden layers of restricted Boltzmann machines that learn the input dataset's probability distribution, rather than the deterministic values. DBN is trained in batches including the unsupervised training phase to obtain initial weights of the neurones and a subsequent supervised phase via back-propagation. The DBN model of carbon capture systems has been shown to have better prediction accuracy than others (Li et al., 2018). Other machine learning algorithms, namely tree regression and Gaussian process regression, have also been used for modelling and simulating solvent-based carbon capture systems, but ANN generally performs better (Shalaby et al., 2021). ANN and other machine algorithms namely support vector machine, gradient boosting and tree regression have also been applied to estimate the CO_2 adsorption capacity for different adsorbents (Yuan et al. 2021; lian et al. 2022) with ANN similarly showing superior predictive capability compared to other algorithms (Fathalian et al. 2022). Many existing machine learning models for CO_2 capture by adsorption are mainly for predicting the CO_2 adsorption capacities for different adsorbents. These models are therefore not suitable for process optimisation and control.

6.6.4. Machine learning for control of the CO_2 capture process

CO_2 capture via chemical absorption exhibits large time inertia due to the high solvent circulation rate and huge volume of the absorber and stripper (Liao et al., 2020). This impacts the capability of the plant to be operated flexibly to follow the rapid dynamics of their host power plant as required, making the process control very challenging and conventional PID controllers insufficient for achieving desired control (Liao et al., 2020). Machine learning-based predictive controllers effectively reach setpoints with zero bias at all conditions (Li et al., 2018;

Akinola et al., 2020; Liao et al., 2020). Conventional model predictive controllers (MPC) are based on first principle models often linearised around the operating point to reduce the associated complexity and computational loads. Although these MPCs show better performance than PID-based controllers, their performance deteriorates quickly due to the linear models. In contrast, the machine learning-based MPC is non-linear; in some cases, the parameters can be conveniently tuned online (Li et al., 2018). The machine learning-based MPC for CO_2 capture has also been assessed for large-scale applications involving a carbon capture plant integrated into a 500 MW coal-fired power plant modelled via the first principle (Liao et al., 2020).

6.6.5. Machine learning for optimisation of the carbon capture process

Process optimisation, which involves an iterative solution of non-linear equations, can be computationally challenging when based on mechanistic models of the process. As a result, reduced-order models are widely used for optimisation (Eason and Biegler, 2020). However, reduced order models sacrifice accuracy and in dynamic scenarios may not capture some critical dynamics of a process, making a case for more accurate machine learning models. Machine learning models of carbon capture systems by chemical absorption using the ANN algorithm have been used for optimising the operating condition of the process using a genetic algorithm and sequential quadratic programming algorithm (Shalaby et al., 2021). More sophisticated systems, involving reinforcement learning using actor-critic neural networks that address the limitation of standard single hidden layer ANN, have also been used to optimize carbon capture systems (Chen and Wang, 2014).

6.6.6. Summary: advantages, limitations and future prospects

Although machine learning has been largely proven for obtaining models of carbon capture and other process systems the models are rarely used. Sipöcz et al. (2011) recommended incorporating machine learning models in component libraries of commercial simulators. This will greatly promote their use and enable hybrid models to leverage the strengths of machine learning and first principle modelling, diminishing their limitations. Machine learning models of carbon capture systems are also mostly obtained from first principle models. While this is sufficient for demonstrating the efficacy of the methodology, the models must be developed using actual operating plant data in practice as assumptions in modelling may oversimplify the practical realities. In addition, overfitting appears to go unnoticed in many reported models showing near-perfect predictions. These studies do not show any rigorous attempt to check for overfitting and the generalisation capability of the models cannot, therefore, be trusted. Finally, machine learning application in CO_2 capture adsorption is limited with many reported models focusing mainly on predicting the capture capacity of different adsorbents without consideration for other operating conditions.

7. Large scale applications of carbon capture technologies

7.1. SaskPower boundary dam CCS facility

7.1.1. Introduction for large scale carbon capture technologies

Given the dominant role that fossil fuels continue to play in primary energy consumption for a prolonged future to come, carbon capture, use and storage (CCUS) will remain a critical greenhouse gas reduction solution. The enormous challenge for implementing CCUS lies in the integration of component technologies through large-scale commercial demonstration projects. CCS is applicable beyond the energy sectors and can be applied to industrial sources of emissions from sectors such as iron, steel, and concrete, which are hard to decarbonize. In recent years, it has been recognized widely recognized by governments and experts that some of the world's most carbon-intensive industries may have no alternatives to CCS for deep emissions reduction.

On 2 October 2014, the first-ever, commercial–scale, coal-fired power plant incorporating amine solvent absorption carbon capture began operation near Estevan, Saskatchewan, Canada. This was a global landmark event, demonstrating a number of high-risk technology and business issues have been overcome. The project has proven to the world that commercial scale carbon dioxide capture at a coal-fired power generating station is possible rather than an elusive future option (Preston, 2015). SaskPower's Boundary Dam 3 Carbon Capture & Storage Facility (BD3 CCS Facility) is fully integrated with a coal-fired power plant. Renowned for being a key part of a full chain operation, the facility includes a power plant burning coal, a CO_2 capture facility, transportation infrastructure (pipelines), use and storage in enhanced oil recovery (EOR), and deep underground storage. The Province of Saskatchewan, Canada, becomes the hub for full-cycle CCUS knowledge, with the large-scale full chain of CCUS operations and demonstration, which is an ideal model for carbon capture, use and storage (CCUS) because the EOR creates revenue from the sale of carbon dioxide (CO_2). Any additional capacity the off-taker of CO_2 does not require can be permanently stored underground.

7.1.2. BD3 CCS project background

BD3 CCS Facility of the SaskPower Boundary Dam Power Station is located in the southeast corner of Saskatchewan near the border with the USA, named after the Boundary Dam Reservoir, which is the surface water source for power plants cooling. The region is endowed with 300-year supply of lignite coal that is affordable, abundant, and accessible and has been fuelling power plants in Saskatchewan for nearly a century. New Canadian greenhouse gas regulations on CO_2 emissions from fossil fuel power generation came into effect on 1 July 2015. Essentially, the regulations require existing and new coal-fired power generation facilities to operate with the same emissions as natural gas-fired plants: 420 tonnes CO_2/GWh. In addition to the performance standard under the Regulation, the current Pan-Canadian Regulation for reducing carbon emission charges a carbon tax at a price of $40 on fossil fuel consumption. Prior to modification, Boundary Dam's Unit #3 emitted 1110 tonnes CO_2/GWh, but at a 90 % capture rate, the plant will, at full capacity, operate with emission at 140 tonnes CO_2/GWh—essentially four times less carbon emissions than a natural gas facility. However, According to SaskPower, the federal government's carbon pricing is having an impact on SaskPower, with emissions payments going up to an estimated $180 million in 2022 from $56 million in 2020. The investment in the BD3 power unit's retrofit and carbon capture plant was C$1.467 billion, of which the carbon capture plant accounted for about 50 %. That gave 30 years of prolonged life to a power unit which could produce 115–120 MW clean base load power 24 h a day (Jonathan and Crawford, 2013).

7.1.3. Technology selection of BD3 CCS project

SaskPower pursued various technology options for carbon capture from oxyfuel combustion to amine solvent absorption that ultimately led to the decision to select the commercially unproven CANSOLV amine solvent carbon dioxide capture process. SaskPower then coupled that technology with Shell Cansolv's proven sulphur dioxide capture process to simplify the capture plant operation and to further reduce emissions. By the end of 2009, Shell Cansolv's CO_2 amine absorption capture process was the leading technology option due, in part, to its proven record of deployment of very similar SO_2 capture technology in coal-fired power plants and other industrial facilities at various global locations. This assured SaskPower of a lower risk of scale-up by selecting the CANSOLV technology for CO_2. SaskPower had forged ahead with the design and construction of the BD3 ICCS retrofit well in advance of GHG Regulations being enacted in Canada, which came into effect on 1 July 2015. This was a strategic and environmentally-responsible decision to ensure the continued use of lignite coal reserves in Saskatchewan that could last 250–500 years.

After it is piped to the adjacent capture plant, the emissions are put through a flue gas cooler to bring the temperature down from 199 $^{\circ}C$ to around 89 $^{\circ}C$, which helps enhance the adsorption of the CO_2 and SO_2.

SaskPower enhances this process by adding a polymer heat exchanger which pre-heats the condenser water used for steam generation in the power plant. The cooler also condenses out the moisture that comes from the lignite–poor-quality coal–burned at the plant. This moisture is not wasted; it is diverted to the cooling tower.

In the tower, the gas first passes through a pre-scrubber that further cools the gas and removes contaminants; then bubbles up through the scrubber, where liquid amines absorb the SO_2. Moreover, the gas is introduced to the caustic polisher section reusing residual caustic generated in the CO_2 capture system to remove the remaining SO_2. The captured CO_2 comes out of the stripper at 16 psi and is passed through an eight-stage compressor to ramp it up to around 2,500 psi, producing supercritical CO_2. A carbon dioxide stripper, made of stainless steel, which weighs roughly 250 tonnes, *44 metresTall* and 26 feet in diameter. The rectangular absorber tower with ceramic tiles inside is even taller, at 54M X11, according to online information.

7.1.4. Design and construction process and considerations

The BD3 capture facility is fully integrated with its host power plant from which it draws its steam and power needs. The BD3 facility includes CO_2 capture, compression, and transport infrastructure. CO_2 produced at the BD3 operation is mainly utilized and stored at nearby enhanced oil recovery (EOR) operations near Weyburn, Saskatchewan, while also providing CO_2 for injection and permanent geological storage at a depth of 3,400 m in a deep saline aquifer at Aquistore Project at the SaskPower Carbon Storage and Research Centre, located near the Boundary Dam Power Station, an onsite CO_2 measurement, monitoring and verification (MMV) project, managed by the Petroleum Technology Research Centre in Regina, Saskatchewan. Key factors contributed to the decision to retrofit BD3 to convert it to clean coal power include the value that would be realized over the next 30 years of operating the retrofitted power plant from the sale of three valuable by-products: carbon dioxide, sulphuric acid and fly ash. This would help to offset the cost of capture. The latter two by-products provide the off-taker market with essential materials for the production of fertilizer and cement, respectively. A 2010 study comparing the cost of building a new NGCC with the retrofit with CCS showed the levelized electricity cost was equal while the clean coal would have one 3rd emission of natural gas. This would satisfy SaskPower's core mission to deliver steady power to its customers, while capturing CO_2, which would mitigate the environmental impact of coal use, with the associated generation of a revenue stream to offset the cost of capture.

7.1.5. Operational status and performances updates

The carbon capture facility at Boundary Dam was designed to be capable of capturing 3,200 metric tons of CO_2 daily, or 1 million metric tons annually. The current performance status of the project, which through a full-scale flue gas post-combustion capture process, produces 115 megawatts (MW) of clean power, captures 90 % of CO_2, 100 % of SO_2, and lowers NOx and PM emissions, and recovers vaporised water from the flue gas to meet half (34 M/H) of the cooling water demand. SaskPower reports that the parasitic energy requirements are 21 %, lower than the typical 24 % to 40 % reported for other CCS schemes (Giannaris et al., 2021).

BD3 CCS Facility has achieved a significant milestone recently with a total of cumulative five million tonnes captured since start-up (Stephenne, 2015). As of the end of 2022, 5,001,707 tonnes of CO_2 have been captured and prevented from entering the atmosphere, and the majority has been stored on oilfield through EOR, with about 10 % permanently sequestered deep underground. The BD3 CCS facility is on track to achieve an 800,000-tonne target for the fiscal year of 2022–23 (Total capture for the 2022 calendar year was 749,035 tonnes).

During the fourth quarter of 2022 (1 October – 31 December), the CCS facility was available 79 % of the time, capturing 192,703 tonnes of CO_2. While online, the facility had a daily average capture rate of 2,631 tonnes in Q4, with a peak one-day capture of 2,874 tonnes. A two-week planned maintenance outage in Q4 allowed SaskPower to undertake scheduled work to enable the facility to run smoothly until the next planned outage in May 2023 (Preston et al., 2018).

Table 7.1
Gas composition list (design value).

Number	Component	Content (mol%)	
		Raw gas components	liquefaction purification
1	H_2	0.5 %	0.012 %
2	N_2	7.3796 %	0.6289 %
3	CO	0.403 %	0.0363 %
4	CO_2	91.62 %	99.2931 %
5	CH_4	0.002 %	0.0003 %
6	Ar	0.07 %	0.0095 %
7	H_2S	0.0004 %	0.0004 %
8	COS	0	0
9	methanol	0.015 %	0.0191 %
10	water	0.01 %	0.0001 %

Table 7.2
Physical parameters (0.1013 MPa (g), 25°C).

Physical parameters	Index
Average molecular weight	42.55
Cp/Cv	1.291
Viscosity (cP)	0.01501
Thermal conductivity (W/m·K)	0.01786
Compressibility factor	0.9950
Density (kg/m$^{3)}$	1.747

7.2. Research and design experience of Qilu Petrochemical-Shengli OilField 1 million tons/year CCUS project capture and transport unit

7.2.1. Project purpose and project scope

Qilu Petrochemical-Shengli Oil Field project is China's first million-tonne CCUS (Carbon Capture, Utilization, and Storage) project and is the largest CCUS full industry chain demonstration base and benchmark project in China. It sets a precedent for the construction of million-tonne CCUS projects in China, and it lays a solid foundation for the large-scale industrial application of CCUS projects. The project is of great significance to constructing the "artificial carbon cycle" model, which will significantly improve China's carbon emission capacity and effectively push forward the achievement of China's "double carbon" target. When completed, the project can reduce CO_2 emissions by 1 million tons each year. This is equivalent to planting nearly 9 million trees each year, stopping nearly 600,000 economy cars from being driven each year, and an additional 2.965 million tons of fuel is expected to be added over the next 15 years. The project is composed of CO_2 capture and CO_2 transportation in Qilu Petrochemical. After being captured in Qilu Petrochemical Company, CO_2 is transported to Shengli Oilfield for oil drive, and sequestered in a green way, realising the integrated application of CO_2 capture, oil drive and storage.

7.2.2. Introduction of construction scale and capture process

7.2.2.1. Gas source and component. The raw gas is supplied by the exhaust gas of the gas installation of the Qilu Petrochemical Company Second Fertilizer Plant, which has a large handling capacity, low inlet pressure and high CO_2 purity. The component of the raw gas, the liquefied and refined gas, are shown in Table 7.1, and the physical properties are shown in Table 7.2.

7.2.2.2. Construction scale and design principles. The project is based on the exhaust gas of the gas installation of the Qilu Petrochemical Company Second Fertilizer Plant to demonstrate CO_2 capture technology, with the designed CO_2 production capacity of 1 million tons/year. Taking the variation in waste gas composition into account, the installation

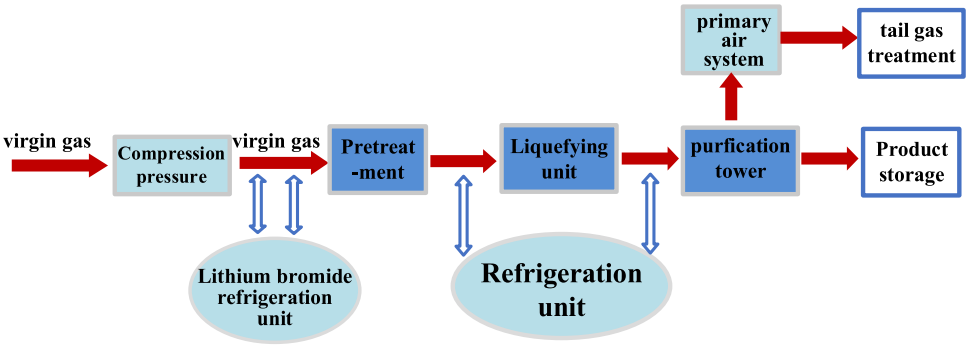

Fig. 7.1. Carbon dioxide recycling process flow chart. (For interpretation of the references to color in this figure legend, the reader is referred to the web version of this article.)

Table 7.3
Gas composition after liquefaction.

Composition	CO_2	H_2S	H_2O
Molar molecular percentage, mol%	≥0.99	≤0.001	≤10 ppm

is intended to run smoothly within 60~105 % of the rated production capacity, with the maximum load of the installation intended to be 105 % of the normal load. The installation has an annual continuous operating time of 8,000 h. Currently, the project team has fully integrated with the owner unit, taking the steam, electricity, recycled water, and other supporting facilities necessary for the 1 million tons/year CO_2 capture into account adequately. The project makes full use of the reserved supporting facilities and land for the CO_2 capture project to reduce reduce the impact on production and engineering investment of Qilu Petrochemical and lay the foundation for the good operation of the CO_2 capture project. The project requires water, electricity and steam to be connected to the main project.

7.2.3. Product programs

7.2.3.1. Product categories. The raw gas is supplied by the exhaust gas of the gas installation of the Qilu Petrochemical Company Second Fertilizer Plant, whose main components are CO_2 and N_2. The Qilu Petrochemical Company Second Fertilizer Plant captures, compresses, dries and liquefies CO_2, eventually obtaining liquid CO_2 with a purity greater than 99 % (mol%). Liquid CO_2 products are transported to Shengli Oilfield via pipelines for oil drive and sequestration.

7.2.3.2. Actual indicators of product quality. The raw gas is dried and liquefied under pressure to obtain liquid CO_2 products with a pressure of 1.9 MPa and a temperature of −27 ˚C. The main component of the product gas is shown in Table 7.3. The product gas meets the purity requirements for on-site geological sequestration.

7.2.4. Process description

7.2.4.1. CO_2 capture process. The process of "compression-condensation-purification" is adopted to recover CO_2. The raw gas is first pressurised by a compressor unit, then passes through a lithium bromide refrigeration unit to recover waste heat for cooling, and then sequentially enters the drying dehydration and liquefaction purification system. The raw gas is condensed and liquefied at low temperatures to obtain a liquid CO_2 product. The liquid CO_2 product is ready to be stored in tanks once it has been qualified.

In accordance with its function, the production process can be divided into compression units, liquid purification units, refrigeration units, tank storage units, loading unit and conveying units. The process flow of CO_2 recycling is shown in Fig. 7.1.

7.2.4.1.1. Compression unit. Compressor is an essential piece of equipment to keep the system running, and its stability is the key factor affecting the normal operation of the system. Currently, centrifugal compressor, reciprocating compressor and screw compressor are the more commonly used types of compressors. The capacity of the unit is key to compressor selection, while the gas composition and final pressure also have a certain influence on compressor selection. Centrifugal compressors are mostly driven by steam, and they are adapted for use in high-flow conditions. Currently, screw compressors and reciprocating compressors are often used to handle the small and medium flow. The project has low gas pressure and high gas volume, so the MCL706 centrifugal compressor is chosen. Horizontal split welded casing is selected, and the speed regulation mode is variable speed when used. The flow ranges from 60 % ~ 105 %. The shaft power of the centrifugal compressor is large. Taking the utility conditions at the project site into consideration, steam turbine is used as the drive mechanism of the centrifugal compressor for this project.

7.2.4.1.2. Liquid purification units. The project has a high concentration of CO_2, so low temperature distillation technology, indicated in Fig. 7.2, is chosen to liquefy and purify CO_2. The selective removal of impurities without the use of chemicals results in dry liquid CO_2.

(1) Dry Dehydration System

The CO_2 raw gas passes through the compression unit and then enters the drying tower for dehydration treatment. The dehydration process is based on a double tower + pre-sorption tower technology.

Commonly used solid desiccants consist of molecular sieve, lithium oxide, activated carbon, alumina, silica gel and compound desiccant. Molecular sieve has poor absorption ability. Lithium oxide has good water absorption properties, but it is corrosive and has a high heat release when absorbing water which affects its cooling capacity. Silica gel has the advantages of good adsorption performance, economic and practical, but it is easy to break after the adsorption of a significant amount of water. Alumina has poor adsorption capacity, only 50 % of silica gel, its regeneration temperature is high, and its regeneration time is long. Composite desiccant is unstable and deliquescent, but its adsorption performance is good.

The CO_2 raw gas is dehydrated using molecular sieves as adsorption carriers, and the water content after dehydration is decreased to less than 10 ppm. When used as a solid desiccant, a molecular sieve carries out gas adsorption by adsorption; that is, water molecules are adsorbed on the surface of the solid. A molecular sieve has a capillary or cylindrical surface, and therefore its adsorption force is more concentrated. When the diameter of the capillary pores approaches that of the adsorbed molecules, Capillary coagulation means that the cohesion starts to concentrate when the diameter of the capillary pores approaches that of the adsorbed molecules. Because of the high cohesion, water can be drawn out from the airflow and condensed into a liquid phase in the capillary pores when the temperature is higher than the boiling point.

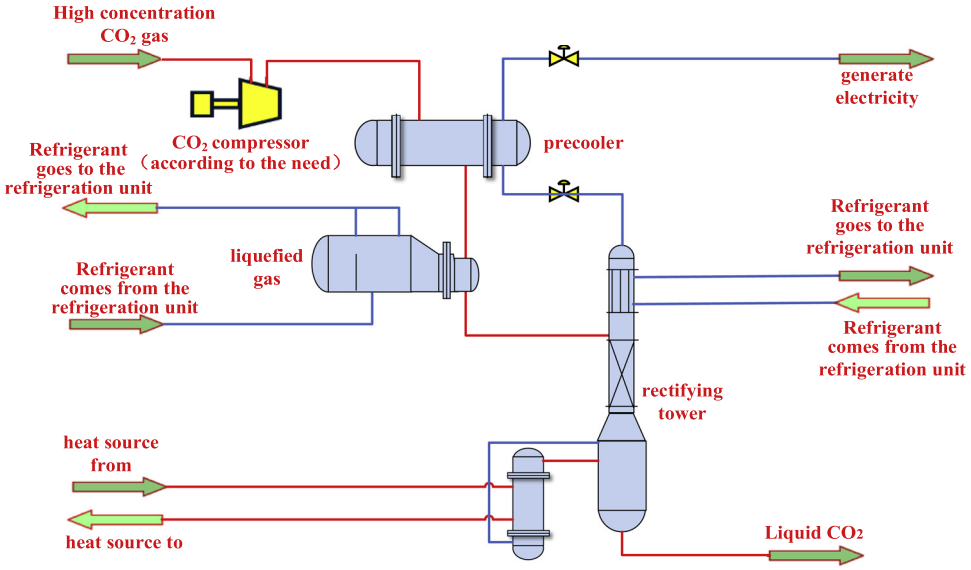

Fig. 7.2. Low-temperature distillation process flow chart. (For interpretation of the references to color in this figure legend, the reader is referred to the web version of this article.)

Table 7.4
Comparison of advantages and disadvantages of common solid desiccants.

Refrigeration circle	Merit	Defect
Lithium oxide desiccant	big amount of water absorption	Corrosive, large heat release when absorbing water, affecting cooling capacity
silica-gel drier	Good adsorption value performance, economical and practical	Easy to crack, high regeneration temperature, long time, limited use times (usually 10-30 times, the first regeneration after the drying effect is almost the same as the original finished product, and the second regeneration effect is reduced to 90 %, after 10-30 times of regeneration, the drying effect is reduced to the original 80 %, generally no desiccant regeneration
Molecular sieve	Strong adsorption, high temperature can still accommodate water molecules, pore size can be controlled by different processes	Relatively low dehydration capacity
Alumina drier	Large water absorption, fast drying speed	Aluminum oxide adsorption capacity is weak, and high regeneration temperature (usually 250-350 °C), long time (3-5 h)
Composite desiccant	Good moisture absorption	Unstable, easy to deliquesce

The advantages and disadvantages of commonly used solid desiccants are shown in Table 7.4 below.

(2) Liquefaction system

After pressurised dehydration, the product gas is cooled to less than −20 °C by a horizontal shell and tube liquefier. Three horizontal shell and tube liquefiers are put into use. The shell medium is propylene, while the tube medium is CO_2. The raw CO_2 gas is condensed into liquid CO_2 due to the evapouration of liquid propylene. CO_2 is completely liquefied and then sent to the purification system for deeper purification.

(3) Purification system

Purify the product gas from the liquefaction system. MellapakPlus TM structured filler is Sulzer's latest generation of structured filler, which effectively increases the handling capacity of the filler. The ripple direction of the upper and lower parts of each filler unit gradually approaches the vertical direction. This can not only reduce the pressure drop and shear force caused by the interaction between vapour and liquid phase, but also reduce the possibility of liquid flooding so as to eliminate local bottlenecks. MellapakPlus TM structured filler also offers significant advantages, such as high mechanical strength and strong corrosion resistance. The new MellapakPlus TM filler design allows for a significant reduction in tower diameter to reduce the customer's upfront investment costs.

(4) Expander

The expansion generator unit recovers the pressure energy of the exhaust gas, and the electricity generated is integrated into the plant grid. The low-temperature exhaust gas, after the expansion is heat exchanged with the raw gas.

Principle of the expansion generator unit: exhaust gas enters the expansion generator unit to be expanded and cooled, and the power output of the expansion generator unit is passed through the gearbox and transmitted to the generator to generate electricity. An emergency shut-off valve is provided at the inlet of the expansion generator unit. When the unit interlocks and shuts down, the emergency shut-off valve immediately cuts off the gas supply to the expansion generator unit. At the same time, the bypass control valve is opened to bring the gas supply directly into the subsequent process to ensure system balance and stability.

(5) Fresh air system

Three fans are put into use, and the flow of each fan is 20000 Nm^3/h. The non-condensable exhaust gas discharged from the expansion generator exchanges heat with air and then enters the exhaust buffer tank. Then it is transported to the RCO unit for exhaust gas treatment.

7.2.4.1.3. Refrigeration units. The main advantages of propylene refrigeration units and lithium bromide refrigeration units are low noise, energy saving and environmental friendliness. In this project, a combination of a centrifugal propylene refrigeration unit and a lithium bromide refrigeration unit is put into use.

Table 7.5
Main equipment of spherical tank area and loading unit.

Equipment name	Quantity	Major parameter
Carbon dioxide spherical tank	2	Volume 4000 m^3, material 07MnNiMoDR, design temperature-45 ~ 50 °C, design pressure 2.2MPa
Carbon dioxide loading pump	2	Flow 30 ~ 120 m^3/h, head 50 m
Carbon dioxide loading crane tube	14	DN50/DN50-304

Table 7.6
Utility consumption.

No.	Name	Unit	Specification	Unit consumption/t products	Time consume	Energy conversion value (kg standard oil)	Energy consumption (kg standard oil/t)
1	Electricity	kWh	6000/380 V	13.428	1180	0.22	2.954
2	Circulating water	t	0.45 MPa	86.373	7590	0.06	5.182
3	Medium- pressure superheated steam	t	4.0 MPaG	0.624	54.6	88	54.912
4	Instrument air	Nm^3	0.7 MPaG	3.414	300	0.038	0.130
5	Medium nitrogen gas	/	1.3 MPa	0.569	50	0.15	0.085
6	Footing	/	/	/	/	/	63.263

The propylene refrigeration unit provides the necessary cryogenic conditions for the condensation and liquefaction of CO_2. The project is processed on a large scale with a turbine-driven centrifugal refrigeration unit.

The lithium bromide aqueous solution absorbs heat by the low boiling point vapourisation of water in a high vacuum state for the purpose of refrigeration. The refrigerant cycle is the cycle of lithium bromide aqueous solution in the machine from dilute to concentrated and concentrated to dilute, refrigerant water from liquid to vapour and from vapour to liquid. The two cycles are carried out simultaneously. The lithium bromide refrigeration unit produces cryogenic cooling water by the waste heat of the final stage outlet of the CO_2 raw gas compressor. The compressed CO_2 raw gas is further cooled to 8 °C using cryogenic cooling water and then transported to subsequent liquefaction and purification installation.

7.2.4.1.4. Spherical tank area and loading units. The CO_2 raw gas is processed by the liquefaction and purification installation to obtain liquid CO_2 product, which is respectively stored in the corresponding spherical tanks and then conveyed by a loading crane. The main equipment of the spherical tanks area and loading units is shown in Table 7.5 below.

7.2.4.1.5. Integrated optimisation of the capture process. The CO_2 capture process of this project adopts two energy-saving processes: the recovery of waste heat by the additional refrigeration unit and the recovery of exhaust pressure energy by the expansion generator. The recovery of waste heat by the additional refrigeration unit can reduce the operating load and electricity consumption of the ice machine and reduce carbon emission. The expansion generator unit recovers the pressure energy of the exhaust gas, and the electricity generated is integrated into the plant grid. The low-temperature exhaust gas, after expansion, can exchange heat with the raw gas to maintain system balance and stability. After the energy-saving process is put into use, the combined energy consumption of capture is 63.263 kg standard oil/tCO_2. In light of the " Standard for Calculation of Energy Consumption for Petrochemical Design " (GB/T50441-2016), the energy consumption is converted to 2.649 GJ/tCO_2. Table 7.6 shows the consumption of utilities for capture and compression drying in each scheme:

7.3. Research and design experience of a 150 kt/a CO_2 capture and purification project

7.3.1. Project purpose and scope

The Guohua Jinjie Power Plant CO_2 capture project relies on the Shenhua Jin Guohua 600 MW sub-critical coal-fired unit to investigate advanced chemical absorption and CO_2 capture processes to capture and store post-combustion CO_2 in a brine layer. The project includes a 150,000 ton/year CO_2 capture system that utilizes a CO_2 capture system built by Shenhua Coal to Oil Company. A storage unit (located in Erdos, Inner Mongolia) was used for geological storage. The successful implementation of this project will help optimize the entire process of post-combustion CO_2 capture and brine storage, mastering various key technologies to achieve near-zero emissions from coal-fired power plants.

Table 7.7
Flue gas composition (design value).

Component	Molecular weight	Mole fraction / (mol %)
CO_2	44.011	11.1
O_2	31.999	6.1
N_2	28.014	70.7
SO_2	64.065	35 mg/Nm^3
SO_3	80.064	/
Dust concentration	—	<10 mg/Nm^3
HCl	36.461	0.0001
HF	20.006	0.0001
H_2O	18.015	12.1
NO_X	—	50 mg/Nm^3

7.3.2. Introduction of construction scale and capture technology

7.3.2.1. Source and composition of the flue gas. The flue gas is introduced from the flue at the outlet of the desulfurization absorption tower of the King Street Power Plant. The composition of the flue gas is shown in Table 7.7.

7.3.2.2. CO_2 stream. The flue gas of the project was introduced from the outlet of the desulfurization absorption tower, and the main components of the flue gas are CO_2 and N_2. After trapping, compression, drying and liquefaction, liquid CO_2 with 99.5 % (V%) purity was obtained at Shenhua Jinjie Power Plant and then transported to the storage site of Shenhua CCS project in Ulanmulun Town, Ijinholuo Banner, Ordos City, Inner Mongolia for geological storage. After pressurizing, drying, and liquefying, the pressure of the product was 2.2 MPag and the temperature was −20 °C. The main components in the product are shown in Table 7.8, and the purity of CO_2 in the product gas meet the requirements for geological storage on site.

7.3.2.3. Process description. For the characteristics of low partial pressure and complex composition of CO_2 in the flue gas of coal-fired power plants, the project integrated and applied design technologies such as a new high-efficiency CO_2 absorber, plastic packed absorption tower, flue

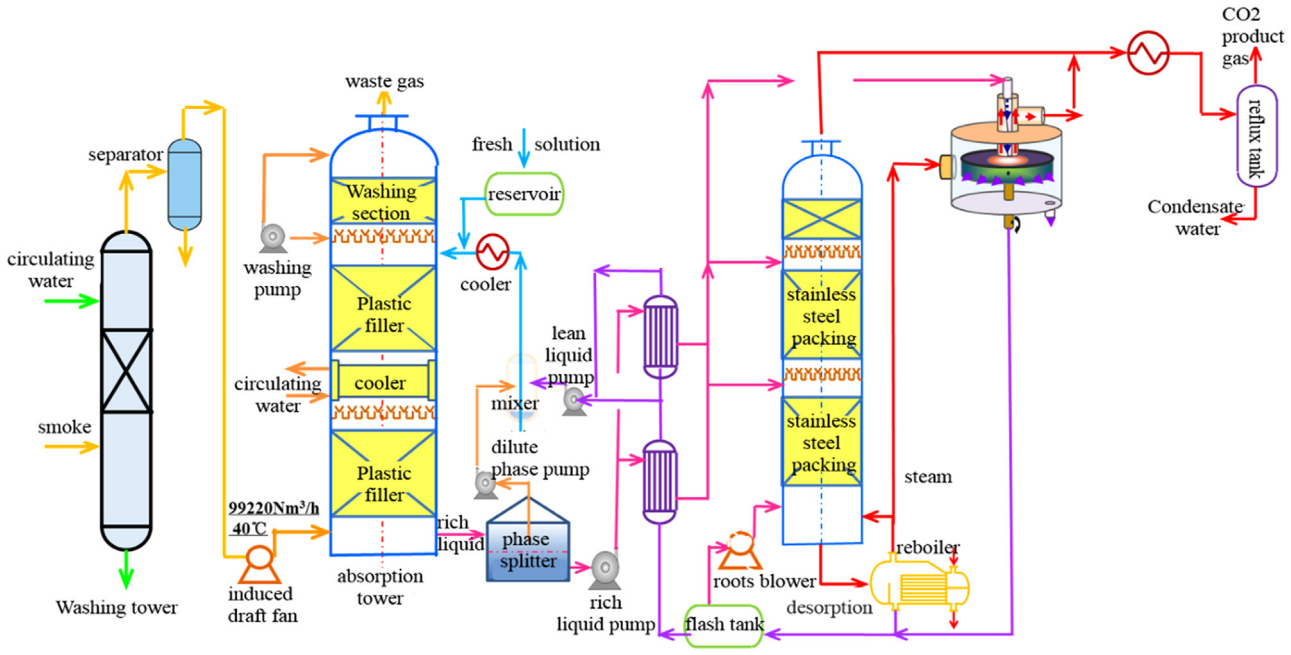

Fig. 7.3. Flow chart showing the low energy CO_2 capture process. (For interpretation of the references to color in this figure legend, the reader is referred to the web version of this article.)

Table 7.8
Composition of the liquefied gas.

Components	Mole percent, mol%
CO_2	0.995
N_2	0.004
O_2	0.001
H_2O	<10 ppm

gas pretreatment process, low-energy CO_2 capture mechanical vapour recompression (MVR) heat pump, and super gravity reactor. The flow chart of the capture link is shown in Fig. 7.3. Depending on the function, the production process can be divided into capture purification, compression, drying, liquefaction and storage units. The refinery site was reserved for the project.

7.3.2.3.1. Integrated optimization of the capture process. As shown in Fig. 7.3, the CO_2 capture project employed three energy-efficient processes, including interstage cooling, split desorption, and an MVR heat pump. The intercooling process improved the absorption load and reduced regeneration energy consumption by cooling the semi-rich liquor from the absorption tower. The rich-liquid split desorption process also recovered waste heat from the regeneration gas by direct heat exchange between the cold rich liquid and the regeneration tower top regeneration gas. In addition, the MVR heat pump process can recover latent heat from the flash vapour by flashing and heating the lean hot liquids back to the regeneration tower. Regeneration energy consumption was reduced by 20 % from 2.9 GJ/ton CO_2 to 2.34 GJ/ton CO_2 and 0.58 GJ/ton CO_2/ton CO_2.

7.3.2.3.2. Process characteristics.

(1) Using new high-efficiency CO_2 capture absorbers (including composite amine absorbers, phase change absorbers and ionic liquids), the energy consumption of the new absorbers was reduced by more than 30 % compared to the regeneration of traditional MEA solvents. At the same time, the loss of absorber was less than 1.0 kg/t CO_2, and the corrosion rate of the absorption tower and desorption tower was less than 0.076 mm/a.

(2) Using flue gas pretreatment technology, the flue gas was pretreated by alkali washing and free water separation before it entered the capture system to reduce the loss of solvent at the back end and maintain the system water balance.

(3) The project process integrated energy-saving processes such as MVR heat pump, inter-stage cooling, and split-desorption, forming a new technology of CO_2 absorption with low cost and low energy consumption, achieving CO_2 capture rate ≥ 90 %, CO_2 purity > 99 %, and regeneration energy consumption ≤ 2.4 GJ/ton CO_2.

(4) Compared with the traditional stainless steel packed absorption tower, the cost of inexpensive plastic-packed absorption tower was reduced by more than 30 %.

7.3.3. Materials consumption

The raw materials, utilities, and main consumption quota are shown in Table 7.9.

7.3.4. Comprehensive energy consumption analysis

In the normal production process, the main electrical equipment in the station included compressors, pump equipment, drying skid silica gel regeneration, indoor and plant lighting, and pipeline electric tracing heat. Steam was mainly used for solution regeneration and intermittent amine recovery heaters. Desalinated water was mainly used for the preparation of chemicals and process system make-up water. Circulating water was mainly used for lean liquid cooling, regenerative cooling and compressor inter-stage cooling. The utility consumption of the capture, compression and drying components in each scenario is shown in Table 7.10.

The project used a compatible design that integrates the physical properties of the composite amine absorber, ionic liquid and phase change absorber. In the design, the calculated total capture power was higher than the actual operating value based on the consideration of full adaptability. The energy consumption was the same for each part of the back-end, starting from compression.

Table 7.9
Raw materials, utilities, and major consumption quotas.

Serial number	Description & specification		Unit	Quantity	Remark
1	Design scale: product gas (dry gas)		Nm^3/h	87217	/
2	Flue gas (dry gas)		Nm^3/h	100000	/
	Chemicals	Amine solvent	t	~80	400 m^3 for original start-up solution
		Corrosion inhibitor	t	~1	
		Antioxidant	t	~0.6	
3	Chemicals	Amine solvent	t/a	~150	Annual operation demand
		Corrosion inhibitor	t/a	~3.75	
		Antioxidant	t/a	~3.75	
		Sodium hydroxide	t/a	~100	
4	Public works	Circulating water	t/h	~2594	1.0 MPag steam for drying skid, and 0.63 MPag steam for amine recovery
		Electric	kwh	~4942.75	
		0.3 MPag steam	t/h	~23.76	
		1.0 MPa steam	t/h	~1.5	
		0.63 MPag steam	t/h	~5	
		Desalted water	t/h	~4.5	
5	Rate of expenditure	Circulating water	t/tCO_2	~115	/
		Electric	kW $/tCO_2$	~263	/
		Steam	t/tCO_2	~1.27	/
		Amine solvent	kg/tCO_2	≤1.0	/
		Corrosion inhibitor	kg/tCO_2	≤0.025	/
		Antioxidants	kg/tCO_2	≤0.025	/
		Sodium hydroxide	kg/tCO_2	≤0.67	/
		Desalted water	kg/tCO_2	~240	/

Table 7.10
Consumption of public works.

Project		Unit	Quantity					Total
			Capture and purification	Compressing components	Drying section	Liquefying part	Storage and loading	
Public works	Circulation water	t/h	~1800	~190	~30	~574	–	2594
	Electrical	kW	~2007.75	~1700	175	~1042	~18	4942.75
	Steam	t/h	~21	–	–	–	–	21
	Desalinated water	t/h	~4.5	–	–	–	–	4.5
	Makeup of the circulating water	t/h	~33	~4	~1	~12	–	50

7.3.5. Estimation of total investment

The construction investment consisted of engineering costs, other engineering construction costs and basic reserve costs. Among them, the engineering cost was 992,322,000 yuan, the engineering secondary cost, including management, design, supervision, protection, seismic assessment and environmental assessment cost was 234,235,000 yuan, and the basic reserve cost was 613,280,000 yuan, totalling 128,788,500 yuan. The project cost was 9,923,220,000 RMB, including 6,995,540,000 RMB for equipment purchase, 1,122,290,000 RMB for main materials, 6,656,680,000 RMB for installation and 113,911,000 RMB for construction. Other expenses: Other costs totalled RMB 2,432,350,000, including construction site acquisition and clearing fees, project construction management fees, project construction technical service fees, complete set of start-up and test freight fees, production preparation fees, and large transportation measures. The basic reserve cost was calculated as 5 % of the sum of construction cost and other costs, totalling 6,132,800 yuan. The project consisted of all own funds and was interest-free during the construction period. The total investment reported and approved was the sum of construction investment and interest and working capital during the construction period. The total investment reported and approved was 13,839,800 yuan.

8. Conclusions and outlook

Carbon capture from flue gas, the primary CO_2 source, is pivotal for achieving net-zero global CO_2 emissions. Post-combustion carbon capture, the most mature and widely utilized technology, presents significant viability and feasibility for existing power plants, requiring no substantial renovation or infrastructure upgrades. The primary post-combustion CO_2 capture technologies encompass absorption separation (physical and chemical), adsorption separation (physical and chemical), and membrane separation. Over 60 % of post-combustion technologies employ absorption-based methods. Particularly, the chemical absorption method, typified by MEA absorption, is highly promising for industrial applications due to its suitability for handling large air volumes and its operational simplicity. It primarily consists of two critical processes: the chemical absorption of CO_2 in the absorption tower and the thermal regeneration of the absorbent in the desorption tower. Nonetheless, CO_2 capture from flue gas sources still faces considerable challenges impeding further development and commercialization. Accordingly, more extensive studies are required to explore the commercial prospects of the pre-combustion CO_2 capture process. Since the late 1990s, large-scale direct air capture (DAC) has been proposed as an additional method for mitigating rising atmospheric CO_2 concentrations. Despite the ambient CO_2 concentrations being extremely low, several DAC approaches have been put forward, utilizing adsorption and absorption technologies. Nevertheless, the topic remains under development. Ensuring efficient operation with reasonable energy consumption is a prerequisite for the practical application of DAC. This review discusses in detail a clear and complete performance evaluation method, focusing on energy consumption and energy efficiency.

Chemical absorption with amine solvents currently serves as a relatively mature post-combustion CO_2 capture method, with practical applications in large fixed emission sources, such as coal/gas-fired power plant flue gas. However, it is still in the industrial demonstration stage due to the absence of large-scale industrial or commercial applications.

Replacing conventional aqueous amine solutions with organic solvents or ionic liquids could provide significant benefits. Additionally, life cycle assessment can be employed to evaluate the environmental and economic impacts of carbon capture and storage. Alkali-metal-based carbonates of K_2CO_3 and Na_2CO_3 are proven as promising candidates for CO_2 capture, while the practical applications of pure carbonates were restricted by their poor capacities and kinetics. As a result, the proper design of efficient K_2CO_3- and Na_2CO_3-based sorbents is of significant importance in broadening their application prospects. The most promising method for modification of K_2CO_3 and Na_2CO_3 is to load them on a porous support, where the optimization of the support materials, K_2CO_3/Na_2CO_3 loading amounts, and preparation methods are expected to improve the texture properties and surface morphology, enhance the dispersion of active K_2CO_3/Na_2CO_3, and hence accelerate the CO_2 adsorption. In spite of the extensive studies on this topic, the influence of the abundant impurities in flue gases, such as sulphur- and chlorine-containing species, on the CO_2 capture performance of alkali-metal-based sorbents was rarely studied systematically, which is critical in evaluating their durability and regeneration efficiency in practical applications.

Apart from liquid-based sorbents, solid sorbents are emerging as potential candidates for large-scale CO_2 capture. These can be categorized as low, medium, and high-temperature solid sorbents. CaO has a high capacity for CO_2 capture. Although it can be deactivated during the CO_2 capture process, the spent CaO could be used for cement industries. One of the key challenges of CaO-based carbon capture is the use of high temperatures (up to 900 °C). MgO is an excellent medium-temperature adsorbent for carbon capture. However, it has very slow reaction kinetics. Key breakthroughs are needed for MgO-based materials development towards its commercial applications.

Furthermore, membrane technology has emerged as a promising alternative for CO_2 capture due to its inherent attributes, such as a smaller footprint, simpler setup and operation, energy savings, and the absence of phase transformation. However, designing a highly permeable membrane remains a significant challenge for efficient CO_2 capture. Other CO_2 capture technologies, including oxy-fuel combustion technology and chemical looping process, have also been reviewed. Techno-economic analysis and process modelling of CO_2 capture technologies are being developed to gain in-depth insights into the CO_2 capture process under various conditions.

The primary factor limiting the commercialization of CO_2 capture technology is its high cost. However, the International Energy Agency (IEA) forecasts that by 2030, the cost of CO_2 capture, such as DAC, is likely to decrease to less than $100/t with the large-scale application of technology. To meet specific climate targets, it is imperative to explore all CO_2 removal technologies thoroughly, as capturing CO_2 at the source, such as power plants, is insufficient. Novel reaction systems such as RPB and process intensification (integrated with CO_2 conversion) and broad system optimization are required. However, for novel high-efficient systems (e.g., RPB), large-scale demonstration is needed to validate process modelling. Process modelling and simulation (e.g., CFD) of carbon capture systems should be further carried out. However, more research is required to enhance the accuracy of modelling and simulation results. Furthermore, extensive process conditions such as adsorption enthalpies should be considered for post-combustion CO_2 capture modelling.

Declaration of Competing Interest

The first author Dr Chunfei Wu is also the Editor-in-Chief of the journal Carbon Capture Science and Technology, however he was not involved in the peer review or handling this paper for the journal. The paper was handled by the Editor Dr. Yeshui Zhang. Furthermore, co-authors Sandra Boetcher, Shijian Lu, Dongdong Feng, Guoping Hu, Paul Webley, Daxin Liang, Aneta Magdziarz, Norbert Miskolczi, Su Shiung Lam, Hongman Sun, Haiping Yang, Mingzhe Sun, Dan Tsang, Jin Shang, Christoph Müller, Lina Liu, Xin Jin, Yongqing Xu, Asim Khan, Haiqing Lin, Xuezhong He, Zhongde Dai, Shouliang Yi, Alar Konist, Xin Tu, Sibudjing Kawi, Chunfeng Song, Meihong Wang, Eni Oko, Li Gao, Hui Zhou are either Editors or board members for this journal, but none of them were involved in the peer review or handling of this paper.

References

Šulc, R., Ditl, P., 2021. A technical and economic evaluation of two different oxygen sources for a small oxy-combustion unit. J. Clean. Prod. 309 (May). doi:10.1016/j.jclepro.2021.127427.

A, S.N., Dodge, B.F., 1946. Removal of carbon dioxide from atmospheric air. Trans. Am. Instit. Chem. Eng. 42 (5-6), 827–848.

Aaron, D., Tsouris, C., 2005. Separation of CO_2 from flue gas: a review. Sep. Sci. Technol. 40 (1-3), 321–348. doi:10.1081/SS-200042244.

Aarti, A., Bhadauria, S., Nanoti, A., Dasgupta, S., Divekar, S., Gupta, P., Chauhan, R., 2016. [Cu3 (BTC)2]-polyethyleneimine: an efficient MOF composite for effective CO_2 separation. RSC Adv. 6 (95), 93003–93009. doi:10.1039/c6ra10465g.

Ababneh, H., Hameed, B.H., 2021. Chitosan-derived hydrothermally carbonized materials and its applications: A review of recent literature. Int. J. Biol. Macromol. 186, 314–327. doi:10.1016/j.ijbiomac.2021.06.161.

Abatzoglou, N., Boivin, S., 2009. A review of biogas purification processes. Biofuels Bioprod. Bioref. 3 (1), 42–71. doi:10.1002/bbb.117.

Abbasi, E., Hassanzadeh, A., Zarghami, S., Arastoopour, H., Abbasian, J., 2014. Regenerable MgO-based sorbent for high temperature CO_2 removal from syngas: 3. CO_2 capture and sorbent enhanced water gas shift reaction. Fuel 137, 260–268. doi:10.1016/j.fuel.2014.07.088.

Abdeen, F.R.H., Mel, M., Jami, M.S., Ihsan, S.I., Ismail, A.F., 2016. A review of chemical absorption of carbon dioxide for biogas upgrading. Chin. J. Chem. Eng. 24 (6), 693–702. doi:10.1016/j.cjche.2016.05.006.

Abdelnaby, M.M., Alloush, A.M., Qasem, N.A., Al-Maythalony, B.A., Mansour, R.B., Cordova, K.E., Al Hamouz, O.C.S., 2018. Carbon dioxide capture in the presence of water by an amine-based crosslinked porous polymer. J. Mater. Chem. A 6 (15), 6455–6462.

Abdelnaby, M.M., Qasem, N.A., Al-Maythalony, B.A., Cordova, K.E., Al Hamouz, O.C.S., 2019. A microporous organic copolymer for selective CO_2 capture under humid conditions. ACS Sustain. Chem. Eng. 7 (16), 13941–13948.

Abián, M., Abad, A., Izquierdo, M.T., Gayán, P., de Diego, L.F., García-Labiano, F., Adánez, J., 2017. Titanium substituted manganese-ferrite as an oxygen carrier with permanent magnetic properties for chemical looping combustion of solid fuels. Fuel 195, 38–48. doi:10.1016/j.fuel.2017.01.030.

Aboudheir, A., Tontiwachwuthikul, P., Chakma, A., Idem, R., 2003. Kinetics of the reactive absorption of carbon dioxide in high CO_2-loaded, concentrated aqueous monoethanolamine solutions. Chem. Eng. Sci. 58 (23-24), 5195–5210. doi:10.1016/j.ces.2003.08.014.

Abu-Zahra, M.R.M., Niederer, J.P.M., Feron, P.H.M., Versteeg, G.F., 2007. CO_2 capture from power plants. Part II. A parametric study of the economical performance based on mono-ethanolamine. Int. J. Greenh. Gas Control 1 (2), 135–142. doi:10.1016/S1750-5836 (07)00032-1.

Achari, A., S, S., Eswaramoorthy, M., 2016. High performance MoS2 membranes: effects of thermally driven phase transition on CO_2 separation efficiency. Energy Environ. Sci. 9 (4), 1224–1228. doi:10.1039/c5ee03856a.

Acosta, E.J., Carr, C.S., Simanek, E.E., Shantz, D.F., 2004. Engineering nanospaces: iterative synthesis of melamine-based dendrimers on amine-functionalized SBA-15 leading to complex hybrids with controllable chemistry and porosity. Adv. Mater. 16 (12), 985–989. doi:10.1002/adma.200306323.

Adelt, M., Wolf, D., Vogel, A., 2011. LCA of biomethane. J. Nat. Gas Sci. Eng. 3 (5), 646–650. doi:10.1016/j.jngse.2011.07.003.

Adeniran, B., Mokaya, R., 2016. Is N-doping in porous carbons beneficial for CO_2 storage? experimental demonstration of the relative effects of pore size and N-doping. Chem. Mater. 28 (3), 994–1001. doi:10.1021/acs.chemmater.5b05020.

Adhikari, B., Orme, C.J., Klaehn, J.R., Stewart, F.F., 2021. Technoeconomic analysis of oxygen-nitrogen separation for oxygen enrichment using membranes. Sep. Purif. Technol. 268. doi:10.1016/j.seppur.2021.118703, 118703-118703.

Administration, U.S.E.I., 2020. Annual Energy Outlook 2020. U.S. Energy Information Administration, Washington, DC, USA.

Afari, D.B., Coker, J., Narku-Tetteh, J., Idem, R., 2018. Comparative kinetic studies of solid absorber catalyst (K/MgO) and solid desorber catalyst (HZSM-5)-aided CO_2 absorption and desorption from aqueous solutions of MEA and blended solutions of BEA-AMP and MEA-MDEA. Ind. Eng. Chem. Res. 57 (46), 15824–15839. doi:10.1021/acs.iecr.8b02931.

Aframehr, W., Molki, B., Bagheri, R., Sarami, N., 2022. Capturing CO_2 by a fixed-site-carrier polyvinylamine-/matrimid-facilitated transport membrane. ACS Appl. Polym. Mater. 4 (5), 3380–3393. doi:10.1021/acsapm.1c01603.

Afzal, R.A., Pennells, J., Yamauchi, Y., Annamalai, P.K., Nanjundan, A.K., Martin, D.J., 2022. Lignocellulosic plant cell wall variation influences the structure and properties of hard carbon derived from sorghum biomass. Carbon Trends 7, 100168. doi:10.1016/j.cartre.2022.100168.

Agarwal, L., et al., 2010. Process intensification in HiGee absorption and distillation: Design procedure and applications. Ind. Eng. Chem. Res. 49 (20), 10046–10058.

Agaton, C.B., Karl, H., 2018. A real options approach to renewable electricity generation in the Philippines. Energy, Sustain. Soc. 8 (1). doi:10.1186/s13705-017-0143-y.

Agee, E.M., Orton, A., 2016. An initial laboratory prototype experiment for sequestration of atmospheric CO_2. J. Appl. Meteorol. Climatol. 55 (8), 1763–1770.

Agee, E., Orton, A., Rogers, J., 2013. CO_2 snow deposition in antarctica to curtail anthropogenic global warming. J. Appl. Meteorol. Clim. 52 (2), 281–288. doi:10.1175/Jamc-D-12-0110.1.

Aghaei, Z., Naji, L., Asl, V.H., Khanbabaei, G., Dezhagah, F., 2018. The influence of fumed silica content and particle size in poly (amide 6-b-ethylene oxide) mixed matrix membranes for gas separation. Sep. Purif. Technol. 199, 47–56. doi:10.1016/j.seppur.2018.01.035.

Aghel, B., Sahraie, S., Heidaryan, E., 2020. Comparison of aqueous and non-aqueous alkanolamines solutions for carbon dioxide desorption in a microreactor. Energy 201, 117618. doi:10.1016/j.energy.2020.117618.

Aghel, B., Behaein, S., Alobaid, F., 2022a. CO_2 capture from biogas by biomass-based adsorbents: A review. Fuel 328, 125276. doi:10.1016/j.fuel.2022.125276.

Aghel, B., Janati, S., Wongwises, S., Shadloo, M.S., 2022b. Review on CO_2 capture by blended amine solutions. Int. J. Greenh. Gas Control 119. doi:10.1016/j.ijggc.2022.103715.

Agrawal, R., Herron, D.M., 2000. Air liquefaction: distillation. Encycl. Sep. Sci. 1895–1910. doi:10.1016/B0-12-226770-2/04821-3.

Aguilar-Lugo, C., Lee, W.H., Miguel, J.s.A., de la Campa, J.G., Prádanos, P., Bae, J.Y., Lee, Y.M., Álvarez, C., Lozano, A.n.E.J.A.A.P.M., 2021. Highly permeable mixed matrix membranes of thermally rearranged polymers and porous polymer networks for gas separations. ACS Appl. Polym. Mater. 3 (10), 5224–5235.

Ahmad, M.Z., Castro-Muñoz, R., Budd, P.M., 2020. Boosting gas separation performance and suppressing the physical aging of polymers of intrinsic microporosity (PIM-1) by nanomaterial blending. Nanoscale 12 (46), 23333–23370. doi:10.1039/D0NR07042D.

Ahmed, E., Deep, A., Kwon, E.E., Brown, R.J.C., Kim, K.-H., 2016. Performance comparison of MOF and other sorbent materials in removing key odorants emitted from pigpen slurry. Sci. Rep. 6 (1), 31283. doi:10.1038/srep31283.

Ahmed, M.B., Zhou, J.L., Ngo, H.H., Guo, W., Chen, M., 2016. Progress in the preparation and application of modified biochar for improved contaminant removal from water and wastewater. Bioresour. Technol. 214, 836–851. doi:10.1016/j.biortech.2016.05.057.

Ahunbay, M.G.k., 2011. Monte Carlo simulation of water adsorption in hydrophobic MFI zeolites with hydrophilic sites. Langmuir 27 (8), 4986–4993.

Ajenifuja, A., Joss, L., Jobson, M., 2020. A new equilibrium shortcut temperature swing adsorption model for fast adsorbent screening. Ind. Eng. Chem. Res. 59 (8), 3485–3497. doi:10.1021/acs.iecr.9b05579.

Ajjawi, I., Verruto, J., Aqui, M., et al., 2017. Lipid production in Nannochloropsis gaditana is doubled by decreasing expression of a single transcriptional regulator. Nat. Biotechnol. 35, 647–652. doi:10.1038/nbt.3865.

Akeeb, O., Wang, L., Xie, W., Davis, R., Alkasrawi, M., Toan, S., 2022. Post-combustion CO_2 capture via a variety of temperature ranges and material adsorption process: A review. J. Environ. Manage. 313, 115026. doi:10.1016/j.jenvman.2022.115026.

Akinola, T.E., Bonilla Prado, P.L., Wang, M., 2022. Experimental studies, molecular simulation and process modelling\simulation of adsorption-based post-combustion carbon capture for power plants: A state-of-the-art review. Appl. Energy 317. doi:10.1016/j.apenergy.2022.119156, 119156-119156.

Aksu, G.O., Erucar, I., Haslak, Z.P., Keskin, S., 2022. Accelerating discovery of COFs for CO_2 capture and H_2 purification using structurally guided computational screening. Chem. Eng. J. 427, 131574.

Al-Hamed, K.H.M., Dincer, I., 2021. A comparative review of potential ammonia-based carbon capture systems. J. Environ. Manage. 287, 112357. doi:10.1016/j.jenvman.2021.112357.

Al-Rowaili, F.N., Khaled, M., Jamal, A., Zahid, U., 2023. Mixed matrix membranes for H2/CO_2 gas separation- a critical review. Fuel 333, 126285. doi:10.1016/j.fuel.2022.126285.

Al-Wabel, M., Elfaki, J., Usman, A., Hussain, Q., Ok, Y.S., 2019. Performance of dry water- and porous carbon-based sorbents for carbon dioxide capture. Environ. Res. 174, 69–79. doi:10.1016/j.envres.2019.04.020.

Alalwan, H.A., Alminshid, A.H., 2021. CO_2 capturing methods: Chemical looping combustion (CLC) as a promising technique. Sci. Total Environ. 788, 147850. doi:10.1016/j.scitotenv.2021.147850.

Alcantara, M.L., Santos, J.P., Loreno, M., Ferreira, P.I.S., Paredes, M.L.L., Cardozo, L., Silva, A.K., Liao, L.M., Pires, C.A.M., Mattedi, S., 2018. Low viscosity protic ionic liquid for CO_2/CH_4 separation: Thermophysical and high-pressure phase equilibria for diethylammonium butanoate. Fluid Phase Equilibria 459, 30–43. doi:10.1016/j.fluid.2017.12.001.

Alebrahim, T., Chakraborty, A., Hu, L., Patil, S., Cheng, S., Acharya, D., Doherty, C.M., Hill, A.J., Cook, T.R., Lin, H., 2022. Gas transport characteristics of supramolecular networks of metal-coordinated highly branched poly (ethylene oxide). J. Membr. Sci. 644, 120063. doi:10.1016/j.memsci.2021.120063.

Ali, S.H., Merchant, S.Q., Fahim, M.A., 2000. Kinetic study of reactive absorption of some primary amines with carbon dioxide in ethanol solution. Sep. Purif. Technol. 18 (3), 163–175.

Ali Saleh Bairq, Z., Gao, H., Huang, Y., Zhang, H., Liang, Z., 2019. Enhancing CO_2 desorption performance in rich MEA solution by addition of SO42−/ZrO2/SiO2 bifunctional catalyst. Appl. Energy 252. doi:10.1016/j.apenergy.2019.113440.

Alivand, M.S., Mazaheri, O., Wu, Y., Stevens, G.W., Scholes, C.A., Mumford, K.A., 2020. Catalytic solvent regeneration for energy-efficient CO_2 capture. ACS Sustain. Chem. Eng. 8 (51), 18755–18788. doi:10.1021/acssuschemeng.0c07066.

Alkhouzaam, A., Khraisheh, M., Atilhan, M., Al-Muhtaseb, S.A., Qi, L., Rooney, D, 2016. High-pressure CO_2/N_2 and CO_2/CH_4 separation using dense polysulfone-supported ionic liquid membranes. J. Nat. Gas Sci. Eng. 36, 472–485.

Allam, R.J., Palmer, M., Brown, G.W., 2013a. System and method for high efficiency power generation using a carbon dioxide circulating working fluid. Google Patents.

Allam, R.J., Palmer, M.R., Brown Jr., G.W., Fetvedt, J., Freed, D., Nomoto, H., Itoh, M., Okita, N., Jones Jr., C., 2013b. High efficiency and low cost of electricity generation from fossil fuels while eliminating atmospheric emissions, including carbon dioxide. Energy Procedia 37, 1135–1149.

Allam, R., Fetvedt, J., Forrest, B., Freed, D., 2014. The oxy-fuel, supercritical CO_2 Allam Cycle: New cycle developments to produce even lower-cost electricity from fossil fuels without atmospheric emissions. In: Turbo Expo: Power for Land, Sea, and Air. American Society of Mechanical Engineers V03BT36A016.

Allam, R., Martin, S., Forrest, B., Fetvedt, J., Lu, X., Freed, D., Brown Jr., G.W., Sasaki, T., Itoh, M., Manning, J., 2017. Demonstration of the Allam Cycle: an update on the development status of a high efficiency supercritical carbon dioxide power process employing full carbon capture. Energy Procedia 114, 5948–5966.

Allen, M., 2019. Technical Summary: Global warming of 1.5 C. An IPCC Special Report on the impacts of global warming of 1.5 C above pre-industrial levels and related global greenhouse gas emission pathways, in the context of strengthening the global response to the threat of climate change, sustainable development, and efforts to eradicate poverty.

Alloush, A.M., Abdelnaby, M.M., Cordova, K.E., Qasem, N.A., Al-Maythalony, B.A., Jalilov, A., Mankour, Y., Al Hamouz, O.C.S., 2020. Selectively capturing carbon dioxide from mixed gas streams using a new microporous organic copolymer. Microporous Mesoporous Mater. 305, 110391.

Almantariotis, D., Gefflaut, T., Padua, A.A.H., Coxam, J.Y., Gomes, M.F.C., 2010. Effect of fluorination and size of the alkyl side-chain on the solubility of carbon dioxide in 1-Alkyl-3-methylimidazolium Bis (trifluoromethylsulfonyl)amide Ionic Liquids. J. Phys. Chem. B 114 (10), 3608–3617. doi:10.1021/jp912176n.

Almeida, R.M.d., Noda, L.c.K., Gonc¸alves, N.S., Meneghetti, S.M.P., Meneghetti, M.R., 2008. Transesterification reaction of vegetable oils, using superacid sulfated TiO2–base catalysts. Appl. Catal. A. 347 (1), 100–105. doi:10.1016/j.apcata.2008.06.006.

Almena, A., Thornley, P., Chong, K., Röder, M., 2022. Carbon dioxide removal potential from decentralised bioenergy with carbon capture and storage (BECCS) and the relevance of operational choices. Biomass Bioenergy 159. doi:10.1016/j.biombioe.2022.106406.

Alvarez, D., Abanades, J.C., 2005. Determination of the critical product layer thickness in the reaction of CaO with CO_2. Ind. Eng. Chem. Res. 44 (15), 5608–5615.

Alvarez, D., Abanades, J.C., 2005. Pore-size and shape effects on the recarbonation performance of calcium oxide submitted to repeated calcination/recarbonation cycles. Energy Fuels 19 (1), 270–278. doi:10.1021/ef049864m.

Amer, N.M., Lahijani, P., Mohammadi, M., Mohamed, A.R., 2022. Modification of biomass-derived biochar: A practical approach towards development of sustainable CO_2 adsorbent. Biomass Conv. Bioref. doi:10.1007/s13399-022-02905-3.

Ammendola, P., Raganati, F., Chirone, R., 2015. Effect of operating conditions on the CO_2 recovery from a fine activated carbon by means of TSA in a fluidized bed assisted by acoustic fields. Fuel Process. Technol. 134, 494–501. doi:10.1016/j.fuproc.2015.03.010.

Anbia, M., Hoseini, V., 2012. Enhancement of CO_2 adsorption on nanoporous chromium terephthalate (MIL-101) by amine modification. J. Nat. Gas Chem. 21 (3), 339–343. doi:10.1016/s1003-9953 (11)60374-5.

Ando, Y., Hirano, Y., Mase, S., Taguchi, H., 1998. Preparation and characterization of monolithic and planar element of zeolite membranes. In: Proc. ICIM, p. 124.

Angelidaki, I., Treu, L., Tsapekos, P., Luo, G., Campanaro, S., Wenzel, H., Kougias, P.G., 2018. Biogas upgrading and utilization: Current status and perspectives. Biotechnol. Adv. 36 (2), 452–466. doi:10.1016/j.biotechadv.2018.01.011.

Anne Julbe, D.F., Guizard, Christian, 2001. Porous ceramic membranes for catalytic reactors — overview and new ideas. J. Membr. Sci. 181, 3–20.

Ansaloni, L., Zhao, Y., Jung, B.T., Ramasubramanian, K., Baschetti, M.G., Ho, W.S.W., 2015. Facilitated transport membranes containing amino-functionalized multi-walled carbon nanotubes for high-pressure CO_2 separations. J. Membr. Sci. 490, 18–28. doi:10.1016/j.memsci.2015.03.097.

Araújo, T., Andrade, M., Bernardo, G., Mendes, A., 2022. Stable cellulose-based carbon molecular sieve membranes with very high selectivities. J. Membr. Sci. 641. doi:10.1016/j.memsci.2021.119852.

Araujo, T., Bernardo, G., Mendes, A., 2020. Cellulose-based carbon molecular sieve membranes for gas separation: a review. Molecules 25 (15). doi:10.3390/molecules25153532.

Arcenegui-Troya, J., Sánchez-Jiménez, P.E., Perejón, A., Valverde, J.M., Chacartegui, R., Pérez-Maqueda, L.A., 2020. Calcium-looping performance of biomineralized CaCO3 for CO_2 capture and thermochemical energy storage. Ind. Eng. Chem. Res. 59 (29), 12924–12933. doi:10.1021/acs.iecr.9b05997.

Arellano, I.H., Huang, J., Pendleton, P., 2015. Synergistic enhancement of CO_2 uptake in highly ordered mesoporous silica-supported zinc-functionalized ionic liquid sorbents. Chem. Eng. J. 281, 119–125. doi:10.1016/j.cej.2015.06.083.

Arias, B., Grasa, G., Abanades, J.C., Manovic, V., Anthony, E.J., 2012. The effect of steam on the fast carbonation reaction rates of CaO. Ind. Eng. Chem. Res. 51 (5), 2478–2482. doi:10.1021/ie202648p.

Arias, A.M., Mores, P.L., Scenna, N.J., Mussati, S.F., 2016. Optimal design and sensitivity analysis of post-combustion CO_2 capture process by chemical absorption with amines. J. Clean. Prod. 115, 315–331. doi:10.1016/j.jclepro.2015.12.056.

Armutlulu, A., Naeem, M.A., Liu, H.J., Kim, S.M., Kierzkowska, A., Fedorov, A., Müller, C.R.J.A.M., 2017. Multishelled CaO microspheres stabilized by atomic layer deposition of Al2O3 for enhanced CO_2 capture performance. Adv. Mater. 29 (41), 1702896.

Aronu, U.E., Gondal, S., Hessen, E.T., Haug-Warberg, T., Hartono, A., Hoff, K.A., Svendsen, H.F., 2011. Solubility of CO_2 in 15, 30, 45 and 60 mass% MEA from 40 to 120°C and model representation using the extended UNIQUAC framework. Chem. Eng. Sci. 66 (24), 6393–6406. doi:10.1016/j.ces.2011.08.042.

Arstad, B., Fjellvåg, H., Kongshaug, K.O., Swang, O., Blom, R., 2008. Amine functionalised metal organic frameworks (MOFs) as adsorbents for carbon dioxide. Adsorption 14 (6), 755–762. doi:10.1007/s10450-008-9137-6.

Aschenbrenner, O., McGuire, P., Alsamaq, S., Wang, J., Supasitmongkol, S., Al-Duri, B., Styring, P., Wood, J., 2011. Adsorption of carbon dioxide on hydrotalcite-like compounds of different compositions. Chem. Eng. Res. Des. 89 (9), 1711–1721. doi:10.1016/j.cherd.2010.09.019.

Ascherl, L., Sick, T., Margraf, J.T., Lapidus, S.H., Calik, M., Hettstedt, C., Karaghiosoff, K., Döblinger, M., Clark, T., Chapman, K.W., 2016. Molecular docking sites designed for the generation of highly crystalline covalent organic frameworks. Nat. Chem. 8 (4), 310–316.

Asghar, H., Ilyas, A., Tahir, Z., Li, X., Khan, A.L., 2018. Fluorinated and sulfonated poly (ether ether ketone) and Matrimid blend membranes for CO_2 separation. Sep. Purif. Technol. 203, 233–241. doi:10.1016/j.seppur.2018.04.047.

Ashokkumar, V., Venkatkarthick, R., Jayashree, S., Chuetor, S., Dharmaraj, S., Kumar, G., Chen, W.H., Ngamcharussrivichai, C., 2022. Recent advances in lignocellulosic biomass for biofuels and value-added bioproducts-A critical review. Bioresour. Technol. 344. doi:10.1016/j.biortech.2021.126195.

Ashtiani, S., Khoshnamvand, M., Bouša, D., Šturala, J., Sofer, Z., Shaliutina-Kolešová, A., Gardenö, D., Friess, K., 2021. Surface and interface engineering in CO_2-philic based UiO-66-NH2-PEI mixed matrix membranes via covalently bridging PVP for effective hydrogen purification. Int. J. Hydrogen Energy 46 (7), 5449–5458. doi:10.1016/j.ijhydene.2020.11.081.

Attou, A., Ferschneider, G., 1999. A two-fluid model for flow regime transition in gas-liquid trickle-bed reactors. Chem. Eng. Sci. 54 (21), 5031–5037. doi:10.1016/S0009-2509 (99)00226-2.

Austgen, D.M, R, G.T.P.X., Chen, C.C., 1989. Model of vapor-liquid equilibria for aqueous acid gas-alkanolamine systems using the electrolyte-NRTL equation. Ind. Eng. Chem. Res. 28, 1060–1073 -1060–1073.

Axelbaum, R., Kumfer, B., Gopan, A., Yang, Z., Phillips, J., Pint, B., 2017. Staged, High–Pressure Oxy-Combustion Technology. Development and Scale-Up Washington Univ, St. Louis, MO (United States).

Azimi, G., Leion, H., Rydén, M., Mattisson, T., Lyngfelt, A., 2013. Investigation of different Mn–Fe oxides as oxygen carrier for chemical-looping with oxygen uncoupling (CLOU). Energy Fuels 27 (1), 367–377. doi:10.1021/ef301120r.

Béarat, H., McKelvy, M.J., Chizmeshya, A.V.G., Sharma, R., Carpenter, R.W., 2002. Magnesium hydroxide dehydroxylation/carbonation reaction processes: implications for carbon dioxide mineral sequestration. 85 (4), 742-748. https://doi.org/10.1111/j.1151-2916.2002.tb00166.x.

Babu, P., Ong, H.W.N., Linga, P., 2016. A systematic kinetic study to evaluate the effect of tetrahydrofuran on the clathrate process for pre-combustion capture of carbon dioxide. Energy 94, 431–442.

Baciocchi, R., Storti, G., Mazzotti, M., 2006. Process design and energy requirements for the capture of carbon dioxide from air. Chem. Eng. Process.: Process Intensif. 45 (12), 1047–1058. doi:10.1016/j.cep.2006.03.015.

Bae, Y.-S., Farha, O.K., Spokoyny, A.M., Mirkin, C.A., Hupp, J.T., Snurr, R.Q., 2008. Carborane-based metal–organic frameworks as highly selective sorbents for CO 2 over methane. Chem. Commun. (35) 4135–4137.

Bae, Y.-S., Hauser, B.G., Farha, O.K., Hupp, J.T., Snurr, R.Q., 2011. Enhancement of CO_2/CH4 selectivity in metal-organic frameworks containing lithium cations. Microporous Mesoporous Mater. 141 (1-3), 231–235. doi:10.1016/j.micromeso.2010.10.048.

Bahamon, D., Vega, L.F., 2016. Systematic evaluation of materials for post-combustion CO 2 capture in a temperature swing adsorption process. Chem. Eng. J. 284, 438–447. doi:10.1016/j.cej.2015.08.098.

Bai, W., Feng, J., Luo, C., Zhang, P., Wang, H., Yang, Y., Zhao, Y., Fan, H., 2021a. A comprehensive review on oxygen transport membranes: development history, current status, and future directions. Int. J. Hydrogen Energy 46, 36257–36290. doi:10.1016/J.IJHYDENE.2021.08.177.

Bai, W., Feng, J., Luo, C., Zhang, P., Wang, H., Yang, Y., Zhao, Y., Fan, H., 2021b. A comprehensive review on oxygen transport membranes: development history, current status, and future directions. Int. J. Hydrogen Energy 46 (73), 36257–36290. doi:10.1016/j.ijhydene.2021.08.177.

Bai, C., Zhang, W., Deng, L., Zhao, Y., Sun, S., Feng, D., Wu, J., 2022. Experimental study of nitrogen conversion during char combustion under a pressurized O_2/H_2O atmosphere. Fuel 311, 122529. doi:10.1016/j.fuel.2021.122529.

Bai, R., Song, X., Yan, W., Yu, J., 2022. Low-energy adsorptive separation by zeolites. Natl. Sci. Rev. doi:10.1093/nsr/nwac064.

Bailera, M., Lisbona, P., Romeo, L.M., 2015. Power to gas-oxyfuel boiler hybrid systems. Int. J. Hydrogen Energy 40 (32), 10168–10175. doi:10.1016/J.IJHYDENE.2015.06.074.

Bailera, M., Lisbona, P., Romeo, L.M., Espatolero, S., 2016. Power to Gas–biomass oxycombustion hybrid system: Energy integration and potential applications. Appl. Energy 167, 221–229. doi:10.1016/J.APENERGY.2015.10.014.

Bailera, M., Lisbona, P., Peña, B., Romeo, L.M., 2020. Energy Storage. Springer International Publishing.

Bailera, M., Peña, B., Lisbona, P., Marín, J., Romeo, L.M., 2021. Lab-scale experimental tests of power to gas-oxycombustion hybridization: System design and preliminary results. Energy 226. doi:10.1016/j.energy.2021.120375, 120375-120375.

Bairq, Z.A.S., Gao, H., Murshed, F.A.M., Tontiwachwuthikul, P., Liang, Z., 2020. Modified heterogeneous catalyst-aided regeneration of CO_2 capture amines: a promising perspective for a drastic reduction in energy consumption. ACS Sustain. Chem. Eng. 8 (25), 9526–9536. doi:10.1021/acssuschemeng.0c02582.

Bakhshi Ani, A., Ale Ebrahim, H., 2021. Comprehensive kinetic study of sulfur dioxide removal by magnesium oxide using TG. J. Therm. Anal. Calorimetry 146 (6), 2587-2599.

Bali, S., Chen, T.T., Chaikittisilp, W., Jones, C.W., 2013. Oxidative stability of amino polymer–alumina hybrid adsorbents for carbon dioxide capture. Energy Fuels 27 (3), 1547–1554. doi:10.1021/ef4001067.

Balice, D.M., Molenaar, C.W.C., Fochesato, M., Venier, C.M., Roghair, I., Deen, N.G., van Sint Annaland, M., 2022. CFD modeling of droplet permeability in fluidized beds. Int. J. Multiph. Flow 152. doi:10.1016/j.ijmultiphaseflow.2022.104069, 104069-104069.

Banaszkiewicz, T., Chorowski, M., 2018. Energy consumption of air-separation adsorption methods. Entropy (Basel, Switz.) 20 (4). doi:10.3390/e20040232, 232-232.

Banaszkiewicz, T., Chorowski, M., Gizicki, W., 2014. Comparative analysis of oxygen production for oxy-combustion application. Energy Procedia 51, 127–134. doi:10.1016/j.egypro.2014.07.014.

Bandehali, S., Ebadi Amooghin, A., Sanaeepur, H., Ahmadi, R., Fuoco, A., Jansen, J.C., Shirazian, S., 2021. Polymers of intrinsic microporosity and thermally rearranged polymer membranes for highly efficient gas separation. Sep. Purif. Technol. 278, 119513. doi:10.1016/j.seppur.2021.119513.

Bao, L., Trachtenberg, M.C., 2006. Facilitated transport of CO_2 across a liquid membrane: Comparing enzyme, amine, and alkaline. J. Membr. Sci. 280 (1), 330–334. doi:10.1016/j.memsci.2006.01.036.

Bao, S.-J., Krishna, R., He, Y.-B., Qin, J.-S., Su, Z.-M., Li, S.-L., Xie, W., Du, D.-Y., He, W.-W., Zhang, S.-R., Lan, Y.-Q., 2015. A stable metal–organic framework with suitable pore sizes and rich uncoordinated nitrogen atoms on the internal surface of micropores for highly efficient CO_2 capture. J. Mater. Chem. A 3 (14), 7361–7367. doi:10.1039/c5ta00256g.

Bararpour, S.T., Karami, D., Mahinpey, N., 2019. Investigation of the effect of alumina-aerogel support on the CO_2 capture performance of K_2CO_3. Fuel 242, 124–132. doi:10.1016/j.fuel.2018.12.123.

Bararpour, S.T., Adanez, J., Mahinpey, N., 2020. Application of core-shell-structured K_2CO_3-based sorbents in postcombustion CO_2 capture: Statistical analysis and optimization using response surface methodology. Energy Fuels 34 (3), 3429–3439. doi:10.1021/acs.energyfuels.9b03442.

Barbera, E., Mio, A., Massi Pavan, A., Bertucco, A., Fermeglia, M., 2022. Fuelling power plants by natural gas: An analysis of energy efficiency, economical aspects and environmental footprint based on detailed process simulation of the whole carbon capture and storage system. Energy Convers. Manage. 252. doi:10.1016/j.enconman.2021.115072.

Barker, R., 2007. The reversibility of the reaction CaCO3 ⇄ CaO+CO_2. J. Appl. Chem. Biotechnol. 23, 733–742. doi:10.1002/jctb.5020231005.

Barpaga, D., Jiang, Y., Zheng, R.F., Malhotra, D., Koech, P.K., Zwoster, A., Mathias, P.M., Heldebrant, D.J., 2022. Evaluation of a third generation single-component water-lean diamine solvent for post-combustion CO_2 capture. ACS Sustain. Chem. Eng. 10 (14), 4522–4528. doi:10.1021/acssuschemeng.1c08401.

Barthomeuf, D., 2003. Framework induced basicity in zeolites. Microporous Mesoporous Mater. 66 (1), 1–14.

Barzagli, F., Mani, F., Peruzzini, M., 2013. Efficient CO_2 absorption and low temperature desorption with non-aqueous solvents based on 2-amino-2-methyl-1-propanol (AMP). Int. J. Greenh. Gas Control 16 (0), 217–223. doi:10.1016/j.ijggc.2013.03.026.

Baskaran, T., Christopher, J., Sakthivel, A., 2015. Progress on layered hydrotalcite (HT) materials as potential support and catalytic materials. RSC Adv. 5 (120), 98853–98875. doi:10.1039/C5RA19909C.

Bassani, A., van Dijk, H.A.J., Cobden, P.D., Spigno, G., Manzolini, G., Manenti, F., 2019. Sorption Enhanced Water Gas Shift for H2 production using sour gases as feedstock. Int. J. Hydrogen Energy 44 (31), 16132–16143. doi:10.1016/j.ijhydene.2019.04.199.

Bastin, L., Bárcia, P.S., Hurtado, E.J., Silva, J.A., Rodrigues, A.E., Chen, B., 2008. A microporous metal– organic framework for separation of CO_2/N_2 and CO_2/CH_4 by fixed-bed adsorption. J. Phys. Chem. C 112 (5), 1575–1581.

Baus, L., Nehr, S., 2022. Potentials and limitations of direct air capturing in the built environment. Build. Environ. 208. doi:10.1016/j.buildenv.2021.108629.

Baxter, L., Baxter, A., Burt, S., 2009. Cryogenic CO_2 capture as a cost-effective CO_2 capture process. In: 26th Annual International Pittsburgh Coal Conference 2009, PCC 2009, p. 1.

Baylin-Stern, A., Beck, L., Beuttler, C., Bolesta, C., Dailey, M., Dixon, T., Edwards, R., 2022. Direct Air Capture A key Technology for Net Zero. International Energy Center.

Bednar, J., Obersteiner, M., Wagner, F., 2019. On the financial viability of negative emissions. Nat. Commun. 10 (1), 1783. doi:10.1038/s41467-019-09782-x.

Bellusci, M., Masi, A., Albino, M., Peddis, D., Petrecca, M., Sangregorio, C., La Barbera, A., Varsano, F., 2021. Fe_3O_4@HKUST-1 magnetic composites by mechanochemical route for induction triggered release of carbon dioxide. Microporous Mesoporous Mater. 328. doi:10.1016/j.micromeso.2021.111458.

Belmabkhout, Y., Serna-Guerrero, R., Sayari, A., 2010. Adsorption of CO_2-containing gas mixtures over amine-bearing pore-expanded MCM-41 silica: application for gas purification. Ind. Eng. Chem. Res. 49 (1), 359–365. doi:10.1021/ie900837t.

Belmabkhout, A.S.Y., 2010. Stabilization of amine-containing CO_2 adsorbents: dramatic effect of water vapour. J. Am. Chem. Soc. 132, 6312–6314.

Ben Petrovic, M.G., Soltani, S.M., 2022. Impact of surface functional groups and their introduction methods on the mechanisms of CO_2 adsorption on porous carbonaceous adsorbents. Carbon Cap. Sci. Technol. 3. doi:10.1016/j.ccst.2022.100045.

Ben Salem, I., El Gamal, M., Sharma, M., Hameedi, S., Howari, F.M., 2021a. Utilization of the UAE date palm leaf biochar in carbon dioxide capture and sequestration processes. J. Environ. Manage. 299. doi:10.1016/j.jenvman.2021.113644.

Ben Salem, I., Saleh, M.B., Iqbal, J., El Gamal, M., Hameed, S., 2021b. Date palm waste pyrolysis into biochar for carbon dioxide adsorption. Energy Rep. 7, 152–159. doi:10.1016/j.egyr.2021.06.027.

Bernabé-Pablo, E., Plascencia-Hernández, F., Yañez-Aulestia, A., Pfeiffer, H., 2020. High and efficient carbon dioxide chemisorption on a new high lithium-content ceramic; hexalithium cobaltate (Li_6CoO_4). Chem. Eng. J. 384, 123291. doi:10.1016/j.cej.2019.123291.

Bernardo, P., Drioli, E., Golemme, G., 2009. Membrane gas separation: a review/state of the art. Ind. Eng. Chem. Res. 48 (10), 4638–4663. doi:10.1021/ie8019032.

Berstad, D., Anantharaman, R., Nekså, P., 2013. Low-temperature CO_2 capture technologies – Applications and potential. Int. J. Refriger. 36 (5), 1403–1416. doi:10.1016/j.ijrefrig.2013.03.017.

Berstad, D., Skaugen, G., Roussanaly, S., Anantharaman, R., Nekså, P., Jordal, K., Trædal, S., Gundersen, T., 2022. CO_2 Capture from IGCC by low-temperature synthesis gas separation. Energies 15 (2), 515. doi:10.3390/en15020515.

Beysel, G., Enhanced Cyrogenic Air Separation. Cottbus, Germany, pp. 38-38.

Bezerra, D.P., Oliveira, R.S., Vieira, R.S., Cavalcante, C.L., Azevedo, D.C.S., 2011. Adsorption of CO_2 on nitrogen-enriched activated carbon and zeolite 13X. Adsorption 17 (1), 235–246. doi:10.1007/s10450-011-9320-z.

Bezerra, D.P., Silva, F.W.M.d., Moura, P.A.S.d., Sousa, A.G.S., Vieira, R.S., Rodriguez-Castellon, E., Azevedo, D.C.S., 2014. CO 2 adsorption in amine-grafted zeolite 13X. Appl. Surf. Sci. 314, 314–321. doi:10.1016/j.apsusc.2014.06.164.

Bezzu, C.G., Fuoco, A., Esposito, E., Monteleone, M., Longo, M., Jansen, J.C., Nichol, G.S., McKeown, N.B., 2021. Ultrapermeable polymers of intrinsic microporosity containing spirocyclic units with fused triptycenes. Adv. Fun. Mater. 31 (37), 2104474. doi:10.1002/adfm.202104474.

Bhagiyalakshmi, M., Lee, J.Y., Jang, H.T., 2010. Synthesis of mesoporous magnesium oxide: Its application to CO_2 chemisorption. Int. J. Greenh. Gas Control 4 (1), 51–56. doi:10.1016/j.ijggc.2009.08.001.

Bhatia, S.K., Perlmutter, D.D., 1983. Effect of the product layer on the kinetics of the CO_2-lime reaction. Aiche J. 29 (1), 79–86. doi:10.1002/aic.690290111.

Bhatt, T.S., Storti, G., Denayer, J.F.M., Rota, R., 2017. Optimal design of dual-reflux pressure swing adsorption units via equilibrium theory: Process configurations employing heavy gas for pressure swing. Chem. Eng. J. 311, 385–406. doi:10.1016/j.cej.2016.11.111.

Bhatt, T.S., Storti, G., Denayer, J.F.M., Rota, R., 2018. Equilibrium theory-based assessment of dual-reflux pressure swing adsorption cycles that utilize light gas for pressure swing. Ind. Eng. Chem. Res. 58 (1), 350–365. doi:10.1021/acs.iecr.8b04415.

Bhattacharyya, S., Shah, F.U., 2016. Ether functionalized choline tethered amino acid ionic liquids for enhanced CO_2 capture. ACS Sustain. Chem. Eng. 4 (10), 5441–5449. doi:10.1021/acssuschemeng.6b00824.

Bhatti, U.H., Shah, A.K., Kim, J.N., You, J.K., Choi, S.H., Lim, D.H., Nam, S., Park, Y.H., Baek, I.H., 2017. Effects of transition metal oxide catalysts on MEA solvent regeneration for the post-combustion carbon capture process. ACS Sustain. Chem. Eng. 5 (7), 5862–5868. doi:10.1021/acssuschemeng.7b00604.

Bhatti, U.H., Nam, S., Park, S., Baek, I.H., 2018a. Performance and mechanism of metal oxide catalyst-aided amine solvent regeneration. ACS Sustain. Chem. Eng. 6 (9), 12079–12087. doi:10.1021/acssuschemeng.8b02422.

Bhatti, U.H., Sivanesan, D., Lim, D.H., Nam, S.C., Park, S., Baek, I.H., 2018b. Metal oxide catalyst-aided solvent regeneration: A promising method to economize post-combustion CO_2 capture process. J. Taiwan Inst. Chem. Eng. 93, 150–157. doi:10.1016/j.jtice.2018.05.029.

Bhatti, U.H., Shah, A.K., Hussain, A., Khan, H.A., Park, C.Y., Nam, S.C., Baek, I.H., 2020. Catalytic activity of facilely synthesized mesoporous HZSM-5 catalysts for optimizing the CO_2 desorption rate from CO_2-rich amine solutions. Chem. Eng. J. 389. doi:10.1016/j.cej.2019.123439.

Bhave, A., Taylor, R.H., Fennell, P., Livingston, W.R., Shah, N., Mac Dowell, N., Dennis, J., Kraft, M., Pourkashanian, M., Insa, M., 2017. Screening and techno-economic assessment of biomass-based power generation with CCS technologies to meet 2050 CO_2 targets. Appl. Energy 190, 481–489.

Bhown, A.S., Freeman, B.C., 2011. Analysis and status of post-combustion carbon dioxide capture technologies. Environ. Sci. Technol. 45 (20), 8624–8632. doi:10.1021/es104291d.

Bhunia, A., Boldog, I., Möller, A., Janiak, C., 2013. Highly stable nanoporous covalent triazine-based frameworks with an adamantane core for carbon dioxide sorption and separation. J. Mater. Chem. A 1 (47), 14990–14999.

Bi, X., Zhang, Y.a., Zhang, F., Zhang, S., Wang, Z., Jin, J., 2020. MOF nanosheet-based mixed matrix membranes with metal–organic coordination interfacial interaction for gas separation. ACS Appl. Mater. Interfaces 12 (43), 49101–49110. doi:10.1021/acsami.0c14639.

Bigdeli, F., Lollar, C.T., Morsali, A., Zhou, H.C., 2020. Switching in metal-organic frameworks. Angew. Chem. Int. Ed. Engl. 59 (12), 4652–4669. doi:10.1002/anie.201900666.

Biliyok, C., Lawal, A., Wang, M., Seibert, F., 2012. Dynamic modelling, validation and analysis of post-combustion chemical absorption CO_2 capture plant. Int. J. Greenh. Gas Control 9, 428–445. doi:10.1016/j.ijggc.2012.05.001.

Biswal, B.P., Chandra, S., Kandambeth, S., Lukose, B., Heine, T., Banerjee, R., 2013. Mechanochemical synthesis of chemically stable isoreticular covalent organic frameworks. J. Am. Chem. Soc. 135 (14), 5328–5331.

Blackwood, J.D., Mcgrory, F., Blackwood, J.D., Mcgrory, F., 1958. The carbon-steam reaction at high pressure. Aust. J. Chem. 11 (1), 16–33.

Blamey, J., Anthony, E., Wang, J., Fennell, P., 2010. The calcium looping cycle for large-scale CO_2 capture. Prog. Energy Combust. 36 (2), 260–279.

Blamey, J., Manovic, V., Anthony, E.J., Dugwell, D.R., Fennell, P.S., 2015. On steam hydration of CaO-based sorbent cycled for CO_2 capture. Fuel 150, 269–277. doi:10.1016/j.fuel.2015.02.026.

D.H. Blanchard, L.A., Beckman, E.J., Brennecke, J.F., 1999. Green processing using ionic liquids and CO_2. Nature 399 (6731), 28–29. doi:10.1038/19887.

Blanco, M.V., Kohopää, K., Snigireva, I., Cova, F., 2018. Low temperature solid state synthesis of Li_5FeO_4 and CO_2 capture mechanism via real time in situ synchrotron X-ray diffraction. Chem. Eng. J. 354, 370–377. doi:10.1016/j.cej.2018.08.017.

Board, O.S., Council, N.R., 2015. Climate Intervention: carbon Dioxide Removal and Reliable Sequestration. National Academies Press.

Boetcher, S.K.S., Traum, M.J., von Hippel, T., 2020. Thermodynamic model of CO_2 deposition in cold climates. Clim. Change 158 (3), 517–530. doi:10.1007/s10584-019-02587-3.

Bollini, P., Didas, S.A., Jones, C.W., 2011. Amine-oxide hybrid materials for acid gas separations. J. Mater. Chem. 21 (39). doi:10.1039/c1jm12522b.

Bollini, P., Brunelli, N.A., Didas, S.A., Jones, C.W., 2012a. Dynamics of CO_2 adsorption on amine adsorbents. 1. Impact of heat effects. Ind. Eng. Chem. Res. 51 (46), 15145–15152. doi:10.1021/ie301790a.

Bollini, P., Brunelli, N.A., Didas, S.A., Jones, C.W., 2012b. Dynamics of CO_2 adsorption on amine adsorbents. 2. insights into adsorbent design. Ind. Eng. Chem. Res. 51 (46), 15153–15162. doi:10.1021/ie3017913.

Bondar, V.I., Freeman, B.D., Pinnau, I., 2000. Gas transport properties of poly (ether-b-amide) segmented block copolymers. J. Polym. Sci. Part B Polym. Phys. 38 (15), 2051–2062. doi:10.1002/1099-0488 (20000801)38:15<2051::AID-POLB100>3.0.CO;2-D.

Bondorf, L., Fiorio, J.L., Bon, V., Zhang, L., Maliuta, M., Ehrling, S., Senkovska, I., Evans, J.D., Joswig, J.-O., Kaskel, S., 2022. Isotope-selective pore opening in a flexible metal-organic framework. Sci. Adv. 8 (15), eabn7035. doi:10.1126/sciadv.abn7035.

Bonetto, R., Latzko, V., 2020. Chapter 8 - Machine learning, in: Fitzek, F.H.P., Granelli, F., Seeling, P.B.T.C.i.C.N. (Eds.), Academic Press, pp. 135-167. https://doi.org/10.1016/B978-0-12-820488-7.00021-9.

Boot-Handford, M.E., Abanades, J.C., Anthony, E.J., Blunt, M.J., Brandani, S., Mac Dowell, N., Fernández, J.R., Ferrari, M.-C., Gross, R., Hallett, J.P., Haszeldine, R.S., Heptonstall, P., Lyngfelt, A., Makuch, Z., Mangano, E., Porter, R.T.J., Pourkashanian, M., Rochelle, G.T., Shah, N., Yao, J.G., Fennell, P.S., 2014. Carbon capture and storage update. Energy Environ. Sci. 7 (1), 130–189. doi:10.1039/c3ee42350f.

Borgwardt, R.H., Bruce, K.R., Blake, J., 1987. An investigation of product-layer diffusivity for calcium oxide sulfation. Ind. Eng. Chem. Res. 26 (10), 1993–1998. doi:10.1021/ie00070a010.

Borhani, T.N., Oko, E., Wang, M., 2018. Process modelling and analysis of intensified CO_2 capture using monoethanolamine (MEA) in rotating packed bed absorber. J. Clean. Prod. 204, 1124–1142.

Borhani, T.N., Oko, E., Wang, M., 2019. Process modelling, validation and analysis of rotating packed bed stripper in the context of intensified CO_2 capture with MEA. J. Ind. Eng. Chem. 75, 285–295.

Bork, A.H., Rekhtina, M., Willinger, E., Castro-Fernandez, P., Drnec, J., Abdala, P.M., Muller, C.R., 2021. Peering into buried interfaces with X-rays and electrons to unveil $MgCO_3$ formation during CO_2 capture in molten salt-promoted MgO. Proc. Natl. Acad. Sci. U S A 118 (26), e2103971118. doi:10.1073/pnas.2103971118.

Boujibar, O., Souikny, A., Ghamouss, F., Achak, O., Dahbi, M., Chafik, T., 2018. CO_2 capture using N-containing nanoporous activated carbon obtained from argan fruit shells. J. Environ. Chem. Eng. 6 (2), 1995–2002. doi:10.1016/j.jece.2018.03.005.

Bounaceur, R., Lape, N., Roizard, D., Vallieres, C., Favre, E., 2006. Membrane processes for post-combustion carbon dioxide capture: A parametric study. Energy 31 (14), 2556–2570. doi:10.1016/j.energy.2005.10.038.

Bower, J.K., Barpaga, D., Prodinger, S., Krishna, R., Schaef, H.T., McGrail, B.P., Derewinski, M.A., Motkuri, R.K., 2018. Dynamic adsorption of CO_2/N_2 on cation-exchanged chabazite SSZ-13: a breakthrough analysis. ACS Appl. Mater. Interfaces 10 (17), 14287–14291.

Boyer, C., Koudil, A., Chen, P., Dudukovic, M.P., 2005. Study of liquid spreading from a point source in a trickle bed via gamma-ray tomography and CFD simulation. Chem. Eng. Sci. 60 (22), 6279–6288. doi:10.1016/j.ces.2005.03.049.

Brúder, P., Grimstvedt, A., Mejdell, T., Svendsen, H.F., 2011. CO_2 capture into aqueous solutions of piperazine activated 2-amino-2-methyl-1-propanol. Chem. Eng. Sci. 66 (23), 6193–6198. doi:10.1016/j.ces.2011.08.051.

Brandani, F., Ruthven, D.M., 2004. The effect of water on the adsorption of CO_2 and C3H8 on type X zeolites. Ind. Eng. Chem. Research 43 (26), 8339–8344.

Bravo, J., Drapanauskaite, D., Sarunac, N., Romero, C., Jesikiewicz, T., Baltrusaitis, J., 2021. Optimization of energy requirements for CO_2 post-combustion capture process through advanced thermal integration. Fuel 283. doi:10.1016/j.fuel.2020.118940.

Breault, R.W., Spenik, J.L., Shadle, L.J., Hoffman, J.S., Gray, M.L., Panday, R., Stehle, R.C., 2016. Carbon capture test unit design and development using amine-based solid sorbent. Chem. Eng. Res. Des. 112, 251–262. doi:10.1016/j.cherd.2016.06.020.

Briones-Hidrovo, A., Copa Rey, J.R., Cláudia Dias, A., Tarelho, L.A.C., Beauchet, S., 2022. Assessing a bio-energy system with carbon capture and storage (BECCS) through dynamic life cycle assessment and land-water-energy nexus. Energy Convers. Manage. 268. doi:10.1016/j.enconman.2022.116014.

Brunetti, A., Cersosimo, M., Kim, J.S., Dong, G., Fontananova, E., Lee, Y.M., Drioli, E., Barbieri, G., 2017. Thermally rearranged mixed matrix membranes for CO_2 separation: An aging study. Int. J. Greenh. Gas Control 61, 16–26. doi:10.1016/j.ijggc.2017.03.024.

Buck, F., Wiegers, K., Schulz, A., Schiestel, T., 2021. MIEC hollow-fibre membranes in a plasma membrane reactor. Interceram - Int. Ceramic Rev. 70 (2), 40–45. doi:10.1007/S42411-021-0445-0, 202170.

Buckingham, J., Reina, T.R., Duyar, M.S., 2022. Recent advances in carbon dioxide capture for process intensification. Carbon Cap. Sci. Technol. 2, 100031. doi:10.1016/j.ccst.2022.100031.

Budd, P.M., McKeown, N.B., 2010. Highly permeable polymers for gas separation membranes. J. Polym. Chem. 1 (1), 63–68.

Budd, P.M., Ghanem, B.S., Makhseed, S., McKeown, N.B., Msayib, K.J., Tattershall, C.E., 2004. Polymers of intrinsic microporosity (PIMs): robust, solution-processable, organic nanoporous materials. Chem. Commun. (2) 230–231. doi:10.1039/B311764B.

Buddin, M., Ahmad, A.L., 2021. A review on metal-organic frameworks as filler in mixed matrix membrane: Recent strategies to surpass upper bound for. J. CO_2 Util. 51, 101616. doi:10.1016/j.jcou.2021.101616.

Budhathoki, S., Ajayi, O., Steckel, J.A., Wilmer, C.E., 2019. High-throughput computational prediction of the cost of carbon capture using mixed matrix membranes. Energy Environ. Sci. 12 (4), 1255–1264. doi:10.1039/c8ee02582g.

Budinis, S., 2022. Direct air capture technology deep dive. https://www.iea.org/reports/direct-air-capture. (Accessed Sep. 2022).

Budzianowski, W.M., Wylock, C.E., Marciniak, P.A., 2017. Power requirements of biogas upgrading by water scrubbing and biomethane compression: Comparative analysis of various plant configurations. Energy Convers. Manage. 141, 2–19. doi:10.1016/j.enconman.2016.03.018.

Buelens, L.C., Galvita, V.V., Poelman, H., Detavernier, C., Marin, G.B., 2016. Super-dry reforming of methane intensifies CO_2 utilization via Le Chatelier's principle. Science 354 (6311), 449–452. doi:10.1126/science.aah7161.

Bui, M., Gunawan, I., Verheyen, V., Feron, P., Meuleman, E., Adeloju, S., 2014. Dynamic modelling and optimisation of flexible operation in post-combustion CO_2 capture plants-A review. Comput. Chem. Eng. 61, 245–265. doi:10.1016/j.compchemeng.2013.11.015.

Bui, M., Adjiman, C.S., Bardow, A., Anthony, E.J., Boston, A., Brown, S., Fennell, P.S., Fuss, S., Galindo, A., Hackett, L.A., 2018. Carbon capture and storage (CCS): the way forward. Energy Environ. Sci.

Burdyny, T., Struchtrup, H., 2010. Hybrid membrane/cryogenic separation of oxygen from air for use in the oxy-fuel process. Energy 35 (5), 1884–1897. doi:10.1016/j.energy.2009.12.033.

Bureekaew, S., Shimomura, S., Kitagawa, S., 2008. Chemistry and application of flexible porous coordination polymers. Sci. Technol. Adv. Mater.

Burns, J.R., Jamil, J.N., Ramshaw, C., 2000. Process intensification: Operating characteristics of rotating packed beds - determination of liquid hold-up for a high-voidage structured packing. Chem. Eng. Sci. 55 (13), 2401–2415. doi:10.1016/S0009-2509(99)00520-5.

Burns, T.D., Pai, K.N., Subraveti, S.G., Collins, S.P., Krykunov, M., Rajendran, A., Woo, T.K., 2020. Prediction of MOF performance in vacuum swing adsorption systems for postcombustion CO_2 capture based on integrated molecular simulations, process optimizations, and machine learning models. Environ. Sci. Technol. 54 (7), 4536–4544. doi:10.1021/acs.est.9b07407.

Buvik, V., Høisæter, K.K., Vevelstad, S.J., Knuutila, H.K., 2021. A review of degradation and emissions in post-combustion CO_2 capture pilot plants. Int. J. Greenh. Gas Control 106. doi:10.1016/j.ijggc.2020.103246.

Cabello, A., Dueso, C., García-Labiano, F., Gayán, P., Abad, A., de Diego, L.F., Adánez, J., 2014. Performance of a highly reactive impregnated Fe2O3/Al2O3 oxygen carrier with CH4 and H2S in a 500Wth CLC unit. Fuel 121, 117–125. doi:10.1016/j.fuel.2013.12.027.

Cacho-Bailo, F., Matito-Martos, I., Perez-Carbajo, J., Etxeberria-Benavides, M., Karvan, O., Sebastian, V., Calero, S., Tellez, C., Coronas, J., 2017. On the molecular mechanisms for the H2/CO_2 separation performance of zeolite imidazolate framework two-layered membranes. Chem. Sci. 8 (1), 325–333. doi:10.1039/c6sc02411d.

Cai, L., Zou, C., Liu, Y., Zhou, K., Han, Q., Zheng, C., 2015. Numerical and experimental studies on the ignition of pulverized coal in O_2/H_2O atmospheres. Fuel 139, 198–205. doi:10.1016/j.fuel.2014.08.038.

Cai, J., Wang, S., Kuang, C., 2017. A modified random pore model for carbonation reaction of CaO-based limestone with CO_2 in different calcination-carbonation cycles. Energy Procedia 105, 1924–1931. doi:10.1016/j.egypro.2017.03.561.

Cai, T., Johnson, J.K., Wu, Y., Chen, X., 2019. Toward understanding the kinetics of CO_2 capture on sodium carbonate. ACS Appl. Mater. Interfaces 11 (9), 9033–9041. doi:10.1021/acsami.8b20000.

Cai, T., Chen, X., Zhong, J., Wu, Y., Ma, J., Liu, D., Liang, C., 2020. Understanding the morphology of supported Na_2CO_3/γ-AlOOH solid sorbent and its CO_2 sorption performance. Chem. Eng. J. 395, 124139. doi:10.1016/j.cej.2020.124139.

Cai, R., Dou, J., Krzystowczyk, E., Richard, A., Li, F., 2022. Chemical looping air separation with Sr0.8Ca0.2Fe0.9Co0.1O3-δ perovskite sorbent: Packed bed modeling, verification, and optimization. Chem. Eng. J. 429. doi:10.1016/J.CEJ.2021.132370, 132370-132370.

Cai, W., Kong, X., Ye, Q., Wang, L., Ren, D., Lu, H., 2022. Numerical modelling of hydrodynamics of molten salt fluid-particles fluidized beds using CFD-DEM and TFM approaches. Powder Technol. 410. doi:10.1016/j.powtec.2022.117882, 117882-117882.

Cailliez, F., Stirnemann, G., Boutin, A., Demachy, I., Fuchs, A.H., 2008. Does water condense in hydrophobic cavities? A molecular simulation study of hydration in heterogeneous nanopores. J. Phys. Chem. C 112 (28), 10435–10445.

Calle, M., Jo, H.J., Doherty, C.M., Hill, A.J., Lee, Y.M., 2015. Cross-linked thermally rearranged poly (benzoxazole-co-imide) membranes prepared from ortho-hydroxycopolyimides containing pendant carboxyl groups and gas separation properties. Macromolecules 48 (8), 2603–2613.

Cantu, D.C., Malhotra, D., Nguyen, M.T., Koech, P.K., Zhang, D., Glezakou, V.A., Rousseau, R., Page, J., Zheng, R., Perry, R.J., Heldebrant, D.J., 2020. Molecular-level overhaul of gamma-aminopropyl aminosilicone/triethylene glycol post-combustion CO (2) -capture solvents. ChemSusChem 13 (13), 3429–3438. doi:10.1002/cssc.202000724.

Cao, X., Harris, W., 2010. Properties of dairy-manure-derived biochar pertinent to its potential use in remediation. Bioresour. Technol. 101 (14), 5222–5228. doi:10.1016/j.biortech.2010.02.052.

Cao, Y., He, B., Ding, G., Su, L., Duan, Z., 2016. Performance modeling of integrated chemical looping air separation and IGCC with CO_2 capture. Energy Fuels 30 (11), 9953–9961. doi:10.1021/ACS.ENERGYFUELS.6B01894.

Cao, X., Wang, Z., Qiao, Z., Zhao, S., Wang, J., 2019. Penetrated COF channels: Amino environment and suitable size for CO_2 preferential adsorption and transport in mixed matrix membranes. ACS Appl. Mater. Interfaces 11 (5), 5306–5315. doi:10.1021/acsami.8b16877.

Cao, Y., Zhang, K., Sanyal, O., Koros, W.J., 2019. Carbon molecular sieve membrane preparation by economical coating and pyrolysis of porous polymer hollow fibers. Angew. Chem. Int. Ed. Engl. 58 (35), 12149–12153. doi:10.1002/anie.201906653.

Cao, M., Zhao, L., Xu, D., Parsley, D., Ciora, R., Liu, P.K.T., Manousiouthakis, V.I., Tsotsis, T.T., 2021. A reactive separation process for pre-combustion CO_2 capture employing oxygen-blown coal gasifier off-gas. Chem. Eng. J. 420, 127694. doi:10.1016/j.cej.2020.127694.

Cao, L.Y., Zhang, X.Y., Xu, Y., Xiang, W., Wang, R., Ding, F.J., Hong, P.Z., Gao, B., 2022. Straw and wood based biochar for CO_2 capture: Adsorption performance and governing mechanisms. Sep. Purif. Technol. 287. doi:10.1016/j.seppur.2022.120592.

Caplow, M., 1968. Kinetics of carbamate formation and breakdown. J. Am. Chem. Soc. 90, 6795–6803.

Caplow, M., 1968. Kinetics of carbamate formation and breakdown. J. Am. Chem. Soc 89, 6795–6803.

Carney, J.E., Finn, J.R., 2016. NETL Technical Report Series. National Energy Technology Lab. (NETL), Albany, OR (United States) 48-48.

Caruana, R., Lawrence, S., C, L.G., 2000. Overfitting in Neural Nets: Backpropagation, Conjugate Gradient, and Early Stopping. Advances in Neural Information Processing Systems 13, 402–408.

Caskey, S.R., Wong-Foy, A.K., Matzger, A.J., 2008. Dramatic tuning of carbon dioxide uptake via metal substitution in a cordination polymer with cylindrical pores. J. Am. Chem. Soc. 130 (33), 10870–10871.

Casleton, K.H., Breault, R.W., Richards, G.A., 2008. System issues and tradeoffs associated with syngas production and combustion. Combust. Sci. Technol. 180 (6), 1013–1052.

Castillo, R., 2011. Thermodynamic analysis of a hard coal oxyfuel power plant with high temperature three-end membrane for air separation. Appl. Energy 88 (5), 1480–1493. doi:10.1016/J.APENERGY.2010.10.044.

Cau, G., Cocco, D., Tola, V., 2014. Performance assessment of USC power plants integrated with CCS and concentrating solar collectors. Energy Convers. Manage. 88, 973–984. doi:10.1016/j.enconman.2014.09.040.

Cavani, F., Trifirò, F., Vaccari, A., 1991. Hydrotalcite-type anionic clays: preparation, properties and applications. Catal. Today 11 (2), 173–301. doi:10.1016/0920-5861(91)80068-K.

Cavka, J.H., Jakobsen, S., Olsbye, U., Guillou, N., Lamberti, C., Bordiga, S., Lillerud, K.P., 2008. A new zirconium inorganic building brick forming metal organic frameworks with exceptional stability. J. Am. Chem. Soc. 130 (42), 13850–13851.

Cecilia, J.A., Vilarrasa-García, E., García-Sancho, C., Saboya, R.M.A., Azevedo, D.C.S., Cavalcante, C.L., Rodríguez-Castellón, E., 2016. Functionalization of hollow silica microspheres by impregnation or grafted of amine groups for the CO_2 capture. Int. J. Greenh. Gas Control 52, 344–356. doi:10.1016/j.ijggc.2016.07.018.

Chacartegui, R., Alovisio, A., Ortiz, C., Valverde, J.M., Verda, V., Becerra, J.A., 2016. Thermochemical energy storage of concentrated solar power by integration of the calcium looping process and a CO_2 power cycle. Appl. Energy 173, 589–605. doi:10.1016/j.apenergy.2016.04.053.

Chagas, J.A.O., Crispim, G.O., Pinto, B.P., San Gil, R.A.S., Mota, C.J.A., 2020. Synthesis, characterization, and CO_2 uptake of adsorbents prepared by hydrothermal carbonization of chitosan. ACS Omega 5 (45), 29520–29529. doi:10.1021/acsomega.0c04470.

Chaikittisilp, W., Kim, H.-J., Jones, C.W., 2011. Mesoporous alumina-supported amines as potential steam-stable adsorbents for capturing CO_2 from simulated flue gas and ambient air. Energy Fuels 25 (11), 5528–5537. doi:10.1021/ef201224v.

Chaikittisilp, W., Lunn, J.D., Shantz, D.F., Jones, C.W., 2011. Poly (L-lysine) brush-mesoporous silica hybrid material as a biomolecule-based adsorbent for CO_2 capture from simulated flue gas and air. Chemistry 17 (38), 10556–10561. doi:10.1002/chem.201101480.

Chakma, A., 1995. An energy efficient mixed solvent for the separation of CO_2. Energy Convers. Manage. 36 (6–9), 427–430. doi:10.1016/0196-8904(95)00036-D.

Chakraborty, A., Maji, T.K., 2014. Mg-MOF-74@SBA-15 hybrids: Synthesis, characterization, and adsorption properties. APL Mater. 2 (12). doi:10.1063/1.4902816.

Chan, H.X.M., Yap, E.H., Ho, J.H., 2013. Overview of axial compression technology for direct capture of CO_2. Adv. Mater. Res. 744, 392–395. doi:10.4028/www.scientific.net/AMR.744.392.

Chan, W., Lei, X., Chang, F., Li, H., 2020. Thermodynamic analysis and optimization of Allam cycle with a reheating configuration. Energy Convers. Manage. 224, 113382.

Chan, W., Li, H., Li, X., Chang, F., Wang, L., Feng, Z., 2021. Exergoeconomic analysis and optimization of the Allam cycle with liquefied natural gas cold exergy utilization. Energy Convers. Manage. 235, 113972.

Chandra, S., Kandambeth, S., Biswal, B.P., Lukose, B., Kunjir, S.M., Chaudhary, M., Babarao, R., Heine, T., Banerjee, R., 2013. Chemically stable multilayered covalent organic nanosheets from covalent organic frameworks via mechanical delamination. J. Am. Chem. Soc. 135 (47), 17853–17861.

Chang, M.-H., Chen, W.-C., Huang, C.-M., Liu, W.-H., Chou, Y.-C., Chang, W.-C., Chen, W., Cheng, J.-Y., Huang, K.-E., Hsu, H.-W., 2014. Design and experimental testing of a 1.9 MWth calcium looping pilot plant. Energy Procedia 63, 2100–2108.

Chao, C., Deng, Y., Dewil, R., Baeyens, J., Fan, X., 2021. Post-combustion carbon capture. Renew. Sustain. Energy Rev. 138, 110490. doi:10.1016/j.rser.2020.110490.

Chatziasteriou, C.C., Kikkinides, E.S., Georgiadis, M.C., 2022. Recent advances on the modeling and optimization of CO_2 capture processes. Comput. Chem. Eng. 165. doi:10.1016/j.compchemeng.2022.107938, 107938-107938.

Chauvy, R., Dubois, L., 2022. Life cycle and techno-economic assessments of direct air capture processes: An integrated review. Int. J. Energy Res. 46 (8), 10320–10344. doi:10.1002/er.7884.

Chavez, H., Larachi, F., 2009. Analysis of flow in rotating packed beds via CFD simulations—Dry pressure drop and gas flow maldistribution. Chemical Engineering Science 64(9), 2113-2126. https://doi.org/10.1016/j.ces.2009.01.019.

Cheah, W.Y., Show, P.L., Chang, J.S., Ling, T.C., Juan, J.C., 2015. Biosequestration of atmospheric CO_2 and flue gas-containing CO_2 by microalgae. Bioresour. Technol. 184, 190–201. doi:10.1016/j.biortech.2014.11.026.

Chen, Y., Ho, W.S.W., 2016. High-molecular-weight polyvinylamine/piperazine glycinate membranes for CO_2 capture from flue gas. J. Membr. Sci. 514, 376–384. doi:10.1016/j.memsci.2016.05.005.

Chen, J., Wang, F., 2014. Cost reduction of CO_2 capture processes using reinforcement learning based iterative design: A pilot-scale absorption-stripping system. Separation and Purification Technology 122, 149–158.

Chen, S.J., Yu, B.Y., 2021. Rigorous simulation and techno-economic evaluation on the hybrid membrane/cryogenic distillation processes for air separation. J. Taiwan Instit. Chem. Eng. 127, 56–68. doi:10.1016/J.JTICE.2021.08.001.

Chen, B., Ji, Y., Xue, M., Fronczek, F.R., Hurtado, E.J., Mondal, J.U., Liang, C., Dai, S., 2008. Metal– organic framework with rationally tuned micropores for selective adsorption of water over methanol. Inorg. Chem. 47 (13), 5543–5545.

Chen, C., Yang, S.T., Ahn, W.S., Ryoo, R., 2009. Amine-impregnated silica monolith with a hierarchical pore structure: enhancement of CO_2 capture capacity. Chem. Commun. (Camb.) (24) 3627–3629. doi:10.1039/b905589d.

Chen, S., Kobayashi, K., Miyata, Y., Imazu, N., Saito, T., Kitaura, R., Shinohara, H., 2009. Morphology and melting behavior of ionic liquids inside single-walled carbon nanotubes. J. Am. Chem. Soc. 131 (41), 14850–14856. doi:10.1021/ja904283d.

Chen, C., Son, W.-J., You, K.-S., Ahn, J.-W., Ahn, W.-S., 2010. Carbon dioxide capture using amine-impregnated HMS having textural mesoporosity. Chem. Eng. J. 161 (1-2), 46–52. doi:10.1016/j.cej.2010.04.019.

Chen, L., Yong, S.Z., Ghoniem, A.F., 2012. Oxy-fuel combustion of pulverized coal: Characterization, fundamentals, stabilization and CFD modeling. Prog. Energy Combust. Sci. 38 (2), 156–214. doi:10.1016/j.pecs.2011.09.003.

Chen, X.Y., Vinh-Thang, H., Rodrigue, D., Kaliaguine, S., 2012. Amine-functionalized MIL-53 metal–organic framework in polyimide mixed matrix membranes for CO_2/CH4 separation. Ind. Eng. Chem. Res. 51 (19), 6895–6906. doi:10.1021/ie3004336.

Chen, C., Kim, S.-S., Cho, W.-S., Ahn, W.-S., 2015. Polyethylenimine-incorporated zeolite 13X with mesoporosity for post-combustion CO_2 capture. Appl. Surf. Sci. 332, 167–171. doi:10.1016/j.apsusc.2015.01.106.

Chen, S., Chen, S., Fei, X., Zhang, Y., Qin, L., 2015. Solubility and Characterization of CO_2 in 40 mass% N-ethylmonoethanolamine solutions: explorations for an efficient nonaqueous solution. Ind. Eng. Chem. Res. 54 (29), 7212–7218. doi:10.1021/acs.iecr.5b01654.

Chen, W., van der Ham, L., Nijmeijer, A., Winnubst, L., 2015. Membrane-integrated oxy-fuel combustion of coal: Process design and simulation. J. Membr. Sci. 492, 461–470. doi:10.1016/J.MEMSCI.2015.05.062.

Chen, S., Chen, S., Zhang, Y., Qin, L., Guo, C., Chen, J., 2016. Species distribution of CO 2 absorption/desorption in aqueous and non-aqueous N -ethylmonoethanolamine solutions. Int. J. Greenh. Gas Control 47, 151–158. doi:10.1016/j.ijggc.2016.01.046.

Chen, X., Xiong, Z., Qin, Y., Gong, B., Tian, C., Zhao, Y., Zhang, J., Zheng, C., 2016. High-temperature CO_2 sorption by Ca-doped Li_4SiO_4 sorbents. Int. J. Hydrogen Energy 41 (30), 13077–13085. doi:10.1016/j.ijhydene.2016.05.267.

Chen, Y., Zhao, L., Wang, B., Dutta, P., Ho, W.S.W., 2016a. Amine-containing polymer/zeolite Y composite membranes for CO_2/N_2 separation. J. Membr. Sci. 497, 21–28.

Chen, Y., Zhao, L., Wang, B., Dutta, P., Winston Ho, W.S., 2016b. Amine-containing polymer/zeolite Y composite membranes for CO_2/N_2 separation. J. Membr. Sci. 497, 21–28. doi:10.1016/j.memsci.2015.09.036.

Chen, C.H., Shimon, D., Lee, J.J., Mentink-Vigier, F., Hung, I., Sievers, C., Jones, C.W., Hayes, S.E., 2018. The "Missing" bicarbonate in CO_2 chemisorption reactions on solid amine sorbents. J. Am. Chem. Soc. 140 (28), 8648–8651. doi:10.1021/jacs.8b04520.

Chen, G., Liu, W., Widenmeyer, M., Ying, P., Dou, M., Xie, W., Bubeck, C., Wang, L., Fyta, M., Feldhoff, A., Weidenkaff, A., 2019. High flux and CO_2-resistance of La0.6Ca0.4Co1−xFexO3−δ oxygen-transporting membranes. J. Membr. Sci. 590, 117082. doi:10.1016/J.MEMSCI.2019.05.007.

Chen, S., Yu, R., Soomro, A., Xiang, W., 2019. Thermodynamic assessment and optimization of a pressurized fluidized bed oxy-fuel combustion power plant with CO_2 capture. Energy 175, 445–455. doi:10.1016/j.energy.2019.03.090.

Chen, J., Duan, L.B., Sun, Z.K., 2020. Review on the development of sorbents for calcium looping. Energy Fuels 34 (7), 7806–7836. doi:10.1021/acs.energyfuels.0c00682.

Chen, X., Zhang, Z., Wu, L., Liu, X., Xu, S., Efome, J.E., Zhang, X., Li, N., 2020. Polymers of intrinsic microporosity having bulky substitutes and cross-linking for gas separation membranes. ACS Appl. Polym. Mater. 2 (2), 987–995.

Chen, Z., Jing, G., Lv, B., Zhou, Z., 2020. An efficient solid–liquid biphasic solvent for CO_2 capture: crystalline powder product and low heat duty. ACS Sustain. Chem. Eng. 8 (38), 14493–14503. doi:10.1021/acssuschemeng.0c04616.

Chen, G., Snyders, R., Britun, N., 2021. CO_2 conversion using catalyst-free and catalyst-assisted plasma-processes: Recent progress and understanding. J. CO_2 Util. 49, 101557. doi:10.1016/J.JCOU.2021.101557.

Chen, J., Duan, L.B., Donat, F., Muller, C.R., 2021. Assessment of the effect of process conditions and material characteristics of alkali metal salt promoted MgO-based sorbents on their CO_2 capture performance. ACS Sustain. Chem. Eng. 9 (19), 6659–6672. doi:10.1021/acssuschemeng.1c00262.

Chen, L.J., Deng, S., Zhao, R.K., Zhao, L., Li, S.J., Guo, Z.H., Lu, Y.N., Zhao, J., Wu, K.L., 2021. The thermodynamics-based benchmarking analysis on energy-efficiency performance of CO_2 capture technology: temperature swing adsorption as case study. Energy Technol. 9 (1). doi:10.1002/ente.202000756.

Chen, R., Sheng, Q., Dai, X., Dong, B., 2021. Upgrading of sewage sludge by low temperature pyrolysis: Biochar fuel properties and combustion behavior. Fuel 300, 121007. doi:10.1016/j.fuel.2021.121007.

Chen, W., Zhang, Z., Yang, C., Liu, J., Shen, H., Yang, K., Wang, Z., 2021. PIM-based mixed-matrix membranes containing MOF-801/ionic liquid nanocomposites for enhanced CO_2 separation performance. J. Membr. Sci. 636, 119581. doi:10.1016/j.memsci.2021.119581.

Chen, G., Feldhoff, A., Weidenkaff, A., Li, C., Liu, S., Zhu, X., Sunarso, J., Huang, K., Wu, X.Y., Ghoniem, A.F., Yang, W., Xue, J., Wang, H., Shao, Z., Duffy, J.H., Brinkman, K.S., Tan, X., Zhang, Y., Jiang, H., Costa, R., Friedrich, K.A., Kriegel, R., 2022. Roadmap for sustainable mixed ionic-electronic conducting membranes. Adv. Funct. Mater. 32, 2105702. doi:10.1002/ADFM.202105702.

Chen, H., Dong, S., Zhang, Y., He, P., 2022. Robust structure regulation of geopolymer as novel efficient amine support to prepare high-efficiency CO_2 capture solid sorbent. Chem. Eng. J. 427. doi:10.1016/j.cej.2021.131577.

Chen, K., Zhang, W., Bai, C., Deng, L., Zhao, Y., Zhang, L., Feng, D., Sun, S., Qin, Y., 2022. Modeling of single-particle char combustion under O_2/H_2O conditions: Effects of temperature and steam concentration. Fuel Process. Technol. 227, 107131. doi:10.1016/j.fuproc.2021.107131.

Cheng, Y., Kondo, A., Noguchi, H., Kajiro, H., Urita, K., Ohba, T., Kaneko, K., Kanoh, H., 2009. Reversible structural change of Cu-MOF on exposure to water and its CO_2 adsorptivity. Langmuir 25 (8), 4510–4513.

Cheng, H.H., Lai, C.C., Tan, C.S., 2013. Thermal regeneration of alkanolamine solutions in a rotating packed bed. Int. J. Greenh. Gas Control 16, 206–216. doi:10.1016/j.ijggc.2013.03.022.

Cheng, Y., Zhai, L., Tong, M., Kundu, T., Liu, G., Ying, Y., Dong, J., Wang, Y., Zhao, D., 2018. Selective gas permeation in mixed matrix membranes accelerated by hollow ionic covalent organic polymers. ACS Sustain. Chem. Eng. 7 (1), 1564–1573. doi:10.1021/acssuschemeng.8b05333.

Cheng, J., Liu, N., Hu, L., Li, Y., Wang, Y., Zhou, J., 2019. Polyethyleneimine entwine thermally-treated Zn/Co zeolitic imidazolate frameworks to enhance CO_2 adsorption. Chem. Eng. J. 364, 530–540. doi:10.1016/j.cej.2019.02.026.

Cheng, Y., Zhai, L., Ying, Y., Wang, Y., Liu, G., Dong, J., Ng, D.Z., Khan, S.A., Zhao, D., 2019. Highly efficient CO_2 capture by mixed matrix membranes containing three-dimensional covalent organic framework fillers. J. Mater. Chem. A 7 (9), 4549–4560. doi:10.1039/C8TA10333J.

Cheng, J., Wang, Y., Hu, L., Liu, N., Xu, J., Zhou, J., 2020a. Using lantern Zn/Co-ZIF nanoparticles to provide channels for CO_2 permeation through PEO-based MMMs. J. Membr. Sci. 597, 117644. doi:10.1016/j.memsci.2019.117644.

Cheng, J., Wang, Y., Liu, N., Hou, W., Zhou, J., 2020b. Enhanced CO_2 selectivity of mixed matrix membranes with carbonized Zn/Co zeolitic imidazolate frameworks. Appl. Energy 272, 115179.

Cheng, H., Song, H., Toan, S., Wang, B., Gasem, K.A.M., Fan, M., Cheng, F., 2021a. Experimental investigation of CO_2 adsorption and desorption on multi-type amines loaded HZSM-5 zeolites. Chem. Eng. J. 406, 126882. doi:10.1016/j.cej.2020.126882.

Cheng, H., Song, H., Toan, S., Wang, B., Gasem, K.A.M., Fan, M., Cheng, F., 2021b. Experimental investigation of CO_2 adsorption and desorption on multi-type amines loaded HZSM-5 zeolites. Chem. Eng. J. 406. doi:10.1016/j.cej.2020.126882.

Cheng, Z., Li, S., Liu, Y., Zhang, Y., Ling, Z., Yang, M., Jiang, L., Song, Y., 2022. Post-combustion CO_2 capture and separation in flue gas based on hydrate technology:a review. Renew. Sustain. Energy Rev. 154. doi:10.1016/j.rser.2021.111806.

Cherbanski, R., Molga, E., 2009. Intensification of desorption processes by use of microwaves-An overview of possible applications and industrial perspectives. Chem. Eng. Process.-Process Intensif. 48 (1), 48–58. doi:10.1016/j.cep.2008.01.004.

Chern, R.T., Koros, W.J., Sanders, E.S., Yui, R., 1983. Second component" effects in sorption and permeation of gases in glassy polymers. J. Membr. Sci. 15 (2), 157–169. doi:10.1016/S0376-7388 (00)80395-6.

Chi, J., Zhao, L., Wang, B., Li, Z., Xiao, Y., Duan, Y., 2014. Thermodynamic performance assessment and comparison of IGCC with solid cycling process for CO_2 capture at high and medium temperatures. Int. J. Hydrog. Energy 39 (12), 6479–6491.

Chi, W.S., Sundell, B.J., Zhang, K., Harrigan, D.J., Hayden, S.C., Smith, Z.P., 2019. Mixed-matrix membranes formed from multi-dimensional metal-organic frameworks for enhanced gas transport and plasticization resistance. ChemSusChem 12 (11), 2355–2360. doi:10.1002/cssc.201900623.

Chichilnisky, G., 2021. 21 Dec NOAH Zurich 2021. Global Thermostat.

Chirone, R., Paulillo, A., Coppola, A., Scala, F., 2022. Carbon capture and utilization via calcium looping, sorption enhanced methanation and green hydrogen: A techno-economic analysis and life cycle assessment study. Fuel 328, 125255. doi:10.1016/j.fuel.2022.125255.

Chisalita, D.-A., Cormos, C.-C., 2019. Techno-economic assessment of hydrogen production processes based on various natural gas chemical looping systems with carbon capture. Energy 181, 331–344.

Chiwaye, N., Majozi, T., Daramola, M.O., 2021. Optimisation of post-combustion carbon dioxide capture by use of a fixed site carrier membrane. Int. J. Greenh. Gas Control 104, 103182. doi:10.1016/j.ijggc.2020.103182.

Cho, S.-H., Park, J.-H., Beum, H.-T., Han, S.-S., Kim, J.-N., 2004. A 2-stage PSA process for the recovery of CO_2 from flue gas and its power consumption. Stud. Surf. Sci. Catal. 153, 405–410.

Choi, E.Y., Park, K., Yang, C.M., Kim, H., Son, J.H., Lee, S.W., Lee, Y.H., Min, D., Kwon, Y.U., 2004. Benzene-templated hydrothermal synthesis of metal–organic frameworks with selective sorption properties. Chem.–A Eur. J. 10 (21), 5535–5540.

Choi, S., Drese, J.H., Jones, C.W., 2009. Adsorbent materials for carbon dioxide capture from large anthropogenic point sources. ChemSusChem 2 (9), 796–854. doi:10.1002/cssc.200900036.

Choi, S., Watanabe, T., Bae, T.H., Sholl, D.S., Jones, C.W., 2012. Modification of the Mg/DOBDC MOF with amines to enhance CO_2 adsorption from ultradilute gases. J. Phys. Chem. Lett. 3 (9), 1136–1141. doi:10.1021/jz300328j.

Choi, W., Min, K., Kim, C., Ko, Y.S., Jeon, J.W., Seo, H., Park, Y.K., Choi, M., 2016. Epoxide-functionalization of polyethyleneimine for synthesis of stable carbon dioxide adsorbent in temperature swing adsorption. Nat. Commun. 7, 12640. doi:10.1038/ncomms12640.

Chorowski, M., Gizicki, W., 2015. Technical and economic aspects of oxygen separation for oxy-fuel purposes. Arch. Thermodyn. 36 (1), 157–170. doi:10.1515/aoter-2015-0011.

Chuah, C.Y., Lee, J., Bao, Y., Song, J., Bae, T.-H., 2021. High-performance porous carbon-zeolite mixed-matrix membranes for CO_2/N_2 separation. J. Membr. Sci. 622. doi:10.1016/j.memsci.2020.119031.

Chuah, C.Y., Lee, J., Song, J., Bae, T.H., 2021. Carbon molecular sieve membranes comprising graphene oxides and porous carbon for CO_2/N_2 separation. Membranes (Basel) 11 (4). doi:10.3390/membranes11040284.

Chungsying Lu, H.B., Wu, B., Su, F., Hwang, J.F., 2008. Comparative study of CO_2 capture by carbon nanotubes, activated carbons, and zeolites. Energy Fuels 22, 3050–3056.

Ciftja, A.F., Hartono, A., Svendsen, H.F., 2014. Experimental study on carbamate formation in the AMP–CO_2–H2O system at different temperatures. Chem. Eng. Sci. 107, 317–327. doi:10.1016/j.ces.2013.12.028.

Clausse, M., Merel, J., Meunier, F., 2011. Numerical parametric study on CO_2 capture by indirect thermal swing adsorption. Int. J. Greenh. Gas Control 5 (5), 1206–1213. doi:10.1016/j.ijggc.2011.05.036.

Clifford, C., 2022. From milligrams to gigatons: Startup that sucks carbon dioxide from the air is building a big plant in Iceland. CNBC.

Clodic, D., Younes, M., 2003. A new method for CO_2 capture: frosting CO_2 at atmospheric pressure. In: Gale, J., Kaya, Y. (Eds.), Greenhouse Gas Control Technologies - 6th International Conference. Pergamon, Oxford, pp. 155–160. doi:10.1016/B978-008044276-1/50025-8.

Clodic, D., Hitti, R.E., Younes, M., Bill, A., Casier, F., 2005a. CO_2 capture by anti-sublimation Thermo-economic process evaluation.

Clodic, D., Younes, M., Bill, A., 2005b. Test results of CO_2 capture by anti-sublimation capture efficiency and energy consumption for boiler plants. In: Rubin, E.S., Keith, D.W., Gilboy, C.F., Wilson, M., Morris, T., Gale, J., Thambimuthu, K. (Eds.), Greenhouse Gas Control Technologies 7. Elsevier Science Ltd, Oxford, pp. 1775–1780. doi:10.1016/B978-008044704-9/50210-X.

Cobden, P.D., Lukashuk, L., de Water, L.v., Lundqvist, M., Manzolini, G., Cormos, C.-C., van Dijk, C., Mancuso, L., Johns, J., Bellqvist, D., 2018. Stepwise project: Sorption-enhanced water-gas shift technology to reduce carbon footprint in the iron and steel industry.

Coenen, K., Gallucci, F., Hensen, E., van Sint Annaland, M., 2019. Kinetic model for adsorption and desorption of H2O and CO_2 on hydrotalcite-based adsorbents. Chem. Eng. J. 355, 520–531. doi:10.1016/j.cej.2018.08.175.

Cohen, D.T., Zhang, C., Fadzen, C.M., Mijalis, A.J., Hie, L.N., Johnson, K.D., Shriver, Z., Plante, O., Miller, S.J., Buchwald, S.L., Pentelute, B.L., 2019. A chemoselective strategy for late-stage functionalization of complex small molecules with polypeptides and proteins. Nat. Chem. 11 (1), 78–85. doi:10.1038/s41557-018-0154-0.

Colelli, G., Chacartegui, R., Ortiz, C., Carro, A., Arena, A.P., Verda, V., 2022. Life cycle and environmental assessment of calcium looping (CaL) in solar thermochemical energy storage. Energy Convers. Manage. 257, 14. doi:10.1016/j.enconman.2022.115428.

Colombo, V., Galli, S., Choi, H.J., Han, G.D., Maspero, A., Palmisano, G., Masciocchi, N., Long, J.R., 2011. High thermal and chemical stability in pyrazolate-bridged metal–organic frameworks with exposed metal sites. Chem. Sci. 2 (7), 1311–1319.

Cooper, A.I., 2009. Conjugated microporous polymers. Adv. Mater. 21 (12), 1291–1295. doi:10.1002/adma.200801971.

Corma, A., Fornés, V., Martín-Aranda, R.M., Rey, F., 1992. Determination of base properties of hydrotalcites: condensation of benzaldehyde with ethyl acetoacetate. J. Catal. 134 (1), 58–65. doi:10.1016/0021-9517 (92)90209-Z.

Cormos, C.-C., 2011. Evaluation of power generation schemes based on hydrogen-fuelled combined cycle with carbon capture and storage (CCS). Int. J. Hydrogen Energy 36 (5), 3726–3738. doi:10.1016/j.ijhydene.2010.12.042.

Cormos, C.-C., 2015. Assessment of chemical absorption/adsorption for post-combustion CO_2 capture from Natural Gas Combined Cycle (NGCC) power plants. Appl. Therm. Eng. 82, 120–128. doi:10.1016/j.applthermaleng.2015.02.054.

Cormos, C.-C., 2018. Techno-economic evaluations of copper-based chemical looping air separation system for oxy-combustion and gasification power plants with carbon capture. Energies 11 (11). doi:10.3390/en11113095, 3095-3095.

Cormos, C.C., 2020. Energy and cost efficient manganese chemical looping air separation cycle for decarbonized power generation based on oxy-fuel combustion and gasification. Energy 191. doi:10.1016/J.ENERGY.2019.116579, 116579-116579.

Cortes Garcia, G.E., van der Schaaf, J., Kiss, A.A., 2017. A review on process intensification in HiGee distillation. J. Chem. Technol. Biotechnol. 92 (6), 1136–1156. doi:10.1002/jctb.5206.

Cote, A.P., Benin, A.I., Ockwig, N.W., O'Keeffe, M., Matzger, A.J., Yaghi, O.M., 2005. Porous, crystalline, covalent organic frameworks. Science 310 (5751), 1166–1170.

Cova, F., Amica, G., Kohopää, K., Blanco, M.V., 2019. Time-resolved synchrotron powder X-ray diffraction studies on the synthesis of Li_8SiO_6 and its reaction with CO_2. Inorg. Chem. 58 (2), 1040–1047. doi:10.1021/acs.inorgchem.8b01297.

Creamer, A.E., Gao, B., Zhang, M., 2014. Carbon dioxide capture using biochar produced from sugarcane bagasse and hickory wood. Chem. Eng. J. 249, 174–179.

Croiset, E., Thambimuthu, K.V., 2001. NOx and SO2 emissions from O_2/CO_2 recycle coal combustion. Fuel 80 (14), 2117–2121. doi:10.1016/S0016-2361 (00)00197-6.

Cui, S., Cheng, W., Shen, X., Fan, M., Russell, A., Wu, Z., Yi, X., 2011. Mesoporous amine-modified SiO2 aerogel: a potential CO_2 sorbent. Energy Environ. Sci. 4 (6). doi:10.1039/c0ee00442a.

Cui, S., Cheng, W.W., Shen, X.D., Fan, M.H., Russell, A., Wu, Z.W., Yi, X.B., 2011. Mesoporous amine-modified SiO2 aerogel: a potential CO_2 sorbent. Energy Environ. Sci. 4 (6), 2070–2074. doi:10.1039/c0ee00442a.

Cui, G., Wang, J., Zhang, S., 2016. Active chemisorption sites in functionalized ionic liquids for carbon capture. Chem. Soc. Rev. 45 (15), 4307–4339. doi:10.1039/c5cs00462d.

Cui, S., Yu, S.W., Lin, B.L., Shen, X.D., Zhang, X., Gu, D.M., 2017. Preparation of amine-modified SiO2 aerogel from rice husk ash for CO_2 adsorption. J. Porous Mater. 24 (2), 455–461. doi:10.1007/s10934-016-0280-2.

Cui, H.J., Zhang, Q.M., Hu, Y.W., Peng, C., Fang, X.C., Cheng, Z.M., Galvita, V.V., Zhou, Z.M., 2018. Ultrafast and stable CO_2 capture using alkali metal salt-promoted MgO-$CaCO_3$ sorbents. ACS Appl. Mater. Interfaces 10 (24), 20611–20620. doi:10.1021/acsami.8b05829.

Cui, H., Cheng, Z., Zhou, Z., 2020. Unravelling the role of alkaline earth metal carbonates in intermediate temperature CO_2 capture using alkali metal salt-promoted MgO-based sorbents. J. Mater. Chem. A 8 (35), 18280–18291. doi:10.1039/D0TA06170K.

Cullinane, J.T., Rochelle, G.T., 2004. Carbon dioxide absorption with aqueous potassium carbonate promoted by piperazine. Chem. Eng. Sci. 59 (17), 3619–3630. doi:10.1016/j.ces.2004.03.029.

Custelcean, R., Garrabrant, K.A., Agullo, P., Williams, N.J., 2021. Direct air capture of CO_2 with aqueous peptides and crystalline guanidines. Cell Rep. Phys. Sci. 2 (4), 100385. doi:10.1016/j.xcrp.2021.100385.

Czaun, M., Goeppert, A., May, R.B., Peltier, D., Zhang, H., Prakash, G.K.S., Olah, G.A., 2013. Organoamines-grafted on nano-sized silica for carbon dioxide capture. J. CO_2 Util. 1, 1–7. doi:10.1016/j.jcou.2013.03.007.

D'Alessandro, D.M., Smit, B., Long, J.R., 2010. Carbon dioxide capture: prospects for new materials. Angew. Chem. Int. Ed. Engl. 49 (35), 6058–6082. doi:10.1002/anie.201000431.

Dai, Z., Ansaloni, L., Deng, L., 2016. Recent advances in multi-layer composite polymeric membranes for CO_2 separation: a review. Green Energy Environ. 1 (2), 102–128. doi:10.1016/j.gee.2016.08.001.

Dai, Z., Deng, J., Ansaloni, L., Janakiram, S., Deng, L., 2019a. Thin-film-composite hollow fiber membranes containing amino acid salts as mobile carriers for CO_2 separation. J. Membr. Sci. 578, 61–68. doi:10.1016/j.memsci.2019.02.023.

Dai, Z., Fabio, S., Giuseppe Marino, N., Riccardo, C., Deng, L., 2019b. Field test of a pre-pilot scale hollow fiber facilitated transport membrane for CO_2 capture. Int. J. Greenh. Gas Control 86, 191–200. doi:10.1016/j.ijggc.2019.04.027.

Dal Pozzo, A., Armutlulu, A., Rekhtina, M., Abdala, P.M., Müller, C.R., 2019. CO_2 uptake and cyclic stability of MgO-based CO_2 sorbents promoted with alkali metal nitrates and their eutectic mixtures. ACS Appl. Energy Mater. 2 (2), 1295–1307. doi:10.1021/acsaem.8b01852.

Danaci, D., et al., 2020. Exploring the limits of adsorption-based CO_2 capture using MOFs with PVSA – from molecular design to process economics. Molecular Systems Design & Engineering 5 (1), 212–231.

Danckwerts, P.V., 1970. Gas-liquid reactions.

Danckwerts, P.V., 1979. The reaction of CO_2 with ethanolamines. Chem. Eng. Sci. 34 (4), 443–446. doi:10.1016/0009-2509 (79)85087-3.

Darde, V., Thomsen, K., van Well, W.J., Stenby, E.H., 2009. Chilled ammonia process for CO_2 capture. Energy Procedia 1 (1), 1035–1042.

Darunte, L.A., Oetomo, A.D., Walton, K.S., Sholl, D.S., Jones, C.W., 2016. Direct air capture of CO_2 using amine functionalized MIL-101 (Cr). ACS Sustain. Chem. Eng. 4 (10), 5761–5768. doi:10.1021/acssuschemeng.6b01692.

Dave, A., Dave, M., Huang, Y., Rezvani, S., Hewitt, N., 2016. Process design for CO_2 absorption from syngas using physical solvent DMEPEG. Int. J. Greenh. Gas Control 49, 436–448. doi:10.1016/j.ijggc.2016.03.015.

Davison, J., 2007. Performance and costs of power plants with capture and storage of CO_2. Energy 32 (7), 1163–1176. doi:10.1016/J.ENERGY.2006.07.039.

Dawson, R., Cooper, A.I., Adams, D.J., 2012. Nanoporous organic polymer networks. Prog. Polym. Sci. 37 (4), 530–563. doi:10.1016/j.progpolymsci.2011.09.002.

Debost, M., Klar, P.B., Barrier, N., Clatworthy, E.B., Grand, J., Laine, F., Brázda, P., Palatinus, L., Nesterenko, N., Boullay, P., 2020. Synthesis of discrete CHA zeolite nanocrystals without organic templates for selective CO_2 capture. Angew. Chem. Int. Ed. 59 (52), 23491–23495.

Decardi-Nelson, B., Akachuku, A., Osei, P., Srisang, W., Pouryousefi, F., Idem, R., 2017. A flexible and robust model for low temperature catalytic desorption of CO 2 from CO 2 -loaded amines over solid acid catalysts. Chem. Eng. Sci. 170, 518–529. doi:10.1016/j.ces.2016.12.068.

Demessence, A., D'Alessandro, D.M., Foo, M.L., Long, J.R., 2009. Strong CO_2 binding in a water-stable, triazolate-bridged metal– organic framework functionalized with ethylenediamine. J. Am. Chem. Soc. 131 (25), 8784–8786.

Deng, L., Hägg, M.-B., 2015. Fabrication and evaluation of a blend facilitated transport membrane for CO_2/CH4 separation. Ind. Eng. Chem. Res. 54 (44), 11139–11150. doi:10.1021/acs.iecr.5b02971.

Deng, L., Kim, T.-J., Hägg, M.-B., 2009. Facilitated transport of CO_2 in novel PVAm/PVA blend membrane. J. Membr. Sci. 340 (1), 154–163. doi:10.1016/j.memsci.2009.05.019.

Deng, S.B., Hu, B.Y., Chen, T., Wang, B., Huang, J., Wang, Y.J., Yu, G., 2015. Activated carbons prepared from peanut shell and sunflower seed shell for high CO_2 adsorption. Adsorpt.-J. Int. Adsorpt. Soc. 21 (1-2), 125–133. doi:10.1007/s10450-015-9655-y.

Deng, J., Dai, Z., Deng, L., 2020a. Effects of the morphology of the ZIF on the CO_2 separation performance of MMMs. Ind. Eng. Chem. Res. 59 (32), 14458–14466.

Deng, J., Dai, Z., Hou, J., Deng, L., 2020b. Morphologically tunable MOF nanosheets in mixed matrix membranes for CO_2 separation. Chem. Mater. 32 (10), 4174–4184. doi:10.1021/acs.chemmater.0c00020.

Deng, G., Wang, Y., Zong, X., Luo, J., Wang, X., Zhang, C., Xue, S., 2021. Structure evolution in carbon molecular sieve membranes derived from binaphthol-6FDA polyimide and their gas separation performance. J. Ind. Eng. Chem. 94, 489–497. doi:10.1016/j.jiec.2020.11.024.

Deng, Y., Li, J., Miao, Y., Izikowitz, D., 2021. A comparative review of performance of nanomaterials for direct air capture. Energy Rep. 7, 3506–3516. doi:10.1016/j.egyr.2021.06.002.

Deng, L., Zhang, W., Sun, S., Bai, C., Zhao, Y., Feng, D., Zhang, L., Wu, J., 2021a. Effect of pressure on the structure and reactivity of demineralized coal during O_2/H_2O thermal conversion process. Energy, 122632 doi:10.1016/j.energy.2021.122632.

Deng, L., Zhang, W., Sun, S., Bai, C., Zhao, Y., Feng, D., Zhang, L., Wu, J., 2021b. Study on the thermal conversion characteristics of demineralized coal char under pressurized O_2/H_2O atmosphere. Fuel, 122429 doi:10.1016/j.fuel.2021.122429.

Deng, L., Zhao, Y., Sun, S., Feng, D., Zhang, W., 2022. Review on thermal conversion characteristics of coal in O_2/H_2O atmosphere. Fuel Process. Technol. 232, 107266. doi:10.1016/j.fuproc.2022.107266.

Deutz, S., Bardow, A., 2021. Life-cycle assessment of an industrial direct air capture process based on temperature-vacuum swing adsorption. Nat. Energy 6 (2), 203–213. doi:10.1038/s41560-020-00771-9.

Dewangan, N., Ashok, J., Sethia, M., Das, S., Pati, S., Kus, H., Kawi, S., 2019. Cobalt-based catalyst supported on different morphologies of alumina for non-oxidative propane dehydrogenation: effect of metal support interaction and lewis acidic sites. ChemCatChem 11 (19), 4923–4934. doi:10.1002/cctc.201900924.

Di Giuliano, A., Gallucci, K., 2018. Sorption enhanced steam methane reforming based on nickel and calcium looping: a review. Chem. Eng. Process. - Process Intensif. 130, 240–252. doi:10.1016/j.cep.2018.06.021.

Diaf, A., Garcia, J.L., Beckman, E.J., 1994. Thermally reversible polymeric sorbents for acid gases: CO_2, SO2, and NOx. J. Appl. Polym. Sci. 53, 857–875.

Diagne, D., Goto, M., Hirose, T., 1994. New PSA process with intermediate feed inlet position operated with dual refluxes: application to carbon dioxide removal and enrichment. J. Chem. Eng. Jpn. 27 (1), 85–89.

Didas, S.A., Choi, S., Chaikittisilp, W., Jones, C.W., 2015. Amine-oxide hybrid materials for CO_2 capture from ambient air. Acc. Chem. Res. 48 (10), 2680–2687. doi:10.1021/acs.accounts.5b00284.

Diego, M.E., Arias, B., 2020. Impact of load changes on the carbonator reactor of a 1.7 MWth calcium looping pilot plant. Fuel Process. Technol. 200, 106307. doi:10.1016/j.fuproc.2019.106307.

Dieter, H., Hawthorne, C., Zieba, M., Scheffknecht, G., 2013. Progress in calcium looping post combustion CO_2 capture: successful pilot scale demonstration. Energy Procedia 37, 48–56. doi:10.1016/j.egypro.2013.05.084.

Dillon, D.J., Panesar, R.S., Wall, R.A., Allam, R.J., White, V., Gibbins, J., Haines, M.R., 2005. Oxy-combustion processes for CO_2 capture from advanced supercritical PF and NGCC power plant. Greenh. Gas Control Technol. 211–220. doi:10.1016/B978-008044704-9/50022-7.

Dillon, D., 2005. Proc 7th Intern. Conf. Greenhouse Gas Control Technol.

Ding, Y., Alpay, E., 2000. Equilibria and kinetics of CO_2 adsorption on hydrotalcite adsorbent. Chem. Eng. Sci. 55 (17), 3461–3474. doi:10.1016/S0009-2509 (99)00596-5.

Ding, Y., Alpay, E., 2001. High temperature recovery of CO_2 from flue gases using hydrotalcite adsorbent. Process. Saf. Environ. Prot. 79 (1), 45–51. doi:10.1205/095758201531130.

Ding, L., Wei, Y., Li, L., Zhang, T., Wang, H., Xue, J., Ding, L.-X., Wang, S., Caro, J., Gogotsi, Y., 2018. MXene molecular sieving membranes for highly efficient gas separation. Nat. Commun. 9 (1). doi:10.1038/s41467-017-02529-6.

Ding, M., Flaig, R.W., Jiang, H.-L., Yaghi, O.M., 2019. Carbon capture and conversion using metal–organic frameworks and MOF-based materials. Chem. Soc. Rev. 48 (10), 2783–2828.

Dissanayake, P.D., You, S.M., Igalavithana, A.D., Xia, Y.F., Bhatnagar, A., Gupta, S., Kua, H.W., Kim, S., Kwon, J.H., Tsang, D.C.W., Ok, Y.S., 2020. Biochar-based adsorbents for carbon dioxide capture: A critical review. Renew. Sustain. Energy Rev. 119. doi:10.1016/j.rser.2019.109582.

Donat, F., Müller, C.R., 2022. Prospects of MgO-based sorbents for CO_2 capture applications at high temperatures. Curr. Opin. Green Sustain. Chem., 100645 doi:10.1016/j.cogsc.2022.100645.

Donat, F., Florin, N.H., Anthony, E.J., Fennell, P.S., 2012. Influence of high-temperature steam on the reactivity of CaO sorbent for CO_2 capture. Environ. Sci. Technol. 46 (2), 1262–1269. doi:10.1021/es202679w.

Dong, Y., Li, D., 2012. Efficient and effective algorithms for training single-hidden-layer neural networks. Patt. Recogn. Lett. 33 (5), 554–558. doi:10.1016/j.patrec.2011.12.002.

Dong, W., Chen, X., Yu, F., Wu, Y., 2015. $Na_2CO_3/MgO/Al_2O_3$ solid sorbents for low-temperature CO_2 capture. Energy Fuels 29 (2), 968–973. doi:10.1021/ef502400s.

Dong, G., Zhang, Y., Hou, J., Shen, J., Chen, V., 2016. Graphene oxide nanosheets based novel facilitated transport membranes for efficient CO_2 capture. Ind. Eng. Chem. Res. 55 (18), 5403–5414. doi:10.1021/acs.iecr.6b01005.

Dong, J., Tang, Y., Nzihou, A., Weiss-Hortala, E., 2020. Effect of steam addition during carbonation, calcination or hydration on re-activation of CaO sorbent for CO_2 capture. J. CO_2 Util. 39, 101167. doi:10.1016/j.jcou.2020.101167.

Dong, H., Cui, H., Zhou, Z., 2022. Promoting effects of Li3PO4 and CaCO3 on the intermediate-temperature CO_2 adsorption over molten NaNO3-promoted MgO-based sorbents. Chem. Eng. J. 442, 136133. doi:10.1016/j.cej.2022.136133.

Doong, S.J., Ho, W.S., Mastondrea, R.P., 1995. Prediction of flux and selectivity in pervapouration through a membrane. J. Membr. Sci. 107 (1), 129–146. doi:10.1016/0376-7388 (95)00109-P.

Drechsler, C., Agar, D.W., 2020. Investigation of water co-adsorption on the energy balance of solid sorbent based direct air capture processes. Energy 192, 116587. doi:10.1016/j.energy.2019.116587.

Du, N., Park, H.B., Robertson, G.P., Dal-Cin, M.M., Visser, T., Scoles, L., Guiver, M.D., 2011. Polymer nanosieve membranes for CO_2-capture applications. Nat. Mater. 10 (5), 372–375. doi:10.1038/nmat2989.

Du, Y., Fan, Z., Guo, T., Xu, J., Han, Z., Pan, Y., Xiao, H., Sun, Y., Yan, Q., 2020. Characteristics of as-prepared biochar derived from catalytic pyrolysis within moderate-temperature ionic liquid for CO_2 uptake. Can. J. Chem. Eng. 98 (3), 690–704. doi:10.1002/cjce.23671.

Duan, K., Wang, J., Zhang, Y., Liu, J., 2019. Covalent organic frameworks (COFs) functionalized mixed matrix membrane for effective CO_2/N_2 separation. J. Membr. Sci. 572, 588–595. doi:10.1016/j.memsci.2018.11.054.

Duan, Y., Duan, L., Wang, J., Anthony, E.J., 2019. Observation of simultaneously low CO, NOx and SO2 emission during oxy-coal combustion in a pressurized fluidized bed. Fuel 242, 374–381. doi:10.1016/j.fuel.2019.01.048.

Duan, D.L., Chen, D.H., Huang, L.Y., Zhang, Y.C., Zhang, Y.Y., Wang, Q., Xiao, G.S., Zhang, W.L., Lei, H.W., Ruan, R., 2021. Activated carbon from lignocellulosic biomass as catalyst: A review of the applications in fast pyrolysis process. J. Analyt. Appl. Pyrol. 158. doi:10.1016/j.jaap.2021.105246.

Dubois, L., Thomas, D., 2018. Comparison of various configurations of the absorption-regeneration process using different solvents for the post-combustion CO_2 capture applied to cement plant flue gases. Int. J. Greenh. Gas Control 69, 20–35. doi:10.1016/j.ijggc.2017.12.004.

Duelli, G., Charitos, A., Diego, M.E., Stavroulakis, E., Dieter, H., Scheffknecht, G., 2015. Investigations at a 10kWth calcium looping dual fluidized bed facility: Limestone calcination and CO_2 capture under high CO_2 and water vapour atmosphere. Int. J. Greenh. Gas Control 33, 103–112. doi:10.1016/j.ijggc.2014.12.006.

Dunn, C.A., Shi, Z., Zhou, R., Gin, D.L., Noble, R.D., 2019. Cross-linked poly (ionic liquid)–ionic liquid–zeolite) mixed-matrix membranes for CO_2/CH_4 gas separations based on curable ionic liquid prepolymers. Ind. Eng. Chem. Res. 58 (11), 4704–4708. doi:10.1021/acs.iecr.8b06464.

Dunne, J., Rao, M., Sircar, S., Gorte, R., Myers, A., 1996. Calorimetric heats of adsorption and adsorption isotherms. 2. O_2, N_2, Ar, CO_2, CH_4, C_2H_6, and SF_6 on NaX, H-ZSM-5, and Na-ZSM-5 zeolites. Langmuir 12 (24), 5896–5904.

Dunstan, M.T., Southon, P.D., Kepert, C.J., Hester, J., Kimpton, J.A., Ling, C.D., 2011. Phase diagram, chemical stability and physical properties of the solid-solution Ba_4Nb_2−xTaxO9. J. Solid State Chem. 184 (10), 2648–2654. doi:10.1016/j.jssc.2011.07.036.

Dunstan, M.T., Liu, W., Pavan, A.F., Kimpton, J.A., Ling, C.D., Scott, S.A., Dennis, J.S., Grey, C.P., 2013. Reversible CO_2 absorption by the 6H perovskite $Ba_4Sb_2O_9$. Chem. Mater. 25 (24), 4881–4891. doi:10.1021/cm402875v.

Dunstan, M.T., Donat, F., Bork, A.H., Grey, C.P., Muller, C.R., 2021. CO_2 capture at medium to high temperature using solid oxide-based sorbents: fundamental aspects, mechanistic insights, and recent advances. Chem. Rev. 121 (20), 12681–12745. doi:10.1021/acs.chemrev.1c00100.

Durá, G., Budarin, V.L., Castro-Osma, J.A., Shuttleworth, P.S., Quek, S.C.Z., Clark, J.H., North, M., 2016. Importance of micropore–mesopore interfaces in carbon dioxide capture by carbon-based materials. Angew. Chem. Int. Ed. 55 (32), 9173–9177. doi:10.1002/anie.201602226.

Duran-Jimenez, G., Kostas, E.T., Stevens, L.A., Meredith, W., Erans, M., Hernandez-Montoya, V., Buttress, A., Uguna, C.N., Binner, E., 2021. Green and simple approach for low-cost bioproducts preparation and CO_2 capture. Chemosphere 279. doi:10.1016/j.chemosphere.2021.130512.

Eason, J.P., Biegler, L.T., 2020. Model reduction in chemical process optimization. De Gruyter, Boston doi:10.1515/9783110499001-001.

Ebner, A.D., Reynolds, S.P., Ritter, J.A., 2006. Understanding the adsorption and desorption behavior of CO_2 on a K-promoted hydrotalcite-like compound (HTlc) through nonequilibrium dynamic isotherms. Ind. Eng. Chem. Res. 45 (18), 6387–6392. doi:10.1021/ie060389k.

Ebner, A.D., Reynolds, S.P., Ritter, J.A., 2007. Nonequilibrium kinetic model that describes the reversible adsorption and desorption behavior of CO_2 in a K-promoted hydrotalcite-like compound. Ind. Eng. Chem. Res. 46 (6), 1737–1744. doi:10.1021/ie061042k.

Ebner, A.D., Gray, M.L., Chisholm, N.G., Black, Q.T., Mumford, D.D., Nicholson, M.A., Ritter, J.A., 2011. Suitability of a solid amine sorbent for CO_2 capture by pressure swing adsorption. Ind. Eng. Chem. Res. 50 (9), 5634–5641. doi:10.1021/ie2000709.

Ebrahimzadeh, E., Matagi, J., Fazlollahi, F., Baxter, L.L., 2016. Alternative extractive distillation system for CO_2–ethane azeotrope separation in enhanced oil recovery processes. Appl. Therm. Eng. 96, 39–47. doi:10.1016/j.applthermaleng.2015.11.082.

Eddaoudi, M., Kim, J., Rosi, N., Vodak, D., Wachter, J., O'Keeffe, M., Yaghi, O.M., 2002. Systematic design of pore size and functionality in isoreticular MOFs and their application in methane storage. Science 295 (5554), 469–472.

El Knidri, H., El Khalfaouy, R., Laajeb, A., Addaou, A., Lahsini, A., 2016. Eco-friendly extraction and characterization of chitin and chitosan from the shrimp shell waste via microwave irradiation. Process. Saf. Environ. Prot. 104, 395–405. doi:10.1016/j.psep.2016.09.020.

El-Kaderi, H.M., Hunt, J.R., Mendoza-Cortés, J.L., Côté, A.P., Taylor, R.E., O'Keeffe, M., Yaghi, O.M., 2007. Designed synthesis of 3D covalent organic frameworks. Science 316 (5822), 268–272.

El-Mahdy, A.F., Kuo, C.-H., Alshehri, A., Young, C., Yamauchi, Y., Kim, J., Kuo, S.-W., 2018. Strategic design of triphenylamine-and triphenyltriazine-based two-dimensional covalent organic frameworks for CO 2 uptake and energy storage. J. Mater. Chem. A 6 (40), 19532–19541.

Elfving, J., Sainio, T., 2021. Kinetic approach to modelling CO_2 adsorption from humid air using amine-functionalized resin: Equilibrium isotherms and

column dynamics. Chem. Eng. Sci. 246, 116885. doi:10.1016/j.ces.2021.116885.
Engels, S., Beggel, F., Modigell, M., Stadler, H., 2010. Simulation of a membrane unit for oxyfuel power plants under consideration of realistic BSCF membrane properties. J. Membr. Sci. 359 (1-2), 93–101. doi:10.1016/J.MEMSCI.2010.01.048.
Eoghan, P., Dillon, C.A.C., Barron, A.R., 2008. Synthesis, characterization, and carbon dioxide adsorption ofcovalently attached polyethyleneimine functionalized single-wall carbon nanotubes. ACS Nano 2 (2), 156–164.
EPRI Report, 2000. Interim Report #1000316 Dec.
Er, H., Xu, Y., Zhao, H., 2019. Properties of mono-protic ionic liquids composed of hexylammonium and hexylethylenediaminium cations with trifluoroacetate and bis (trifluoromethylsulfonyl) imide anions. J. Mol. Liq. 276, 379–384. doi:10.1016/j.molliq.2018.11.132.
Erans, M., Manovic, V., Anthony, E.J., 2016. Calcium looping sorbents for CO_2 capture. Appl. Energy 180, 722–742. doi:10.1016/j.apenergy.2016.07.074.
Erucar, I., Keskin, S., 2016. Computational methods for MOF/polymer membranes. Chem. Rec. 16, 703–718. doi:10.1002/tcr.201500275.
Esfilar, R., Mehrpooya, M., Moosavian, S.M.A., 2018. Thermodynamic assessment of an integrated biomass and coal co-gasification, cryogenic air separation unit with power generation cycles based on LNG vapourization. Energy Conver. Manage. 157, 438–451. doi:10.1016/j.enconman.2017.12.026.
Etxeberria-Benavides, M., Johnson, T., Cao, S., Zornoza, B., Coronas, J., Sanchez-Lainez, J., Sabetghadam, A., Liu, X., Andres-Garcia, E., Kapteijn, F., 2020. PBI mixed matrix hollow fiber membrane: Influence of ZIF-8 filler over $H2/CO_2$ separation performance at high temperature and pressure. Sep. Purif. Technol. 237, 116347.
Férey, G., Serre, C., Mellot-Draznieks, C., Millange, F., Surblé, S., Dutour, J., Margiolaki, I., 2004. A hybrid solid with giant pores prepared by a combination of targeted chemistry, simulation, and powder diffraction. Angew. Chem. 116 (46), 6456–6461.
Férey, G., Mellot-Draznieks, C., Serre, C., Millange, F., Dutour, J., Surblé, S., Margiolaki, I., 2005. A chromium terephthalate-based solid with unusually large pore volumes and surface area. Science 309 (5743), 2040–2042.
Fagerlund, J., Highfield, J., Zevenhoven, R., 2012. Kinetics studies on wet and dry gas–solid carbonation of MgO and Mg (OH)2 for CO_2 sequestration. RSC Adv. 2 (27), 10380–10393. doi:10.1039/C2RA21428H.
Fajardy, M., Morris, J., Gurgel, A., Herzog, H., Mac Dowell, N., Paltsev, S., 2021. The economics of bioenergy with carbon capture and storage (BECCS) deployment in a 1.5°C or 2°C world. Glob. Environ. Change 68. doi:10.1016/j.gloenvcha.2021.102262.
Fan, Y., Jia, X., 2022. Progress in amine-functionalized silica for CO_2 capture: important roles of support and amine structure. Energy Fuels 36 (3), 1252–1270. doi:10.1021/acs.energyfuels.1c03788.
Fan, L.-S., Zeng, L., Wang, W., Luo, S., 2012. Chemical looping processes for CO 2 capture and carbonaceous fuel conversion–prospect and opportunity. Energy Environ. Sci. 5 (6), 7254–7280.
Fan, X., Zhang, L., Zhang, G., Shu, Z., Shi, J., 2013. Chitosan derived nitrogen-doped microporous carbons for high performance CO_2 capture. Carbon 61, 423–430. doi:10.1016/j.carbon.2013.05.026.
Fan, H., Mundstock, A., Feldhoff, A., Knebel, A., Gu, J., Meng, H., Caro, J.r., 2018. Covalent organic framework–covalent organic framework bilayer membranes for highly selective gas separation. J. Am. Chem. Soc. 140 (32), 10094–10098. doi:10.1021/jacs.8b05136.
Fan, H., Peng, M., Strauss, I., Mundstock, A., Meng, H., Caro, J., 2021. MOF-in-COF molecular sieving membrane for selective hydrogen separation. Nat. Commun. 12 (1), 38.
Fan, D., Ozcan, A., Ramsahye, N.A., Maurin, G., Semino, R., 2022a. Putting Forward NUS-8-CO_2H/PIM-1 as a Mixed Matrix Membrane for CO_2 Capture. ACS Appl. Mater. Interfaces 14 (14), 16820–16829. doi:10.1021/acsami.2c00090.
Fan, D., Ozcan, A., Shekhah, O., Semino, R., Eddaoudi, M., Maurin, G., 2022b. Engineering MOF surface defects in mixed matrix membranes: an effective strategy to enhance MOF/polymer adhesion and control interfacial gas transport. J. Membr. Sci. Lett. 2 (2), 100029.
Fang, W., Liang, F., Cao, Z., Steinbach, F., Feldhoff, A., 2015. A mixed ionic and electronic conducting dual-phase membrane with high oxygen permeability. Angew. Chem. Int. Ed. 54, 4847–4850. doi:10.1002/anie.201411963.
Fang, M., He, Z., Merkel, T.C., Okamoto, Y., 2018. High-performance perfluorodioxolane copolymer membranes for gas separation with tailored selectivity enhancement. J. Mater. Chem. A 6 (2), 652–658. doi:10.1039/C7TA09047A.
Fang, X., Men, Y., Wu, F., Zhao, Q., Singh, R., Xiao, P., Du, T., Webley, P.A., 2019. Promoting CO_2 hydrogenation to methanol by incorporating adsorbents into catalysts: Effects of hydrotalcite. Chem. Eng. J. 378, 122052. doi:10.1016/j.cej.2019.122052.
Fang, M., Yi, N., Di, W., Wang, T., Wang, Q., 2020. Emission and control of flue gas pollutants in CO_2 chemical absorption system – A review. Int. J. Greenh. Gas Control 93. doi:10.1016/j.ijggc.2019.102904.
Fang, Q.X., Huang, W.Q., Wang, H.N., 2020. Role of additives in silica-supported polyethylenimine adsorbents for CO_2 adsorption. Mater. Res. Exp. 7 (3) 10.10882053-1591/ab80eb.
Farha, O.K., Yazaydin, A.O., Eryazici, I., Malliakas, C.D., Hauser, B.G., Kanatzidis, M.G., Nguyen, S.T., Snurr, R.Q., Hupp, J.T., 2010. De novo synthesis of a metal-organic framework material featuring ultrahigh surface area and gas storage capacities. Nat. Chem. 2 (11), 944–948. doi:10.1038/nchem.834.
Farmahini, A.H., Krishnamurthy, S., Friedrich, D., Brandani, S., Sarkisov, L., 2018. From crystal to adsorption column: challenges in multiscale computational screening of materials for adsorption separation processes. Ind. Eng. Chem. Res. 57 (45), 15491–15511. doi:10.1021/acs.iecr.8b03065.
Farooqui, A., Bose, A., Ferrero, D., Llorca, J., Santarelli, M., 2018. Techno-economic and exergetic assessment of an oxy-fuel power plant fueled by syngas produced by chemical looping CO_2 and H2O dissociation. J. CO_2 Util. 27, 500–517.
Fasihi, M., Efimova, O., Breyer, C., 2019. Techno-economic assessment of CO_2 direct air capture plants. J. Clean. Prod. 224, 957–980. doi:10.1016/j.jclepro.2019.03.086.
Favre, E., 2007. Carbon dioxide recovery from post-combustion processes: Can gas permeation membranes compete with absorption? J. Membr. Sci. 294 (1-2), 50–59. doi:10.1016/j.memsci.2007.02.007.
Fayaz, M., Sayari, A., 2017. Long-term effect of steam exposure on CO_2 capture performance of amine-grafted silica. ACS Appl. Mater. Interfaces 9 (50), 43747–43754. doi:10.1021/acsami.7b15463.
Fazlollahi, F., Bown, A., Ebrahimzadeh, E., Baxter, L.L., 2015. Design and analysis of the natural gas liquefaction optimization process- CCC-ES (energy storage of cryogenic carbon capture). Energy 90, 244–257. doi:10.1016/j.energy.2015.05.139.
Feng, D., Zhao, Y., Zhang, Y., Zhang, Z., Zhang, L., Gao, J., Sun, S., 2017. Synergetic effects of biochar structure and AAEM species on reactivity of H2O-activated biochar from cyclone air gasification. Int. J. Hydrogen Energy 42 (25), 16045–16053. doi:10.1016/j.ijhydene.2017.05.153.
Feng, S., Bu, M., Pang, J., Fan, W., Fan, L., Zhao, H., Yang, G., Guo, H., Kong, G., Sun, H., 2020. Hydrothermal stable ZIF-67 nanosheets via morphology regulation strategy to construct mixed-matrix membrane for gas separation. J. Membr. Sci. 593, 117404. doi:10.1016/j.memsci.2019.117404.
Fennell, P.S., Pacciani, R., Dennis, J.S., Davidson, J.F., Hayhurst, A.N., 2007. The effects of repeated cycles of calcination and carbonation on a variety of different limestones, as measured in a hot fluidized bed of sand. Energy Fuels 21 (4), 2072–2081. doi:10.1021/ef060506o.
Feron, P.H.M., Jansen, A.E., 2002. CO_2 separation with polyolefin membrane contactors and dedicated absorption liquids: performances and prospects. Sep. Purif. Technol. 27 (3), 231–242. doi:10.1016/S1383-5866 (01)00207-6.
Feron, P.H.M., Cousins, A., Jiang, K., Zhai, R., Garcia, M., 2020. An update of the benchmark post-combustion CO_2-capture technology. Fuel 273. doi:10.1016/j.fuel.2020.117776.
Ferreira, T.J., Ribeiro, R.P.P.L., Mota, J.P.B., Rebelo, L.s.P.N., Esperança, J.M.S.S., Esteves, I.A.A.C., 2019. Ionic liquid-impregnated metal–organic frameworks for CO_2/CH_4 separation. ACS Appl. Nano Mater. doi:10.1021/acsanm.9b01936.s001.
Figueroa, J.D., Fout, T., Plasynski, S., McIlvried, H., Srivastava, R.D., 2008. Advances in CO_2 capture technology—The U.S. department of energy's carbon sequestration program. Int. J. Greenh. Gas Control 2 (1), 9–20. doi:10.1016/s1750-5836 (07)00094-1.
Finsy, V., Ma, L., Alaerts, L., De Vos, D.E., Baron, G.V., Denayer, J.F.M., 2009. Separation of CO_2/CH4 mixtures with the MIL-53 (Al) metal–organic framework. Microporous Mesoporous Mater. 120 (3), 221–227. doi:10.1016/j.micromeso.2008.11.007.
Flores-Segura, H., Torres, L.A., 1997. Enthalpies of formation of primary, secondary, and tertiary amineborane adducts in tetrahydrofuran solution. Struct. Chem. 8.
Florio, C., Fiorentino, G., Corcelli, F., Ulgiati, S., Dumontet, S., Güsewell, J., Eltrop, L., 2019. A life cycle assessment of biomethane production from waste feedstock through different upgrading technologies, Energies.
Foong, S.Y., Liew, R.K., Yang, Y., Cheng, Y.W., Yek, P.N.Y., Wan Mahari, W.A., Lee, X.Y., Han, C.S., Vo, D.-V.N., Van Le, Q., Aghbashlo, M., Tabatabaei, M., Sonne, C., Peng, W., Lam, S.S., 2020. Valorization of biomass waste to engineered activated biochar by microwave pyrolysis: Progress, challenges, and future directions. Chem. Eng. J. 389, 124401. doi:10.1016/j.cej.2020.124401.
Forano, C., Costantino, U., Prévot, V., Gueho, C.T., 2013. Chapter 14.1 - layered double hydroxides (LDH). In: Bergaya, F., Lagaly, G. (Eds.), Developments in Clay Science. Elsevier, pp. 745–782. doi:10.1016/B978-0-08-098258-8.00025-0.
Forero, C., Gayán, P., García-Labiano, F., De Diego, L., Abad, A., Adánez, J., 2010. Effect of gas composition in chemical-looping combustion with copper-based oxygen carriers: fate of sulphur. Int. J. Greenh. Gas Control 4 (5), 762–770.
Forse, A.C., Milner, P.J., 2020. New chemistry for enhanced carbon capture: beyond ammonium carbamates. Chem. Sci. 12 (2), 508–516. doi:10.1039/d0sc06059c.
Forse, A.C., Milner, P.J., Lee, J.H., Redfearn, H.N., Oktawiec, J., Siegelman, R.L., Martell, J.D., Dinakar, B., Zasada, L.B., Gonzalez, M.I., Neaton, J.B., Long, J.R., Reimer, J.A., 2018. Elucidating CO_2 chemisorption in diamine-appended metal-organic frameworks. J. Am. Chem. Soc. 140 (51), 18016–18031. doi:10.1021/jacs.8b10203.
Fourati, M., Roig, V., Raynal, L., 2013. Liquid dispersion in packed columns: Experiments and numerical modeling. Chem. Eng. Sci. 100, 266–278. doi:10.1016/j.ces.2013.02.041.
Freeman, B.D., 1999. Basis of permeability/selectivity tradeoff relations in polymeric gas separation membranes. Macromolecules 32 (2), 375–380. doi:10.1021/MA9814548.
Friebe, S., Mundstock, A., Unruh, D., Renz, F., Caro, J., 2016. NH2-MIL-125 as membrane for carbon dioxide sequestration: Thin supported MOF layers contra Mixed-Matrix-Membranes. J. Membr. Sci. 516, 185–193. doi:10.1016/j.memsci.2016.06.015.
Frisch, H.L., 1970. "Diffusion in polymers" edited by J. Crank and G. S. Park, Academic Press, London and New York, 1968; 452 pg. 14 (6), 1657-1657. https://doi.org/10.1002/app.1970.070140623.
Fu, J., Das, S., Xing, G., Ben, T., Valtchev, V., Qiu, S., 2016. Fabrication of COF-MOF composite membranes and their highly selective separation of $H2/CO_2$. J. Am. Chem. Soc. 138 (24), 7673–7680.
Fu, K., Zhang, P., Wang, L., Huang, X., Fu, D., 2020. Viscosity of 2-ethylhexan-1-amine (EHA)-diglyme, EHA-triglyme and EHA-tetraglyme non-aqueous solutions and its effect on initial absorption rate. J. Mol. Liq. 302. doi:10.1016/j.molliq.2020.112518.
Fu, S., Angelidaki, I., Zhang, Y., 2021. In situ biogas upgrading by CO_2-to-CH4 bioconversion. Trends Biotechnol. 39 (4), 336–347. doi:10.1016/j.tibtech.2020.08.006.
Fujikawa, S., Selyanchyn, R., Kunitake, T., 2020. A new strategy for membrane-based direct air capture. Polym. J. 53, 111–119.

Fujikawa, S., Selyanchyn, R., Kunitake, T., 2021. A new strategy for membrane-based direct air capture. Polym. J. 53 (1), 111–119. doi:10.1038/s41428-020-00429-z.

Fujishiro, F., Fukasawa, K., Hashimoto, T., 2011. CO_2 absorption and desorption properties of single phase $Ba_2Fe_2O_5$ and analysis of their mechanism using thermodynamic calculation. J. Am. Ceramic Soc. 94 (11), 3675–3678. doi:10.1111/j.1551-2916.2011.04842.x.

Fulong, C.R.P., Liu, J., Pastore, V.J., Lin, H., Cook, T.R., 2018. Mixed-matrix materials using metal–organic polyhedra with enhanced compatibility for membrane gas separation. Dalton Trans. 47 (24), 7905–7915. doi:10.1039/C8DT00082D.

Furukawa, H., Yaghi, O.M., 2009. Storage of hydrogen, methane, and carbon dioxide in highly porous covalent organic frameworks for clean energy applications. J. Am. Chem. Soc. 131 (25), 8875–8883.

Furukawa, H., Ko, N., Go, Y.B., Aratani, N., Choi, S.B., Choi, E., Yazaydin, A.Ö., Snurr, R.Q., M, O.K., Kim, J., Yaghi, O.M., 2010. Ultrahigh porosity in_metal-organic frameworks. Science 329 (5990), 424–428.

Gómez-Garduño, N., Pfeiffer, H., 2019. Thermokinetic evaluation of iron addition on lithium metazirconate (Fe-Li_2ZrO_3) for enhancing carbon dioxide capture at high temperatures. Thermochim. Acta 673, 129–137. doi:10.1016/j.tca.2019.01.017.

Gaikwad, S., Kim, S.-J., Han, S., 2019. CO_2 capture using amine-functionalized bimetallic MIL-101 MOFs and their stability on exposure to humid air and acid gases. Microporous Mesoporous Mater. 277, 253–260. doi:10.1016/j.micromeso.2018.11.001.

Gaikwad, S., Kim, Y., Gaikwad, R., Han, S., 2021. Enhanced CO_2 capture capacity of amine-functionalized MOF-177 metal organic framework. J. Environ. Chem. Eng. 9 (4). doi:10.1016/j.jece.2021.105523.

Galindo, R., López-Delgado, A., Padilla, I., Yates, M., 2015. Synthesis and characterisation of hydrotalcites produced by an aluminium hazardous waste: a comparison between the use of ammonia and the use of triethanolamine. Appl. Clay Sci. 115, 115–123. doi:10.1016/j.clay.2015.07.032.

Galusnyak, S.C., Petrescu, L., Cormos, C.C., 2022. Environmental impact assessment of post-combustion CO_2 capture technologies applied to cement production plants. J. Environ. Manage. 320, 10. doi:10.1016/j.jenvman.2022.115908.

Galven, C., Fourquet, J.-L., Suard, E., Crosnier-Lopez, M.-P., Le Berre, F., 2010. Mechanism of a reversible CO_2 capture monitored by the layered perovskite $Li_2SrTa_2O_7$. Dalton Trans. 39 (17), 4191–4197. doi:10.1039/C002223N.

Gan, Q., Zou, Y., Rooney, D., Nancarrow, P., Thompson, J., Liang, L., Lewis, M., 2011. Theoretical and experimental correlations of gas dissolution, diffusion, and thermodynamic properties in determination of gas permeability and selectivity in supported ionic liquid membranes. Adv. Colloid Interface Sci. 164 (1), 45–55. doi:10.1016/j.cis.2011.01.005.

Ganapathy, H., Shooshtari, A., Dessiatoun, S., Alshehhi, M., Ohadi, M., 2014. Fluid flow and mass transfer characteristics of enhanced CO_2 capture in a minichannel reactor. Appl. Energy 119, 43–56. doi:10.1016/j.apenergy.2013.12.047.

Ganapathy, H., Shooshtari, A., Dessiatoun, S., Ohadi, M.M., Alshehhi, M., 2015. Hydrodynamics and mass transfer performance of a microreactor for enhanced gas separation processes. Chem. Eng. J. 266, 258–270. doi:10.1016/j.cej.2014.12.028.

Ganapathy, H., Steinmayer, S., Shooshtari, A., Dessiatoun, S., Ohadi, M.M., Alshehhi, M., 2016. Process intensification characteristics of a microreactor absorber for enhanced CO_2 capture. Appl. Energy 162, 416–427. doi:10.1016/j.apenergy.2015.10.010.

Gao, N., Li, J., Qi, B., Li, A., Duan, Y., Wang, Z., 2014. Thermal analysis and products distribution of dried sewage sludge pyrolysis. J. Analyt. Appl. Pyrol. 105, 43–48. doi:10.1016/j.jaap.2013.10.002.

Gao, J., Zhang, Y., Feng, D., Du, Q., Yu, M., Xie, M., Sun, L., Wu, S., 2015. A new technique of carbon capture by ammonia with the reinforced crystallization at low carbonized ratio and initial experimental research. Fuel Process. Technol. 135, 207–211. doi:10.1016/j.fuproc.2015.02.008.

Gao, H., Xu, B., Han, L., Luo, X., Liang, Z., 2017. Mass transfer performance and correlations for CO_2 absorption into aqueous blended of DEEA/MEA in a random packed column. AIChE J. 63 (7), 3048–3057. doi:10.1002/aic.15673.

Gao, H., Liu, S., Gao, G., Luo, X., Liang, Z., 2018. Hybrid behavior and mass transfer performance for absorption of CO_2 into aqueous DEEA/PZ solutions in a hollow fiber membrane contactor. Sep. Purif. Technol. 201, 291–300. doi:10.1016/j.seppur.2018.03.027.

Gao, Q., Li, X., Ning, G.-H., Xu, H.-S., Liu, C., Tian, B., Tang, W., Loh, K.P., 2018. Covalent organic framework with frustrated bonding network for enhanced carbon dioxide storage. Chem. Mater. 30 (5), 1762–1768.

Gao, W., Zhou, T., Gao, Y., Wang, Q., Lin, W., 2018. Study on MNO_3/NO_2 (M = Li, Na, and K)/MgO composites for intermediate-temperature CO_2 capture. Energy Fuels 33 (3), 1704–1712. doi:10.1021/acs.energyfuels.8b02749.

Gao, Y., Qiao, Z., Zhao, S., Wang, Z., Wang, J., 2018. In situ synthesis of polymer grafted ZIFs and application in mixed matrix membrane for CO_2 separation. J. Mater. Chem. A 6 (7), 3151–3161. doi:10.1039/C7TA10322K.

Gao, H., Huang, Y., Zhang, X., Bairq, Z., Huang, Y., Tontiwachwuthikul, P., Liang, Z., 2020. Catalytic performance and mechanism of SO42/ZrO2/SBA-15 catalyst for CO_2 desorption in CO_2-loaded monoethanolamine solution. Appl. Energy 259.

Gao, H., Huang, Y., Zhang, X., Bairq, Z.A.S., Huang, Y., Tontiwachwuthikul, P., Liang, Z., 2020. Catalytic performance and mechanism of SO42−/ZrO2/SBA-15 catalyst for CO_2 desorption in CO_2-loaded monoethanolamine solution. Appl. Energy 259. doi:10.1016/j.apenergy.2019.114179.

Gao, W., Liang, S., Wang, R., Jiang, Q., Zhang, Y., Zheng, Q., Xie, B., Toe, C.Y., Zhu, X., Wang, J., Huang, L., Gao, Y., Wang, Z., Jo, C., Wang, Q., Wang, L., Liu, Y., Louis, B., Scott, J., Roger, A.-C., Amal, R., Heh, H., Park, S.-E., 2020. Industrial carbon dioxide capture and utilization: state of the art and future challenges. Chem. Soc. Rev. 49 (23), 8584–8686. doi:10.1039/d0cs00025f.

Gao, W., Vasiliades, M.A., Damaskinos, C.M., Zhao, M., Fan, W., Wang, Q., Reina, T.R., Efstathiou, A.M., 2021. Molten salt-promoted MgO adsorbents for CO_2 capture: transient kinetic studies. Environ. Sci. Technol. 55 (8), 4513–4521. doi:10.1021/acs.est.0c08731.

Gao, Z., Liang, L., Zhang, X., Xu, P., Sun, J., 2021. Facile one-pot synthesis of Zn/Mg-MOF-74 with unsaturated coordination metal centers for efficient CO_2 adsorption and conversion to cyclic carbonates. ACS Appl. Mater. Interfaces 13 (51), 61334–61345. doi:10.1021/acsami.1c20878.

Gao, W., Xiao, J., Wang, Q., Li, S., Vasiliades, M.A., Huang, L., Gao, Y., Jiang, Q., Niu, Y., Zhang, B.J.A.M., 2021. Unravelling the mechanism of intermediate-temperature CO_2 interaction with molten NaNO3 salt promoted MgO. 2106677.

Gao, X., Wang, Z., Chen, T., Hu, L., Yang, S., Kawi, S., 2022a. State-of-art designs and synthesis of zeolite membranes for CO_2 capture. Carbon Cap. Sci. Technol. 5, 100073. doi:10.1016/j.ccst.2022.100073.

Gao, X., Yang, S., Hu, L., Cai, S., Wu, L., Kawi, S., 2022b. Carbonaceous materials as adsorbents for CO_2 capture: synthesis and modification. Carbon Cap. Sci. Technol. 3, 100039. doi:10.1016/j.ccst.2022.100039.

García-Labiano, F., de Diego, L.F., Gayan, P., Adanez, J., Abad, A., Dueso, C., 2009. Effect of fuel gas composition in chemical-looping combustion with Ni-based oxygen carriers. 1. Fate of sulfur. Ind. Eng. Chem. Res. 48 (5), 2499–2508.

García-Luna, S., Ortiz, C., Carro, A., Chacartegui, R., Pérez-Maqueda, L.A., 2022. Oxygen production routes assessment for oxy-fuel combustion. Energy 254 (September), 1–58. doi:10.1016/j.energy.2022.124303.

Garcia-Abuin, A., Gomez-Diaz, D., Navaza, J.M., Vidal-Tato, I., 2010. CO_2 capture by aqueous solutions of glucosamine in a bubble column reactor. Chem. Eng. J. 162 (1), 37–42. doi:10.1016/j.cej.2010.04.050.

Garcia-Fayos, J., Serra, J.M., Luiten-Olieman, M.W.J., Meulenberg, W.A., 2020. Gas separation ceramic membranes. Adv. Ceram. Energy Convers. Storage 321–385. doi:10.1016/B978-0-08-102726-4.00008-9.

Gargiulo, N., Peluso, A., Caputo, D., 2020. MOF-based adsorbents for atmospheric emission control: a review. Processes 8 (5). doi:10.3390/pr8050613.

Gaspar, J., Cormos, A.M., 2012. Dynamic modeling and absorption capacity assessment of CO_2 capture process. Int. J. Greenh. Gas Control 8, 45–55. doi:10.1016/j.ijggc.2012.01.016.

Gaultois, M.W., Dunstan, M.T., Bateson, A.W., Chan, M.S.C., Grey, C.P., 2018. Screening and characterization of ternary oxides for high-temperature carbon capture. Chem. Mater. 30 (8), 2535–2543. doi:10.1021/acs.chemmater.7b04679.

Gawande, M.B., Monga, Y., Zboril, R., Sharma, R.K., 2015. Silica-decorated magnetic nanocomposites for catalytic applications. Coord. Chem. Rev. 288, 118–143. doi:10.1016/j.ccr.2015.01.001.

Gazzani, M., Romano, M.C., Manzolini, G., 2015. CO_2 capture in integrated steelworks by commercial-ready technologies and SEWGS process. Int. J. Greenh. Gas Control 41, 249–267. doi:10.1016/j.ijggc.2015.07.012.

Gbadago, D.Q., Oh, H.T., Oh, D.H., Lee, C.H., Oh, M., 2020. CFD simulation of a packed bed industrial absorber with interbed liquid distributors. Int. J. Greenh. Gas Control 95. doi:10.1016/j.ijggc.2020.102983, 102983-102983.

Ge, L., Wei, J., Geng, L., Chen, S., Liao, L., 2021. Amine-bifunctionalized ZSM-5/SBA-16 composite for CO_2 adsorption. J. Porous Mater. 29 (1), 19–31. doi:10.1007/s10934-021-01146-5.

Gebald, C., Wurzbacher, J.A., Borgschulte, A., Zimmermann, T., Steinfeld, A., 2014. Single-component and binary CO_2 and H2O adsorption of amine-functionalized cellulose. Environ. Sci. Technol. 48 (4), 2497–2504. doi:10.1021/es404430g.

Gelles, T., Lawson, S., Rownaghi, A.A., Rezaei, F., 2019. Recent advances in development of amine functionalized adsorbents for CO_2 capture. Adsorption 26 (1), 5–50. doi:10.1007/s10450-019-00151-0.

Geng, S.Y., Wei, J.Y., Jonasson, S., Hedlund, J., Oksman, K., 2020. Multifunctional carbon aerogels with hierarchical anisotropic structure derived from lignin and cellulose nanofibers for CO_2 capture and energy storage. ACS Appl. Mater. Interfaces 12 (6), 7432–7441. doi:10.1021/acsami.9b19955.

Gentile, G., Bonalumi, D., Pieterse, J.A.Z., Sebastiani, F., Lucking, L., Manzolini, G., 2022. Techno-economic assessment of the FReSMe technology for CO_2 emissions mitigation and methanol production from steel plants. J. CO_2 Util. 56, 101852. doi:10.1016/j.jcou.2021.101852.

Ghahramaninezhad, M., Soleimani, B., Niknam Shahrak, M., 2018. A simple and novel protocol for Li-trapping with a POM/MOF nano-composite as a new adsorbent for CO_2 uptake. New J. Chem. 42 (6), 4639–4645. doi:10.1039/c8nj00274f.

Ghanbari, S., Kamath, G., 2019. Dynamic simulation and mass transfer study of carbon dioxide capture using biochar and MgO-impregnated activated carbon in a swing adsorption process. Energy Fuels 33 (6), 5452–5463. doi:10.1021/acs.energyfuels.9b00923.

Gholidoust, A., Atkinson, J.D., Hashisho, Z., 2017. Enhancing CO_2 adsorption via amine-impregnated activated carbon from oil sands coke. Energy Fuels 31 (2), 1756–1763. doi:10.1021/acs.energyfuels.6b02800.

Giannaris, S., Janowczyk, D., Ruffini, J., Hill, K., Jacobs, B., Bruce, C., Feng, Y., Srisang, W., 2021. SaskPower's Boundary Dam Unit 3 Carbon Capture Facility - The Journey to Achieving Reliability. Social Science Electronic Publishing.

Gibon, T., Wood, R., Arvesen, A., Bergesen, J.D., Suh, S., Hertwich, E.G., 2015. A methodology for integrated, multiregional life cycle assessment scenarios under large-scale technological change. Environ. Sci. Technol. 49 (18), 11218–11226. doi:10.1021/acs.est.5b01558.

Gibson, J.A.A., Gromov, A.V., Brandani, S., Campbell, E.E.B., 2015. The effect of pore structure on the CO_2 adsorption efficiency of polyamine impregnated porous carbons. Microporous Mesoporous Mater. 208, 129–139. doi:10.1016/j.micromeso.2015.01.044.

Gielen, D., Taibi, E., Miranda, R., 2019. Hydrogen: a renewable energy perspective.

Gil, A., Arrieta, E., Vicente, M.A., Korili, S.A., 2018. Synthesis and CO_2 adsorption properties of hydrotalcite-like compounds prepared from aluminum saline slag wastes. Chem. Eng. J. 334, 1341–1350. doi:10.1016/j.cej.2017.11.100.

Giordano, L., Roizard, D., Bounaceur, R., Favre, E., 2017. Energy penalty of a single stage gas permeation process for CO_2 capture in post-combustion: a rigorous parametric analysis of temperature, humidity and membrane performances. Energy Procedia 114, 636–641. doi:10.1016/j.egypro.2017.03.1206.

Giordano, L., Roizard, D., Favre, E., 2018. Life cycle assessment of post-combustion CO 2 capture: A comparison between membrane separation and chemical absorption processes. Int. J. Greenh. Gas Control 68, 146–163. doi:10.1016/j.ijggc.2017.11.008.

Glasser, L., Jenkins, H.D.B., 2000. Lattice energies and unit cell volumes of complex ionic solids. J. Am. Chem. Soc. 122 (4), 632–638.

Gnanasekaran, L., Priya, A.K., Thanigaivel, S., Hoang, T.K.A., Soto-Moscoso, M., 2022. The conversion of biomass to fuels via cutting-edge technologies: Explorations from natural utilization systems. Fuel 331. doi:10.1016/j.fuel.2022.125668.

Goeppert, A., Czaun, M., May, R.B., Prakash, G.K., Olah, G.A., Narayanan, S.R., 2011. Carbon dioxide capture from the air using a polyamine based regenerable solid adsorbent. J. Am. Chem. Soc. 133 (50), 20164–20167. doi:10.1021/ja2100005.

Goeppert, A., Czaun, M., Surya Prakash, G.K., Olah, G.A., 2012. Air as the renewable carbon source of the future: an overview of CO_2 capture from the atmosphere. Energy Environ. Sci. 5 (7), 7833–7853. doi:10.1039/C2EE21586A.

Goff, F., Lackner, K., 1998. Carbon dioxide sequestering using ultramafic rocks. Environ. Geosci. 5 (3), 89–101.

Gomez, A., Jayakumar, A., Mahinpey, N., 2016. Experimental verification of the reaction mechanism of solid K_2CO_3 during postcombustion CO_2 capture. Ind. Eng. Chem. Res. 55 (41), 11022–11028. doi:10.1021/acs.iecr.6b02916.

Gonçalves, C., Ferreira, N., Lourenço, L., 2021. Production of low molecular weight chitosan and chitooligosaccharides (COS): A review. Polymers 13 (15). doi:10.3390/polym13152466.

González, B., Blamey, J., McBride-Wright, M., Carter, N., Dugwell, D., Fennell, P., Abanades, J.C., 2011. Calcium looping for CO_2 capture: sorbent enhancement through doping. Energy Procedia 4, 402–409. doi:10.1016/j.egypro.2011.01.068.

González, A.S., Plaza, M.G., Rubiera, F., Pevida, C., 2013. Sustainable biomass-based carbon adsorbents for post-combustion CO_2 capture. Chem. Eng. J. 230, 456–465. doi:10.1016/j.cej.2013.06.118.

Gopan, A., Kumfer, B.M., Phillips, J., Thimsen, D., Smith, R., Axelbaum, R.L., 2014. Process design and performance analysis of a staged, pressurized oxy-combustion (SPOC) power plant for carbon capture. Appl. Energy 125, 179–188. doi:10.1016/j.apenergy.2014.03.032.

Gopan, A., Verma, P., Yang, Z., Axelbaum, R.L., 2020. Quantitative analysis of the impact of flue gas recirculation on the efficiency of oxy-coal power plants. Int. J. Greenh. Gas Control 95, 102936. doi:10.1016/j.ijggc.2019.102936.

Grande, C.A., Rodrigues, A.E., 2008. Electric Swing Adsorption for CO_2 removal from flue gases. Int. J. Greenh. Gas Control 2 (2), 194–202. doi:10.1016/S1750-5836(07)00116-8.

Grande, C.A., Ribeiro, R.P.L., Oliveira, E.L.G., Rodrigues, A.E., 2009. Electric swing adsorption as emerging CO_2 capture technique. Energy Procedia 1 (1), 1219–1225. doi:10.1016/j.egypro.2009.01.160.

Grande, C.A., Poplow, F., Rodrigues, A.E., 2010. Vacuum pressure swing adsorption to produce polymer-grade propylene. Sep. Sci. Technol. 45 (9), 1252–1259.

Grant, T., Anderson, C., Hooper, B., 2014. Comparative life cycle assessment of potassium carbonate and monoethanolamine solvents for CO 2 capture from post combustion flue gases. Int. J. Greenh. Gas Control 28, 35–44. doi:10.1016/j.ijggc.2014.06.020.

Grasa, G.S., Abanades, J.C., 2006. CO_2 capture capacity of CaO in long series of carbonation/calcination cycles. Ind. Eng. Chem. Res. 45 (26), 8846–8851. doi:10.1021/ie0606946.

Grasa, G.S., Alonso, M., Abanades, J.C., 2008. Sulfation of CaO particles in a carbonation/calcination loop to capture CO_2. Ind. Eng. Chem. Res. 47 (5), 1630–1635. doi:10.1021/ie070937+.

Grosser, K., Carbonell, R.G., Sundaresan, S., 1988. Onset of pulsing in two-phase cocurrent downflow through a packed bed. AIChE J. 34 (11), 1850–1860. doi:10.1002/aic.690341111.

Gu, F., et al., 2004. CFD simulation of liquid film flow on inclined plates. Chemical Engineering and Technology 27 (10), 1099–1104.

Gudena, K., Rangaiah, G.P., Lakshminarayanan, S., 2013. HiGee stripper-membrane system for decentralized bioethanol recovery and purification. Ind. Eng. Chem. Res. 52 (12), 4572–4585. doi:10.1021/ie302557f.

Gunjal, P.R., Kashid, M.N., Ranade, V.V., Chaudhari, R.V., 2005. Hydrodynamics of trickle-bed reactors: experiments and CFD modeling. Ind. Eng. Chem. Res. 44 (16), 6278–6294. doi:10.1021/ie0491037.

Guo, H., Zhu, G., Li, H., Zou, X., Yin, X., Yang, W., Qiu, S., Xu, R., 2006. Hierarchical growth of large-scale ordered zeolite silicalite-1 membranes with high permeability and selectivity for recycling CO_2. Angew. Chem. Int. Ed. 45 (42), 7053–7056.

Guo, C., Chen, S., Zhang, Y., Wang, G., 2014. Solubility of CO_2 in Nonaqueous Absorption System of 2- (2-Aminoethylamine)ethanol + Benzyl Alcohol. J. Chem. Eng. Data 59 (6), 1796–1801. doi:10.1021/je401028g.

Guo, X., Huang, H., Ban, Y., Yang, Q., Xiao, Y., Li, Y., Yang, W., Zhong, C., 2015. Mixed matrix membranes incorporated with amine-functionalized titanium-based metal-organic framework for CO_2/CH4 separation. J. Membr. Sci. 478, 130–139. doi:10.1016/j.memsci.2015.01.007.

Guo, T.-Y., et al., 2016. Computational Fluid Dynamics Analysis of the Micromixing Efficiency in a Rotating-Packed-Bed Reactor. Ind. Eng. Chem. Res. 55 (17), 4856–4866.

Guo, T.-Y., Cheng, K.-P., Wen, L.-X., Andersson, R., Chen, J.-F., 2017. Three-dimensional simulation on liquid flow in a rotating packed bed reactor. Ind. Eng. Chem. Res. 56 (28), 8169–8179. doi:10.1021/acs.iecr.7b01759.

Guo, T.X., Ma, N., Pan, Y.F., Bedane, A.H., Xiao, H.N., Eic, M., Du, Y.R., 2018. Characteristics of CO_2 adsorption on biochar derived from biomass pyrolysis in molten salt. Can. J. Chem. Eng. 96 (11), 2352–2360. doi:10.1002/cjce.23153.

Guo, Y.F., Zhao, C.W., Sun, J., Li, W.L., Lu, P., 2018. Facile synthesis of silica aerogel supported K2CO3 sorbents with enhanced CO_2 capture capacity for ultra-dilute flue gas treatment. Fuel 215, 735–743. doi:10.1016/j.fuel.2017.11.113.

Guo, Y., Zhao, C., Sun, J., Li, W., Lu, P., 2018. Facile synthesis of silica aerogel supported K_2CO_3 sorbents with enhanced CO_2 capture capacity for ultra-dilute flue gas treatment. Fuel 215, 735–743. doi:10.1016/j.fuel.2017.11.113.

Guo, X., Qiao, Z., Liu, D., Zhong, C., 2019. Mixed-matrix membranes for CO_2 separation: role of the third component. J. Mater. Chem. A 7 (43), 24738–24759. doi:10.1039/C9TA09012F.

Guo, X.Y., Qiao, Z.H., Liu, D.H., Zhong, C.L., 2019. Mixed-matrix membranes for CO_2 separation: role of the third component. J. Mater. Chem. A 7 (43), 24738–24759. doi:10.1039/c9ta09012f.

Guo, W., Mahurin, S.M., Wang, S., Meyer, H.M., Luo, H., Hu, X., Jiang, D.-e., Dai, S., 2020. Ion-gated carbon molecular sieve gas separation membranes. J. Membr. Sci. 604. doi:10.1016/j.memsci.2020.118013.

Guo, X., Xu, S., Sun, Y., Qiao, Z., Huang, H., Zhong, C., 2021. Metal-organic polyhedron membranes for molecular separation. J. Membr. Sci. 632, 119354. doi:10.1016/j.memsci.2021.119354.

Guo, Y., Hu, G., Chen, K., Guo, J., Webley, P.A., Li, G.K., 2021. Capture of dilute methane with a novel dynamic-feed dual-reflux pressure swing adsorption process. AIChE J. 68, e17390. doi:10.1002/aic.17390.

Guo, F., Li, D., Ding, R., Gao, J., Ruan, X., Jiang, X., He, G., Xiao, W., 2022. Constructing MOF-doped two-dimensional composite material ZIF-90@C3N4 mixed matrix membranes for CO_2/N_2 separation. Sep. Purif. Technol. 280. doi:10.1016/j.seppur.2021.119803.

Guo, H., Cui, J., Li, J., 2022. Biomass power generation in China: status, policies and recommendations. Energy Rep. 8, 687–696. doi:10.1016/j.egyr.2022.08.072.

Guo, S., Li, Y., Wang, Y., Wang, L., Sun, Y., Liu, L., 2022. Recent advances in biochar-based adsorbents for CO_2 capture. Carbon Cap. Sci. Technol., 100059.

Guo, W., Tran, T.N., Mondal, H., Schaefer, S., Huang, L., Lin, H., 2022. Superior CO_2/N_2 separation performance of highly branched Poly (1,3 dioxolane) plasticized by polyethylene glycol. J. Membr. Sci. 648, 120352. doi:10.1016/j.memsci.2022.120352.

Gupta, S., Li, L., 2022. The potential of machine learning for enhancing CO_2 sequestration, storage, transportation, and utilization-based processes: a brief perspective. JOM 74 (2), 414–428. doi:10.1007/s11837-021-05079-x.

Gupta, S., Adams, J.J., Wilson, J.R., Eddings, E.G., Mahapatra, M.K., Singh, P., 2016. Performance and post-test characterization of an OTM system in an experimental coal gasifier. Appl. Energy 165, 72–80. doi:10.1016/J.APENERGY.2015.12.077.

Gutierrez-Ortega, A., Nomen, R., Sempere, J., Parra, J.B., Montes-Morán, M.A., Gonzalez-Olmos, R., 2022. A fast methodology to rank adsorbents for CO_2 capture with temperature swing adsorption. Chem. Eng. J. 435. doi:10.1016/j.cej.2022.134703.

Guyomard-Lack, A., Buchtová, N., Humbert, B., Le Bideau, J., 2015. Ion segregation in an ionic liquid confined within chitosan based chemical ionogels. Phys. Chem. Chem. Phys. 17 (37), 23947–23951. doi:10.1039/C5CP04198H.

Hägg, M.B., Lindbråthen, A., He, X., Nodeland, S.G., Cantero, T., 2017. Pilot demonstration-reporting on CO_2 capture from a cement plant using hollow fiber process. Energy Procedia 114, 6150–6165. doi:10.1016/j.egypro.2017.03.1752.

H, H., 2003. Assessing the Feasibility of Capturing CO_2 from the Air. Massachusetts Institute of Technology, Laboratory for Energy and the Environment Publication No. LFEE 2.

Haase, F., Gottschling, K., Stegbauer, L., Germann, L., Gutzler, R., Duppel, V., Vyas, V., Kern, K., Dinnebier, R., Lotsch, B., 2017. Tuning the stacking behaviour of a 2D covalent organic framework through non-covalent interactions. Mater. Chem. Front. 1 (7), 1354–1361.

Haddad, S., Rivera-Tinoco, R., Bouallou, C., 2019. Modelling of CO_2 frost formation and growth on a flat plate. Chem. Eng. Trans. doi:10.3303/cet1976112.

Haghpanah, R., Majumder, A., Nilam, R., Rajendran, A., Farooq, S., Karimi, I.A., Amanullah, M., 2013. Multiobjective optimization of a four-step adsorption process for post-combustion CO_2 capture via finite volume simulation. Ind. Eng. Chem. Res. 52 (11), 4249–4265. doi:10.1021/ie302658y.

Haghshenas Fard, M., et al., 2007. CFD Simulation of Mass Transfer Efficiency and Pressure Drop in a Structured Packed Distillation Column. Chemical Engineering & Technology 30 (7), 854–861.

Hahn, M.W., Jelic, J., Berger, E., Reuter, K., Jentys, A., Lercher, J.A., 2016. Role of amine functionality for CO_2 chemisorption on silica. J. Phys. Chem. B 120 (8), 1988–1995. doi:10.1021/acs.jpcb.5b10012.

Haizhou, Lin, Hui, Yang, Haizhong, Luo, Aiguo, Pei, Mengxiang, F., 2019. Research progress on amine absorbent for CO_2 capture from flue gas. South. Energy Construct. 6 (01), 16–21.

Halabi, M.H., de Croon, M.H.J.M., van der Schaaf, J., Cobden, P.D., Schouten, J.C., 2012. High capacity potassium-promoted hydrotalcite for CO_2 capture in H2 production. Int. J. Hydrogen Energy 37 (5), 4516–4525. doi:10.1016/j.ijhydene.2011.12.003.

Haldar, R., Heinke, L., Woll, C., 2019. Advanced photoresponsive materials using the metal-organic framework approach. Adv. Mater., e1905227 doi:10.1002/adma.201905227.

Halder, K., Neumann, S., Bengtson, G., Khan, M.M., Filiz, V., Abetz, V., 2018. Polymers of intrinsic microporosity postmodified by vinyl groups for membrane applications. Macromolecules 51 (18), 7309–7319. doi:10.1021/acs.macromol.8b01252.

Hamm, J.B.S., Ambrosi, A., Griebeler, J.G., Marcilio, N.R., Tessaro, I.C., Pollo, L.D., 2017. Recent advances in the development of supported carbon membranes for gas separation. Int. J. Hydrogen Energy 42 (39), 24830–24845. doi:10.1016/j.ijhydene.2017.08.071.

Hamon, L., Jolimaitre, E., Pirngruber, G.D., 2010. CO_2 and CH4 separation by adsorption using Cu-BTC metal-organic_framework. Ind. Eng. Chem. Res. 49, 7497–7503.

Han, Y., Ho, W.S.W., 2018. Recent advances in polymeric membranes for CO_2 capture. Chin. J. Chem. Eng. 26 (11), 2238–2254. doi:10.1016/j.cjche.2018.07.010.

Han, Y., Ho, W.S.W., 2020. Recent advances in polymeric facilitated transport membranes for carbon dioxide separation and hydrogen purification. J. Polym. Sci. 58 (18), 2435–2449. doi:10.1002/pol.20200187.
Han, Y., Ho, W.S.W., 2021a. Facilitated transport membranes for H2 purification from coal-derived syngas: A techno-economic analysis. J. Membr. Sci. 636, 119549. doi:10.1016/j.memsci.2021.119549.
Han, Y., Ho, W.S.W., 2021b. Polymeric membranes for CO_2 separation and capture. J. Membr. Sci. 628, 119244. doi:10.1016/j.memsci.2021.119244.
Han, Y., Ho, W.S.W., 2022. Mitigated carrier saturation of facilitated transport membranes for decarbonizing dilute CO_2 sources: An experimental and techno-economic study. J. Membr. Sci. Lett. 2 (1), 100014. doi:10.1016/j.memlet.2022.100014.
Han, A.-J., He, H.-Y., Guo, J., Yu, H., Huang, Y.-F., Long, Y.-C., 2005. Studies on structure and acid–base properties of high silica MFI-type zeolite modified with methylamine. Microporous Mesoporous Mater. 79 (1-3), 177–184.
Han, S.S., Jung, D.-H., Heo, J., 2013. Interpenetration of metal organic frameworks for carbon dioxide capture and hydrogen purification: Good or bad? J. Phys. Chem. C 117 (1), 71–77.
Han, S.J., Bang, Y., Kwon, H.J., Lee, H.C., Hiremath, V., Song, I.K., Seo, J.G., 2014. Elevated temperature CO_2 capture on nano-structured MgO-Al2O3 aerogel: Effect of Mg/Al molar ratio. Chem. Eng. J. 242, 357–363. doi:10.1016/j.cej.2013.12.092.
Han, J., Du, Z., Zou, W., Li, H., Zhang, C., 2015. Moisture-responsive hydrogel impregnated in porous polymer foam as CO_2 adsorbent in high-humidity flue gas. Ind. Eng. Chem. Res. 54 (31), 7623–7631. doi:10.1021/acs.iecr.5b01305.
Han, Y., Wu, D., Ho, W.S.W., 2018. Nanotube-reinforced facilitated transport membrane for CO_2/N_2 separation with vacuum operation. J. Membr. Sci. 567, 261–271. doi:10.1016/j.memsci.2018.08.061.
Han, Y., Salim, W., Chen, K.K., Wu, D., Ho, W.S.W., 2019a. Field trial of spiral-wound facilitated transport membrane module for CO_2 capture from flue gas. J. Membr. Sci. 575, 242–251. doi:10.1016/j.memsci.2019.01.024.
Han, Y., Wu, D., Ho, W.S.W., 2019b. Simultaneous effects of temperature and vacuum and feed pressures on facilitated transport membrane for CO_2/N_2 separation. J. Membr. Sci. 573, 476–484. doi:10.1016/j.memsci.2018.12.028.
Han, Y., Wu, D., Ho, W.S.W., 2019c. Simultaneous effects of temperature and vacuum and feed pressures on facilitated transport membrane for CO_2/N_2 separation. J. Membr. Sci. 573, 476–484.
Han, Y., Yang, Y., Ho, W.S.W., 2020. Recent progress in the engineering of polymeric membranes for CO_2 capture from flue gas. Membranes (Basel) 10 (11). doi:10.3390/membranes10110365.
Han, Y., Tian, M., Wang, C., Kang, Y., Kang, L., Su, Y., Huang, C., Zong, T., Lin, J., Hou, B., Pan, X., Wang, X., 2021. Highly active and anticoke Ni/CeO2 with ultralow ni loading in chemical looping dry reforming via the strong metal–support interaction. ACS Sustain. Chem. Eng. 9 (51), 17276–17288. doi:10.1021/acssuschemeng.1c06079.
Han, N., Shen, Z., Zhao, X., Chen, R., Thakur, V.K., 2022. Perovskite oxides for oxygen transport: Chemistry and material horizons. Sci. Total Environ. 806, 151213. doi:10.1016/J.SCITOTENV.2021.151213.
Han, R., Wang, Y., Xing, S., Pang, C.H., Hao, Y., Song, C.F., Liu, Q.L., 2022. Progress in reducing calcination reaction temperature of Calcium-Looping CO_2 capture technology: a critical review. Chem. Eng. J. 450, 15. doi:10.1016/j.cej.2022.137952.
Hanak, D.P., Anthony, E.J., Manovic, V., 2015a. A review of developments in pilot-plant testing and modelling of calcium looping process for CO_2 capture from power generation systems. Energy Environ. Sci. 8 (8), 2199–2249. doi:10.1039/C5EE01228G.
Hanak, D.P., Biliyok, C., Manovic, V., 2015b. Rate-based model development, validation and analysis of chilled ammonia process as an alternative CO_2 capture technology for coal-fired power plants. Int. J. Greenh. Gas Control 34, 52–62. doi:10.1016/j.ijggc.2014.12.013.
Hanioka, S., Maruyama, T., Sotani, T., Teramoto, M., Matsuyama, H., Nakashima, K., Hanaki, M., Kubota, F., Goto, M.J., 2008. CO_2 separation facilitated by task-specific ionic liquids using a supported liquid membrane. J. Membr. Sci. 314 (1-2), 1-4.
Harada, T., Hatton, T.A., 2015. Colloidal nanoclusters of MgO coated with alkali metal nitrates/nitrites for rapid, high capacity CO_2 capture at moderate temperature. Chem. Mater. 27 (23), 8153–8161. doi:10.1021/acs.chemmater.5b03904.
Harada, T., Hatton, T.A., 2017. Tri-lithium borate (Li3BO3); a new highly regenerable high capacity CO_2 adsorbent at intermediate temperature. J. Mater. Chem. A 5 (42), 22224–22233. doi:10.1039/C7TA06167F.
Harada, T., Simeon, F., Hamad, E.Z., Hatton, T.A., 2015. Alkali metal nitrate-promoted high-capacity MgO adsorbents for regenerable CO_2 capture at moderate temperatures. Chem. Mater. 27 (6), 1943–1949. doi:10.1021/cm503295g.
Harami, H.R., Fini, F.R., Rezakazemi, M., Shirazian, S., 2019. Sorption in mixed matrix membranes: experimental and molecular dynamic simulation and grand canonical Monte Carlo method. J. Mol. Liq. 282, 566–576. doi:10.1016/j.molliq.2019.03.047.
Haroun, Y., Raynal, L., Legendre, D., 2012. Mass transfer and liquid hold-up determination in structured packing by CFD. Chem. Eng. Sci. 75, 342–348.
Harrison, D.P., 2008. Sorption-enhanced hydrogen production: a review. Ind. Eng. Chem. Res. 47 (17), 6486–6501. doi:10.1021/ie800298z.
Harun, N., Douglas, P.L., Ricardez-Sandoval, L., Croiset, E., 2011. Dynamic simulation of MEA absorption processes for CO_2 capture from fossil fuel power plant. Energy Procedia 1478–1485.
Hasan, M.M.F., First, E.L., Floudas, C.A., 2013. Cost-effective CO_2 capture based on in silico screening of zeolites and process optimization. Phys. Chem. Chem. Phys. 15 (40), 17601–17618. doi:10.1039/c3cp53627k.
Haseli, Y., 2021. Approximate relations for optimum turbine operating parameters in allam cycle. J. Eng. Gas Turbines Power 143 (6), 064501.
Hashemi, S.E., Sarker, S., Lien, K.M., Schnell, S.K., Austbø, B., 2019. Cryogenic vs. absorption biogas upgrading in liquefied biomethane production – An energy efficiency analysis. Fuel 245, 294–304. doi:10.1016/j.fuel.2019.01.172.
Hashemi, S.M., Sedghkerdar, M.H., Mahinpey, N., 2022. Calcium looping carbon capture: progress and prospects. Can. J. Chem. Eng. 100 (9), 2140–2171. doi:10.1002/cjce.24480.
Hasib-ur-Rahman, M., Larachi, F., 2013. Kinetic behavior of carbon dioxide absorption in diethanolamine/ionic-liquid emulsions. Sep. Purif. Technol. 118, 757–761. doi:10.1016/j.seppur.2013.08.027.
Hasib-ur-Rahman, M., Siaj, M., Larachi, F., 2012. CO_2 capture in alkanolamine/room-temperature ionic liquid emulsions: A viable approach with carbamate crystallization and curbed corrosion behavior. Int. J. Greenh. Gas Control 6, 246–252. doi:10.1016/j.ijggc.2011.10.014.
Hassan, M.M., Ruthven, D.M., Raghavan, N.S., 1986. Air separation by pressure swing adsorption on a carbon molecular sieve. Chem. Eng. Sci. 41 (5), 1333–1343. doi:10.1016/0009-2509 (86)87106-8.
Hassanlouei, R.N., Pelalak, R., Daraei, A., 2013. Wettability study in CO_2 capture from flue gas using nano porous membrane contactors. Int. J. Greenh. Gas Control 16, 233–240. doi:10.1016/j.ijggc.2013.03.018.
Hazazi, K., Ma, X., Wang, Y., Ogieglo, W., Alhazmi, A., Han, Y., Pinnau, I., 2019. Ultra-selective carbon molecular sieve membranes for natural gas separations based on a carbon-rich intrinsically microporous polyimide precursor. J. Membr. Sci. 585, 1–9. doi:10.1016/j.memsci.2019.05.020.
He, X., Hägg, M.-B., 2011. Hollow fiber carbon membranes: investigations for CO_2 capture. J. Membr. Sci. 378 (1-2), 1–9. doi:10.1016/j.memsci.2010.10.070.
He, X., Arvid Lie, J., Sheridan, E., Hägg, M.-B., 2009. CO_2 capture by hollow fibre carbon membranes: Experiments and process simulations. Energy Procedia 1 (1), 261–268. doi:10.1016/j.egypro.2009.01.037.
He, F., Li, X., Zhao, K., Huang, Z., Wei, G., Li, H., 2013. The use of La1−xSrxFeO3 perovskite-type oxides as oxygen carriers in chemical-looping reforming of methane. Fuel 108, 465–473. doi:10.1016/j.fuel.2012.11.035.
He, D., Shao, Y., Qin, C., Pu, G., Ran, J., Zhang, L., 2016. Understanding the sulfation pattern of CaO-based sorbents in a novel process for sequential CO_2 and SO_2 capture. Ind. Eng. Chem. Res. 55 (39), 10251–10262.
He, X., Lindbråthen, A., Kim, T.-J., Hägg, M.-B., 2017a. Pilot testing on fixed-site-carrier membranes for CO_2 capture from flue gas. Int. J. Greenh. Gas Control 64, 323–332. doi:10.1016/j.ijggc.2017.08.007.
He, X., Lindbråthen, A., Kim, T.-J., Hägg, M.-B., 2017b. Pilot testing on fixed-site-carrier membranes for CO 2 capture from flue gas. Int. J. Greenh. Gas Control 64, 323–332. doi:10.1016/j.ijggc.2017.08.007.
He, R., Cong, S., Wang, J., Liu, J., Zhang, Y., 2019. Porous graphene oxide/porous organic polymer hybrid nanosheets functionalized mixed matrix membrane for efficient CO_2 capture. ACS Appl. Mater. Interfaces 11 (4), 4338–4344. doi:10.1021/acsami.8b17599.
He, S., Jiang, X., Li, S., Ran, F., Long, J., Shao, L., 2020. Intermediate thermal manipulation of polymers of intrinsic microporous (PIMs) membranes for gas separations. AIChE J. 66 (10), e16543.
He, D., Gong, H., Chen, Y., Jiao, Z., Liu, Y., Zhang, X., Qin, C., Yin, H., 2021. Experimental and density functional theory study of the synergistic effect between steam and SO2 on CO_2 capture of calcium-based sorbents. Fuel 295, 120634.
He, X., Chen, D., Liang, Z., Yang, F., 2022. Insight and comparison of energy-efficient membrane processes for CO_2 capture from flue gases in power plant and energy-intensive industry. Carbon Cap. Sci. Technol. 2. doi:10.1016/j.ccst.2021.100020.
He, X., 2021. Polyvinylamine-based facilitated transport membranes for post-combustion CO_2 capture: challenges and perspectives from materials to processes. Engineering 7 (1), 124–131. doi:10.1016/j.eng.2020.11.001.
Healey, K., Liang, W., Southon, P.D., Church, T.L., D'Alessandro, D.M., 2016. Photoresponsive spiropyran-functionalised MOF-808: postsynthetic incorporation and light dependent gas adsorption properties. J. Mater. Chem. A 4 (28), 10816–10819. doi:10.1039/c6ta04160d.
Hecht, E.S., Shaddix, C.R., Geier, M., Molina, A., Haynes, B.S., 2012. Effect of CO 2 and steam gasification reactions on the oxy-combustion of pulverized coal char. Combust. Flame 159 (11), 3437–3447.
Hedin, N., Andersson, L., Bergström, L., Yan, J., 2013. Adsorbents for the post-combustion capture of CO_2 using rapid temperature swing or vacuum swing adsorption. Appl. Energy 104, 418–433. doi:10.1016/j.apenergy.2012.11.034.
Hefti, M., Mazzotti, M., 2018. Postcombustion CO_2 capture from wet flue gas by temperature swing adsorption. Ind. Eng. Chem. Res. 57, 15542–15555. doi:10.1021/acs.iecr.8b03580.
Heinke, L., Wöll, C., 2019. Surface-mounted metal–organic frameworks: crystalline and porous molecular assemblies for fundamental insights and advanced applications. Adv. Mater. 31 (26). doi:10.1002/adma.201806324.
Heldebrant, D.J., Koech, P.K., Yonker, C.R., 2010. A reversible zwitterionic SO2-binding organic liquid. Energy Environ. Sci. 3 (1), 111–113. doi:10.1039/b916550a.
Heldebrant, D.J., Koech, P.K., Rousseau, R., Glezakou, V.-A., Cantu, D., Malhotra, D., Zheng, F., Whyatt, G., Freeman, C.J., Bearden, M.D., 2017. Are water-lean solvent systems viable for post-combustion CO_2 capture? Energy Procedia 114, 756–763. doi:10.1016/j.egypro.2017.03.1218.
Hellums, M.W., Koros, W.J., Husk, G.R., Paul, D.R., 1989. Fluorinated polycarbonates for gas separation applications. J. Membr. Sci. 46 (1), 93–112. doi:10.1016/S0376-7388(00)81173-4.
Hemmatifar, A., Kang, J.S., Ozbek, N., Tan, K.-J., Hatton, T.A., 2022. Electrochemically mediated direct CO_2 capture by a stackable bipolar cell. ChemSusChem 15 (6), e202102533. doi:10.1002/cssc.202102533.
Hepworth, T., 1892. Oxygen for limelight. Nature 47 (1208), 176–177.
Heydari-Gorji, A., Sayari, A., 2012. Thermal, oxidative, and co2-induced degradation of supported polyethylenimine adsorbents. Ind. Eng. Chem. Res. 51 (19), 6887–6894. doi:10.1021/ie3003446.

Heydari-Gorji, A., Belmabkhout, Y., Sayari, A., 2011a. Degradation of amine-supported CO_2 adsorbents in the presence of oxygen-containing gases. Microporous Mesoporous Mater. 145 (1-3), 146–149. doi:10.1016/j.micromeso.2011.05.010.

Heydari-Gorji, A., Belmabkhout, Y., Sayari, A., 2011b. Polyethylenimine-impregnated mesoporous silica: effect of amine loading and surface alkyl chains on CO_2 adsorption. Langmuir 27 (20), 12411–12416. doi:10.1021/la202972t.

Higginbotham, P., White, V., Fogash, K., Guvelioglu, G., 2011. Oxygen supply for oxyfuel CO_2 capture. Int. J. Greenh. Gas Control 5 (SUPPL. 1), S194–S203. doi:10.1016/J.IJGGC.2011.03.007.

Hiloidhari, M., Kumari, S., 2021. Chapter 15 - Biogas upgrading and life cycle assessment of different biogas upgrading technologies. In: Aryal, N., Mørck Ottosen, L.D., Wegener Kofoed, M.V., Pant, D. (Eds.), Emerging Technologies and Biological Systems for Biogas Upgrading. Academic Press, pp. 413–445. doi:10.1016/B978-0-12-822808-1.00015-5.

Hilz, J., Helbig, M., Haaf, M., Daikeler, A., Ströhle, J., Epple, B., 2017. Long-term pilot testing of the carbonate looping process in 1MWth scale. Fuel 210, 892–899. doi:10.1016/j.fuel.2017.08.105.

Himeno, S., Tomita, T., Suzuki, K., Yoshida, S., 2007. Characterization and selectivity for methane and carbon dioxide adsorption on the all-silica DD3R zeolite. Microporous Mesoporous Mater. 98 (1-3), 62–69.

HINO, M., ARATA, K., 1979. Solid catalyst treated with anion. 2. Reactions of butane and isobutane catalyzed by zirconium oxide treated with sulfate ion. Solid superacid catalyst. Chem. Soc. Jpn. 101 (21), 6439–6441.

Hiremath, V., Trivino, M.L.T., Seo, J.G.J.J.o.E.S., 2019. Eutectic mixture promoted CO_2 sorption on MgO-TiO2 composite at elevated temperature. 76, 80-88.

Ho, N.A.D., Leo, C.P., 2021. A review on the emerging applications of cellulose, cellulose derivatives and nanocellulose in carbon capture. Environ. Res. 197. doi:10.1016/j.envres.2021.111100.

Ho, M.T., Allinson, G.W., Wiley, D.E., 2008. Reducing the cost of CO_2 capture from flue gases using pressure swing adsorption. Ind. Eng. Chem. Res. 47 (14), 4883–4890. doi:10.1021/ie070831e.

Hoang, V.T., Kaliaguine, S., 2013. Predictive models for mixed-matrix membrane performance: a review. Chem. Rev. 113 (7), 4980–5028. doi:10.1021/cr3003888.

Hoegh-Guldberg, O., Jacob, D., Taylor, M., Guillen Bolanos, T., Bindi, M., Brown, S., Camilloni, I.A., Diedhiou, A., Djalante, R., Ebi, K., Engelbrecht, F., Guiot, J., Hijioka, Y., Mehrotra, S., Hope, C.W., Payne, A.J., Portner, H.O., Seneviratne, S.I., Thomas, A., Warren, R., Zhou, G., 2019. The human imperative of stabilizing global climate change at 1.5 degrees C. Science 365 (6459). doi:10.1126/science.aaw6974.

Hofs, B., Ogier, J., Vries, D., Beerendonk, E.F., Cornelissen, E.R., 2011. Comparison of ceramic and polymeric membrane permeability and fouling using surface water. Sep. Purif. Technol. 79 (3), 365–374. doi:10.1016/J.SEPPUR.2011.03.025.

Holmes, A.S., Ryan, J.M., 1982. Cryogenic Distillative Separation of Acid Gases from Methane. Koch Press Systems, Inc., United States.

Homonnay, Z., Nomura, K., Juhász, G., Gál, M., Sólymos, K., Hamakawa, S., Hayakawa, T., Vértes, A., 2002. Simultaneous probing of the Fe and Co sites in the CO_2-absorber perovskite $Sr_{0.95}Ca_{0.05}Co_{0.5}Fe_{0.5}O_3$-$\delta$: a Mössbauer study. Chem. Mater. 14 (3), 1127–1135. doi:10.1021/cm011190v.

Hong, J., Chaudhry, G., Brisson, J.G., Field, R., Gazzino, M., Ghoniem, A.F., 2009. Analysis of oxy-fuel combustion power cycle utilizing a pressurized coal combustor. Energy 34 (9), 1332–1340. doi:10.1016/j.energy.2009.05.015.

Hong, J., Field, R., Gazzino, M., Ghoniem, A.F., 2010. Operating pressure dependence of the pressurized oxy-fuel combustion power cycle. Energy 35 (12), 5391–5399. doi:10.1016/j.energy.2010.07.016.

Hong, X.J., Wei, Q., Cai, Y.P., Zheng, S.R., Yu, Y., Fan, Y.Z., Xu, X.Y., Si, L.P., 2017. 2-fold interpenetrating bifunctional Cd-metal-organic frameworks: highly selective adsorption for CO_2 and sensitive luminescent sensing of nitro aromatic 2,4,6-trinitrophenol. ACS Appl. Mater. Interfaces 9 (5), 4701–4708. doi:10.1021/acsami.6b14051.

Hong, W.Y., 2022. A techno-economic review on carbon capture, utilisation and storage systems for achieving a net-zero CO_2 emissions future. Carbon Cap. Sci. Technol. 3, 100044. doi:10.1016/j.ccst.2022.100044.

Horn, F.L., Steinberg, M., 1982. Control of carbon dioxide emissions from a power plant (and use in enhanced oil recovery). Fuel 61 (5), 415–422. doi:10.1016/0016-2361(82)90064-3.

Hoshino, Y., Utsunomiya, T., Abe, O., 1981. The thermal-decomposition of sodium-nitrate and the effects of several oxides on the decomposition. B Chem. Soc. Jpn. 54 (5), 1385–1391. doi:10.1246/bcsj.54.1385.

Hoskins, B.F., Robson, R., 1990. Design and construction of a new class of scaffolding-like materials comprising infinite polymeric frameworks of 3D-linked molecular rods. A reappraisal of the zinc cyanide and cadmium cyanide structures and the synthesis and structure of the diamond-related frameworks [N (CH3) 4][CuIZnII (CN) 4] and CuI [4, 4′, 4″, 4‴-tetracyanotetraphenylmethane] BF4. xC6H5NO2. J. Am. Chem. Soc. 112 (4), 1546–1554.

Hosono, N., Guo, W., Omoto, K., Yamada, H., Kitagawa, S., 2019. Bottom-up synthesis of defect-free mixed-matrix membranes by using polymer-grafted metal–organic polyhedra. Chem. Lett. 48 (6), 597–600. doi:10.1246/cl.190131.

Hossain, M.M., de Lasa, H.I., 2007. Reactivity and stability of Co-Ni/Al2O3 oxygen carrier in multicycle CLC. AIChE J. 53 (7), 1817–1829. doi:10.1002/aic.11188.

Hossain, M.K., Strezov, V., Chan, K.Y., Ziolkowski, A., Nelson, P.F., 2011. Influence of pyrolysis temperature on production and nutrient properties of wastewater sludge biochar. J. Environ. Manage. 92 (1), 223–228. doi:10.1016/j.jenvman.2010.09.008.

Hossain, M.A., Nabavi, S.A., Ranganathan, P., Könözsy, L., Manovic, V., 2020. 3D CFD modelling of liquid dispersion in structured packed bed column for CO_2 capture. Chem. Eng. Sci. 225. doi:10.1016/j.ces.2020.115800, 115800-115800.

Hosseini, S.H., Shojaee, S., Ahmadi, G., Zivdar, M., 2012. Computational fluid dynamics studies of dry and wet pressure drops in structured packings. J. Ind. Eng. Chem. 18 (4), 1465–1473. doi:10.1016/j.jiec.2012.02.012.

Hosseini, S.S., Najari, S., Kundu, P.K., Tan, N.R., Roodashti, S.M., 2015. Simulation and sensitivity analysis of transport in asymmetric hollow fiber membrane permeators for air separation. RSC Adv. 5 (105), 86359–86370. doi:10.1039/C5RA13943K.

Hou, X., 2016. Smart gating multi-scale pore/channel-based membranes. Adv. Mater. 28 (33), 7049–7064. doi:10.1002/adma.201600797.

House, K.Z., Baclig, A.C., Ranjan, M., van Nierop, E.A., Wilcox, J., Herzog, H.J., 2011. Economic and energetic analysis of capturing CO_2 from ambient air. Proc. Natl. Acad. Sci. 108 (51), 20428–20433. doi:10.1073/pnas.1012253108.

Hsa, B., Mc, C., Jf, A., Wd, A., Min, H.A., Jh, A., Lq, A., Pt, B., Zlb, D., 2021. Application of "coordinative effect" into tri-solvent MEA+BEA+AMP blends at concentrations of 0.1 + 2 + 20.5 + 2 + 2 mol/L with absorption, desorption and mass transfer analyses - ScienceDirect. Int. J. Greenh. Gas Control 107.

Hu, Y., Yan, J., 2012. Characterization of flue gas in oxy-coal combustion processes for CO_2 capture. Appl. Energy 90 (1), 113–121. doi:10.1016/j.apenergy.2011.03.005.

Hu, Y., Liu, Z., Xu, J., Huang, Y., Song, Y., 2013. Evidence of pressure enhanced CO_2 storage in ZIF-8 probed by FTIR spectroscopy. J. Am. Chem. Soc. 135 (25), 9287–9290. doi:10.1021/ja403635b.

Hu, H., Li, F., Xia, Q., Li, X., Liao, L., Fan, M., 2014. Research on influencing factors and mechanism of CO_2 absorption by poly-amino-based ionic liquids. Int. J. Greenh. Gas Control 31, 33–40. doi:10.1016/j.ijggc.2014.09.021.

Hu, Y., Verdegaal, W.M., Yu, S.H., Jiang, H.L., 2014. Alkylamine-tethered stable metal-organic framework for CO (2) capture from flue gas. ChemSusChem 7 (3), 734–737. doi:10.1002/cssc.201301163.

Hu, Y., Liu, W., Chen, H., Zhou, Z., Wang, W., Sun, J., Yang, X., Li, X., Xu, M., 2016. Screening of inert solid supports for CaO-based sorbents for high temperature CO_2 capture. Fuel 181, 199–206.

Hu, Z., Gami, A., Wang, Y., Zhao, D., 2017a. A triphasic modulated hydrothermal approach for the synthesis of multivariate metal–organic frameworks with hydrophobic moieties for highly efficient moisture-resistant CO_2 capture. Adv. Sustain. Syst. 1 (11), 1700092.

Hu, Z., Wang, Y., Farooq, S., Zhao, D., 2017b. A highly stable metal-organic framework with optimum aperture size for CO_2 capture. AIChE J. 63 (9), 4103–4114.

Hu, J., Galvita, V.V., Poelman, H., Marin, G.B., 2018. Advanced chemical looping materials for CO_2 utilization: a review. Materials 11 (7), 1187.

Hu, L., Liu, J., Zhu, L., Hou, X., Huang, L., Lin, H., Cheng, J., 2018. Highly permeable mixed matrix materials comprising ZIF-8 nanoparticles in rubbery amorphous poly (ethylene oxide) for CO_2 capture. Sep. Purif. Technol. 205, 58–65. doi:10.1016/j.seppur.2018.05.012.

Hu, Y.C., Guo, Y.F., Sun, J., Li, H.L., Liu, W.Q., 2019. Progress in MgO sorbents for cyclic CO_2 capture: a comprehensive review. J. Mater. Chem. A 7 (35), 20103–20120. doi:10.1039/c9ta06930e.

Hu, Y.W., Cui, H.J., Cheng, Z.M., Zhou, Z.M., 2019. Sorption-enhanced water gas shift reaction by *in situ* CO_2 capture on an alkali metal salt-promoted MgO-$CaCO_3$ sorbent. Chem. Eng. J. 377, 119823 10.1016j.cej.2018.08.209.

Hu, J., Poelman, H., Marin, G.B., Detavernier, C., Kawi, S., Galvita, V.V., 2020. FeO controls the sintering of iron-based oxygen carriers in chemical looping CO_2 conversion. J. CO_2 Util. 40, 101216. doi:10.1016/j.jcou.2020.101216.

Hu, X., Liu, L., Luo, X., Xiao, G., Shiko, E., Zhang, R., Fan, X., Zhou, Y., Liu, Y., Zeng, Z., Li, C.e., 2020. A review of N-functionalized solid adsorbents for post-combustion CO_2 capture. Appl. Energy 260. doi:10.1016/j.apenergy.2019.114244.

Hu, X., Lee, W.H., Zhao, J., Kim, J.S., Wang, Z., Yan, J., Zhuang, Y., Lee, Y.M.J., 2020. Thermally rearranged polymer membranes containing highly rigid biphenyl ortho-hydroxyl diamine for hydrogen separation. J. Membr. Sci. 604, 118053.

Hu, C., Cheng, P., Chou, S., Lai, C., Huang, S., Tsai, H., Hung, W., Lee, K., 2020. Separation behavior of amorphous amino-modified silica nanoparticle/polyimide mixed matrix membranes for gas separation. J. Membr. Sci. 595, 117542. doi:10.1016/j.memsci.2019.117542.

Hu, Y.C., Lu, H.Y., Liu, W.Q., Yang, Y.D., Li, H.L., 2020. Incorporation of CaO into inert supports for enhanced CO_2 capture: a review. Chem. Eng. J. 396, 16. doi:10.1016/j.cej.2020.125253.

Hu, J., Galvita, V.V., Poelman, H., Wang, Z., Marin, G.B., Kawi, S., 2021a. Coupling CO_2 utilization and NO reduction in chemical looping manner by surface carbon. Appl. Catal. B: Environ. 297, 120472. doi:10.1016/j.apcatb.2021.120472.

Hu, J., Hongmanorom, P., Chirawatkul, P., Kawi, S., 2021b. Efficient integration of CO_2 capture and conversion over a Ni supported CeO2-modified CaO microsphere at moderate temperature. Chem. Eng. J. 426, 130864. doi:10.1016/j.cej.2021.130864.

Hu, J., Hongmanorom, P., Galvita, V.V., Li, Z., Kawi, S., 2021c. Bifunctional Ni-Ca based material for integrated CO_2 capture and conversion via calcium-looping dry reforming. Appl. Catal. B: Environ. 284, 119734. doi:10.1016/j.apcatb.2020.119734.

Hu, H.T., Fang, M.X., Liu, F., Wang, T., Xia, Z.X., Zhang, W., Ge, C.L., Yuan, J.J., 2022. Novel alkanolamine-based biphasic solvent for CO_2 capture with low energy consumption and phase change mechanism analysis. Appl. Energy 324. doi:10.1016/j.apenergy.2022.119570.

Hu, L., Bui, V.T., Pal, S., Guo, W., Subramanian, A., Kisslinger, K., Fan, S., Nam, C.Y., Ding, Y., Lin, H., 2022a. In situ growth of crystalline and polymer-incorporated amorphous ZIFs in polybenzimidazole achieving hierarchical nanostructures for carbon capture. Small, 2201982 doi:10.1002/smll.202201982.

Hu, L., Clark, K., Alebrahim, T., Lin, H., 2022b. Mixed matrix membranes for post-combustion carbon capture: From materials design to membrane engineering. J. Membr. Sci. 644, 120140. doi:10.1016/j.memsci.2021.120140.

Huang, Q., Wu, C., 2022. Photoswitching metal organic frameworks development and applications on environmental related topics. Mater. Today Sustain. 18. doi:10.1016/j.mtsust.2022.100149.

Huang, A., Dou, W., Caro, J.r., 2010. Steam-stable zeolitic imidazolate framework ZIF-90 membrane with hydrogen selectivity through covalent functionalization. J. Am. Chem. Soc. 132 (44), 15562–15564. doi:10.1021/ja108774v.
Huang, Y.-F., Chiueh, P.-T., Shih, C.-H., Lo, S.-L., Sun, L., Zhong, Y., Qiu, C., 2015. Microwave pyrolysis of rice straw to produce biochar as an adsorbent for CO_2 capture. Energy 84, 75–82. doi:10.1016/j.energy.2015.02.026.
Huang, X., Lu, J., Wang, W., Wei, X., Ding, J., 2016. Experimental and computational investigation of CO_2 capture on amine grafted metal-organic framework NH2-MIL-101. Appl. Surf. Sci. 371, 307–313. doi:10.1016/j.apsusc.2016.02.154.
Huang, H.-j., Yang, T., Lai, F.-y., Wu, G.-q., 2017. Co-pyrolysis of sewage sludge and sawdust/rice straw for the production of biochar. J. Analyt. Appl. Pyrol. 125, 61–68. doi:10.1016/j.jaap.2017.04.018.
Huang, L., Zhang, Y., Gao, W., Harada, T., Qin, Q., Zheng, Q., Hatton, T.A., Wang, Q., 2017. Alkali carbonate molten salt coated calcium oxide with highly improved carbon dioxide capture capacity. Energy Technol..
Huang, Q., Jing, G., Zhou, X., Lv, B., Zhou, Z., 2018. A novel biphasic solvent of amino-functionalized ionic liquid for CO_2 capture: High efficiency and regenerability. J. CO_2 Util. 25, 22–30. doi:10.1016/j.jcou.2018.03.001.
Huang, G., Isfahani, A.P., Muchtar, A., Sakurai, K., Shrestha, B.B., Qin, D., Yamaguchi, D., Sivaniah, E., Ghalei, B., 2018. Pebax/ionic liquid modified graphene oxide mixed matrix membranes for enhanced CO_2 capture. J. Membr. Sci. 565, 370–379. doi:10.1016/j.memsci.2018.08.026.
Huang, J., Liu, W., Yang, Y., Liu, B., 2018. High-performance Ni–Fe redox catalysts for selective CH4 to syngas conversion via chemical looping. ACS Catal. 8 (3), 1748–1756. doi:10.1021/acscatal.7b03964.
Huang, Q., Luo, Q., Wang, Y., Pentzer, E., Gurkan, B., 2019. Hybrid ionic liquid capsules for rapid CO_2 capture. Ind. Eng. Chem. Res. 58 (24), 10503–10509. doi:10.1021/acs.iecr.9b00314.
Huang, Y.F., Chiueh, P.T., Lo, S.L., 2019. CO_2 adsorption on biochar from co-torrefaction of sewage sludge and leucaena wood using microwave heating. Innov. Solut. Energy Trans. 158, 4435–4440. doi:10.1016/j.egypro.2019.01.772.
Huang, L., Liu, J., Lin, H., 2020. Thermally stable, homogeneous blends of cross-linked poly (ethylene oxide) and crown ethers with enhanced CO_2 permeability. J. Membr. Sci. 610, 118253. doi:10.1016/j.memsci.2020.118253.
Huang, L., Ding, L., Wang, H., 2021. MXene-based membranes for separation applications. Small Sci. 1 (7), 2100013. doi:10.1002/smsc.202100013.
Huang, Q., Mu, J., Zhan, Z., Wang, F., Jin, S., Tan, B., Wu, C., 2022. Steric hindrance alleviation strategy to enhance the photo switching efficiency of azobenzene functionalized metal-organic framework toward tailorable carbon dioxide capture. J. Mater. Chem. A doi:10.1039/d1ta09270g.
Hufton, J.R., Mayorga, S., Sircar, S., 1999. Sorption-enhanced reaction process for hydrogen production. Process. Saf. Environ. Protect. 45 (2), 248–256. doi:10.1002/aic.690450205.
S.J.W. Hufton, J., Nataraj, S., Rao, M., Sircar, S., 1999. Proceedings of the 1999 US DOE Hydrogen Program Review National Renewable Energy Lab. (NREL), Golden, CO (United States).
Hunsom, M., Autthanit, C., 2013. Adsorptive purification of crude glycerol by sewage sludge-derived activated carbon prepared by chemical activation with H3PO4, K2CO3 and KOH. Chem. Eng. J. 229, 334–343. doi:10.1016/j.cej.2013.05.120.
Husebye, J., et al., 2012. Techno Economic Evaluation of Amine based CO_2 Capture: Impact of CO_2 Concentration and Steam Supply. Energy Procedia 23, 381–390.
Hussain, A., Hägg, M.-B., 2010. A feasibility study of CO_2 capture from flue gas by a facilitated transport membrane. J. Membr. Sci. 359 (1), 140–148. doi:10.1016/j.memsci.2009.11.035.
Hussain, S., Dong, H., Zeng, S., Ahmad, M.U., Shehzad, F.K., Wu, H., Zhang, Y., 2021. Investigation uncovered the impact of anions on CO_2 absorption by low viscous ether functionalized pyridinium ionic liquids. J. Mol. Liq. 336. doi:10.1016/j.molliq.2021.116362.
Hutson, N.D., Attwood, B.C., 2008. High temperature adsorption of CO_2 on various hydrotalcite-like compounds. Adsorption 14 (6), 781–789. doi:10.1007/s10450-007-9085-6.
Hwang, K.-S., Park, S.-W., Park, D.-W., Oh, K.-J., Kim, S.-S., 2010. Absorption of carbon dioxide into diisopropanolamine solutions of polar organic solvents. J. Taiwan Instit. Chem. Eng. 41 (1), 16–21.
Iarikov, D., Hacarlioglu, P., Oyama, S.T., 2011. Supported room temperature ionic liquid membranes for CO_2/CH4 separation. Chem. Eng. J. 166 (1), 401-406.
Ibrahim, M., Hameed, B.H., Ouakouak, A., Din, A.T.M., 2022. Effect of hydrothermal carbonization parameters and performance of carbon dioxide adsorption on pineapple peel waste biochar. Chem. Eng. Technol. doi:10.1002/ceat.202200089.
Agency, I.E., CO_2 capture: an examination of potential gas-solid adsorption technologies for the capture of CO_2 and other greenhouse gases arising from power generation using fossil fuel. 1992.
IEA, 2021. Net zero by 2050: A roadmap for the global energy sector. https://www.iea.org/reports/net-zero-by-2050 (Accessed Oct. 2021).
Igalavithana, A.D., Choi, S.W., Dissanayake, P.D., Shang, J., Wang, C.-H., Yang, X., Kim, S., Tsang, D.C.W., Lee, K.B., Ok, Y.S., 2020a. Gasification biochar from biowaste (food waste and wood waste) for effective CO_2 adsorption. J. Hazard. Mater. 391, 121147. doi:10.1016/j.jhazmat.2019.121147.
Igalavithana, A.D., Choi, S.W., Shang, J., Hanif, A., Dissanayake, P.D., Tsang, D.C., Kwon, J.-H., Lee, K.B., Ok, Y.S., 2020b. Carbon dioxide capture in biochar produced from pine sawdust and paper mill sludge: Effect of porous structure and surface chemistry. Sci. Total Environ. 739, 139845.
Igalavithana, A.D., Choi, S.W., Shang, J., Hanif, A., Dissanayake, P.D., Tsang, D.C.W., Kwon, J.-H., Lee, K.B., Ok, Y.S., 2020c. Carbon dioxide capture in biochar produced from pine sawdust and paper mill sludge: Effect of porous structure and surface chemistry. Sci. Total Environ. 739, 139845. doi:10.1016/j.scitotenv.2020.139845.
Ignat'ev, N.V., Finze, M., Sprenger, J.A.P., Kerpen, C., Bernhardt, E., Willner, H., 2015. New hydrophobic ionic liquids with perfluoroalkyl phosphate and cyanofluoroborate anions. J. Fluorine Chem. 177, 46–54. doi:10.1016/j.jfluchem.2015.03.007.
Iliuta, I., Petre, C.F., Larachi, F., 2004. Hydrodynamic continuum model for two-phase flow structured-packing- containing columns. Chem. Eng. Sci. 59 (4), 879–888. doi:10.1016/j.ces.2003.11.020.
Iliuta, I., Hasib-ur-Rahman, M., Larachi, F., 2014. CO_2 absorption in diethanolamine/ionic liquid emulsions - Chemical kinetics and mass transfer study. Chem. Eng. J. 240, 16–23. doi:10.1016/j.cej.2013.11.063.
Iliuta, I., Larachi, F., Fourati, M., Raynal, L., Roig, V., 2014. Flooding limit in countercurrent gas-liquid structured packed beds-Prediction from a linear stability analysis of an Eulerian two-fluid model. Chem. Eng. Sci. 120, 49–58. doi:10.1016/j.ces.2014.08.053.
Im, D., Jung, H., Lee, J.H., 2020. Modeling, simulation and optimization of the rotating packed bed (RPB) absorber and stripper for MEA-based carbon capture. Comput. Chem. Eng. 143. doi:10.1016/j.compchemeng.2020.107102, 107102-107102.
Ioannidi, A., Vroulias, D., Kallitsis, J., Ioannides, T., Deimede, V., 2021. Synthesis and characterization of poly (ethylene oxide) based copolymer membranes for efficient gas/vapour separation: effect of PEO content and chain length. J. Membr. Sci. 632, 119353. doi:10.1016/j.memsci.2021.119353.
Iora, P., Chiesa, P., 2009. High efficiency process for the production of pure oxygen based on solid oxide fuel cell–solid oxide electrolyzer technology. J. Power Sources 190 (2), 408–416. doi:10.1016/J.JPOWSOUR.2009.01.045.
Isanejad, M., Mohammadi, T., 2018. Effect of amine modification on morphology and performance of poly (ether-block-amide)/fumed silica nanocomposite membranes for CO_2/CH4 separation. Mater. Chem. Phys. 205, 303–314.
Izquierdo, M.T., García-Labiano, F., Abad, A., Cabello, A., Gayán, P., de Diego, L.F., Adánez, J., 2021. On the optimization of physical and chemical stability of a Cu/Al2O3 impregnated oxygen carrier for chemical looping combustion. Fuel Process. Technol. 215, 106740. doi:10.1016/j.fuproc.2021.106740.
Jacobson, M.Z., 2009. Review of solutions to global warming, air pollution, and energy security. Energy Environ. Sci. 2 (2), 148–173.
R.V.C. Jadhav, P.D., Biniwale, R.B., Labhsetwar, N.K., Devotta, S., Rayalu, S.S., 2007. Monoethanol Amine Modified Zeolite 13X for CO_2 Adsorption at Different Temperatures. Energy Fuels 21, 3555–3559.
Jafari, T., Moharreri, E., Toloueinia, P., Amin, A.S., Sahoo, S., Khakpash, N., Noshadi, I., Alpay, S.P., Suib, S.L., 2017. Microwave-assisted synthesis of amine functionalized mesoporous polydivinylbenzene for CO_2 adsorption. J. CO_2 Util. 19, 79–90. doi:10.1016/j.jcou.2017.03.004.
Jahandar Lashaki, M., Ziaei-Azad, H., Sayari, A., 2017. Insights into the hydrothermal stability of triamine-functionalized SBA-15 silica for CO_2 adsorption. ChemSusChem 10 (20), 4037–4045. doi:10.1002/cssc.201701439.
Jahandar Lashaki, M., Khiavi, S., Sayari, A., 2019. Stability of amine-functionalized CO_2 adsorbents: a multifaceted puzzle. Chem. Soc. Rev. 48 (12), 3320–3405. doi:10.1039/c8cs00877a.
Jaiboon, O.-a., Chalermsinsuwan, B., Mekasut, L., Piumsomboon, P., 2013. Effect of flow patterns/regimes on CO_2 capture using K_2CO_3 solid sorbent in fluidized bed/circulating fluidized bed. Chem. Eng. J. 219, 262–272. doi:10.1016/j.cej.2012.12.081.
Jalalabadi, T., Glenn, M., Tremain, P., Moghtaderi, B., Donne, S., Allen, J., 2019. Modification of biochar formation during slow pyrolysis in the presence of alkali metal carbonate additives. Energy Fuels 33 (11), 11235–11245. doi:10.1021/acs.energyfuels.9b02865.
James, I.I.I.R.E., Keairns, D., Turner, M., Woods, M., Kuehn, N., Zoelle, A., 2019. Cost and Performance Baseline for Fossil Energy Plants Volume 1: Bituminous Coal and Natural Gas to Electricity. National Energy Technology Laboratory, United States.
Jana, A.K., 2016. A new divided-wall heat integrated distillation column (HIDiC) for batch processing: feasibility and analysis. Appl. Energy 172, 199–206. doi:10.1016/j.apenergy.2016.03.117.
Janakiram, S., Espejo, Martín, Juan, L., Høisæter, K.K., Lindbråthen, A., Ansaloni, L., Deng, L., 2020. Three-phase hybrid facilitated transport hollow fiber membranes for enhanced CO_2 separation. Appl. Mater. Today 21, 100801. doi:10.1016/j.apmt.2020.100801.
Jankowski, A., Grabiec, E., Nocoń-Szmajda, K., Marcinkowski, A., Janeczek, H., Wolińska-Grabczyk, A., 2021. Polyimide-based membrane materials for CO_2 separation: a comparison of segmented and aromatic (Co)polyimides. 11 (4), 274.
Jansen, D., Gazzani, M., Manzolini, G., Dijk, E.v., Carbo, M., 2015. Pre-combustion CO_2 capture. Int. J. Greenh. Gas Control 40, 167–187. doi:10.1016/j.ijggc.2015.05.028.
Janusz-Szymańska, K., Dryjańska, A., 2015. Possibilities for improving the thermodynamic and economic characteristics of an oxy-type power plant with a cryogenic air separation unit. Energy 85, 45–61. doi:10.1016/J.ENERGY.2015.03.049.
Jasieńko-Hałat, M., Kędzior, K., 2005. Comparison of molecular sieve properties in microporous chars from low-rank bituminous coal activated by steam and carbon dioxide. Carbon 43 (5), 944–953.
Jassim, M.S., Rochelle, G., Eimer, D., Ramshaw, C., 2007. Carbon dioxide absorption and desorption in aqueous monoethanolamine solutions in a rotating packed bed. Ind. Eng. Chem. Res. 46 (9), 2823–2833. doi:10.1021/ie051104r.
Jensen, M.J., Russell, C.S., Bergeson, D., Hoeger, C.D., Frankman, D.J., Bence, C.S., Baxter, L.L., 2015. Prediction and validation of external cooling loop cryogenic carbon capture (CCC-ECL) for full-scale coal-fired power plant retrofit. Int. J. Greenh. Gas Control 42, 200–212. doi:10.1016/j.ijggc.2015.04.009.
Jeon, H., Min, Y.J., Ahn, S.H., Hong, S.-M., Shin, J.-S., Kim, J.H., Lee, K.B., 2012. Graft copolymer templated synthesis of mesoporous MgO/TiO_2 mixed oxide nanoparticles and their CO_2 adsorption capacities. Colloids Surf. A: Physicochem. Eng. Aspects 414, 75–81.
Jeon, D.H., Min, B.G., Oh, J.G., Nah, C., Park, S.J., 2015. Influence of Nitro-

gen moieties on CO_2 capture of Carbon Aerogel. Carbon Lett. 16 (1), 57–61. doi:10.5714/Cl.2015.16.1.057.
Jeon, J.W., Kim, D.-G., Sohn, E.-h., Yoo, Y., Kim, Y.S., Kim, B.G., Lee, J.-C., 2017. Highly carboxylate-functionalized polymers of intrinsic microporosity for CO_2-selective polymer membranes. Macromolecules 50 (20), 8019–8027. doi:10.1021/acs.macromol.7b01332.
Ji, L., et al., 2022. Metal oxyhydroxide catalysts promoted CO_2 absorption and desorption in amine-based carbon capture: a feasibility study. ACS Omega 7 (49), 44620–44630. doi:10.1021/acsomega.2c02851.
Ji, G., Memon, M.Z., Zhuo, H., Zhao, M., 2017. Experimental study on CO_2 capture mechanisms using Na2ZrO3 sorbents synthesized by soft chemistry method. Chem. Eng. J. 313, 646–654.
Ji, C., Yuan, S., Huffman, M., El-Halwagi, M.M., Wang, Q., 2021. Post-combustion carbon capture for tank to propeller via process modeling and simulation. J. CO_2 Util. 51. doi:10.1016/j.jcou.2021.101655.
Jia, X., Qiao, Z., He, B., Zhong, C., 2020. Highly selective filler–polymer gaps in situ fabricated in mixed matrix membranes for gas separation. J. Mater. Chem. A 8 (24), 11928–11932. doi:10.1039/D0TA03378B.
Jia, P., Liu, J., Kong, J., Hu, M., Qi, N., Chen, Z., Xu, S., Li, N., 2022. Tailoring the micropore structure of 6FDA-based polyimide membrane for gas permselectivity studied by positron annihilation. Sep. Purif. Technol. 282, 120044.
Jia, Y., Wei, J., Yuan, Y., Geng, L., Chen, S., Liao, L., 2022. Tetraethylenepentamine impregnated composite material ZSM-5/SBA-16 for CO_2 adsorption. J. Mater. Res. 37 (2), 543–553. doi:10.1557/s43578-021-00469-y.
Jiang, Y., Khadilkar, M.R., Al-Dahhan, M.H., Dudukovic, M.P., 2002. CFD of multiphase flow in packed-bed reactors: II. Results and applications. AIChE J. 48 (4), 716–730. doi:10.1002/aic.690480407.
Jiang, B., Wang, X., Gray, M.L., Duan, Y., Luebke, D., Li, B., 2013. Development of amino acid and amino acid-complex based solid sorbents for CO_2 capture. Appl. Energy 109, 112–118. doi:10.1016/j.apenergy.2013.03.070.
Jiang, J., Lu, Z., Zhang, M., Duan, J., Zhang, W., Pan, Y., Bai, J., 2018. Higher symmetry multinuclear clusters of metal-organic frameworks for highly selective CO_2 capture. J. Am. Chem. Soc. 140 (51), 17825–17829. doi:10.1021/jacs.8b07589.
Jiang, K., Li, K., Yu, H., Feron, P.H.M., 2018. Piperazine-promoted aqueous-ammonia-based CO_2 capture: process optimisation and modification. Chem. Eng. J. 347, 334–342. doi:10.1016/j.cej.2018.04.103.
Jiang, Y., Tan, P., Qi, S.C., Liu, X.Q., Yan, J.H., Fan, F., Sun, L.B., 2019. Metal-organic frameworks with target-specific active sites switched by photoresponsive motifs: efficient adsorbents for tailorable CO_2 capture. Angew. Chem. Int. Ed. Engl. 58 (20), 6600–6604. doi:10.1002/anie.201900141.
Jiang, Y., Zhang, Z., Fan, J., Yang, L., Liu, J., 2020. Experimental study on postcombustion systems including a hollow fiber membrane and a packed column. ACS Omega 5 (28), 17692–17702. doi:10.1021/acsomega.0c02251.
Jiang, X., He, S., Han, G., Long, J., Li, S., Lau, C.H., Zhang, S., Shao, L., 2021. Aqueous one-step modulation for synthesizing monodispersed ZIF-8 nanocrystals for mixed-matrix membrane. ACS Appl. Mater. Interfaces 13 (9), 11296–11305. doi:10.1021/acsami.0c22910.
Jiang, C., Fan, M., Gao, G., Jiang, W., Li, X., Luo, C., Zhang, L., Wu, F., 2022. Nanostructured AlOOH - A promising catalyst to reduce energy consumption for amine-based CO_2 capture. Sep. Purif. Technol. 303. doi:10.1016/j.seppur.2022.122232.
Jilvero, H., Normann, F., Andersson, K., Johnsson, F., 2015. Ammonia-based post combustion–The techno-economics of controlling ammonia emissions. Int. J. Greenh. Gas Control 37, 441–450.
Jin, H., Capareda, S., Chang, Z., Gao, J., Xu, Y., Zhang, J., 2014. Biochar pyrolytically produced from municipal solid wastes for aqueous As (V) removal: Adsorption property and its improvement with KOH activation. Bioresour. Technol. 169, 622–629. doi:10.1016/j.biortech.2014.06.103.
Jin, S., Ho, K., Vu, A.-T., Lee, C.-H., 2017. Salt-composition-controlled precipitation of triple-salt-promoted MgO with enhanced CO_2 sorption rate and working capacity. Energy Fuels 31 (9), 9725–9735.
Jo, S.I., An, Y.I., Kim, K.Y., Choi, S.Y., Kwak, J.S., Oh, K.R., Kwon, Y.U., 2017. Mechanisms of absorption and desorption of CO_2 by molten $NaNO_3$-promoted MgO. Phys. Chem. Chem. Phys. 19 (8), 6224–6232. doi:10.1039/c6cp07787k.
Joel, A.S., Wang, M., Ramshaw, C., Oko, E., 2014. Process analysis of intensified absorber for post-combustion CO_2 capture through modelling and simulation. Int. J. Greenh. Gas Control 21, 91–100. doi:10.1016/j.ijggc.2013.12.005.
Joel, A.S., Wang, M., Ramshaw, C., Oko, E., 2017. Modelling, simulation and analysis of intensified regenerator for solvent based carbon capture using rotating packed bed technology. Appl. Energy 203, 11–25. doi:10.1016/j.apenergy.2017.05.157.
Jonathan, C., 2013. SaskPower expects 30 % savings in carbon capture following Boundary Dam project. SNL Energy Coal Rep..
Jones, S.C., Bauer, C.A., 2009. Diastereoselective heterogeneous bromination of stilbene in a porous metal– organic framework. J. Am. Chem. Soc. 131 (35), 12516–12517.
Jones, C.L., Tansell, A.J., Easun, T.L., 2016. The lighter side of MOFs: structurally photoresponsive metal–organic frameworks. J. Mater. Chem. A 4 (18), 6714–6723. doi:10.1039/c5ta09424k.
Jones, N., 2009. Climate crunch: sucking it up. Nature 458 1094+.
Jones, C.W., 2011. CO_2 Capture from dilute gases as a component of modern global carbon management. Ann. Rev.Chem. Biomol. Eng. 2 (1), 31–52. doi:10.1146/annurev-chembioeng-061010-114252.
Joss, L., Gazzani, M., Mazzotti, M., 2017. Rational design of temperature swing adsorption cycles for post-combustion CO_2 capture. Chem. Eng. Sci. 158, 381–394. doi:10.1016/j.ces.2016.10.013.
Juhasz, G., Homonnay, Z.o., Nomura, K., Hayakawa, T., Hamakawa, S., Vértes, A., 2001. Microstructural study of the CO_2 absorption in $SrxCa_1-xFe_{0.5}Co_{0.5}O_3-\delta$. Solid State Ionics 139, 219–231. doi:10.1016/S0167-2738 (01)00690-7.
Jung, K.-W., Ahn, K.-H., 2016. Fabrication of porosity-enhanced MgO/biochar for removal of phosphate from aqueous solution: Application of a novel combined electrochemical modification method. Bioresour. Technol. 200, 1029–1032. doi:10.1016/j.biortech.2015.10.008.
Jung, W., Lee, K.S., 2020. Isotherm and kinetics modeling of simultaneous CO_2 and H2O adsorption on an amine-functionalized solid sorbent. J. Nat. Gas Sci. Eng. 84, 103489. doi:10.1016/j.jngse.2020.103489.
Jung, W., Lee, J., 2022a. Economic evaluation for four different solid sorbent processes with heat integration for energy-efficient CO_2 capture based on PEI-silica sorbent. Energy 238. doi:10.1016/j.energy.2021.121864, 121864-121864.
Jung, W., Lee, J., 2022b. Pseudo counter-current turbulent fluidized bed process with sensible heat recovery for energy-efficient CO_2 capture using an amine-functionalized solid sorbent. Energy 240. doi:10.1016/j.energy.2021.122803, 122803-122803.
Jung, H., Jeon, S., Jo, D.H., Huh, J., Kim, S.H., 2017. Effect of crosslinking on the CO_2 adsorption of polyethyleneimine-impregnated sorbents. Chem. Eng. J. 307, 836–844. doi:10.1016/j.cej.2016.09.005.
Jung, S., Park, Y.-K., Kwon, E.E., 2019. Strategic use of biochar for CO_2 capture and sequestration. J. CO_2 Util. 32, 128–139. doi:10.1016/j.jcou.2019.04.012.
Kárászová, M., Zach, B., Petrusová, Z., Červenka, V., Bobák, M., Šyc, M., Izák, P., 2020. Post-combustion carbon capture by membrane separation, Review. Sep. Purif. Technol. 238, 116448. doi:10.1016/j.seppur.2019.116448.
Küsgens, P., Rose, M., Senkovska, I., Fröde, H., Henschel, A., Siegle, S., Kaskel, S., 2009. Characterization of metal-organic frameworks by water adsorption. Microporous Mesoporous Mater. 120 (3), 325–330.
K, U.K., 1979. Porous Silica. Elsevier.
Kadam, R., Panwar, N.L., 2017. Recent advancement in biogas enrichment and its applications. Renew. Sustain. Energy Rev. 73, 892–903. doi:10.1016/j.rser.2017.01.167.
Kadi, M.W., El Salam, H.M.A., Zaki, T., Mohamed, R.M., 2020. Adsorption of carbon dioxide on CuxMgy (BTC)2 MOFs: influence of Cu/Mg ratio. J. Nanoparticle Res. 22 (6). doi:10.1007/s11051-020-04855-1.
Kagunya, W., Hassan, Z., Jones, W., 1996. Catalytic properties of layered double hydroxides and their calcined derivatives. Inorg. Chem. 35 (21), 5970–5974. doi:10.1021/ic960047e.
Kalantari, S., Omidkhah, M., Ebadi Amooghin, A., Matsuura, T., 2020. Superior interfacial design in ternary mixed matrix membranes to enhance the CO_2 separation performance. Appl. Mater. Today 18, 100491. doi:10.1016/j.apmt.2019.100491.
Kammakakam, I., O'Harra, K.E., Jackson, E.M., Bara, J.E.J.P., 2021. Synthesis of imidazolium-mediated Poly (benzoxazole) Ionene and composites with ionic liquids as advanced gas separation membranes. 214, 123239.
Kamran, U., Park, S.J., 2020. Tuning ratios of KOH and NaOH on acetic acid-mediated chitosan-based porous carbons for improving their textural features and CO_2uptakes. J. CO_2 Util. 40. doi:10.1016/j.jcou.2020.101212.
Kandambeth, S., Mallick, A., Lukose, B., Mane, M.V., Heine, T., Banerjee, R., 2012. Construction of crystalline 2D covalent organic frameworks with remarkable chemical (acid/base) stability via a combined reversible and irreversible route. J. Am. Chem. Soc. 134 (48), 19524–19527.
Kandambeth, S., Shinde, D.B., Panda, M.K., Lukose, B., Heine, T., Banerjee, R., 2013. Enhancement of chemical stability and crystallinity in porphyrin-containing covalent organic frameworks by intramolecular hydrogen bonds. Angew. Chem. Int. Ed. 52 (49), 13052–13056.
Kandambeth, S., Venkatesh, V., Shinde, D.B., Kumari, S., Halder, A., Verma, S., Banerjee, R., 2015. Self-templated chemically stable hollow spherical covalent organic framework. Nat. Commun. 6 (1), 1–10.
Kanehashi, S., Nagai, K., 2005. Analysis of dual-mode model parameters for gas sorption in glassy polymers. J. Membr. Sci. 253 (1-2), 117–138.
Kanehashi, S., Chen, G.Q., Scholes, C.A., Ozcelik, B., Hua, C., Ciddor, L., Southon, P.D., D'Alessandro, D.M., Kentish, S.E., 2015. Enhancing gas permeability in mixed matrix membranes through tuning the nanoparticle properties. J. Membr. Sci. 482, 49–55.
Kanezashi, M., Tomarino, Y., Nagasawa, H., Tsuru, T., 2019. Tailoring the molecular sieving properties and thermal stability of carbonized membranes containing polyhedral oligomeric silsesquioxane (POSS)-polyimide via the introduction of norbornene. J. Membr. Sci. 582, 59–69. doi:10.1016/j.memsci.2019.04.003.
Kang, J.-L., Sun, K., Wong, D.S.-H., Jang, S.-S., Tan, C.-S., 2014. Modeling studies on absorption of CO_2 by monoethanolamine in rotating packed bed. Int. J. Greenh. Gas Control. 25, 141–150. doi:10.1016/j.ijggc.2014.04.011.
Kang, Z., Peng, Y., Hu, Z., Qian, Y., Chi, C., Yeo, L.Y., Tee, L., Zhao, D., 2015. Mixed matrix membranes composed of two-dimensional metal–organic framework nanosheets for pre-combustion CO_2 capture: a relationship study of filler morphology versus membrane performance. J. Mater. Chem. A 3 (41), 20801–20810. doi:10.1039/C5TA03739E.
Kang, M., Min, H.J., Kim, N.U., Kim, J.H., 2021a. Amphiphilic micelle-forming PDMS-PEGBEM comb copolymer self-assembly to tailor the interlamellar nanospaces of defective poly (ethylene oxide) membranes. Sep. Purif. Technol. 257, 117892. doi:10.1016/j.seppur.2020.117892.
Kang, M., Min, H.J., Kim, N.U., Kim, J.H., 2021b. Amphiphilic micelle-forming PDMS-PEGBEM comb copolymer self-assembly to tailor the interlamellar nanospaces of defective poly (ethylene oxide) membranes. Sep. Purif. Technol. 257, 117892.
Kanniche, M., Gros-Bonnivard, R., Jaud, P., Valle-Marcos, J., Amann, J.-M., Bouallou, C., 2010. Pre-combustion, post-combustion and oxy-combustion in thermal power plant for CO_2 capture. Appl. Therm. Eng. 30 (1), 53–62.
Kapoor, R., Ghosh, P., Kumar, M., Vijay, V.K., 2019. Evaluation of biogas upgrading technologies and future perspectives: a review. Environ. Sci. Pollut. Res. 26 (12), 11631–11661. doi:10.1007/s11356-019-04767-1.
Karimi, M., Hillestad, M., Svendsen, H.F., 2011. Capital costs and energy considerations of different alternative stripper configurations for post combustion CO_2

capture. Chem. Eng. Res. Des. 89 (8), 1229–1236. doi:10.1016/j.cherd.2011.03.005.
Karimi, M., Hillestad, M., Svendsen, H.F., 2012. Investigation of the dynamic behavior of different stripper configurations for post-combustion CO 2 capture. Int. J. Greenh. Gas Control 7, 230–239. doi:10.1016/j.ijggc.2011.10.008.
Karimi, M., de Tuesta, J.L.D., Goncalves, C., Gomes, H.T., Rodrigues, A.E., Silva, J.A.C., 2020. Compost from municipal solid wastes as a source of biochar for CO_2 capture. Chem. Eng. Technol. 43 (7), 1336–1349. doi:10.1002/ceat.201900108.
Karimi, M., Shirzad, M., Silva, J.A.C., Rodrigues, A.E., 2022. Biomass/Biochar carbon materials for CO_2 capture and sequestration by cyclic adsorption processes: A review and prospects for future directions. J. Co2 Util. 57. doi:10.1016/j.jcou.2022.101890.
Karousos, D.S., Vangeli, O.C., Athanasekou, C.P., Sapalidis, A.A., Kouvelos, E.P., Romanos, G.E., Kanellopoulos, N.K., 2016. Physically bound and chemically grafted activated carbon supported 1-hexyl-3-methylimidazolium bis (trifluoromethylsulfonyl)imide and 1-ethyl-3-methylimidazolium acetate ionic liquid absorbents for SO2/CO_2 gas separation. Chem. Eng. J. 306, 146–154. doi:10.1016/j.cej.2016.07.040.
Karousos, D.S., Lei, L., Lindbråthen, A., Sapalidis, A.A., Kouvelos, E.P., He, X., Favvas, E.P., 2020. Cellulose-based carbon hollow fiber membranes for high-pressure mixed gas separations of CO_2/CH4 and CO_2/N_2. Sep. Purif. Technol. 253. doi:10.1016/j.seppur.2020.117473.
Kasahara, S., Kamio, E., Otani, A., Matsuyama, H., 2014. Fundamental investigation of the factors controlling the CO_2 permeability of facilitated transport membranes containing amine-functionalized task-specific ionic liquids. Ind. Eng. Chem. Res. 53, 2422–2431. doi:10.1021/ie403116t.
Katare, A., Kumar, S., Kundu, S., Sharma, S., Kundu, L.M., Mandal, B., 2023. Mixed matrix membranes for carbon capture and sequestration: challenges and scope. ACS Omega 8 (20), 17511–17522. doi:10.1021/acsomega.3c01666.
Katekomol, P., Roeser, J.r.m., Bojdys, M., Weber, J., Thomas, A., 2013. Covalent triazine frameworks prepared from 1, 3, 5-tricyanobenzene. Chem. Mater. 25 (9), 1542–1548.
Katoh, M., Yoshikawa, T., Tomonari, T., Katayama, K., Tomida, T., 2000. Adsorption characteristics of ion-exchanged ZSM-5 zeolites for CO_2/N_2 mixtures. J. Colloid Interface Sci. 226 (1), 145–150.
Kattula, M., Ponnuru, K., Zhu, L., Jia, W., Lin, H., Furlani, E.P., 2015. Designing ultra-thin film composite membranes: the impact of a gutter layer. Sci. Rep. 5, 15016. doi:10.1038/srep15016.
Kaviani, S., Kolahchyan, S., Hickenbottom, K.L., Lopez, A.M., Nejati, S., 2018. Enhanced solubility of carbon dioxide for encapsulated ionic liquids in polymeric materials. Chem. Eng. J. 354, 753–757. doi:10.1016/j.cej.2018.08.086.
Kaya, N., Uzun, Z.Y., 2021. Investigation of effectiveness of pine cone biochar activated with KOH for methyl orange adsorption and CO_2 capture. Biomass Conv. Bioref. 11 (3), 1067–1083. doi:10.1007/s13399-020-01063-8.
Kaye, S.S., Dailly, A., Yaghi, O.M., Long, J.R., 2007. Impact of preparation and handling on the hydrogen storage properties of Zn4O (1, 4-benzenedicarboxylate) 3 (MOF-5). J. Am. Chem. Soc. 129 (46), 14176–14177.
Kazemi, A., Hosseini, M., Mehrabani-Zeinabad, A., Faizi, V., 2016. Evaluation of different vapour recompression distillation configurations based on energy requirements and associated costs. Appl. Therm. Eng. 94, 305–313. doi:10.1016/j.applthermaleng.2015.10.042.
Kazemi, H., Shahhosseini, S., Bazyari, A., Amiri, M., 2020. A study on the effects of textural properties of γ-Al_2O_3 support on CO_2 capture capacity of Na_2CO_3. Process. Saf. Environ. Prot. 138, 176–185. doi:10.1016/j.psep.2020.03.001.
Kearns, D.T., Webley, P.A., 2006a. Modelling and evaluation of dual-reflux pressure swing adsorption cycles: Part I. Mathematical models. Chem. Eng. Sci. 61 (22), 7223–7233. doi:10.1016/j.ces.2006.07.040.
Kearns, D.T., Webley, P.A., 2006b. Modelling and evaluation of dual reflux pressure swing adsorption cycles: part II. productivity and energy consumption. Chem. Eng. Sci. 61 (22), 7234–7239. doi:10.1016/j.ces.2006.07.043.
Keith, D.W., Ha-Duong, M., Stolaroff, J.K., 2006. Climate strategy with Co2 capture from the air. Clim. Change 74 (1), 17–45. doi:10.1007/s10584-005-9026-x.
Keith, D.W., Holmes, G., St Angelo, D., Heidel, K., 2018. A process for capturing CO_2 from the atmosphere. Joule 2 (8), 1573–1594. doi:10.1016/j.joule.2018.05.006.
Keith, D.W., 2009. Why Capture CO_2 from the atmosphere? Science 325 (5948), 1654–1655. doi:10.1126/science.1175680.
Keller, L., Ohs, B., Lenhart, J., Abduly, L., Blanke, P., Wessling, M., 2018. High capacity polyethylenimine impregnated microtubes made of carbon nanotubes for CO_2 capture. Carbon 126, 338–345. doi:10.1016/j.carbon.2017.10.023.
Kelley, B.T., Valencia, J.A., Northrop, P.S., Mart, C.J., 2011. Controlled Freeze Zone™ for developing sour gas reserves. Energy Procedia 4, 824–829. doi:10.1016/j.egypro.2011.01.125.
Kenig, E.Y., Schneider, R., Górak, A., 2001. Reactive absorption: optimal process design via optimal modelling. Chem. Eng. Sci. 56 (2), 343–350. doi:10.1016/S0009-2509(00)00234-7.
Keshavarz, L., Ghaani, M.R., MacElroy, J.M.D., English, N.J., 2021. A comprehensive review on the application of aerogels in CO_2-adsorption: Materials and characterisation. Chem. Eng. J. 412, 128604. doi:10.1016/j.cej.2021.128604.
Keshavarz, L., Ghaani, M.R., MacElroy, J.M.D., English, N.J., 2021. A comprehensive review on the application of aerogels in CO_2-adsorption: Materials and characterisation. Chem. Eng. J. 412. doi:10.1016/j.cej.2021.128604.
Kezibri, N., Bouallou, C., 2017. Conceptual design and modelling of an industrial scale power to gas-oxy-combustion power plant. Int. J. Hydrogen Energy 42 (30), 19411–19419. doi:10.1016/J.IJHYDENE.2017.05.133.
Khalifa, O., Alkhatib, I.I.I., Bahamon, D., Alhajaj, A., Abu-Zahra, M.R.M., Vega, L.F., 2022. Modifying absorption process configurations to improve their performance for Post-Combustion CO_2 capture – What have we learned and what is still Missing? Chem. Eng. J. 430. doi:10.1016/j.cej.2021.133096.
Khalil, S.H., Aroua, M.K., Daud, W.M.A.W., 2012. Study on the improvement of the capacity of amine-impregnated commercial activated carbon beds for CO_2 adsorbing. Chem. Eng. J. 183, 15–20. doi:10.1016/j.cej.2011.12.011.
Khan, F.M., Krishnamoorthi, V., Mahmud, T., 2011. Modelling reactive absorption of CO_2 in packed columns for post-combustion carbon capture applications. Chem. Eng. Res. Des. 89 (9), 1600–1608. doi:10.1016/j.cherd.2010.09.020.
Khan, I.U., Othman, M.H.D., Jilani, A., Ismail, A.F., Hashim, H., Jaafar, J., Rahman, M.A., Rehman, G.U., 2018. Economical, environmental friendly synthesis, characterization for the production of zeolitic imidazolate framework-8 (ZIF-8) nanoparticles with enhanced CO_2 adsorption. Arab. J. Chem. 11 (7), 1072–1083. doi:10.1016/j.arabjc.2018.07.012.
Khan, M.U., Lee, J.T.E., Bashir, M.A., Dissanayake, P.D., Ok, Y.S., Tong, Y.W., Shariati, M.A., Wu, S., Ahring, B.K., 2021. Current status of biogas upgrading for direct biomethane use: A review. Renew. Sustain. Energy Rev. 149, 111343. doi:10.1016/j.rser.2021.111343.
Khatami, R., Stivers, C., Joshi, K., Levendis, Y.A., Sarofim, A.F., 2012. Combustion behavior of single particles from three different coal ranks and from sugar cane bagasse in O_2/N_2 and O_2/CO_2 atmospheres. Combust. Flame 159 (3), 1253–1271. doi:10.1016/j.combustflame.2011.09.009.
Khosa, A.A., Xu, T.X., Xia, B.Q., Yan, J., Zhao, C.Y., 2019. Technological challenges and industrial applications of CaCO3/CaO based thermal energy storage system - A review. Sol. Energy 193, 618–636. doi:10.1016/j.solener.2019.10.003.
Khurana, M., Farooq, S., 2016a. Adsorbent screening for postcombustion CO_2 capture: A method relating equilibrium isotherm characteristics to an optimum vacuum swing adsorption process performance. Ind. Eng. Chem. Res. 55 (8), 2447–2460. doi:10.1021/acs.iecr.5b04531.
Khurana, M., Farooq, S., 2016b. Simulation and optimization of a 6-step dual-reflux VSA cycle for post-combustion CO_2 capture. Chem. Eng. Sci. 152, 507–515. doi:10.1016/j.ces.2016.06.033.
Khurana, M., Farooq, S., 2019. Integrated adsorbent process optimization for minimum cost of electricity including carbon capture by a VSA process. AIChE J. 65 (1), 184–195. doi:10.1002/aic.16362.
Kianfar, E., Cao, V., 2021. Polymeric membranes on base of PolyMethyl methacrylate for air separation: a review. J. Mater. Res. Technol. 10, 1437–1461. doi:10.1016/j.jmrt.2020.12.061.
Kiełbasa, K., Bayar, Ş., Varol, E.A., Sreńscek-Nazzal, J., Bosacka, M., Michalkiewicz, B., 2022. Thermochemical conversion of lignocellulosic biomass - olive pomace - into activated biocarbon for CO_2 adsorption. Ind. Crops Prod. 187, 115416. doi:10.1016/j.indcrop.2022.115416.
Kiebach, R., Pirou, S., Martinez Aguilera, L., Haugen, A.B., Kaiser, A., Hendriksen, P.V., Balaguer, M., García-Fayos, J., Serra, J.M., Schulze-Küppers, F., Christie, M., Fischer, L., Meulenberg, W.A., Baumann, S., 2022. A review on dual-phase oxygen transport membranes: from fundamentals to commercial deployment. J. Mater. Chem. A 10, 2152–2195. doi:10.1039/D1TA07898D.
Kierzkowska, A.M., Pacciani, R., Müller, C.R., 2013. CaO-Based CO_2 sorbents: from fundamentals to the development of new, highly effective materials. ChemSusChem 6 (7), 1130–1148.
Kim, S., Lee, Y.M.J.P.i.P.S., 2015. Rigid and microporous polymers for gas separation membranes. 43, 1-32.
Kim, H., Lee, K.S., 2016. Design guidance for an energy-thrift absorption process for carbon capture: Analysis of thermal energy consumption for a conventional process configuration. Int. J. Greenh. Gas Control 47, 291–302. doi:10.1016/j.ijggc.2016.02.003.
Kim, T.-J., Li, B., Hägg, M.-B., 2004. Novel fixed-site–carrier polyvinylamine membrane for carbon dioxide capture. 42 (23), 4326-4336. https://doi.org/10.1002/polb.20282.
Kim, J.-Y., Kim, J., Yang, S.-T., Ahn, W.-S., 2013. Mesoporous SAPO-34 with amine-grafting for CO_2 capture. Fuel 108, 515–520. doi:10.1016/j.fuel.2012.12.020.
Kim, T.-J., Vrålstad, H., Sandru, M., Hägg, M.-B., 2013. Separation performance of PVAm composite membrane for CO_2 capture at various pH levels. J. Membr. Sci. 428, 218–224. doi:10.1016/j.memsci.2012.10.009.
Kim, C., Cho, H.S., Chang, S., Cho, S.J., Choi, M., 2016. An ethylenediamine-grafted Y zeolite: a highly regenerable carbon dioxide adsorbent via temperature swing adsorption without urea formation. Energy Environ. Sci. 9 (5), 1803–1811. doi:10.1039/c6ee00601a.
Kim, J., Pham, D.A., Lim, Y.I., 2016. Gas-liquid multiphase computational fluid dynamics (CFD) of amine absorption column with structured-packing for CO_2 capture. Comput. Chem. Eng. 88, 39–49. doi:10.1016/j.compchemeng.2016.02.006.
Kim, J., Choi, J., Soo Kang, Y., Won, J., 2016. Matrix effect of mixed-matrix membrane containing CO_2-selective MOFs. 133 (1). https://doi.org/10.1002/app.42853.
Kim, J., Pham, D.A., Lim, Y.I., 2017. Effect of gravity center position on amine absorber with structured packing under offshore operation: Computational fluid dynamics approach. Chem. Eng. Res. Des. 121, 99–112. doi:10.1016/j.cherd.2017.03.008.
Kim, S.M., Liao, W.-C., Kierzkowska, A.M., Margossian, T., Hosseini, D., Yoon, S., Broda, M., Copéret, C., Müller, C.R., 2018. In Situ XRD and dynamic nuclear polarization surface enhanced NMR spectroscopy unravel the deactivation mechanism of CaO-based, Ca3Al2O6-stabilized CO_2 sorbents. Chem. Mater. 30 (4), 1344–1352. doi:10.1021/acs.chemmater.7b05034.
Kim, S., Hou, J., Wang, Y., Ou, R., Simon, G.P., Seong, J.G., Lee, Y.M., Wang, H.J.J.o.M.C.A., 2018. Highly permeable thermally rearranged polymer composite membranes with a graphene oxide scaffold for gas separation. 6 (17), 7668-7674.
Kim, C., Choi, W., Choi, M., 2019. SO2-resistant amine-containing CO_2 adsorbent with a surface protection layer. ACS Appl. Mater. Interfaces 11 (18), 16586–16593. doi:10.1021/acsami.9b02831.

Kim, H., Sohail, M., Yim, K., Park, Y.C., Chun, D.H., Kim, H.J., Han, S.O., Moon, J.-H., 2019. Effective CO_2 and CO separation using [M2 (DOBDC)] (M= Mg, Co, Ni) with unsaturated metal sites and excavation of their adsorption sites. ACS Appl. Mater. Interfaces 11 (7), 7014–7021.

Kim, N., Park, B., Lee, J., Kim, J., 2019. High-performance ultrathin mixed-matrix membranes based on an adhesive PGMA-co-POEM comb-like copolymer for CO_2 capture. J. Mater. Chem. A 7 (24), 14723–14731. doi:10.1039/C9TA02962A.

Kim, S.M., Armutlulu, A., Kierzkowska, A.M., Müller, C.R., 2019. Inverse opal-like, Ca3Al2O6-stabilized, CaO-based CO_2 Sorbent: stabilization of a highly porous structure to improve its cyclic CO_2 uptake. ACS Appl. Energy Mater. 2 (9), 6461–6471. doi:10.1021/acsaem.9b01058.

RL Kim, E.S., Jiang, H.Z.H., Forse, A.C., 2020. Cooperative carbon capture and steam regeneration with tetraamine-appended metal–organic frameworks. Science 369 (6502), 392–396. doi:10.1126/science.abb3976.

Kim, N.U., Park, B.J., Guiver, M.D., Kim, J.H., 2020. Use of non-selective, high-molecular-weight poly (ethylene oxide) membrane for CO_2 separation by incorporation of comb copolymer. J. Membr. Sci. 605, 118092. doi:10.1016/j.memsci.2020.118092.

Kim, Y., Lim, H.S., Kim, H.S., Lee, M., Lee, J.W., Kang, D., 2022. Carbon dioxide splitting and hydrogen production using a chemical looping concept: A review. J. CO_2 Util. 63, 102139. doi:10.1016/j.jcou.2022.102139.

Kinik, F.P., Altintas, C., Balci, V., Koyuturk, B., Uzun, A., Keskin, S., 2016. [BMIM][PF6] Incorporation doubles CO_2 selectivity of ZIF-8: elucidation of interactions and their consequences on performance. ACS Appl. Mater. Interfaces 8 (45), 30992–31005. doi:10.1021/acsami.6b11087.

Kishor, R., Ghoshal, A.K., 2016. Polyethylenimine functionalized As-synthesized KIT-6 adsorbent for highly CO_2/N_2 selective separation. Energy Fuels 30 (11), 9635–9644. doi:10.1021/acs.energyfuels.6b02082.

Kiss, A.A., 2014. Distillation technology - still young and full of breakthrough opportunities. J. Chem. Technol. Biotechnol. 89 (4), 479–498. doi:10.1002/jctb.4262.

Kizzie, A.C., Wong-Foy, A.G., Matzger, A.J., 2011. Effect of humidity on the performance of microporous coordination polymers as adsorbents for CO_2 capture. Langmuir 27 (10), 6368–6373.

Klemm, A., Lee, Y.-Y., Mao, H., Gurkan, B., 2020. Facilitated Transport Membranes With Ionic Liquids for CO_2 Separations. 8. https://doi.org/10.3389/fchem.2020.00637.

Klinthong, W., Huang, C.-H., Tan, C.-S., 2016. One-Pot synthesis and pelletizing of polyethylenimine-containing mesoporous silica powders for CO_2 capture. Ind. Eng. Chem. Res. 55 (22), 6481–6491. doi:10.1021/acs.iecr.6b00644.

Knapik, E., Kosowski, P., Stopa, J., 2018. Cryogenic liquefaction and separation of CO_2 using nitrogen removal unit cold energy. Chem. Eng. Res. Des. 131, 66–79. doi:10.1016/j.cherd.2017.12.027.

Knebel, A., Bavykina, A., Datta, S.J., Sundermann, L., Garzon-Tovar, L., Lebedev, Y., Durini, S., Ahmad, R., Kozlov, S.M., Shterk, G., 2020. Solution processable metal–organic frameworks for mixed matrix membranes using porous liquids. Nat. Mater. 19 (12), 1346–1353. doi:10.1038/s41563-020-0764-y.

Knowles, G.P., Chaffee, A.L., 2016. Aminopropyl-functionalized silica CO_2 adsorbents via sonochemical methods. J. Chem. 2016, 1–10. doi:10.1155/2016/1070838.

Ko, Y.G., Lee, H.J., Oh, H.C., Choi, U.S., 2013. Amines immobilized double-walled silica nanotubes for CO_2 capture. J. Hazard Mater. 250-251, 53–60. doi:10.1016/j.jhazmat.2013.01.035.

Kołodziej, A., Łojewska, J., 2009. Experimental and modelling study on flow resistance of wire gauzes. Chem. Eng. Process.: Process Intensif. 48 (3), 816–822. doi:10.1016/j.cep.2008.10.009.

Kolle, J.M., Fayaz, M., Sayari, A., 2021. Understanding the effect of water on CO_2 adsorption. Chem. Rev. 121 (13), 7280–7345. doi:10.1021/acs.chemrev.0c00762.

Kong, Y., Shen, X.D., Cui, S., Fan, M.H., 2015. Development of monolithic adsorbent via polymeric sol-gel process for low-concentration CO_2 capture. Appl. Energy 147, 308–317. doi:10.1016/j.apenergy.2015.03.011.

Kong, Y., Shen, X., Fan, M., Yang, M., Cui, S., 2016. Dynamic capture of low-concentration CO_2 on amine hybrid silsesquioxane aerogel. Chem. Eng. J. 283, 1059–1068. doi:10.1016/j.cej.2015.08.034.

Kong, Y., Zhang, J.Y., Shen, X.D., 2017. One-pot sol-gel synthesis of amine hybrid titania/silsesquioxane composite aerogel for CO_2 capture. J. Sol-Gel Sci. Technol. 84 (3), 422–431. doi:10.1007/s10971-017-4516-7.

Kong, Y.K., Ruan, S., Kurumisawa, K., 2022. Recycling of calcined carbonated cement pastes as cementitious materials: Proposed CCUS technology for calcium looping. J. Environ. Chem. Eng. 10 (5), 11. doi:10.1016/j.jece.2022.108247.

Koronaki, I.P., Prentza, L., Papaefthimiou, V., 2015. Modeling of CO_2 capture via chemical absorption processes - An extensive literature review. Renew. Sustain. Energy Rev. 50, 547–566. doi:10.1016/j.rser.2015.04.124.

Koros, W.J., Zhang, C., 2017. Materials for next-generation molecularly selective synthetic membranes. Nat. Mater. 16 (3), 289–297. doi:10.1038/nmat4805.

Kou, S.G., Peters, L.M., Mucalo, M.R., 2021. Chitosan: A review of sources and preparation methods. Int. J. Biol. Macromol. 169, 85–94. doi:10.1016/j.ijbiomac.2020.12.005.

Krödel, M., Landuyt, A., Abdala, P.M., Müller, C.R.J.C., 2020. Mechanistic understanding of CaO-based sorbents for high-temperature CO2 capture: advanced characterization and prospects. 13 (23), 6259-6272.

Krödel, M., Oing, A., Negele, J., Landuyt, A., Kierzkowska, A., Bork, A.H., Donat, F., Müller, C.R., 2022. Yolk–shell-type CaO-based sorbents for CO_2 capture: assessing the role of nanostructuring for the stabilization of the cyclic CO_2 uptake. Nanoscale 14 (45), 16816–16828. doi:10.1039/D2NR04492G.

Krekel, D., Samsun, R.C., Peters, R., Stolten, D., 2018. The separation of CO_2 from ambient air – A techno-economic assessment. Appl. Energy 218, 361–381. doi:10.1016/j.apenergy.2018.02.144.

Krishna, R., van Baten, J.M., 2010. In silico screening of zeolite membranes for CO_2 capture. J. Membr. Sci. 360 (1-2), 323–333.

Krishnamurthy, S., Haghpanah, R., Rajendran, A., Farooq, S., 2014a. Simulation and optimization of a dual-Adsorbent, two-bed vacuum swing adsorption process for CO_2 capture from wet flue gas. Ind. Eng. Chem. Res. 53 (37), 14462–14473. doi:10.1021/ie5024723.

Krishnamurthy, S., Rao, V.R., Guntuka, S., Sharratt, P., Haghpanah, R., Rajendran, A., Amanullah, M., Karimi, A., Farooq, S., 2014b. CO_2 capture from dry flue gas by vacuum swing adsorption: A pilot plant study. AIChE J. 60 (5), 1830–1842. doi:10.1002/aic.14435.

Kuhn, P., Antonietti, M., Thomas, A., 2008. Porous, covalent triazine-based frameworks prepared by ionothermal synthesis. Angew. Chem. Int. Ed. 47 (18), 3450–3453.

Kumakiri, X.H.a.I., 2020. Carbon membrane technology: fundamentals and applications.

Kumar, S., Prasad, K., Gil, J.M., Sobral, A.J.F.N., Koh, J., 2018. Mesoporous zeolite-chitosan composite for enhanced capture and catalytic activity in chemical fixation of CO_2. Carbohydr. Polym. 198, 401–406. doi:10.1016/j.carbpol.2018.06.100.

Kumar, A., Singh, E., Mishra, R., Lo, S.L., Kumar, S., 2022. A green approach towards sorption of CO2 on waste derived biochar. Environ. Res. 214. doi:10.1016/j.envres.2022.113954.

Kunalan, S., Palanivelu, K., 2022. Polymeric composite membranes in carbon dioxide capture process: a review. Environ. Sci. Pollut. Res. Int. 29 (26), 38735–38767. doi:10.1007/s11356-022-19519-x.

Kundu, P.K., Chakma, A., Feng, X., 2014. Effectiveness of membranes and hybrid membrane processes in comparison with absorption using amines for post-combustion CO_2 capture. Int. J. Greenh. Gas Control 28, 248–256. doi:10.1016/j.ijggc.2014.06.031.

Kung, H.H., Ko, E.I., 1996. Preparation of oxide catalysts and catalyst supports — a review of recent advances. Chem. Eng. J. Biochem. Eng. J. 64 (2), 203–214. doi:10.1016/S0923-0467 (96)03139-9.

Kurlov, A., Broda, M., Hosseini, D., Mitchell, S.J., Pérez-Ramírez, J., Müller, C.R., 2016. Mechanochemically activated, calcium oxide-based, magnesium oxide-stabilized carbon dioxide sorbents. ChemSusChem 9 (17), 2380–2390. doi:10.1002/cssc.201600510.

Kurlov, A., Armutlulu, A., Donat, F., Studart, A.R., Müller, C.R., 2020a. CaO-Based CO_2 sorbents with a hierarchical porous structure made via microfluidic droplet templating. Ind. Eng. Chem. Res. 59 (15), 7182–7188. doi:10.1021/acs.iecr.9b05996.

Kurlov, A., Kierzkowska, A.M., Huthwelker, T., Abdala, P.M., Müller, C.R.J.P.C.C.P., 2020b. Na 2 CO 3-modified CaO-based CO 2 sorbents: the effects of structure and morphology on CO 2 uptake. 22 (42), 24697-24703.

Kvamsdal, H.M., Jakobsen, J.P., Hoff, K.A., 2009. Dynamic modeling and simulation of a CO_2 absorber column for post-combustion CO_2 capture. Chem. Eng. Process.: Process Intensif. 48 (1), 135–144. doi:10.1016/j.cep.2008.03.002.

Kwon, G., Cho, D.-W., Hyun Moon, D., Kwon, E.E., Song, H., 2019. Beneficial use of CO_2 in pyrolysis of chicken manure to fabricate a sorptive material for CO_2. Appl. Therm. Eng. 154, 469–475. doi:10.1016/j.applthermaleng.2019.03.110.

Kwon, G., Cho, D.W., Moon, D.H., Kwon, E.E., Song, H., 2019. Beneficial use of CO_2 in pyrolysis of chicken manure to fabricate a sorptive material for CO_2. Appl. Therm. Eng. 154, 469–475. doi:10.1016/j.applthermaleng.2019.03.110.

Kwon, D.-i., Kim, J.-C., Lee, H., Lee, W., Jo, C., 2022. Engineering micropore walls of beta zeolites by post-functionalization for CO_2 adsorption performance screening under humid conditions. Chem. Eng. J. 427. doi:10.1016/j.cej.2021.131461.

López, T., Bosch, P., Tzompantzi, F., Gómez, R., Navarrete, J., López-Salinas, E., Llanos, M.E., 2000. Effect of sulfation methods on TiO2−SiO2 sol−gel catalyst acidity. Appl. Catal., A. 197, 107–117.

López, R., Fernández, C., Martínez, O., Sánchez, M.E., 2016. Techno-economic analysis of a 15MW corn-rape oxy-combustion power plant. Fuel Process. Technol. 142, 296–304. doi:10.1016/j.fuproc.2015.10.020.

Z.X. Lü, B, Li, X, et al., 2021. Mechanism of CO_2 capture into amino-azolyl dual-functionalized ionic liquid biphasic solvent. Sci. China: Chem. 51 (12), 1660–1670. doi:10.1360/SSC-2021-0026.

Laassiri, S., Zeinalipour-Yazdi, C.D., Catlow, C.R.A., Hargreaves, J.S., 2018. The potential of manganese nitride based materials as nitrogen transfer reagents for nitrogen chemical looping. Appl. Catal. B: Environ. 223, 60–66.

Labreche, Y., Fan, Y., Lively, R.P., Jones, C.W., Koros, W.J., 2015. Direct dual layer spinning of aminosilica/T orlon® hollow fiber sorbents with a lumen layer for CO_2 separation by rapid temperature swing adsorption. J. Appl. Polym. Sci. 132 (17).

Lackner, K., Ziock, H.-J., Grimes, P., 1999. Carbon Dioxide Extraction from Air: Is It An Option? United States.

Lackner, K.S., Brennan, S., Matter, J.M., Park, A.H.A., Wright, A., van der Zwaan, B., 2012. The urgency of the development of CO_2 capture from ambient air. P Natl. Acad. Sci. USA 109 (33), 13156–13162. doi:10.1073/pnas.1108765109.

Lackner, K.S., 2003. A guide to CO_2 sequestration. Science 300 (5626), 1677–1678.

Lahijani, P., Mohammadi, M., Mohamed, A.R., 2018. Metal incorporated biochar as a potential adsorbent for high capacity CO_2 capture at ambient condition. J. Co2 Util. 26, 281–293. doi:10.1016/j.jcou.2018.05.018.

Lai, J.Y., Ngu, L.H., Hashim, S.S., 2021. A review of CO_2 adsorbents performance for different carbon capture technology processes conditions. Greenh. Gases 11 (5), 1076–1117. doi:10.1002/ghg.2112.

Lail, M., Tanthana, J., Coleman, L., 2014. Non-aqueous solvent (NAS) CO_2 capture process. Energy Proc. 63, 580–594. doi:10.1016/j.egypro.2014.11.063.

Lam, S.S., Liew, R.K., Cheng, C.K., Rasit, N., Ooi, C.K., Ma, N.L., Ng, J.-H., Lam, W.H., Chong, C.T., Chase, H.A., 2018. Pyrolysis production of fruit peel biochar for potential use in treatment of palm oil mill effluent. J. Environ. Manage. 213, 400–408. doi:10.1016/j.jenvman.2018.02.092.

Landelle, A., Tauveron, N., Haberschill, P., Revellin, R., Colasson, S., 2017. Organic Rankine cycle design and performance comparison based on experimental database. Appl. Energy 204, 1172–1187. doi:10.1016/j.apenergy.2017.04.012.

Landuyt, A., Kumar, P., Yuwono, J., Bork, A.H., Abdala, P., Müller, C., 2022. Uncovering the CO_2 capture mechanism of alkali metal nitrate promoted MgO by 18O isotope labeling. [Manuscript submitted for publication.

Lappalainen, K., Manninen, M., Alopaeus, V., 2009. CFD modeling of radial spreading of flow in trickle-bed reactors due to mechanical and capillary dispersion. Chem. Eng. Sci. 64 (2), 207–218. doi:10.1016/j.ces.2008.10.009.

Lappalainen, K., Gorshkova, E., Manninen, M., Alopaeus, V., 2011. Characteristics of liquid and tracer dispersion in trickle-bed reactors: effect on CFD modeling and experimental analyses. Comput. Chem. Eng. 35 (1), 41–49. doi:10.1016/j.compchemeng.2010.06.006.

Lara-García, H.A., Ovalle-Encinia, O., Ortiz-Landeros, J., Lima, E., Pfeiffer, H., 2019. Synthesis of $Li_4{}^+xSi_1-xFexO_4$ solid solution by dry ball milling and its highly efficient CO_2 chemisorption in a wide temperature range and low CO_2 concentrations. J. Mater. Chem. A 7 (8), 4153–4164. doi:10.1039/C8TA12359D.

Lasek, J.A., Janusz, M., Zuwała, J., Głód, K., Iluk, A., 2013. Oxy-fuel combustion of selected solid fuels under atmospheric and elevated pressures. Energy 62, 105–112. doi:10.1016/j.energy.2013.04.079.

Lawal, A., Wang, M., Stephenson, P., Yeung, H., 2009. Dynamic modelling of CO_2 absorption for post combustion capture in coal-fired power plants. Fuel 88 (12), 2455–2462. doi:10.1016/j.fuel.2008.11.009.

Lawal, A., Wang, M., Stephenson, P., Koumpouras, G., Yeung, H., 2010. Dynamic modelling and analysis of post-combustion CO_2 chemical absorption process for coal-fired power plants. Fuel 89 (10), 2791–2801. doi:10.1016/j.fuel.2010.05.030.

Lawal, A., Wang, M., Stephenson, P., Obi, O., 2012. Demonstrating full-scale post-combustion CO 2 capture for coal-fired power plants through dynamic modelling and simulation. Fuel 101, 115–128. doi:10.1016/j.fuel.2010.10.056.

Lawson, S., Rownaghi, A.A., Rezaei, F., 2018. Carbon hollow fiber-supported metal–organic framework composites for gas adsorption. Energy Technol. 6 (4), 694–701. doi:10.1002/ente.201700657.

Laycock, D.E., Collacott, R.J., Alan Skelton, D., Tchir, M.F., 1991. Stereospecific polymerization of propylene oxide on thermally activated synthetic hydrotalcite. J. Catal. 130 (2), 354–358. doi:10.1016/0021-9517 (91)90119-O.

León, M., Díaz, E., Bennici, S., Vega, A., Ordóñez, S., Auroux, A., 2010. Adsorption of CO_2 on hydrotalcite-derived mixed oxides: sorption mechanisms and consequences for adsorption irreversibility. Ind. Eng. Chem. Res. 49 (8), 3663–3671. doi:10.1021/ie902072a.

C.B. Leal, O., Ovalles, C., Garcia, J.J., Espidel, Y., 1995. Reversible adsorption of carbon dioxide on amine surface-bonded silica gel. Inorg. Chim. Acta 240, 183–189.

Leavitt, F., 1992. Duplex adsorption process: US Patent 5,085,674.

Lee, Y., Gurkan, B., 2021. Graphene oxide reinforced facilitated transport membranes with poly (ionic liquid) and ionic liquid carriers for CO_2/N_2 separation. J. Membr. Sci. 638, 119652. doi:10.1016/j.memsci.2021.119652.

Lee, A., Miller, D.C., 2013. A one-dimensional (1-D) three-region model for a bubbling fluidized-bed adsorber. Ind. Eng. Chem. Res. 52 (1), 469–484. doi:10.1021/ie300840q.

Lee, J.H., Park, S.J., 2020. Recent advances in preparations and applications of carbon aerogels: A review. Carbon 163, 1–18. doi:10.1016/j.carbon.2020.02.073.

Lee, S.W., Kim, H.J., Lee, Y.K., Park, K., Son, J.-H., Kwon, Y.-U., 2003. Triply interpenetrating coordination polymers based on paddle-wheel type secondary-building units of M2 (CO_2R) 4:[Ni3 (2, 6-NDC) 3 (bipy) 1.5],[Co3 (2, 6-NDC) 3 (bipy) 1.5], and [Co (1, 3-BDC) (bipyen)] (2, 6-NDC= 2, 6-naphthalenedicarboxylate; 1, 3-BDC= 1, 3-benzenedicarboxylate; bipy= 4, 4′-bipyridine; bipyen= trans-1, 2-bis (4-pyridyl) ethylene). Inorg. Chim. Acta 353, 151–158.

Lee, K.B., Verdooren, A., Caram, H.S., Sircar, S., 2007. Chemisorption of carbon dioxide on potassium-carbonate-promoted hydrotalcite. J. Colloid. Interface Sci. 308 (1), 30–39. doi:10.1016/j.jcis.2006.11.011.

Lee, S.C., Chae, H.J., Lee, S.J., Choi, B.Y., Yi, C.K., Lee, J.B., Ryu, C.K., Kim, J.C., 2008. Development of regenerable MgO-based sorbent promoted with K_2CO_3 for CO_2 capture at low temperatures. Environ. Sci. Technol. 42 (8), 2736–2741. doi:10.1021/es702693c.

Lee, J.M., Min, Y.J., Lee, K.B., Jeon, S.G., Na, J.G., Ryu, H.J., 2010. Enhancement of CO_2 sorption uptake on hydrotalcite by impregnation with K2CO3. Langmuir 26 (24), 18788–18797. doi:10.1021/la102974s.

Lee, D., Jin, Y., Jung, N., Lee, J., Lee, J., Jeong, Y.S., Jeon, S., 2011. Gravimetric analysis of the adsorption and desorption of CO_2 on amine-functionalized mesoporous silica mounted on a microcantilever array. Environ. Sci. Technol. 45 (13), 5704–5709. doi:10.1021/es200680v.

Lee, C.S., Ong, Y.L., Aroua, M.K., Daud, W.M.A.W., 2013. Impregnation of palm shell-based activated carbon with sterically hindered amines for CO_2 adsorption. Chem. Eng. J. 219, 558–564. doi:10.1016/j.cej.2012.10.064.

Lee, S.C., Kwon, Y.M., Chae, H.J., Jung, S.Y., Lee, J.B., Ryu, C.K., Yi, C.K., Kim, J.C., 2013. Improving regeneration properties of potassium-based alumina sorbents for carbon dioxide capture from flue gas. Fuel 104, 882–885. doi:10.1016/j.fuel.2012.05.037.

Lee, S.C., Cho, M.S., Jung, S.Y., Ryu, C.K., Kim, J.C., 2014. Effects of alumina phases on CO_2 sorption and regeneration properties of potassium-based alumina sorbents. Adsorption 20 (2), 331–339. doi:10.1007/s10450-013-9596-2.

Lee, W.R., Hwang, S.Y., Ryu, D.W., Lim, K.S., Han, S.S., Moon, D., Choi, J., Hong, C.S., 2014. Diamine-functionalized metal–organic framework: exceptionally high CO_2capacities from ambient air and flue gas, ultrafast CO_2uptake rate, and adsorption mechanism. Energy Environ. Sci. 7 (2), 744–751. doi:10.1039/c3ee42328j.

Lee, M.-S., Lee, S.-Y., Park, S.-J., 2015. Preparation and characterization of multi-walled carbon nanotubes impregnated with polyethyleneimine for carbon dioxide capture. Int. J. Hydrogen Energy 40 (8), 3415–3421. doi:10.1016/j.ijhydene.2014.12.104.

Lee, W.R., Jo, H., Yang, L.-M., Lee, H., Ryu, D.W., Lim, K.S., Song, J.H., Min, D.Y., Han, S.S., Seo, J.G., Park, Y.K., Moon, D., Hong, C.S., 2015. Exceptional CO_2 working capacity in a heterodiamine-grafted metal–organic framework. Chem. Sci. 6 (7), 3697–3705. doi:10.1039/c5sc01191d.

Lee, A., Elam, J.W., Darling, S.B., 2016. Membrane materials for water purification: design, development, and application. Environ. Sci.: Water Res. Technol. 2 (1), 17–42.

Lee, J.H., Lee, J., Jo, H.J., Seong, J.G., Kim, J.S., Lee, W.H., Moon, J., Lee, D., Oh, W.J., Yeo, J.-g.J.J.o.M.S., 2017. Wet CO_2/N_2 permeation through a crosslinked thermally rearranged poly (benzoxazole-co-imide) (XTR-PBOI) hollow fiber membrane module for CO_2 capture. 539, 412-420.

Lee, C.H., Choi, S.W., Yoon, H.J., Kwon, H.J., Lee, H.C., Jeon, S.G., Lee, K.B.J.C.E.J., 2018. Na2CO3-doped CaO-based high-temperature CO_2 sorbent and its sorption kinetics. 352, 103-109.

Lee, E.J., Bae, J., Choi, K.M., Jeong, N.C., 2019. Exploiting microwave chemistry for activation of metal−organic frameworks. ACS Appl. Mater. Interfaces 11, 35155–35161. doi:10.1021/acsami.9b12201.

Lee, J., Kim, J.S., Kim, J.F., Jo, H.J., Park, H., Seong, J.G., Lee, Y.M.J.J.o.m.s., 2019. Densification-induced hollow fiber membranes using crosslinked thermally rearranged (XTR) polymer for CO_2 capture. 573, 393-402.

Lee, J., Satheeshkumar, C., Yu, H.J., Kim, S., Lee, J.S., Seo, M., Kim, M., 2020. Pore engineering of covalently connected metal-organic framework nanoparticle-mixed-matrix membrane composites for molecular separation. ACS Appl. Nano Mater. doi:10.1021/acsanm.0c01982.

Lee, Y.-Y., Edgehouse, K., Klemm, A., Mao, H., Pentzer, E., Gurkan, B., 2020. Capsules of reactive ionic liquids for selective capture of carbon dioxide at low concentrations. ACS Appl. Mater. Interfaces 12 (16), 19184–19193. doi:10.1021/acsami.0c01622.

Lee, J., Kim, J.S., Moon, S.-y., Park, C.Y., Kim, J.F., Lee, Y.M.J.J.o.M.S., 2020. Dimensionally-controlled densification in crosslinked thermally rearranged (XTR) hollow fiber membranes for CO_2 capture. 595, 117535.

Lee, T.H., Ozcan, A., Park, I., Fan, D., Jang, J.K., Mileo, P.G., Yoo, S.Y., Roh, J.S., Kang, J.H., Lee, B.K., 2021a. Disclosing the Role of defect-engineered metal-organic frameworks in mixed matrix membranes for efficient CO_2 separation: a joint experimental-computational exploration. Adv. Funct. Mater. 31 (38), 2103973. doi:10.1002/adfm.202103973.

Lee, T.H., Ozcan, A., Park, I., Fan, D., Jang, J.K., Mileo, P.G., Yoo, S.Y., Roh, J.S., Kang, J.H., Lee, B.K., 2021b. Disclosing the role of defect-engineered metal–organic frameworks in mixed matrix membranes for efficient CO_2 separation: a joint experimental-computational exploration. Adv. Funct. Mater. 31 (38), 2103973.

Lee, C.S., Kang, M., Kim, K.C., Kim, J.H., 2022. In-situ formation of asymmetric thin-film, mixed-matrix membranes with ZIF-8 in dual-functional imidazole-based comb copolymer for high-performance CO_2 capture. J. Membr. Sci. 642, 119913. doi:10.1016/j.memsci.2021.119913.

Lee, W.M., 1980. Selection of barrier materials from molecular structure. 20 (1), 65-69. https://doi.org/10.1002/pen.760200111.

Lei, L., Bai, L., Lindbråthen, A., Pan, F., Zhang, X., He, X., 2020. Carbon membranes for CO_2 removal: Status and perspectives from materials to processes. Chem. Eng. J. 401. doi:10.1016/j.cej.2020.126084.

Lei, L., Pan, F., Lindbrathen, A., Zhang, X., Hillestad, M., Nie, Y., Bai, L., He, X., Guiver, M.D., 2021. Carbon hollow fiber membranes for a molecular sieve with precise-cutoff ultramicropores for superior hydrogen separation. Nat. Commun. 12 (1), 268. doi:10.1038/s41467-020-20628-9.

Leites, I.L., 1998. Thermodynamics of CO_2 solubility in mixtures monoethanolamine with organic solvents and water and commercial experience of energy saving gas purification technology. Energy Convers. Manage. 39 (16-18), 1665–1674. doi:10.1016/S0196-8904 (98)00076-4.

Leng, L., Xiong, Q., Yang, L., Li, H., Zhou, Y., Zhang, W., Jiang, S., Li, H., Huang, H., 2021. An overview on engineering the surface area and porosity of biochar. Sci. Total Environ. 763, 144204. doi:10.1016/j.scitotenv.2020.144204.

Lenzi, D., 2018. The ethics of negative emissions. Glob. Sustain. 1, e7. doi:10.1017/sus.2018.5.

Leperi, K.T., Snurr, R.Q., You, F., 2016. Optimization of Two-Stage Pressure/Vacuum Swing Adsorption with Variable Dehydration Level for Postcombustion Carbon Capture. Ind. Eng. Chem. Res. 55 (12), 3338–3350.

Leperi, K.T., Chung, Y.G., You, F., Snurr, R.Q., 2019. Development of a general evaluation metric for rapid screening of adsorbent materials for postcombustion CO_2 capture. ACS Sustain. Chem. Eng. 7 (13), 11529–11539. doi:10.1021/acssuschemeng.9b01418.

Leppänen, P., Inha, T., Pentti, M., 2014. An experimental study on the effect of design flue gas temperature on the fire safety of chimneys. Fire Technol. 51 (4), 847–866. doi:10.1007/s10694-014-0415-4.

Leukel, S., Panthöfer, M., Mondeshki, M., Kieslich, G., Wu, Y., Krautwurst, N., Tremel, W., 2018. Mechanochemical access to defect-stabilized amorphous calcium carbonate. Chem. Mater. 30 (17), 6040–6052.

Leung, D.Y.C., Caramanna, G., Maroto-Valer, M.M., 2014. An overview of current status of carbon dioxide capture and storage technologies. Renew. Sustain. Energy Rev. 39, 426–443. doi:10.1016/j.rser.2014.07.093.

Lewis, W.K., Gilliland, E.R., 1954. Production of pure carbon dioxide. Google Patents.

Lewis, T., Nielsen, L., 1970. Dynamic mechanical properties of particulate-filled composites. J. Appl. Polym. Sci. 14 (6), 1449–1471.

Li, G., Bai, P., 2012a. New operation strategy for separation of ethanol–water by extractive distillation. Ind. Eng. Chem. Res. 51 (6), 2723–2729. doi:10.1021/IE2026579.

Li, G., Bai, P., 2012b. New operation strategy for separation of ethanol–water by extractive distillation. Ind. Eng. Chem. Res. 51 (6), 2723–2729. doi:10.1021/ie2026579.

Li, H., Hill, M.R., 2017. Low-energy CO_2 release from metal-organic frameworks triggered by external stimuli. Acc. Chem. Res. 50 (4), 778–786. doi:10.1021/acs.accounts.6b00591.

Li, H., Hill, M.R., 2017. Low-energy CO_2 release from metal–organic frameworks triggered by external stimuli. Accounts Chemi. Res. 50 (4), 778–786.

Li, G., Pidko, E.A., 2019. The nature and catalytic function of cation sites in zeolites: a computational perspective. ChemCatChem 11 (1), 134–156.

Li, Y., Yang, R.T., 2007. Gas adsorption and storage in metal– organic framework MOF-177. Langmuir 23 (26), 12937–12944.
Li, H.L., Eddaoudi, M., Groy, T.L., Yaghi, O.M., 1998. Establishing microporosity in open metal-organic_frameworks_ gas sorption isotherms for Zn (BDC)_ (BDC) 1,4-benzenedicarboxylate). J. Am. Chem. Soc. 120 (33), 8571–8572.
Li, Z.-s., Cai, N.-s., Huang, Y.-y., 2006. Effect of preparation temperature on cyclic CO_2 capture and multiple carbonation−calcination cycles for a new Ca-based CO_2 sorbent. Ind. Eng. Chem. Res. 45 (6), 1911–1917. doi:10.1021/ie0512111.
Li, F., Li, Y., Chung, T.-S., Kawi, S., 2010. Facilitated transport by hybrid POSS®–Matrimid®–Zn2+ nanocomposite membranes for the separation of natural gas. J. Membr. Sci. 356 (1), 14–21. doi:10.1016/j.memsci.2010.03.021.
Li, L., Li, Y., Wen, X., Wang, F., Zhao, N., Xiao, F., Wei, W., Sun, Y., 2011. CO_2 capture over $K_2CO3/MgO/Al_2O_3$ dry sorbent in a fluidized bed. Energy Fuels 25 (8), 3835–3842. doi:10.1021/ef200499b.
Li, Z.-s., Fang, F., Tang, X.-y., Cai, N.-s., 2012. Effect of temperature on the carbonation reaction of CaO with CO_2. Energy Fuels 26 (4), 2473–2482. doi:10.1021/ef201543n.
Li, J., You, C., Chen, L., Ye, Y., Qi, Z., Sundmacher, K., 2012. Dynamics of CO_2 absorption and desorption processes in alkanolamine with cosolvent polyethylene glycol. Ind. Eng. Chem. Res. 51 (37), 12081–12088.
Li, H., Moullec, Y.L., Lu, J., Chen, J., Marcos, J.C.V., Chen, G., 2014. Solubility and energy analysis for CO_2 absorption in piperazine derivatives and their mixtures. Int. J. Greenh. Gas Control 31, 25–32. doi:10.1016/j.ijggc.2014.09.012.
Li, L.-J., Liao, P.-Q., He, C.-T., Wei, Y.-S., Zhou, H.-L., Lin, J.-M., Li, X.-Y., Zhang, J.-P., 2015. Grafting alkylamine in UiO-66 by charge-assisted coordination bonds for carbon dioxide capture from high-humidity flue gas. J. Mater. Chem. A 3 (43), 21849–21855. doi:10.1039/c5ta05997f.
Li, X., Cheng, Y., Zhang, H., Wang, S., Jiang, Z., Guo, R., Wu, H., 2015. Efficient CO_2 capture by functionalized graphene oxide nanosheets as fillers to fabricate multi-permselective mixed matrix membranes. ACS Appl. Mater. Interfaces 7 (9), 5528–5537. doi:10.1021/acsami.5b00106.
Li, Y., Wang, S., He, G., Wu, H., Pan, F., Jiang, Z., 2015. Facilitated transport of small molecules and ions for energy-efficient membranes. Chem. Soc. Rev. 44 (1), 103–118. doi:10.1039/C4CS00215F.
Li, Q., Wang, T., Dai, C., Lei, Z., 2016. Hydrodynamics of novel structured packings: an experimental and multi-scale CFD study. Chem. Eng. Sci. 143, 23–35. doi:10.1016/j.ces.2015.12.014.
Li, D., Zhou, Y., Shen, Y., Sun, W., Fu, Q., Yan, H., Zhang, D., 2016. Experiment and simulation for separating CO_2/N_2 by dual-reflux pressure swing adsorption process. Chem. Eng. J. 297, 315–324. doi:10.1016/j.cej.2016.03.075.
Li, H., Hill, M.R., Doblin, C., Lim, S., Hill, A.J., Falcaro, P., 2016. Visible light triggered CO_2 liberation from silver nanocrystals incorporated metal-organic frameworks. Adv. Funct. Mater. 26 (27), 4815–4821. doi:10.1002/adfm.201600827.
Li, K., Jiang, J., Chen, X., Gao, Y., Yan, F., Tian, S., 2016. Research on urea linkages formation of amine functional adsorbents during CO_2 capture process: two key factors analysis, temperature and moisture. J. Phys. Chem. C 120 (45), 25892–25902. doi:10.1021/acs.jpcc.6b08788.
Li, S., Ding, J., Zhang, X., Cheng, D., Hu, X., Li, X., 2016. A feasible energy-saving analysis of a new system for CO_2 cryogenic capture. Int. J. Low-Carbon Technol. 11 (2), 235–239. doi:10.1093/ijlct/ctt065.
Li, Z.-H., Wang, Y., Xu, K., Yang, J.-Z., Niu, S.-B., Yao, H., 2016. Effect of steam on CaO regeneration, carbonation and hydration reactions for CO_2 capture. Fuel Process. Technol. 151, 101–106. doi:10.1016/j.fuproc.2016.05.019.
Li, H., Sadiq, M.M., Suzuki, K., Ricco, R., Doblin, C., Hill, A.J., Lim, S., Falcaro, P., Hill, M.R., 2016a. Magnetic metal-organic frameworks for efficient carbon dioxide capture and remote trigger release. Adv. Mater. 28 (9), 1839–1844. doi:10.1002/adma.201505320.
Li, H., Wang, K., Feng, D., Chen, Y.P., Verdegaal, W., Zhou, H.C., 2016b. Incorporation of alkylamine into metal-organic frameworks through a bronsted acid-base reaction for CO_2 capture. ChemSusChem 9 (19), 2832–2840. doi:10.1002/cssc.201600768.
Li, P., Liu, W., Dennis, J.S., Zeng, H.C., 2017. Synthetic architecture of MgO/C nanocomposite from hierarchical-structured coordination polymer toward enhanced CO_2 capture. ACS Appl. Mater. Interfaces 9 (11), 9592–9602.
Li, Y., Li, L., Yu, J., 2017. Applications of zeolites in sustainable chemistry. Chem 3 (6), 928–949.
Li, C., Chew, J.J., Mahmoud, A., Liu, S., Sunarso, J., 2018. Modelling of oxygen transport through mixed ionic-electronic conducting (MIEC) ceramic-based membranes: An overview. J. Membr. Sci. 567, 228–260. doi:10.1016/J.MEMSCI.2018.09.016.
Li, H., Li, H., Dai, Q., Li, H., Brédas, J.L., 2018. Hydrolytic stability of boronate ester-linked covalent organic frameworks. Adv. Theor. Simul. 1 (2), 1700015.
Li, M., Tang, Y., Ren, N., Zhang, Z., Cao, Y., 2018. Effect of mineral constituents on temperature-dependent structural characterization of carbon fractions in sewage sludge-derived biochar. J. Clean. Prod. 172, 3342–3350. doi:10.1016/j.jclepro.2017.11.090.
Li, S., Jiang, X., Sun, H., He, S., Zhang, L., Shao, L., 2019. Mesoporous dendritic fibrous nanosilica (DFNS) stimulating mix matrix membranes towards superior CO_2 capture. J. Membr. Sci. 586, 185–191. doi:10.1016/j.memsci.2019.05.069.
Li, H., Wang, K., Hu, Z., Chen, Y.-P., Verdegaal, W., Zhao, D., Zhou, H.-C., 2019. Harnessing solvent effects to integrate alkylamine into metal–organic frameworks for exceptionally high CO_2 uptake. J. Mater. Chem. A 7 (13), 7867–7874. doi:10.1039/c8ta11300a.
Li, H., Zhao, Z., Xiouras, C., Stefanidis, G.D., Li, X., Gao, X., 2019. Fundamentals and applications of microwave heating to chemicals separation processes. Renew. Sustain. Energy Rev. 114, 109316. doi:10.1016/j.rser.2019.109316.
Li, H.M., Li, J.H., Thomas, A., Liao, Y.Z., 2019. Ultra-high surface area nitrogen-doped carbon aerogels derived from a schiff-base porous organic polymer aerogel for CO_2 storage and supercapacitors. Adv. Funct. Mater. 29 (40). doi:10.1002/adfm.201904785.
Li, N., Chang, Z., Huang, H., Feng, R., He, W.W., Zhong, M., Madden, D.G., Zaworotko, M.J., Bu, X.H., 2019. Specific K (+) binding sites as CO_2 traps in a porous MOF for enhanced CO_2 selective sorption. Small 15 (22), e1900426. doi:10.1002/smll.201900426.
Li, S., Prasetya, N., Ladewig, B.P., 2019. Investigation of Azo-COP-2 as a photoresponsive low-energy CO_2 adsorbent and porous filler in mixed matrix membranes for CO_2/N_2 separation. Ind. Eng. Chem. Res. 58 (23), 9959–9969. doi:10.1021/acs.iecr.9b00762.
Li, W., Goh, K., Chuah, C.Y., Bae, T.-H., 2019. Mixed-matrix carbon molecular sieve membranes using hierarchical zeolite: A simple approach towards high CO_2 permeability enhancements. J. Membr. Sci. 588. doi:10.1016/j.memsci.2019.117220.
Li, Z., Shan, X.W., Yang, P.P., Gao, Z.Z., Fang, Q.R., Xue, M., Qiu, S.L., 2019. Preparation, characterization and gas adsorption properties of metal-organic aerogels. Chem. J. Chin. U 40 (6), 1116–1120. doi:10.7503/cjcu20190102.
Li, H., Liu, B., Yang, M., Zhu, D., Huang, Z., Chen, W., Yang, L., Chen, G., 2020. CO_2 separation performance of zeolitic imidazolate framework-8 porous slurry in a pilot-scale packed tower. Ind. Eng. Chem. Res. 59 (13), 6154–6163. doi:10.1021/acs.iecr.9b06897.
Li, Y.W., Jia, P.P., Xu, J., Wu, Y., Jiang, H., Li, Z., 2020. The aminosilane functionalization of cellulose nanofibrils and the mechanical and CO_2 adsorption characteristics of their aerogel. Ind. Eng. Chem. Res. 59 (7), 2874–2882. doi:10.1021/acs.iecr.9b04253.
Li, X., Ding, S., Zhang, J., Wei, Z.J.I.J.o.G.G.C., 2020. Optimizing microstructure of polymer composite membranes by tailoring different ionic liquids to accelerate CO_2 transport. 101, 103136.
Li, B., Wang, S.-s., Qiao, J., Wang, B., Song, L., 2021. Thermodynamic analysis and optimization of a dual-pressure Allam cycle integrated with the regasification of liquefied natural gas. Energy Convers. Manage. 246, 114660.
Li, D., Motz, A.R., Bae, C., Fujimoto, C., Yang, G., Zhang, F.-Y., Ayers, K.E., Kim, Y.S., 2021. Durability of anion exchange membrane water electrolyzers. Energy Environ. Sci. 14 (6), 3393–3419. doi:10.1039/d0ee04086j.
Li, X., Zhou, X., Wei, J., Fan, Y., Liao, L., Wang, H., 2021. Reducing the energy penalty and corrosion of carbon dioxide capture using a novel nonaqueous monoethanolamine-based biphasic solvent. Sep. Purif. Technol. 265. doi:10.1016/j.seppur.2021.118481.
Li, B., Mbeugang, C.F.M., Huang, Y., Liu, D.J., Wang, Q., Zhang, S., 2022. A review of CaO based catalysts for tar removal during biomass gasification. Energy 244, 12. doi:10.1016/j.energy.2022.123172.
Li, J., Bao, A., Chen, J., Bao, Y., 2022. A green route to CO_2 adsorption on biomass chitosan derived nitrogen-doped micropore-dominated carbon nanosheets by different activators. J. Environ. Chem. Eng. 10 (1), 107021. doi:10.1016/j.jece.2021.107021.
Li, K., Xu, R., Sun, J., Cui, Y., Liu, J., Yang, S., Wang, R., Zhou, Z., Nie, X., 2022. Comparative investigation on thermochemical energy storage stability of Zr/Al-supported dark CaO-based composites under harsh energy storage mode. Carbon Cap. Sci. Technol. 5, 100076. doi:10.1016/j.ccst.2022.100076.
Li, R., Lian, S., Zhang, Z., Song, C., Han, R., Liu, Q., 2022. Techno-economic evaluation of a novel membrane-cryogenic hybrid process for carbon capture. Appl. Therm. Eng. 200, 117688. doi:10.1016/j.applthermaleng.2021.117688.
Li, S., Chang, S.-M., Yin, M.-J., Zhang, W.-H., Sun, W.-S., Shiue, A., An, Q.-F., 2022. Build up 'highway' in membrane via solvothermal annealing for high-efficient CO_2 capture. J. Membr. Sci. 652, 120444. doi:10.1016/j.memsci.2022.120444.
Li, T., Yang, C., Tantikhajorngosol, P., Sema, T., Tontiwachwuthikul, P., 2022. Studies on advanced configurations of post-combustion CO_2 capture process applied to cement plant flue gases. Carbon Cap. Sci. Technol. 4, 100064. doi:10.1016/J.CCST.2022.100064.
Li, W.L., Liang, H.W., Wang, J.H., Shao, L., Chu, G.W., Xiang, Y., 2022. CFD modeling on the chemical absorption of CO_2 in a microporous tube-in-tube microchannel reactor. Fuel 327. doi:10.1016/j.fuel.2022.125064, 125064-125064.
Li, Y.B., Wen, Z.N., Sun, B.C., Luo, Y., Gao, K.J., Chu, G.W., 2022. Flow patterns, liquid holdup, and wetting behavior of viscous liquids in a disk-distributor rotating packed bed. Chem. Eng. Sci. 252. doi:10.1016/j.ces.2021.117256, 117256-117256.
Lian, G., Zhong, W., 2022. CFD–DEM modeling of oxy-char combustion in a fluidized bed. Powder Technol. 407. doi:10.1016/j.powtec.2022.117698, 117698-117698.
Lian, S., Song, C., Liu, Q., Duan, E., Ren, H., Kitamura, Y., 2021. Recent advances in ionic liquids-based hybrid processes for CO_2 capture and utilization. J. Environ. Sci. 99, 281–295. doi:10.1016/j.jes.2020.06.034.
Liang, Z., Fu, K., Idem, R., Tontiwachwuthikul, P., 2016a. Review on current advances, future challenges and consideration issues for post-combustion CO_2 capture using amine-based absorbents. Chin. J. Chem. Eng. 24 (2), 278–288.
Liang, Z., Idem, R., Tontiwachwuthikul, P., Yu, F., Liu, H., Rongwong, W., 2016b. Experimental study on the solvent regeneration of a CO_2-loaded MEA solution using single and hybrid solid acid catalysts. AlChE J. 62 (3), 753–765. doi:10.1002/aic.15073.
Liang, J., Liang, Z., Zou, R., Zhao, Y., 2017. Heterogeneous catalysis in zeolites, mesoporous silica, and metal-organic frameworks. Adv. Mater. 29 (30). doi:10.1002/adma.201701139.
Liang, W., Huang, J., Xiao, P., Singh, R., Guo, J., Dehdari, L., Li, G.K., 2022. Amine-immobilized HY zeolite for CO_2 capture from hot flue gas. Chin. J. Chem. Eng. 43, 335–342. doi:10.1016/j.cjche.2022.02.004.
Liao, J., Wang, Z., Gao, C., Li, S., Qiao, Z., Wang, M., Zhao, S., Xie, X., Wang, J., Wang, S., 2014. Fabrication of high-performance facilitated transport membranes for CO_2 separation. Chem. Sci. 5 (7), 2843–2849. doi:10.1039/C3SC53334D.
Liao, H., Gao, H., Xu, B., Liang, Z., 2017. Mass transfer performance studies of aqueous blended DEEA-MEA solution using orthogonal array design in a packed column. Sep. Purif. Technol. 183, 117–126. doi:10.1016/j.seppur.2017.03.064.
Liao, Z., Hu, Y., Wang, J., Yang, Y., You, F., 2019. Systematic design and optimization of a membrane-cryogenic hybrid system for CO_2 capture. ACS Sustain. Chem. Eng. 7 (20), 17186–17197. doi:10.1021/acssuschemeng.9b03727.

Liao, P., Li, Y., Wu, X., Wang, M., Oko, E., 2020. Flexible operation of large-scale coal-fired power plant integrated with solvent-based post-combustion CO_2 capture based on neural network inverse control. Int. J. Greenh. Gas Control 95. doi:10.1016/j.ijggc.2020.102985.

Liew, R.K., Azwar, E., Yek, P.N.Y., Lim, X.Y., Cheng, C.K., Ng, J.H., Jusoh, A., Lam, W.H., Ibrahim, M.D., Ma, N.L., Lam, S.S., 2018. Microwave pyrolysis with KOH/NaOH mixture activation: A new approach to produce micro-mesoporous activated carbon for textile dye adsorption. Bioresour. Technol. 266, 1–10. doi:10.1016/j.biortech.2018.06.051.

Liew, R.K., Chai, C., Yek, P.N.Y., Phang, X.Y., Chong, M.Y., Nam, W.L., Su, M.H., Lam, W.H., Ma, N.L., Lam, S.S., 2019. Innovative production of highly porous carbon for industrial effluent remediation via microwave vacuum pyrolysis plus sodium-potassium hydroxide mixture activation. J. Clean. Prod. 208, 1436–1445. doi:10.1016/j.jclepro.2018.10.214.

Lillia, S., Bonalumi, D., Grande, C., Manzolini, G., 2018. A comprehensive modeling of the hybrid temperature electric swing adsorption process for CO_2 capture. Int. J. Greenh. Gas Control 74, 155–173. doi:10.1016/j.ijggc.2018.04.012.

Lillia, S., Bonalumi, D., Fosbøl, P.L., Thomsen, K., Jayaweera, I., Valenti, G., 2019. Thermodynamic and kinetic properties of NH3-K2CO3-CO_2-H2O system for carbon capture applications. Int. J. Greenh. Gas Control 85, 121–131. doi:10.1016/j.ijggc.2019.03.019.

Lim, G., Lee, K.B., Ham, H.C., 2016. Effect of N-containing functional groups on CO_2 adsorption of carbonaceous materials: a density functional theory approach. J. Phys. Chem. C 120 (15), 8087–8095. doi:10.1021/acs.jpcc.5b12090.

Lin, H., Wagner, E.V., Swinnea, J.S., Freeman, B.D., Pas, S.J., Hill, A.J., Kalakkunnath, S., Kalika, D.S., 2006. Transport and structural characteristics of crosslinked poly (ethylene oxide) rubbers. J. Membr. Sci. 276 (1), 145–161. doi:10.1016/j.memsci.2005.09.040.

Lin, Y., Yan, Q., Kong, C., Chen, L., 2013. Polyethyleneimine incorporated metal-organic frameworks adsorbent for highly selective CO_2 capture. Sci. Rep. 3, 1859. doi:10.1038/srep01859.

Lin, Y.F., Chen, C.H., Tung, K.L., Wei, T.Y., Lu, S.Y., Chang, K.S., 2013. Mesoporous fluorocarbon-modified silica aerogel membranes enabling long-term continuous CO_2 capture with large absorption flux enhancements. Chemsuschem 6 (3), 437–442. doi:10.1002/cssc.201200837.

Lin, R., Hernandez, B.V., Ge, L., Zhu, Z., 2018. Metal organic framework based mixed matrix membranes: An overview on filler/polymer interfaces. J. Mater. Chem. A 6 (2), 293–312.

Lin, J.-B., Nguyen, T.T.T., Vaidhyanathan, R., Burner, J., Taylor, J.M., Durekova, H., Akhtar, F., Mah, R.K., Ghaffari-Nik, O., Marx, S., Fylstra, N., Iremonger, S.S., Dawson, K.W., Sarkar, P., Hovington, P., Rajendran, A., Woo, T.K., Shimizu, G.K.H., 2021. A scalable metal-organic framework as a durable physisorbent for carbon dioxide capture. Science 374, 1464–1469.

Lin, Q., Liao, Z., Hu, Y., Sun, J., Jiang, B., Wang, J., Yang, Y., 2021. Optimal design of a subambient membrane separation system with work and heat integration for CO_2 capture. Ind. Eng. Chem. Res. 60 (42), 15194–15207. doi:10.1021/acs.iecr.1c02303.

Lindqvist, K., Jordal, K., Haugen, G., Hoff, K.A., Anantharaman, R., 2014. Integration aspects of reactive absorption for post-combustion CO_2 capture from NGCC (natural gas combined cycle) power plants. Energy 78, 758–767. doi:10.1016/j.energy.2014.10.070.

Linneen, N.N., Pfeffer, R., Lin, Y.S., 2014. CO_2 adsorption performance for amine grafted particulate silica aerogels. Chem. Eng. J. 254, 190–197. doi:10.1016/j.cej.2014.05.087.

Littel, R.J., Versteeg, G.F., Van Swaaij, W.P.M., 1992. Kinetics of CO_2 with primary and secondary amines in aqueous solutions-I. Zwitterion deprotonation kinetics for DEA and DIPA in aqueous blends of alkanolamines. Chem. Eng. Sci. 47 (8), 2027–2035. doi:10.1016/0009-2509 (92)80319-8.

Liu, S.-H., Huang, Y.-Y., 2018. Valorization of coffee grounds to biochar-derived adsorbents for CO_2 adsorption. J. Clean. Prod. 175, 354–360. doi:10.1016/j.jclepro.2017.12.076.

Liu, S.H., Huang, Y.Y., 2018. Valorization of coffee grounds to biochar-derived adsorbents for CO_2 adsorption. J. Clean. Prod. 175, 354–360. doi:10.1016/j.jclepro.2017.12.076.

Liu, B., Smit, B., 2010. Molecular simulation studies of separation of CO_2/N_2, CO_2/CH_4, and CH_4/N_2 by ZIFs. J. Phys. Chem. C 114 (18), 8515–8522.

Liu, Y., Wilcox, J., 2012. Effects of surface heterogeneity on the adsorption of CO_2 in microporous carbons. Environ. Sci. Technol. 46 (3), 1940–1947. doi:10.1021/es204071g.

Liu, S., Zhang, X., Li, J., Zhao, N., Wei, W., Sun, Y., 2008. Preparation and application of stabilized mesoporous MgO–ZrO2 solid base. Catal. Commun. 9 (7), 1527–1532. doi:10.1016/j.catcom.2007.12.007.

Liu, W., Feng, B., Wu, Y., Wang, G., Barry, J., Diniz da Costa, J., 2010. Synthesis of sintering-resistant sorbents for CO_2 capture. Environ. Sci. Technol. 44 (8), 3093–3097.

Liu, J., Wang, Y., Benin, A.I., Jakubczak, P., Willis, R.R., LeVan, M.D., 2010. CO_2/H2O adsorption equilibrium and rates on metal– organic frameworks: HKUST-1 and Ni/DOBDC. Langmuir 26 (17), 14301–14307.

Liu, J., Benin, A.I., Furtado, A.M., Jakubczak, P., Willis, R.R., LeVan, M.D., 2011. Stability effects on CO_2 adsorption for the DOBDC series of metal–organic frameworks. Langmuir 27 (18), 11451–11456.

Liu, W.-J., Jiang, H., Tian, K., Ding, Y.-W., Yu, H.-Q., 2013. Mesoporous carbon stabilized MgO nanoparticles synthesized by pyrolysis of MgCl2 preloaded waste biomass for highly efficient CO_2 capture. Environ. Sci. Technol. 47 (16), 9397–9403.

Liu, C., Xing, W., Zhou, J., Zhuo, S.-p., 2013. N-containing activated carbons for CO_2 capture. Int. J. Smart Nano Mater. 4 (1), 55–61. doi:10.1080/19475411.2012.668861.

Liu, H., Dai, S., Jiang, D., 2013. Insights into CO_2/N_2 separation through nanoporous graphene from molecular dynamics. Nanoscale 5 (20), 9984–9987. doi:10.1039/C3NR02852F.

Liu, Y., Yu, S., Wu, H., Li, Y., Wang, S., Tian, Z., Jiang, Z., 2014. High permeability hydrogel membranes of chitosan/poly ether-block-amide blends for CO_2 separation. J. Membr. Sci. 469, 198–208. doi:10.1016/j.memsci.2014.06.050.

Liu, L., Qiu, W., Sanders, E.S., Ma, C., Koros, W.J., 2016. Post-combustion carbon dioxide capture via 6FDA/BPDA-DAM hollow fiber membranes at sub-ambient temperatures. J. Membr. Sci. 510, 447–454. doi:10.1016/j.memsci.2016.03.027.

Liu, X., Gao, F., Xu, J., Zhou, L., Liu, H., Hu, J., 2016. Zeolite@Mesoporous silica-supported-amine hybrids for the capture of CO_2 in the presence of water. Microporous Mesoporous Mater. 222, 113–119. doi:10.1016/j.micromeso.2015.10.006.

Liu, Y., Luo, Y., Chu, G.W., Luo, J.Z., Arowo, M., Chen, J.F., 2017. 3D numerical simulation of a rotating packed bed with structured stainless steel wire mesh packing. Chem. Eng. Sci. 170, 365–377. doi:10.1016/j.ces.2017.01.033.

Liu, X., Wang, X., Bavykina, A., Chu, L., Shan, M., Sabetghadam, A., Miro, H., Kapteijn, F., Gascon, J., 2018. Molecular-scale hybrid membranes derived from metal-organic polyhedra for gas separation. ACS Appl. Mater. Interfaces 10, 21381–21389. doi:10.1021/acsami.8b07045.

Liu, J., Wang, Z., Wang, Z., Song, J., Li, G., Xu, Q., You, J., Cheng, H., Lu, X., 2019. Alkali carbonates promote CO_2 capture by sodium orthosilicate. Phys. Chem. Chem. Phys. 21 (24), 13135–13143. doi:10.1039/C9CP01306G.

Liu, F., Fang, M., Yi, N., Wang, T., 2019a. Research on alkanolamine-based physical–chemical solutions as biphasic solvents for CO_2 capture. Energy Fuels 33 (11), 11389–11398. doi:10.1021/acs.energyfuels.9b02392.

Liu, F., Fang, M., Yi, N., Wang, T., Wang, Q., 2019b. Biphasic behaviors and regeneration energy of a 2- (diethylamino)-ethanol and 2- ((2-aminoethyl)amino) ethanol blend for CO_2 capture. Sustain. Energy Fuels 3 (12), 3594–3602. doi:10.1039/c9se00821g.

Liu, M., Nothling, M.D., Webley, P.A., Jin, J., Fu, Q., Qiao, G.G., 2020. High-throughput CO_2 capture using PIM-1@MOF based thin film composite membranes. Chem. Eng. J. 396, 125328. doi:10.1016/j.cej.2020.125328.

Liu, L., Jin, S., Ko, K., Kim, H., Ahn, I.-S., Lee, C.-H., 2020. Alkyl-functionalization of (3-Aminopropyl)triethoxysilane-grafted zeolite beta for carbon dioxide capture in temperature swing adsorption. Chem. Eng. J. 382. doi:10.1016/j.cej.2019.122834.

Liu, B., Yang, X., Chiang, P.-C., Wang, T., 2020. Energy consumption analysis of cryogenic-membrane hybrid process for CO_2 capture from CO_2-EOR extraction gas. Aerosol. Air Qual. Res. 20 (4), 820–832. doi:10.4209/aaqr.2020.02.0047.

Liu, F., Shen, Y., Shen, L., Sun, C., Chen, L., Wang, Q., Li, S., Li, W., 2020. Novel amino-functionalized ionic liquid/organic solvent with low viscosity for CO_2 capture. Environ. Sci. Technol. 54 (6), 3520–3529. doi:10.1021/acs.est.9b06717.

Liu, J., Fulong, C.R.P., Hu, L., Huang, L., Zhang, G., Cook, T.R., Lin, H., 2020. Interpenetrating networks of mixed matrix materials comprising metal-organic polyhedra for membrane CO_2 capture. J. Membr. Sci. 606, 118122. doi:10.1016/j.memsci.2020.118122.

Liu, Y., Wu, H., Wu, S., Song, S., Guo, Z., Ren, Y., Zhao, R., Yang, L., Wu, Y., Jiang, Z., 2021. Multifunctional covalent organic framework (COF)-Based mixed matrix membranes for enhanced CO_2 separation. J. Membr. Sci. 618, 118693. doi:10.1016/j.memsci.2020.118693.

Liu, Z.Y., Ma, R., Du, W.J., Yang, G., Chen, T., 2021. Radiation-initiated high strength chitosan/lithium sulfonate double network hydrogel/aerogel with porosity and stability for efficient CO_2 capture. RSC Adv. 11 (33), 20486–20497. doi:10.1039/d1ra03041h.

Liu, B., Li, Z., Li, D., Sun, H., Yao, J., 2021. Polyzwitterion-grafted UiO-66-PEI incorporating polyimide membrane for high efficiency CO_2/CH4 separation. Sep. Purif. Technol. 267, 118617. doi:10.1016/j.seppur.2021.118617.

Liu, K., Li, H., Zhao, Z.-y., Wang, X.-j., Li, X.-g., Gao, X., 2021. Microwave-induced spray evapouration process for separation intensification of azeotropic system. Sep. Purif. Technol. 279. doi:10.1016/j.seppur.2021.119702.

Liu, M., Nothling, M.D., Zhang, S., Fu, Q., Qiao, G.G., 2022. Thin film composite membranes for postcombustion carbon capture: Polymers and beyond. Progress Polym. Sci. 126. doi:10.1016/j.progpolymsci.2022.101504.

Liu, N., Cheng, J., Hu, L., Hou, W., Yang, X., Luo, M., Zhang, H., Ye, B., Zhou, J., 2022. Boosting CO_2 transport of poly (ethylene oxide) membranes by hollow Rubik-like "expressway" channels with anion pillared hybrid ultramicroporous materials. Chem. Eng. J. 427, 130845. doi:10.1016/j.cej.2021.130845.

Liu, Q., Zhong, W., Yu, A., Wang, C.-H., 2022. Co-firing of coal and biomass under pressurized oxy-fuel combustion mode: Experimental test in a 10 kWth fluidized bed. Chem. Eng. J. 431, 133457. doi:10.1016/j.cej.2021.133457.

Liu, F., Huang, K., Yoo, C.-J., Okonkwo, C., Tao, D.-J., Jones, C.W., Dai, S., 2017. Facilely synthesized meso-macroporous polymer as support of poly (ethyleneimine) for highly efficient and selective capture of CO_2. Chem. Eng. J. 314, 466–476. doi:10.1016/j.cej.2016.12.004.

Liu, H., Zhang, X., Gao, H., Liang, Z., Idem, R., Tontiwachwuthikul, P., 2017. Investigation of CO_2 regeneration in single and blended amine solvents with and without catalyst. Ind. Eng. Chem. Res. 56 (27), 7656–7664. doi:10.1021/acs.iecr.7b00778.

Liu, S.H., 2019. Waste-Derived Biochar for CO_2 Sequestration. Biochar Biomass Waste: Fundament. Appl. 295–304. doi:10.1016/b978-0-12-811729-3.00016-9.

Lively, R.P., Chance, R.R., Kelley, B.T., Deckman, H.W., Drese, J.H., Jones, C.W., Koros, W.J., 2009. Hollow fiber adsorbents for CO_2 removal from flue gas. Ind. Eng. Chem. Res. 48, 7314–7324.

Lively, R.P., Chance, R.R., Koros, W.J., 2010. Enabling low-cost CO_2 capture via heat integration. Ind. Eng. Chem. Res. 49, 7550–7562.

Lively, R.P., Chance, R.R., Mysona, J.A., Babu, V.P., Deckman, H.W., Leta, D.P., Thomann, H., Koros, W.J., 2012. CO_2 sorption and desorption performance of thermally cycled hollow fiber sorbents. Int. J. Greenh. Gas Control 10, 285–294. doi:10.1016/j.ijggc.2012.06.019.

Llewellyn, P.L., Bourrelly, S., Serre, C., Vimont, A., Daturi, M., Hamon, L., Weireld, G.D., Chang, J.S., Hong, D.Y., Hwang, Y.K., Jhung, S.H., Fe´rey, G., 2008. High Uptakes of CO_2 and CH4 in Mesoporous MetalsOrganic_Frameworks MIL-100 and MIL-101. Langmuir 24 (14), 7245–7250.

Loganathan, S., Ghoshal, A.K., 2017. Amine tethered pore-expanded MCM-41: A promising adsorbent for CO 2 capture. Chem. Eng. J. 308, 827–839. doi:10.1016/j.cej.2016.09.103.

Lu, H., Kim, J.P., Son, S.H., Park, J.H., 2011. Novel $SrCo_{1-2x}$ (Fe,Nb)$xO_3-\delta$ (x=0.05, 0.10) oxides targeting CO_2 capture and O_2 enrichment: structural stability and oxygen sorption properties. Mater. Lett. 65 (19), 2858–2860. doi:10.1016/j.matlet.2011.06.062.

Lu, W., Sculley, J.P., Yuan, D., Krishna, R., Wei, Z., Zhou, H.C., 2012. Polyamine-tethered porous polymer networks for carbon dioxide capture from flue gas. Angew. Chem. Int. Ed. Engl. 51 (30), 7480–7484. doi:10.1002/anie.201202176.

Lu, X., Forrest, B., Martin, S., Fetvedt, J., McGroddy, M., Freed, D., 2016. Integration and optimization of coal gasification systems with a near-zero emissions supercritical carbon dioxide power cycle. In: Turbo Expo: Power for Land, Sea, and Air. American Society of Mechanical Engineers V009T036A019.

Lu, X., Xie, P., Ingham, D.B., Ma, L., Pourkashanian, M., 2019. Modelling of CO_2 absorption in a rotating packed bed using an Eulerian porous media approach. Chem. Eng. Sci. 199, 302–318. doi:10.1016/j.ces.2019.01.029.

Lu, J., Zhang, X., Xu, L., Zhang, G., Zheng, J., Tong, Z., Shen, C., Meng, Q., 2021. Preparation of amino-functional UiO-66/PIMs mixed matrix membranes with [bmim][Tf_2N] as regulator for enhanced gas separation. Membranes 11 (1), 35. doi:10.3390/membranes11010035.

Lu, W., Shi, X., Zhou, H., Luo, W., Wang, L., He, H., 2022. Tailoring and properties of a novel solar energy-triggered regenerative bionic fiber adsorbent for CO_2 capture. Chem. Eng. J. 449. doi:10.1016/j.cej.2022.137885.

Luberti, M., Oreggioni, G.D., Ahn, H., 2017. Design of a rapid vacuum pressure swing adsorption (RVPSA) process for post-combustion CO_2 capture from a biomass-fuelled CHP plant. J. Environ. Chem. Eng. 5 (4), 3973–3982. doi:10.1016/j.jece.2017.07.029.

Luca, A.V., Petrescu, L., 2021. Membrane technology applied to steel production: Investigation based on process modelling and environmental tools. J. Clean. Prod. 294. doi:10.1016/j.jclepro.2021.126256.

Lukin, I., Pietzka, L., Groß, K., Górak, A., Schembecker, G., 2020. Economic evaluation of rotating packed bed use for aroma absorption from bioreactor off-gas. Chem. Eng. Process. - Process Intensif. 154 (December 2019). doi:10.1016/j.cep.2020.108011, 108011-108011.

Lunn, J.D., Shantz, D.F., 2009. Peptide brush—Ordered mesoporous silica nanocomposite materials. Chem. Mater. 21 (15), 3638–3648. doi:10.1021/cm901025n.

Luo, H., Kanoh, H., 2017. Fundamentals in CO_2 capture of Na_2CO_3 under a moist condition. J. Energy Chem. 26 (5), 972–983. doi:10.1016/j.jechem.2017.08.005.

Luo, Q., Pentzer, E., 2020. Encapsulation of Ionic Liquids for Tailored Applications. ACS Appl. Mater. Interfaces 12 (5), 5169–5176. doi:10.1021/acsami.9b16546.

Luo, F., Fan, C.B., Luo, M.B., Wu, X.L., Zhu, Y., Pu, S.Z., Xu, W.Y., Guo, G.C., 2014. Photoswitching CO (2) capture and release in a photochromic diarylethene metal-organic framework. Angew. Chem. Int. Ed. Engl. 53 (35), 9298–9301. doi:10.1002/anie.201311124.

Luo, S., Bayham, S., Zeng, L., McGiveron, O., Chung, E., Majumder, A., Fan, L.-S., 2014. Conversion of metallurgical coke and coal using a coal direct chemical looping (CDCL) moving bed reactor. Appl. Energy 118, 300–308. doi:10.1016/j.apenergy.2013.11.068.

Luo, S., Stevens, K.A., Park, J.S., Moon, J.D., Liu, Q., Freeman, B.D., Guo, R., 2016. Highly CO_2-selective gas separation membranes based on segmented copolymers of poly (Ethylene oxide) reinforced with pentiptycene-containing polyimide hard segments. ACS Appl. Mater. Interfaces 8 (3), 2306–2317. doi:10.1021/acsami.5b11355.

Luo, W., Guo, D., Zheng, J., Gao, S., Chen, J., 2016. CO_2 absorption using biphasic solvent: Blends of diethylenetriamine, sulfolane, and water. Int. J. Greenh. Gas Control 53, 141–148. doi:10.1016/j.ijggc.2016.07.036.

Luo, X., Liu, S., Gao, H., Liao, H., Tontiwachwuthikul, P., Liang, Z., 2016. An improved fast screening method for single and blended amine-based solvents for post-combustion CO_2 capture. Sep. Purif. Technol. 169, 279–288. doi:10.1016/j.seppur.2016.06.018.

Luo, X.Y., Fan, X., Shi, G.L., Li, H.R., Wang, C.M., 2016. Decreasing the viscosity in CO_2 capture by amino-functionalized ionic liquids through the formation of intramolecular hydrogen bond. J. Phys. Chem. B 120 (10), 2807–2813. doi:10.1021/acs.jpcb.5b10553.

Luo, M., Yi, Y., Wang, S., Wang, Z., Du, M., Pan, J., Wang, Q., 2018. Review of hydrogen production using chemical-looping technology. Renew. Sustain. Energy Rev. 81, 3186–3214. doi:10.1016/j.rser.2017.07.007.

Luo, J., Emelogu, O., Morosuk, T., Tsatsaronis, G., 2021. Exergy-based investigation of a coal-fired allam cycle. Energy 218, 119471.

Luo, X., Wang, M., Lee, J., Hendry, J., 2021. Dynamic modelling based on surface renewal theory, model validation and process analysis of rotating packed bed absorber for carbon capture. Appl. Energy 301 (March). doi:10.1016/j.apenergy.2021.117462, 117462-117462.

Luo, H., Wang, X., Liu, X., Wu, X., Shi, X., Xiong, Q., 2022. A review on CFD simulation of biomass pyrolysis in fluidized bed reactors with emphasis on particle-scale models. J. Analyt. Appl. Pyrol. 162. doi:10.1016/j.jaap.2022.105433, 105433-105433.

Lv, B., Jing, G., Qian, Y., Zhou, Z., 2016a. An efficient absorbent of amine-based amino acid-functionalized ionic liquids for CO_2 capture: High capacity and regeneration ability. Chem. Eng. J. 289, 212–218. doi:10.1016/j.cej.2015.12.096.

Lv, B., Jing, G., Qian, Y., Zhou, Z., 2016b. An efficient absorbent of amine-based amino acid-functionalized ionic liquids for CO 2 capture: High capacity and regeneration ability. Chem. Eng. J. 289, 212–218. doi:10.1016/j.cej.2015.12.096.

Lv, B., Zhou, X., Zhou, Z., Jing, G., 2019. Kinetics and thermodynamics of CO_2 absorption into a novel DETA-AMP-PMDETA biphasic solvent. ACS Sustain. Chem. Eng. 7 (15), 13400–13410. doi:10.1021/acssuschemeng.9b02700.

Lv, B.H., Huang, Q.S., Zhou, Z.M., Jing, G.H., 2020. Novel biphasic amino-functionalized ionic liquid solvent for CO_2 capture: kinetics and regeneration heat duty. Environ. Sci. Pollut. Res. 27 (21), 26965–26973. doi:10.1007/s11356-020-09039-x.

Lyndon, R., Konstas, K., Ladewig, B.P., Southon, P.D., Kepert, P.C., Hill, M.R., 2013. Dynamic photo-switching in metal-organic frameworks as a route to low-energy carbon dioxide capture and release. Angew. Chem. Int. Ed. Engl. 52 (13), 3695–3698. doi:10.1002/anie.201206359.

Lyndon, R., Konstas, K., Evans, R.A., Keddie, D.J., Hill, M.R., Ladewig, B.P., 2015a. Tunable photodynamic switching of DArE@PAF-1 for carbon capture. Adv. Funct. Mater. 25 (28), 4405–4411. doi:10.1002/adfm.201502069.

Lyndon, R., Konstas, K., Thornton, A.W., Seeber, A.J., Ladewig, B.P., Hill, M.R., 2015b. Visible light-triggered capture and release of CO_2 from stable metal organic frameworks. Chem. Mater. 27 (23), 7882–7888. doi:10.1021/acs.chemmater.5b02211.

Lyngfelt, A., Leckner, B., Mattisson, T., 2001. A fluidized-bed combustion process with inherent CO_2 separation; application of chemical-looping combustion. Chem. Eng. Sci. 56 (10), 3101–3113.

Lyngfelt, A., Brink, A., Langørgen, Ø., Mattisson, T., Rydén, M., Linderholm, C., 2019. 11,000 h of chemical-looping combustion operation—Where are we and where do we want to go? Int. J. Greenh. Gas Control 88, 38–56. doi:10.1016/j.ijggc.2019.05.023.

Ma, S., Chen, G., Zhu, S., Wen, J., Gao, R., Ma, L., Chai, J., 2016. Experimental study of mixed additive of Ni (II) and piperazine on ammonia escape in CO_2 capture using ammonia solution. Appl. Energy 169, 597–606.

Ma, C., Liu, C., Lu, X., Ji, X., 2018. Techno-economic analysis and performance comparison of aqueous deep eutectic solvent and other physical absorbents for biogas upgrading. Appl. Energy 225, 437–447. doi:10.1016/j.apenergy.2018.04.112.

Ma, L., Svec, F., Lv, Y., Tan, T., 2019. In situ bottom–up growth of metal–organic frameworks in a crosslinked poly (ethylene oxide) layer with ultrahigh loading and superior uniform distribution. J. Mater. Chem. A 7 (35), 20293–20301. doi:10.1039/C9TA05401D.

Ma, X., Wu, X., Caro, J., Huang, A., 2019. Polymer composite membrane with penetrating ZIF-7 sheets displays high hydrogen permselectivity. Angew. Chem. Int. Ed. 58 (45), 16156–16160. doi:10.1002/anie.201911226.

Ma, Y., Jue, M.L., Zhang, F., Mathias, R., Jang, H.Y., Lively, R.P., 2019. Creation of well-defined "Mid-Sized" micropores in carbon molecular sieve membranes. Angew. Chem. Int. Ed. Engl. 58 (38), 13259–13265. doi:10.1002/anie.201903105.

Ma, J., Wang, Y.T., Yang, X.Q., Zhu, M.X., Wang, B.H., 2021. DFT study on the chemical absorption mechanism of CO_2 in diamino protic ionic liquids. J. Phys. Chem. B 125 (5), 1416–1428. doi:10.1021/acs.jpcb.0c08500.

Ma, Q.X., Chen, W.H., Jin, Z.H., Chen, L., Zhou, Q.Y., Jiang, X., 2021. One-step synthesis of microporous nitrogen-doped biochar for efficient removal of CO_2 and H2S. Fuel 289. doi:10.1016/j.fuel.2020.119932.

Ma, X., Li, Y., Huang, X., Feng, T., Mu, M., 2021. Sorption-enhanced reaction process using advanced Ca-based sorbents for low-carbon hydrogen production. Process. Saf. Environ. Prot. 155, 325–342. doi:10.1016/j.psep.2021.09.009.

Mac Dowell, N., Llovell, F., Adjiman, C.S., Jackson, G., Galindo, A., 2010. Modeling the fluid phase behavior of carbon dioxide in aqueous solutions of monoethanolamine using transferable parameters with the SAFT-VR approach. Ind. Eng. Chem. Res. 49 (4), 1883–1899. doi:10.1021/ie901014t.

Machida, M., Kawada, T., Fujii, H., Hinokuma, S., 2015. The role of CeO2 as a gateway for oxygen storage over CeO2-grafted Fe2O3 composite materials. J. Phys. Chem. C 119 (44), 24932–24941. doi:10.1021/acs.jpcc.5b09876.

Macneil, S., Basu, P., 1998. Effect of pressure on char combustion in a pressurized circulating fluidized bed boiler. Fuel 77 (4), 269–275.

Madejski, P., Chmiel, K., Subramanian, N., Kus, T., 2022. Methods and techniques for CO_2 capture: review of potential solutions and applications in modern energy technologies. Energies 15 (3), 21. doi:10.3390/en15030887.

Madzaki, H., KarimGhani, W., Rebitanim, N., Alias, A., 2016. Carbon dioxide adsorption on sawdust biochar. In: Proceeding of 4th International Conference on Process Engineering and Adv. Mater. (Icpeam 2016), 148, pp. 718–725. doi:10.1016/j.proeng.2016.06.591.

Mahdipoor, H.R., Halladj, R., Ganji Babakhani, E., Amjad-Iranagh, S., Sadeghzadeh Ahari, J., 2021. Synthesis, characterization, and CO_2 adsorption properties of metal organic framework Fe-BDC. RSC Adv. 11 (9), 5192–5203. doi:10.1039/d0ra09292d.

Mahr, B., Mewes, D., 2008. Two-phase flow in structured packings: Modeling and calculation on a macroscopic scale. AIChE J. 54 (3), 614–626. doi:10.1002/aic.11400.

Maina, J.W., Pringle, J.M., Razal, J.M., Nunes, S., Vega, L., Gallucci, F., Dumee, L.F., 2021. Strategies for integrated capture and conversion of CO_2 from dilute flue gases and the atmosphere. ChemSusChem 14 (8), 1805–1820. doi:10.1002/cssc.202100010.

Maity, R., Singh, H.D., Yadav, A.K., Chakraborty, D., Vaidhyanathan, R., 2019. Water-stable adenine-based MOFs with polar pores for selective CO_2 capture. Chem. Asian J. 14 (20), 3736–3741. doi:10.1002/asia.201901020.

Majchrzak-Kuceba, I., Soltysik, M., 2020. The potential of biocarbon as CO_2 adsorbent in VPSA unit. J. Therm. Anal. Calorim. 142 (1), 267–273. doi:10.1007/s10973-020-09858-7.

Maleki, H., 2016. Recent advances in aerogels for environmental remediation applications: a review. Chem. Eng. J. 300, 98–118. doi:10.1016/j.cej.2016.04.098.

Malhi, G.S., Kaur, M., Kaushik, P., 2021. Impact of climate change on agriculture and its mitigation strategies: a review. Sustainability 13 (3). doi:10.3390/su13031318.

Mangun, C.L., Benak, K.R., Economy, J., Foster, K.L., 2001. Surface chemistry, pore sizes and adsorption properties of activated carbon fibers and precursors treated with ammonia. Carbon 39 (12), 1809–1820. doi:10.1016/S0008-6223 (00)00319-5.

Mannan, H.A., Mukhtar, H., Shahrun, M.S., Bustam, M.A., Man, Z., Bakar, M.Z.A., 2016. Effect of [EMIM][Tf2N] Ionic Liquid on Ionic Liquid-polymeric Membrane (ILPM) for CO_2/CH4 Separation. Proc. Eng. 148, 25–29. doi:10.1016/j.proeng.2016.06.477.

Manuel Vicent-Luna, J., Jose Gutierrez-Sevillano, J., Antonio Anta, J., Calero, S., 2013. Effect of room-temperature ionic liquids on CO_2 separation by a Cu-BTC metal-organic framework. J. Phys. Chem. C 117 (40), 20762–20768. doi:10.1021/jp407176j.

Manyà, J.J., González, B., Azuara, M., Arner, G., 2018. Ultra-microporous adsorbents prepared from vine shoots-derived biochar with high CO_2 uptake and CO_2/N_2 selectivity. Chem. Eng. J. 345, 631–639. doi:10.1016/j.cej.2018.01.092.

Manya, J.J., Gonzalez, B., Azuara, M., Arner, G., 2018. Ultra-microporous adsorbents prepared from vine shoots-derived biochar with high CO_2 uptake and CO_2/N-2 selectivity. Chem. Eng. J. 345, 631–639. doi:10.1016/j.cej.2018.01.092.

Manya, J.J., Garcia-Morcate, D., Gonzalez, B., 2020. Adsorption performance of physically activated biochars for postcombustion CO_2 capture from dry and humid flue gas. Appl. Sci.-Basel 10 (1). doi:10.3390/app10010376.

Manzolini, G., Giuffrida, A., Cobden, P.D., van Dijk, H.A.J., Ruggeri, F., Consonni, F., 2020. Techno-economic assessment of SEWGS technology when applied to integrated steel-plant for CO_2 emission mitigation. Int. J. Greenh. Gas Control 94, 102935. doi:10.1016/j.ijggc.2019.102935.

Maqsood, K., Ali, A., Shariff, A.B.M., Ganguly, S., 2014a. Synthesis of conventional and hybrid cryogenic distillation sequence for purification of natural gas. J. Appl. Sci. 14 (21), 2722–2729. doi:10.3923/jas.2014.2722.2729.

Maqsood, K., Mullick, A., Ali, A., Kargupta, K., Ganguly, S., 2014b. Cryogenic carbon dioxide separation from natural gas: a review based on conventional and novel emerging technologies. Rev. Chem. Eng. 30 (5). doi:10.1515/revce-2014-0009.

Maqsood, K., Pal, J., Turunawarasu, D., Pal, A.J., Ganguly, S., 2014c. Performance enhancement and energy reduction using hybrid cryogenic distillation networks for purification of natural gas with high CO_2 content. Korean J. Chem. Eng. 31 (7), 1120–1135. doi:10.1007/s11814-014-0038-y.

Maqsood, K., Ali, A., Shariff, A.B.M., Ganguly, S., 2017. Process intensification using mixed sequential and integrated hybrid cryogenic distillation network for purification of high CO_2 natural gas. Chem. Eng. Res. Des. 117, 414–438. doi:10.1016/j.cherd.2016.10.011.

Marin, O., et al., 2003. National Energy Technology Laboratory. Cost and performance for low-rank pulverized. In: Proc. 28th Intern. Tech. Conf. Coal Util. Fuel Systems, Cl March.

Maring, B.J., Webley, P.A., 2013a. A new simplified pressure/vacuum swing adsorption model for rapid adsorbent screening for CO_2 capture applications. Int. J. Greenh. Gas Control 15, 16–31. doi:10.1016/j.ijggc.2013.01.009.

Maring, B.J., Webley, P.A., 2013b. A new simplified pressure/vacuum swing adsorption model for rapid adsorbent screening for CO_2 capture applications. Int. J. Greenh. Gas Control 15, 16–31. doi:10.1016/j.ijggc.2013.01.009.

Markewitz, P., Marx, J., Schreiber, A., Zapp, P., 2013. Ecological evaluation of coal-fired oxyfuel power plants -cryogenic versus membrane-based air separation. Energy Proc. 37, 2864–2876. doi:10.1016/j.egypro.2013.06.172.

Marono, M., Torreiro, Y., Cillero, D., Maria Sanchez, J., 2015. Experimental studies of CO_2 capture by a hybrid catalyst/adsorbent system applicable to IGCC processes. Appl. Therm. Eng. 74, 28–35. doi:10.1016/j.applthermaleng.2014.02.068.

Marques, L.M., Carrott, P.J.M., Carrott, M.M.L.R., 2013. Amine-modified Carbon Aerogels for CO_2 capture. Adsorpt. Sci. Technol. 31 (2-3), 223–232. doi:10.1260/0263-6174.31.2-3.223.

Martínez, F., Sanz, R., Orcajo, G., Briones, D., Yángüez, V., 2016. Amino-impregnated MOF materials for CO 2 capture at post-combustion conditions. Chem. Eng. Sci. 142, 55–61. doi:10.1016/j.ces.2015.11.033.

Martínez-Cruz, M.A., Yañez-Aulestia, A., Ramos-Sánchez, G., Oliver-Tolentino, M., Vera, M., Pfeiffer, H., Ramírez-Rosales, D., González, I., 2020. Unraveling the effects on lithium-ion cathode performance by cation doping M–Li2CuO_2 solid solution samples (M = Mn, Fe and Ni). Dalton Trans. 49 (14), 4549–4558. doi:10.1039/D0DT00273A.

Martínez-dlCruz, L., Pfeiffer, H., 2012. Microstructural thermal evolution of the Na_2CO_3 phase produced during a Na_2ZrO_3–CO_2 chemisorption process. J. Phys. Chem. C 116 (17), 9675–9680. doi:10.1021/jp301917a.

Mashhadikhan, S., Moghadassi, A., Ebadi Amooghin, A., Sanaeepur, H., 2020. Interlocking a synthesized polymer and bifunctional filler containing the same polymer's monomer for conformable hybrid membrane systems. J. Mater. Chem. A 8 (7), 3942–3955. doi:10.1039/c9ta13375e.

Mason, J.A., Sumida, K., Herm, Z.R., Krishna, R., Long, J.R., 2011. Evaluating metal–organic frameworks for post-combustion carbon dioxide capture via temperature swing adsorption. Energy Environ. Sci. 4 (8). doi:10.1039/c1ee01720a.

Mason, J.A., McDonald, T.M., Bae, T.-H., Bachman, J.E., Sumida, K., Dutton, J.J., Kaye, S.S., Long, J.R., 2015. Application of a high-throughput analyzer in evaluating solid adsorbents for post-combustion carbon capture via multicomponent adsorption of CO_2, N_2, and H_2O. J. Am. Chem. Soc. 137 (14), 4787–4803.

Masoud, N., Bordanaba-Florit, G., van Haasterecht, T., Bitter, J.H., 2021. Effect of support surface properties on CO_2 capture from air by carbon-supported potassium carbonate. Ind. Eng. Chem. Res. 60 (38), 13749–13755. doi:10.1021/acs.iecr.1c01229.

Masoudi Soltani, S., Lahiri, A., Bahzad, H., Clough, P., Gorbounov, M., Yan, Y., 2021. Sorption-enhanced steam methane reforming for combined CO_2 capture and hydrogen production: a state-of-the-art review. Carbon Cap. Sci. Technol. 1, 100003. doi:10.1016/j.ccst.2021.100003.

Masuda, S., Osaka, Y., Tsujiguchi, T., Kodama, A., 2021. CO_2 capture from a simulated dry exhaust gas by internally heated and cooled temperature swing adsorption. J. Chem. Eng. Jpn. 54 (5), 248–254. doi:10.1252/jcej.20we112.

Masuda, S., Osaka, Y., Tsujiguchi, T., Kodama, A., 2022. Carbon dioxide recovery from a simulated dry exhaust gas by an internally heated and cooled temperature swing adsorption packed with a typical hydrophobic adsorbent. Sep. Purif. Technol. 284. doi:10.1016/j.seppur.2021.120249.

Matsumoto, K., Endo, T., 2008. Confinement of ionic liquid by networked polymers based on multifunctional epoxy resins. Macromolecules 41 (19), 6981–6986. doi:10.1021/ma801293j.

Matteucci, S., Raharjo, R.D., Kusuma, V.A., Swinnea, S., Freeman, B.D., 2008. Gas permeability, solubility, and diffusion coefficients in 1, 2-polybutadiene containing magnesium oxide. Macromolecules 41 (6), 2144–2156. doi:10.1021/ma702459k.

Matthews, L., Lipiński, W., 2012. Thermodynamic analysis of solar thermochemical CO_2 capture via carbonation/calcination cycle with heat recovery. Energy 45 (1), 900–907. doi:10.1016/j.energy.2012.06.072.

Mattisson, T., Lyngfelt, A., Leion, H., 2009. Chemical-looping with oxygen uncoupling for combustion of solid fuels. Int. J. Greenh. Gas Control 3 (1), 11–19.

Mattisson, T., Keller, M., Linderholm, C., Moldenhauer, P., Rydén, M., Leion, H., Lyngfelt, A., 2018. Chemical-looping technologies using circulating fluidized bed systems: Status of development. Fuel Process. Technol. 172, 1–12. doi:10.1016/j.fuproc.2017.11.016.

Mattisson, T., 2013. Materials for Chemical-Looping with Oxygen Uncoupling. ISRN Chem. Eng. 2013, 1–19. doi:10.1155/2013/526375.

Maurin, G., Llewellyn, P., Bell, R., 2005. Adsorption mechanism of carbon dioxide in faujasites: grand canonical Monte Carlo simulations and microcalorimetry measurements. J. Phys. Chem. B 109 (33), 16084–16091.

Maurya, M., Singh, J.K., 2019. Effect of ionic liquid impregnation in highly water-stable metal–organic frameworks, covalent organic frameworks, and carbon-based adsorbents for post-combustion flue gas treatment. Energy Fuels 33 (4), 3421–3428. doi:10.1021/acs.energyfuels.9b00179.

May, E.F., Zhang, Y., Saleman, T.L.H., Xiao, G., Li, G., Young, B.R., 2017. Demonstration and optimisation of the four dual-reflux pressure swing adsorption configurations. Sep. Purif. Technol. 177, 161–175. doi:10.1016/j.seppur.2016.12.007.

Mazzotti, M., Baciocchi, R., Desmond, M.J., Socolow, R.H., 2013. Direct air capture of CO_2 with chemicals: optimization of a two-loop hydroxide carbonate system using a countercurrent air-liquid contactor. Clim. Change 118 (1), 119–135. doi:10.1007/s10584-012-0679-y.

McBain, J.W., 2002. The sorption of gases and vapours by solids. J. Phys. Chem. 37 (1), 149–150.

McCarthy, M.C., Varela-Guerrero, V., Barnett, G.V., Jeong, H.-K., 2010. Synthesis of zeolitic imidazolate framework films and membranes with controlled microstructures. Langmuir 26 (18), 14636–14641.

McCollom, T., 2011. Carbon Dioxide. In: Gargaud, M., Amils, R., Quintanilla, J.C., Cleaves, H.J., Irvine, W.M., Pinti, D.L., Viso, M. (Eds.), Encyclopedia of Astrobiology. Springer Berlin Heidelberg, Berlin, Heidelberg, pp. 239–240. doi:10.1007/978-3-642-11274-4_1737.

McDonald, T.M., Lee, W.R., Mason, J.A., Wiers, B.M., Hong, C.S., Long, J.R., 2012. Capture of carbon dioxide from air and flue gas in the alkylamine-appended metal–organic framework mmen-Mg2 (dobpdc). J. Am. Chem. Soc. 134 (16), 7056–7065.

McDonald, T.M., Mason, J.A., Kong, X., Bloch, E.D., Gygi, D., Dani, A., Crocella, V., Giordanino, F., Odoh, S.O., Drisdell, W.S., Vlaisavljevich, B., Dzubak, A.L., Poloni, R., Schnell, S.K., Planas, N., Lee, K., Pascal, T., Wan, L.F., Prendergast, D., Neaton, J.B., Smit, B., Kortright, J.B., Gagliardi, L., Bordiga, S., Reimer, J.A., Long, J.R., 2015. Cooperative insertion of CO_2 in diamine-appended metal-organic frameworks. Nature 519 (7543), 303–308. doi:10.1038/nature14327.

McDonald, T., 2011. D, Alessandro, DM; Krishna, R. Long, JR. Chem. Sci. 2 (10), 2022–2028.

McEwen, J., Hayman, J.-D., Ozgur Yazaydin, A., 2013. A comparative study of CO_2, CH_4 and N_2 adsorption in ZIF-8, Zeolite-13X and BPL activated carbon. Chem. Phys. 412, 72–76. doi:10.1016/j.chemphys.2012.12.012.

McKeown, N., 2012. Polymers of intrinsic microporosity. ISRN Mater. Sci. 2012. doi:10.5402/2012/513986.

Medina-Carrasco, S., Valverde, J.M., 2022. The Calcium Looping process for energy storage: Insights from in situ XRD analysis. Chem. Eng. J. 429, 132244.

Mehrpooya, M., Ghorbani, B., Manizadeh, A., 2020. Cryogenic biogas upgrading process using solar energy (process integration, development, and energy analysis). Energy 203, 117834. doi:10.1016/j.energy.2020.117834.

Mei, X., Yang, S., Lu, P., Zhang, Y., Zhang, J., 2020. Improving the selectivity of ZIF-8/Polysulfone-mixed matrix membranes by polydopamine modification for H2/CO_2 separation. Front. Chem. 8. doi:10.3389/fchem.2020.00528.

Meis, D., Neumann, S., Filiz, V., 2022. Thermal rearrangement in thermal cascade reaction polymers via ortho-carbonate ester functionalization of polyimides and their gas separation performance. J. Membr. Sci. 655, 120586.

Meixia Shan, X.L., Wang, X., Yarulina, I., Seoane, B., Freek Kapteijn, J.G., 2018. Facile manufacture of porous organic framework membranes for precombustion CO 2 capture. Sci. Adv. 4.

Meldon, J.H., Stroeve, P., Grégoire, C.E., 1982. Facilitated transport of carbon dioxide: a review. Chem. Eng. Commun. 16, 263–300.

Mendes, D.N.D.L., Gaspar, A., Ferreira, I., Mota, J.P.B., Ribeiro, R.P.P.L., 2021. 3D-printed hybrid zeolitic/carbonaceous electrically conductive adsorbent structures. Chem. Eng. Res. Des. 174, 442–453. doi:10.1016/j.cherd.2021.08.020.

Meng, Y., Ju, T., Meng, F., Han, S., Song, M., Jiang, J., 2021. Insights into the critical role of abundant-porosity supports in polyethylenimine functionalization as efficient and stable CO_2 adsorbents. ACS Appl. Mater. Interfaces 13 (45), 54018–54031. doi:10.1021/acsami.1c17132.

Merkel, T.C., Freeman, B.D., Spontak, R.J., He, Z., Pinnau, I., Meakin, P., Hill, A.J., 2002. Ultrapermeable, reverse-selective nanocomposite membranes. Science 296, 519–522. doi:10.1126/science.1069580.

Merkel, T.C., Pinnau, I., Prabhakar, R., Freeman, B.D. 2006. https://doi.org/10.1002/047002903X.ch9.

Merkel, T.C., Lin, H., Wei, X., Baker, R., 2010. Power plant post-combustion carbon dioxide capture: An opportunity for membranes. J. Membr. Sci. 359 (1-2), 126–139. doi:10.1016/j.memsci.2009.10.041.

Merkel, T.C., Lin, H., Wei, X., Baker, R., 2010. Power plant post-combustion carbon dioxide capture: An opportunity for membranes. J. Membr. Sci. 359 (1-2), 126–139.

Merrick, M.M., Sujanani, R., Freeman, B.D., 2020. Glassy polymers: Historical findings, membrane applications, and unresolved questions regarding physical aging. Polymer 211, 123176. doi:10.1016/j.polymer.2020.123176.

Miccio, F., Murri, A.N., Landi, E., 2016. High-temperature capture of CO_2 by strontium oxide sorbents. Ind. Eng. Chem. Res. 55 (23), 6696–6707. doi:10.1021/acs.iecr.6b00184.

Michael E Parker, P.E., Northrop, S., Valencia, J.A., Foglesong, R.E., Duncan, W.T., 2011. CO_2 management at ExxonMobil's LaBarge field, Wyoming, USA. Energy Procedia 4, 5455–5470. doi:10.1016/j.egypro.2011.02.531.

Mikkelsen, M., Jørgensen, M., Krebs, F.C., 2010. The teraton challenge. A review of fixation and transformation of carbon dioxide. Energy Environ. Sci. 3 (1), 43–81.

Mikulčić, H., Ridjan Skov, I., Dominković, D.F., Wan Alwi, S.R., Manan, Z.A., Tan, R., Duić, N., Hidayah Mohamad, S.N., Wang, X., 2019. Flexible carbon capture and utilization technologies in future energy systems and the utilization pathways of captured CO_2. Renew. Sustain. Energy Rev. 114, 109338. doi:10.1016/j.rser.2019.109338.

Millward, A.R., Yaghi, O.M., 2005. Metal-organic frameworks with exceptionally high capacity for storage of_carbon dioxide at room temperature. J. Am. Chem. Soc. 127 (51), 17998–17999.

Milner, P.J., Siegelman, R.L., Forse, A.C., Gonzalez, M.I., Runcevski, T., Martell, J.D., Reimer, J.A., Long, J.R., 2017. A diaminopropane-appended metal-organic framework enabling efficient CO_2 capture from coal flue gas via a mixed adsorption mechanism. J. Am. Chem. Soc. 139 (38), 13541–13553. doi:10.1021/jacs.7b07612.

Min, K., Choi, W., Kim, C., Choi, M., 2018. Oxidation-stable amine-containing adsorbents for carbon dioxide capture. Nat. Commun. 9 (1), 726. doi:10.1038/s41467-018-03123-0.

Min, H.J., Kang, M., Lee, C.S., Kim, J.H., 2021. Dual-functional interconnected pebble-like structures in highly crystalline poly (ethylene oxide) membranes for CO_2 separation. Sep. Purif. Technol. 263, 118363. doi:10.1016/j.seppur.2021.118363.

Miricioiu, M.G., Zaharioiu, A., Oancea, S., Bucura, F., Raboaca, M.S., Filote, C., Ionete, R.E., Niculescu, V.C., Constantinescu, M., 2021. Sewage sludge derived materials for CO_2 adsorption. Appl. Sci. 11 (15), 7139. doi:10.3390/app11157139.

Mirzaie, M., Talebizadeh, A.R., Hashemipour, H., 2020. CFD simulation of benzene adsorption on pistachio activated carbon porous media. Frontiers in Heat and Mass Transfer 14, 1–7.

Miyamoto, M., Fujioka, Y., Yogo, K., 2012. Pure silica CHA type zeolite for CO 2 separation using pressure swing adsorption at high pressure. J. Mater. Chem. 22 (38), 20186–20189.

Mletzko, J., Ehlers, S., Kather, A., 2016. Comparison of natural gas combined cycle power plants with post combustion and oxyfuel technology at different CO_2 capture rates. Energy Procedia 86, 2–11. doi:10.1016/j.egypro.2016.01.001.

Moško, J., Pohořelý, M., Skoblia, S., Fajgar, R., Straka, P., Soukup, K., Beňo, Z., Farták, J., Bičáková, O., Jeremiáš, M., Šyc, M., Meers, E., 2021. Structural and chemical changes of sludge derived pyrolysis char prepared under different process temperatures. J. Analyt. Appl. Pyrol. 156, 105085. doi:10.1016/j.jaap.2021.105085.

Modak, A., Jana, S., 2019. Advancement in porous adsorbents for post-combustion CO_2 capture. Microporous Mesoporous Mater. 276, 107–132.

Moghadam, F., Kamio, E., Matsuyama, H., 2017. High CO_2 separation performance of amino acid ionic liquid-based double network ion gel membranes in low CO_2 concentration gas mixtures under humid conditions. J. Membr. Sci. 525, 290–297.

Mohamed, A.M.O., Moncho, S., Krokidas, P., Kakosimos, K., Brothers, E.N., Economou, I.G., 2019. Computational investigation of the performance of ZIF-8 with encapsulated ionic liquids towards CO_2 capture. Mol. Phys. 117 (23-24), 3791–3805. doi:10.1080/00268976.2019.1666170.

Mohamedali, M., Ibrahim, H., Henni, A., 2018. Incorporation of acetate-based ionic liquids into a zeolitic imidazolate framework (ZIF-8) as efficient sorbents for carbon dioxide capture. Chem. Eng. J. 334, 817–828. doi:10.1016/j.cej.2017.10.104.

Monsalve-Bravo, G.M., Bhatia, S.K., 2018. Modeling permeation through mixed-matrix membranes: A review. Processes 6 (9), 172. doi:10.3390/pr6090172.

Moon, H.R., Kobayashi, N., Suh, M.P., 2006. Porous metal– organic framework with coordinatively unsaturated MnII sites: sorption properties for various gases. Inorg. Chem. 45 (21), 8672–8676.

Moore, C.C.S., Autunes, C.H., Kulay, L., 2022. Economic, environmental and energy analysis of carbon capture systems coupled in coal power plants for the reduction of CO_2 emissions in Brazil. Int. J. Greenh. Gas Control 114, 11. doi:10.1016/j.ijggc.2022.103606.

Moors, J.H.J., 1999. Pulverised char combustion and gasification at high temperatures and pressures. Technische Universiteit Eindhoven.

Moreira, R.F.P.M., Soares, J.L., Casarin, G.L., Rodrigues, A.E., 2006. Adsorption of CO_2 on hydrotalcitelike compounds in a fixed bed. Sep. Sci. Technol. 41 (2), 341–357. doi:10.1080/01496390500496827.

Mori, G., Coccolo, S., Castello, R., Scartezzini, J.-L., 2019. Geospatial analysis and optimization of the incoming and stored CO_2 emissions within the EPFL campus. J. Phys.: Conf. Ser. 1343 (1), 012118. doi:10.1088/1742-6596/1343/1/012118.

Mostafavi, E., Ashrafi, O., Navarri, P., 2021. Assessment of process modifications for amine-based post-combustion carbon capture processes. Clean. Eng. Technol. 4. doi:10.1016/j.clet.2021.100249, 100249-100249.

Motahari, F., Raisi, A., 2020. UV irradiation-assisted cross-linking of high molecular weight poly (ethylene oxide) with poly (ethylene glycol) diacrylate to prepare CO_2 selective membranes. Polymer 205, 122821. doi:10.1016/j.polymer.2020.122821.

Mubashir, M., Yeong, Y.F., Lau, K.K., Chew, T.L., Norwahyu, J., 2018. Efficient CO_2/N_2 and CO_2/CH4 separation using NH2-MIL-53 (Al)/cellulose acetate (CA) mixed matrix membranes. Sep. Purif. Technol. 199, 140–151. doi:10.1016/j.seppur.2018.01.038.

Muchan, P., Saiwan, C., Narku-Tetteh, J., Idem, R., Supap, T., Tontiwachwuthikul, P., 2017. Screening tests of aqueous alkanolamine solutions based on primary, secondary, and tertiary structure for blended aqueous amine solution selection in post combustion CO 2 capture. Chem. Eng. Sci. 170, 574–582. doi:10.1016/j.ces.2017.02.031.

Mukherjee, S., Kumar, P., Yang, A., Fennell, P., 2015. Energy and exergy analysis of chemical looping combustion technology and comparison with pre-combustion and oxy-fuel combustion technologies for CO_2 capture. J. Environ. Chem. Eng. 3 (3), 2104–2114.

Mukherjee, S., Sikdar, N., O'Nolan, D., Franz, D.M., Gascón, V., Kumar, A., Kumar, N., Scott, H.S., Madden, D.G., Kruger, P.E., Space, B., Zaworotko, M.J., 2019. Trace CO_2 capture by an ultramicroporous physisorbent with low water affinity. Sci. Adv. 5 (11), eaax9171. doi:10.1126/sciadv.aax9171.

Mukherjee, A., Borugadda, V.B., Dynes, J.J., Niu, C., Dalai, A.K., 2021. Carbon dioxide capture from flue gas in biochar produced from spent coffee grounds: Effect of surface chemistry and porous structure. J. Environ. Chem. Eng. 9 (5). doi:10.1016/j.jece.2021.106049.

Mukhopadhyay, R.D., Praveen, V.K., Ajayaghosh, A., 2014. Photoresponsive metal–organic materials: exploiting the azobenzene switch. Mater. Horiz. 1 (6), 572–576. doi:10.1039/c4mh00122b.

Mukhtar, A., Saqib, S., Mellon, N.B., Babar, M., Rafiq, S., Ullah, S., Bustam, M.A., Al-Sehemi, A.G., Muhammad, N., Chawla, M., 2020. CO_2 capturing, thermokinetic principles, synthesis and amine functionalization of covalent organic polymers for CO_2 separation from natural gas: A review. J. Nat. Gas Sci. Eng. 77. doi:10.1016/j.jngse.2020.103203.

Mulgundmath, V.P., Jones, R.A., Tezel, F.H., Thibault, J., 2012. Fixed bed adsorption for the removal of carbon dioxide from nitrogen: Breakthrough behaviour and modelling for heat and mass transfer. Sep. Purif. Technol. 85, 17–27. doi:10.1016/j.seppur.2011.07.038.

Mungse, P., Saravanan, G., Rayalu, S., Labhsetwar, N., 2015. Mixed oxides of iron and manganese as potential low-cost oxygen carriers for chemical looping combustion. Energy Technol. 3 (8), 856–865. doi:10.1002/ente.201500035.

Munro, S., Åhlén, M., Cheung, O., Sanna, A., 2020. Tuning Na_2ZrO_3 for fast and stable CO_2 adsorption by solid state synthesis. Chem. Eng. J. 388, 124284. doi:10.1016/j.cej.2020.124284.

Murali, R.S., Sankarshana, T., Sridhar, S., 2013. Air separation by polymer-based membrane technology. Sep. Purif. Rev. 42 (2), 130–186. doi:10.1080/15422119.2012.686000.

Murge, P., Dinda, S., Roy, S., 2019. Zeolite-based sorbent for CO_2 capture: preparation and performance evaluation. Langmuir 35 (46), 14751–14760. doi:10.1021/acs.langmuir.9b02259.

Muriithi, G.N., Petrik, L.F., Gitari, W.M., Doucet, F.J., 2017. Synthesis and characterization of hydrotalcite from South African Coal fly ash. Powder Technol. 312, 299–309. doi:10.1016/j.powtec.2017.02.018.

Murugiah, P.S., Oh, P.C., Lau, K.K., 2018. Facilitated transport graphene oxide based PPOdm mixed matrix membrane for CO_2 separation. Mater. Today: Proc. 5 (10, Part 2), 21818–21824. doi:10.1016/j.matpr.2018.07.037.

Muschi, M., Devautour-Vinot, S., Aureau, D., Heymans, N., Sene, S., Emmerich, R., Ploumistos, A., Geneste, A., Steunou, N., Patriarche, G., De Weireld, G., Serre, C., 2021. Metal–organic framework/graphene oxide composites for CO_2 capture by microwave swing adsorption. J. Mater. Chem. A 9 (22), 13135–13142. doi:10.1039/d0ta12215g.

Mutyala, S., Jonnalagadda, M., Mitta, H., Gundeboyina, R., 2019a. CO_2 capture and adsorption kinetic study of amine-modified MIL-101 (Cr). Chem. Eng. Res. Des. 143, 241–248. doi:10.1016/j.cherd.2019.01.020.

Mutyala, S., Yakout, S.M., Ibrahim, S.S., Jonnalagadda, M., Mitta, H., 2019b. Enhancement of CO_2 capture and separation of CO_2/N_2 using post-synthetic modified MIL-100 (Fe). N. J. Chem. 43 (24), 9725–9731. doi:10.1039/c9nj02258a.

Nabipour, N., Qasem, S.N., Salwana, E., Baghban, A., 2020. Evolving LSSVM and ELM models to predict solubility of non-hydrocarbon gases in aqueous electrolyte systems. Measurement: J. Int. Measur. Confed. 164. doi:10.1016/j.measurement.2020.107999, 107999-107999.

Nadeali, A., Zamani Pedram, M., Omidkhah, M., Yarmohammadi, M., 2019. Promising performance for efficient CO_2 separation with the p-tert-Butylcalix [4] arene/Pebax-1657 mixed matrix membrane. ACS Sustain. Chem. Eng. 7 (23), 19015–19026. doi:10.1021/acssuschemeng.9b04641.

Naeem, M.A., Armutlulu, A., Imtiaz, Q., Müller, C.R., 2017. CaO-based CO_2 sorbents effectively stabilized by metal oxides. ChemPhysChem 18 (22), 3280–3285.

Naeem, M.A., Armutlulu, A., Imtiaz, Q., Donat, F., Schäublin, R., Kierzkowska, A., Müller, C.R., 2018. Optimization of the structural characteristics of CaO and its effective stabilization yield high-capacity CO_2 sorbents. Nat. Commun. 9 (1), 2408. doi:10.1038/s41467-018-04794-5.

Nagarajan, S., Skillen, N.C., Irvine, J.T.S., Lawton, L.A., Robertson, P.K.J., 2017. Cellulose II as bioethanol feedstock and its advantages over native cellulose. Renew. Sustain. Energy Rev. 77, 182–192. doi:10.1016/j.rser.2017.03.118.

Nahak, B.K., Preetam, S., Sharma, D., Shukla, S.K., Syvajarvi, M., Toncu, D.C., Tiwari, A., 2022. Advancements in net-zero pertinency of lignocellulosic biomass for climate neutral energy production. Renew. Sustain. Energy Rev. 161. doi:10.1016/j.rser.2022.112393.

Naquash, A., Qyyum, M.A., Haider, J., Bokhari, A., Lim, H., Lee, M., 2022. State-of-the-art assessment of cryogenic technologies for biogas upgrading: Energy, economic, and environmental perspectives. Renew. Sustain. Energy Rev. 154. doi:10.1016/j.rser.2021.111826.

Narku-Tetteh, J., Muchan, P., Saiwan, C., Supap, T., Idem, R., 2017. Selection of components for formulation of amine blends for post combustion CO 2 capture based on the side chain structure of primary, secondary and tertiary amines. Chem. Eng. Sci. 170, 542–560. doi:10.1016/j.ces.2017.02.036.

Narku-Tetteh, J., Afari, D.B., Coker, J., Idem, R., 2018. Evaluation of the Roles of Absorber and Desorber Catalysts in the Heat Duty and Heat of CO_2Desorption from Butylethanolamine–2-Amino-2-methyl-1-propanol and Monoethanolamine–Methyldiethanolamine Solvent Blends in a Bench-Scale CO_2Capture Pilot Plant. Energy Fuels 32 (9), 9711–9726. doi:10.1021/acs.energyfuels.8b02205.

Natewong, P., Prasongthum, N., Reubroycharoen, P., Idem, R., 2019. Evaluating the CO_2 capture performance using a BEA-AMP biblend amine solvent with novel high-performing absorber and desorber catalysts in a bench-scale CO_2 capture pilot plant. Energy Fuels 33 (4), 3390–3402. doi:10.1021/acs.energyfuels.8b04466.

Nauels, N., Herzog, S., Modigell, M., Broeckmann, C., 2019. Membrane module for pilot scale oxygen production. J. Membr. Sci. 574, 252–261. doi:10.1016/J.MEMSCI.2018.12.061.

Neal, L., Shafiefarhood, A., Li, F., 2015. Effect of core and shell compositions on MeOx@LaySr1−yFeO3 core–shell redox catalysts for chemical looping reforming of methane. Appl. Energy 157, 391–398. doi:10.1016/j.apenergy.2015.06.028.

Neumann, K., Gladyszewski, K., Groß, K., Qammar, H., Wenzel, D., Górak, A., Skiborowski, M., 2018. A guide on the industrial application of rotating packed beds. Chem. Eng. Res. Des. 134, 443–462. doi:10.1016/j.cherd.2018.04.024.

Ngamou, P.H.T., Ivanova, M.E., Guillon, O., Meulenberg, W.A., 2019. High-performance carbon molecular sieve membranes for hydrogen purification and pervaporation dehydration of organic solvents. J. Mater. Chem. A 7 (12), 7082–7091. doi:10.1039/c8ta09504c.

Nguyen, M.V., Lee, B.K., 2016. A novel removal of CO_2 using nitrogen doped biochar beads as a green adsorbent. Process. Saf. Environ. Prot. 104, 490–498. doi:10.1016/j.psep.7016.04.007.

Nguyen, N.T., Furukawa, H., Gándara, F., Nguyen, H.T., Cordova, K.E., Yaghi, O.M., 2014. Selective capture of carbon dioxide under humid conditions by hydrophobic chabazite-type zeolitic imidazolate frameworks. Angew. Chem. Int. Ed. 53 (40), 10645–10648.

Nicolas, C.H., Pera-Titus, M., 2012. Nanocomposite MFI-alumina hollow fiber membranes: influence of NO x and propane on CO_2/N_2 separation properties. Ind. Eng. Chem. Res. 51 (31), 10451–10461.

Nie, H., Jiang, H., Chong, D., Wu, Q., Xu, C., Zhou, H., 2013. Comparison of water scrubbing and propylene carbonate absorption for biogas upgrading process. Energy Fuels 27 (6), 3239–3245. doi:10.1021/ef400233w.

Nigar, H., Garcia-Baños, B., Peñaranda-Foix, F.L., Catalá-Civera, J.M., Mallada, R., Santamaría, J., 2016. Amine-functionalized mesoporous silica: A material capable of CO_2 adsorption and fast regeneration by microwave heating. AIChE J. 62 (2), 547–555. doi:10.1002/aic.15118.

Nik, O.G., Nohair, B., Kaliaguine, S., 2011. Aminosilanes grafting on FAU/EMT zeolite: Effect on CO_2 adsorptive properties. Microporous Mesoporous Mater. 143 (1), 221–229. doi:10.1016/j.micromeso.2011.03.002.

Nikam, S., Mandal, D., Dabhade, P., 2022. LDF based parametric optimization to model fluidized bed adsorption of trichloroethylene on activated carbon particles. Particuology 65, 72–92.

Nikolaidis, G.N., Kikkinides, E.S., Georgiadis, M.C., 2018. A model-based approach for the evaluation of new zeolite 13X-based adsorbents for the efficient post-combustion CO_2 capture using P/VSA processes. Chem. Eng. Res. Des. 131, 362–374. doi:10.1016/j.cherd.2017.06.016.

Nithin Mithra, S., Ahankari, S.S., 2022. Nanocellulose-based membranes for CO_2 separation from biogas through the facilitated transport mechanism: a review. Mater. Today Sustain., 100191 doi:10.1016/j.mtsust.2022.100191.

Nittaya, T., Douglas, P.L., Croiset, E., Ricardez-Sandoval, L.A., 2014. Dynamic modelling and controllability studies of a commercial-scale MEA absorption processes for CO_2 capture from coal-fired power plants. Energy Procedia 63, 1595–1600. doi:10.1016/j.egypro.2014.11.169.

Niu, H., Pan, L., Su, H., Wang, S., 2009. Effects of design and operating parameters on CO_2 absorption in microchannel contactors. Ind. Eng. Chem. Res. 48 (18), 8629–8634. doi:10.1021/ie8018966.

Niu, M., Yang, H., Zhang, X., Wang, Y., Tang, A., 2016. Amine-impregnated mesoporous silica nanotube as an emerging nanocomposite for CO_2 capture. ACS Appl. Mater. Interfaces 8 (27), 17312–17320. doi:10.1021/acsami.6b05044.

NOAA, 2022. Carbon dioxide peaks near 420 parts per million at Muana Loa observatory.

Noble, R.D.J, 1990. Analysis of facilitated transport with fixed site carrier membranes. J. Membr. Sci. 50 (2), 207–214.

Nomura, K., Ujihira, Y., Hayakawa, T., Takehira, K., 1996. CO_2 absorption properties and characterization of perovskite oxides, (Ba,Ca) (Co,Fe) $O_{3-\delta}$. Appl. Catal. A 137 (1), 25–36. doi:10.1016/0926-860X (95)00317-7.

Norouzbahari, S., Shahhosseini, S., Ghaemi, A., 2015. Modeling of CO_2 loading in aqueous solutions of piperazine: Application of an enhanced artificial neural network algorithm. J. Nat. Gas Sci. Eng. 24, 18–25. doi:10.1016/j.jngse.2015.03.011.

Notz, R.J., Tönnies, I., McCann, N., Scheffknecht, G., Hasse, H., 2011. CO_2 capture for fossil fuel-fired power plants. Chem. Eng. Technol. 34 (2), 163–172. doi:10.1002/ceat.201000491.

Ntiamoah, A., Ling, J., Xiao, P., Webley, P.A., Zhai, Y., 2015. CO_2 capture by vacuum swing adsorption: role of multiple pressure equalization steps. Adsorption 21 (6-7), 509–522. doi:10.1007/s10450-015-9690-8.

Ntiamoah, A., Ling, J., Xiao, P., Webley, P.A., Zhai, Y., 2016. CO_2 capture by temperature swing adsorption: Use of hot CO_2-rich gas for regeneration. Ind. Eng. Chem. Res. 55 (3), 703–713. doi:10.1021/acs.iecr.5b01384.

Nwaoha, C., Saiwan, C., Supap, T., Idem, R., Tontiwachwuthikul, P., Rongwong, W., Al-Marri, M.J., Benamor, A., 2016a. Carbon dioxide (CO_2) capture performance of aqueous tri-solvent blends containing 2-amino-2-methyl-1-propanol (AMP) and methyldiethanolamine (MDEA) promoted by diethylenetriamine (DETA). Int. J. Greenh. Gas Control 53, 292–304. doi:10.1016/j.ijggc.2016.08.012.

Nwaoha, C., Saiwan, C., Tontiwachwuthikul, P., Supap, T., Rongwong, W., Idem, R., Al-Marri, M.J., Benamor, A., 2016b. Carbon dioxide (CO_2) capture: Absorption-desorption capabilities of 2-amino-2-methyl-1-propanol (AMP), piperazine (PZ) and monoethanolamine (MEA) tri-solvent blends. J. Nat. Gas Sci. Eng. 33, 742–750. doi:10.1016/j.jngse.2016.06.002.

Nwaoha, C., Idem, R., Supap, T., Saiwan, C., Tontiwachwuthikul, P., Rongwong, W., Al-Marri, M.J., Benamor, A., 2017. Heat duty, heat of absorption, sensible heat and heat of vapourization of 2–Amino–2–Methyl–1–Propanol (AMP), Piperazine (PZ) and Monoethanolamine (MEA) tri–solvent blend for carbon dioxide (CO_2) capture. Chem. Eng. Sci. 170, 26–35. doi:10.1016/j.ces.2017.03.025.

Obergassel, W., Arens, C., Hermwille, L., Kreibich, N., Mersmann, F., Ott, H.E., Wang-Helmreich, H., 2016. Phoenix from the ashes: an analysis of the Paris Agreement to the United Nations framework convention on climate change. Wuppertal Institut für Klima, Umwelt, Energie.

Oexmann, J., Kather, A., 2010. Minimising the regeneration heat duty of post-combustion CO_2 capture by wet chemical absorption: The misguided focus on low heat of absorption solvents. Int. J. Greenh. Gas Control 4 (1), 36–43.

Oexmann, J., Hensel, C., Kather, A., 2008. Post-combustion CO_2-capture from coal-fired power plants: Preliminary evaluation of an integrated chemical absorption process with piperazine-promoted potassium carbonate. Int. J. Greenh. Gas Control 2 (4), 539–552. doi:10.1016/j.ijggc.2008.04.002.

Ogieglo, W., Furchner, A., Ma, X., Hazazi, K., Alhazmi, A.T., Pinnau, I., 2019. Thin composite carbon molecular sieve membranes from a polymer of intrinsic microporosity precursor. ACS Appl. Mater. Interfaces 11 (20), 18770–18781. doi:10.1021/acsami.9b04602.

Oh, H.T., Ju, Y., Chung, K., Lee, C.H., 2020. Techno-economic analysis of advanced stripper configurations for post-combustion CO_2 capture amine processes. Energy 206. doi:10.1016/j.energy.2020.118164, 118164-118164.

Oko, E., Wang, M., Joel, A.S., 2017. Current status and future development of solvent-based carbon capture. Int J. Coal Sci. Technol. 4 (1), 5–14. doi:10.1007/s40789-017-0159-0.

Oko, E., Ramshaw, C., Wang, M., 2018. Study of intercooling for rotating packed bed absorbers in intensified solvent-based CO_2 capture process. Appl. Energy 223, 302–316.

Olabi, A.G., Obaideen, K., Elsaid, K., Wilberforce, T., Sayed, E.T., Maghrabie, H.M., Abdelkareem, M.A., 2022. Assessment of the pre-combustion carbon capture contribution into sustainable development goals SDGs using novel indicators. Renew. Sustain. Energy Rev. 153, 111710. doi:10.1016/j.rser.2021.111710.

Olajire, A.A., 2017. Recent advances in the synthesis of covalent organic frameworks for CO_2 capture. J. CO_2 Util. 17, 137–161.

Olaleye, A.K., Oko, E., Wang, M., Kelsall, G., 2016. Dynamic modelling and analysis of supercritical coal-fired power plant integrated with post-combustion CO_2 capture. In: Clean Coal Technology and Sustainable Development - Proceedings of the 8th International Symposium on Coal Combustion,2015. Springer, pp. 359–363.

Oliveira, E.L.G., Grande, C.A., Rodrigues, A.E., 2008. CO_2 sorption on hydrotalcite and alkali-modified (K and Cs) hydrotalcites at high temperatures. Sep. Purif. Technol. 62 (1), 137–147. doi:10.1016/j.seppur.2008.01.011.

Omodolor, I.S., Otor, H.O., Andonegui, J.A., Allen, B.J., Alba-Rubio, A.C., 2020. Dual-function materials for CO_2 capture and conversion: a review. Ind. Eng. Chem. Res. 59 (40), 17612–17631. doi:10.1021/acs.iecr.0c02218.

Onda, K., Takeuchi, H., Okumoto, Y., 1968. Mass transfer coefficients between gas and liquid phases in packed columns. Journal of Chemical Engineering of Japan 1 (1), 56–62.

Oreggioni, G.D., Brandani, S., Luberti, M., Baykan, Y., Friedrich, D., Ahn, H., 2015. CO_2 capture from syngas by an adsorption process at a biomass gasification CHP plant: Its comparison with amine-based CO_2 capture. Int. J. Greenh. Gas Control 35, 71–81. doi:10.1016/j.ijggc.2015.01.008.

Orthman, J., Zhu, H., Lu, G., 2003. Use of anion clay hydrotalcite to remove coloured organics from aqueous solutions. Sep. Purif. Technol. 31 (1), 53–59.

Ortiz, C., Valverde, J.M., Chacartegui, R., Perez-Maqueda, L.A., Gimenez, P., 2019. The Calcium-Looping (CaCO3/CaO) process for thermochemical energy storage in Concentrating Solar Power plants. Renew. Sustain. Energy Rev. 113, 18. doi:10.1016/j.rser.2019.109252.

Osman, A.I., Hefny, M., Abdel Maksoud, M.I.A., Elgarahy, A.M., Rooney, D.W., 2021. Recent advances in carbon capture storage and utilisation technologies: a review. Environ. Chem. Lett. 19 (2), 797–849. doi:10.1007/s10311-020-01133-3.

Othman, M.R., Helwani, Z., Martunus, Fernando, W.J.N., 2009. Synthetic hydrotalcites from different routes and their application as catalysts and gas adsorbents: a review. Appl. Organ. Chem. 23 (9), 335–346. doi:10.1002/aoc.1517.

Otitoju, O., Oko, E., Wang, M., 2021. Technical and economic performance assessment of post-combustion carbon capture using piperazine for large scale natural gas combined cycle power plants through process simulation. Appl. Energy 292. doi:10.1016/j.apenergy.2021.116893, 116893-116893.

Otitoju, O., Oko, E., Wang, M., 2023. Modelling, scale-up and techno-economic assessment of rotating packed bed absorber for CO_2 capture from a 250 MWe combined cycle gas turbine power plant. Applied Energy 335, 120747 -120747.

Otitoju, O.S., 2022. Modelling, Simulation and Performance Evaluation of Post-Combustion Carbon Capture based on Chemical Absorption. The University of Sheffield, United Kingdom.

Ozkan, M., Nayak, S.P., Ruiz, A.D., Jiang, W., 2022. Current status and pillars of direct air capture technologies. iScience 25 (4), 103990. doi:10.1016/j.isci.2022.103990.

Pérez-Francisco, J.M., Santiago-García, J.L., Loría-Bastarrachea, M.I., Paul, D.R., Freeman, B.D., Aguilar-Vega, M., 2020. CMS membranes from PBI/PI blends: Temperature effect on gas transport and separation performance. J. Membr. Sci. 597. doi:10.1016/j.memsci.2019.117703.

Pachauri, R., Meyer, L., 2014. Climate change 2014: Synthesis report. In: Contribution of Working Groups I, II and III to the Fifth Assessment Report of the Intergovernmental Panel on Climate Change.

Pachitsas, S., Bonalumi, D., 2022. Parametric investigation of CO_2 capture from industrial flue gases using aqueous mixtures of ammonia (NH3) and potassium carbonate (K2CO3). Int. J. Greenh. Gas Control 114, 103567. doi:10.1016/j.ijggc.2021.103567.

Pai, K.N., Prasad, V., Rajendran, A., 2021. Practically achievable process performance limits for pressure-vacuum swing adsorption-based postcombustion CO_2 capture. ACS Sustain. Chem. Eng. 9 (10), 3838–3849. doi:10.1021/acssuschemeng.0c08933.

Pakizeh, M., Moradi, A., Ghassemi, T., 2021. Chemical extraction and modification of chitin and chitosan from shrimp shells. Eur. Polym. J. 159. doi:10.1016/j.eurpolymj.2021.110709.

Pal, A., Chand, S., Das, M.C., 2017. A water-stable twofold interpenetrating microporous MOF for selective CO_2 adsorption and separation. Inorg. Chem. 56 (22), 13991–13997. doi:10.1021/acs.inorgchem.7b02136.

Pallarés, J., González-Cencerrado, A., Arauzo, I., 2018. Production and characterization of activated carbon from barley straw by physical activation with carbon dioxide and steam. Biomass Bioenergy 115, 64–73. doi:10.1016/j.biombioe.2018.04.015.

Palomino, M., Corma, A., Rey, F., Valencia, S., 2010. New Insights on CO_2– Methane separation using LTA zeolites with different Si/Al ratios and a first comparison with MOFs. Langmuir 26 (3), 1910–1917.

Pan, X., Clodic, D., Toubassy, J., 2013. CO_2 capture by antisublimation process and its technical economic analysis. Greenh. Gas Sci. Technol. 3 (1), 8–20. doi:10.1002/ghg.1313.

Pan, W., Galvin, J., Huang, W.L., Xu, Z., Sun, X., Fan, Z., Liu, K., 2018. Device-scale CFD modeling of gas-liquid multiphase flow and amine absorption for CO_2 capture. Greenh. Gases: Sci. Technol. 8 (3), 603–620. doi:10.1002/ghg.1770.

Panda, D., Kumar, E.A., Singh, S.K., 2019. Amine modification of binder-containing zeolite 4A bodies for post-combustion CO_2 capture. Ind. Eng. Chem. Res. 58 (13), 5301–5313. doi:10.1021/acs.iecr.8b03958.

Pang, Z.-F., Xu, S.-Q., Zhou, T.-Y., Liang, R.-R., Zhan, T.-G., Zhao, X., 2016. Construction of covalent organic frameworks bearing three different kinds of pores through the heterostructural mixed linker strategy. J. Am. Chem. Soc. 138 (14), 4710–4713.

Pang, S.H., Lively, R.P., Jones, C.W., 2018. Oxidatively-stable linear poly (propylenimine)-containing adsorbents for CO_2 capture from ultradilute streams. ChemSusChem 11 (15), 2628–2637. doi:10.1002/cssc.201800438.

Papalas, T., Polychronidis, I., Antzaras, A.N., Lemonidou, A.A., 2021. Enhancing the intermediate-temperature CO_2 capture efficiency of mineral MgO via molten alkali nitrates and $CaCO_3$: Characterization and sorption mechanism. J. CO_2 Util. 50, 101605. doi:10.1016/j.jcou.2021.101605.

Park, H.J., Suh, M.P., 2013. Enhanced isosteric heat, selectivity, and uptake capacity of CO 2 adsorption in a metal-organic framework by impregnated metal ions. Chem. Sci. 4 (2), 685–690.

Park, S.W., Lee, J.W., Choi, B.S., Lee, J.W., 2005. Reaction kinetics of carbon dioxide with diethanolamine in polar organic solvents. Sep. Sci. Technol. 40 (9), 1885–1898.

Park, S.-W., Choi, B.-S., Lee, J.-W., 2006. Chemical absorption of carbon dioxide with triethanolamine in non-aqueous solutions. Korean J. Chem. Eng. 23 (1), 138–143.

Park, S.W., Lee, J.W., Choi, B.S., Lee, J.W., 2006. Absorption of carbon dioxide into non-aqueous solutions of N-methyldiethanolamine. Korean J. Chem. Eng. 23 (5), 806–811. doi:10.1007/bf02705932.

Park, H.B., Jung, C.H., Lee, Y.M., Hill, A.J., Pas, S.J., Mudie, S.T., Van Wagner, E., Freeman, B.D., Cookson, D.J., 2007. Polymers with cavities tuned for fast selective transport of small molecules and ions. Science (New York, N.Y.) 318 (5848), 254–258. doi:10.1126/science.1146744.

Park, Y.-I., Kim, B.-S., Byun, Y.-H., Lee, S.-H., Lee, E.-W., Lee, J.-M.J.D., 2009. Preparation of supported ionic liquid membranes (SILMs) for the removal of acidic gases from crude natural gas. Desalianation 236 (1-3), 342–348.

Park, J., Yuan, D., Pham, K.T., Li, J.R., Yakovenko, A., Zhou, H.C., 2012. Reversible alteration of CO_2 adsorption upon photochemical or thermal treatment in a metal-organic framework. J. Am. Chem. Soc. 134 (1), 99–102. doi:10.1021/ja209197f.

Park, S.H., Lee, S.J., Lee, J.W., Chun, S.N., Lee, J.B., 2015. The quantitative evaluation of two-stage pre-combustion CO_2 capture processes using the physical solvents with various design parameters. Energy 81, 47–55. doi:10.1016/j.energy.2014.10.055.

Park, J.H., Celedonio, J.M., Seo, H., Park, Y.K., Ko, Y.S., 2016. A study on the effect of the amine structure in CO_2 dry sorbents on CO_2 capture. Catal. Today 265, 68–76. doi:10.1016/j.cattod.2015.10.015.

Park, S., Cho, K., Jeong, H.-K., 2020. Polyimide/ZIF-7 mixed-matrix membranes: understanding the in situ confined formation of the ZIF-7 phases inside a polymer and their effects on gas separations. J. Mater. Chem. A 8 (22), 11210–11217. doi:10.1039/D0TA02761H.

Pate, S.G., Xu, H., O'Brien, C.P., 2022. Operando observation of CO_2 transport intermediates in polyvinylamine facilitated transport membranes, and the role of water in the formation of intermediates, using transmission FTIR spectroscopy. J. Mater. Chem. A 10 (8), 4418–4427. doi:10.1039/D1TA10015G.

Patel, H.A., Je, S.H., Park, J., Chen, D.P., Jung, Y., Yavuz, C.T., Coskun, A., 2013. Unprecedented high-temperature CO_2 selectivity in N_2-phobic nanoporous covalent organic polymers. Nat. Commun. 4 (1), 1–8. doi:10.1038/ncomms2359.

Patil, T., Dharaskar, S., Sinha, M., Jampa, S.S., 2022. Effectiveness of ionic liquid-supported membranes for carbon dioxide capture: a review. Environ. Sci. Pollut. Res. Int. 29 (24), 35723–35745. doi:10.1007/s11356-022-19586-0.

Paul, D., Kemp, D., 1973. The diffusion time lag in polymer membranes containing adsorptive fillers. J. Polym. Sci.: Polym. Symp. 79–93 Wiley Online Library.

Peh, S.B., Farooq, S., Zhao, D., 2022. A metal-organic framework (MOF)-based temperature swing adsorption cycle for postcombustion CO_2 capture from wet flue gas. Chem. Eng. Sci. 250. doi:10.1016/j.ces.2021.117399.

Pehnt, M., Henkel, J., 2009. Life cycle assessment of carbon dioxide capture and storage from lignite power plants. Int. J. Greenh. Gas Control 3 (1), 49–66. doi:10.1016/j.ijggc.2008.07.001.

Pellegrini, G., Strube, R., Manfrida, G., 2010. Comparative study of chemical absorbents in postcombustion CO_2 capture. Energy 35 (2), 851–857.

Pellegrini, L.A., De Guido, G., Langé, S., 2018. Biogas to liquefied biomethane via cryogenic upgrading technologies. Renew. Energy 124, 75–83. doi:10.1016/j.renene.2017.08.007.

Peltola, P., Ritvanen, J., Tynjälä, T., Pröll, T., Hyppänen, T., 2013. One-dimensional modelling of chemical looping combustion in dual fluidized bed reactor system. Int. J. Greenh. Gas Control 16, 72–82.

Peltzer, D., Mùnera, J., Cornaglia, L., Strumendo, M., 2018. Characterization of potassium doped Li_2ZrO_3 based CO_2 sorbents: Stability properties and CO_2 desorption kinetics. Chem. Eng. J. 336, 1–11. doi:10.1016/j.cej.2017.10.177.

Peltzer, D., Múnera, J., Cornaglia, L., 2019. The effect of the Li:Na molar ratio on the structural and sorption properties of mixed zirconates for CO_2 capture at high temperature. J. Environ. Chem. Eng. 7 (2), 102927. doi:10.1016/j.jece.2019.102927.

Peng, X., Ye, L.L., Wang, C.H., Zhou, H., Sun, B., 2011. Temperature- and duration-dependent rice straw-derived biochar: Characteristics and its effects on soil properties of an Ultisol in southern China. Soil and Tillage Res. 112 (2), 159–166. doi:10.1016/j.still.2011.01.002.

Peng, D., Wang, S., Tian, Z., Wu, X., Wu, Y., Wu, H., Xin, Q., Chen, J., Cao, X., Jiang, Z., 2017. Facilitated transport membranes by incorporating graphene nanosheets with high zinc ion loading for enhanced CO_2 separation. J. Membr. Sci. 522, 351–362. doi:10.1016/j.memsci.2016.09.040.

Peng, H.-L., Zhang, J.-B., Zhang, J.-Y., Zhong, F.-Y., Wu, P.-K., Huang, K., Fan, J.-P., Liu, F., 2019. Chitosan-derived mesoporous carbon with ultrahigh pore volume for amine impregnation and highly efficient CO_2 capture. Chem. Eng. J. 359, 1159–1165. doi:10.1016/j.cej.2018.11.064.

Peng, L., Shi, M., Zhang, X., Xiong, W., Hu, X., Tu, Z., Wu, Y., 2022. Facilitated transport separation of CO_2 and H2S by supported liquid membrane based on task-specific protic ionic liquids. Green Chem. Eng. 3 (3), 259–266. doi:10.1016/j.gce.2021.12.005.

Pera-Titus, M., 2014. Porous inorganic membranes for CO_2 capture: present and prospects. Chem. Rev. 114 (2), 1413–1492.

Pereira, A., Ferreira, A.F.P., Rodrigues, A., Ribeiro, A.M., Regufe, M.J., 2022. Evaluation of the potential of a 3D-printed hybrid zeolite 13X/activated carbon material for CO_2/N_2 separation using electric swing adsorption. Chem. Eng. J. 450. doi:10.1016/j.cej.2022.138197.

Perejón, A., Romeo, L.M., Lara, Y., Lisbona, P., Martínez, A., Valverde, J.M.J.A.E., 2016. The Calcium-Looping technology for CO_2 capture: On the important roles of energy integration and sorbent behavior. Appl. Energy 162, 787–807.

Perejon, A., Romeo, L.M., Lara, Y., Lisbona, P., Martinez, A., Valverde, J.M., 2016. The calcium-looping technology for CO_2 capture: On the important roles of energy integration and sorbent behavior. Appl. Energy 162, 787–807. doi:10.1016/j.apenergy.2015.10.121.

Peres, C.B., Rosa, A.H., de Morais, L.C., 2022. CO_2 adsorption of bagasse waste feedstock using thermogravimetric analyses. J. Therm. Anal. Calorim. 147 (10), 5973–5984. doi:10.1007/s10973-021-10949-2.

Perinu, C., Bernhardsen, I.M., Svendsen, H.F., Jens, K.-J., 2017. CO_2 Capture by Aqueous 3- (Methylamino)propylamine in Blend with Tertiary Amines: An NMR Analysis. Energy Proc. 114, 1949–1955. doi:10.1016/j.egypro.2017.03.1326.

Perot, G., Guisnet, M., 1990. Advantages and disadvantages of zeolites as catalysts in organic chemistry. J. Mol. Catal. 61 (2), 173–196. doi:10.1016/0304-5102(90)85154-A.

Perskin, J.B., Traum, M.J., von Hippel, T., Boetcher, S.K.S., 2022. On the feasibility of precompression for direct atmospheric cryogenic carbon capture. Carbon Cap. Sci. Technol. 4, 100063. doi:10.1016/j.ccst.2022.100063.

Peters, A., 2022. A startup in Hawaii just launched the world's first ocean-assisted carbon removal plant. https://www.fastcompany.com/90750797/a-startup-in-hawaii-just-launched-the-worlds-first-ocean-assisted-carbon-removal-plant. (Accessed 2022.05.22.

Petre, C.F., Larachi, F., Iliuta, I., Grandjean, B.P.A., 2003. Pressure drop through structured packings: Breakdown into the contributing mechanisms by CFD modeling. Chem. Eng. Sci. 58 (1), 163–177. doi:10.1016/S0009-2509(02)00473-6.

Petrescu, L., Cormos, C.-C., 2017. Environmental assessment of IGCC power plants with pre-combustion CO_2 capture by chemical & calcium looping methods. J. Clean. Prod. 158, 233–244. doi:10.1016/j.jclepro.2017.05.011.

Petrescu, L., Bonalumi, D., Valenti, G., Cormos, A.-M., Cormos, C.-C., 2017. Life Cycle Assessment for supercritical pulverized coal power plants with post-combustion carbon capture and storage. J. Clean. Prod. 157, 10–21. doi:10.1016/j.jclepro.2017.03.225.

Pfaff, I., Kather, A., 2009. Comparative thermodynamic analysis and integration issues of CCS steam power plants based on oxy-combustion with cryogenic or membrane based air separation. Energy Procedia 1 (1), 495–502. doi:10.1016/j.egypro.2009.01.066.

Pham, D.A., Lim, Y.I., Jee, H., Ahn, E., Jung, Y., 2015. Effect of ship tilting and motion on amine absorber with structured-packing for CO_2 removal from natural gas. AIChE J. 61 (12), 4412–4425. doi:10.1002/aic.14962.

Pham, D.A., Lim, Y.I., Jee, H., Ahn, E., Jung, Y., 2015. Porous media Eulerian computational fluid dynamics (CFD) model of amine absorber with structured-packing for CO_2 removal. Chem. Eng. Sci. 132, 259–270. doi:10.1016/j.ces.2015.04.009.

Pi, S., Zhang, Z., He, D., Qin, C., Ran, J.J.E., 2019. Novel binders-promoted extrusion-spheronized CaO-based pellets for high-temperature CO_2 capture. Fuels 33 (3), 2381–2389.

Pinto, D.D.D., Knuutila, H., Fytianos, G., Haugen, G., Mejdell, T., Svendsen, H.F., 2014a. CO_2 post combustion capture with a phase change solvent. Pilot plant campaign. Int. J. Greenh. Gas Control 31, 153–164. doi:10.1016/j.ijggc.2014.10.007.

Pinto, D.D.D., Zaidy, S.A.H., Hartono, A., Svendsen, H.F., 2014b. Evaluation of a phase change solvent for CO 2 capture: Absorption and desorption tests. Int. J. Greenh. Gas Control 28, 318–327. doi:10.1016/j.ijggc.2014.07.002.

Pirngruber, G.D., Guillou, F., Gomez, A., Clausse, M., 2013. A theoretical analysis of the energy consumption of post-combustion CO_2 capture processes by temperature swing adsorption using solid sorbents. Int. J. Greenh. Gas Control 14, 74–83. doi:10.1016/j.ijggc.2013.01.010.

Plant, D., Maurin, G., Deroche, I., Gaberova, L., Llewellyn, P.L., 2006. CO_2 adsorption in alkali cation exchanged Y faujasites: a quantum chemical study compared to experiments. Chem. Phys. Lett. 426 (4-6), 387–392.

Plaza, M.G., Rubiera, F., 2019. Evaluation of a novel multibed heat-integrated vacuum and temperature swing adsorption post-combustion CO_2 capture process. Appl. Energy 250, 916–925. doi:10.1016/j.apenergy.2019.05.079.

Plaza, M.G., Pevida, C., Arias, B., Fermoso, J., Casal, M.D., Martín, C.F., Rubiera, F., Pis, J.J., 2009. Development of low-cost biomass-based adsorbents for postcombustion CO_2 capture. Fuel 88 (12), 2442–2447. doi:10.1016/j.fuel.2009.02.025.

Plaza, M.G., Pevida, C., Martín, C.F., Fermoso, J., Pis, J.J., Rubiera, F., 2010. Developing almond shell-derived activated carbons as CO_2 adsorbents. Sep. Purif. Technol. 71 (1), 102–106. doi:10.1016/j.seppur.2009.11.008.

Plaza, M.G., García, S., Rubiera, F., Pis, J.J., Pevida, C., 2011. Evaluation of ammonia modified and conventionally activated biomass based carbons as CO_2 adsorbents in postcombustion conditions. Sep. Purif. Technol. 80 (1), 96–104. doi:10.1016/j.seppur.2011.04.015.

Plaza, M.G., Martinez, S., Rubiera, F., 2020. CO_2 capture, use, and storage in the cement industry: state of the art and expectations. Energies 13 (21), 28. doi:10.3390/en13215692.

Plazaola, A.A., Labella, A.C., Liu, Y., Porras, N.B., Tanaka, D.A.P., Annaland, M.V.S., Gallucci, F., 2019. Mixed ionic-electronic conducting membranes (MIEC) for their application in membrane reactors: a review. Processes 7, 128. doi:10.3390/PR7030128, 2019, Vol. 7, Page 128.

Pohako-Esko, K., Bahlmann, M., Schulz, P.S., Wasserscheid, P., 2016. Chitosan containing supported ionic liquid phase materials for CO_2 absorption. Ind. Eng. Chem. Res. 55 (25), 7052–7059. doi:10.1021/acs.iecr.6b00862.

Pokhrel, J., Bhoria, N., Anastasiou, S., Tsoufis, T., Gournis, D., Romanos, G., Karanikolos, G.N., 2018. CO_2 adsorption behavior of amine-functionalized ZIF-8, graphene oxide, and ZIF-8/graphene oxide composites under dry and wet conditions. Microporous Mesoporous Mater. 267, 53–67. doi:10.1016/j.micromeso.2018.03.012.

Policicchio, A., Zhao, Y., Zhong, Q., Agostino, R.G., Bandosz, T.J., 2014. Cu-BTC/aminated graphite oxide composites as high-efficiency CO_2 capture media. ACS Appl. Mater. Interfaces 6 (1), 101–108. doi:10.1021/am404952z.

Portillo, E., Alonso-Fariñas, B., Vega, F., Cano, M., Navarrete, B., 2019. Alternatives for oxygen-selective membrane systems and their integration into the oxy-fuel combustion process: A review. Sep. Purif. Technol. 229. doi:10.1016/j.seppur.2019.115708, 115708-115708.

Prabhakar, R., Freeman, B., 2002. Application of hydrocarbon—fluorocarbon interactions in membrane-based gas separations. Desalination 144 (1), 79–83. doi:10.1016/S0011-9164 (02)00292-8.

Prashar, A.K., Seo, H., Choi, W.C., Kang, N.Y., Park, S., Kim, K., Min, D.Y., Kim, H.M., Park, Y.K., 2016. Factors affecting the rate of CO_2 absorption after partial desorption in $NaNO_3$-promoted MgO. Energy Fuels 30 (4), 3298–3305.

Prasongthum, N., Natewong, P., Reubroycharoen, P., Idem, R., 2019. Solvent regeneration of a CO_2-Loaded BEA–AMP Bi-blend amine solvent with the aid of a solid Brønsted Ce (SO4)2/ZrO2 superacid catalyst. Energy Fuels 33 (2), 1334–1343. doi:10.1021/acs.energyfuels.8b03580.

Prationo, W., Zhang, J., Cui, J., Wang, Y., Zhang, L., 2015. Clarifying the influence of moisture on the ignition and combustion of wet Victorian brown coal in air-firing and oxy-fuel modes: Part 2: Contribution of gasification reaction to char oxidation rate. Fuel Process. Technol. 138, 680–686.

Presser, V., McDonough, J., Yeon, S.-H., Gogotsi, Y., 2011. Effect of pore size on carbon dioxide sorption by carbide derived carbon. Energy Environ. Sci. 4 (8), 3059–3066. doi:10.1039/C1EE01176F.

Preston, C.K., Bruce, C., Monea, M.J., 2018. An update on the integrated CCS project at Saskpower's boundary dam power station.

Preston, C., 2015. IEA GHG Report #2015-06 "Integrated carbon capture and storage project at saskpower's boundary dam power station". IEA GHG report #2015-06 "integrated carbon capture and storage project at saskpower's boundary dam power station".

Primo, A., Forneli, A., Corma, A., García, H., 2012. From biomass wastes to highly efficient CO_2 adsorbents: Graphitisation of chitosan and alginate biopolymers. ChemSusChem 5 (11), 2207–2214. doi:10.1002/cssc.201200366.

Prosser, N.M., Shah, M.M., 2011. Current and Future Oxygen (O 2) Supply Technologies for Oxy-Fuel Combustion. Elsevier, pp. 195–227.

Pruna, A., Carcel, A., Benedito, A., Gimenez, E., 2021. Hydrothermal-freeze-casting of poly (amidoamine)-modified graphene aerogels towards CO_2 adsorption. Int. J. Mol. Sci. 22 (17). doi:10.3390/ijms22179333.

Przepiórski, J., Skrodzewicz, M., Morawski, A.W., 2004. High temperature ammonia treatment of activated carbon for enhancement of CO_2 adsorption. Appl. Surf. Sci. 225 (1), 235–242. doi:10.1016/j.apsusc.2003.10.006.

Pu, Y., Yang, Z., Wee, V., Wu, Z., Jiang, Z., Zhao, D., 2022. Amino-functionalized NUS-8 nanosheets as fillers in PIM-1 mixed matrix membranes for CO_2 separations. J. Membr. Sci. 641, 119912. doi:10.1016/j.memsci.2021.119912.

Qasem, N.A.A., Qadir, N.U., Ben-Mansour, R., Said, S.A.M., 2017. Synthesis, characterization, and CO 2 breakthrough adsorption of a novel MWCNT/MIL-101 (Cr) composite. J. CO_2 Util. 22, 238–249. doi:10.1016/j.jcou.2017.10.015.

Qasem, N.A.A., Ben-Mansour, R., Habib, M.A., 2018. An efficient CO_2 adsorptive storage using MOF-5 and MOF-177. Appl. Energy 210, 317–326. doi:10.1016/j.apenergy.2017.11.011.

Qi, T., Yang, Y., Wu, Y., Wang, J., Li, P., Yu, J., 2018. Sorption-enhanced methanol steam reforming for hydrogen production by combined copper-based catalysts with hydrotalcites. Chem. Eng. Process. - Process Intensif. 127, 72–82. doi:10.1016/j.cep.2018.03.022.

Qiao, Z., Zhao, S., Wang, J., Wang, S., Wang, Z., Guiver, M.D., 2016. A highly permeable aligned montmorillonite mixed-matrix membrane for CO_2 separation. Angew. Chem. Int. Ed. 128 (32), 9467–9471. doi:10.1002/anie.201603211.

Qiao, Y.Q., Wang, J.Y., Zhang, Y., Gao, W.L., Harada, T., Huang, L., Hatton, T.A., Wang, Q., 2017. Alkali nitrates molten salt modified commercial MgO for intermediate-temperature CO_2 capture: optimization of the Li/Na/K ratio. Ind. Eng. Chem. Res. 56 (6), 1509–1517. doi:10.1021/acs.iecr.6b04793.

Qiao, Y.T., Zhang, S.M., Quan, C., Gao, N.B., Josnston, C., Wu, C.F., 2020. One-pot synthesis of digestate-derived biochar for carbon dioxide capture. Fuel 279. doi:10.1016/j.fuel.2020.118525.

Qiao, Y., Bailey, J.J., Huang, Q., Ke, X., Wu, C., 2022. Potential photo-switching sorbents for CO_2 capture – A review. Renew. Sustain. Energy Rev. 158. doi:10.1016/j.rser.2022.112079.

Qin, C., Yin, J., Ran, J., Zhang, L., Feng, B., 2014. Effect of support material on the performance of K_2CO3-based pellets for cyclic CO_2 capture. Appl. Energy 136, 280–288. doi:10.1016/j.apenergy.2014.09.043.

Qin, Q., Liu, H., Zhang, R., Ling, L., Fan, M., Wang, B., 2018. Application of density functional theory in studying CO_2 capture with TiO_2-supported K_2CO_3 being an example. Appl. Energy 231, 167–178. doi:10.1016/j.apenergy.2018.09.114.

Qiu, W., Vaughn, J., Liu, G., Xu, L., Brayden, M., Martinez, M., Fitzgibbons, T., Wenz, G., Koros, W.J., 2019. Hyperaging tuning of a carbon molecular-sieve hollow fiber membrane with extraordinary gas-separation performance and stability. Angew. Chem. Int. Ed. Engl. 58 (34), 11700–11703. doi:10.1002/anie.201904913.

Qiu, H., Liu, H., Liu, X., Yao, H., 2022. Synthesis of Novel Al_2O_3 nanoparticle organic hybrid Materials for enhancing the CO_2-separation performance of prepared Al_2O_3-NOHMs/Pebax mixed matrix membrane. Mater. Lett., 132854 doi:10.1016/j.matlet.2022.132854.

Qiu, Y., Lamers, P., Daioglou, V., McQueen, N., de Boer, H.-S., Harmsen, M., Wilcox, J., Bardow, A., Suh, S., 2022. Environmental trade-offs of direct air capture technologies in climate change mitigation toward 2100. Nat. Commun. 13 (1), 3635. doi:10.1038/s41467-022-31146-1.

Qu, Z., Zhao, R., Wu, H., Ren, Y., Liu, Y., Guo, Z., Wu, Y., Yang, L., Liang, X., Jiang, Z., 2020. Polyelectrolyte membranes with tunable hollow CO_2-philic clusters via sacrificial template for biogas upgrading. J. Membr. Sci. 612, 118445. doi:10.1016/j.memsci.2020.118445.

Quan, C., Su, R., Gao, N., 2020. Preparation of activated biomass carbon from pine sawdust for supercapacitor and CO_2 capture. Int. J. Energy Res. 44 (6), 4335–4351. doi:10.1002/er.5206.

Quang, D.V., Dindi, A., Abu-Zahra, M.R.M., 2017. One-step process using CO_2 for the preparation of amino-functionalized mesoporous silica for CO_2 capture application. ACS Sustain. Chem. Eng. 5 (4), 3170–3178. doi:10.1021/acssuschemeng.6b02961.

Que, H., Chen, C.-C., 2011. Thermodynamic modeling of the NH3–CO_2–H2O system with electrolyte NRTL model. Ind. Eng. Chem. Res. 50 (19), 11406–11421.

Radfarnia, H.R., Iliuta, M.C., 2013. Metal oxide-stabilized calcium oxide CO_2 sorbent for multicycle operation. Chem. Eng. J. 232, 280–289. doi:10.1016/j.cej.2013.07.049.

Rafiq, S., Deng, L., Hägg, M.-B., 2016. Role of facilitated transport membranes and composite membranes for efficient CO_2 capture – a review. ChemBioEng. Rev. 3 (2), 68–85. doi:10.1002/cben.201500013.

Rafizah, W., Ismail, A., 2008. Effect of carbon molecular sieve sizing with poly (vinyl pyrrolidone) K-15 on carbon molecular sieve–polysulfone mixed matrix membrane. J. Membr. Sci. 307 (1), 53–61.

Raganati, F., Chirone, R., Ammendola, P., 2020. CO_2 capture by temperature swing adsorption: Working capacity as affected by temperature and CO_2 partial pressure. Ind. Eng. Chem. Res. 59 (8), 3593–3605. doi:10.1021/acs.iecr.9b04901.

Raganati, F., Miccio, F., Ammendola, P., 2021. Adsorption of carbon dioxide for post-combustion capture: a review. Energy Fuels 35 (16), 12845–12868. doi:10.1021/acs.energyfuels.1c01618.

Rahimi, M., Moosavi, S.M., Smit, B., Hatton, T.A., 2021. Toward smart carbon capture with machine learning. Cell Rep. Phys. Sci. 2 (4). doi:10.1016/j.xcrp.2021.100396, 100396-100396.

Rahimpour, M.R., Kashkooli, A.Z., 2004. Enhanced carbon dioxide removal by promoted hot potassium carbonate in a split-flow absorber. Chem. Eng. Process.: Process Intensif. 43 (7), 857–865. doi:10.1016/S0255-2701 (03)00106-5.

Rahman, F.A., Aziz, M.M.A., Saidur, R., Bakar, W.A.W.A., Hainin, M.R., Putrajaya, R., Hassan, N.A., 2017. Pollution to solution: Capture and sequestration of carbon dioxide (CO 2) and its utilization as a renewable energy source for a sustainable future. Renew. Sustain. Energy Rev. 71, 112–126. doi:10.1016/j.rser.2017.01.011.

Rahman, M.M., Abetz, C., Shishatskiy, S., Martin, J., Müller, A.J., Abetz, V., 2018. CO_2 selective PolyActive membrane: thermal transitions and gas permeance as a function of thickness. ACS Appl. Mater. Interfaces 10 (31), 26733–26744. doi:10.1021/acsami.8b09259.

Rajagopalan, A.K., Avila, A.M., Rajendran, A., 2016. Do adsorbent screening metrics predict process performance? A process optimisation based study for post-combustion capture of CO_2. Int. J. Greenh. Gas Control 46, 76–85. doi:10.1016/j.ijggc.2015.12.033.

Ram Reddy, M.K., Xu, Z.P., Lu, G.Q., Diniz da Costa, J.C., 2006. Layered double hydroxides for CO_2 capture: structure evolution and regeneration. Ind. Eng. Chem. Res. 45 (22), 7504–7509. doi:10.1021/ie060757k.

Ram Reddy, M.K., Xu, Z.P., Diniz da Costa, J.C., 2008. Influence of water on high-temperature CO_2 capture using layered double hydroxide derivatives. Ind. Eng. Chem. Res. 47 (8), 2630–2635. doi:10.1021/ie0716060.

Ramasubramanian, K., Zhao, Y., Winston Ho, W.S., 2013. CO_2 capture and H2 purification: Prospects for CO_2-selective membrane processes. Chem. Eng. Pract. 59 (4), 1033–1045. doi:10.1002/aic.14078.

Raphael Idem, M.W., Paitoon Tontiwachwuthikul, A.C., Amornvadee Veawab, A.A., Gelowitz, A.D., 2006. Pilot plant studies of the CO_2 capture performance of aqueous MEA and mixed MEA/MDEA solvents at the university of regina CO_2 capture technology development plant and the boundary dam CO_2 capture demonstration plant. Ind. Eng. Chem. Res. 45, 2414–2420.

Rastogi, N.K., Nayak, C.A., 2011. Membranes for Forward Osmosis in Industrial Applications. Elsevier, pp. 680–717.

Ray, B., Churipard, S.R., Peter, S.C., 2021. An overview of the materials and methodologies for CO_2 capture under humid conditions. J. Mater. Chem. A 9 (47), 26498–26527. doi:10.1039/d1ta08862a.

Raynal, L., Boyer, C., Ballaguet, J.P., 2004. Liquid holdup and pressure drop determination in structured packing with CFD simulations. Can. J. Chem. Eng. 82 (5), 871–879. doi:10.1002/cjce.5450820502.

Raynal, L., Bouillon, P.-A., Gomez, A., Broutin, P., 2011. From MEA to demixing solvents and future steps, a roadmap for lowering the cost of post-combustion carbon capture. Chem. Eng. J. 171 (3), 742–752. doi:10.1016/j.cej.2011.01.008.

Razi, N., Svendsen, H.F., Bolland, O., 2013. Validation of mass transfer correlations for CO_2 absorption with MEA using pilot data. Int. J. Greenh. Gas Control 19, 478–491. doi:10.1016/j.ijggc.2013.10.006.

Realmonte, G., Drouet, L., Gambhir, A., Glynn, J., Hawkes, A., Köberle, A.C., Tavoni, M., 2019. An inter-model assessment of the role of direct air capture in deep mitigation pathways. Nat. Commun. 10 (1), 3277. doi:10.1038/s41467-019-10842-5.

Regmi, C., Ashtiani, S., Průša, F., Friess, K., 2022. Synergistic effect of hybridized TNT@GO fillers in CTA-based mixed matrix membranes for selective CO_2/CH4 separation. Sep. Purif. Technol. 282, 120128. doi:10.1016/j.seppur.2021.120128.

Reichle, W.T., 1985. Catalytic reactions by thermally activated, synthetic, anionic clay minerals. J. Catal. 94 (2), 547–557. doi:10.1016/0021-9517 (85)90219-2.

Reijers, H.T.J., Valster-Schiermeier, S.E.A., Cobden, P.D., van den Brink, R.W., 2006. Hydrotalcite as CO_2 sorbent for sorption-enhanced steam reforming of methane. Ind. Eng. Chem. Res. 45 (8), 2522–2530. doi:10.1021/ie050563p.

Rekhtina, M., Dal Pozzo, A., Stoian, D., Armutlulu, A., Donat, F., Blanco, M.V., Wang, Z.J., Willinger, M.G., Fedorov, A., Abdala, P.M., Muller, C.R., 2020. Effect of molten sodium nitrate on the decomposition pathways of hydrated magnesium hydroxycarbonate to magnesium oxide probed by *in situ* total scattering. Nanoscale 12 (31), 16462–16473. doi:10.1039/d0nr01760d.

Ren, S., Bojdys, M.J., Dawson, R., Laybourn, A., Khimyak, Y.Z., Adams, D.J., Cooper, A.I., 2012. Porous, fluorescent, covalent triazine-based frameworks via room-temperature and microwave-assisted synthesis. Adv. Mater. 24 (17), 2357–2361.

Ren, J., Li, Z., Chen, Y., Yang, Z., Lu, X., 2018. Supported ionic liquid sorbents for CO_2 capture from simulated flue-gas. Chin. J. Chem. Eng. 26 (11), 2377–2384. doi:10.1016/j.cjche.2018.04.025.

Ren, X., Kanezashi, M., Nagasawa, H., Xu, R., Zhong, J., Tsuru, T., 2019. Ceramic-supported polyhedral oligomeric silsesquioxane–organosilica nanocomposite membrane for efficient gas separation. Ind. Eng. Chem. Res. 58 (47), 21708–21716. doi:10.1021/acs.iecr.9b05251.

Ren, W., Wei, Z.Z., Xia, X.X., Hong, Z.W., Li, S., 2020. CO_2 adsorption performance of CuBTC/graphene aerogel composites. J. Nanopart. Res. 22 (7). doi:10.1007/s11051-020-04933-4.

Research, G.S., 2019. Carbonomics: the future of energy in the age of climate change.

Rezaei, N., Mohebbi, V., Feyzi, V., 2022. Hybrid hydrate processes for CO_2/H2 mixture purification: A techno-economic analysis. Int. J. Hydrog. Energy 47 (18), 10137–10155. doi:10.1016/j.ijhydene.2022.01.102.

Rezakazemi, M., Mohammadi, T., 2013. Gas sorption in H_2-selective mixed matrix membranes: experimental and neural network modeling. Int. J. Hydrog. Energy 38 (32), 14035–14041. doi:10.1016/j.ijhydene.2013.08.062.

Rhodes, C.J., 2016. The 2015 Paris climate change conference: COP21. Sci. Prog. 99 (1), 97–104.

Rindfleisch, F., DiNoia, T.P., McHugh, M.A., 1996. Solubility of polymers and copolymers in supercritical CO_2. J. Phys. Chem. 100 (38), 15581–15587. doi:10.1021/jp9615823.

Robertson, C., Mokaya, R., 2013. Microporous activated carbon aerogels via a simple subcritical drying route for CO_2 capture and hydrogen storage. Microporous Mesoporous Mater. 179, 151–156. doi:10.1016/j.micromeso.2013.05.025.

Robeson, L.M., Freeman, B.D., Paul, D.R., Rowe, B.W., 2009. An empirical correlation of gas permeability and permselectivity in polymers and its theoretical basis. J. Membr. Sci. 341 (1), 178–185. doi:10.1016/j.memsci.2009.06.005.

Robeson, L.M., Liu, Q., Freeman, B.D., Paul, D.R., 2015. Comparison of transport properties of rubbery and glassy polymers and the relevance to the upper bound relationship. J. Membr. Sci. 476, 421–431. doi:10.1016/J.MEMSCI.2014.11.058.

Robeson, L.M., 1991. Correlation of separation factor versus permeability for polymeric membranes. J. Membr. Sci. 62 (2), 165–185. doi:10.1016/0376-7388 (91)80060-J.

Robeson, L.M., 2008. The upper bound revisited. J. Membr. Sci. 320 (1-2), 390–400.

Robeson, L.M., 2008. The upper bound revisited. J. Membr. Sci. 320 (1), 390–400. doi:10.1016/j.memsci.2008.04.030.

Rocco, M.V., Lange, S., Pigoli, L., Colombo, E., Pellegrini, L.A., 2019. Assessing the energy intensity of alternative chemical and cryogenic natural gas purification processes in LNG production. J. Clean. Prod. 208, 827–840. doi:10.1016/j.jclepro.2018.10.108.

Rochelle, G.T., 2009. Amine Scrubbing for CO_2 Capture. Science 325 (5948), 1652–1654. doi:10.1126/science.1176731.

Rodríguez-Mosqueda, R., Bramer, E.A., Brem, G., 2018. CO_2 capture from ambient air using hydrated Na_2CO_3 supported on activated carbon honeycombs with application to CO_2 enrichment in greenhouses. Chem. Eng. Sci. 189, 114–122. doi:10.1016/j.ces.2018.05.043.

Rodríguez Hervás, G., Petrakopoulou, F., 2019. Exergoeconomic analysis of the allam cycle. Energy Fuels 33 (8), 7561–7568.

Rodrigues, S.C., Andrade, M., Moffat, J., Magalhães, F.D., Mendes, A., 2019. Preparation of carbon molecular sieve membranes from an optimized ionic liquid-regenerated cellulose precursor. J. Membr. Sci. 572, 390–400. doi:10.1016/j.memsci.2018.11.027.

Rogelj, J., den Elzen, M., Höhne, N., Fransen, T., Fekete, H., Winkler, H., Schaeffer, R., Sha, F., Riahi, K., Meinshausen, M., 2016. Paris Agreement climate proposals need a boost to keep warming well below 2 °C. Nature 534, 631. doi:10.1038/nature18307. https://www.nature.com/articles/nature18307#supplementary-information.

Roongrat, Sakwattanapong, Adisorn, Aroonwilas, Veawab, A., 2005. Behavior of reboiler heat duty for CO_2 capture plants using regenerable single and blended alkanolamines. Ind. Eng. Chem. Res 44, 4465–4473.

Rose, I., Bezzu, C.G., Carta, M., Comesaña-Gándara, B., Lasseuguette, E., Ferrari, M.C., Bernardo, P., Clarizia, G., Fuoco, A., Jansen, J.C., Hart, Kyle E., Liyana-Arachchi, T.P., Colina, C.M., McKeown, N.B., 2017. Polymer ultrapermeability from the inefficient packing of 2D chains. Nat. Mater. 16 (9), 932–937. doi:10.1038/nmat4939.

Rossi, E., Storti, G., Rota, R., 2020. Influence of the main operating parameters on the DRPSA process design based on the equilibrium theory. Adsorption 27 (1), 27–39. doi:10.1007/s10450-020-00274-9.

Rostamizadeh, M., Rezakazemi, M., Shahidi, K., Mohammadi, T., 2013. Gas permeation through H_2-selective mixed matrix membranes: experimental and neural network modeling. Int. J. Hydrog. Energy 38 (2), 1128–1135. doi:10.1016/j.ijhydene.2012.10.069.

Roussanaly, S., Anantharaman, R., Lindqvist, K., Zhai, H., Rubin, E., 2016. Membrane properties required for post-combustion CO_2 capture at coal-fired power plants. J. Membr. Sci. 511, 250–264. doi:10.1016/j.memsci.2016.03.035.

Ruan, X., He, G., Li, B., Yan, X., Dai, Y., 2014. Chemical potential analysis for directing the optimal design of gas membrane separation frameworks. Chem. Eng. Sci. 107, 245–255. doi:10.1016/j.ces.2013.11.046.

Rubin, E.S., Mantripragada, H., Marks, A., Versteeg, P., Kitchin, J., 2012. The outlook for improved carbon capture technology. Prog. Energy Combust. Sci. 38 (5), 630–671. doi:10.1016/j.pecs.2012.03.003.

Rufford, T.E., Smart, S., Watson, G.C.Y., Graham, B.F., Boxall, J., Diniz da Costa, J.C., May, E.F., 2012. The removal of CO_2 and N_2 from natural gas: A review of conventional and emerging process technologies. J. Petrol. Sci. Eng. 94-95, 123–154. doi:10.1016/j.petrol.2012.06.016.

Ruminski, A.M., Jeon, K.-J., Urban, J.J., 2011. Size-dependent CO_2 capture in chemically synthesized magnesium oxide nanocrystals. J. Mater. Chem. 21 (31), 11486–11491.

Rungta, M., Wenz, G.B., Zhang, C., Xu, L., Qiu, W., Adams, J.S., Koros, W.J., 2017. Carbon molecular sieve structure development and membrane performance relationships. Carbon 115, 237–248. doi:10.1016/j.carbon.2017.01.015.

Ruthven, D.M., Farooq, S., 1990. Air separation by pressure swing adsorption. Gas Sep. Purif. 4 (3), 141–148. doi:10.1016/0950-4214 (90)80016-E.

Ruuskanen, V., Givirovskiy, G., Elfving, J., Kokkonen, P., Karvinen, A., Järvinen, L., Sillman, J., Vainikka, M., Ahola, J., 2021. Neo-carbon food concept: A pilot-scale hybrid biological–inorganic system with direct air capture of carbon dioxide. J. Clean. Prod. 278, 123423. doi:10.1016/j.jclepro.2020.123423.

Rydén, M., Cleverstam, E., Johansson, M., Lyngfelt, A., Mattisson, T., 2010. Fe2O3 on Ce-, Ca-, or Mg-stabilized ZrO2 as oxygen carrier for chemical-looping combustion using NiO as additive. AIChE J. 56 (8), 2211–2220. doi:10.1002/aic.12143.

Rydén, M., Jing, D., Källén, M., Leion, H., Lyngfelt, A., Mattisson, T., 2014. CuO-Based oxygen-carrier particles for chemical-looping with oxygen uncoupling – experiments in batch reactor and in continuous operation. Ind. Eng. Chem. Res. 53 (15), 6255–6267. doi:10.1021/ie4039983.

Ryder, M.R., Civalleri, B., Bennett, T.D., Henke, S., Rudić, S., Cinque, G., Fernandez-Alonso, F., Tan, J.-C., 2014. Identifying the role of terahertz vibrations in metal-organic frameworks: from gate-opening phenomenon to shear-driven structural destabilization. Phys. Rev. Lett. 113 (21), 215502. doi:10.1103/PhysRevLett.113.215502.

Sánchez-Laínez, J., Zornoza, B., Téllez, C., Coronas, J., 2018. Asymmetric polybenzimidazole membranes with thin selective skin layer containing ZIF-8 for H2/CO_2 separation at pre-combustion capture conditions. J. Membr. Sci. 563, 427–434.

Sönnichsen, N., 2022. Production of biogas worldwide from 2000 to 2020.

Sabetghadam, A., Liu, X., Gottmer, S., Chu, L., Gascon, J., Kapteijn, F., 2019. Thin mixed matrix and dual layer membranes containing metal-organic framework nanosheets and Polyactive™ for CO_2 capture. J. Membr. Sci. 570, 226–235. doi:10.1016/j.memsci.2018.10.047.

Sada, E., Kumazawa, H., Han, Z.Q., Matsuyama, H., 1985. Chemical kinetics of the reaction of carbon dioxide with ethanolamines in nonaqueous solvents. AIChE J. 31 (8), 1297–1303. doi:10.1002/aic.690310808.

Sadiq, M.M., Li, H., Hill, A.J., Falcaro, P., Hill, M.R., Suzuki, K., 2016. Magnetic induction swing adsorption: An energy efficient route to porous adsorbent regeneration. Chem. Mater. 28 (17), 6219–6226. doi:10.1021/acs.chemmater.6b02409.

Sadiq, M.M., Batten, M.P., Mulet, X., Freeman, C., Konstas, K., Mardel, J.I., Tanner, J., Ng, D., Wang, X., Howard, S., Hill, M.R., Thornton, A.W., 2020. A pilot-scale demonstration of mobile direct air capture using metal-organic frameworks. Adv. Sustain. Syst. 4 (12), 2000101. doi:10.1002/adsu.202000101.

Saeed, M., Rafiq, S., Bergersen, L.H., Deng, L., 2017. Tailoring of water swollen PVA membrane for hosting carriers in CO_2 facilitated transport membranes. Sep. Purif. Technol. 179, 550–560. doi:10.1016/j.seppur.2017.02.022.

Safaei, S., Zeynali, R., Safaei, B., 2021. Modeling study of propane/propylene membrane separation using CFD method. Macromol. Theory Simul. 30 (2), 2000092. doi:10.1002/mats.202000092.

Safdarnejad, S.M., Hedengren, J.D., Baxter, L.L., 2015. Plant-level dynamic optimization of Cryogenic Carbon Capture with conventional and renewable power sources. Appl. Energy 149, 354–366. doi:10.1016/j.apenergy.2015.03.100.

Said Al Hoqani, H.A., Al-Shaqsi, N., Hossain, M.A., Al Sibani, M.A., 2020. Isolation and optimization of the method for industrial production of chitin and chitosan from Omani shrimp shell. Carbohydr. Res. 492. doi:10.1016/j.carres.2020.108001.

Said, W., Nemer, M., Clodic, D., 2011. Modeling of dry pressure drop for fully developed gas flow in structured packing using CFD simulations. Chem. Eng. Sci. 66 (10), 2107–2117.
Said, R.B., Kolle, J.M., Essalah, K., Tangour, B., Sayari, A., 2020. A Unified approach to CO_2-amine reaction mechanisms. ACS Omega 5 (40), 26125–26133. doi:10.1021/acsomega.0c03727.
Sajjadi, B., Chen, W.-Y., Egiebor, N.O., 2019a. A comprehensive review on physical activation of biochar for energy and environmental applications. Rev. Chem. Eng. 35 (6), 735–776. doi:10.1515/revce-2017-0113.
Sajjadi, B., Zubatiuk, T., Leszczynska, D., Leszczynski, J., Chen, W.Y., 2019b. Chemical activation of biochar for energy and environmental applications: a comprehensive review. Rev. Chem. Eng. 35 (7), 777–815.
Sakhiya, A.K., Baghel, P., Anand, A., Vijay, V.K., Kaushal, P., 2021. A comparative study of physical and chemical activation of rice straw derived biochar to enhance Zn+2 adsorption. Bioresour. Technol. Rep. 15, 100774. doi:10.1016/j.biteb.2021.100774.
Salam, M., Hossain, T., Papri, N., Ahmed, K., Habib, M., Uddin, M., Wilckens, R., 2020. Hydrogen production performances via steam reforming over hydrotalcite derived catalyst: a sustainable energy production review. Adv. Chem. Eng. Sci. 10 (4), 259–296.
Salaudeen, S.A., Acharya, B., Dutta, A., 2018. CaO-based CO_2 sorbents: A review on screening, enhancement, cyclic stability, regeneration and kinetics modelling. J. CO_2 Util. 23, 179–199. doi:10.1016/j.jcou.2017.11.012.
Salvador, C., 2007. Modeling design and pilot-scale experiments of CANMET'S advanced oxy-fuel/steam burner. In: International oxy-combustion reserch network 2nd workshop, USA, p. 26.
Samanta, A., et al., 2011. Post-combustion CO_2 capture using solid sorbents: a review. Ind. Eng. Chem. Res. 51 (4), 1438–1463.
Samanta, A., Zhao, A., Shimizu, G.K.H., Sarkar, P., Gupta, R., 2012. Post-combustion CO_2 capture using solid sorbents: a review. Ind. Eng. Chem. Res. 51 (4), 1438–1463. doi:10.1021/ie200686q.
Sanaeepur, H., Ahmadi, R., Amooghin, A.E., Ghanbari, D., 2019. A novel ternary mixed matrix membrane containing glycerol-modified poly (ether-block-amide) (Pebax 1657)/copper nanoparticles for CO_2 separation. J. Membr. Sci. 573, 234–246. doi:10.1016/j.memsci.2018.12.012.
Sanchez-Jimenez, P.E., Perez-Maqueda, L.A., Valverde, J.M., 2014. Nanosilica supported CaO: A regenerable and mechanically hard CO_2 sorbent at Ca-looping conditions. Appl. Energy 118, 92–99. doi:10.1016/j.apenergy.2013.12.024.
Sanders, D.F., Smith, Z.P., Guo, R., Robeson, L.M., McGrath, J.E., Paul, D.R., Freeman, B.D., 2013. Energy-efficient polymeric gas separation membranes for a sustainable future: A review. Polymer 54 (18), 4729–4761.
Sangon, S., Hunt, A.J., Attard, T.M., Mengchang, P., Ngernyen, Y., Supanchaiyamat, N., 2018. Valorisation of waste rice straw for the production of highly effective carbon based adsorbents for dyes removal. J. Clean. Prod. 172, 1128–1139. doi:10.1016/j.jclepro.2017.10.210.
Sangroniz, L., Wang, B., Su, Y., Liu, G., Cavallo, D., Wang, D., Müller, A.J., 2021. Fractionated crystallization in semicrystalline polymers. Prog. Polym. Sci. 115, 101376. doi:10.1016/j.progpolymsci.2021.101376.
Sanpasertparnich, T., Idem, R., Bolea, I., deMontigny, D., Tontiwachwuthikul, P., 2010. Integration of post-combustion capture and storage into a pulverized coal-fired power plant. Int. J. Greenh. Gas Control 4 (3), 499–510. doi:10.1016/j.ijggc.2009.12.005.
Santiago, R., Lemus, J., Moreno, D., Moya, C., Larriba, M., Alonso-Morales, N., Gilarranz, M.A., Rodríguez, J.J., Palomar, J., 2018. From kinetics to equilibrium control in CO_2 capture columns using Encapsulated Ionic Liquids (ENILs). Chem. Eng. J. 348, 661–668. doi:10.1016/j.cej.2018.05.029.
Santos, M.P.S., Hanak, D.P., 2022. Carbon capture for decarbonisation of energy-intensive industries: a comparative review of techno-economic feasibility of solid looping cycles. Front. Chem. Sci. Eng. 16 (9), 1291–1317. doi:10.1007/s11705-022-2151-5.
Sanz-Pérez, E.S., Murdock, C.R., Didas, S.A., Jones, C.W., 2016. Direct capture of CO_2 from ambient air. Chem. Rev. 116 (19), 11840–11876. doi:10.1021/acs.chemrev.6b00173.
Sanz-Perez, E.S., Murdock, C.R., Didas, S.A., Jones, C.W., 2016a. Direct capture of CO_2 from ambient air. Chem. Rev. 116 (19), 11840–11876. doi:10.1021/acs.chemrev.6b00173.
Sanz-Perez, E.S., Murdock, C.R., Didas, S.A., Jones, C.W., 2016b. Direct capture of CO_2 from ambient air. Chem. Rev. 116 (19), 11840–11876. doi:10.1021/acs.chemrev.6b00173.
Saravanan, A., Kumar, P.S., Jeevanantham, S., Karishma, S., Vo, D.V.N., 2022. Recent advances and sustainable development of biofuels production from lignocellulosic biomass. Bioresour. Technol. 344. doi:10.1016/j.biortech.2021.126203.
Sartori, G., Savage, D.W.J.I., Fundamentals, E.C., 1983. Sterically hindered amines for carbon dioxide removal from gases. 22, 239-249.
Sasikumar, B., Bisht, S., Arthanareeswaran, G., Ismail, A.F., Othman, M.H.D., 2021. Performance of polysulfone hollow fiber membranes encompassing ZIF-8, SiO2/ZIF-8, and amine-modified SiO2/ZIF-8 nanofillers for CO_2/CH4 and CO_2/N_2 gas separation. Sep. Purif. Technol. 264, 118471. doi:10.1016/j.seppur.2021.118471.
Sateesh, C., Nandakishora, Y., Sahoo, R.K., Murugan, S., 2021. Study of cryogenic CO_2 capture with solar-assisted VAR system. Clean. Eng. Technol. 5, 100351. doi:10.1016/j.clet.2021.100351.
T Satyapal, S.F., Trela, J, Strange, J, 2001. Performance and properties of a solid amine sorbent for carbon dioxide removal in space life support applications. Energy Fuels 15 (2), 250–255. doi:10.1021/ef0002391.
Saunier, F., Fradette, S., Clerveaux, F., Lefebvre, S., Madore, É., Veilleux, G., Bulle, C., Surprenant, R., 2019. Comparison of life-cycle assessment between bio-catalyzed and promoted potassium carbonate processes and amine-based carbon capture technologies. Int. J. Greenh. Gas Control 88, 134–155. doi:10.1016/j.ijggc.2019.05.009.
Sayari, A., Heydari-Gorji, A., Yang, Y., 2012. CO_2-induced degradation of amine-containing adsorbents: reaction products and pathways. J. Am. Chem. Soc. 134 (33), 13834–13842. doi:10.1021/ja304888a.
Sayari, N., Sila, A., Abdelmalek, B.E., Abdallah, R.B., Ellouz-Chaabouni, S., Bougatef, A., Balti, R., 2016. Chitin and chitosan from the Norway lobster by-products: Antimicrobial and anti-proliferative activities. Int. J. Biol. Macromol. 87, 163–171. doi:10.1016/j.ijbiomac.2016.02.057.
Sayari, P.J.E.H.a.A., 2006. Applications of pore-expanded mesoporous silicas. 3. triamine silane grafting for enhanced CO_2 adsorption. Ind. Eng. Chem. Res 45 (9), 3248–3255.
Sazali, N., Wan Salleh, W.N., Ismail, A.F., Ismail, N.H., Kadirgama, K., 2021. A brief review on carbon selective membranes from polymer blends for gas separation performance. Rev. Chem. Eng. 37 (3), 339–362. doi:10.1515/revce-2018-0086.
Scaccabarozzi, R., Gatti, M., Martelli, E., 2016. Thermodynamic analysis and numerical optimization of the NET Power oxy-combustion cycle. Appl. Energy 178, 505–526.
Schach, M.-O., Oyarzún, B., Schramm, H., Schneider, R., Repke, J.-U., 2011. Feasibility study of CO_2 capture by anti-sublimation. Energy Procedia 4, 1403–1410. doi:10.1016/j.egypro.2011.02.005.
Schakel, W., Meerman, H., Talaei, A., Ramírez, A., Faaij, A., 2014. Comparative life cycle assessment of biomass co-firing plants with carbon capture and storage. Appl. Energy 131, 441–467. doi:10.1016/j.apenergy.2014.06.045.
Scheffknecht, G., Al-Makhadmeh, L., Schnell, U., Maier, J., 2011. Oxy-fuel coal combustion—A review of the current state-of-the-art. Int. J. Greenh. Gas Control 5, S16–S35. doi:10.1016/j.ijggc.2011.05.020.
Scheidema, M.N., Taskinen, P., 2011. Decomposition thermodynamics of magnesium sulfate. Ind. Eng. Chem. Res. 50 (16), 9550–9556. doi:10.1021/ie102554f.
Scholes, C.A., Bacus, J., Chen, G.Q., Tao, W.X., Li, G., Qader, A., Stevens, G.W., Kentish, S.E., 2012. Pilot plant performance of rubbery polymeric membranes for carbon dioxide separation from syngas. J. Membr. Sci. 389, 470–477.
Scholes, C.A., Ho, M.T., Wiley, D.E., Stevens, G.W., Kentish, S.E., 2013. Cost competitive membrane-cryogenic post-combustion carbon capture. Int. J. Greenh. Gas Control 17, 341–348. doi:10.1016/j.ijggc.2013.05.017.
Scholes, C.A., Stevens, G.W., Kentish, S.E., 2016. Impact of heavy hydrocarbons on natural gas sweetening using perfluorinated polymeric membranes. Ind. Eng. Chem. Res. 55 (28), 7696–7703. doi:10.1021/acs.iecr.6b01823.
Scholz, M., Frank, B., Stockmeier, F., Falß, S., Wessling, M., 2013. Techno-economic analysis of hybrid processes for biogas upgrading. Ind. Eng. Chem. Res. 52 (47), 16929–16938. doi:10.1021/ie402660s.
Schröck, K., Schröder, F., Heyden, M., Fischer, R., Havenith, M., 2008. Characterization of interfacial water in MOF-5 (Zn 4 (O) (BDC) 3)—a combined spectroscopic and theoretical study. Phys. Chem. Chem. Phys. 10 (32), 4732–4739.
Schreiber, A., Marx, J., Zapp, P., 2013. Environmental assessment of a membrane-based air separation for a coal-fired oxyfuel power plant. J. Membr. Sci. 440, 122–133. doi:10.1016/j.memsci.2013.03.026.
Schultz, J.S., Goddard, J.D., Suchdeo, S.R.J.A.J., 1974. Facilitated transport via carrier-mediated diffusion in membranes: Part I. Mechanistic aspects, experimental systems and characteristic regimes. 20 (3), 417-445.
Scofield, J.M.P., Gurr, P.A., Kim, J., Fu, Q., Kentish, S.E., Qiao, G.G., 2016a. Blends of fluorinated additives with highly selective thin-film composite membranes to increase CO_2 permeability for CO_2/N_2 gas separation applications. Ind. Eng. Chem. Res. 55 (30), 8364–8372. doi:10.1021/acs.iecr.6b02167.
Scofield, J.M.P., Gurr, P.A., Kim, J., Fu, Q., Kentish, S.E., Qiao, G.G., 2016b. Development of novel fluorinated additives for high performance CO_2 separation thin-film composite membranes. J. Membr. Sci. 499, 191–200. doi:10.1016/j.memsci.2015.10.035.
Sebastiani, F., James, J., van Dijk, H., Pieterse, J.A., Boon, J., Cobden, P., 2021. Modelling of CO 2 and H 2 O interaction during adsorption cycles on hydrotalcite for SEWGS applications. In: Proceedings of the 15th Greenhouse Gas Control Technologies Conference, pp. 15–18.
Seema, H., Kemp, K.C., Le, N.H., Park, S.-W., Chandra, V., Lee, J.W., Kim, K.S., 2014. Highly selective CO_2 capture by S-doped microporous carbon materials. Carbon 66, 320–326. doi:10.1016/j.carbon.2013.09.006.
Seepana, S., Jayanti, S., 2010. Steam-moderated oxy-fuel combustion. Energy Convers. Manage. 51 (10), 1981–1988. doi:10.1016/j.enconman.2010.02.031.
Seggiani, M., Stefanelli, E., Puccini, M., Vitolo, S., 2018. CO_2 sorption/desorption performance study on K_2CO_3-doped Li_4SiO_4-based pellets. Chem. Eng. J. 339, 51–60. doi:10.1016/j.cej.2018.01.117.
Seki, S., Kobayashi, T., Kobayashi, Y., Takei, K., Miyashiro, H., Hayamizu, K., Tsuzuki, S., Mitsugi, T., Umebayashi, Y., 2010. Effects of cation and anion on physical properties of room-temperature ionic liquids. J. Mol. Liq. 152 (1-3), 9–13. doi:10.1016/j.molliq.2009.10.008.
Sema, T., Naami, A., Fu, K., Edali, M., Liu, H., Shi, H., Liang, Z., Idem, R., Tontiwachwuthikul, P., 2012. Comprehensive mass transfer and reaction kinetics studies of CO_2 absorption into aqueous solutions of blended MDEA–MEA. Chem. Eng. J. 209, 501–512. doi:10.1016/j.cej.2012.08.016.
Sengupta, S., Amte, V., Dongara, R., Das, A.K., Bhunia, H., Bajpai, P.K., 2015. Effects of the adsorbent preparation method for CO_2 capture from flue gas using K_2CO_3/Al_2O_3 adsorbents. Energy Fuels 29 (1), 287–297. doi:10.1021/ef501792c.
Seo, H., Rahimi, M., Hatton, T.A., 2022. Electrochemical carbon dioxide capture and release with a redox-active amine. J. Am. Chem. Soc. 144 (5), 2164–2170. doi:10.1021/jacs.1c10656.
Serafin, J., Narkiewicz, U., Morawski, A.W., Wróbel, R.J., Michalkiewicz, B., 2017. Highly microporous activated carbons from biomass for CO_2 capture and effective micropores at different conditions. J. CO_2 Util. 18, 73–79. doi:10.1016/j.jcou.2017.01.006.
E Serna-Guerrero, R.D.n., Sayari, A, 2008. New insights into the interactions of CO_2 with amine-functionalized silica. Ind. Eng. Chem. Res. 47 (23), 9406–9412. doi:10.1021/ie801186g.
Serna-Guerrero, R., Belmabkhout, Y., Sayari, A., 2010. Modeling CO_2 adsorption on amine-functionalized mesoporous silica: 1. A semi-empirical equi-

librium model. Chem. Eng. J. 161 (1-2), 173–181. doi:10.1016/j.cej.2010.04.024.
Service, R.F., 2017. Fossil Power, Guilt Free. American Association for the Advancement of Science.
Shafawi, A.N., Mohamed, A.R., Lahijani, P., Mohammadi, M., 2021. Recent advances in developing engineered biochar for CO_2 capture: An insight into the biochar modification approaches. J. Environ. Chem. Eng. 9 (6). doi:10.1016/j.jece.2021.106869.
Shafeeyan, M.S., Daud, W.M.A.W., Houshmand, A., Shamiri, A., 2010. A review on surface modification of activated carbon for carbon dioxide adsorption. J. Analyt. Appl. Pyrol. 89 (2), 143–151. doi:10.1016/j.jaap.2010.07.006.
Shafeeyan, M.S., Wan Daud, W.M.A., Houshmand, A., Arami-Niya, A., 2012. The application of response surface methodology to optimize the amination of activated carbon for the preparation of carbon dioxide adsorbents. Fuel 94, 465–472. doi:10.1016/j.fuel.2011.11.035.
Shafeeyan, M.S., Wan Daud, W.M.A., Shamiri, A., 2014. A review of mathematical modeling of fixed-bed columns for carbon dioxide adsorption. Chem. Eng. Res. Des. 92 (5), 961–988. doi:10.1016/j.cherd.2013.08.018.
Shah, K., Moghtaderi, B., Zanganeh, J., Wall, T., 2013. Integration options for novel chemical looping air separation (ICLAS) process for oxygen production in oxy-fuel coal fired power plants. Fuel 107, 356–370. doi:10.1016/J.FUEL.2013.01.007.
Shah, K., Zhou, C., Song, H., Doroodchi, E., Moghtaderi, B., 2015. A novel hybrid chemical-looping oxy combustor process for the combustion of solid and gaseous fuels: thermodynamic analysis. Energy Fuels 29 (2), 602–617. doi:10.1021/EF502389T.
Shah, S., Shah, M., Shah, A., Shah, M., 2020. Evolution in the membrane-based materials and comprehensive review on carbon capture and storage in industries. Emergent Mater. 3 (1), 33–44. doi:10.1007/s42247-020-00069-2.
Shah, G., Ahmad, E., Pant, K.K., Vijay, V.K., 2021. Comprehending the contemporary state of art in biogas enrichment and CO_2 capture technologies via swing adsorption. Int. J. Hydrog. Energy 46 (9), 6588–6612. doi:10.1016/j.ijhydene.2020.11.116.
Shahkarami, S., Azargohar, R., Dalai, A.K., Soltan, J., 2015. Breakthrough CO_2 adsorption in bio-based activated carbons. J. Environ. Sci. 34, 68–76. doi:10.1016/j.jes.2015.03.008.
Shahkaramipour, N., Adibi, M., Seifkordi, A., Fazli, Y.J.J.o.m.s., 2014. Separation of CO_2/CH4 through alumina-supported geminal ionic liquid membranes. 455, 229-235.
Shalaby, A., Elkamel, A., Douglas, P.L., Zhu, Q., Zheng, Q.P., 2021. A machine learning approach for modeling and optimization of a CO_2 post-combustion capture unit. Energy 215. doi:10.1016/j.energy.2020.119113, 119113-119113.
Shamair, Z., Habib, N., Gilani, M.A., Khan, A.L., 2020. Theoretical and experimental investigation of CO_2 separation from CH_4 and N_2 through supported ionic liquid membranes. Appl. Energy 268, 115016. doi:10.1016/j.apenergy.2020.115016.
Shamsabadi, A.A., Seidi, F., Salehi, E., Nozari, M., Rahimpour, A., Soroush, M., 2017. Efficient CO_2-removal using novel mixed-matrix membranes with modified TiO_2 nanoparticles. J. Mater. Chem. A 5 (8), 4011–4025. doi:10.1039/C6TA09990D.
Shamsabadi, A.A., Isfahani, A.P., Salestan, S.K., Rahimpour, A., Ghalei, B., Sivaniah, E., Soroush, M., 2019. Pushing rubbery polymer membranes to be economic for CO_2 separation: embedment with $Ti_3C_2T_x$ MXene nanosheets. ACS Appl. Mater. Interfaces 12 (3), 3984–3992. doi:10.1021/acsami.9b19960.
Shang, J., Li, G., Singh, R., Gu, Q., Nairn, K.M., Bastow, T.J., Medhekar, N., Doherty, C.M., Hill, A.J., Liu, J.Z., 2012. Discriminative separation of gases by a “molecular trapdoor” mechanism in chabazite zeolites. J. Am. Chem. Soc. 134 (46), 19246–19253.
Shang, J., Li, G., Singh, R., Xiao, P., Liu, J.Z., Webley, P.A., 2013. Determination of composition range for “molecular trapdoor” effect in chabazite zeolite. J. Phys. Chem. C 117 (24), 12841–12847.
Shao, N., Gavriilidis, A., Angeli, P., 2010. Mass transfer during Taylor flow in microchannels with and without chemical reaction. Chem. Eng. J. 160 (3), 873–881. doi:10.1016/j.cej.2010.02.049.
Shao, Z.D., Cheng, X., Zheng, Y.M., 2018. Facile co-precursor sol-gel synthesis of a novel amine-modified silica aerogel for high efficiency carbon dioxide capture. J. Colloid. Interface Sci. 530, 412–423. doi:10.1016/j.jcis.2018.06.094.
Sharma, I., Hoadley, A.F.A., Mahajani, S.M., Ganesh, A., 2016. Multi-objective optimisation of a Rectisol (TM) process for carbon capture. J. Clean. Prod. 119, 196–206. doi:10.1016/j.jclepro.2016.01.078.
Shash, M.M., 2011. Capturing CO_2 from Oxy-Fuel Combustion Flue Gas. In: International Oxy-Combustion Research Network for CO 2 Capture Report on Inaugural (1 st) Workshop. Cottbus, Germany.
Shaw, R., Mukherjee, S., 2022. The development of carbon capture and storage (CCS) in India: A critical review. Carbon Cap. Sci. Technol. 2, 100036. doi:10.1016/J.CCST.2022.100036.
Shayegh, S., Bosetti, V., Tavoni, M., 2021. Future prospects of direct air capture technologies: insights from an expert elicitation survey. Front. Clim. 3.
Shen, W., Fan, W., 2013. Nitrogen-containing porous carbons: synthesis and application. J. Mater. Chem. A 1 (4), 999–1013.
Shen, C., Grande, C.A., Li, P., Yu, J., Rodrigues, A.E., 2010. Adsorption equilibria and kinetics of CO_2 and N_2 on activated carbon beads. Chem. Eng. J. 160 (2), 398–407. doi:10.1016/j.cej.2009.12.005.
Shen, C., Liu, Z., Li, P., Yu, J., 2012. Two-stage VPSA process for CO_2 capture from flue gas using activated carbon beads. Ind. Eng. Chem. Res. 51 (13), 5011–5021. doi:10.1021/ie202097y.
Shen, Y., Linville, J.L., Ignacio-de Leon, P.A.A., Schoene, R.P., Urgun-Demirtas, M., 2016. Towards a sustainable paradigm of waste-to-energy process: Enhanced anaerobic digestion of sludge with woody biochar. J. Clean. Prod. 135, 1054–1064. doi:10.1016/j.jclepro.2016.06.144.
Shen, Y., Zhou, Y., Li, D., Fu, Q., Zhang, D., Na, P., 2017. Dual-reflux pressure swing adsorption process for carbon dioxide capture from dry flue gas. Int. J. Greenh. Gas Control 65, 55–64. doi:10.1016/j.ijggc.2017.08.020.
Shen, Y., Shi, W., Zhang, D., Na, P., Fu, B., 2018. The removal and capture of CO_2 from biogas by vacuum pressure swing process using silica gel. J. CO_2 Util. 27, 259–271. doi:10.1016/j.jcou.2018.08.001.
Shen, Q., Cong, S., He, R., Wang, Z., Jin, Y., Li, H., Cao, X., Wang, J., Van der Bruggen, B., Zhang, Y., 2019. SIFSIX-3-Zn/PIM-1 mixed matrix membranes with enhanced permeability for propylene/propane separation. J. Membr. Sci. 588, 117201. doi:10.1016/j.memsci.2019.117201.
Shen, R.X., Lu, J.W., Yao, Z.L., Zhao, L.X., Wu, Y.L., 2021. The hydrochar activation and biocrude upgrading from hydrothermal treatment of lignocellulosic biomass. Bioresour. Technol. 342. doi:10.1016/j.biortech.2021.125914.
Shen, M.H., Tong, L.G., Yin, S.W., Liu, C.P., Wang, L., Feng, W.J., Ding, Y.L., 2022. Cryogenic technology progress for CO_2 capture under carbon neutrality goals: A review. Sep. Purif. Technol. 299. doi:10.1016/j.seppur.2022.121734.
Shen, X., Li, H., Zhao, Z., Li, X., Liu, K., Gao, X., 2022. Imaging of liquid temperature distribution during microwave heating via thermochromic metal organic frameworks. Int. J. Heat Mass Transf. 189. doi:10.1016/j.ijheatmasstransfer.2022.122667.
Shi, X., Xiang, Y., Wen, L.X., Chen, J.F., 2013. CFD analysis of liquid phase flow in a rotating packed bed reactor. Chem. Eng. J. 228, 1040–1049. doi:10.1016/j.cej.2013.05.081.
Shi, H., Idem, R., Naami, A., Gelowitz, D., Tontiwachwuthikul, P., 2014a. Catalytic solvent regeneration using hot water during amine based CO_2 capture process. Energy Procedia 63, 266–272. doi:10.1016/j.egypro.2014.11.028.
Shi, H., Naami, A., Idem, R., Tontiwachwuthikul, P., 2014b. Catalytic and non catalytic solvent regeneration during absorption-based CO_2 capture with single and blended reactive amine solvents. Int. J. Greenh. Gas Control 26, 39–50. doi:10.1016/j.ijggc.2014.04.007.
Shi, H., Zheng, L., Huang, M., Zuo, Y., Li, M., Jiang, L., Idem, R., Tontiwachwuthikul, P., 2018. CO_2 desorption tests of blended monoethanolamine-diethanolamine solutions to discover novel energy efficient solvents. Asia-Pac. J. Chem. Eng. 13 (3). doi:10.1002/apj.2186.
Shi, Y., Zhong, W., Shao, Y., Liu, X., 2019. Energy efficiency analysis of pressurized oxy-coal combustion system utilizing circulating fluidized bed. Appl. Therm. Eng. 150, 1104–1115. doi:10.1016/j.applthermaleng.2019.01.085.
Shi, H., Fu, J., Wu, Q., Huang, M., Jiang, L., Cui, M., Idem, R., Tontiwachwuthikul, P., 2020. Studies of the coordination effect of DEA-MEA blended amines (within 1 + 4 to 2 + 3 M) under heterogeneous catalysis by means of absorption and desorption parameters. Sep. Purif. Technol. 236. doi:10.1016/j.seppur.2019.116179.
Shi, Y., Liang, B., Lin, R.-B., Zhang, C., Chen, B., 2020. Gas separation via hybrid metal–organic framework/polymer membranes. Trends Chem. 2 (3), 254–269.
Shi, F., Sun, J., Wang, J., Liu, M., Yan, Z., Zhu, B., Li, Y., Cao, X., 2021. MXene versus graphene oxide: Investigation on the effects of 2D nanosheets in mixed matrix membranes for CO_2 separation. J. Membr. Sci. 620, 118850. doi:10.1016/j.memsci.2020.118850.
Shi, H., Cheng, X., Peng, J., Feng, H., Tontiwachwuthikul, P., Hu, J., 2022. The CO_2 absorption and desorption analysis of tri-solvent MEA + EAE + AMP compared with MEA + BEA + AMP along with "coordination effects" evaluation. Environ. Sci. Pollut. Res. Int. 29 (27), 40686–40700. doi:10.1007/s11356-022-18792-0.
Shi, H., Peng, J., Cheng, X., Yang, X., Jin, J., Hu, J., 2022. The CO_2 desorption analysis of tri-solvent MEA+BEA+DEEA with several commercial solid acid catalysts. Int. J. Greenh. Gas Control 116. doi:10.1016/j.ijggc.2022.103647.
Shin, D., Kang, S., 2018. Numerical analysis of an ion transport membrane system for oxy–fuel combustion. Appl. Energy 230, 875–888. doi:10.1016/J.APENERGY.2018.09.016.
Shin, D.W., Hyun, S.H., Cho, C.H., Han, M.H., 2005. Synthesis and CO_2/N_2 gas permeation characteristics of ZSM-5 zeolite membranes. Microporous Mesoporous Mater. 85 (3), 313–323.
Shin, J.E., Lee, S.K., Cho, Y.H., Park, H.B., 2019. Effect of PEG-MEA and graphene oxide additives on the performance of Pebax® 1657 mixed matrix membranes for CO_2 separation. J. Membr. Sci. 572, 300–308. doi:10.1016/j.memsci.2018.11.025.
Shulman, A., Cleverstam, E., Mattisson, T., Lyngfelt, A., 2009. Manganese/Iron, Manganese/Nickel, and Manganese/Silicon oxides used in chemical-looping with oxygen uncoupling (clou) for combustion of methane. Energy Fuels 23 (10), 5269–5275. doi:10.1021/ef9005466.
Shulman, A., Cleverstam, E., Mattisson, T., Lyngfelt, A., 2011. Chemical – Looping with oxygen uncoupling using Mn/Mg-based oxygen carriers – Oxygen release and reactivity with methane. Fuel 90 (3), 941–950. doi:10.1016/j.fuel.2010.11.044.
Shuyi, H., Ke, W., Yong, H., Yaling, Q., Ling, H., Shenghua, J., 2014. Research progress of natural gas decarbonization and desulfurization based on alkanolamine. Nat. Gas and Oil 32 (03), 19–22. doi:10.3969/j.issn.1006-5539.2014.03.006, +8.
Siahpoosh, M., Fatemi, S., Vatani, A., 2009. Mathematical modeling of single and multi-component adsorption fixed beds to rigorously predict the mass transfer zone and breakthrough curves. Iran. J. Chem. Chem. Eng. 28 (3), 25–44.
Sidhikku Kandath Valappil, R., Ghasem, N., Al-Marzouqi, M., 2021. Current and future trends in polymer membrane-based gas separation technology: A comprehensive review. J. Ind. Eng. Chem. 98, 103–129. doi:10.1016/J.JIEC.2021.03.030.
Siefert, N.S., Agarwal, S., Shi, F., Shi, W., Roth, E.A., Hopkinson, D., Kusuma, V.A., Thompson, R.L., Luebke, D.R., Nulwala, H.B., 2016. Hydrophobic physical solvents for pre-combustion CO_2 capture: Experiments, computational simulations, and techno-economic analysis. Int. J. Greenh. Gas Control 49, 364–371. doi:10.1016/j.ijggc.2016.03.014.
Siegelman, R.L., McDonald, T.M., Gonzalez, M.I., Martell, J.D., Milner, P.J., Mason, J.A., Berger, A.H., Bhown, A.S., Long, J.R., 2017. Controlling cooperative CO_2 adsorption in diamine-appended Mg2 (dobpdc) metal-organic frameworks. J. Am. Chem. Soc. 139 (30), 10526–10538. doi:10.1021/jacs.7b05858.
Siegelman, R.L., Kim, E.J., Long, J.R., 2021. Porous materials for carbon dioxide separations. Nat. Mater. 20 (8), 1060–1072. doi:10.1038/s41563-021-01054-8.

Sikarwar, V.S., Pfeifer, C., Ronsse, F., Pohořelý, M., Meers, E., Kaviti, A.K., Jeremiáš, M., 2022. Progress in in-situ CO_2-sorption for enhanced hydrogen production. Prog. Energy Combust. Sci. 91, 101008. doi:10.1016/j.pecs.2022.101008.

Silva, F.W.M.d., Magalhães, G.M., Jardim, E.O., Silvestre-Albero, J., Sepúlveda-Escribano, A., de Azevedo, D.C.S., de Lucena, S.M.P., 2015. CO_2 adsorption on ionic liquid—modified Cu-BTC: experimental and simulation study. Adsorpt. Sci. Technol. 33 (2), 223–242. doi:10.1260/0263-6174.33.2.223.

Silva, L.P., Moya, C., Sousa, M., Santiago, R., Sintra, T.E., Carreira, A.R.F., Palomar, J., Coutinho, J.A.P., Carvalho, P.J., 2020. Encapsulated amino-acid-based ionic liquids for CO_2 capture. Eur. J. Inorg. Chem. 2020 (33), 3158–3166. doi:10.1002/ejic.202000364.

Simo, M., Brown, C.J., Hlavacek, V., 2008. Simulation of pressure swing adsorption in fuel ethanol production process. Comput. Chem. Eng. 32 (7), 1635–1649. doi:10.1016/j.compchemeng.2007.07.011.

Singh, R., Ram Reddy, M.K., Wilson, S., Joshi, K., Diniz da Costa, J.C., Webley, P., 2009. High temperature materials for CO_2 capture. Energy Procedia 1 (1), 623–630. doi:10.1016/j.egypro.2009.01.082.

Singh, G., Lakhi, K.S., Sil, S., Bhosale, S.V., Kim, I., Albahily, K., Vinu, A., 2019. Biomass derived porous carbon for CO_2 capture. Carbon 148, 164–186. doi:10.1016/j.carbon.2019.03.050.

Singh, S., Kumar, V., Dhanjal, D.S., Datta, S., Bhatia, D., Dhiman, J., Samuel, J., Prasad, R., Singh, J., 2020. A sustainable paradigm of sewage sludge biochar: Valorization, opportunities, challenges and future prospects. J. Clean. Prod. 269, 122259. doi:10.1016/j.jclepro.2020.122259.

Singh, E., Mishra, R., Kumar, A., Shukla, S.K., Lo, S.-L., Kumar, S., 2022. Circular economy-based environmental management using biochar: Driving towards sustainability. Process. Saf. Environ. Prot. 163, 585–600. doi:10.1016/j.psep.2022.05.056.

Singto, S., Supap, T., Idem, R., Tontiwachwuthikul, P., Tantayanon, S., Al-Marri, M.J., Benamor, A., 2016. Synthesis of new amines for enhanced carbon dioxide (CO_2) capture performance: The effect of chemical structure on equilibrium solubility, cyclic capacity, kinetics of absorption and regeneration, and heats of absorption and regeneration. Sep. Purif. Technol. 167, 97–107. doi:10.1016/j.seppur.2016.05.002.

Sinha, A., Realff, M.J., 2019. A parametric study of the techno-economics of direct CO_2 air capture systems using solid adsorbents. AIChE J. 65 (7), e16607. doi:10.1002/aic.16607.

Sinha, A., Darunte, L.A., Jones, C.W., Realff, M.J., Kawajiri, Y., 2017. Systems design and economic analysis of direct air capture of CO_2 through temperature vacuum swing adsorption using MIL-101 (Cr)-PEI-800 and mmen-Mg2 (dobpdc) MOF adsorbents. Ind. Eng. Chem. Res. 56 (3), 750–764. doi:10.1021/acs.iecr.6b03887.

Sinha, A., Darunte, L.A., Jones, C.W., Realff, M.J., Kawajiri, Y., 2020. Correction to "systems design and economic analysis of direct air capture of CO_2 through temperature vacuum swing adsorption using MIL-101 (Cr)-PEI-800 and mmen-Mg2 (dobpdc) MOF adsorbents". Ind. Eng. Chem. Res. 59 (1), 503–505. doi:10.1021/acs.iecr.9b06779.

Sipöcz, N., Tobiesen, F.A., Assadi, M., 2011. The use of Artificial Neural Network models for CO_2 capture plants. Applied Energy 88 (7), 2368–2376.

Sircar, S., Kratz, W., 1988. Simultaneous production of hydrogen and carbon dioxide from steam reformer off-gas by pressure swing adsorption. Sep. Sci. Technol. 23 (14-15), 2397–2415.

Siriwardane, R.V., Shen, M.-S., Fisher, E.P., Poston, J.A., 2001. Adsorption of CO_2 on molecular sieves and activated carbon. Energy Fuels 15 (2), 279–284. doi:10.1021/ef000241s.

Siriwardane, R.V., Shen, M.S., Fisher, E.P., Losch, J, 2005. Adsorption of CO_2on zeolites at moderate temperatures. Energy Fuels 19, 1153–1159.

Skarstrom, C.W., Attorney, O.-O.I., 1958. Method and apparatus for fractionating gaseous mixtures by adsorption.

Skarstrom, C.W., 1960. Method and Apparatus for Fractionating Gaseous Mixtures by Adsorption, in: US (Ed.). ExxonMobil Research and Engineering Co., US.

Skorek-Osikowska, A., Bartela, Ł., Kotowicz, J., 2015. A comparative thermodynamic, economic and risk analysis concerning implementation of oxy-combustion power plants integrated with cryogenic and hybrid air separation units. Energy Convers. Manage. 92, 421–430. doi:10.1016/J.ENCONMAN.2014.12.079.

Skulimowska, A., Di Felice, L., Kamińska-Pietrzak, N., Celińska, A., Pławecka, M., Hercog, J., Krauz, M., Aranda, A., 2017. Chemical looping with oxygen uncoupling (CLOU) and chemical looping combustion (CLC) using copper-enriched oxygen carriers supported on fly ash. Fuel Process. Technol. 168, 123–130. doi:10.1016/j.fuproc.2017.08.035.

Slater, A.G., Cooper, A.I., 2015. Porous materials. Function-led design of new porous materials. Science 348 (6238), aaa8075. doi:10.1126/science.aaa8075.

Smith, A.R., Klosek, J., 2001. A review of air separation technologies and their integration with energy conversion processes. Fuel Process. Technol. 70 (2), 115–134. doi:10.1016/S0378-3820 (01)00131-X.

Smith, K., Lee, A., Mumford, K., Li, S., Indrawan, Thanumurthy, N., Temple, N., Anderson, C., Hooper, B., Kentish, S., Stevens, G., 2015. Pilot plant results for a precipitating potassium carbonate solvent absorption process promoted with glycine for enhanced CO_2 capture. Fuel Process. Technol. 135, 60–65. doi:10.1016/j.fuproc.2014.10.013.

Smith, S.J., Hou, R., Lau, C.H., Konstas, K., Kitchin, M., Dong, G., Lee, J., Lee, W.H., Seong, J.G., Lee, Y.M., 2019. Highly permeable thermally rearranged mixed matrix membranes (TR-MMM). J. Membr. Sci. 585, 260–270. doi:10.1016/j.memsci.2019.05.046.

Smith, S.J., Hou, R., Konstas, K., Akram, A., Lau, C.H., Hill, M.R., 2020. Control of physical aging in super-glassy polymer mixed matrix membranes. Acc. Chem. Res. 53 (7), 1381–1388. doi:10.1021/acs.accounts.0c00256.

Smith, K.H., Ashkanani, H.E., Morsi, B.I., Siefert, N.S., 2022. Physical solvents and techno-economic analysis for pre-combustion CO_2 capture: A review. Int. J. Greenh. Gas Control 118, 103694. doi:10.1016/j.ijggc.2022.103694.

Sneha, B.R., Thangadurai, V., 2007. Synthesis of nano-sized crystalline oxide ion conducting fluorite-type Y_2O_3-doped CeO_2 using perovskite-like $BaCe_{0.9}Y_{0.1}O_{2.95}$ (BCY) and study of CO_2 capture properties of BCY. J. Solid State Chem. 180 (10), 2661–2669. doi:10.1016/j.jssc.2007.07.016.

Soares, J.L., Moreira, R.F.P.M., José, H.J., Grande, C.A., Rodrigues, A.E., 2005. Hydrotalcite materials for carbon dioxide adsorption at high temperatures: characterization and diffusivity measurements. Sep. Sci. Technol. 39 (9), 1989–2010. doi:10.1081/SS-120039307.

Socolow, R., Desmond, M., Aines, R., Blackstock, J., Bolland, O., Kaarsberg, T., Lewis, N., Mazzotti, M., Pfeffer, A., Sawyer, K., Siirola, J., Smit, B., Wilcox, J., 2011. Direct Air Capture of CO_2 with Chemicals: A Technology Assessment for the APS Panel on Public Affairs. American Physical Society.

Socolow, R., Desmond, M., Aines, R., Blackstock, J., Bolland, O., Kaarsberg, T., Newis, N., Mazzotti, M., Pfeffer, A., Sawyer, K., Siirola, J., Smit, B., Wilcox, J., 2011. Directair capture of co2 with chemicals. a technology assessment for the aps panelon public affairs, in: Society, A.P. (Ed.)

Soetemans, L., Uyttebroek, M., Bastiaens, L., 2020. Characteristics of chitin extracted from black soldier fly in different life stages. Int. J. Biol. Macromol. 165, 3206–3214. doi:10.1016/j.ijbiomac.2020.11.041.

Sohail, M., An, H., Choi, W., Singh, J., Yim, K., Kim, B.H., Park, Y.C., Lee, J.S., Kim, H., 2021. Sorption-enhanced thin film composites with metal-organic polyhedral nanocages for CO_2 separation. J. Membr. Sci. 620, 118826. doi:10.1016/j.memsci.2020.118826.

Solomenko, Z., Haroun, Y., Fourati, M., Larachi, F., Boyer, C., Augier, F., 2015. Liquid spreading in trickle-bed reactors: Experiments and numerical simulations using Eulerian-Eulerian two-fluid approach. Chem. Eng. Sci. 126, 698–710. doi:10.1016/j.ces.2015.01.013.

Son, W.-J., Choi, J.-S., Ahn, W.-S., 2008. Adsorptive removal of carbon dioxide using polyethyleneimine-loaded mesoporous silica materials. Microporous Mesoporous Mater. 113 (1-3), 31–40. doi:10.1016/j.micromeso.2007.10.049.

Song, C.F., Kitamura, Y., Li, S.H., 2012a. Evaluation of Stirling cooler system for cryogenic CO_2 capture. Appl. Energy 98, 491–501. doi:10.1016/j.apenergy.2012.04.013.

Song, C.F., Kitamura, Y., Li, S.H., Jiang, W.Z., 2012b. Parametric analysis of a novel cryogenic CO_2 capture system based on Stirling coolers. Environ. Sci. Technol. 46 (22), 12735–12741. doi:10.1021/es3025947.

Song, C.F., Kitamura, Y., Li, S.H., Ogasawara, K., 2012c. Design of a cryogenic CO_2 capture system based on Stirling coolers. Int. J. Greenh. Gas Control 7, 107–114. doi:10.1016/j.ijggc.2012.01.004.

Song, C., Kitamura, Y., Li, S., 2014. Energy analysis of the cryogenic CO_2 capture process based on Stirling coolers. Energy 65, 580–589. doi:10.1016/j.energy.2013.10.087.

Song, C., Kansha, Y., Fu, Q., Ishizuka, M., Tsutsumi, A., 2016. Reducing energy consumption of advanced PTSA CO_2 capture process—Experimental and numerical study. J. Taiwan Instit. Chem. Eng. 64, 69–78. doi:10.1016/j.jtice.2015.12.006.

Song, C., Liu, Q., Ji, N., Deng, S., Zhao, J., Li, Y., Kitamura, Y., 2017. Reducing the energy consumption of membrane-cryogenic hybrid CO_2 capture by process optimization. Energy 124, 29–39. doi:10.1016/j.energy.2017.02.054.

Song, C.F., Liu, Q.L., Ji, N., Deng, S., Zhao, J., Kitamura, Y., 2017. Advanced cryogenic CO_2 capture process based on Stirling coolers by heat integration. Appl. Therm. Eng. 114, 887–895. doi:10.1016/j.applthermaleng.2016.12.049.

Song, C., Fan, Z., Li, R., Liu, Q., Kitamura, Y., 2018a. Efficient biogas upgrading by a novel membrane-cryogenic hybrid process: Experiment and simulation study. J. Membr. Sci. 565, 194–202. doi:10.1016/j.memsci.2018.08.027.

Song, C., Liu, Q., Ji, N., Deng, S., Zhao, J., Li, Y., Song, Y., Li, H., 2018b. Alternative pathways for efficient CO_2 capture by hybrid processes—A review. Renew. Sustain. Energy Rev. 82, 215–231. doi:10.1016/j.rser.2017.09.040.

Song, C., Liu, J., Xie, M., Qiu, Y., Chen, G., Qi, Y., Kitamura, Y., 2019a. Intensification of a novel absorption-microalgae hybrid CO_2 utilization process via fed-batch mode optimization. Int. J. Greenh. Gas Control 82, 1–7. doi:10.1016/j.ijggc.2019.01.001.

Song, C., Liu, Q., Deng, S., Li, H., Kitamura, Y., 2019b. Cryogenic-based CO_2 capture technologies: State-of-the-art developments and current challenges. Renew. Sustain. Energy Rev. 101, 265–278. doi:10.1016/j.rser.2018.11.018.

Song, C., Xie, M., Qiu, Y., Liu, Q., Sun, L., Wang, K., Kansha, Y., 2019c. Integration of CO_2 absorption with biological transformation via using rich ammonia solution as a nutrient source for microalgae cultivation. Energy 179, 618–627. doi:10.1016/j.energy.2019.05.039.

Soubeyrand-Lenoir, E., Vagner, C., Yoon, J.W., Bazin, P., Ragon, F., Hwang, Y.K., Serre, C., Chang, J.S., Llewellyn, P.L., 2012. How water fosters a remarkable 5-fold increase in low-pressure CO_2 uptake within mesoporous MIL-100 (Fe). J. Am. Chem. Soc. 134 (24), 10174–10181. doi:10.1021/ja302787x.

Soundararajan, R., Gundersen, T., 2013. Coal based power plants using oxy-combustion for CO_2 capture: Pressurized coal combustion to reduce capture penalty. Appl. Therm. Eng. 61 (1), 115–122. doi:10.1016/j.applthermaleng.2013.04.010.

Spiegl, N., Long, X., Berrueco, C., Paterson, N., Millan, M., 2021. Oxy-fuel co-gasification of coal and biomass for negative CO_2 emissions. Fuel 306, 121671. doi:10.1016/j.fuel.2021.121671.

Spitler, E.L., Giovino, M.R., White, S.L., Dichtel, W.R., 2011. A mechanistic study of Lewis acid-catalyzed covalent organic framework formation. Chem. Sci. 2 (8), 1588–1593.

Spitoni, M., Pierantozzi, M., Comodi, G., Polonara, F., Arteconi, A., 2019. Theoretical evaluation and optimization of a cryogenic technology for carbon dioxide separation and methane liquefaction from biogas. J. Nat. Gas Sci. Eng. 62, 132–143. doi:10.1016/j.jngse.2018.12.007.

Sreedhar, I., Nahar, T., Venugopal, A., Srinivas, B., 2017. Carbon capture by absorption – Path covered and ahead. Renew. Sustain. Energy Rev. 76, 1080–1107. doi:10.1016/j.rser.2017.03.109.

Srisang, W., Pouryousefi, F., Osei, P.A., Decardi-Nelson, B., Akachuku, A., Tontiwachwuthikul, P., Idem, R., 2017. Evaluation of the heat duty of catalyst-aided amine-based post combustion CO 2 capture. Chem. Eng. Sci. 170, 48–57. doi:10.1016/j.ces.2017.01.049.

Srisang, W., Pouryousefi, F., Osei, P.A., Decardi-Nelson, B., Akachuku, A., Tontiwachwuthikul, P., Idem, R., 2018. CO_2 capture efficiency and heat duty of solid acid catalyst-aided CO_2 desorption using blends of primary-tertiary amines. Int. J. Greenh. Gas Control 69, 52–59. doi:10.1016/j.ijggc.2017.12.010.

Stöhr, B., Boehm, H.P., Schlögl, R., 1991. Enhancement of the catalytic activity of activated carbons in oxidation reactions by thermal treatment with ammonia or hydrogen cyanide and observation of a superoxide species as a possible intermediate. Carbon 29 (6), 707–720. doi:10.1016/0008-6223 (91)90006-5.

Stadler, H., Beggel, F., Habermehl, M., Persigehl, B., Kneer, R., Modigell, M., Jeschke, P., 2011. Oxyfuel coal combustion by efficient integration of oxygen transport membranes. Int. J. Greenh. Gas Control 5 (1), 7–15. doi:10.1016/J.IJGGC.2010.03.004.

Stanger, R., Wall, T., Spörl, R., Paneru, M., Grathwohl, S., Weidmann, M., Scheffknecht, G., McDonald, D., Myöhänen, K., Ritvanen, J., Rahiala, S., Hyppänen, T., Mletzko, J., Kather, A., Santos, S., 2015. Oxyfuel combustion for CO_2 capture in power plants. Int. J. Greenh. Gas Control 40, 55–125. doi:10.1016/j.ijggc.2015.06.010.

Stanovsky, P., Zitkova, A., Karaszova, M., Šyc, M., Jansen, J.C., Comesaña Gándara, B., McKeown, N., Izak, P., 2020. Flue gas purification with membranes based on the polymer of intrinsic microporosity PIM-TMN-Trip. Sep. Purif. Technol. 242, 116814. doi:10.1016/j.seppur.2020.116814.

Starr, K., Gabarrell, X., Villalba, G., Talens, L., Lombardi, L., 2012. Life cycle assessment of biogas upgrading technologies. Waste Manage. 32 (5), 991–999. doi:10.1016/j.wasman.2011.12.016.

Steinberg, M., Dang, V.-D., 1977. Production of synthetic methanol from air and water using controlled thermonuclear reactor power—I. technology and energy requirement. Energy Convers. 17 (2), 97–112. doi:10.1016/0013-7480 (77)90080-8.

Stephenne, K., 2015. Start-Up of World's first commercial post-combustion coal fired CCS Project: Contribution of shell cansolv to SaskPower boundary dam ICCS project. In: International Conference on Greenhouse Gas Control Technologies.

Stiernet, P., Mazaj, M., Kovačič, S., Debuigne, A., 2022. Bifunctional imidazolium/amine polymer foams: One-pot synthesis and synergistic promotion of CO_2 sorption. Chem. Eng. J. 446. doi:10.1016/j.cej.2022.137012.

Stolaroff, J.K., Keith, D.W., Lowry, G.V., 2008. Carbon dioxide capture from atmospheric air using sodium hydroxide spray. Environ. Sci. Technol. 42 (8), 2728–2735. doi:10.1021/es702607w.

Ströhle, J., Lasheras, A., Galloy, A., Epple, B., 2009. Simulation of the carbonate looping process for post-combustion CO_2 capture from a coal-fired power plant. Chem. Eng. Technol. 32 (3), 435–442. doi:10.1002/CEAT.200800569.

Ströhle, J., Hilz, J., Epple, B., 2020. Performance of the carbonator and calciner during long-term carbonate looping tests in a 1 MWth pilot plant. J. Environ. Chem. Eng. 8 (1), 103578. doi:10.1016/j.jece.2019.103578.

Stylianou, M., Christou, A., Dalias, P., Polycarpou, P., Michael, C., Agapiou, A., Papanastasiou, P., Fatta-Kassinos, D., 2020. Physicochemical and structural characterization of biochar derived from the pyrolysis of biosolids, cattle manure and spent coffee grounds. J. Energy Instit. 93 (5), 2063–2073. doi:10.1016/j.joei.2020.05.002.

Su, F., Lu, C., 2012. CO_2 capture from gas stream by zeolite 13X using a dual-column temperature/vacuum swing adsorption. Energy Environ. Sci. 5 (10). doi:10.1039/c2ee22647b.

Su, F., Lu, C., Cnen, W., Bai, H., Hwang, J.F., 2009. Capture of CO_2 from flue gas via multiwalled carbon nanotubes. Sci Total Environ. 407 (8), 3017–3023. doi:10.1016/j.scitotenv.2009.01.007.

Su, F., Lu, C., Kuo, S.-C., Zeng, W., 2010. Adsorption of CO_2 on amine-functionalized Y-type zeolites. Energy Fuels 24 (2), 1441–1448. doi:10.1021/ef901077k.

Su, F., Lu, C., Chen, H.S., 2011. Adsorption, desorption, and thermodynamic studies of CO_2 with high-amine-loaded multiwalled carbon nanotubes. Langmuir 27 (13), 8090–8098. doi:10.1021/la201745y.

Su, X., Bromberg, L., Martis, V., Simeon, F., Huq, A., Hatton, T.A., 2017. Postsynthetic functionalization of Mg-MOF-74 with tetraethylenepentamine: structural characterization and enhanced CO_2 adsorption. ACS Appl. Mater. Interfaces 9 (12), 11299–11306. doi:10.1021/acsami.7b02471.

Sublet, J., Pera-Titus, M., Guilhaume, N., Farrusseng, D., Schrive, L., Chanaud, P., Siret, B., Durécu, S., 2012. Technico-economical assessment of MFI-type zeolite membranes for CO_2 capture from postcombustion flue gases. AIChE J. 58 (10), 3183–3194.

Subramanian Balashankar, V., Rajendran, A., 2019. Process optimization-based screening of zeolites for post-combustion CO_2 capture by vacuum swing adsorption. ACS Sustain. Chem. Eng. 7 (21), 17747–17755. doi:10.1021/acssuschemeng.9b04124.

Subramanian Balashankar, V., Rajagopalan, A.K., de Pauw, R., Avila, A.M., Rajendran, A., 2019. Analysis of a batch adsorber analogue for rapid screening of adsorbents for postcombustion CO_2 capture. Ind. Eng. Chem. Res. 58 (8), 3314–3328. doi:10.1021/acs.iecr.8b05420.

Subraveti, S.G., Li, Z., Prasad, V., Rajendran, A., 2019a. Machine learning-based multiobjective optimization of pressure swing adsorption. Ind. Eng. Chem. Res. 58 (44), 20412–20422. doi:10.1021/acs.iecr.9b04173.

Subraveti, S.G., Pai, K.N., Rajagopalan, A.K., Wilkins, N.S., Rajendran, A., Jayaraman, A., Alptekin, G., 2019b. Cycle design and optimization of pressure swing adsorption cycles for pre-combustion CO_2 capture. Appl. Energy 254, 113624. doi:10.1016/j.apenergy.2019.113624.

Subraveti, S.G., Roussanaly, S., Anantharaman, R., Riboldi, L., Rajendran, A., 2021. Techno-economic assessment of optimised vacuum swing adsorption for post-combustion CO_2 capture from steam-methane reformer flue gas. Sep. Purif. Technol. 256. doi:10.1016/j.seppur.2020.117832, 117832-117832.

Subraveti, S.G., Roussanaly, S., Anantharaman, R., Riboldi, L., Rajendran, A., 2022. How much can novel solid sorbents reduce the cost of post-combustion CO_2 capture? A techno-economic investigation on the cost limits of pressure–vacuum swing adsorption. Appl. Energy 306. doi:10.1016/j.apenergy.2021.117955, 11795-11795.

Subrenat, A.S., Le Cloirec, P.A., 2006. Volatile organic compound (Voc) removal by adsorption onto activated carbon fiber cloth and electrothermal desorption: An industrial application. Chem. Eng. Commun. 193 (4), 478–486. doi:10.1080/00986440500191768.

Sudhoff, D., Leimbrink, M., Schleinitz, M., Górak, A., Lutze, P., 2015. Modelling, design and flexibility analysis of rotating packed beds for distillation. Chem. Eng. Res. Des. 94, 72–89. doi:10.1016/j.cherd.2014.11.015.

Suhas, Gupta, V.K., Carrott, P.J.M., Singh, R., Chaudhary, M., Kushwaha, S., 2016. Cellulose: A review as natural, modified and activated carbon adsorbent. Bioresour. Technol. 216, 1066–1076. doi:10.1016/j.biortech.2016.05.106.

Sujan, A.R., Koh, D.-Y., Zhu, G., Babu, V.P., Stephenson, N., Rosinski, A., Du, H., Luo, Y., Koros, W.J., Lively, R.P., 2018. High-temperature activation of zeolite-loaded fiber orbents. Ind. Eng. Chem. Res. 57 (34), 11757–11766. doi:10.1021/acs.iecr.8b02210.

Sun, P., Grace, J.R., Lim, C.J., Anthony, E.J., 2007. The effect of CaO sintering on cyclic CO_2 capture in energy systems. Aiche J. 53 (9), 2432–2442. doi:10.1002/aic.11251.

Sun, Y., Cui, F., Shi, K., Wang, J., Niu, M., Ma, R., 2009. The effect of chitosan molecular weight on the characteristics of spray-dried methotrexate-loaded chitosan microspheres for nasal administration. Drug Dev. Ind. Pharm. 35 (3), 379–386. doi:10.1080/03639040802395185.

Sun, X.F., Liu, S.Y., Khan, A., Zhao, C., Yan, C.Y., Mu, T.C., 2014. Ionicity of acetate-based protic ionic liquids: evidence for both liquid and gaseous phases. New J. Chem. 38 (8), 3449–3456. doi:10.1039/c4nj00384e.

Sun, J., Liu, W., Hu, Y., Li, M., Yang, X., Zhang, Y., Xu, M., 2015. Structurally improved, core-in-shell, CaO-based sorbent pellets for CO_2 capture. Energy Fuels 29 (10), 6636–6644. doi:10.1021/acs.energyfuels.5b01419.

Sun, J., Liang, C., Tong, X., Guo, Y., Li, W., Zhao, C., Zhang, J., Lu, P., 2019. Evaluation of high-temperature CO_2 capture performance of cellulose-templated CaO-based pellets. Fuel 239, 1046–1054. doi:10.1016/j.fuel.2018.11.123.

Sun, H., Wang, J., Liu, X., Shen, B., Parlett, Christopher, M.A., Adwek, G.O., John Anthony, E., Williams, P.T., Wu, C., 2019. Fundamental studies of carbon capture using CaO-based materials. J. Mater. Chem. A 7 (16), 9977–9987. doi:10.1039/C8TA10472G.

Sun, M., Gu, Q., Hanif, A., Wang, T., Shang, J., 2019. Transition metal cation-exchanged SSZ-13 zeolites for CO_2 capture and separation from N_2. Chem. Eng. J. 370, 1450–1458.

Sun, B., Bhatelia, T., Utikar, R.P., Evans, G.M., Pareek, V.K., 2021. Study on hydrodynamic performance of structured packings for gas-liquid flow: Effects of geometry parameters. Chem. Eng. Res. Des. 167, 6–9. doi:10.1016/j.cherd.2021.01.003.

Sun, Q., Mao, Y., Gao, H., Sema, T., Liang, Z., 2021. Efficient nickel-based catalysts for amine regeneration of CO2 capture: From experimental to calculations verifications.

Sunarso, J., Baumann, S., Serra, J.M., Meulenberg, W.A., Liu, S., Lin, Y.S., Diniz da Costa, J.C., 2008. Mixed ionic–electronic conducting (MIEC) ceramic-based membranes for oxygen separation. J. Membr. Sci. 320, 13–41. doi:10.1016/J.MEMSCI.2008.03.074.

Suroutseua, D., Amin, R., Barifcani, A., 2011. Design and operation of pilot plant for CO_2 capture from IGCC flue gases by combined cryogenic and hydrate method. Chem. Eng. Res. Des. 89 (9), 1752–1757. doi:10.1016/j.cherd.2010.08.016.

Sutrisna, P.D., Hou, J., Li, H., Zhang, Y., Chen, V., 2017. Improved operational stability of Pebax-based gas separation membranes with ZIF-8: A comparative study of flat sheet and composite hollow fibre membranes. J. Membr. Sci. 524, 266–279. doi:10.1016/j.memsci.2016.11.048.

Sutrisna, P.D., Hou, J., Zulkifli, M.Y., Li, H., Zhang, Y., Liang, W., D'Alessandro, D.M., Chen, V., 2018. Surface functionalized UiO-66/Pebax-based ultrathin composite hollow fiber gas separation membranes. J. Mater. Chem. A 6 (3), 918–931. doi:10.1039/C7TA07512J.

Suzuki, T.J.P., 2021. Gas transport properties of thermally rearranged (TR) polybenzoxazole–silica hybrid membranes. 214, 123274.

Swati, I.K., Sohaib, Q., Cao, S., Younas, M., Liu, D., Gui, J., Rezakazemi, M., 2021. Protic/aprotic ionic liquids for effective CO_2 separation using supported ionic liquid membrane. Chemosphere 267, 128894. doi:10.1016/j.chemosphere.2020.128894.

Syeda Saba Fatima, A.B., Ayoub, M., Abd Ghani, N., 2021. Development and progress of functionalized silica-based adsorbents for CO_2 capture. J. Mol. Liq. 338, 116913. doi:10.1016/j.molliq.2021.116913.

Tailor, R., Sayari, A., 2016. Grafted propyldiethanolamine for selective removal of SO 2 in the presence of CO 2. Chem. Eng. J. 289, 142–149. doi:10.1016/j.cej.2015.12.084.

Tajima, H., Yamasaki, A., Kiyono, F., 2004. Energy consumption estimation for greenhouse gas separation processes by clathrate hydrate formation. Energy 29 (11), 1713–1729. doi:10.1016/j.energy.2004.03.003.

Takuo, N., Hitoshi, K., Shinzo, Y., Shinzo, K., 1979. The polymerization of β-propiolactone by calcined synthetic hydrotalcite. 52 (8), 2449-2450. https://doi.org/10.1246/bcsj.52.2449.

Tan, X., Wang, Z., Meng, B., Meng, X., Li, K., 2010. Pilot-scale production of oxygen from air using perovskite hollow fibre membranes. J. Membr. Sci. 352, 189–196. doi:10.1016/J.MEMSCI.2010.02.015.

Tan, J., Shao, H., Xu, J., Du, L., Luo, G., 2011. Mixture absorption system of monoethanolamine–triethylene glycol for CO_2 capture. Ind. Eng. Chem. Res. 50 (7), 3966–3976. doi:10.1021/ie101810a.

Tan, Y., Nookuea, W., Li, H., Thorin, E., Yan, J., 2017. Cryogenic technology for biogas upgrading combined with carbon capture - a review of systems and property impacts. Energy Procedia 142, 3741–3746. doi:10.1016/j.egypro.2017.12.270.

Tan, H., Wen, N., Ding, Z., 2021. Computational fluid dynamics simulation of multi-phase flow characteristics in an industrial-scale randomly packed tower. Asia-Pac. J. Chem. Eng. 16 (6). doi:10.1002/apj.2708, e2708-e2708.

Tanaka, K., Kita, H., Okano, M., Okamoto, K.-i., 1992. Permeability and permselectivity of gases in fluorinated and non-fluorinated polyimides. Polymer 33 (3), 585–592. doi:10.1016/0032-3861 (92)90736-G.

Tang, Z., Han, Z., Yang, G., Yang, J., 2013. Polyethylenimine loaded nanoporous carbon with ultra-large pore volume for CO_2 capture. Appl. Surf. Sci. 277, 47–52. doi:10.1016/j.apsusc.2013.03.142.

Tang, B., White, S.P., Frisbie, C.D., Lodge, T.P., 2015. Synergistic increase in ionic conductivity and modulus of triblock copolymer ion gels. Macromolecules 48 (14), 4942–4950. doi:10.1021/acs.macromol.5b00882.

Tao, M., Gao, J., Zhang, W., Li, Y., He, Y., Shi, Y., 2018. A novel phase-changing nonaqueous solution for CO_2 capture with high capacity, thermostability, and regeneration efficiency. Ind. Eng. Chem. Res. 57 (28), 9305–9312. doi:10.1021/acs.iecr.8b01775.

Tawalbeh, M., Al-Ismaily, M., Kruczek, B., Tezel, F.H., 2021. Modeling the transport of CO_2, N_2, and their binary mixtures through highly permeable silicalite-1 membranes using Maxwell– Stefan equations. Chemosphere 263, 127935.

Teixeira, P., Bacariza, C., Correia, P., Pinheiro, C.I.C., Cabrita, I., 2022. Hydrogen production with in situ CO_2 capture at high and medium temperatures using solid sorbents. Energies 15 (11), 44. doi:10.3390/en15114039.

Tepe, J., Dodge, B., 1943. Absorption of carbon dioxide by sodium hydroxide solutions in a packed column. Trans. Am. Inst. Chem. Eng. 39, 255–276.

Teramoto, M., Nakai, K., Ohnishi, N., Huang, Q., Watari, T., Matsuyama, H., 1996. Facilitated transport of carbon dioxide through supported liquid membranes of aqueous amine solutions. Ind. Eng. Chem. Res. 35 (2), 538–545. doi:10.1021/ie950112c.

Teramoto, M., Huang, Q., Watari, T., Tokunaga, Y., Nakatani, R., Maeda, T., Matsuyama, H., 1997. Facilitated transport of CO_2 through supported liquid membranes of various amine solutions—Effects of rate and equilibrium of reaction between CO_2 and Amine—. J. Chem. Eng. Jpn. 30 (2), 328–335. doi:10.1252/jcej.30.328.

Thakkar, H., Issa, A., Rownaghi, A.A., Rezaei, F., 2017. CO_2 capture from air using amine-functionalized kaolin-based zeolites. Chem. Eng. Technol. 40 (11), 1999–2007. doi:10.1002/ceat.201700188.

Thankamony, R.L., Li, X., Das, S.K., Ostwal, M.M., Lai, Z., 2019. Porous covalent triazine piperazine polymer (CTPP)/PEBAX mixed matrix membranes for CO_2/N_2 and CO_2/CH_4 separations. J. Membr. Sci. 591, 117348. doi:10.1016/j.memsci.2019.117348.

Thiels, M., et al., 2016. Modelling and Design of Carbon Dioxide Absorption in Rotating Packed Bed and Packed Column. IFAC-PapersOnLine 49 (7), 895–900.

Thompson, J.A., Brunelli, N.A., Lively, R.P., Johnson, J.R., Jones, C.W., Nair, S., 2013. Tunable CO_2 adsorbents by mixed-linker synthesis and postsynthetic modification of zeolitic imidazolate frameworks. J. Phys. Chem. C 117 (16), 8198–8207. doi:10.1021/jp312590r.

Thomsen, K., Rasmussen, P., 1999. Modeling of vapour–liquid–solid equilibrium in gas–aqueous electrolyte systems. Chem. Eng. Sci. 54 (12), 1787–1802.

Tian, H., Guo, Q., Chang, J., 2008. Investigation into decomposition behavior of CaSO4 in chemical-looping combustion. Energy Fuels 22 (6), 3915–3921. doi:10.1021/ef800508w.

Tian, H., Simonyi, T., Poston, J., Siriwardane, R., 2009. Effect of hydrogen sulfide on chemical looping combustion of coal-derived synthesis gas over bentonite-supported metal–oxide oxygen carriers. Ind. Eng. Chem. Res. 48 (18), 8418–8430. doi:10.1021/ie900638p.

Tian, X., Wei, Y., Zhao, H., 2017. Evaluation of a hierarchically-structured CuO@TiO2-Al2O3 oxygen carrier for chemical looping with oxygen uncoupling. Fuel 209, 402–410. doi:10.1016/j.fuel.2017.08.022.

Tian, L., Liang, F., Dong, L.H., Li, J.Y., Jia, Q.L., Zhang, H.J., Yan, S., Zhang, S.W., 2021. Preparation and enhanced adsorption properties for CO (2)and dyes of amino-decorated hierarchical porous BCN aerogels. J. Am. Ceram. Soc. 104 (2), 1110–1119. doi:10.1111/jace.17501.

Tian, M., Wang, C., Han, Y., Wang, X., 2021. Recent advances of oxygen carriers for chemical looping reforming of methane. ChemCatChem 13 (7), 1615–1637. doi:10.1002/cctc.202001481.

Tian, J., Shen, Y., Zhang, D., Tang, Z., 2021. CO_2 capture by vacuum pressure swing adsorption from dry flue gas with a structured composite adsorption medium. J. Environ. Chem. Eng. 9 (5), 106037. doi:10.1016/j.jece.2021.106037.

Tian, H., Wei, Y., Cheng, S., Huang, Z., Qing, M., Chen, Y., Yang, H., Yang, Y., 2022. Optimizing the gasification reactivity of biochar: The composition, structure and kinetics of biochar derived from biomass lignocellulosic components and their interactions during gasification process. Fuel 324, 124709. doi:10.1016/j.fuel.2022.124709.

Tilford, R.W., Gemmill, W.R., zur Loye, H.-C., Lavigne, J.J., 2006. Facile synthesis of a highly crystalline, covalently linked porous boronate network. Chem. Mater. 18 (22), 5296–5301.

Tinnirello, M., Papurello, D., Santarelli, M., Fiorilli, S., 2020. Thermal activation of digested sewage sludges for carbon dioxide removal from biogas. Fuels 1 (1), 30–46. doi:10.3390/fuels1010004.

Titirici, M.M., Antonietti, M., 2010. Chemistry and materials options of sustainable carbon materials made by hydrothermal carbonization. Chem. Soc. Rev. 39 (1), 103–116. doi:10.1039/B819318P.

Tiwari, S.C., Pant, K.K., Upadhyayula, S., 2021. Efficient CO_2 absorption in aqueous dual functionalized cyclic ionic liquids. J. Co2 Util. 45. doi:10.1016/j.jcou.2020.101416.

Toftegaard, M.B., Brix, J., Jensen, P.A., Glarborg, P., Jensen, A.D., 2010. Oxy-fuel combustion of solid fuels. Prog. Energy Combust. Sci. 36 (5), 581–625. doi:10.1016/j.pecs.2010.02.001.

Togashi, N., Okumura, T., Oh-Ishi, K., 2007. Synthesis and CO_2 absorption property of Li_4TiO_4 as a novel CO_2 absorbent. J. Ceram. Soc. Jpn. 115, 324–328. doi:10.2109/jcersj.115.324.

Tomé, L.C., Marrucho, I., 2016. Ionic liquid-based materials: A platform to design engineered CO_2 separation membranes. Chem. Soc. Rev. 45. doi:10.1039/C5CS00510H.

Tome, L.C., Marrucho, I.M., 2016. Ionic liquid-based materials: a platform to design engineered CO_2 separation membranes. Chem. Soc. Rev. 45 (10), 2785–2824. doi:10.1039/c5cs00510h.

Tong, Z., Ho, W.S.W., 2017. Facilitated transport membranes for CO_2 separation and capture. Sep. Sci. Technol. 52 (2), 156–167.

Tong, Z., Ho, W.S.W., 2017a. Facilitated transport membranes for CO_2 separation and capture. Sep. Sci. Technol. 52 (2), 156–167. doi:10.1080/01496395.2016.1217885.

Tong, Z., Ho, W.S.W., 2017b. New sterically hindered polyvinylamine membranes for CO_2 separation and capture. J. Membr. Sci. 543, 202–211. doi:10.1016/j.memsci.2017.08.057.

Tong, S., Zhang, S., Yin, H., Wang, J., Chen, M., 2021. Study on co-hydrothermal treatment combined with pyrolysis of rice straw/sewage sludge: Biochar properties and heavy metals behavior. J. Analyt. Appl. Pyrol. 155, 105074. doi:10.1016/j.jaap.2021.105074.

Tranier, J.-P., Dubettier, R., Darde, A., Perrin, N., 2011. Air separation, flue gas compression and purification units for oxy-coal combustion systems. Energy Procedia 4, 966–971. doi:10.1016/j.egypro.2011.01.143.

Trapp, C., Thomaser, T., van Dijk, H.A.J., Colonna, P., 2015. Design optimization of a pre-combustion CO_2 capture plant embedding experimental knowledge. Fuel 157, 126–139. doi:10.1016/j.fuel.2015.04.007.

Tregambi, C., Troiano, M., Montagnaro, F., Solimene, R., Salatino, P., 2021. Fluidized beds for concentrated solar thermal technologies-a review. Front. Energy Res. 9, 26. doi:10.3389/fenrg.2021.618421.

Trivedi, T.J., Bhattacharjya, D., Yu, J.-S., Kumar, A., 2015. Functionalized agarose self-healing ionogels suitable for supercapacitors. ChemSusChem 8 (19), 3294–3303. doi:10.1002/cssc.201500648.

Troy, S., Schreiber, A., Zapp, P., 2016. Life cycle assessment of membrane-based carbon capture and storage. Clean Technol. Environ. Policy 18 (6), 1641–1654. doi:10.1007/s10098-016-1208-x.

Trzpit, M., Soulard, M., Patarin, J., Desbiens, N., Cailliez, F., Boutin, A., Demachy, I., Fuchs, A., 2007. The effect of local defects on water adsorption in silicalite-1 zeolite: A joint experimental and molecular simulation study. Langmuir 23 (20), 10131–10139.

Tseng, H.-H., Itta, A.K., 2012. Modification of carbon molecular sieve membrane structure by self-assisted deposition carbon segment for gas separation. J. Membr. Sci. 389, 223–233. doi:10.1016/j.memsci.2011.10.031.

Tseng, H.-H., Wang, C.-T., Zhuang, G.-L., Uchytil, P., Reznickova, J., Setnickova, K., 2016. Enhanced H2/CH4 and H2/CO_2 separation by carbon molecular sieve membrane coated on titania modified alumina support: Effects of TiO2 intermediate layer preparation variables on interfacial adhesion. J. Membr. Sci. 510, 391–404. doi:10.1016/j.memsci.2016.02.036.

Tu, Z., Liu, P., Zhang, X., Shi, M., Zhang, Z., Luo, S., Zhang, L., Wu, Y., Hu, X.J.S., Technology, P., 2021a. Highly-selective separation of CO_2 from N_2 or CH_4 in task-specific ionic liquid membranes: Facilitated transport and salting-out effect. 254, 117621.

Tu, Z., Shi, M., Zhang, X., Liu, P., Wu, Y., Hu, X., 2021b. Selective membrane separation of CO_2 using novel epichlorohydrin-amine-based crosslinked protic ionic liquids: Crosslinking mechanism and enhanced salting-out effect. J. CO_2 Util. 46, 101473. doi:10.1016/j.jcou.2021.101473.

Tuinier, M.J., van Sint Annaland, M., 2012. Biogas purification using cryogenic packed-bed technology. Ind. Eng. Chem. Res. 51 (15), 5552–5558. doi:10.1021/ie202606g.

Tuinier, M.J., van Sint Annaland, M., Kramer, G.J., Kuipers, J.A.M., 2010. Cryogenic CO_2 capture using dynamically operated packed beds. Chem. Eng. Sci. 65 (1), 114–119. doi:10.1016/j.ces.2009.01.055.

Tuinier, M.J., Hamers, H.P., van Sint Annaland, M., 2011a. Techno-economic evaluation of cryogenic CO_2 capture—A comparison with absorption and membrane technology. Int. J. Greenh. Gas Control 5 (6), 1559–1565. doi:10.1016/j.ijggc.2011.08.013.

Tuinier, M.J., van Sint Annaland, M., Kuipers, J.A.M., 2011b. A novel process for cryogenic CO_2 capture using dynamically operated packed beds—An experimental and numerical study. Int. J. Greenh. Gas Control 5 (4), 694–701. doi:10.1016/j.ijggc.2010.11.011.

Tung, H.H., Mah, R.S.H., 1985. Modeling liquid mass transfer in higee separation process. Chemical Engineering Communications 39 (1-6), 147–153.

Turnbull, E., Kossakowski, E.R., Davidson, J.F., Hopes, R.B., Blackshaw, H.W., Goodyer, P.T.Y., 1984. Effect of pressure on combustion of char in fluidised beds. Chem. Eng. Res. Des. 62 (4), 223–234.

Uehara, Y., Karami, D., Mahinpey, N., 2018. Roles of cation and anion of amino acid anion-functionalized ionic liquids immobilized into a porous support for CO_2 capture. Energy Fuels 32 (4), 5345–5354. doi:10.1021/acs.energyfuels.8b00190.

Ullah, A., Saleem, M.W., Kim, W.-S., 2017. Performance and energy cost evaluation of an integrated NH3-based CO_2 capture-capacitive deionization process. Int. J. Greenh. Gas Control 66, 85–96. doi:10.1016/j.ijggc.2017.09.013.

Ullah Khan, I., Hafiz Dzarfan Othman, M., Hashim, H., Matsuura, T., Ismail, A.F., Rezaei-DashtArzhandi, M., Wan Azelee, I., 2017. Biogas as a renewable energy fuel – A review of biogas upgrading, utilisation and storage. Energy Convers. Manage. 150, 277–294. doi:10.1016/j.enconman.2017.08.035.

Uribe-Romo, F.J., Hunt, J.R., Furukawa, H., Klöck, C., O'Keeffe, M., Yaghi, O.M., 2009. A crystalline imine-linked 3-D porous covalent organic framework. J. Am. Chem. Soc. 131 (13), 4570–4571.

Uribe-Romo, F.J., Doonan, C.J., Furukawa, H., Oisaki, K., Yaghi, O.M., 2011. Crystalline covalent organic frameworks with hydrazone linkages. J. Am. Chem. Soc. 133 (30), 11478–11481.

Uwitonze, H., Lee, I., Suh, S.B., Lee, I., 2021. CFD study of oscillatory motion effect on liquid flow distribution into structured packed divided wall column. Chem. Eng. Process. - Process Intensif. 165. doi:10.1016/j.cep.2021.108429, 108429-108429.

Vaccari, A., 1998. Preparation and catalytic properties of cationic and anionic clays. Catal. Today 41 (1), 53–71. doi:10.1016/S0920-5861 (98)00038-8.

Valenciano, R., Aylón, E., Izquierdo, M.T., 2015. A critical short review of equilibrium and kinetic adsorption models for vocs breakthrough curves modelling. Adsorpt. Sci. Technol. 33 (10), 851–870. doi:10.1260/0263-6174.33.10.851.

Valverde, J.M., Sanchez-Jimenez, P.E., Perez-Maqueda, L.A., 2015. Ca-looping for post-combustion CO_2 capture: a comparative analysis on the performances of dolomite and limestone. Appl. Energy 138, 202–215.

Valverde, J.M., 2018. The Ca-looping process for CO_2 capture and energy storage: role of nanoparticle technology. J. Nanopart. Res. 20 (2), 16. doi:10.1007/s11051-017-4092-3.

Van Den Bergh, J., Mittelmeijer-Hazeleger, M., Kapteijn, F., 2010. Modeling permeation of CO_2/CH_4, N_2/CH_4, and CO_2/air mixtures across a DD3R zeolite membrane. J. Phys. Chem. C 114 (20), 9379–9389.

Van Der Jagt, R., Vasileiadis, A., Veldhuizen, H., Shao, P., Feng, X., Ganapathy, S., Habisreutinger, N.C., van der Veen, M.A., Wang, C., Wagemaker, M., 2021. Synthesis and structure–property relationships of polyimide covalent organic frameworks for carbon dioxide capture and (aqueous) sodium-ion batteries. Chem. Mater. 33 (3), 818–833.

van Dijk, H.A.J., Walspurger, S., Cobden, P.D., van den Brink, R.W., de Vos, F.G., 2011. Testing of hydrotalcite-based sorbents for CO_2 and H2S capture for use in sorption enhanced water gas shift. Int. J. Greenh. Gas Control 5 (3), 505–511. doi:10.1016/j.ijggc.2010.04.011.

Van Gerven, T., Stankiewicz, A., 2009. Structure, energy, synergy, time-the fundamentals of process intensification. Ind. Eng. Chem. Res. 48 (5), 2465–2474. doi:10.1021/ie801501y.

Veerabhadrappa, M.G., Maroto-Valer, M.M., Chen, Y., Garcia, S., 2021. Layered double hydroxides-based mixed metal oxides: development of novel structured sorbents for CO_2 capture applications. ACS Appl. Mater. Interfaces 13 (10), 11805–11813. doi:10.1021/acsami.0c20457.

Vega, F., Baena-Moreno, F.M., Gallego Fernández, L.M., Portillo, E., Navarrete, B., Zhang, Z., 2020. Current status of CO_2 chemical absorption research applied to CCS: Towards full deployment at industrial scale. Appl. Energy 260. doi:10.1016/j.apenergy.2019.114313.

Veneman, R., Frigka, N., Zhao, W., Li, Z., Kersten, S., Brilman, W., 2015. Adsorption of H2O and CO_2 on supported amine sorbents. Int. J. Greenh. Gas Control 41, 268–275. doi:10.1016/j.ijggc.2015.07.014.

Vera, E., García, S., Maroto-Valer, M.M., Pfeiffer, H., 2019. CO_2–CO capture and kinetic analyses of sodium cobaltate under various partial pressures. Adsorption doi:10.1007/s10450-019-00167-6.

Verdoliva, V., Saviano, M., De Luca, S., 2019. Zeolites as acid/basic solid catalysts: recent synthetic developments. Catalysts 9 (3), 248.

Verma, P., Kuwahara, Y., Mori, K., Raja, R., Yamashita, H., 2020. Functionalized mesoporous SBA-15 silica: recent trends and catalytic applications. Nanoscale 12 (21), 11333–11363. doi:10.1039/d0nr00732c.

Verougstraete, B., Martín-Calvo, A., Van der Perre, S., Baron, G., Finsy, V., Denayer, J.F.M., 2020. A new honeycomb carbon monolith for CO_2 capture by rapid temperature swing adsorption using steam regeneration. Chem. Eng. J. 383. doi:10.1016/j.cej.2019.123075.

Verougstraete, B., Schoukens, M., Sutens, B., Vanden Haute, N., De Vos, Y., Rombouts, M., Denayer, J.F.M., 2022. Electrical swing adsorption on 3D-printed activated carbon monoliths for CO_2 capture from biogas. Sep. Purif. Technol. 299. doi:10.1016/j.seppur.2022.121660.

Versteeg, P., Rubin, E.S., 2011. A technical and economic assessment of ammonia-based post-combustion CO_2 capture at coal-fired power plants. Int. J. Greenh. Gas Control 5 (6), 1596–1605. doi:10.1016/j.ijggc.2011.09.006.

Versteeg, G., van Swaaij, W.b., 1988. On the kinetics between CO_2 and alkanolamines both in aqueous and non-aqueous solutions—II. Tertiary amines. Chem. Eng. Sci. 43 (3), 587–591.

Veselovskaya, J.V., Derevschikov, V.S., Kardash, T.Y., Stonkus, O.A., Trubitsina, T.A., Okunev, A.G., 2013. Direct CO_2 capture from ambient air using K2CO3/Al2O3 composite sorbent. Int. J. Greenh. Gas Control 17, 332–340. doi:10.1016/j.ijggc.2013.05.006.

Vicent-Luna, J.M., Gutiérrez-Sevillano, J.J., Hamad, S., Anta, J., Calero, S., 2018. Role of ionic liquid [EMIM]+[SCN]− in the adsorption and diffusion of gases in metal–organic frameworks. ACS Appl. Mater. Interfaces 10 (35), 29694–29704. doi:10.1021/acsami.8b11842.

Vinayakumar, K., Palliyarayil, A., Kumar, N.S., Sil, S., 2022a. Processing of aerogels and their applications toward CO_2 adsorption and electrochemical reduction: a review. Environ. Sci. Pollut. Res. doi:10.1007/s11356-022-20355-2.

Vinayakumar, K., Palliyarayil, A., Kumar, N.S., Sil, S., 2022b. Processing of aerogels and their applications toward CO_2 adsorption and electrochemical reduction: a review. Environ. Sci. Pollut. Res. 29 (32), 47942–47968. doi:10.1007/s11356-022-20355-2.

Vlahostergios, Z., Misirlis, D., Papadopoulos, A.I., Seferlis, P., 2020. Investigation of the flow field development inside a rotating packed bed with the use of CFD. Chem. Eng. Trans. 81, 883–888. doi:10.3303/CET2081148.

Volkart, K., Bauer, C., Boulet, C., 2013. Life cycle assessment of carbon capture and storage in power generation and industry in Europe. Int. J. Greenh. Gas Control 16, 91–106. doi:10.1016/j.ijggc.2013.03.003.

von Hippel, T., 2018. Thermal removal of carbon dioxide from the atmosphere: energy requirements and scaling issues. Clim. Change 148 (4), 491–501. doi:10.1007/s10584-018-2208-0.

Voon, B.K., Shen Lau, H., Liang, C.Z., Yong, W.F., 2022. Functionalized two-dimensional g-C3N4 nanosheets in PIM-1 mixed matrix membranes for gas separation. Sep. Purif. Technol. 296. doi:10.1016/j.seppur.2022.121354.

Vu, A.-T., Ho, K., Jin, S., Lee, C.-H., 2016. Double sodium salt-promoted mesoporous MgO sorbent with high CO 2 sorption capacity at intermediate temperatures under dry and wet conditions. Chem. Eng. J. 291, 161–173.

Wahono, S.K., Dwiatmoko, A.A., Cavallaro, A., Indirathankam, S.C., Addai-Mensah, J., Skinner, W., Vinu, A., Vasilev, K., 2021. Amine-functionalized natural zeolites prepared through plasma polymerization for enhanced carbon dioxide adsorption. Plasma Processes Polym. 18 (8). doi:10.1002/ppap.202100028.

Wai, S.K., Nwaoha, C., Saiwan, C., Idem, R., Supap, T., 2018. Absorption heat, solubility, absorption and desorption rates, cyclic capacity, heat duty, and absorption kinetic modeling of AMP–DETA blend for post–combustion CO_2 capture. Sep. Purif. Technol. 194, 89–95. doi:10.1016/j.seppur.2017.11.024.

Wall, T., Liu, Y., Spero, C., Elliott, L., Khare, S., Rathnam, R., Zeenathal, F., Moghtaderi, B., Buhre, B., Sheng, C., 2009a. An overview on oxyfuel coal combustion—State of the art research and technology development. Chem. Eng. Res. Des. 87 (8), 1003–1016.

Wall, T., Liu, Y., Spero, C., Elliott, L., Khare, S., Rathnam, R., Zeenathal, F., Moghtaderi, B., Buhre, B., Sheng, C., 2009b. An overview on oxyfuel coal combustion—State of the art research and technology development. Chem. Eng. Res. Des. 87 (8), 1003–1016.

Walters, M.S., Edgar, T.F., Rochelle, G.T., 2016. Dynamic modeling and control of an intercooled absorber for post-combustion CO_2 capture. Chem. Eng. Process.: Process Intensif. 107, 1–10. doi:10.1016/j.cep.2016.05.012.

Walton, K.S., Abney, M.B., LeVan, M.D., 2006. CO_2 adsorption in Y and X zeolites modified by alkali metal cation exchange. Microporous Mesoporous Mater. 91 (1-3), 78–84.

Wan, S., Guo, J., Kim, J., Ihee, H., Jiang, D., 2008. A belt-shaped, blue luminescent, and semiconducting covalent organic framework. Angew. Chem. Int. Ed. 47 (46), 8826–8830.

Wang, Z., Cohen, S.M., 2007. Postsynthetic covalent modification of a neutral metal–organic framework. J. Am. Chem. Soc. 129 (41), 12368–12369.

Wang, B., Gan, Z.H., 2014. Feasibility analysis of cryocooler based small scale CO_2 cryogenic capture. Comment on “Energy analysis of the cryogenic CO_2 process based on Stirling coolers” Song CF, Kitamura Y, Li SH [Energy 2014; 65: 580–89]. Energy 68, 1000–1003. doi:10.1016/j.energy.2014.02.032.

Wang, X., Song, C., 2020a. Carbon capture from flue gas and the atmosphere: a perspective. Front. Energy Res. 8. doi:10.3389/fenrg.2020.560849.

Wang, X., Song, C., 2020b. Carbon capture from flue gas and the atmosphere: A perspective. Front. Energy Res. 8, 560849.

Wang, S., Yan, S., Ma, X., Gong, J., 2011. Recent advances in capture of carbon dioxide using alkali-metal-based oxides. Energy Environ. Sci. 4 (10), 3805–3819.

Wang, M., Lawal, A., Stephenson, P., Sidders, J., Ramshaw, C., 2011. Post-combustion CO_2 capture with chemical absorption: A state-of-the-art review. Chem. Eng. Res. Des. 89 (9), 1609–1624. doi:10.1016/j.cherd.2010.11.005.

Wang, Q., Luo, J., Zhong, Z., Borgna, A., 2011. CO_2 capture by solid adsorbents and their applications: current status and new trends. Energy Environ. Sci. 4 (1), 42–55. doi:10.1039/C0EE00064G.

Wang, L., Liu, Z., Li, P., Yu, J., Rodrigues, A.E., 2012. Experimental and modeling investigation on post-combustion carbon dioxide capture using zeolite 13X-APG by hybrid VTSA process. Chem. Eng. J. 197, 151–161. doi:10.1016/j.cej.2012.05.017.

Wang, X., Li, H., Hou, X.-J., 2012. Amine-functionalized metal organic framework as a highly selective adsorbent for CO_2 over CO. J. Phys. Chem. C 116 (37), 19814–19821. doi:10.1021/jp3052938.

Wang, J., Wang, M., Zhao, B., Qiao, W., Long, D., Ling, L., 2013. Mesoporous carbon-supported solid amine sorbents for low-temperature carbon dioxide capture. Ind. Eng. Chem. Res. 52 (15), 5437–5444. doi:10.1021/ie303388h.

Wang, X., Akhmedov, N.G., Duan, Y., Luebke, D., Li, B., 2013. Immobilization of amino acid ionic liquids into nanoporous microspheres as robust sorbents for CO_2 capture. J. Mater. Chem. A 1 (9), 2978–2982. doi:10.1039/C3TA00768E.

Wang, Y., Chen, J., Larachi, F., 2013. Modelling and simulation of trickle-bed reactors using computational fluid dynamics: A state-of-the-art review. Canadian Journal of Chemical Engineering 91 (1), 136–180.

Wang, L., Yang, Y., Shen, W., Kong, X., Li, P., Yu, J., Rodrigues, A.E., 2013a. CO_2 capture from flue gas in an existing coal-fired power plant by two successive pilot-scale VPSA units. Ind. Eng. Chem. Res. 52 (23), 7947–7955. doi:10.1021/ie4009716.

Wang, L., Yang, Y., Shen, W., Kong, X., Li, P., Yu, J., Rodrigues, A.E., 2013b. Experimental evaluation of adsorption technology for CO_2 capture from flue gas in an existing coal-fired power plant. Chem. Eng. Sci. 101, 615–619. doi:10.1016/j.ces.2013.07.028.

Wang, C., Zhou, X., Jia, L., Tan, Y., 2014. Sintering of limestone in calcination/carbonation cycles. Ind. Eng. Chem. Res. 53 (42), 16235–16244. doi:10.1021/ie502069d.

Wang, T., Huang, J., He, X., Wu, J., Fang, M., Cheng, J., 2014. CO_2 fertilization system integrated with a low-cost direct air capture technology. Energy Procedia 63, 6842–6851. doi:10.1016/j.egypro.2014.11.718.

Wang, X., Song, C., Gaffney, A.M., Song, R., 2014. New molecular basket sorbents for CO_2 capture based on mesoporous sponge-like TUD-1. Catal. Today 238, 95–102. doi:10.1016/j.cattod.2014.02.022.

Wang, J.Y., Huang, L., Yang, R.Y., Zhang, Z., Wu, J.W., Gao, Y.S., Wang, Q., O'Hare, D., Zhong, Z.Y., 2014. Recent advances in solid sorbents for CO_2 capture and new development trends. Energy Environ. Sci. 7 (11), 3478–3518. doi:10.1039/c4ee01647e.

Wang, J., Huang, H., Wang, M., Yao, L., Qiao, W., Long, D., Ling, L., 2015. Direct capture of low-concentration CO_2 on mesoporous carbon-supported solid amine adsorbents at ambient temperature. Ind. Eng. Chem. Res. 54 (19), 5319–5327. doi:10.1021/acs.iecr.5b01060.

Wang, M., Joel, A.S., Ramshaw, C., Eimer, D., Musa, N.M., 2015. Process intensification for post-combustion CO_2 capture with chemical absorption: A critical review. Appl. Energy 158, 275–291. doi:10.1016/j.apenergy.2015.08.083.

Wang, S., Li, X., Wu, H., Tian, Z., Xin, Q., He, G., Peng, D., Chen, S., Yin, Y., Jiang, Z., Guiver, M.D., 2016. Advances in high permeability polymer-based membrane materials for CO_2 separations. Energy Environ. Sci. 9 (6), 1863–1890. doi:10.1039/C6EE00811A.

Wang, T., Yu, W., Liu, F., Fang, M., Farooq, M., Luo, Z., 2016. Enhanced CO_2 absorption and desorption by monoethanolamine (MEA)-based nanoparticle suspensions. Ind. Eng. Chem. Res. 55 (28), 7830–7838. doi:10.1021/acs.iecr.6b00358.

Wang, J., Zhao, J., Wang, Y., Deng, S., Sun, T., Li, K., 2017. Application potential of solar-assisted post-combustion carbon capture and storage (CCS) in China: A life cycle approach. J. Clean. Prod. 154, 541–552. doi:10.1016/j.jclepro.2017.04.021.

Wang, L., Zhou, Z.M., Hu, Y.W., Cheng, Z.M., Fang, X.C., 2017. Nanosheet MgO-Based CO_2 sorbent promoted by mixed-alkali-metal nitrate and carbonate: performance and mechanism. Ind. Eng. Chem. Res. 56 (20), 5802–5812. doi:10.1021/acs.iecr.7b00483.

Wang, S., Guo, W., Gao, F., Yang, R., 2017. Characterization and Pb (II) removal potential of corn straw- and municipal sludge-derived biochars. R. Soc. Open Sci. 4 (9), 170402. doi:10.1098/rsos.170402.

Wang, Z., Ren, H., Zhang, S., Zhang, F., Jin, J.J., 2017. Polymers of intrinsic microporosity/metal–organic framework hybrid membranes with improved interfacial interaction for high-performance CO 2 separation. 5 (22), 10968-10977.

Wang, F., Zhao, J., Miao, H., Zhao, J., Zhang, H., Yuan, J., Yan, J., 2018. Current status and challenges of the ammonia escape inhibition technologies in ammonia-based CO_2 capture process. Appl. Energy 230, 734–749.

Wang, H., He, S., Qin, X., Li, C., Li, T., 2018. Interfacial engineering in metal–organic framework-based mixed matrix membranes using covalently grafted polyimide brushes. J. Am. Chem. Soc. 140 (49), 17203–17210. doi:10.1021/jacs.8b10138.

Wang, H., Zhang, J., Wang, G., Wang, Q., Song, T., 2018. High-temperature capture of CO_2 by Li_4SiO_4 prepared with blast furnace slag and kinetic analysis. J. Therm. Anal. Calorim. 133 (2), 981–989. doi:10.1007/s10973-018-7167-1.

Wang, C., Cao, F., Ruan, Y., Jia, X., Zhen, W., Jiang, X., 2019. Specific generation of singlet oxygen through the russell mechanism in hypoxic tumors and GSH depletion by Cu-TCPP nanosheets for cancer therapy. Angew. Chem. Int. Ed. 131 (29), 9951–9955. doi:10.1002/anie.201903981.

Wang, P., Sun, J., Guo, Y., Zhao, C., Li, W., Wang, G., Lei, S., Lu, P., 2019. Structurally improved, urea-templated, K_2CO_3-based sorbent pellets for CO_2 capture. Chem. Eng. J. 374, 20–28. doi:10.1016/j.cej.2019.05.091.

Wang, R., Liu, S., Wang, L., Li, Q., Zhang, S., Chen, B., Jiang, L., Zhang, Y., 2019. Superior energy-saving splitter in monoethanolamine-based biphasic solvents for CO_2 capture from coal-fired flue gas. Appl. Energy 242, 302–310. doi:10.1016/j.apenergy.2019.03.138.

Wang, S., Bai, P., Sun, M., Liu, W., Li, D., Wu, W., Yan, W., Shang, J., Yu, J., 2019. Fabricating mechanically robust binder-free structured zeolites by 3d printing coupled with zeolite soldering: a superior configuration for CO_2 capture. Adv. Sci. 6 (17), 1901317.

Wang, X., Shan, M., Liu, X., Wang, M., Doherty, C.M., Osadchii, D., Kapteijn, F., 2019. High-performance polybenzimidazole membranes for helium extraction from natural gas. ACS Appl. Mater. Interfaces 11 (22), 20098–20103. doi:10.1021/acsami.9b05548.

Wang, X., Shang, D., Zeng, S., Wang, Y., Zhang, X., Zhang, X., Liu, J., 2019. Enhanced CO_2 capture by binary systems of pyridinium-based ionic liquids and porous ZIF-8 particles. J. Chem. Thermodyn. 128, 415–423. doi:10.1016/j.jct.2018.08.038.

Wang, K., Hong, J., Zhou, Z., Lin, Z., Zhao, P., 2019. Development of alkali nitrate-containing Li_4SiO_4 for high-temperature CO_2 capture. Energy Technol. 7 (2), 325–332. doi:10.1002/ente.201800229.

Wang, W.J., Chen, M., Huang, D.L., Zeng, G.M., Zhang, C., Lai, C., Zhou, C.Y., Yang, Y., Cheng, M., Hu, L., Xiong, W.P., Li, Z.H., Wang, Z.W., 2019a. An overview on nitride and nitrogen-doped photocatalysts for energy and environmental applications. Composit. Part B-Eng. 172, 704–723. doi:10.1016/j.compositesb.2019.05.097.

Wang, W.J., Motuzas, J., Zhao, X.S., da Costa, J.C.D., 2019b. 2D/3D amine functionalised sorbents containing graphene silica aerogel and mesoporous silica with improved CO_2 sorption. Sep. Purif. Technol. 222, 381–389. doi:10.1016/j.seppur.2019.04.050.

Wang, B., Qiao, Z., Xu, J., Wang, J., Liu, X., Zhao, S., Wang, Z., Guiver, M.D., 2020. Unobstructed ultrathin gas transport channels in composite membranes by interfacial self-assembly. Adv. Mater. 32 (22), 1907701. doi:10.1002/adma.201907701.

Wang, C., Guo, F., Li, H., Xu, J., Hu, J., Liu, H., Wang, M., 2020. A porous ionic polymer bionic carrier in a mixed matrix membrane for facilitating selective CO_2 permeability. J. Membr. Sci. 598, 117677. doi:10.1016/j.memsci.2019.117677.

Wang, T., Wang, X., Hou, C., Liu, J., 2020. Quaternary functionalized mesoporous adsorbents for ultra-high kinetics of CO_2 capture from air. Sci. Rep. 10 (1), 21429. doi:10.1038/s41598-020-77477-1.

Wang, Y.L., Guo, B.H., Guo, J.N., Zhang, M., Yang, H.R., Jin, Y., 2020. K2CO3-impregnated Al/Si aerogel prepared by ambient pressure drying for CO (2)Capture: synthesis, characterization and adsorption characteristics. Materials 13 (17). doi:10.3390/ma13173741.

Wang, Z., Shen, Q., Liang, J., Zhang, Y., Jin, J., 2020. Adamantane-grafted polymer of intrinsic microporosity with finely tuned interchain spacing for improved CO_2 separation performance. Sep. Purif. Technol. 233, 116008.

Wang, H., Wang, H., Liu, G., Yan, Q., 2021. In-situ pyrolysis of Taihu blue algae biomass as appealing porous carbon adsorbent for CO_2 capture: Role of the intrinsic N. Sci. Total Environ. 771, 145424. doi:10.1016/j.scitotenv.2021.145424.

Wang, J., Fu, J., Zeng, X., 2021. Research on dynamic modelling of amine-based carbon capture pilot plant based on gCCS. Proc. CSEE 41 (18), 6340–6350. doi:10.13334/j.0258-8013.pcsee.201642.

Wang, J., Guo, Z., Deng, S., Zhao, R., Chen, L., Xue, J., 2021. A rapid multi-objective optimization of pressure and temperature swing adsorption for CO_2 capture based on simplified equilibrium model. Sep. Purif. Technol. 279. doi:10.1016/j.seppur.2021.119663.

Wang, Y., Zhang, N., Wu, H., Ren, Y., Yang, L., Wang, X., Wu, Y., Liu, Y., Zhao, R., Jiang, Z., 2021. Exfoliation-free layered double hydroxides laminates intercalated with amino acids for enhanced CO_2 separation of mixed matrix membrane. J. Membr. Sci. 618, 118691. doi:10.1016/j.memsci.2020.118691.

Wang, J., Chen, S., Xu, J.-y., Liu, L.-c., Zhou, J.-c., Cai, J.-j., 2021. High-surface-area porous carbons produced by the mild KOH activation of a chitosan hydrochar and their CO_2 capture. New Carbon Mater. 36 (6), 1081–1090. doi:10.1016/S1872-5805(21)60074-4.

Wang, S., Wu, J., Ma, N., Chen, S., 2021. High molecular weight polyethylenimine encapsulated into a porous polymer monolithic by one-step polymerization for CO_2 capture. New J. Chem. 45 (28), 12538–12548. doi:10.1039/d1nj01288f.

Wang, Y., Pan, Z., Zhang, W., Borhani, T.N., Li, R., Zhang, Z., 2022. Life cycle assessment of combustion-based electricity generation technologies integrated with carbon capture and storage: A review. Environ. Res. 207, 112219. doi:10.1016/j.envres.2021.112219.

Wang, S., Qiu, X., Chen, Y., Chen, S., 2022. Preparation and structure tuning of CO_2 adsorbent based on in-situ amine-functionalized hierarchical porous polymer. Microporous Mesoporous Mater. 330. doi:10.1016/j.micromeso.2021.111585.

Ward, J., Habgood, H., 1966. The infrared spectra of carbon dioxide adsorbed on zeolite X. J. Phys. Chem. 70 (4), 1178–1182.

Wawrzyńczak, D., Majchrzak-Kucęba, I., Srokosz, K., Kozak, M., Nowak, W., Zdeb, J., Smółka, W., Zajchowski, A., 2019. The pilot dual-reflux vacuum pressure swing adsorption unit for CO_2 capture from flue gas. Sep. Purif. Technol. 209, 560–570. doi:10.1016/j.seppur.2018.07.079.

Webley, P.A., 2014. Adsorption technology for CO_2 separation and capture: a perspective. Adsorption 20 (2-3), 225–231. doi:10.1007/s10450-014-9603-2.

Wei, J., Shi, J., Pan, H., Zhao, W., Ye, Q., Shi, Y., 2008. Adsorption of carbon dioxide on organically functionalized SBA-16. Microporous Mesoporous Mater. 116 (1-3), 394–399. doi:10.1016/j.micromeso.2008.04.028.

Wei, L., Guo, R.F., Tang, Y.Q., Zhu, J.M., Liu, M.Y., Chen, J.Q., Xu, Y., 2020. Properties of aqueous amine based protic ionic liquids and its application for CO_2 quick capture. Sep. Purif. Technol. 239. doi:10.1016/j.seppur.2020.116531.

Weidong, Z., Dong, Z., Kezhong, T., 2009. Carbon capture and sequestration technology. Sino-Glob. Energy 14 (11), 7–14.

Wen, X., et al., 2007. CFD modeling of columns equipped with structured packings: I. Approach based on detailed packing geometry. Asia-Pacific Journal of Chemical Engineering 2 (4), 336–344.

Wen, J.J., Gu, F.N., Wei, F., Zhou, Y., Lin, W.G., Yang, J., Yang, J.Y., Wang, Y., Zou, Z.G., Zhu, J.H., 2010. One-pot synthesis of the amine-modified meso-structured monolith CO_2 adsorbent. J. Mater. Chem. 20 (14). doi:10.1039/b920027d.

White, J.C., Dutta, P.K., Shqau, K., Verweij, H., 2010. Synthesis of ultrathin zeolite Y membranes and their application for separation of carbon dioxide and nitrogen gases. Langmuir 26 (12), 10287–10293.

Widenmeyer, M., Wiegers, K.S., Chen, G., Yoon, S., Feldhoff, A., Weidenkaff, A., 2020. Engineering of oxygen pathways for better oxygen permeability in Cr-substituted Ba2In2O5 membranes. J. Membr. Sci. 595, 117558. doi:10.1016/J.MEMSCI.2019.117558.

Wijmans, J.G., Baker, R.W., 1995. The solution-diffusion model: a review. J. Membr. Sci. 107 (1-2), 1–21. doi:10.1016/0376-7388 (95)00102-I.

Wilcox, J., Haghpanah, R., Rupp, E.C., He, J., Lee, K., 2014. Advancing adsorption and membrane separation processes for the gigaton carbon capture challenge. Annu. Rev. Chem. Biomol. Eng. 5, 479–505. doi:10.1146/annurev-chembioeng-060713-040100.

Williams, R., Burt, L.A., Esposito, E., Jansen, J.C., Tocci, E., Rizzuto, C., Lanč, M., Carta, M., McKeown, N.B.J.J.o.M.C.A., 2018. A highly rigid and gas selective methanopentacene-based polymer of intrinsic microporosity derived from Tröger's base polymerization. 6 (14), 5661-5667.

Wilm, L.F.B., Das, M., Janssen-Muller, D., Muck-Lichtenfeld, C., Glorius, F., Dielmann, F., 2022. Photoswitchable nitrogen superbases: using light for reversible carbon dioxide capture. Angew. Chem. Int. Ed. Engl. 61 (3), e202112344. doi:10.1002/anie.202112344.

Wirawan, S.K., Creaser, D., 2006a. CO_2 adsorption on silicalite-1 and cation exchanged ZSM-5 zeolites using a step change response method. Microporous Mesoporous Mater. 91 (1-3), 196–205.

Wirawan, S.K., Creaser, D., 2006b. Multicomponent H2/CO/CO_2 adsorption on BaZSM-5 zeolite. Sep. Purif. Technol. 52 (2), 224–231.

Wirawan, S.K., Creaser, D., Lindmark, J., Hedlund, J., Bendiyasa, I.M., Sediawan, W.B., 2011. H2/CO_2 permeation through a silicalite-1 composite membrane. J. Membr. Sci. 375 (1-2), 313–322.

Woo, K.T., Dong, G., Lee, J., Kim, J.S., Do, Y.S., Lee, W.H., Lee, H.S., Lee, Y.M., 2016a. Ternary mixed-gas separation for flue gas CO_2 capture using high performance thermally rearranged (TR) hollow fiber membranes. J. Membr. Sci. 510, 472–480.

Woo, K.T., Lee, J., Dong, G., Kim, J.S., Do, Y.S., Jo, H.J., Lee, Y.M., 2016b. Thermally rearranged poly (benzoxazole-co-imide) hollow fiber membranes for CO_2 capture. J. Membr. Sci. 498, 125–134.

Wormeyer, K., Smirnova, I., 2013. Adsorption of CO_2, moisture and ethanol at low partial pressure using aminofunctionalised silica aerogels. Chem. Eng. J. 225, 350–357. doi:10.1016/j.cej.2013.02.022.

Wormeyer, K., Alnaief, M., Smirnova, I., 2012. Amino functionalised Silica-Aerogels for CO_2-adsorption at low partial pressure. Adsorpt.-J. Int. Adsorpt. Soc. 18 (3-4), 163–171. doi:10.1007/s10450-012-9390-6.

Wu, Y., Wang, C., Tan, Y., Jia, L., Anthony, E.J., 2011. Characterization of ashes from a 100kWth pilot-scale circulating fluidized bed with oxy-fuel combustion. Appl. Energy 88 (9), 2940–2948. doi:10.1016/j.apenergy.2011.03.007.

Wu, H., Chua, Y.S., Krungleviciute, V., Tyagi, M., Chen, P., Yildirim, T., Zhou, W., 2013. Unusual and highly tunable missing-linker defects in zirconium metal–organic framework UiO-66 and their important effects on gas adsorption. J. Am. Chem. Soc. 135 (28), 10525–10532. doi:10.1021/ja404514r.

Wu, H., Li, X., Li, Y., Wang, S., Guo, R., Jiang, Z., Wu, C., Xin, Q., Lu, X., 2014. Facilitated transport mixed matrix membranes incorporated with amine functionalized MCM-41 for enhanced gas separation properties. J. Membr. Sci. 465, 78–90. doi:10.1016/j.memsci.2014.04.023.

Wu, X., Tian, Z., Wang, S., Peng, D., Yang, L., Wu, Y., Xin, Q., Wu, H., Jiang, Z., 2017. Mixed matrix membranes comprising polymers of intrinsic microporosity and covalent organic framework for gas separation. J. Membr. Sci. 528, 273–283. doi:10.1016/j.memsci.2017.01.042.

Wu, F., Argyle, M.D., Dellenback, P.A., Fan, M., 2018. Progress in O_2 separation for oxy-fuel combustion–A promising way for cost-effective CO_2 capture: A review. Prog. Energy Combust. Sci. 67, 188–205. doi:10.1016/j.pecs.2018.01.004.

Wu, Q., Gao, M., Zhang, G., Zhang, Y., Liu, S., Xie, C., Yu, H., Liu, Y., Huang, L., Yu, S., 2019. Preparation and application performance study of biomass-based carbon materials with various morphologies by a hydrothermal/soft template method. Nanotechnology 30 (18). doi:10.1088/1361-6528/ab0042.

Wu, J., Lv, B., Wu, X., Zhou, Z., Jing, G., 2019. Aprotic heterocyclic anion-based dual-functionalized ionic liquid solutions for efficient CO_2 uptake: quantum chemistry calculation and experimental research. ACS Sustain. Chem. Eng. 7 (7), 7312–7323. doi:10.1021/acssuschemeng.9b00420.

Wu, X., Wang, M., Liao, P., Shen, J., Li, Y., 2020. Solvent-based post-combustion CO_2 capture for power plants: A critical review and perspective on dynamic modelling, system identification, process control and flexible operation. Appl. Energy 257. doi:10.1016/j.apenergy.2019.113941.

Wu, Y., Chen, X., Ma, J., Wu, Y., Liu, D., Xie, W., 2020. System integration optimization for coal-fired power plant with CO_2 capture by Na_2CO_3 dry sorbents. Energy 211, 118554. doi:10.1016/j.energy.2020.118554.

Wu, J.J., Qiu, X.Y., Chen, S.X., 2022. Preparation and characterization of an amine-modified graphene aerogel for enhanced carbon dioxide adsorption. J. Mater. Sci. 57 (3), 1727–1737. doi:10.1007/s10853-021-06768-3.

Wurzbacher, J.A., Gebald, C., Steinfeld, A., 2011. Separation of CO_2 from air by temperature-vacuum swing adsorption using diamine-functionalized silica gel. Energy Environ. Sci. 4 (9). doi:10.1039/c1ee01681d.

Wurzbacher, J.A., Gebald, C., Piatkowski, N., Steinfeld, A., 2012. Concurrent separation of CO_2 and H2O from air by a temperature-vacuum swing adsorption/desorption cycle. Environ. Sci. Technol. 46 (16), 9191–9198. doi:10.1021/es301953k.

Wurzbacher, J.A., Gebald, C., Brunner, S., Steinfeld, A., 2016. Heat and mass transfer of temperature–vacuum swing desorption for CO_2 capture from air. Chem. Eng. J. 283, 1329–1338. doi:10.1016/j.cej.2015.08.035.

X Li, J.H., Guo, R., Wang, Z., Zhang, J., 2019. Constructing unique cross-sectional structured mixed matrix membranes by incorporating ultrathin microporous nanosheets for efficient CO_2 separation. ACS Appl. Mater. Interfaces 11 (27), 24618–24626. doi:10.1021/acsami.9b07815.

Xia, Y., Zhu, Y., Tang, Y., 2012. Preparation of sulfur-doped microporous carbons for the storage of hydrogen and carbon dioxide. Carbon 50 (15), 5543–5553. doi:10.1016/j.carbon.2012.07.044.

Xian, S., Wu, Y., Wu, J., Wang, X., Xiao, J., 2015a. Enhanced dynamic CO_2 adsorption capacity and CO_2/CH4 selectivity on polyethylenimine-impregnated UiO-66. Ind. Eng. Chem. Res. 54 (44), 11151–11158. doi:10.1021/acs.iecr.5b03517.

Xian, S., Xu, F., Ma, C., Wu, Y., Xia, Q., Wang, H., Li, Z., 2015b. Vapor-enhanced CO_2 adsorption mechanism of composite PEI@ZIF-8 modified by polyethyleneimine for CO_2/N_2 separation. Chem. Eng. J. 280, 363–369. doi:10.1016/j.cej.2015.06.042.

Xiao, M., Liu, H., Idem, R., Tontiwachwuthikul, P., Liang, Z., 2016. A study of structure–activity relationships of commercial tertiary amines for post-combustion CO_2 capture. Appl. Energy 184, 219–229. doi:10.1016/j.apenergy.2016.10.006.

Xiao, J., Wang, Y., Zhang, T.C., Ouyang, L., Yuan, S., 2022. Phytic acid-induced self-assembled chitosan gel-derived N, P–co-doped porous carbon for high-performance CO_2 capture and supercapacitor. J. Power Sources 517, 230727. doi:10.1016/j.jpowsour.2021.230727.

Xiao, Y., Raheem, A., Ding, L., Chen, W.-H., Chen, X., Wang, F., Lin, S.-L., 2022. Pretreatment, modification and applications of sewage sludge-derived biochar for resource recovery- A review. Chemosphere 287, 131969. doi:10.1016/j.chemosphere.2021.131969.

Xie, Y., Zhang, Y., Lu, X., Ji, X., 2014. Energy consumption analysis for CO_2 separation using imidazolium-based ionic liquids. Appl. Energy 136, 325–335. doi:10.1016/j.apenergy.2014.09.046.

Xie, W.J., Yu, M.Q., Wang, R., 2017. CO_2 capture behaviors of amine-modified resorcinol-based carbon aerogels adsorbents. Aerosol. Air Qual. Res. 17 (11), 2715–2725. doi:10.4209/aaqr.2016.12.0597.

Xie, K., Fu, Q., Webley, P.A., Qiao, G.G., 2018. MOF scaffold for a high-performance mixed-matrix membrane. Angew. Chem. Int. Ed. 130 (28), 8733–8738. doi:10.1002/anie.201804162.

Xie, P., et al., 2019. A mesoscale 3D CFD analysis of the liquid flow in a rotating packed bed. Chemical Engineering Science 199, 528–545.

Xie, Y.Q., Wang, L., Li, H.L., Westholm, L.J., Carvalho, L., Thorin, E., Yu, Z.X., Yu, X.H., Skreiberg, O., 2022. A critical review on production, modification and utilization of biochar. J. Analyt. Appl. Pyrol. 161. doi:10.1016/j.jaap.2021.105405.

Xing, L., Wei, K., Li, Y., Fang, Z., Li, Q., Qi, T., An, S., Zhang, S., Wang, L., 2021. TiO2 coating strategy for robust catalysis of the metal–organic framework toward energy-efficient CO_2 capture. Environ. Sci. Technol. 55 (16), 11216–11224. doi:10.1021/acs.est.1c02452.

Xiong, J., Zhao, H., Zheng, C., 2011. Exergy analysis of a 600 MWe oxy-combustion pulverized-coal-fired power plant. Energy Fuels 25 (8), 3854–3864. doi:10.1021/EF200702K.

Xiong, J., Zhao, H., Zheng, C., 2012. Thermoeconomic cost analysis of a 600 MWe oxy-combustion pulverized-coal-fired power plant. Int. J. Greenh. Gas Control 9, 469–483. doi:10.1016/J.IJGGC.2012.05.012.

Xiong, Z., Shihong, Z., Haiping, Y., Tao, S., Yingquan, C., Hanping, C., 2013. Influence of $NH3/CO_2$ modification on the characteristic of biochar and the CO_2 capture. Bioenerg. Res. 6 (4), 1147–1153. doi:10.1007/s12155-013-9304-9.

Xiong, Q., Wu, X., Lv, H., Liu, S., Hou, H., Wu, X., 2021. Influence of rice husk addition on phosphorus fractions and heavy metals risk of biochar derived from sewage sludge. Chemosphere 280, 130566. doi:10.1016/j.chemosphere.2021.130566.

C Xu, X.S., Andresen, J.M, Miller, B.G, Scaroni, A.W., 2002. Novel polyethyleneimine–modified mesoporous molecular sieve of MCM-41 type as high-capacity adsorbent for CO_2 capture. Energy Fuels 16, 1463–1469.

S.C. Xu, X., Miller, B.G., Scaroni, A.W., 2005. Influence of Moisture on CO_2 Separation from Gas Mixture by a Nanoporous Adsorbent Based on Polyethylenimine-Modified Molecular Sieve MCM-41. Ind. Eng. Chem. Res. 44 (21), 8113–8119.

Xu, L., Rungta, M., Hessler, J., Qiu, W., Brayden, M., Martinez, M., Barbay, G., Koros, W.J., 2014. Physical aging in carbon molecular sieve membranes. Carbon 80, 155–166. doi:10.1016/j.carbon.2014.08.051.

Xu, X.Y., Kan, Y., Zhao, L., Cao, X.D., 2016. Chemical transformation of CO_2 during its capture by waste biomass derived biochars. Environ. Pollut. 213, 533–540. doi:10.1016/j.envpol.2016.03.013.

Xu, Y., Luo, C., Zheng, Y., Ding, H., Zhou, D., Zhang, L., 2017. Natural calcium-based sorbents doped with sea salt for cyclic CO_2 capture. J. Chem. Eng. 40 (3), 522–528.

Xu, Y., Ding, H., Luo, C., Zheng, Y., Zhang, Q., Li, X., Sun, J., Zhang, L., 2018. Potential synergy of chlorine and potassium and sodium elements in carbonation enhancement of CaO-based sorbents. ACS Sustain. Chem. Eng. 6 (9), 11677–11684. doi:10.1021/acssuschemeng.8b01941.

Xu, Y., He, Q., Chen, Y.G., 2018. A rational design of microporous aerogel for excellent CO_2 capture and selectivities via Co-synergistic effects of electrostatic in-plane and pi-pi stacking interactions (1, 2). Polym. Sci. Ser. B+ 60 (3), 317–323. doi:10.1134/S1560090418030193.

Xu, J., Wang, Z., Qiao, Z., Wu, H., Dong, S., Zhao, S., Wang, J., 2019. Post-combustion CO_2 capture with membrane process: Practical membrane performance and appropriate pressure. J. Membr. Sci. 581, 195–213. doi:10.1016/j.memsci.2019.03.052.

Xu, Y., Cui, D., Zhang, S., Xu, G., Su, Z., 2019. Facile synthesis of conjugated microporous polymer-based porphyrin units for adsorption of CO_2 and organic vapours. Polym. Chem. 10 (7), 819–822. doi:10.1039/C8PY01476K.

Xu, Y., Jin, B., Chen, X., Zhao, Y., 2019. Performance of CO_2 absorption in a spray tower using blended ammonia and piperazine solution: Experimental studies and comparisons. Int. J. Greenh. Gas Control 82, 152–161. doi:10.1016/j.ijggc.2019.01.008.

Xu, Y.C., Li, Y.B., Liu, Y.Z., Luo, Y., Chu, G.W., Zhang, L.L., Chen, J.F., 2019. Liquid jet impaction on the single-layer stainless steel wire mesh in a rotating packed bed reactor. AIChE J. 65 (6). doi:10.1002/aic.16597, e16597-e16597.

Xu, M., Wang, S., Xu, L., 2019. Screening of physical-chemical biphasic solvents for CO_2 absorption. Int. J. Greenh. Gas Control 85, 199–205. doi:10.1016/j.ijggc.2019.03.015.

Xu, X., Myers, M.B., Versteeg, F.G., Pejcic, B., Heath, C., Wood, C.D., 2020. Direct air capture (DAC) of CO_2 using polyethylenimine (PEI) “snow”: a scalable strategy. Chem. Commun. 56 (52), 7151–7154. doi:10.1039/D0CC02572K.

Xu, X.Y., Xu, Z.B., Gao, B., Zhao, L., Zheng, Y.L., Huang, J.S., Tsang, D.C.W., Ok, Y.S., Cao, X.D., 2020. New insights into CO_2 sorption on biochar/Fe oxyhydroxide composites: kinetics, mechanisms, and in situ characterization. Chem. Eng. J. 384. doi:10.1016/j.cej.2019.123289.

Xu, Y., Jin, B., Jiang, H., Li, L., Wei, J., 2020. Investigation of the regeneration of a CO_2-loaded ammonia solution with solid acid catalysts: A promising alternative for reducing regeneration energy. Fuel Process. Technol. 205, 106452.

Xu, Y., Yang, Z., Zhang, G., Zhao, P., 2020. Excellent CO_2 adsorption performance of nitrogen-doped waste biocarbon prepared with different activators. J. Clean. Prod. 264, 121645. doi:10.1016/j.jclepro.2020.121645.

Xu, J., Jia, P.P., Wang, X.J., Xie, Z.Y., Chen, Z.Y., Jiang, H., 2021. The aminosilane functionalization of cellulose nanocrystal aerogel via vapour-phase reaction and its CO_2 adsorption characteristics. J. Appl. Polym. Sci. 138 (35). doi:10.1002/app.50891.

Xu, Y., Shen, C., Lu, B., Luo, C., Wu, F., Li, X., Zhang, L., 2021. Study on the effect of NaBr modification on CaO-based sorbent for CO_2 capture and SO2 capture. Carbon Cap. Sci. Technol. 1, 100015. doi:10.1016/j.ccst.2021.100015.

Xu, Y., Donat, F., Luo, C., Chen, J., Kierzkowska, A., Awais Naeem, M., Zhang, L., Müller, C.R., 2023. Investigation of K2CO3-modified CaO sorbents for CO_2 capture using in-situ X-ray diffraction. Chem. Eng. J. 453, 139913. doi:10.1016/j.cej.2022.139913.

Xuan, Y., Yu, Q., Qin, Q., Wang, K., Duan, W., Liu, K., Zhang, P., 2018. Selection of desulfurizer and control of reaction products on flue-gas desulfurization using chemical-looping technology. Energy Fuels 32 (1), 889–900.

Xue, J., Liao, Q., Chen, W., Bouwmeester, H.J.M., Wang, H., Feldhoff, A., 2015. A new CO_2-resistant Ruddlesden–Popper oxide with superior oxygen transport: A-site deficient (Pr0.9La0.1)1.9 (Ni0.74Cu0.21Ga0.05)O4+δ. J. Mater. Chem. A 3, 19107–19114. doi:10.1039/C5TA02514A.

Xuepeng, B., 2014. CO_2 capture technologies and application. Clean Coal Technol. 20 (05) 9-13+19.

Yañez-Aulestia, A., Wang, Q., Pfeiffer, H., 2020. Enhancing CO_2 chemisorption on lithium cuprate (Li_2CuO_2) at moderate temperatures and different pressures by alkaline nitrate addition. Phys. Chem. Chem. Phys. 22 (5), 2803–2813. doi:10.1039/C9CP05512F.

Yadav, S., Mondal, S.S., 2022. A review on the progress and prospects of oxy-fuel carbon capture and sequestration (CCS) technology. Fuel 308. doi:10.1016/J.FUEL.2021.122057, 122057-122057.

Yamazaki, T., Katoh, M., Ozawa, S., Ogino, Y., 1993. Adsorption of CO_2 over univalent cation-exchanged ZSM-5 zeolites. Mol. Phys. 80 (2), 313–324.

Yan, X., Zhang, L., Zhang, Y., Qiao, K., Yan, Z., Komarneni, S., 2011a. Amine-modified mesocellular silica foams for CO_2 capture. Chem. Eng. J. 168 (2), 918–924. doi:10.1016/j.cej.2011.01.066.

Yan, X., Zhang, L., Zhang, Y., Yang, G., Yan, Z., 2011b. Amine-modified SBA-15: effect of pore structure on the performance for CO_2 capture. Ind. Eng. Chem. Res. 50 (6), 3220–3226. doi:10.1021/ie101240d.

Yan, Q., Lin, Y., Kong, C., Chen, L., 2013. Remarkable CO_2/CH4 selectivity and CO_2 adsorption capacity exhibited by polyamine-decorated metal-organic framework adsorbents. Chem. Commun. (Camb.) 49 (61), 6873–6875. doi:10.1039/c3cc43352h.

Yan, X., Komarneni, S., Yan, Z., 2013. CO_2 adsorption on santa barbara amorphous-15 (SBA-15) and amine-modified santa barbara amorphous-15 (SBA-15) with and without controlled microporosity. J. Colloid. Interface Sci. 390 (1), 217–224. doi:10.1016/j.jcis.2012.09.038.

Yan, X., Komarneni, S., Zhang, Z., Yan, Z., 2014. Extremely enhanced CO_2 uptake by HKUST-1 metal–organic framework via a simple chemical treatment. Microporous Mesoporous Mater. 183, 69–73. doi:10.1016/j.micromeso.2013.09.009.

Yan, H., Fu, Q., Zhou, Y., Li, D., Zhang, D., 2016. CO_2 capture from dry flue gas by pressure vacuum swing adsorption: A systematic simulation and optimization. Int. J. Greenh. Gas Control 51, 1–10. doi:10.1016/j.ijggc.2016.04.005.

Yan, S., Zhu, D., Zhang, Z., Li, H., Chen, G., Liu, B., 2019. A pilot-scale experimental study on CO_2 capture using Zeolitic imidazolate framework-8 slurry under normal pressure. Appl. Energy 248, 104–114. doi:10.1016/j.apenergy.2019.04.097.

Yan, Y., Borhani, T.N., Subraveti, S.G., Pai, K.N., Prasad, V., Rajendran, A., Nkulikiyinka, P., Asibor, J.O., Zhang, Z., Shao, D., Wang, L., Zhang, W., Yan, Y., Ampomah, W., You, J., Wang, M., Anthony, E.J., Manovic, V., Clough, P.T., 2021. Harnessing the power of machine learning for carbon capture, utilisation, and storage (CCUS)-a state-of-the-art review. Energy Environ. Sci. 14 (12), 6122–6157. doi:10.1039/d1ee02395k.

Yan, Y.-T., Wu, G., Chen, S.-C., Wang, Y.-Z., 2022. Controlled synthesis and closed-loop chemical recycling of biodegradable copolymers with composition-dependent properties. Sci. China Chem. 65 (5), 943–953. doi:10.1007/s11426-021-1196-7.

Yang, J.-I., Kim, J.-N., 2006. Hydrotalcites for adsorption of CO_2 at high temperature. Korean J. Chem. Eng. 23 (1), 77–80. doi:10.1007/BF02705695.

Yang, Q., Lin, Y.S., 2006. Kinetics of carbon dioxide sorption on perovskite-type metal oxides. Ind. Eng. Chem. Res. 45 (18), 6302–6310. doi:10.1021/ie060264f.

Yang, Z., Lin, Y.S., Zeng, Y., 2002. High-temperature sorption process for air separation and oxygen removal. Ind. Eng. Chem. Res. 41 (11), 2775–2784. doi:10.1021/IE010736K.

Yang, D., Wang, Z., Wang, J., Wang, S., 2009. Potential of two-stage membrane system with recycle stream for CO_2 capture from postcombustion gas†. Energy Fuels 23 (10), 4755–4762. doi:10.1021/ef801109p.

Yang, Q., Wiersum, A.D., Llewellyn, P.L., Guillerm, V., Serre, C., Maurin, G., 2011. Functionalizing porous zirconium terephthalate UiO-66 (Zr) for natural gas upgrading: a computational exploration. Chem. Commun. (Camb.) 47 (34), 9603–9605. doi:10.1039/c1cc13543k.

Yang, S.-T., Kim, J.-Y., Kim, J., Ahn, W.-S., 2012. CO_2 capture over amine-functionalized MCM-22, MCM-36 and ITQ-2. Fuel 97, 435–442. doi:10.1016/j.fuel.2012.03.034.

Yang, D., Hou, M., Ning, H., Zhang, J., Ma, J., Han, B., 2013. Efficient SO2 capture by amine functionalized PEG. Phys. Chem. Chem. Phys. 15 (41). doi:10.1039/c3cp52911h.

Yang, M., Song, Y., Jiang, L., Liu, Y., Li, Y., 2014. CO_2 hydrate formation characteristics in a water/brine-saturated silica gel. Ind. Eng. Chem. Res. 53 (26), 10753–10761. doi:10.1021/ie5012728.

Yang, N., Yu, H., Xu, D.y., Conway, W., Maeder, M., Feron, P., 2014. Amino acids/NH3 mixtures for CO_2 capture: Effect of neutralization methods on CO_2 mass transfer and NH3 vapour loss. Energy Procedia 63, 773–780.

Yang, J., Pruvost, S., Livi, S., Duchet-Rumeau, J., 2015. Understanding of versatile and tunable nanostructuration of ionic liquids on fluorinated copolymer. Macromolecules 48 (13), 4581–4590. doi:10.1021/acs.macromol.5b00931.

Yang, Y., Xiang, Y., Li, Y., Chu, G., Zou, H., Arowo, M., Chen, J., 2015. 3D CFD modelling and optimization of single-phase flow in rotating packed beds. Can. J. Chem. Eng. 93 (6), 1138–1148. doi:10.1002/cjce.22183.

Yang, X., Zhao, L., Liu, Y., Sun, Z., Xiao, Y., 2016. Carbonation performance of NaNO3 modified MgO sorbents. Ind. Eng. Chem. Res. 56 (1), 342–350.

Yang, X., Liu, W., Sun, J., Hu, Y., Wang, W., Chen, H., Zhang, Y., Li, X., Xu, M., 2016a. Alkali-doped lithium orthosilicate sorbents for carbon dioxide capture. ChemSusChem 9 (17), 2480–2487. doi:10.1002/cssc.201600737.

Yang, X., Liu, W., Sun, J., Hu, Y., Wang, W., Chen, H., Zhang, Y., Li, X., Xu, M., 2016b. Preparation of novel Li_4SiO_4 sorbents with superior performance at low CO_2 concentration. ChemSusChem 9 (13), 1607–1613. doi:10.1002/cssc.201501699.

Yang, L., Tian, Z., Zhang, X., Wu, X., Wu, Y., Wang, Y., Peng, D., Wang, S., Wu, H., Jiang, Z., 2017. Enhanced CO_2 selectivities by incorporating CO_2-philic PEG-POSS into polymers of intrinsic microporosity membrane. J. Membr. Sci. 543, 69–78. doi:10.1016/j.memsci.2017.08.050.

Yang, Z., Yi, H., Tang, X., Zhao, S., Yu, Q., Gao, F., Zhou, Y., Wang, J., Huang, Y., Yang, K., Shi, Y., 2017. Potential demonstrations of "hot spots" presence by adsorption-desorption of toluene vapour onto granular activated carbon under microwave radiation. Chem. Eng. J. 319, 191–199. doi:10.1016/j.cej.2017.02.157.

Yang, Y., Lin, X., Chen, X., Guo, W., Wang, Y., Zhang, J., Kawa, O., 2018. Investigation on the effects of different forms of sodium, chlorine and sulphur and various pretreatment methods on the deposition characteristics of Na species during pyrolysis of a Na-rich coal. Fuel 234, 872–885. doi:10.1016/j.fuel.2018.07.130.

Yang, Y., Chuah, C.Y., Bae, T.-H., 2019. Polyamine-appended porous organic polymers for efficient post-combustion CO_2 capture. Chem. Eng. J. 358, 1227–1234. doi:10.1016/j.cej.2018.10.122.

Yang, H., Yang, L., Wang, H., Xu, Z., Zhao, Y., Luo, Y., Nasir, N., Song, Y., Wu, H., Pan, F., 2019. Covalent organic framework membranes through a mixed-dimensional assembly for molecular separations. Nat. Commun. 10 (1), 1–10. doi:10.1038/s41467-019-10157-5.

Yang, Z., Zhang, G., Xu, Y., Zhao, P., 2019. One step N-doping and activation of biomass carbon at low temperature through NaNH2: An effective approach to CO_2 adsorbents. J. CO_2 Util. 33, 320–329. doi:10.1016/j.jcou.2019.06.021.

Yang, Z., Guo, W., Mahurin, S.M., Wang, S., Chen, H., Cheng, L., Jie, K., Meyer, H.M., Jiang, D.-e., Liu, G., Jin, W., Popovs, I., Dai, S., 2020. Surpassing robeson upper limit for CO_2/N_2 separation with fluorinated carbon molecular sieve membranes. Chem 6 (3), 631–645. doi:10.1016/j.chempr.2019.12.006.

Yang, C., Zhang, B., Zhang, S., Wu, Y., Wang, T., Qiu, J., 2021. Highly permeable and selective sepiolite hybrid mixed matrix carbon membranes supported on plate carbon substrates for gas separation. Chem. Eng. Res. Des. 174, 319–330. doi:10.1016/j.cherd.2021.08.012.

Yang, Y., Li, Y.J., Yan, X.Y., Zhao, J.L., Zhang, C.X., 2021. Development of thermochemical heat storage based on CaO/CaCO3 cycles: a review. Energies 14 (20), 26. doi:10.3390/en14206847.

Yang, Z., Khatri, D., Verma, P., Li, T., Adeosun, A., Kumfer, B.M., Axelbaum, R.L., 2021. Experimental study and demonstration of pilot-scale, dry feed, oxy-coal combustion under pressure. Appl. Energy 285, 116367. doi:10.1016/j.apenergy.2020.116367.

Yang, C., Zhao, T., Pan, H., Liu, F., Cao, J., Lin, Q., 2022. Facile preparation of N-doped porous carbon from chitosan and NaNH2 for CO_2 adsorption and conversion. Chem. Eng. J. 432, 134347. doi:10.1016/j.cej.2021.134347.

Yang, F., Ge, T., Zhu, X., Wu, J., Wang, R., 2022. Study on CO_2 capture in humid flue gas using amine-modified ZIF-8. Sep. Purif. Technol. 287. doi:10.1016/j.seppur.2022.120535.

Yang, Z., Ying, Y., Pu, Y., Wang, D., Yang, H., Zhao, D., 2022. Poly (ionic liquid)-functionalized UiO-66- $(OH)_2$: Improved interfacial compatibility and separation ability in mixed matrix membranes for CO_2 separation. Ind. Eng. Chem. Res. 61 (22), 7626–7633. doi:10.1021/acs.iecr.1c04648.

Yanuka-Golub, K., Baransi-Karkaby, K., Szczupak, A., Reshef, L., Rishpon, J., Shechter, R., Gophna, U., Sabbah, I., 2019. An electrode-assisted anaerobic digestion process for the production of high-quality biogas. Water Sci. Technol. 79 (11), 2145–2155. doi:10.2166/wst.2019.214.

Yao, Q., Su, J., Cheung, O., Liu, Q., Hedin, N., Zou, X., 2012. Interpenetrated metal–organic frameworks and their uptake of CO_2 at relatively low pressures. J. Mater. Chem. 22 (20). doi:10.1039/c2jm15933c.

Yassin, M.M., Anderson, J.A., Dimitrakis, G.A., Martin, C.F., 2021. Effects of the heating source on the regeneration performance of different adsorbents under post-combustion carbon capture cyclic operations. A comparative analysis. Sep. Purif. Technol. 276. doi:10.1016/j.seppur.2021.119326.

Yave, W., Car, A., Funari, S.S., Nunes, S.P., Peinemann, K.-V., 2010. CO_2-philic polymer membrane with extremely high separation performance. Macromolecules 43 (1), 326–333. doi:10.1021/ma901950u.

Yay, B., Gizli, N., 2019. A review on silica aerogels for CO_2 capture applications. Pamukkale Univ. J. Eng. Sci.-Pamukkale Univ. Muhendislik Bilimleri Dergisi 25 (7), 907–913. doi:10.5505/pajes.2018.35651.

Yazaydin, A.O., Benin, A.I., Faheem, S.A., Jakubczak, P., Low, J.J., Willis, R.R., Snurr, R.Q., 2009. Enhanced CO_2 adsorption in metal-organic frameworks via_occupation of open-metal sites by coordinated water molecules. Chem. Mater. 21, 1425–1430.

Ye, Q., Wang, X., Lu, Y., 2015. Screening and evaluation of novel biphasic solvents for energy-efficient post-combustion CO_2 capture. Int. J. Greenh. Gas Control 39, 205–214. doi:10.1016/j.ijggc.2015.05.025.

Ye, L., Jie, X., Wang, L., Xu, G., Sun, Y., Kang, G., Cao, Y., 2021. Preparation and gas separation performance of thermally rearranged poly (benzoxazole-co-amide) (TR-PBOA) hollow fiber membranes deriving from polyamides. Sep. Purif. Technol. 257, 117870.

Yek, P.N.Y., Peng, W., Wong, C.C., Liew, R.K., Ho, Y.L., Wan Mahari, W.A., Azwar, E., Yuan, T.Q., Tabatabaei, M., Aghbashlo, M., Sonne, C., Lam, S.S., 2020. Engineered biochar via microwave CO_2 and steam pyrolysis to treat carcinogenic Congo red dye. J. Hazard. Mater. 395, 122636. doi:10.1016/j.jhazmat.2020.122636.

Yi, C.-K., Jo, S.-H., Seo, Y., Lee, J.-B., Ryu, C.-K., 2007. Continuous operation of the potassium-based dry sorbent CO_2 capture process with two fluidized-bed reactors. Int. J. Greenh. Gas. Con. 1 (1), 31–36. doi:10.1016/s1750-5836 (07)00014-x.

Yi, F., Zou, H.K., Chu, G.W., Shao, L., Chen, J.F., 2009. Modeling and experimental studies on absorption of CO_2 by Benfield solution in rotating packed bed. Chem. Eng. J. 145 (3), 377–384. doi:10.1016/j.cej.2008.08.004.

Yi, J., Schroeder, M., Weirich, T., Mayer, J., 2010. Behavior of Ba (Co, Fe, Nb)O_3-δ Perovskite in CO_2-containing atmospheres: degradation mechanism and materials design. Chem. Mater. 22 (23), 6246–6253. doi:10.1021/cm101665r.

Yi, J., Weirich, T.E., Schroeder, M., 2013. CO_2 corrosion and recovery of perovskite-type BaCo1−x−yFexNbyO3−δ membranes. J. Membr. Sci. 437, 49–56. doi:10.1016/j.memsci.2013.02.049.

Yin, J.-Z., Zhen, M.-Y., Cai, P., Zhou, D., Li, Z.-J., Zhu, H.-Y., Xu, Q.-Q., 2018. Supercritical CO_2 preparation of SBA-15 supported ionic liquid and its adsorption for CO_2. Mater. Res. Exp. 5 (6), 065060. doi:10.1088/2053-1591/aacdb4.

Yin, X., Xi, M., Li, Y., Kong, F., Jiang, Z., 2021. Improvements in physicochemical and nutrient properties of sewage sludge biochar by the co-pyrolysis with organic additives. Sci. Total Environ. 779, 146565. doi:10.1016/j.scitotenv.2021.146565.

Yin, Y., Chen, W., Wu, C., Zhang, X., Fu, T., Zhu, C., Ma, Y., 2022. Bubble dynamics and mass transfer enhancement in split–and–recombine (SAR) microreactor with rapid chemical reaction. Sep. Purif. Technol. 287, 120573. doi:10.1016/j.seppur.2022.120573.

Ying, Z., Zheng, X., Cui, G., 2016. Pressurized oxy-fuel combustion performance of pulverized coal for CO_2 capture. Appl. Therm. Eng. 99, 411–418. doi:10.1016/j.applthermaleng.2016.01.023.

Ying, W., Cai, J., Zhou, K., Chen, D., Ying, Y., Guo, Y., Kong, X., Xu, Z., Peng, X., 2018. Ionic liquid selectively facilitates CO_2 transport through graphene oxide membrane. ACS Nano 12 (6), 5385–5393. doi:10.1021/acsnano.8b00367.

Yong, Z., Rodrigues, A., 2002. Hydrotalcite-like compounds as adsorbents for carbon dioxide. Energy Convers. Manage. 43, 1865–1876. doi:10.1016/S0196-8904 (01)00125-X.
Yong, Z., Mata, Rodrigues, A.E., 2001. Adsorption of carbon dioxide onto hydrotalcite-like compounds (HTlcs) at high temperatures. Ind. Eng. Chem. Res. 40 (1), 204–209. doi:10.1021/ie000238w.
Yoo, D.K., Jhung, S.H., 2022. Selective CO_2 adsorption at low pressure with a Zr-based UiO-67 metal–organic framework functionalized with aminosilanes. J. Mater. Chem. A 10 (16), 8856–8865. doi:10.1039/d1ta09772e.
Yoshimura, T., Tamenori, Y., Suzuki, A., Kawahata, H., Iwasaki, N., Hasegawa, H., Nguyen, L.T., Kuroyanagi, A., Yamazaki, T., Kuroda, J., Ohkouchi, N., 2017. Altervalent substitution of sodium for calcium in biogenic calcite and aragonite. Geochim. Cosmochim. Acta 202, 21–38. doi:10.1016/j.gca.2016.12.003.
Younas, M., Rezakazemi, M., Daud, M., Wazir, M.B., Ahmad, S., Ullah, N., Inamuddin, Ramakrishna, S., 2020. Recent progress and remaining challenges in post-combustion CO_2 capture using metal-organic frameworks (MOFs). Prog. Energy Combust. Sci. 80. doi:10.1016/j.pecs.2020.100849.
Young, B., Krynock, M., Carlson, D., Hawkins, T.R., Marriott, J., Morelli, B., Jamieson, M., Cooney, G., Skone, T.J., 2019. Comparative environmental life cycle assessment of carbon capture for petroleum refining, ammonia production, and thermoelectric power generation in the United States. Int. J. Greenh. Gas Control 91. doi:10.1016/j.ijggc.2019.102821.
Young, J., Garcia-Diez, E., Garcia, S., van der Spek, M., 2021. The impact of binary water-CO_2 isotherm models on the optimal performance of sorbent-based direct air capture processes. Energy Environ. Sci. 14 (10), 5377–5394. doi:10.1039/d1ee01272j.
Yousef, A.M., El-Maghlany, W.M., Eldrainy, Y.A., Attia, A., 2018a. Low-temperature distillation process for CO_2/CH4 separation: a study for avoiding CO_2 freeze-out. J. Heat Transf. 140 (4), 042001. doi:10.1115/1.4038193.
Yousef, A.M., El-Maghlany, W.M., Eldrainy, Y.A., Attia, A., 2018b. New approach for biogas purification using cryogenic separation and distillation process for CO_2 capture. Energy 156, 328–351. doi:10.1016/j.energy.2018.05.106.
Yousef, A.M., El-Maghlany, W.M., Eldrainy, Y.A., Attia, A., 2019. Upgrading biogas to biomethane and liquid CO_2: A novel cryogenic process. Fuel 251, 611–628. doi:10.1016/j.fuel.2019.03.127.
Yu, J., Balbuena, P.B., 2013. Water effects on postcombustion CO_2 capture in Mg-MOF-74. J. Phys. Chem. C 117 (7), 3383–3388.
Yu, J., Wang, S., 2015. Modeling analysis of energy requirement in aqueous ammonia based CO_2 capture process. Int. J. Greenh. Gas Control 43, 33–45. doi:10.1016/j.ijggc.2015.10.010.
Yu, K., Curcic, I., Gabriel, J., Tsang, S., 2008. Recent advances in CO_2 capture and utilization. ChemSusChem 1 (11), 893–899.
Yu, X., Wang, Z., Wei, Z., Yuan, S., Zhao, J., Wang, J., Wang, S., 2010. Novel tertiary amino containing thin film composite membranes prepared by interfacial polymerization for CO_2 capture. J. Membr. Sci. 362 (1-2), 265–278.
Yu, M., Funke, H.H., Noble, R.D., Falconer, J.L., 2011. H2 separation using defect-free, inorganic composite membranes. J. Am. Chem. Soc. 133 (6), 1748–1750. doi:10.1021/ja108681n.
Yu, C.-H., Huang, C.-H., Tan, C.-S., 2012. A review of CO_2 capture by absorption and adsorption. Aerosol. Air Qual. Res. 12 (5), 745–769. doi:10.4209/aaqr.2012.05.0132.
Yu, Y.S., Lu, H.F., Zhang, T.T., Zhang, Z.X., Wang, G.X., Rudolph, V., 2013. Determining the performance of an efficient nonaqueous CO_2 capture process at desorption temperatures below 373 K. Ind. Eng. Chem. Res. 52 (35), 12622–12634. doi:10.1021/ie400353f.
Yu, Y., Mai, J., Wang, L., Li, X., Jiang, Z., Wang, F., 2014. Ship-in-a-bottle synthesis of amine-functionalized ionic liquids in NaY zeolite for CO_2 capture. Sci. Rep. 4, 5997. doi:10.1038/srep05997.
Yu, Y., Mai, J., Huang, L., Wang, L., Li, X., 2014. Ship in a bottle synthesis of ionic liquids in NaY supercages for CO_2 capture. RSC Adv. 4 (25), 12756–12762. doi:10.1039/C3RA46971A.
Yu, G., Zou, X., Sun, L., Liu, B., Wang, Z., Zhang, P., Zhu, G., 2019. Constructing connected paths between UiO-66 and PIM-1 to improve membrane CO_2 separation with crystal-Like gas selectivity. Adv. Mater. 31 (15), 1806853. doi:10.1002/adma.201806853.
Yu, Z., Yang, Y., Yang, S., Zhang, Q., Zhao, J., Fang, Y., Hao, X., Guan, G., 2019. Iron-based oxygen carriers in chemical looping conversions: A review. Carbon Resour. Convers. 2 (1), 23–34. doi:10.1016/j.crcon.2018.11.004.
Yu, Y., Wang, J., Wang, Y., Pan, W., Liu, C., Liu, P., Liang, L., Xu, C., Liu, Y., 2020. Polyethyleneimine-functionalized phenolphthalein-based cardo poly (ether ether ketone) membrane for CO_2 separation. J. Ind. Eng. Chem. 83, 20–28. doi:10.1016/j.jiec.2019.10.007.
Yu, H., Gundersen, T., Gençer, E., 2021. Optimal liquified natural gas (LNG) cold energy utilization in an Allam cycle power plant with carbon capture and storage. Energy Convers. Manage. 228, 113725.
Yu, H., 2018. Recent developments in aqueous ammonia-based post-combustion CO_2 capture technologies. Chin. J. Chem. Eng. 26 (11), 2255–2265.
Yuan, H., Lu, T., Huang, H., Zhao, D., Kobayashi, N., Chen, Y., 2015. Influence of pyrolysis temperature on physical and chemical properties of biochar made from sewage sludge. J. Analyt. Appl. Pyrol. 112, 284–289. doi:10.1016/j.jaap.2015.01.010.
Yuan, J., Zhu, H., Sun, J., Mao, Y., Liu, G., Jin, W., 2017. Novel ZIF-300 mixed–matrix membranes for efficient CO_2 capture. ACS Appl. Mater. Interfaces 9 (44), 38575–38583.
Yuan, Y., Qiao, Z., Xu, J., Wang, J., Zhao, S., Cao, X., Wang, Z., Guiver, M.D.J.J.o.M.S., 2021. Mixed matrix membranes for CO_2 separations by incorporating microporous polymer framework fillers with amine-rich nanochannels. J. Membr. Sci. 620, 118923.
Yue, M.B., Chun, Y., Cao, Y., Dong, X., Zhu, J.H., 2006. CO_2 capture by as-prepared SBA-15 with an occluded organic template. Adv. Funct. Mater. 16 (13), 1717–1722. doi:10.1002/adfm.200600427.
Yue, J., Chen, G., Yuan, Q., Luo, L., Gonthier, Y., 2007. Hydrodynamics and mass transfer characteristics in gas–liquid flow through a rectangular microchannel. Chem. Eng. Sci. 62 (7), 2096–2108. doi:10.1016/j.ces.2006.12.057.
Yue, B., Liu, S., Chai, Y., Wu, G., Guan, N., Li, L., 2022. Zeolites for separation: Fundamental and application. J. Energy Chem. 71, 288–303. doi:10.1016/j.jechem.2022.03.035.
Zafar, Q., Mattisson, T., Gevert, B., 2006. Redox investigation of some oxides of transition-state metals Ni, Cu, Fe, and Mn supported on SiO2 and MgAl2O4. Energy Fuels 20 (1), 34–44. doi:10.1021/ef0501389.
Zahedi, R., Ayazi, M., Aslani, A., 2022. Comparison of amine adsorbents and strong hydroxides soluble for direct air CO_2 capture by life cycle assessment method. Environ. Technol. Innov. 28. doi:10.1016/j.eti.2022.102854.
Zakuciová, K., Štefanica, J., Carvalho, A., Kočí, V., 2020. Environmental assessment of a coal power plant with carbon dioxide capture system based on the activated carbon adsorption process: a case study of the Czech Republic. Energies 13 (9). doi:10.3390/en13092251.
Zalewski, M., Krawczyk, T., Siewniak, A., Sobolewski, A., 2021. Carbon dioxide capture using water-imidazolium ionic liquids-amines ternary systems. Int. J. Greenh. Gas Control 105. doi:10.1016/j.ijggc.2020.103210.
Zan, H., Chen, X., Ma, J., Liu, D., Wu, Y., 2020. Experimental study of NOx formation in a high-steam atmosphere during a pressurized oxygen-fuel combustion process. ACS Omega 5 (26), 16037–16044. doi:10.1021/acsomega.0c01480.
Zanco, S.E., Joss, L., Hefti, M., Gazzani, M., Mazzotti, M., 2017. Addressing the criticalities for the deployment of adsorption-based CO_2 capture processes. Energy Procedia 114, 2497–2505. doi:10.1016/j.egypro.2017.03.1407.
Zapata Ballesteros, A., De Witte, N., Denayer, J.F.M., Van Assche, T.R.C., 2022. Effect of pellet size on PSA performance: monolayer and multilayer bed case study for biogas upgrading. Adsorption doi:10.1007/s10450-022-00365-9.
Zarghami, S., Hassanzadeh, A., Arastoopour, H., Abbasian, J., 2015. Effect of steam on the reactivity of MgO-based sorbents in precombustion CO_2 capture processes. Ind. Eng. Chem. Res. 54 (36), 8860–8866. doi:10.1021/acs.iecr.5b01175.
Zelenak, V., Halamova, D., Gaberova, L., Bloch, E., Llewellyn, P., 2008. Amine-modified SBA-12 mesoporous silica for carbon dioxide capture: Effect of amine basicity on sorption properties. Microporous Mesoporous Mater. 116 (1-3), 358–364. doi:10.1016/j.micromeso.2008.04.023.
Zeman, F., Lackner, K., 2004. Capturing carbon dioxide directly from the atmosphere. World Resour. Rev. 16 (2), 157–172.
Zeman, F., 2007. Energy and material balance of CO_2 capture from ambient air. Environ. Sci. Technol. 41 (21), 7558–7563. doi:10.1021/es070874m.
Zeng, W., Bai, H., 2015. High-performance CO_2 capture on amine-functionalized hierarchically porous silica nanoparticles prepared by a simple template-free method. Adsorption 22 (2), 117–127. doi:10.1007/s10450-015-9698-0.
Zeng, Y., Zou, R., Zhao, Y., 2016. Covalent organic frameworks for CO_2 capture. Adv. Mater. 28 (15), 2855–2873.
Zeng, Y., Li, K., Zhu, Q., Wang, J., Cao, Y., Lu, S., 2018. Capture of CO_2 in carbon nanotube bundles supported with room-temperature ionic liquids: A molecular simulation study. Chem. Eng. Sci. 192, 94–102. doi:10.1016/j.ces.2018.07.025.
Zeng, L., Cheng, Z., Fan, J.A., Fan, L.-S., Gong, J., 2018. Metal oxide redox chemistry for chemical looping processes. Nat. Rev. Chem. 2 (11), 349–364. doi:10.1038/s41570-018-0046-2.
Zeng, P., Zhao, C., Wang, X., Wei, X., Sun, J., Wang, R., Guo, Y., 2022. One-step synthesis of structurally improved, Al_2O_3-supported K_2CO_3 pellets via graphite-casting method for low-temperature CO_2 capture. Sep. Purif. Technol. 292, 120929. doi:10.1016/j.seppur.2022.120929.
Zhai, L., Huang, N., Xu, H., Chen, Q., Jiang, D., 2017. A backbone design principle for covalent organic frameworks: the impact of weakly interacting units on CO 2 adsorption. Chem. Commun. 53 (30), 4242–4245.
Zhan, G., Bai, L., Zeng, S., Bai, Y., Su, H., Wu, B., Cao, F., Shang, D., Li, Z., Zhang, X., Zhang, S., 2020. Dynamic process simulation and assessment of CO_2 removal from confined spaces using pressure swing adsorption. Ind. Eng. Chem. Res. 59 (37), 16407–16419. doi:10.1021/acs.iecr.0c02255.
Zhan, G., Bai, L., Wu, B., Cao, F., Duan, Y., Chang, F., Shang, D., Bai, Y., Li, Z., Zhang, X., Zhang, S., 2021. Dynamic process simulation and optimization of CO_2 removal from confined space with pressure and temperature swing adsorption. Chem. Eng. J. 416. doi:10.1016/j.cej.2021.129104.
Zhang, C., Bokil, A., 1997. A quasi-three-dimensional approach to simulate the two-phase fluid flow and heat transfer in condensers. Int. J. Heat Mass Transf. 40 (15), 3537–3546. doi:10.1016/S0017-9310 (97)00014-8.
Zhang, C., Koros, W.J., 2017. Ultraselective carbon molecular sieve membranes with tailored synergistic sorption selective properties. Adv. Mater. 29 (33). doi:10.1002/adma.201701631.
Zhang, H., Liu, Z., 2013. Research progress of CO_2 capture materials for post-combustion. Modern Chem. Ind. 33 (05). doi:10.16606/j.cnki.issn0253-4320.2013.05.034, 17-20+22.
Zhang, W., Xie, P., Li, Y., Zhu, J., 2022. Modeling of gas-liquid flow in a rotating packed bed using an Eulerian multi-fluid approach. AIChE Journal 68 (4). doi:10.1002/aic.17561, e17561–e17561.
Zhang, J., Webley, P.A., Xiao, P., 2008. Effect of process parameters on power requirements of vacuum swing adsorption technology for CO_2 capture from flue gas. Energy Conversion and Management 49 (2), 346–356.
Zhang, Y., Chen, H., Chen, C.C., Plaza, J.M., Dugas, R., Rochelle, G.T., 2009. Rate-based process modeling study of CO_2 Capture with aqueous monoethanolamine solution. Ind. Eng. Chem. Res. 48 (20), 9233–9246. doi:10.1021/ie900068k.
Zhang, X., Zheng, X., Zhang, S., Zhao, B., Wu, W., 2012. AM-TEPA impregnated disordered mesoporous silica as CO_2 capture adsorbent for balanced adsorption–desorption properties. Ind. Eng. Chem. Res. 51 (46), 15163–15169. doi:10.1021/ie300180u.

Zhang, K.L., Li, X.H.S., Duan, Y.H., King, D.L., Singh, P., Li, L.Y., 2013. Roles of double salt formation and $NaNO_3$ in Na_2CO_3-promoted MgO absorbent for intermediate temperature CO_2 removal. Int. J. Greenh. Gas Control 12, 351–358. doi:10.1016/j.ijggc.2012.11.013.

Zhang, Z., Xian, S., Xia, Q., Wang, H., Li, Z., Li, J., 2013. Enhancement of CO_2 adsorption and CO_2/N_2 selectivity on ZIF-8 via postsynthetic modification. AIChE J. 59 (6), 2195–2206. doi:10.1002/aic.13970.

Zhang, B., Dang, X., Wu, Y., Liu, H., Wang, T., Qiu, J., 2014. Structure and gas permeation of nanoporous carbon membranes based on RF resin/F-127 with variable catalysts. J. Mater. Res. 29 (23), 2881–2890. doi:10.1557/jmr.2014.327.

Zhang, K., Li, X.S., Li, W.-Z., Rohatgi, A., Duan, Y., Singh, P., Li, L., King, D.L., 2014. Phase transfer-catalyzed fast CO_2 absorption by MgO-based absorbents with high cycling capacity. Adv. Mater. Interfaces 1 (3), 1400030. doi:10.1002/admi.201400030.

Zhang, X., Singh, B., He, X., Gundersen, T., Deng, L., Zhang, S., 2014. Post-combustion carbon capture technologies: Energetic analysis and life cycle assessment. Int. J. Greenh. Gas Control 27, 289–298. doi:10.1016/j.ijggc.2014.06.016.

Zhang, X.P., Singh, B., He, X.Z., Gundersen, T., Deng, L.Y., Zhang, S.J., 2014. Post-combustion carbon capture technologies: energetic analysis and life cycle assessment. Int. J. Greenh. Gas Control 27, 289–298. doi:10.1016/j.ijggc.2014.06.016.

Zhang, K., Li, X.S., Chen, H., Singh, P., King, D.L., 2015. Molten salt promoting effect in double salt CO_2 absorbents. J. Phys. Chem. C 120 (2), 1089–1096.

Zhang, R., Liang, Z., Liu, H., Rongwong, W., Luo, X., Idem, R., Yang, Q., 2016. Study of formation of bicarbonate ions in CO_2-loaded aqueous single 1DMA2P and MDEA tertiary amines and blended MEA–1DMA2P and MEA–MDEA amines for low heat of regeneration. Ind. Eng. Chem. Res. 55 (12), 3710–3717. doi:10.1021/acs.iecr.5b03097.

Zhang, W., Liu, H., Sun, Y., Cakstins, J., Sun, C., Snape, C.E., 2016. Parametric study on the regeneration heat requirement of an amine-based solid adsorbent process for post-combustion carbon capture. Appl. Energy 168, 394–405. doi:10.1016/j.apenergy.2016.01.049.

Zhang, X., Wu, J., Yang, H., Shao, J., Wang, X., Chen, Y., Zhang, S., Chen, H., 2016. Preparation of nitrogen-doped microporous modified biochar by high temperature CO 2–NH 3 treatment for CO_2 adsorption: effects of temperature. RSC Adv. 6 (100), 98157–98166.

Zhang, Y., Ji, X., Xie, Y., Lu, X., 2016. Screening of conventional ionic liquids for carbon dioxide capture and separation. Appl. Energy 162, 1160–1170. doi:10.1016/j.apenergy.2015.03.071.

Zhang, C., Sunarso, J., Liu, S., 2017. Designing CO_2-resistant oxygen-selective mixed ionic-electronic conducting membranes: Guidelines, recent advances, and forward directions. Chem. Soc. Rev. R. Soc. Chem. 2941–3005.

Zhang, J.P., Luo, Y., Chu, G.W., Sang, L., Liu, Y., Zhang, L.L., Chen, J.F., 2017. A hydrophobic wire mesh for better liquid dispersion in air. Chem. Eng. Sci. 170, 204–212. doi:10.1016/j.ces.2017.03.058.

Zhang, M., Li, Y., Li, Y., Han, H., Teng, L., 2017. Numerical simulations on the effect of sloshing on liquid flow maldistribution of randomly packed column. Appl. Therm. Eng. 112, 585–594. doi:10.1016/j.applthermaleng.2016.10.049.

Zhang, S., Zhang, J., Zhang, Y., Deng, Y., 2017. Nanoconfined ionic liquids. Chem. Rev. 117 (10), 6755–6833. doi:10.1021/acs.chemrev.6b00509.

Zhang, W., Chen, J., Luo, X., Wang, M., 2017. Modelling and process analysis of post-combustion carbon capture with the blend of 2-amino-2-methyl-1-propanol and piperazine. Int. J. Greenh. Gas Control 63, 37–46. doi:10.1016/j.ijggc.2017.04.018.

Zhang, X., Liu, H., Liang, Z., 2017. CO_2 desorption in single and blended amine solvents with and without catalyst. Energy Procedia 114, 1862–1868. doi:10.1016/j.egypro.2017.03.1316.

Zhang, X.-M., Tu, Z.-H., Li, H., Li, L., Wu, Y.-T., Hu, X.-B., 2017a. Supported protic-ionic-liquid membranes with facilitated transport mechanism for the selective separation of CO_2. J. Membr. Sci. 527, 60–67. doi:10.1016/j.memsci.2017.01.006.

Zhang, X.-M., Tu, Z.-H., Li, H., Li, L., Wu, Y.-T., Hu, X.-B., 2017b. Supported protic-ionic-liquid membranes with facilitated transport mechanism for the selective separation of CO_2. J. Membr. Sci. 527, 60–67.

Zhang, B., Wei, M., Mao, H., Pei, X., Alshmimri, S.A., Reimer, J.A., Yaghi, O.M., 2018. Crystalline dioxin-linked covalent organic frameworks from irreversible reactions. J. Am. Chem. Soc. 140 (40), 12715–12719.

Zhang, H., Tian, H., Zhang, J., Guo, R., Li, X., 2018. Facilitated transport membranes with an amino acid salt for highly efficient CO_2 separation. Int. J. Greenh. Gas Control 78, 85–93. doi:10.1016/j.ijggc.2018.07.014.

Zhang, S., Shen, Y., Shao, P., Chen, J., Wang, L., 2018. Kinetics, thermodynamics, and mechanism of a novel biphasic solvent for CO_2 capture from flue gas. Environ. Sci. Technol. 52 (6), 3660–3668. doi:10.1021/acs.est.7b05936.

Zhang, X., Hong, J., Liu, H., Luo, X., Olson, W., Tontiwachwuthikul, P., Liang, Z., 2018a. SO42−/ZrO2 supported on γ-Al2O3 as a catalyst for CO_2 desorption from CO_2-loaded monoethanolamine solutions. AlChE J. 64 (11), 3988–4001. doi:10.1002/aic.16380.

Zhang, X., Liu, H., Liang, Z., Idem, R., Tontiwachwuthikul, P., Jaber Al-Marri, M., Benamor, A., 2018b. Reducing energy consumption of CO_2 desorption in CO_2-loaded aqueous amine solution using Al2O3/HZSM-5 bifunctional catalysts. Appl. Energy 229, 562–576. doi:10.1016/j.apenergy.2018.07.035.

Zhang, X., Zhang, R., Liu, H., Gao, H., Liang, Z., 2018c. Evaluating CO_2 desorption performance in CO_2-loaded aqueous tri-solvent blend amines with and without solid acid catalysts. Appl. Energy 218, 417–429. doi:10.1016/j.apenergy.2018.02.087.

Zhang, M., Li, J., Wang, Y., Yang, C., 2019. Impacts of different biochar types on the anaerobic digestion of sewage sludge. RSC Adv. 9 (72), 42375–42386. doi:10.1039/C9RA08700A.

Zhang, P., Xu, R., Li, H., Gao, H., Liang, Z., 2019. Mass transfer performance for CO_2 absorption into aqueous blended DMEA/MEA solution with optimized molar ratio in a hollow fiber membrane contactor. Sep. Purif. Technol. 211, 628–636. doi:10.1016/j.seppur.2018.10.034.

Zhang, W., Gao, E., Li, Y., Bernards, M.T., He, Y., Shi, Y., 2019. CO_2 capture with polyamine-based protic ionic liquid functionalized mesoporous silica. J. CO_2 Util. 34, 606–615. doi:10.1016/j.jcou.2019.08.012.

Zhang, X., Xiong, W., Tu, Z., Peng, L., Wu, Y., Hu, X., 2019. Supported ionic liquid membranes with dual-site interaction mechanism for efficient separation of CO_2. ACS Sustain. Chem. Eng. 7. doi:10.1021/acssuschemeng.9b01604.

Zhang, Y., Feng, D., Gao, J., Du, Q., Wu, S., 2019. Thermodynamic properties in ternary system of NH4HCO3–H2O–ethanol based on antisolvent method to strengthen crystallization of carbonized ammonia. Adsorpt. Sci. Technol. 37 (1-2), 127–138.

Zhang, J., Xin, Q., Li, X., Yun, M., Xu, R., Wang, S., Li, Y., Lin, L., Ding, X., Ye, H., 2019a. Mixed matrix membranes comprising aminosilane-functionalized graphene oxide for enhanced CO_2 separation. J. Membr. Sci. 570, 343–354. doi:10.1016/j.memsci.2018.10.075.

Zhang, X., Huang, Y., Gao, H., Luo, X., Liang, Z., Tontiwachwuthikul, P., 2019a. Zeolite catalyst-aided tri-solvent blend amine regeneration: An alternative pathway to reduce the energy consumption in amine-based CO_2 capture process. Appl. Energy 240, 827–841. doi:10.1016/j.apenergy.2019.02.089.

Zhang, X., Huang, Y., Gao, H., Luo, X., Liang, Z., Tontiwachwuthikul, P., 2019a. Zeolite catalyst-aided tri-solvent blend amine regeneration: An alternative pathway to reduce the energy consumption in amine-based CO_2 capture process. Appl. Energy 240 (APR.15), 827–841.

Zhang, X., Zhu, Z., Sun, X., Yang, J., Gao, H., Huang, Y., Luo, X., Liang, Z., Tontiwachwuthikul, P., 2019b. Reducing energy penalty of CO_2 capture using Fe promoted SO4 (2-)/ZrO2/MCM-41 catalyst. Environ. Sci. Technol. 53 (10), 6094–6102. doi:10.1021/acs.est.9b01901.

Zhang, X., Zhu, Z., Sun, X., Yang, J., Gao, H., Huang, Y., Luo, X., Liang, Z., Tontiwachwuthikul, P., 2019b. Reducing energy penalty of CO_2 capture using Fe promoted SO42-/ZrO2/MCM-41 catalyst. Environ. Sci. Technol. 53 (10), 6094–6102. doi:10.1021/acs.est.9b01901.

Zhang, J., Xin, Q., Li, X., Yun, M., Xu, R., Wang, S., Li, Y., Lin, L., Ding, X., Ye, H., Zhang, Y., 2019b. Mixed matrix membranes comprising aminosilane-functionalized graphene oxide for enhanced CO_2 separation. J. Membr. Sci. 570-571, 343–354. doi:10.1016/j.memsci.2018.10.075.

Zhang, T.M., Zhang, W.W., Zhang, Y., Shen, M.X., Zhang, J.F., 2020. Gas phase synthesis of aminated nanocellulose aerogel for carbon dioxide adsorption. Cellulose 27 (6), 2953–2958. doi:10.1007/s10570-020-03035-7.

Zhang, W., Xie, P., Li, Y., Teng, L., Zhu, J., 2020. CFD analysis of the hydrodynamic characteristics in a rotating packed bed with multi-nozzles. Chem. Eng. Process. - Process Intensif. 158. doi:10.1016/j.cep.2020.108107, 108107-108107.

Zhang, W.D., Sun, S.Z., Zhao, Y.J., Zhao, Z.J., Wang, P.X., Feng, D.D., Li, P.F., 2020. Effects of total pressure and CO_2 partial pressure on the physicochemical properties and reactivity of pressurized coal char produced at rapid heating rate. Energy 208. doi:10.1016/j.energy.2020.118297.

Zhang, W., Li, Y.J., Li, B.Y., Wang, Y.Z., Qian, Y.Q., Wang, Z.Y., 2020a. Simultaneous NO/CO_2 removal by Cu-modified biochar/CaO in carbonation step of calcium looping process. Chem. Eng. J. 392. doi:10.1016/j.cej.2019.123659.

Zhang, W., Li, Y.J., Ma, X.T., Qian, Y.Q., Wang, Z.Y., 2020b. Simultaneous NO/CO_2 removal performance of biochar/limestone in calcium looping process. Fuel 262. doi:10.1016/j.fuel.2019.116428.

Zhang, B., Yan, Q., Chen, G., Yi, C., Qi, S., Yang, B., 2021. Fabrication of mixed matrix membranes with zinc ion loaded titanium dioxide for improved CO_2 separation. Sep. Purif. Technol. 254, 117472. doi:10.1016/j.seppur.2020.117472.

Zhang, W., Xie, P., Li, Y., Teng, L., Zhu, J., 2021. 3D CFD simulation of the liquid flow in a rotating packed bed with structured wire mesh packing. Chem. Eng. J. 427. doi:10.1016/j.cej.2021.130874, 130874-130874.

Zhang, Z., Rao, S., Han, Y., Pang, R., Ho, W.S.W., 2021. CO_2-selective membranes containing amino acid salts for CO_2/N_2 separation. J. Membr. Sci. 638, 119696. doi:10.1016/j.memsci.2021.119696.

Zhang, Q., Zhou, M., Liu, X., Zhang, B., 2021a. Pebax/two-dimensional MFI nanosheets mixed-matrix membranes for enhanced CO_2 separation. J. Membr. Sci. 636. doi:10.1016/j.memsci.2021.119612.

Zhang, Q., Zhou, M., Liu, X., Zhang, B., 2021b. Pebax/two-dimensional MFI nanosheets mixed-matrix membranes for enhanced CO_2 separation. J. Membr. Sci. 636, 119612.

Zhang, B., Peng, J., Li, Y., Shi, H., Jin, J., Hu, J., Lu, S., 2022. Evaluating CO_2 desorption activity of tri-solvent MEA + EAE + AMP with various commercial solid acid catalysts. Catalysts 12 (7). doi:10.3390/catal12070723.

Zhang, G., Tran, T.N., Huang, L., Deng, E., Blevins, A., Guo, W., Ding, Y., Lin, H., 2022. Thin-film composite membranes based on hyperbranched poly (ethylene oxide) for CO_2/N_2 separation. J. Membr. Sci. 644, 120184. doi:10.1016/j.memsci.2021.120184.

Zhang, J.J., Huang, D.R., Shao, J.A., Zhang, X., Zhang, S.H., Yang, H.P., Chen, H.P., 2022. A new nitrogen-enriched biochar modified by ZIF-8 grafting and annealing for enhancing CO_2 adsorption. Fuel Process. Technol. 231. doi:10.1016/j.fuproc.2022.107250.

Zhang, P., Xin, Y., He, Y., et al., 2022. Exploring a blue-light-sensing transcription factor to double the peak productivity of oil in nannochloropsis oceanica. Nat. Commun. 13 (1664). doi:10.1038/s41467-022-29337-x.

Zhang, X., Rong, M., Qin, P., Tan, T., 2022. PEO-based CO_2-philic mixed matrix membranes compromising N-rich ultramicroporous polyaminals for superior CO_2 capture. J. Membr. Sci. 644, 120111. doi:10.1016/j.memsci.2021.120111.

Zhang, X., Zhang, F., Song, Z., Lin, L., Zhao, X., Sun, J., Mao, Y., Wang, W., 2022. Review of chemical looping process for carbonaceous feedstock conversion: rational design of oxygen carriers. Fuel 325, 124964.

Zhang, X.Y., Cao, L.Y., Xiang, W., Xu, Y., Gao, B., 2022. Preparation and evaluation of fine-tuned micropore biochar by lignin impregnation for CO_2 and VOCs adsorption. Sep. Purif. Technol. 295. doi:10.1016/j.seppur.2022.121295.

Zhang, Y., Ma, L., Lv, Y., Tan, T., 2022. Facile manufacture of COF-based mixed

matrix membranes for efficient CO_2 separation. Chem. Eng. J. 430, 133001. doi:10.1016/j.cej.2021.133001.
Zhang, Y., Wang, S.Z., Feng, D.D., Gao, J.M., Dong, L.H., Zhao, Y.J., Sun, S.Z., Huang, Y.D., Qin, Y.K., 2022. Functional biochar synergistic solid/liquid-phase CO_2 capture: a review. Energy Fuels 36 (6), 2945–2970. doi:10.1021/acs.energyfuels.1c04372.
Zhang, Z., Zheng, Y., Qian, L., Luo, D., Dou, H., Wen, G., Yu, A., Chen, Z., 2022. Emerging trends in sustainable CO_2-management materials. Adv. Mater. 34 (29), 2201547. doi:10.1002/adma.202201547.
Zhang, G., Ingham, D., Ma, L., Pourkashanian, M., 2022. Modelling of 3D liquid dispersion in a rotating packed bed using an Eulerian porous medium approach. Chem. Eng. Sci. 250. doi:10.1016/j.ces.2021.117393, 117393-117393.
Zhang, C., Li, Y., Yang, L., Fan, X., Chu, L., 2022. Analysis on H2 production process integrated CaO/Ca (OH) 2 heat storage and sorption enhanced staged gasification using calcium looping. Energy Convers. Manage. 253, 115169.
Zhang, G., Ma, L., Pourkashanian, M., 2023. A porous medium approach to the 3D modelling of an entire rotating packed bed for post-combustion carbon capture. Chem. Eng. Sci. 274. doi:10.1016/j.ces.2023.118687, 118687-118687.
Zhang, Z., Guo, K., Luo, H., Song, J., Qian, Z., 2014. Characteristics of mass transfer between gas-liquid phases in a higee reactor. Chemical Industry and Chemical Engineering Quarterly 20 (4), 523–530. doi:10.2298/CICEQ130729034Z.
Zhao, Y., Ho, W.W., 2012. Steric hindrance effect on amine demonstrated in solid polymer membranes for CO_2 transport. J. Membr. Sci. 415, 132–138.
Zhao, Y., Winston Ho, W.S., 2012. Steric hindrance effect on amine demonstrated in solid polymer membranes for CO_2 transport. J. Membr. Sci. 415-416, 132–138. doi:10.1016/j.memsci.2012.04.044.
Zhao, J., Wang, Z., Wang, J., Wang, S., 2006. Influence of heat-treatment on CO_2 separation performance of novel fixed carrier composite membranes prepared by interfacial polymerization. J. Membr. Sci. 283 (1), 346–356. doi:10.1016/j.memsci.2006.07.004.
Zhao, T., Ochoa-Fernández, E., Rønning, M., Chen, D., 2007. Preparation and high-temperature CO_2 capture properties of nanocrystalline Na2ZrO3. Chem. Mater. 19 (13), 3294–3301.
Zhao, L., Bacsik, Z., Hedin, N., Wei, W., Sun, Y., Antonietti, M., Titirici, M.M., 2010. Carbon dioxide capture on amine-rich carbonaceous materials derived from glucose. ChemSusChem 3 (7), 840–845. doi:10.1002/cssc.201000044.
Zhao, Y., Ding, H., Zhong, Q., 2012. Preparation and characterization of aminated graphite oxide for CO_2 capture. Appl. Surf. Sci. 258 (10), 4301–4307. doi:10.1016/j.apsusc.2011.12.085.
Zhao, Y., Yao, K.X., Teng, B., Zhang, T., Han, Y., 2013. A perfluorinated covalent triazine-based framework for highly selective and water–tolerant CO_2 capture. Energy Environ. Sci. 6 (12), 3684–3692.
Zhao, M., Bilton, M., Brown, A.P., Cunliffe, A.M., Dvininov, E., Dupont, V., Comyn, T.P., Milne, S.J., 2014. Durability of CaO–CaZrO3 sorbents for high-temperature CO_2 capture prepared by a wet chemical method. Energy Fuels 28 (2), 1275–1283. doi:10.1021/ef4020845.
Zhao, R., Deng, S., Zhao, L., Liu, Y., Tan, Y., 2015. Energy-saving pathway exploration of CCS integrated with solar energy: Literature research and comparative analysis. Energy Convers. Manage. 102, 66–80. doi:10.1016/J.ENCONMAN.2015.01.018.
Zhao, S., Feron, P.M., Deng, L., Favre, E., Chabanon, E., Yan, S., Hou, J., Chen, V., Qi, H., 2016. Status and progress of membrane contactors in post-combustion carbon capture: A state-of-the-art review of new developments. J. Membr. Sci. 511, 180–206. doi:10.1016/j.memsci.2016.03.051.
Zhao, L., Chen, Y., Wang, B., Sun, C., Chakraborty, S., Ramasubramanian, K., Dutta, P.K., Ho, W.W., 2016. Multilayer polymer/zeolite Y composite membrane structure for CO_2 capture from flue gas. J. Membr. Sci. 498, 1–13.
Zhao, B., Liu, F., Cui, Z., Liu, C., Yue, H., Tang, S., Liu, Y., Lu, H., Liang, B., 2017. Enhancing the energetic efficiency of MDEA/PZ-based CO_2 capture technology for a 650 MW power plant: Process improvement. Appl. Energy 185, 362–375. doi:10.1016/j.apenergy.2016.11.009.
Zhao, M., Lu, Q., Ma, Q., Zhang, H., 2017. Two-dimensional metal-organic framework nanosheets. Small Methods 1 (1-2), 1600030. doi:10.1039/C8CS00268A.
Zhao, X., Zhou, H., Sikarwar, V.S., Zhao, M., Park, A.-H.A., Fennell, P.S., Shen, L., Fan, L.-S., 2017. Biomass-based chemical looping technologies: the good, the bad and the future. Energy Environ. Sci. 10 (9), 1885–1910. doi:10.1039/C6EE03718F.
Zhao, Q., Wu, F., He, Y., Xiao, P., Webley, P.A., 2017. Impact of operating parameters on CO_2 capture using carbon monolith by Electrical Swing Adsorption technology (ESA). Chem. Eng. J. 327, 441–453. doi:10.1016/j.cej.2017.06.123.
Zhao, R., Deng, S., Liu, Y., Zhao, Q., He, J., Zhao, L., 2017a. Carbon pump: Fundamental theory and applications. Energy 119, 1131–1143. doi:10.1016/j.energy.2016.11.076.
Zhao, R., Deng, S., Zhao, L., Zhao, Y., Li, S., Zhang, Y., Yu, Z., 2017b. Experimental study and energy-efficiency evaluation of a 4-step pressure-vacuum swing adsorption (PVSA) for CO_2 capture. Energy Convers. Manage. 151, 179–189. doi:10.1016/j.enconman.2017.08.057.
Zhao, R., Zhao, L., Deng, S., Song, C., He, J., Shao, Y., Li, S., 2017c. A comparative study on CO_2 capture performance of vacuum-pressure swing adsorption and pressure-temperature swing adsorption based on carbon pump cycle. Energy 137, 495–509. doi:10.1016/j.energy.2017.01.158.
Zhao, Q., Wu, F., Xie, K., Singh, R., Zhao, J., Xiao, P., Webley, P.A., 2018. Synthesis of a novel hybrid adsorbent which combines activated carbon and zeolite NaUSY for CO_2 capture by electric swing adsorption (ESA). Chem. Eng. J. 336, 659–668. doi:10.1016/j.cej.2017.11.167.
Zhao, T.X., Zhang, X.M., Tu, Z.H., Wu, Y.T., Hu, X.B., 2018. Low-viscous diamino protic ionic liquids with fluorine-substituted phenolic anions for improving CO_2 reversible capture. J. Mol. Liq. 268, 617–624. doi:10.1016/j.molliq.2018.07.096.
Zhao, X., Ji, G.Z., Liu, W., He, X., Anthony, E.J., Zhao, M., 2018. Mesoporous MgO promoted with $NaNO_3$/$NaNO_2$ for rapid and high-capacity CO_2 capture at moderate temperatures. Chem. Eng. J. 332 (Supplement C), 216–226. doi:10.1016/j.cej.2017.09.068.
Zhao, Y., Kuang, Y., Liu, M., Wang, J., Pei, R., 2018. Synthesis of metal-organic framework nanosheets with high relaxation rate and singlet oxygen yield. Chem. Mater. 30 (21), 7511–7520. doi:10.1021/acs.chemmater.8b02467.
Zhao, H., Luo, X., Zhang, H., Sun, N., Wei, W., Sun, Y., 2018. Carbon-based adsorbents for post-combustion capture: a review. Greenh. Gases: Sci. Technol. 8 (1), 11–36. doi:10.1002/ghg.1758.
Zhao, J., Xie, K., Liu, L., Liu, M., Qiu, W., Webley, P.A., 2019. Enhancing plasticization-resistance of mixed-matrix membranes with exceptionally high CO_2/CH_4 selectivity through incorporating ZSM-25 zeolite. J. Membr. Sci. 583, 23–30. doi:10.1016/j.memsci.2019.03.073.
Zhao, Q., Wu, F., Men, Y., Fang, X., Zhao, J., Xiao, P., Webley, P.A., Grande, C.A., 2019. CO_2 capture using a novel hybrid monolith (H-ZSM5/activated carbon) as adsorbent by combined vacuum and electric swing adsorption (VESA). Chem. Eng. J. 358, 707–717. doi:10.1016/j.cej.2018.09.196.
Zhao, Y., Feng, D., Li, B., Sun, S., Zhang, S., 2019. Combustion characteristics of char from pyrolysis of Zhundong sub-bituminous coal under O_2/steam atmosphere: Effects of mineral matter. Int. J. Greenh. Gas Control 80, 54–60. doi:10.1016/j.ijggc.2018.12.001.
Zhao, R., Liu, L., Zhao, L., Deng, S., Li, S., Zhang, Y., 2019a. A comprehensive performance evaluation of temperature swing adsorption for post-combustion carbon dioxide capture. Renew. Sustain. Energy Rev. 114. doi:10.1016/j.rser.2019.109285, 109285-109285.
Zhao, R., Liu, L., Zhao, L., Deng, S., Li, S., Zhang, Y., Li, H., 2019b. Thermodynamic exploration of temperature vacuum swing adsorption for direct air capture of carbon dioxide in buildings. Energy Convers. Manage. 183, 418–426. doi:10.1016/j.enconman.2019.01.009.
Zhao, H., Li, H., Li, X., Gao, X., 2021. Process intensification for improving the uniformity and efficiency of microwave heating reactor by bubbles-enhanced flow method. Appl. Therm. Eng. 197. doi:10.1016/j.applthermaleng.2021.117346.
Zhao, Z., Li, H., Zhao, K., Wang, L., Gao, X., 2022a. Microwave-assisted synthesis of MOFs: Rational design via numerical simulation. Chem. Eng. J. 428. doi:10.1016/j.cej.2021.131006.
Zhao, Z., Shen, X., Li, H., Liu, K., Wu, H., Li, X., Gao, X., 2022b. Watching microwave-induced microscopic hot spots via the thermosensitive fluorescence of Europium/Terbium mixed-metal organic complexes. Angew. Chem.-Int. Ed. 61 (6). doi:10.1002/anie.202114340.
Zheng, C., Tan, J., Wang, Y., Luo, G., 2012. CO_2 solubility in a mixture absorption system of 2-amino-2-methyl-1-propanol with glycol. Ind. Eng. Chem. Res. 51 (34), 11236–11244.
Zheng, H., Wang, Z., Deng, X., Zhao, J., Luo, Y., Novak, J., Herbert, S., Xing, B., 2013. Characteristics and nutrient values of biochars produced from giant reed at different temperatures. Bioresour. Technol. 130, 463–471. doi:10.1016/j.biortech.2012.12.044.
Zheng, F., Heldebrant, D.J., Mathias, P.M., Koech, P., Bhakta, M., Freeman, C.J., Bearden, M.D., Zwoster, A., 2016. Bench-scale testing and process performance projections of CO_2 capture by CO_2–binding organic liquids (CO_2BOLs) with and without polarity-swing-assisted regeneration. Energy Fuels doi:10.1021/acs.energyfuels.5b02437.
Zheng, W.T., Zhang, F., Wu, Y.T., Hu, X.B., 2017. Concentrated aqueous solutions of protic ionic liquids as effective CO_2 absorbents with high absorption capacities. J. Mol. Liq. 243, 169–177. doi:10.1016/j.molliq.2017.08.035.
Zheng, W.-T., Huang, K., Dai, S., 2019. Solvothermal and template-free synthesis of N-Functionalized mesoporous polymer for amine impregnation and CO_2 adsorption. Microporous Mesoporous Mater. 290. doi:10.1016/j.micromeso.2019.109653.
Zheng, X., Fukuhara, K., Hijikata, Y., Pirillo, J., Sato, H., Takahashi, K., Noro, S., Nakamura, T., 2020. Understanding the interactions between the bis (trifluoromethylsulfonyl)imide anion and absorbed CO_2 using X-ray diffraction analysis of a soft crystal surrogate. Commun. Chem. 3 (1). doi:10.1038/s42004-020-00390-1.
Zheng, S., Zeng, S., Li, Y., Bai, L., Bai, Y., Zhang, X., Liang, X., Zhang, S., 2021. State of the art of ionic liquid-modified adsorbents for CO_2 capture and separation. AIChE J. 68 (2). doi:10.1002/aic.17500.
Zheng, W., Liu, Z., Ding, R., Dai, Y., Li, X., Ruan, X., He, G., 2022. Constructing continuous and fast transport pathway by highly permeable polymer electrospun fibers in composite membrane to improve CO_2 capture. Sep. Purif. Technol. 285, 120332. doi:10.1016/j.seppur.2021.120332.
Zheng, Q., Xie, Y., Tan, J., Xu, Z., Luo, P., Wang, T., Liu, Z., Liu, F., Zhang, K., Fang, Z., Zhang, G., Jin, W., 2022. Coupling of dielectric barrier discharge plasma with oxygen permeable membrane for highly efficient low-temperature permeation. J. Membr. Sci. 641, 119896. doi:10.1016/J.MEMSCI.2021.119896.
Zhou, S., Chen, X., Nguyen, T., Voice, A.K., Rochelle, G.T., 2010. Aqueous ethylenediamine for CO_2 capture. ChemSusChem 3 (8), 913–918. doi:10.1002/cssc.200900293.
Zhou, C., Shah, K., Moghtaderi, B., 2015a. Techno-economic assessment of integrated chemical looping air separation for oxy-fuel combustion: An Australian case study. Energy Fuels 29 (4), 2074–2088. doi:10.1021/EF5022076/SUPPL_FILE/EF5022076_SI_001.PDF.
Zhou, C., Shah, K., Song, H., Zanganeh, J., Doroodchi, E., Moghtaderi, B., 2015b. Integration options and economic analysis of an integrated chemical looping air separation process for oxy-fuel combustion. Energy Fuels 30 (3), 1741–1755. doi:10.1021/ACS.ENERGYFUELS.5B02209.
Zhou, C., Shah, K., Song, H., Zanganeh, J., Doroodchi, E., Moghtaderi, B., 2016. Integration options and economic analysis of an integrated chemical looping air separation process for oxy-fuel combustion. Energy Fuels 30 (3), 1741–1755. doi:10.1021/ACS.ENERGYFUELS.5B02209/ASSET/IMAGES/LARGE/EF-2015-02209K_0023.JPEG.
Zhou, Z., Zhou, X., Jing, G., Lv, B., 2016. Evaluation of the multi-amine functionalized

ionic liquid for efficient postcombustion CO_2 capture. Energy Fuels 30 (9), 7489–7495. doi:10.1021/acs.energyfuels.6b00692.
Zhou, K., Chaemchuen, S., Verpoort, F., 2017. Alternative materials in technologies for biogas upgrading via CO_2 capture. Renew. Sustain. Energy Rev. 79, 1414–1441. doi:10.1016/j.rser.2017.05.198.
Zhou, X., Liu, F., Lv, B., Zhou, Z., Jing, G., 2017. Evaluation of the novel biphasic solvents for CO 2 capture: Performance and mechanism. Int. J. Greenh. Gas Control 60, 120–128. doi:10.1016/j.ijggc.2017.03.013.
Zhou, Z., Anderson, C.M., Butler, S.K., Thompson, S.K., Whitty, K.J., Shen, T.C., Stowers, K.J., 2017. Stability and efficiency of CO_2 capture using linear amine polymer modified carbon nanotubes. J. Mater. Chem. A 5 (21), 10486–10494. doi:10.1039/c7ta02576a.
Zhou, Z., Balijepalli, S.K., Nguyen-Sorenson, A.H.T., Anderson, C.M., Park, J.L., Stowers, K.J., 2018. Steam-stable covalently bonded polyethylenimine modified multiwall carbon nanotubes for carbon dioxide capture. Energy Fuels 32 (11), 11701–11709. doi:10.1021/acs.energyfuels.8b02864.
Zhou, H., Zhao, B., Fu, C., Wu, Z., Wang, C., Ding, Y., Han, B.-H., Hu, A., 2019. Synthesis of conjugated microporous polymers through cationic cyclization polymerization. Macromolecules 52 (10), 3935–3941. doi:10.1021/acs.macromol.9b00437.
Zhou, S., Zhao, Y., Zheng, J., Zhang, S., 2019. High-performance functionalized polymer of intrinsic microporosity (PIM) composite membranes with thin and stable interconnected layer for organic solvent nanofiltration. J. Membr. Sci. 591, 117347. doi:10.1016/j.memsci.2019.117347.
Zhou, X., Jing, G., Lv, B., Liu, F., Zhou, Z., 2019. Low-viscosity and efficient regeneration of carbon dioxide capture using a biphasic solvent regulated by 2-amino-2-methyl-1-propanol. Appl. Energy 235, 379–390. doi:10.1016/j.apenergy.2018.10.118.
Zhou, H.C., Xu, X., Chen, X.C., Yu, G.R., 2020. Novel ionic liquids phase change solvents for CO_2 capture. Int. J. Greenh. Gas Control 98. doi:10.1016/j.ijggc.2020.103068.
Zhou, X., Li, X., Wei, J., Fan, Y., Liao, L., Wang, H., 2020. Novel nonaqueous liquid-liquid biphasic solvent for energy-efficient carbon dioxide capture with low corrosivity. Environ. Sci. Technol. 54 (24), 16138–16146. doi:10.1021/acs.est.0c05774.
Zhou, S., Sun, Y., Xue, B., Li, S., Zheng, J., Zhang, S., 2020a. Controlled superacid-catalyzed self-cross-linked polymer of intrinsic microporosity for high-performance CO_2 separation. Macromolecules 53 (18), 7988–7996.
Zhou, S., Sun, Y., Xue, B., Li, S., Zheng, J., Zhang, S., 2020b. Controlled superacid-catalyzed self-cross-linked polymer of intrinsic microporosity for high-performance CO_2 separation. Macromolecules 53 (18), 7988–7996.
Zhou, G., Wang, K.L., Liu, R.L., Tian, Y., Kong, B., Qi, G.S., 2021. Synthesis and CO_2 adsorption performance of TEPA-loaded cellulose whisker/silica composite aerogel. Colloid Surf. A 631. doi:10.1016/j.colsurfa.2021.127675.
Zhou, Q., Fu, X., Hui Lim, K., Li, Z., Liao, M., Lu, J., Liu, F., Kawi, S., 2022. Complete confinement of Ce/Ni within SiO2 nanotube with high oxygen vacancy concentration for CO_2 methane reforming. Fuel 325, 124819. doi:10.1016/j.fuel.2022.124819.
Zhu, L., Fan, Y., 2011. A real options-based CCS investment evaluation model: Case study of China's power generation sector. Appl. Energy 88 (12), 4320–4333. doi:10.1016/j.apenergy.2011.04.005.
Zhu, Y., Zhang, W., 2014. Reversible tuning of pore size and CO_2 adsorption in azobenzene functionalized porous organic polymers. Chem. Sci. 5 (12), 4957–4961. doi:10.1039/c4sc02305f.
Zhu, L., Zhang, Y.-B., 2017. Crystallization of covalent organic frameworks for gas storage applications. Molecules 22 (7), 1149.
Zhu, W., Hrabanek, P., Gora, L., Kapteijn, F., Moulijn, J.A., 2006. Role of adsorption in the permeation of CH4 and CO_2 through a silicalite-1 membrane. Ind. Eng. Chem. Res. 45 (2), 767–776.
Zhu, Y., Liu, X., Zhou, Z., 2006. Optimization of cryogenic air separation distillation columns. In: Proceedings of the World Congress on Intelligent Control and Automation (WCICA), 2, pp. 7702–7705. doi:10.1109/WCICA.2006.1713466.
Zhu, X., Tian, C., Chai, S., Nelson, K., Han, K.S., Hagaman, E.W., Veith, G.M., Mahurin, S.M., Liu, H., Dai, S., 2013. New tricks for old molecules: development and application of porous N-doped, carbonaceous membranes for CO_2 separation. Adv. Mater. 25 (30), 4152–4158. doi:10.1002/adma.201300793.
Zhu, L., Swihart, M.T., Lin, H., 2017. Tightening polybenzimidazole (PBI) nanostructure via chemical cross-linking for membrane H 2/CO 2 separation. J. Mater. Chem. A 5 (37), 19914–19923.
Zhu, X., Song, M.L., Xu, Y.J., 2017. DBU-based protic ionic liquids for CO_2 capture. ACS Sustain. Chem. Eng. 5 (9), 8192–8198. doi:10.1021/acssuschemeng.7b01839.
Zhu, J., He, B., Huang, J., Li, C., Ren, T., 2018. Effect of immobilization methods and the pore structure on CO_2 separation performance in silica-supported ionic liquids. Microporous Mesoporous Mater. 260, 190–200. doi:10.1016/j.micromeso.2017.10.035.
Zhu, L., Swihart, M.T., Lin, H., 2018. Unprecedented size-sieving ability in polybenzimidazole doped with polyprotic acids for membrane H2/CO_2 separation. Energy Environ. Sci. 11 (1), 94–100. doi:10.1039/c7ee02865b.
Zhu, Z., Chen, Y., Wu, J., Zhang, S., Zheng, S., 2019a. A modified Allam cycle without compressors realizing efficient power generation with peak load shifting and CO_2 capture. Energy 174, 478–487.
Zhu, Z., Chen, Y., Wu, J., Zheng, S., Zhao, W., 2019b. Performance study on s-CO_2 power cycle with oxygen fired fuel of s-water gasification of coal. Energy Convers. Manage. 199, 112058.
Zhu, W.K., Yao, Y., Zhang, Y., Jiang, H., Wang, Z., Chen, W., Xue, Y.Y., 2020. Preparation of an amine-modified cellulose nanocrystal aerogel by chemical vapour deposition and its application in CO_2 capture. Ind. Eng. Chem. Res. 59 (38), 16660–16668. doi:10.1021/acs.iecr.0c02687.
Zhu, X., Chen, L., Chen, Y., Cao, Q., Liu, X., Li, D., 2020. Effect of H2 addition on the microbial community structure of a mesophilic anaerobic digestion system. Energy 198, 117368. doi:10.1016/j.energy.2020.117368.
Zhu, X., Imtiaz, Q., Donat, F., Müller, C.R., Li, F., 2020. Chemical looping beyond combustion – a perspective. Energy Environ. Sci. 13 (3), 772–804. doi:10.1039/C9EE03793D.
Zhu, X., Ge, T., Yang, F., Wang, R., 2021. Design of steam-assisted temperature vacuum-swing adsorption processes for efficient CO_2 capture from ambient air. Renew. Sustain. Energy Rev. 137, 110651. doi:10.1016/j.rser.2020.110651.
Zhu, L., Yin, D., Qin, Y., Konda, S., Zhang, S., Zhu, A., Liu, S., Xu, T., Swihart, M.T., Lin, H., 2019. Sorption-enhanced mixed matrix membranes with facilitated hydrogen transport for hydrogen purification and CO_2 capture. Adv. Funct. Mater. 29 (36), 1904357.
Zhuang, Q., Clements, B., 2018. CO_2 capture by biphasic absorbent—absorption performance and VLE 2 characteristic. Energy 147, 169. doi:10.1016/j.energy.
Zhuang, Y., Seong, J.G., Lee, W.H., Do, Y.S., Lee, M.J., Wang, G., Guiver, M.D., Lee, Y.M., 2015. Mechanically tough, thermally rearranged (TR) random/block poly (benzoxazole-co-imide) gas separation membranes. Macromolecules 48 (15), 5286–5299.
Zhuo, H., Hu, Y.J., Tong, X., Zhong, L.X., Peng, X.W., Sun, R.C., 2016. Sustainable hierarchical porous carbon aerogel from cellulose for high-performance supercapacitor and CO_2 capture. Ind. Crops Prod. 87, 229–235. doi:10.1016/j.indcrop.2016.04.041.
Ziółkowski, P., Zakrzewski, W., Kaczmarczyk, O., Badur, J., 2013. Thermodynamic analysis of the double Brayton cycle with the use of oxy combustion and capture of CO_2. Arch. Thermodyn. 34 (2), 23–38. doi:10.2478/aoter-2013-0008.
Ziaii, S., Rochelle, G.T., Edgar, T.F., 2009. Dynamic modeling to minimize energy use for CO 2 capture in power plants by aqueous monoethanolamine. Ind. Eng. Chem. Res. 48 (13), 6105–6111. doi:10.1021/ie801385q.
Zoghlami, A., Paes, G., 2019. Lignocellulosic biomass: understanding recalcitrance and predicting hydrolysis. Front. Chem. 7. doi:10.3389/fchem.2019.00874.
Zornoza, B., Téllez, C., Coronas, J., Esekhile, O., Koros, W.J., 2015. Mixed matrix membranes based on 6FDA polyimide with silica and zeolite microsphere dispersed phases. AIChE J. 61 (12), 4481–4490.
Zou, C., Zhang, L., Cao, S., Zheng, C., 2014a. A study of combustion characteristics of pulverized coal in O_2/H_2O atmosphere. Fuel 115, 312–320. doi:10.1016/j.fuel.2013.07.025.
Zou, C., Zhang, L., Cao, S., Zheng, C., 2014b. A study of combustion characteristics of pulverized coal in O 2 /H 2 O atmosphere. Fuel 115, 312–320.
Zou, C., Cai, L., Wu, D., Liu, Y., Liu, S., Zheng, C., 2015a. Ignition behaviors of pulverized coal particles in O_2/N_2 and O_2/H_2O mixtures in a drop tube furnace using flame monitoring techniques. Proc. Combust. Instit. 35 (3), 3629–3636. doi:10.1016/j.proci.2014.06.067.
Zou, C., Cai, L., Wu, D., Liu, Y., Liu, S., Zheng, C., 2015b. Ignition behaviors of pulverized coal particles in O 2 /N 2 and O 2 /H 2 O mixtures in a drop tube furnace using flame monitoring techniques. Proc. Combust. Instit. 35 (3), 3629–3636.
Zou, L., Sun, Y., Che, S., Yang, X., Wang, X., Bosch, M., Wang, Q., Li, H., Smith, M., Yuan, S., Perry, Z., Zhou, H.C., 2017. Porous organic polymers for post-combustion carbon capture. Adv. Mater. 29 (37). doi:10.1002/adma.201700229.
Zubbri, N.A., Mohamed, A.R., Kamiuchi, N., Mohammadi, M., 2020. Enhancement of CO_2 adsorption on biochar sorbent modified by metal incorporation. Environ. Sci. Pollut. Res. 27 (11), 11809–11829. doi:10.1007/s11356-020-07734-3.
Zubbri, N.A., Mohamed, A.R., Lahijani, P., Mohammadi, M., 2021. Low temperature CO_2 capture on biomass-derived KOH-activated hydrochar established through hydrothermal carbonization with water-soaking pre-treatment. J. Environ. Chem. Eng. 9 (1). doi:10.1016/j.jece.2021.105074.
Zydney, A.L., 1995. Membrane handbook edited by W. S. Winston Ho, and Kamalesh K. Sirkar, Van Nostrand Reinhold, New York, 1992, 954 pp. $131.95. 41 (10), 2343-2344. https://doi.org/10.1002/aic.690411024.